# Seismic base isolation using natural materials - experimental and numerical verification

**Banović, Ivan**

# UNIVERSITY OF SPLIT

## FACULTY OF CIVIL ENGINEERING, ARCHITECTURE AND GEODESY

**Ivan Banović, mag. ing. aedif.**


# SEISMIC BASE ISOLATION USING NATURAL MATERIALS – EXPERIMENTAL AND NUMERICAL VERIFICATION

**Doctoral Dissertation**


**Split, 2021.**

Ivan Banović, mag. ing. aedif.
Serial number: 052

**This dissertation has been submitted for evaluation to the University of Split, Faculty of Civil Engineering, Architecture and Geodesy, for the purpose of obtaining the doctoral degree in Technical Sciences, field of Civil Engineering.**

**Supervisor:** Prof. Jure Radnić, PhD

**Committee for the doctoral dissertation assessment:**

Prof. Alen Harapin, PhD
Prof. Boris Trogrlić, PhD
Prof. Damir Varevac, PhD

**Committee for the doctoral dissertation defense:**

Prof. Alen Harapin, PhD

Prof. Boris Trogrlić, PhD

Prof. Damir Varevac, PhD

The doctoral dissertation has been defended on March 26, 2021.

Secretary:

Saša Delić, LL.M.

**This doctoral dissertation contains:**

240 pages
201 figures
17 tables
143 references

***Dedicated to my family***

This research was carried out at the Seismic Testing Centre of the Faculty of Civil Engineering, Architecture and Geodesy, at the University of Split. The work has been fully supported by the Croatian Science Foundation under the project *"Seismic base isolation of a building by using natural materials – shake table testing and numerical modelling*" [IP-06-2016-5325]. Furthermore, the work of doctoral student Ivan Banović has been fully supported by the *"Young researchers' career development project – training of doctoral students"* of the Croatian Science Foundation funded by the European Union from the European Social Fund. Their support is gratefully acknowledged. The opinions expressed in the dissertation are those of the author only and do not necessarily reflect those of the funders.

*Throughout the writing of this dissertation I have received a great deal of support.*

*First, I would like to express my deepest gratitude to my supervisor, Prof. Jure Radnić, for the continuous support, patience, motivation, and his immense knowledge. Countless discussions, corrections, advices and help are invaluable. I am deeply grateful for all that he did for me on personal and professional level.*

*Besides my supervisor, I would like to thank my dissertation committee: Prof. Alen Harapin, Prof. Boris Trogrlić, and Prof. Damir Varevac, for their insightful comments and suggestions that have increased the dissertation quality.*

*Many thanks also to Asst. Prof. Nikola Grgić, for discussions, advices, and help. His valuable guidance throughout my research is deeply appreciated. Also, thanks to lab technician Krešimir Vranješ for his help during experimental tests.*

*I would like to acknowledge my colleagues: Ante Buzov, PhD, Asst. Prof. Marija Smilović Zulim, and Asst. Prof. Marina Sunara for support and advices. Many thanks!*

*I would like to thank my parents and my brother. Their support, not only through last few years but for my whole life was enormous.*

*Finally, I would like to thank the most important people of life, my wife Ivanica and my children Toma and Marijeta for their support, patience, and loving along the process.*

*Thank you, dear God for giving me patience and will, for such a venture.*

UDC 624.042.7:624.591.14:691.22]:519.87](043.3)

Ivan Banović, mag. ing. aedif.

# Seismic base isolation using natural materials – experimental and numerical verification

**Abstract:**

The problem under consideration is the earthquake impact on structures. The subject of the performed research is the efficiency of seismic base isolation using layers of predominantly natural materials below the foundation, as well as the development of a numerical model for seismic analysis of structures with such isolation. The aseismic layers below foundation are made of limestone sand – *ASL-1*, stone pebbles – *ASL-2*, and stone pebbles combined with layers of geogrid and geomembrane – *ASL-3*. The experimental research methodology is based on the use of shake-table and other modern equipment for dynamic and static testing of structures. Experiments were conducted on the basis of detailed research plan and program.

Efficiency of the limestone sand layer – *ASL-1* was tested on cantilever concrete columns, under seismic excitations up to failure, varying the sand thickness and intensity of seismic excitation.

Influence of several layer parameters on the efficiency of stone pebble layer – *ASL-2* was investigated. For each considered layer parameter, a rigid model $M_0$ was exposed to four different accelerograms, with three levels of peak ground acceleration (0.2 g, 0.4 g and 0.6 g), while all other layer parameters were kept constant. On the basis of test results, the optimal pebble layer was adopted. Afterwards, the optimal *ASL-2* efficiency was tested on various model parameters: stiffness (deformable models $M_1$-$M_4$), foundation size (small and large), excitation type (four earthquake accelerograms), and stress level in the model (elastic and up to failure).

In the *ASL-3* composite aseismic layer, the optimal *ASL-2* is combined with a thin additional layer of sliding material (geogrid, geomembrane above limestone sand layer), in order to achieve greater efficiency of this layer than that of the *ASL-2*. A total of eleven different aseismic layers were considered. To determine the optimal *ASL-3*, the $M_0$ model was used, like for the *ASL-2*. On the basis of test results, the optimal *ASL-3* layer was adopted (one higher strength geogrid at the pebble layer top). The optimal *ASL-3* is tested on various model parameters, analogous to the optimal *ASL-2*.

A numerical model for reliable seismic analysis of concrete, steel, and masonry structures with seismic base isolation using *ASL-2* was developed, with innovative constitutive model for

seismic isolation. The model can simulate the main nonlinear effects of mentioned materials, and was verified on performed experimental tests.

In relation to the rigid base – *RB* without seismic isolation, model based on the *ASL-1* had an average reduction in seismic force and strain/stress by approximately 10% at lower *PGA* levels and approximately 14% at model failure. Due to the effect of sand calcification over time, the long-term seismic efficiency of such a layer is questionable.

It was concluded that the aseismic layers *ASL-2* and *ASL-3* are not suitable for models of medium-stiff structure $M_3$ and soft structure $M_4$.

In relation to the *RB* without seismic isolation, the $M_1$ (very stiff structure) and $M_2$ (stiff structure) based on the *ASL-2* had an average reduction in seismic force and strain/stress by approximately 13% at lower *PGA* levels and approximately 25% at model failure.

In relation to the *RB* without seismic isolation, the $M_1$ and $M_2$ based on the *ASL-3* had an average reduction in seismic force and strain/stress by approximately 25% at lower *PGA* levels and approximately 34% at model failure.

In relation to the *RB* without seismic isolation, the *ASL-2* and *ASL-3* did not result in major $M_1$ and $M_2$ model displacements, which was also favourable. It is concluded that the *ASL-2* and especially *ASL-3* have great potential for seismic base isolation of very stiff and stiff structures, as well as small bridges based on solid ground, but further research is needed.

In addition, it was concluded that the developed numerical model has great potential for practical application. Finally, further verification of the created numerical model on the results of other experimental tests is needed, but also improvement of the developed constitutive models.

**Keywords:** seismic base isolation, limestone sand, stone pebbles, geosynthetics, shake-table testing, numerical modelling

UDK 624.042.7:624.591.14:691.22]:519.87](043.3)

Ivan Banović, mag. ing. aedif.

# Seizmička izolacija osnove građevine uporabom prirodnih materijala – eksperimentalna i numerička provjera

**Sažetak:**

Problem koji se razmatra je utjecaj potresa na građevine. Predmet istraživanja je efikasnost seizmičke izolacije osnove građevine uporabom prirodnih materijala, kao i razvoj numeričkog modela za dinamičku analizu konstrukcija s predmetnom seizmičkom izolacijom. Aseizmički slojevi ispod temelja izrađeni su od vapnenačkog pijeska – *ASL-1*, kamenih oblutaka – *ASL-2* i kamenih oblutaka u kombinaciji s geomrežama i geomembranom – *ASL-3*. Metodologija eksperimentalnih istraživanja temelji se na korištenju potresne platforme i ostale moderne opreme za statička i dinamička ispitivanja konstrukcija. Eksperimenti su provedeni prema detaljnom planu i programu ispitivanja.

Efikasnost sloja *ASL-1* testirana je na konzolnim armiranobetonskim stupovima izloženim seizmičkom djelovanju do sloma, gdje je varirana debljina sloja pijeska i intenzitet seizmičke pobude.

Istražen je utjecaj više parametara sloja oblutaka *ASL-2* na njegovu aseizmičku efikasnost. Za svaki razmatrani parametar model krute zgrade $M_0$ izložen je djelovanju četiriju različitih akcelerograma, s tri razine vršnog ubrzanja (0.2 g, 0.4 g i 0.6 g), dok su ostali parametri sloja nepromjenjivi. Na temelju rezultata testova odabran je optimalni sloj *ASL-2*. Potom je efikasnost optimalnog sloja *ASL-2* testirana pod utjecajem raznih parametara modela: krutost (deformabilni modeli $M_1$-$M_4$), veličina temelja (mali, veliki), tip potresa (četiri različita akcelerograma) i razina naprezanja (elastična, do sloma).

Da bi se dobio još efikasniji aseizmički sloj *ASL-3*, optimalnom sloju *ASL-2* dodavani su razni klizni slojevi (geomreže, geomembrana na sloju pijeska). Kreirano je jedanaest različitih kompozitnih slojeva *ASL-3* čija je efikasnost testirana na modelu krute zgrade $M_0$ kao kod sloja *ASL-2*. Na temelju rezultata testova određen je optimalni sloj *ASL-3* (*ASL-2* s jednom geomrežom veće površine na vrhu sloja). Potom je efikasnost optimalnog sloj *ASL-3* testirana pod utjecajem raznih parametara modela, kao kod testiranja sloja *ASL-2*.

Razvijen je pouzdani numerički model za seizmičku analizu betonskih, čeličnih i zidanih konstrukcija sa seizmičkom izolacijom baze pomoću sloja *ASL-2*, s inovativnim konstitutivnim

modelom aseizmičkog sloja. Model može simulirati najvažnije nelinearne efekte u navedenim materijalima, a provjeren je na rezultatima provedenih eksperimentalnih testova.

Zaključeno je da, u odnosu na krutu podlogu, sloj *ASL-1* može povećati sigurnost testiranih modela za približno 10% pri nižim razinama ubrzanja podloge te približno 14% pri slomu modela. Zbog efekta kalcifikacije pijeska dugotrajna efikasnost ovog sloja je upitna.

Zaključeno je da razmatrane aseizmičke podloge *ASL-2* i *ASL-3* nisu prikladne kod modela srednje krutih $M_3$ i mekih konstrukcija $M_4$.
U odnosu na krutu podlogu – *RB*, modeli $M_1$ (vrlo kruta konstrukcija) i $M_2$ (kruta konstrukcija) s aseizmičkim slojem *ASL-2* imali su prosječno smanjenje potresnih sila i naprezanja/deformacija od 13% pri nižim razinama ubrzanja podloge te približno 25% pri slomu modela.
U odnosu na *RB* modeli $M_1$ i $M_2$ sa aseizmičkim slojem *ASL-3* imali su prosječno smanjenje potresnih sila i naprezanja/deformacija od 25% pri nižim razinama ubrzanja podloge, te približno 34% pri slomu modela.
U odnosu na *RB* modeli $M_1$ i $M_2$ oslonjeni na *ASL-2* i *ASL-3* nisu imali veće pomake, što je povoljno. Zaključeno je da slojevi *ASL-2* i *ASL-3* imaju veliki potencijal za praktičnu primjenu kod vrlo krutih i krutih zgrada, kao i mostova manjih raspona temeljenih na čvrstom tlu. Ipak, potrebna su daljnja istraživanja.

Također, zaključeno je da razvijeni numerički model ima veliki potencijal za praktičnu primjenu. Potrebna je daljnja verifikacija kreiranog modela na rezultatima eksperimentalnih testova, kao i poboljšanje razvijenih konstitutivnih modela.

**Ključne riječi:** seizmička izolacija osnove građevine, vapnenački pijesak, kameni oblutci, geosintetici, testiranje potresnom platformom, numeričko modeliranje

## LIST OF APPENDED PAPERS AND MY CONTRIBUTION

The doctoral dissertation is based on eight papers (see Appendix), referred by Roman numerals in the text of the dissertation:

| No. | Paper Title | JCR Rank* |
|---|---|---|
| [I] | **Banović I.**, Radnić J., Grgić N., Matešan D., *The use of limestone sand for the seismic base isolation of structures*, Advances in Civil Engineering, Article ID 9734283, 12 pages, 2018., doi:10.1155/2018/9734283 | Q3 |
| [II] | **Banović I.**, Radnić J., Grgić N., *Geotechnical seismic isolation system based on sliding mechanism using stone pebble layer: shake-table experiments*, Shock and Vibration, Article ID 9346232, 26 pages, 2019., doi:10.1155/2019/9346232 | Q2 |
| [III] | **Banović I.**, Radnić J., Grgić N., *Shake table study on the efficiency of seismic base isolation using natural stone pebbles*, Advances in Materials Science and Engineering, Article ID 1012527, 20 pages, 2018., doi:10.1155/2018/1012527 | Q3 |
| [IV] | **Banović I.**, Radnić J., Grgić N., *Effect of structural stiffness on the efficiency of seismic base isolation using layers of stone pebbles*, Ingegneria Sismica, Vol. 37 (2), 66-91, 2020. | Q2 |
| [V] | **Banović I.**, Radnić J., Grgić N., *Foundation size effect on the efficiency of seismic base isolation using a layer of stone pebbles*, Earthquakes and Structures, Vol. 19 (2), 103-117, 2020., doi:10.12989/eas.2020.19.2.103 | Q3 |
| [VI] | **Banović I.**, Radnić J., Grgić N., *Effectiveness of several low-cost composite seismic base isolations: A shake table study*, 2020., submitted for publication to WoS journal | |
| [VII] | **Banović I.**, Radnić J., Grgić N., *Effect of geogrid on the efficiency of seismic base isolation using natural stone pebbles: A shake table study*, 2020., submitted for publication to WoS journal | |
| [VIII] | **Banović I.**, Radnić J., Grgić N., *Numerical model for dynamic analysis of structures with seismic base isolation using a layer of stone pebbles*, 2020., submitted for publication to WoS journal | |

*****Quartiles are determined for the year of the paper submission or the paper publication, according to the more favourable classification for the candidate

**My contributions to the listed papers:**

- Participation in research planning and testing programme
- Participation in preparation and realization of experimental tests
- Participation in design of the updated numerical model
- Participation in analysis of the experimental and numerical results
- Design of drawings, diagrams and tables based on the experimental and numerical results
- Participation in the development of the research findings/conclusions
- Participation in the creation and writing of all papers

# TABLE OF CONTENT

# 1. INTRODUCTION

## 1.1 Problem and subject of the research

An earthquake is a natural disaster that causes great material and human casualties. Many countries, including Croatia, are in earthquake-prone area. Past and present are witness of strong earthquake disastrous consequences.

Earthquake-resistant design of the load-bearing structure in an earthquake-prone area is a mandatory activity of a civil engineer who participates in the building design (in the case of a new or rehabilitation/strengthening of an existing building). The verification of the building load-bearing structure is usually performed according to the following two approaches:

(i) The earthquake-generated acceleration/force is transmitted directly to the load-bearing structure (foundations) of the building. Based on the external force, displacement and stress (internal force) in the load-bearing structure are calculated. In such an approach, the load-bearing structure of a building receives a large part of the earthquake energy, which is dissipated by plastic deformation and damage to the structural elements. This approach often results in a high cost of load-bearing structure. Furthermore, this traditional approach is still predominantly used in the building design.

(ii) With various solutions, the earthquake-generated acceleration/force tends to be reduced as much as possible before being transmitted to the load-bearing structure. This modern approach is at the beginning of wider application. With this approach, different technological solutions dissipate the earthquake energy under the foundation before transmission to the building.

Seismic base isolation techniques using various types of bearings (elastomeric, spherical, metal "springs", etc.) have been intensively researched for more than half a century, and have found application in the construction of bridges and some important buildings. Unfortunately, a large number of complex devices for seismic force reduction are expensive and rarely applied. The costs of realization of such systems can sometimes be higher than the reduction of the load-bearing structure cost due to the reduction of seismic forces, so their application is not economically justified. Furthermore, such devices require intensive maintenance and their service life is significantly shorter than the operating time of a building. For "rubber" devices, the aging effect can significantly reduce the isolation efficiency.

The idea that a building can be uncoupled from the damaging effects of the ground movement produced by a strong earthquake has appealed to inventors and engineers long time ago (Kelly [K.4]). In the seismic base isolation approach, the load-bearing structure is separated from the movement of the indigenous soil due to an earthquake with various shear "soft" material or device. In general, the basic concept of seismic base isolation is to shift basic period of structure oscillation beyond the dominant frequency range of expected earthquakes. The consequence of using this approach results with increase in the displacement of the structure in the event of an earthquake. Such an approach enables the reduction of seismic load and greater safety of considered building.

Owing to limited resources for earthquake-resistant design of structures, developing countries are more vulnerable to earthquake hazard. In addition, people live in areas at high risk from natural disasters (unsafe urban areas), and the housing was poorly built and can be easily damaged in the event of a disaster (Zorn [Z.4]). Tsang [T.4] reported that earthquakes have killed an average of over 20,000 people a year throughout the world in the past century, with 90% of fatalities occurring in developing countries. Nevertheless, according to OECD report [O.1], earthquakes kill to about 60,000 people a year worldwide – around 90% of which occur in developing countries. Therefore, one of the most important tasks of earthquake engineering is to design safe facilities to protect the lives of people in these marginalized communities. Application of conventional base isolation using complex devices in low-income regions is not viable due to significant limitations: highly-engineered product, maintenance and significant up-front cost (Tsiavos *et al.* [T.9]). In this background, viable low-cost and environmentally friendly seismic base isolation for these regions is the starting point of research within this doctoral dissertation.

It is of particular interest to investigate the possibility of applying a layer of natural materials under the foundations of buildings, bridges and other structures in order to reduce seismic forces and increase their seismic resistance. It is desirable to use materials that can be easily found in nature and that have large stocks. The purpose of such seismic base isolation would be fulfilled even if it allows a lower level of seismic force reduction, compared to more complex and expensive devices. This is especially desirable for less developed countries and rural regions. By analysing the content of the available literature, it can be concluded that there are no detailed and systematic studies of the use of natural materials for seismic base isolation.

In accordance with the above, the subject of research in this dissertation is twofold:

(i) Systematic experimental verification of the efficiency of a thin aseismic layer under the structural model foundation. The aseismic layers are made of:
   - limestone sand
   - stone pebbles (river gravel)
   - stone pebbles with geogrid and geomembrane

(ii) Development of a reliable numerical model for dynamic analysis of structures with seismic base isolation using a layer of stone pebbles.

In general, the problem under consideration is the earthquake impact on structures. The subject of the research is the efficiency of seismic base isolation using layers of predominantly natural materials, as well as the development of a numerical model for seismic analysis of structures with such seismic isolation.

## 1.2 An overview of previous knowledge in the research field

Research in this dissertation is dominant in the field of efficiency of techniques for reducing seismic forces on buildings using the concept of aseismic layer under the foundation of the building, based on experimental tests using a shake-table, and to a lesser extent in the field of numerical modelling of structures with such seismic isolation. In accordance with the above, a review of the literature in the field of research is presented below.

Seismic base isolation techniques using various types of devices, including elastomeric bearings, lead rubber bearings, rubber bearings, friction pendulum bearings, pure-friction sliding isolators and various dampers have been intensively researched since the 1960s and are regularly used in developed countries (Ahmad *et al.* [A.1], Avossa and Pianese [A.8], Calvi *et al.* [C.1], Castaldo and Ripani [C.2], Chang and Spencer [C.3], De Domenico *et al.* [D.1], Eatherton *et al.* [E.1], Kelly [K.4], Lomiento *et al.* [L.1], Morgan *et al.* [M.4], Nanda *et al.* [N.2, N.3], Petrone *et al.* [P.9], Qamaruddin and Ahmad [Q.1], Tashkov *et al.* [T.1]). A state-of-the-art review on the historical development, theory and application of base isolation, with described testing programmes and research needs can be found in literature (Calvi and Calvi [C.1], Kelly [K.4], Makris [M.1], Naiem and Kelly [N.1], Stanton and Roeder [S.8], Warn and Ryan [W.2]). Lately, the lattice metamaterials as innovative energy dissipation devices are presented (Amendola *et al.* [A.1, A.2], Fabbrocino *et al.* [F.1], Fraternali *et al.* [F.5], Titirla *et al.* [T.3]).

Possible solution is a seismic base isolation with a unique, engineered layer below building foundation for seismic hazard mitigation, known as the Geotechnical Seismic Isolation (*GSI*) system (Tsang [T.5]). This solution is particularly relevant for developing countries due to its

rationality and simplicity, with an acceptable reduction of seismic forces on the structure. Namely, low-cost seismic base isolation can be defined as a technological approach that involves the use of a continuous layer of low-modulus materials below the building foundation to mitigate the earthquake hazards on low-rise buildings constructed on rigid soil. In this seismic isolation approach, dissipation of earthquake energy is primarily achieved by reducing the friction under the foundation and its horizontal sliding on the substrate and sliding between the low-modulus material sub-layers (Banović *et al.* [B.5, B.6, B.7], Tsang and Pitilakis [T.6]). Earthquake energy can also be dissipated by reducing the rocking stiffness (Tsang and Pitilakis [T.6]), taking the advantages of rocking isolation, which is a well-known seismic isolation technique (Chen *et al.* [C.11], Chung *et al.* [C.12], Deviprasad and Dodagoudar [D.3], Feng *et al.* [F.2], Hung *et al.* [H.4], Makris [M.2], Masoud *et al.* [M.3], Sarand and Jalali [S.1], Sorrentino *et al.* [S.6, S.7], Tsatsis and Anastasopoulos [T.8], Wang *et al.* [W.1], Xu and Fatahi [X.4]). This isolation method development goes in several directions, using different materials below the foundation. The most important studies dealing low-cost seismic isolation are presented in-detail below.

Carpani [C.7] reported that the idea of loosening the tie between the ground and the structure has its roots in antiquity, as evidenced by a set of construction practices like the interposition of sand or clay layers under the foundations. Furthermore, many scholars reported that throughout history builders utilized natural materials, including layers of gravel, stone, and wood for seismic hazard mitigation (Carpani [C.8], Kulukčija and Humo [K.8], Kulukčija *et al.* [K.9], Przewłócki *et al.* [P.1]). In detail, Kulukčija *et al.* [K.9] provided detailed research on multi-layered timber grillage foundations of two masonry arch bridges dating from the Ottoman period in Bosnia and Herzegovina. The development of seismic isolators for low-cost buildings analysed Kelly [K.5] and Kelly and Taniwangsa [K.6]. They presented experimental and analytical studies of base isolation applications for low-cost housing, especially natural rubber isolation systems.

Based on experimental study results, Tehrani and Hasani [T.2] concluded that clay and sand are acceptable material for base isolation of buildings in Iran. Radnić *et al.* [R.1] also reported that layer of sand reduced earthquake-induced stress in concrete columns tested on shake-table. Anastasopoulos *et al.* [A.5] studied the seismic performance of a rocking-isolated bridge pier on surface foundation, resting on sand. Author conducted series of reduced-scale shaking table tests, comparing the performance of a rocking-isolated system to a pier founded on conventionally designed foundation. The rocking-isolated pier was effectively protected, surviving all seismic excitations without structural damage, at the expense of increased foundation settlement due to a low static factor of safety ($FS_v$). Following this study, Anastasopoulos *et al.* [A.6] conducted further experimental study on the rocking response of single-degree-of-freedom systems on

shallow improved sand. In this study, shallow soil improvement was considered as an alternative to prevent unforeseen inadequate $FS_V$. Authors reported that shallow soil improvement is quite effective provided that its depth is equal to the width of the foundation. In this context, Masoud *et al.* [M.3] investigated performance of geogrid and geocell as soil reinforcement elements at different depth ratios on the rocking isolation potential of high-rise bridge foundations. They reported that using a geocell at depth ratios of less than 0.25 effectively reduced settlements.

In order to improve the seismic performance of low-rise buildings by the introduction of a simple, low-cost seismic isolation system, Xiao *et al.* [X.1] tested performance of sand, lighting ridge pebble, polypropylene and PVC sheet, and polythene membrane as isolation materials. Patil *et al.* [P.2, P.3] tested clean river sand as base isolation material and performed shake-table tests on model with raft foundation. They reported that the degree of isolation varied depending on the soil properties and magnitude of the ground motion. The isolation proved to be higher as magnitude of ground acceleration was higher. Recently, Tsiavos *et al.* [T.10] conducted a large-scale experimental study that explores the beneficial effect of the encapsulation of sand grains between two PVC surfaces on the initiation of sliding and the dissipation of seismic energy between the surfaces. The experimentally derived response of the seismically isolated structure is compared with the response of the corresponding fixed-base structure. They reported that the seismic isolation system set an upper bound to the response of the structure for ground motion excitations exceeding the design level. Further, Tsiavos *et al.* [T.11] investigated the effect of the deformability of a sliding layer on the sliding displacement and acceleration response of structures subjected to harmonic and pulse ground motion excitations. They presented a novel, generalized and dimensionless mathematical formulation that reduced drastically the complexity of the variables compared to the existing formulations. Authors reported that use of deformable layer is beneficial for seismic and vibration isolation of structures as it leads to a significant reduction of their maximum acceleration response compared to the rigid-plastic sliding layer case.

Zhao *el al.* [Z.2] performed numerical investigation of the foundation base pressure and gravel cushion thickness on the layer isolation effect. They reported that the isolation effect of the cushion increased with the layer thickness increase and decreased with the base pressure increase. Zhang [Z.1] also experimentally tested performance of gravel as base isolation material to reduce the seismic response of an upper structure. The Rio–Antirion Bridge (Pecker [P.7]) in Greece, the Vasco de Gama Bridge (Pecker *et al*. [P.8]) in Portugal, and the Izmit Bay Bridge (Steenfelt *et al.* [S.9]) in Turkey have pylons founded on caisson-cushion-pile composite foundation.

Tsang [T.5] proposed use of rubber-soil mixtures (*RSM*) around the foundation of structures for absorbing seismic energy as a promising seismic isolation method particularly suitable for developing countries. The author pointed out that the distinctive advantage of the proposed method is significant reduction of the shaking level due to vertical ground motion, at which an increasing attention has been paid in the earthquake engineering community. In addition, Tsang carried out series of numerical simulations and a parametric study. Furthermore, as mentioned earlier, Tsang [T.5] proposed that the seismic isolation methods involving geotechnics could be collectively termed *Geotechnical Seismic Isolation (GSI)*, in contrast to the commonly used *Structural Seismic Isolation*. Owing the possibility to consume a stockpile of waste tires worldwide, the concept of *GSI* using *RSM* layer has attracted a lot of research interest in the last decade. Based on aforementioned parametric numerical study [T.5], Xiong and Li [X.2] and Xiong *et al.* [X.3] conducted shaking-table experiments to validate *RSM* dynamic performance during earthquakes. The present experimental results showed that the *GSI* system has potential to significantly mitigate seismic hazards, and authors reported that this system attenuated structural response, in terms of the maximal output acceleration, by 30–50%. Hence, the seismic isolation performance of the *GSI* technique has increased with an increase in the intensity of the input acceleration.

Bandyopadhyay *et al.* [B.4] also conducted shake-table test to evaluate seismic performance of sand and *RSM* layer as low-cost base isolators. They reported that the performance of a composite consisting of sand and 50% shredded rubber tire placed under the footing is found to be most promising as a low-cost effective base isolator. More recently, Tsiavos *et al.* [T.9] experimentally tested a sliding layer consisting of a deformable sand-rubber granular mixture as a seismic isolation strategy for low-rise, small footprint buildings in developing countries. They performed direct shear tests to quantify the angle of friction of three different sand-rubber mixtures subjected to different vertical stress levels. Also, they identified the frictional characteristics of sliding between a sand-rubber layer and a timber interface. Finally, they determined the optimum grain size ratio and the height of the sand-rubber layer, that corresponds to the lower (and more favourable from a seismic isolation view point) friction coefficient between the sand-rubber layer and the foundation. Dhanya *et al.* [D.4, D.5] evaluated the seismic performance of *GSI* by experimental and numerical tests. They focused on the use of geogrid reinforcement to improve the bearing capacity, settlement, and rotational aspects of a shallow foundation resting on a *RSM* layer under static loading. Further, finite-element-based numerical modelling of the footing on the *RSM* system with geogrid was also carried out, and the computed results were compared with those measured from the experiments. They reported that the bearing

capacity of the *RSM* layer can be increased up to three times by providing double-layered geogrid reinforcements with a substantial reduction in the settlement.

Ravi and Gourav [R.5] also explore the viability of using waste tire chips and combined waste tire chips, geogrid reinforcement for improving load-carrying capacity of sand. They highlighted that this technique has an advantage of enabling shallow foundations in situations that either demand use of deep foundations or costly ground improvement techniques thus providing economy in construction as well as safe disposals of large stockpiles of waste tires.

In addition to the aforementioned experimental studies, the performance of the *GSI* system using *RSM* layer has been studied in a number of numerical studies (Brunet *et al.* [B.15], Forcellini [F.3, F.4], Hernández *et al.* [H.2], Mavronicola *et al.* [M.4], Nanda *et al.* [N.4], Panjamani *et al.* [P.1], Pistolas *et al.* [P.10], Pitilakis *et al.* [P.11], Tsang [T.4, T.5], Tsang and Pilitakis [T.6], Tsang *et al.* [T.7], Tsiavos *et al.* [T.9, T.11, T.12]). In detail, Pitilakis *et al.* [P.11] assessed the effectiveness of utilizing *RSM* in the foundation soil of different moment resisting frames typologies through numerical simulations. Dynamic analyses of the soil–structure systems were performed for different input motions considering the variation in the *RSM* layer thickness and the building's height. Pistolas *et al.* [P.10] also performed numerical investigation on the seismic isolation potential of *RSM.* They examined the influence of the *RSM* layer on the fundamental variables of the seismic response: the base shear and the total drift displacement of the structure on deformable soil. Recently, Tsang and Pitilakis [T.6] developed a simple and efficient lumped-parameter analytical model for analysing the dynamic soil-foundation-structure interaction of the *GSI* system. They pointed out that the seismic isolation capability of the *GSI* system is founded on the reduced lateral stiffness of the *RSM* layer and the lower modulus of *RSM* that reduces the rocking stiffness. Hernández *et al.* [H.2] aim to develop eco-rubber seismic-isolation foundation system consisting of *RSM* layer and a basement raft made of steel-fibre-reinforced rubberized concrete to enhance the flexibility of the foundation under differential displacement demand.

Kuvat and Sadoglu [K.10] noticed, inter alia, that the major disadvantage of the *RSM* is that the addition of rubber leads to significant reduction in stiffness of the granular soil. Therefore, they proposed asphalt-sand mixtures as an alternative *GSI* material. They performed triaxial tests to determine dynamic properties of sand and bitumen mixtures which can be used as damping materials in *GSI* systems. Hadad *et al.* [H.1] reported on the performance of economic base isolators using tyres filled with elastomeric recycled materials. They tested isolators made of kart tyres filled with different recycled elastomeric materials and aggregates. Dynamic and static tests proved acceptable vertical to horizontal stiffness ratio of the bearings and shake-table tests

showed an excellent enhancement of the base isolated structural response compared to the corresponding fixed base structure. Karatzia *et al.* [K.2] proposed seismic protection of structures on liquefied ground using shallow (instead of deep) foundations. The proposed geotechnical approach exploits the presence of natural liquefiable soil as a natural base isolation system that de-amplifies the seismic ground motion and hence reduces the seismic demand on the superstructure. Doudoumis *et al.* [D.6] proposed an artificial soil layer with a low shearing resistance that allows the slipping of the building under the action of strong seismic motions based on analytical study results.

Geosynthetics have a wide application spectrum in various civil engineering areas, including waterproofing, filtration, soil drainage, separation, and reinforcement. In this background, many researchers studied geosynthetic interface behaviour under dynamic loading (Arab and Kavazanjian Jr [A.7], Briançon *et al.* [B.13, B.14], Carbone *et al.* [C.3, C.4], Cardile *et al.* [C.5, C.6], De and Zimmie [D.1], Kalpakcı *et al.* [K.1], Nanda *et al.* [N.5, N.6], Narjabadifam and Chavoshi [N.7], Pavanello and Carrubba [P.4], Pavanello *et al.* [P.5, P.6], Wasti and Özdüzgün [W.3], Yegian and Catan [Y.1], Yegian and Kadakal [Y.2, Y.3], Yegian and Lahlaf [Y.4, Y.5], Ziegler [Z.3]).

In detail, Yegian and Lahlaf [Y.5] demonstrated by shake-table tests that two sheets of smooth high-density polyethylene geomembrane (*HDPE*) can serve as material for base isolation in earthquake hazard mitigation. The test results showed that limited shear force can be transmitted from one geomembrane to another. Nevertheless, Yegian and Lahlaf [Y.4] conducted shake-table tests to measure the dynamic interface shear strength properties between geotextiles and geomembranes. They observed that there is a limited shear stress, hence a limited acceleration, which can be transmitted from one geosynthetic to another. Further, they reported that the dynamic interface friction angles measured at the onset of relative displacement between the geosynthetics are not appreciably different from those obtained from static tests. They pointed out that further exploration of this application of geosynthetics may lead to products that can provide varying degrees of base isolation, especially in geotechnical earthquake engineering. Further research on this issue on various geosynthetic-geosynthetic and geosynthetic-soil interfaces performed Yegian and Kadakal [Y.2]. Same authors, based on cyclic and shake-table tests, proposed a high strength, nonwoven geotextile placed over an ultrahigh molecular weight polyethylene, *UHMWPE* (geotextile/*UHMWPE*) constitutes a liner that is well suited for base isolation application [Y.3].

Based on the study of Yegian and Kadakal [Y.2], Kalpakci *et al.* [K.1] evaluate the effect of the geomembrane/geotextile interface on the seismic response of small-to-moderate height structures using shake-table test setup. Nanda *et al.* [N.5] investigated the concept of seismic isolation for vibration control of masonry buildings by separating the superstructure from the foundation at plinth level by a sliding earthquake energy reducing friction layer in the form of green marble/geotextile sliding couple. They observed that the frictional base isolation provided by the geotextile limits the earthquake energy transmission to the superstructure during a strong earthquake. Same authors performed further study [N.6] and tested sliding friction interface in the form of a nonwoven geotextile–smooth marble. They also reported that the use of geotextiles as frictional base isolation was quite effective in mitigating earthquake-induced vibrations.

Azinović *et al.* [A.9] performed an extensive parametric study of the seismic behaviour of buildings founded on thermal insulation (*TI*) made of extruded polystyrene (*XPS*). Modern passive and low-energy houses, which strictly follow the requirements of passive house standards for the prevention of thermal bridges, are often founded on a *TI* layer, which is placed under the building's foundation slab. They reported no critical negative effects were observed in the case of regular buildings having up to three storeys due to *XPS* layer below foundation. Following this parametric study, same authors performed further research on this issue [A.10]. They reported that the total base shear that might act on the superstructure could be reduced by permitting sliding between the layers of *TI* boards, thus reducing or even preventing the occurrence of damage. Other interesting contributions on this topic and application of geofoam for seismic base isolation can be found in literature (Azzam *et al.* [A.11], Karatzia and Mylonakis [K.1], Koren and Kilar [K.7], Murillo *et al*. [M.6]).

A review of the literature shows that this isolation method development goes in several directions, using different materials below the foundation including, sand, gravel, rubber-soil mixtures (*RSM*), geosynthetics, and geofoam. Moreover, there is limited systematic research on the use of sand, and there are not any research papers on the use of natural stone pebbles for seismic base isolation, which is the topic of this research. The ultimate goal is for the concept of seismic isolation to find wide application in various types of buildings, and especially in seismic areas of low-income countries with large population where stronger earthquakes take many human lives. Therefore, a further experimental investigation of this seismic base isolation concept is welcome, as well as the development of numerical models for reliable dynamic analysis of structures with such seismic isolation. The research conducted in this doctoral dissertation is also a valuable contribution.

## 1.3 The purpose and objective of the research

The purpose of the research is to create and experimentally test the efficiency of an aseismic layer of predominantly natural materials under the building foundation (sand, stone pebbles and stone pebbles with combinations of geogrid and geomembrane for additional reduction of layer shear stiffness) to reduce seismic response of very stiff and stiff buildings, as well as bridges of smaller span based on solid ground. Also, the purpose of a part of the research is to develop a reliable numerical model for dynamic analysis of structures with an aseismic layer of stone pebbles.

The intention is that the considered concepts of seismic base isolation to be sufficiently efficient, rational and easy to implement, and to have a wide application in practice. Also, the intention is that the developed numerical model to find practical application.

As a confirmation of the validity of the conducted research, the goal is for most of them to be published in leading civil engineering journals.
The individual research goals are:

(i) Experimental research

- Determination of the limestone sand aseismic layer efficiency (*ASL*-1)
- Determining the effect of numerous parameters on the efficiency of the stone pebbles aseismic layer (*ASL-2*): layer thickness, layer compaction, grain size, moisture, etc.
- Defining the optimal *ASL-2* aseismic layer
- Determining the effect of structural stiffness on the efficiency of the *ASL-2* aseismic layer
- Determining the foundation size effect on the efficiency of the *ASL-2* aseismic layer
- Determining the effect of several parameters on the efficiency of the *ASL-3* aseismic layer: combination of stone pebbles and the sliding geogrid and geomembrane layers
- Determining the effect of structural stiffness on the efficiency of the *ASL-3* aseismic layer

(ii) Numerical research

- Development of a numerical model for dynamic analysis of structures with seismic isolation *ASL-2*, and its verification on the results of experimental tests

## 1.4 Research methodology

The planned research is mostly experimental and to a lesser extent numerical. The methodology of the experimental research is based on modern equipment for dynamic testing of structures (shake-table, equipment for measuring physical quantities, equipment for data collection and processing, etc.). The experiments were conducted on the basis of detailed research plan and program, in accordance with modern achievements and knowledge in the implementation of experimental research. It can be noted that properly planned and successfully conducted experimental research is generally more reliable than research using numerical models. Due to the availability of quality equipment for dynamic testing of structures (shake-table), a more intensive experimental research is preferred over numerical.

In addition to experimental research, a numerical model for reliable seismic analysis of structures with the tested seismic base isolation has been developed.

The methodology of the experimental and numerical research is briefly described below.

### 1.4.1 Experimental research

#### A. Application of limestone sand for seismic base isolation – layer *ASL-1*

The possibility of applying a layer of limestone sand for the seismic base isolation was experimentally investigated. Cantilevered reinforced concrete columns with different foundation support conditions were tested: (i) foundation on a rigid base, (ii) foundation supported on a thin layer of sand, and (iii) foundation supported on a thick layer of sand. The column was exposed to a set of horizontal base accelerations of artificial accelerogram (*AA*) until structure collapse. The research is a continuation of previous experimental research on this issue (Grgić [G.1], Grgić *et al.* [G.2, G.3]). Only the most important research results are presented, and the main conclusions are highlighted.

#### B. Application of stone pebbles for seismic base isolation – layer *ASL-2*

This layer for seismic base isolation is made only of natural stone pebbles **–** *ASL-2*.

- ***Effect of several parameters on the efficiency of the stone pebble layer for seismic base isolation***

The effects of several stone pebble layer parameters including the pebbles fraction, the layer thickness, the pebble compaction, the pebble moisture, the vertical contact stress below the foundation, and the effect of repeated excitations on layer aseismic efficiency were investigated

experimentally. For each considered parameter, the rigid building model ($M_0$) was exposed to four accelerograms, with three levels of peak ground acceleration (*PGA*), while the other layer parameters were kept constant. A $M_0$ model was adopted to expedite the study. This should not have a major impact on the conclusions reached as the proposed concept is primarily intended for very stiff and stiff structures. In addition, only the relative effect of some layer parameters was investigated. Namely, a building is approximated by a rigid concrete block with mass $m$ = 2000 kg, and dimensions of 1.0 m x 2.0 m x 0.4 m. The block was made of prefabricated elements, rigidly coupled with prestressed bolts. The block had a reduced area in contact with the aseismic layer, in order to achieve the desired magnitude of contact stress. An aseismic layer of stone pebbles was made within a rigid frame with plan dimensions of 2.5 m x 2.5 m, which was fixed for the shake-table. Characteristic displacements and accelerations of the model were measured. The most important research results and important conclusions regarding the optimal pebble layer were presented.

- ***Behaviour of deformable building models on the optimal ASL-2 aseismic layer***

The efficiency of the optimal pebble layer, selected as part of previous research, was experimentally tested on the deformable building models ($M_1$-$M_4$). Like in previous research, stone pebble layer was made within a rigid frame with plan dimensions of 2.5 m x 2.5 m, fixed for the shake-table. Two pebble layer thicknesses were tested: $h_p$ = 0.3 m and $h_p$ = 0.6 m.

Four models of different stiffness were tested, simulating the behaviour a wide range of building stiffness. Namely, model $M_1$ represents a very stiff structure ($T$ = 0.05 s), $M_2$ a stiff structure ($T$ = 0.3 s), $M_3$ a medium-stiff structure ($T$ = 0.6 s) and $M_4$ a soft structure ($T$ = 1.4 s), wherein $T$ is the fundamental vibration period. A concrete block ($m$ = 1000 kg) rigidly coupled to the column top was adopted for all tested samples. The column is a square hollow hot-rolled steel tube (S355), of variable cross-sectional stiffness. The cross-sectional characteristics were selected so that the models have the stated target periods $T$. The column is rigidly coupled with a concrete foundation (0.7 m x 0.5 m x 0.3 m), which is of equal dimensions for all tested models.

The same models were then tested with significantly larger foundation dimensions (1.2 m x 0.7 m x 0.3 m), to gain insight into the seismic base isolation efficiency with little effect of foundation uplifting (rocking). All the samples were first tested for the case of classical support on a rigid base, without seismic isolation. For this support case, the horizontal displacement of the foundation in relation to the base (shake-table) is prevented, while the rocking and uplifting of the foundation are allowed. Subsequently, the samples were tested on the considered aseismic layers. All models were exposed to four accelerogram. The maximum accelerations of the

accelerogram were taken at lower levels so that the stress in the models remains in the linear range. On this manner, the efficiency of the seismic isolation is clearly demonstrated without the influence of nonlinearity in the model material. Part of the tests was performed by gradually increasing the *PGA* for the most unfavourable accelerogram until the structure collapsed. The purpose of these tests was to determine the difference in the ultimate bearing capacity of the structural model with and without seismic isolation. Characteristic accelerations, displacements and strains of the model were measured.

To evaluate the efficiency of seismic isolation, the measured acceleration, displacement, and strain on the tested structural model based on seismic isolation and on the corresponding model on rigid base were compared. Thus, in addition to each model based on the aseismic layer, the same model based on the rigid base (without the aseismic layer) was also tested. For the indicator (coefficient) of seismic isolation efficiency, the ratio of the measured peak horizontal acceleration in the mass centre at the column top for both mentioned cases was adopted. In addition to acceleration, the most important indicator of isolation efficiency were determined by strain/stress reduction in the isolated structural model. The most important results of the research are presented and the main conclusions are highlighted.

### C. Application of stone pebbles with additional sliding layer for seismic base isolation - layer *ASL-3*

In the *ASL-3* aseismic layer, the optimal stone pebble layer *ASL-2* described in Section 2.2.2 are combined with a thin additional layer of sliding material, in order to achieve greater efficiency of this layer than that of the *ASL-2* layer.

- ***Effect of several parameters on the efficiency of the ASL-3 aseismic layer***

Several parameters of the additional sliding material were varied with experimental verification, in order to find the highest efficiency of the entire aseismic layer. For each parameter considered, $M_0$ was exposed to four accelerogram, with three levels of *PGA*, while the other parameters were kept constant. Characteristic displacements and accelerations of the model were measured. The most important research results and important conclusions regarding the optimal layer were presented.

- ***Behaviour of deformable building models on the optimal aseismic layer ASL-3***

The efficiency of the optimal *ASL-3* aseismic layer, determined in previous research, was experimentally tested on models $M_1$-$M_4$. All models are exposed to four accelerogram, wherein

the maximum accelerations are scaled so that the stress in the models remains in the elastic range. As previously stated, the efficiency of seismic isolation without the influence of nonlinearity in the material is clearly demonstrated. Part of the tests was performed by gradually increasing the *PGA* for the most unfavourable accelerogram until the structure collapsed. The purpose of these tests was to determine the difference in the ultimate bearing capacity of the structural model with and without seismic isolation. Characteristic accelerations, displacements and strains of the model were measured. For the isolation efficiency indicator, the same methodology was used as for the *ASL-2* isolation layer study. The most important results of the research are presented and the main conclusions are highlighted.

### 1.4.2 Numerical model

A numerical model for reliable seismic analysis of planar structures with seismic base isolation using *ASL-2* layer has been developed. The model can analyse planar structures made of concrete, steel and masonry, including a combination of these materials, interacting with the soil. Numerical model, developed by Radnić *et al.* [R.2], and later improved by (Baloević *et al.* [B.1, B.2, B.3], Radnić *et al.* [R.3, R.4], and Smilović *et al.* [S.3, S.4, S.5]) was used, supplemented by an adequate simulation of the behaviour of the aseismic layer. The model is based on the finite element method (*FEM*) and simulates the most important nonlinear effects of individual structural material, the effect of large displacements and structure construction in stages. The *ASL-2* isolation layer was simulated by an anisotropic material model, with different properties in the horizontal and vertical directions. Emphasis is placed on the most credible modelling of shear stiffness (deformability) and bearing capacity of the isolation layer, and some parameters of the material model are defined based on the experimental test results. The coupled numerical model was verified on the simulation of several conducted experimental tests of the $M_1$ and $M_2$ models on the *ASL-2* isolation layer.

# 2. EXPERIMENTAL RESEARCH

## 2.1 General

In Sections 2.2 to 2.5, basic data related to the implementation of all experimental research (considered seismic base isolation, tested models, applied base accelerations and measured quantities) is presented. Section 2.6 presents summaries of published papers and papers submitted for publication in the field of experimental research.

The main results of the conducted experimental research are presented in Section 2.7. They represent the synthesis and sublimation of papers [I to VII]. Furthermore, the results are presented simply and clearly, all for the purpose of the reader's insight into the actual seismic potential of the considered seismic isolations. The main conclusions of the experimental research are presented in Section 2.8.

In terms of the scope of the experimental investigations performed, they were conducted much more broadly and more systematically for the *ASL-2* and *ASL-3* isolation layers, compared to the *ASL-1* limestone sand isolation layer.

The term seismic isolation efficiency is often used in this dissertation. Seismic isolation efficiency is defined as the ratio of the measured acceleration (inertial force), strain and displacement on the model based on seismic isolation, in relation to the quantity measured on the corresponding model on rigid base.

## 2.2 Considered seismic base isolations

As mentioned in Section 1.3, three types of seismic base isolation were considered, i.e three types of isolation layers under the model foundation: (i) a thin layer of limestone sand, (ii) a layer of stone pebbles and (iii) a layer of stone pebbles with a sliding geogrid and geomembrane layers (Figures 2.1 to 2.3). To evaluate the efficiency of seismic isolation, the considered structural models were also tested on a rigid base.

### 2.2.1 Limestone sand aseismic layer – *ASL-1*

Limestone sand of 0-4 mm fraction is adopted. Models were isolated with a 20 mm thick and a 100 mm thick isolation layer (Figure 2.1). The sand had a moisture content of 10% and was slightly statically compacted (homogenized) on declared layer thicknesses. The isolation layer is formed directly above the shake-table. In order to prevent the sand slipping on the metal surface, a rough cement syringe was applied.

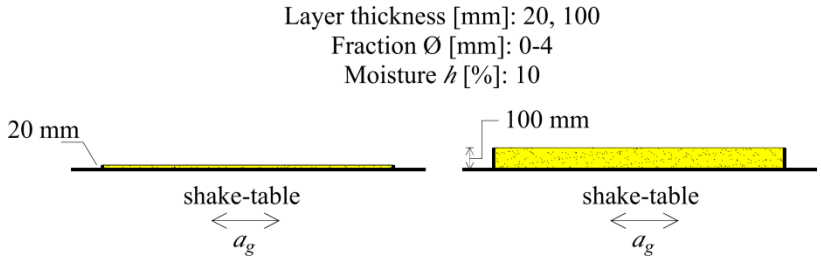


*Figure 2.1* Considered limestone sand aseismic layers

## 2.2.2 Stone pebble aseismic layer – *ASL-2*

Stone pebbles (river gravel) fractions 4-8 mm, 8-16 mm, and 16-32 mm were used (Figure 2.2). The pebbles were predominantly of high-strength limestone, with rounded outer surfaces and washed of fine particles. Two-layer thicknesses were used: $h_p$ = 0.30 m (so-called thin substrate) and $h_p$ = 0.60 m (so-called thick substrate). The effects of several layer parameters on seismic isolation efficiency were investigated: the pebbles fraction, the layer thickness, the pebble compaction, the pebble moisture, the vertical contact stress below the foundation, and the effect of repeated excitations on layer aseismic efficiency. A layer of stone pebbles was placed inside a rigid box with plan dimension of 2.5 m x 2.5 m, which was fixed to the shake-table. A total of 9 different stone pebble isolation layers were considered. Stone pebbles are a natural material that is widespread and has large reserves.

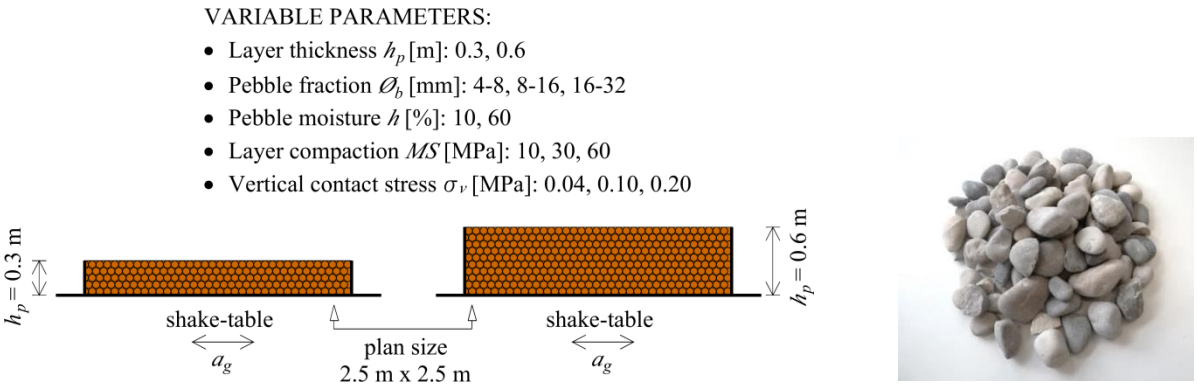


(a) (b)

*Figure 2.2* Considered stone pebble isolation layer: (a) Varied parameters; (b) Photo of $\phi_b$ = 16-32 mm stone pebbles

## 2.2.3 Stone pebble layer with sliding geogrid and geomembrane layers – *ASL-3*

The optimal stone pebble layer from Section 2.2.2 is combined with a thin sliding layer of different elements/materials (geogrid, geomembrane above limestone sand layer). Different thicknesses of the pebble layer, position and tensile strength of the geogrid and geomembrane

within the pebble layer were varied. A total of eleven different aseismic layers were considered (Figure 2.3a).

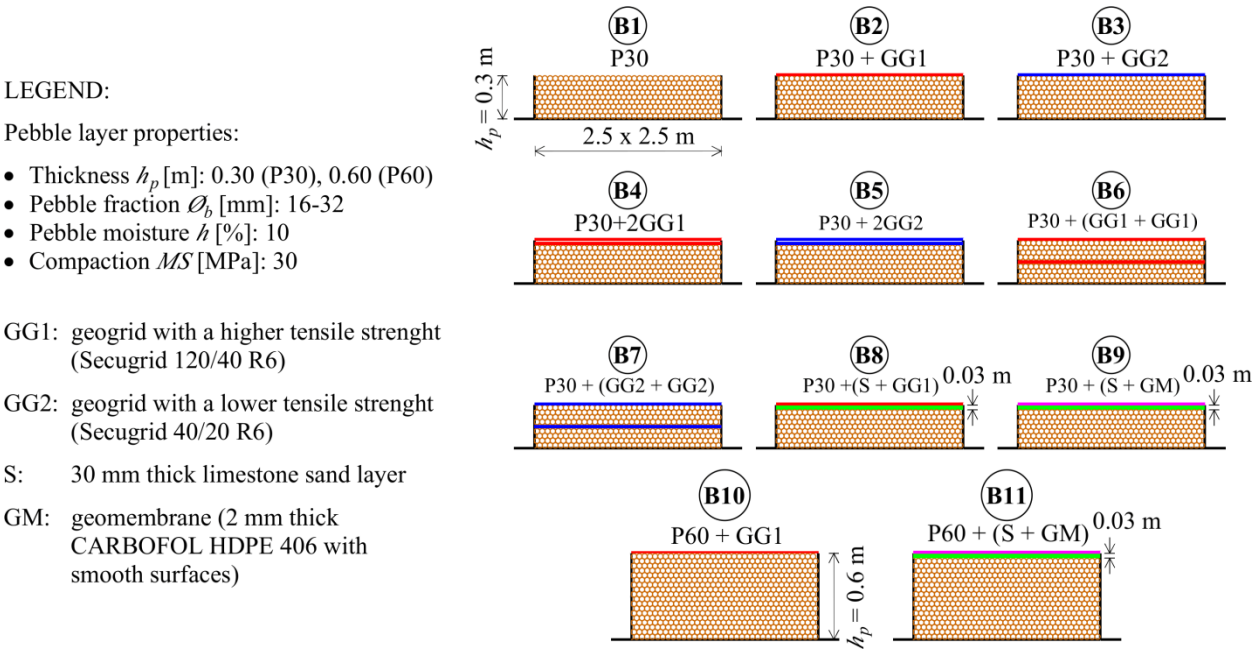


(a)

Limestone sand

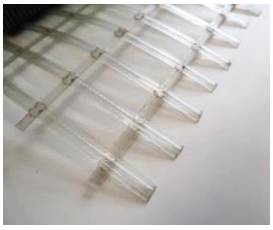

Geogrid GG1

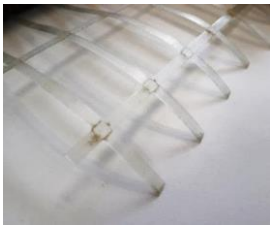

Geogrid GG2

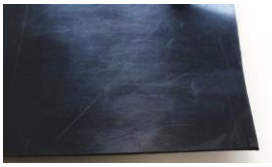

Geomembrane HDPE 406

(b)

*Figure 2.3 ASL-3* aseismic layers: (a) Composite seismic base isolations considered in this study; (b) Adopted materials for the sliding layer

## 2.3 Considered structural models

### 2.3.1 Model on aseismic layer *ASL-1*

In order to test the efficiency of seismic base isolation with a limestone sand layer *ASL-1*, a simple model of cantilevered concrete column according to Figure 2.4 was used. The column is 1.08 m high, with a square cross-section of 0.1 m x 0.1 m. It is rigidly constrained at the foundation with dimensions: 0.75 m (length) x 0.5 m (width) x 0.3 m (height). At the top of the column is a centrically placed concrete block measuring 1.0 m x 1.0 m x 0.8 m and weighing 2000 kg, which is rigidly coupled to the column top.

The column and foundation were made of concrete. The compressive strength of the concrete was 37.2 MPa, the flexural tensile strength of concrete was 3.9 MPa, and the Young's modulus was 33.2 GPa. The column was reinforced with vertical bars 4Φ8 mm ($A_s$ = 201.1 mm$^2$, i.e., 2% of the concrete cross section area) and Φ4.2 mm stirrups at a spacing of 50 mm. The ultimate strength of the steel was 653 MPa, and the Young's modulus was 205 GPa.

The foundation of the column is placed on a shake table according to each of the following conditions: (i) fixed to the shake table – *C1*, (ii) over a 20-mm thick layer of limestone sand – *C2*, and (iii) over a 100-mm thick layer of limestone sand – *C3* (Figure 2.1).

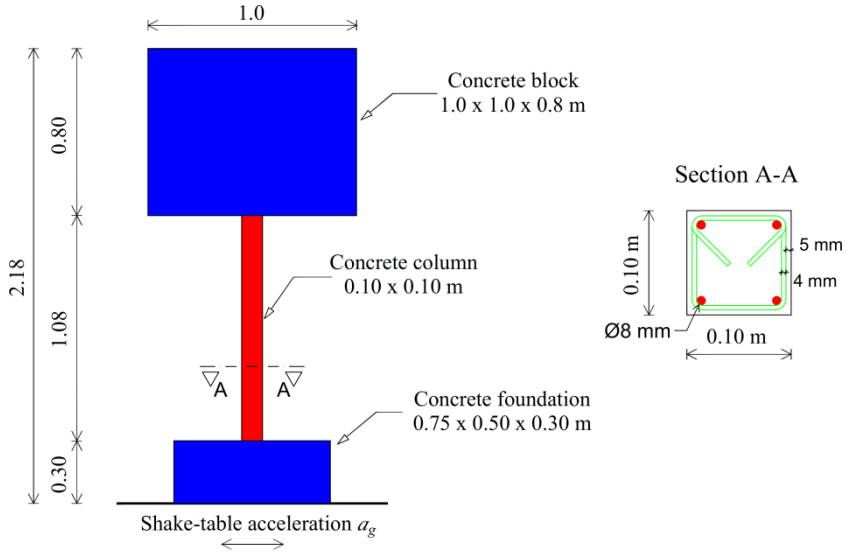


*Figure 2.4* Model of cantilever concrete column tested on aseismic layer *ASL-1*

## 2.3.2 Models on aseismic layers *ASL-2* and *ASL-3*

The considered simple structural models for testing the efficiency of seismic isolation *ASL-2* and *ASL-3* are presented in Figure 2.5. In order to investigate the effect of several parameters on the efficiency of these seismic isolation layers, the rigid model $M_0$ shown in Figure 2.5a was used. It is considered that $M_0$ can well represent very stiff structures with a small fundamental period, *i.e.* credibly test the effect of each varied layer parameter on the seismic isolation efficiency. The model is a rigid concrete block measuring 1.0 m x 2.0 m x 0.4 m, with a reduced contact area of the lower prefabricated segment (based on the isolation layer) in order to achieve the desired contact stress at the top of the substrate. The model (concrete block) is formed in height by prefabricated elements, rigidly coupled with prestressed bolts.

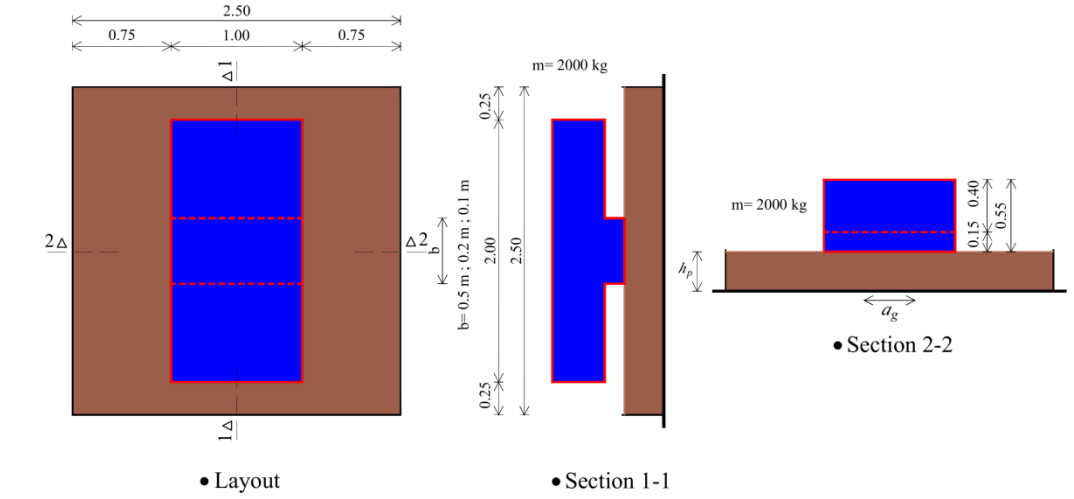


(a)

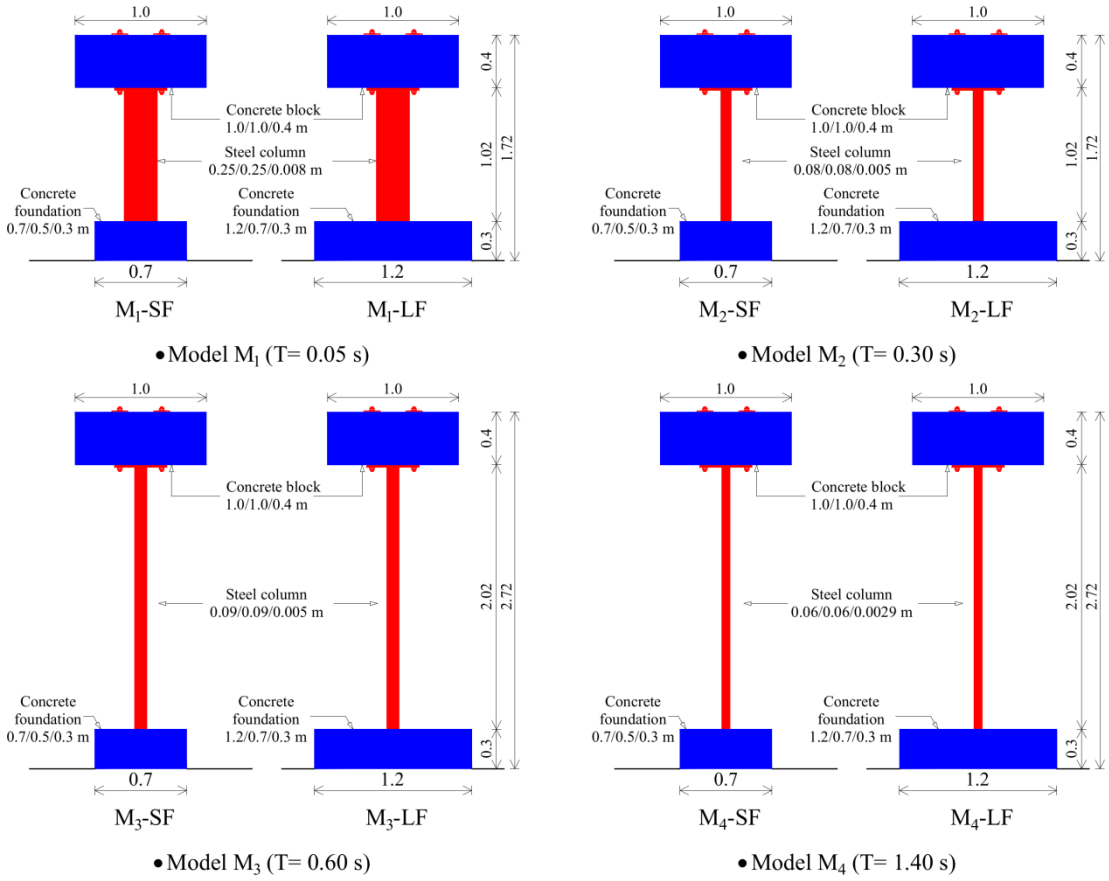


(b)

*Figure 2.5* Tested models on aseismic layers *ASL-2* and *ASL-3*: (a) Rigid model $M_0$; (b) Deformable models $M_1$-$M_4$

Four simple models ($M_1$, $M_2$, $M_3$, and $M_4$) were adopted to test the effect of structural stiffness on the efficiency of seismic base isolation using *ASL-2* and *ASL-3* layers. The models are a cantilevered steel columns embedded in a concrete foundation, with a centric concrete block (mass) at the column top (Figure 2.5b), and with two variants of the foundation ground plan dimension. The columns are square hollow hot-rolled steel tubes (S355), with fundamental

periods $T$: $T$ = 0.05 s (for $M_1$), $T$ = 0.30 s (for $M_2$), $T$ = 0.60 s (for $M_3$), and $T$ = 1.40 s (for $M_4$). The fundamental periods of the models are shown in the elastic response spectrum according to EC 8 [E.2] for earthquake type 1 and soil type A (Figure 2.6).

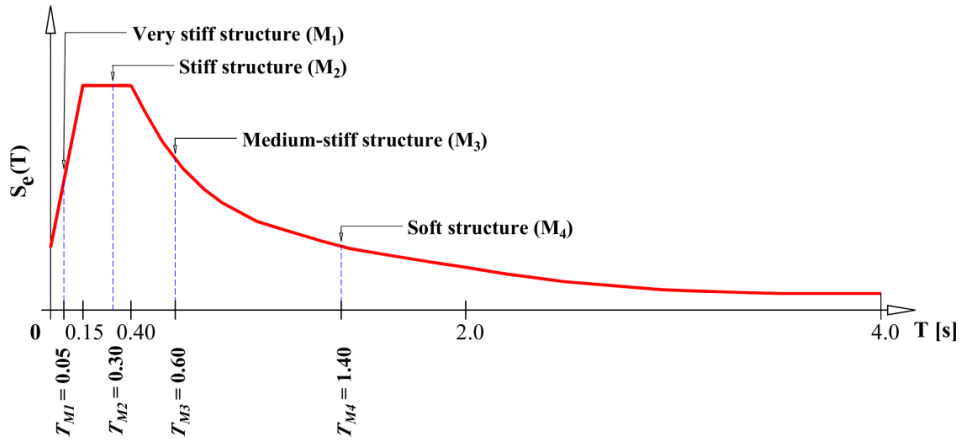


*Figure 2.6* The fundamental periods of the models and elastic response spectrum according to EC 8 (earthquake type 1 and soil type A)

The intention is for the $M_1$ to represent a very stiff structure, $M_2$ a stiff structure, $M_3$ a medium-stiff structure, and $M_4$ a soft structure. A mass m = 1000 kg at the column top, in the form of a concrete block measuring 1.0 m x 1.0 m x 0.4 m, was adopted, which was rigidly coupled with the column top. The adopted square hollow cross-section dimensions of the steel column are such that the stresses during the tests with lower *PGA* levels remain elastic. In this case, the effect of the nonlinearity (energy dissipation) in the construction material is excluded. In this way, the efficiency of seismic isolation is most clearly demonstrated.

To analyse the foundation size effect on the efficiency of the seismic isolation layers, two sizes of the foundation were considered: (i) the so-called small foundation – *SF* (length b = 0.7 m, width 0.5 m, and height 0.3 m) and (ii) the so-called large foundation – *LF* (length b = 1.2 m, width 0.7 m, and height 0.3 m).

All considered structural models were first tested on a rigid base (without seismic isolation). For this support case, the horizontal displacement of the foundation in relation to the base (shake-table) is prevented, while the rocking and uplifting of the foundation are allowed. This support case is more realistic than the fixed base support case, in which displacement and rotation of the foundation in relation to the base do not occur. Also, compared to the fixed base, rigid base support case produces lower seismic forces on the model, which gives more conservative seismic base isolation efficiency. Subsequently, the samples were tested on the considered aseismic layers.

## 2.4 Applied base excitations

It is well known that the choice of relevant excitations, *i.e.* the selection of reference accelerograms in experimental test of structural models is extremely important and requires great attention. The results obtained and the conclusions reached regarding the behaviour of the model depend on this choice. It is desirable to test the model with as many different real accelerograms as possible, which are unfavourable for the considered structure. It is clear that as the number of accelerograms increases, the duration and complexity of the study increases. Therefore, the question remains with what minimum number of relevant accelerograms the considered model should be examined in order to obtain reliable research conclusions. It should be noted that different accelerograms are not equally unfavourable (relevant) for the considered structural model. Therefore, a larger number of selected accelerograms, which are less relevant for the tested model, may be of less use than only one, which is far more authoritative. According to previous experience, the application of adequate artificial accelerogram of sufficient duration, which covers a wide spectrum of possible model frequencies, can give fairly reliable results for acceptable research conclusions.

The adopted horizontal excitations in this research are shown in Figure 2.7a. An artificial accelerogram – *AA* was created to match the elastic response spectrum according to Eurocode 8 [E.2], for earthquake type 1 and soil type A. The *AA* is generated using SIMQKE software [S.2], as a superposition of sine functions. The N-S accelerogram of the Petrovac earthquake – *AP*, Montenegro 1979, (Ambraseys *et al.* [A.2]), as well as *AA*, represent long-lasting earthquakes with a relatively longer predominant period (for *AP* it is longer than for *AA*). The N-S accelerogram of the Stone earthquake – *AS*, Croatia 1996, (Ambraseys *et al.* [A.2]), and the N-S accelerogram of the Banja Luka earthquake – *ABL*, BiH 1981, (Ambraseys *et al.* [A.2]), represent short impact earthquakes with a short predominant period. It is expected that *AA* and *AP* cause a stronger vibration of the structure and bring more earthquake energy into the system, and cause a greater bending effect. Accelerograms *AS* and *ABL* are impact-acting and should have a more pronounced shear effect. The intention was that the applied accelerograms cover a wider range of possible structural frequencies that will change during the action of the excitation, passing a wide range of structural behaviour, from linear to deeply nonlinear. The presented ground motions are scaled to the equal acceleration values.

An elastic response spectrum of adopted excitations is presented in Figure 2.7b. By analysing the spectral quantities, it can be concluded that the selected excitations cover the fundamental periods of tested models, as well as the increased periods of models when nonlinearities appear

in the system. Although *AS* and *ABL* seem very close at first sight, it can be seen from Figure 2.7b that their spectral values are quite different. The results of the experimental tests performed confirmed quite different structural response for *AS* and *ABL* excitations. Only the *AA* excitation was used to test the model base on *ASL-1* layer, while all four accelerograms from Figure 2.7 were used to test the models based on *ASL-2* and *ASL-3* layers.

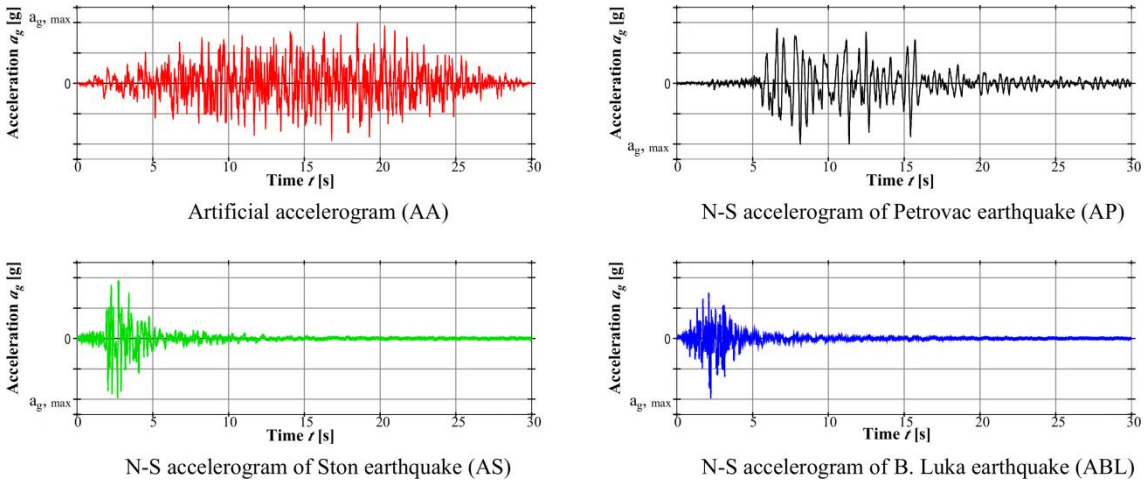


(a)

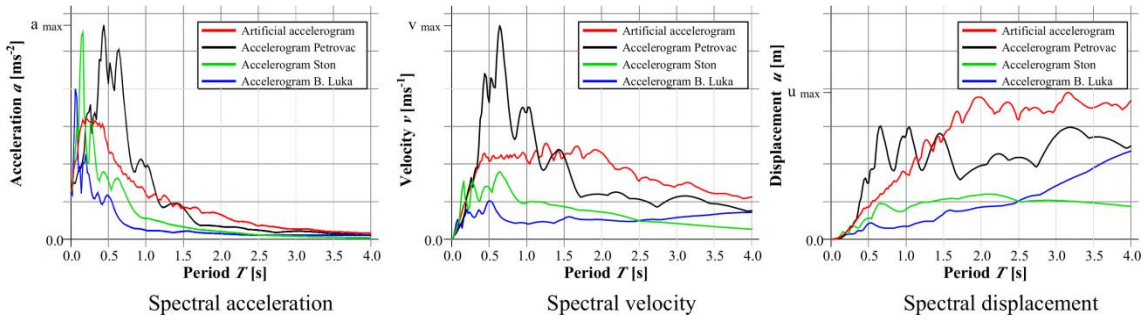


(b)

*Figure 2.7* Adopted base excitations: (a) Horizontal base accelerograms; (b) Elastic response spectra

## 2.5 Measured quantities

### 2.5.1 Model tested on *ASL-1*

Characteristic displacements, accelerations and strains (Figure 2.8) were measured for all tested substrates and base excitations.

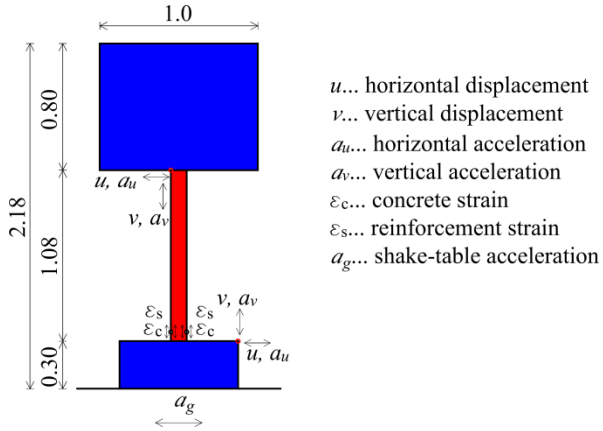


*Figure 2.8* Measured quantities on the model tested on *ASL-1* layer

## 2.5.2 Models tested on *ASL-2* and *ASL-3*

### (i) Rigid model $M_0$

The behaviour of tested model is described by measured characteristic displacements and accelerations (Figure 2.9).

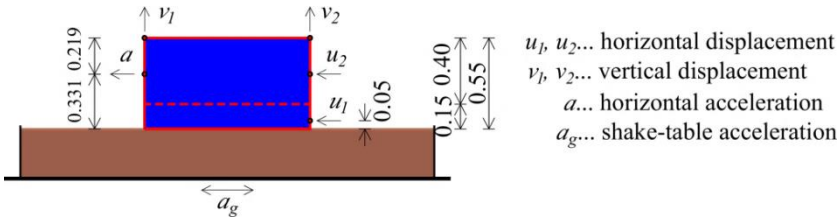


*Figure 2.9* Measured quantities on the rigid model $M_0$ tested on *ASL-2* and *ASL-3*

### (ii) Deformable models $M_1$, $M_2$, $M_3$, and $M_4$

Measured characteristic displacements, accelerations and strains are presented on Figure 2.10.

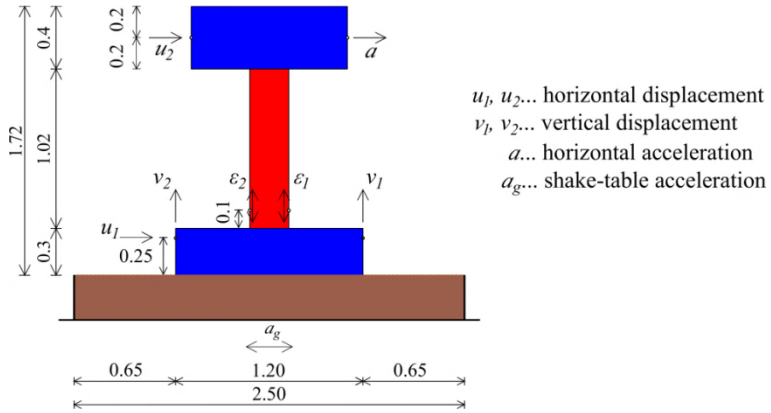


*Figure 2.10* Measured quantities on the $M_1$, $M_2$, $M_3$, and $M_4$ models on *ASL-2* and *ASL-3*

## 2.6 Test equipment

A uniaxial shake-table at the University of Split, Faculty of Civil Engineering, Architecture and Geodesy (Croatia) was used to test the models. The shake-table had a layout size of 4 m × 4 m, maximum capacity 20 000 kg, a maximum displacement of ±150 mm, a maximum acceleration of up to 5 g, and frequencies ranging from 0-20 Hz. The shake-table is controlled by acceleration, and the acceleration function can be arbitrary. Weight of test samples, shake-table displacement (acceleration) and the oscillation frequency are mutually dependent.

The model behaviour was monitored using sensors, *i.e.* strain gauge of type 6/120 LY11 (Hottinger Baldwin Messtechnik-*HBM*) for steel strains, strain gauge of type 60/120 LY11 (*HBM*) for concrete strains; analogue displacement sensors of type PB-25-S10-N0S-10C (Uni Measure) for displacements; and a piezoelectric low-frequency accelerometer-type 4610 (Measurement Specialties) sensor for accelerations. A video camera (Canon EOS M5) was used to monitor and record the tests. For data collection and processing, a 16-channel Quantum-x mx 840A (*HBM*) high-speed data acquisition system was used. The sampling rate during the tests was 200 Hz.

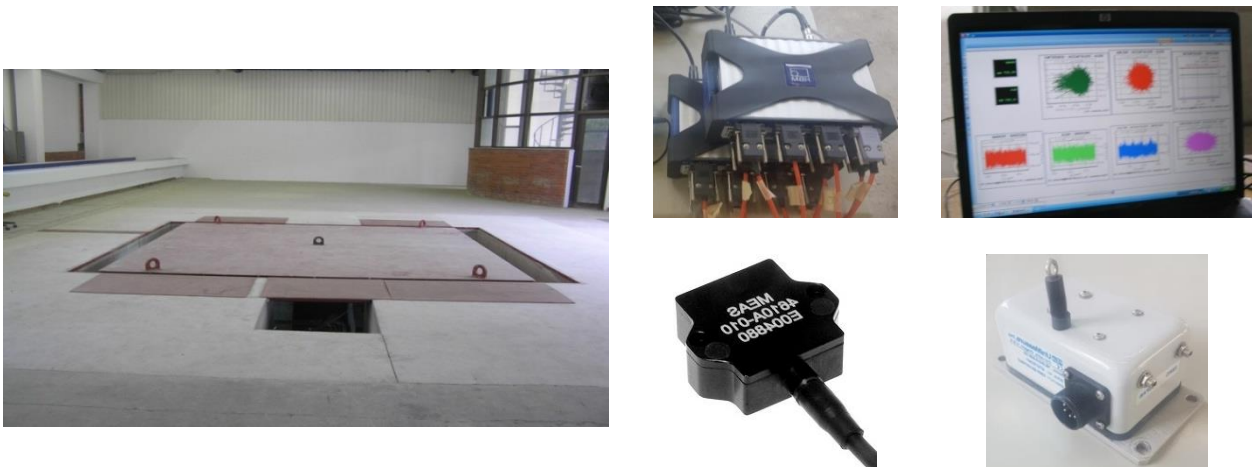

(a) (b)

*Figure 2.11* Test equipment: (a) Uniaxial shake-table; (b) Data acquisition system and some sensors for measuring mechanical values

## 2.7 Summary of research results presented in appended papers

Below is an abstract of published papers and those in the process of publication, on which this doctoral dissertation is based. Namely, these papers are the result of research related to the efficiency of using seismic base isolation from the considered natural materials (aseismic layers *ASL-1*, *ASL-2*, and *ASL-3*).

The results of an experimental study to determine the effectiveness of limestone sand under the foundation of a cantilever concrete column to increase its seismic resistance were published in the paper by Banović *et al.* [B.11], also referred as [I]. A simple model of a free-standing cantilever concrete column was adopted, with a concrete foundation and a centrically supported mass at the column top (in the form of a concrete block). The behaviour of the column was tested at three different substrates: rigid base (foundation model was fixed), 20 mm thick layer of sand (thin layer) and 100 mm thick layer of sand (thick layer). The model is exposed to horizontal accelerations of an *AA*, with a successive increase in *PGA* to column failure. Characteristic displacements, accelerations and strains of the model were measured. The test results showed that the rigid based model had the lowest safety (collapsed at *PGA* = 0.35 g), while the models on both sand layers had the same safety (collapsed at *PGA* = 0.40 g). The column based on a thicker layer of sand had more favourable strains for the previous *PGA* increment. It was concluded that the limited research range is necessary to expand. Furthermore, a thin layer of sand under the foundation can increase the safety of the model by approximately 10%, and it is not possible to reliably define which sand layer thickness is more favourable.

Within the application of seismic base isolation using a layer of stone pebbles, the influence of several parameters (thickness and compaction of the pebble layer, pebbles fraction and moisture, size of contact stress on the top of the pebble layer and the effect of repeated excitations) on the efficiency of seismic isolation was investigated. The research results are presented in the paper by Banović *et al.* [B.6], also referred as [II]. For each considered parameter, a $M_0$ on an aseismic layer was exposed to four different accelerograms, with three levels of *PGA*: 0.2 g, 0.4 g and 0.6 g, while all other layer parameters were kept constant. It was concluded that the seismic isolation efficiency and the effects of all observed layer parameters are significantly dependent on the type of applied excitation and *PGA*. Moreover, variations in parameter values did not significantly affect the efficiency of the aseismic layer. Considering the simplicity and speed of the construction, as well as layer rationality, the following parameters of the pebble layer were adopted as optimal: the pebble fraction $\Phi_b$ = 16-32 mm, the pebble layer compaction *MS* = 30 MPa and the pebble moisture $h$ = 10%.

The results of experimental investigations of the efficiency of a stone pebble isolation layer on models of a stiff and medium-stiff building (cantilever steel columns with mass at the column top, rigidly coupled in a relatively small concrete foundation) are presented in paper Banović *et al.* [B.5], also referred as [III]. The efficiency of seismic isolation was determined on a comparison of the measured values of acceleration, strain and displacement on the isolated model and on model supported on rigid base. Each model was exposed to the horizontal

acceleration of four different earthquake accelerograms. It was concluded that the effectiveness of the stone pebble layer significantly depends on the type of the applied excitation and depends relatively little on the layer thickness and pebbles fraction. It was found that the pebble layer can significantly reduce seismic force and strain/stress in the isolated model in relation to model on rigid base. Seismic isolation has proven to be more effective for the stiff building model than for the medium-stiff building model. The need for further research is stated in order to better understand the effectiveness of the tested seismic isolation.

The paper Banović *et al.* [B.8], also referred as [IV], presents the results of a shake-table study of the effect of structural stiffness on the efficiency of seismic base isolation using an optimal layer of pebbles, determined in paper [II]. Four structural models were tested: very stiff $M_1$, stiff $M_2$, medium-stiff $M_3$ and soft $M_4$. Stiffness is defined over the fundamental period of the oscillations of an individual model. The model is a free-standing steel column with relatively small concrete foundation and mass at the column top. The models are exposed to the horizontal acceleration of four different accelerograms (*AA*, *AP*, *AS* and *ABL*). A part of the study was carried out for the lower maximum acceleration of the shake-table with the stresses of the model in the elastic range, and part of the study for the most unfavourable accelerogram was carried out by incremental base acceleration tests to the collapse of the model. The highest seismic isolation efficiency was for $M_1$, followed in order by those for $M_2$, $M_3$, and $M_4$. Furthermore, the isolation efficiency is greater as the structural stiffness increases.

The seismic isolation efficiency coefficients are defined through the acceleration in the block centre $c_a$ and the strains in the bottom of the column $c_\varepsilon$. The efficiency of seismic isolation was highly dependent on the type of applied accelerogram, regardless of the tested model. Thus, according to the above conclusions, the coefficients $c_a$ for AA were 0.47 ($M_1$), 0.57 ($M_2$), 0.54 ($M_3$), and 0.64 ($M_4$), and the coefficients $c_{\varepsilon 1,2}$ were 0.44 ($M_1$), 0.52 ($M_2$), 0.54 ($M_3$), and 0.64 ($M_4$). For the impact-type accelerogram *AS*, the coefficient $c_a$ were 0.83 ($M_1$), 0.86 ($M_2$), 0.97 ($M_3$), and 0.98 ($M_4$), and the coefficients $c_{\varepsilon 1,2}$ were 0.74 ($M_1$), 0.97 ($M_2$), 0.97 ($M_3$), and 1.07 ($M_4$). It is important to outline that the acceleration and strain in the models for the *AA* accelerogram were far greater than for the *AS* accelerogram. That is, the *AS* and *ABL* impact-type accelerograms were not relevant for the tested models. Also, it was found that reducing the stiffness of the model increases model displacements. In the other part of the study, each tested sample was exposed to a set of incremental base acceleration tests with *AA* by scaling *PGA* for $\Delta a_{g,max}$ = 0.05 g until the structure collapsed. The ratios of acceleration at which the model

collapsed on the seismic isolation and acceleration at which the model collapsed on a rigid base were 1.50:1.25:1.25:1.20 for models $M_1$, $M_2$, $M_3$, and $M_4$.

The results of the foundation size effect on the efficiency of seismic base isolation using a layer of stone pebbles were published in the paper by Banović *et al.* [B.7], also denoted as [V]. The paper is based on the results of previous research in [II] and [IV]. In this case, models $M_1$, $M_2$, $M_3$, and $M_4$ were additionally tested as in [IV], but with larger ground plan dimensions of the foundation, which allows less rotation of the foundation (rocking) during a stronger earthquake. In [IV], the models were based on a foundation 0.75 m long and 0.5 m wide (small foundation), and in [V] additionally on a foundation 1.2 m long and 0.70 m wide (large foundation). Everything else (seismic isolation layers, applied base accelerations, tests performed, etc.) was taken as in [IV].

For the case of the one-time base acceleration of the adopted excitation with elastic strain/stress in the model column it was found that models with larger foundations result in higher accelerations, larger column strains, significantly smaller foundation and column top displacements, and significantly smaller vertical foundation displacements. For example, for the artificial accelerogram *AA*, the seismic isolation efficiency coefficient $c_\varepsilon$ for the larger foundation models $M_1$-*LF*, $M_2$-*LF*, $M_3$-*LF*, and $M_4$-*LF* were 0.78, 0.68, 1.00, and 1.01. This is significantly less favourable than for the same models (columns) with a smaller foundation [IV]. Similar conclusions apply for the *AP*, *AS*, and *ABL* excitations.

Every model was exposed to a set of repeated *AA* by scaling the *PGA* until the structure collapsed or lost stability. The ratios of the acceleration $a_{g,max}$ (load-bearing capacity) of the considered models for the foundation supported on the stone pebble layer and the foundation supported on a rigid base for the *LF* case, for $M_1$-*LF*, $M_2$-*LF*, $M_3$-*LF*, and $M_4$-*LF* the ratios were 1.38, 1.29, 1.13, and 1.00. This is significantly less favourable than for the same models (columns) with a smaller foundation [IV]. Also, it was stated that for the models $M_3$-*LF* and $M_4$-*LF* seismic base isolation using a layer of stone pebbles does not make practical sense, while for stiffer models based on rigid soil (fundamental period up to 0.3 s - 0.4 s) still has a significant capacity to reduce seismic forces and strain/stress in the structure (although the efficiency is lower than for a *SF* [IV]).

The findings of an experimental investigation of the efficiency of several low-cost frictional composite seismic base isolations is presented in Banović *et al.* [B.9], also referred as [VI]. A total of eleven different aseismic layers were considered. One layer was made of stone pebbles only – *B1*, whereas the remaining ten layers (*B2*-*B11*) were composite containing combinations

of stone pebbles with different types and positions of sliding elements (geogrid, geomembrane over limestone sand layer). The presented research is a continuation of the ones started in [II], [IV] and [V], with analogous solutions related to pebbles. The $M_0$ model as in [II] was used, as well as the adopted base accelerations (*PGA* = 0.2 g, 0.4 g, and 0.6 g, respectively).

The research results showed that average composite seismic base isolations have higher efficiency than the *B1* isolation, but some of them are less efficient than *B1*. The most efficient composite seismic isolations were those with one geogrid at the pebble layer top (*B2* and *B10* isolations). The *B2* composite seismic isolation was selected as most straightforward and most practical application. Furthermore, the maximum acceleration of the $M_0$ model based on *B2* and *B10* isolation averaged over all the excitations and PGA levels were 16% lower than that based solely on the *B1* isolation from stone pebbles.

The research results on the effect of geogrid on the efficiency of seismic base isolation using a layer of stone pebbles are presented in the paper by Banović *et al.* [B.10], also referred as [VII]. Four different foundation support cases (rigid base – *RB*, 0.3 m thick layer of stone pebbles – *BI1*, 0.3 m thick layer of stone pebbles with geogrid at the layer top – *BI2*, and 0.6 m thick layer of stone pebbles with geogrid at the layer top – *BI3*) were tested on four models of different stiffness. The same models ($M_1$, $M_2$, $M_3$, and $M_4$) and the same base accelerations (*AA*, *AP*, *AS*, and *ABL*) as in paper [V] were adopted. The efficiency of the seismic isolations for the *AA* excitation to the model collapse was also investigated. It was concluded that the application of seismic isolations *BI1*, *BI2*, and *BI3* are not effective for some structural models ($M_3$ and $M_4$). The average seismic isolation efficiency coefficient for models $M_1$ and $M_2$, for which this isolation is applicable, was as follows: *BI2* compared to *RB* = 0.75, *BI2* compared to *BI1* = 0.90, and *BI2* compared to *BI3* = 0.92. The displacements of model $M_1$ and $M_2$ on *BI1*, and in particular on *BI2* and *BI3*, were larger than on *RB*, which was unfavourable. The ratio of *PGA* at which the sample collapsed was *RB:BI:BI2:BI3* = 1.00:1.38:1.62:1.50 for model $M_1$, and *RB:BI1:BI2:BI3* = 1.00:1.29:1.43:1.43 for model $M_2$. Composite seismic isolation *BI2* proved to be the most efficient, with the largest reduction of inertial force and strain/stress in the column. Tested on four different earthquake accelerograms, this reduction was 25%, which is considered very encouraging for possible practical application. However, for the practical application of this seismic isolation, which is highly promising for low-rise rigid buildings resting on solid ground, broader studies on more realistic building models are required.

## 2.8 Main research results

### 2.8.1 Limestone sand aseismic layer – *ASL-1*

At the outset, it should be noted that a small range of experimental tests were conducted to investigate the efficiency of seismic base isolation using a layer of limestone sand. Some of the most important research results on the behaviour of a cantilevered concrete column supported on a rigid base – *C1*, a 20 mm layer of limestone sand – *C2* and a 100 mm layer of limestone sand – *C3* are presented in Figure 2.12. Column *C1* failure occurred at *PGA* = 0.35 g (practically at *PGA* = 0.30 g), while column *C2* and *C3* failure occurred at *PGA* = 0.40 g. Column *C3* had a more favourable behaviour than column *C2* before the collapse. Based on the above, it follows that the columns isolated with limestone sand layer had approximately 10% higher load-bearing capacity than the column on rigid base.

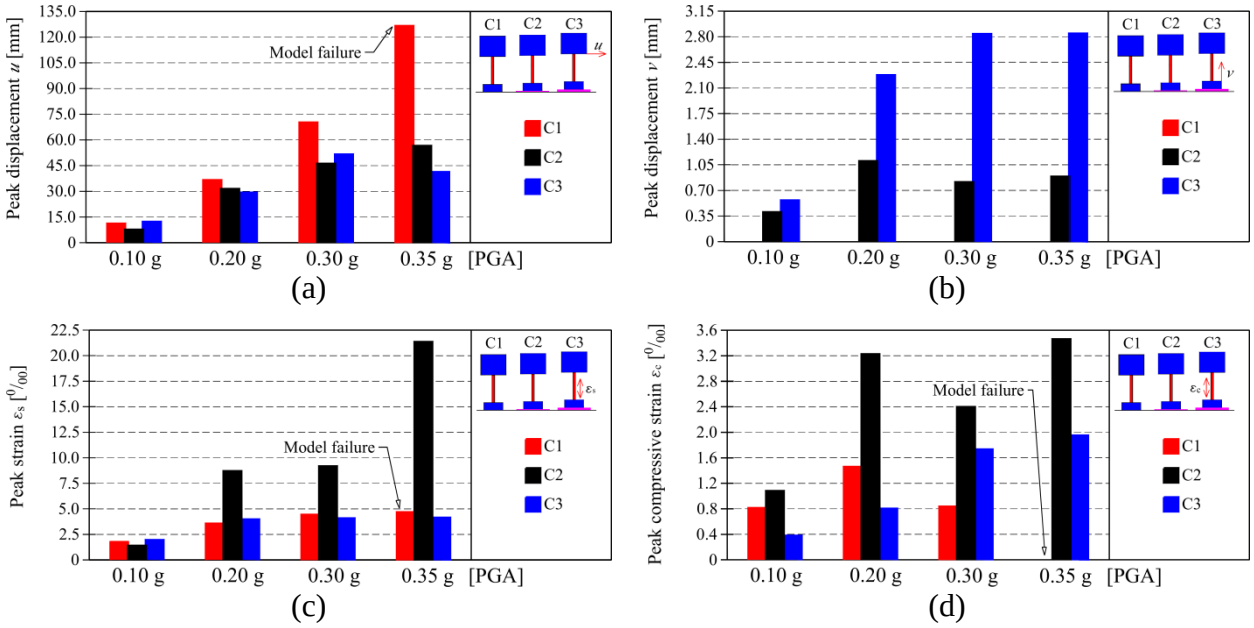


*Figure 2.12* Some results of tested models isolated with limestone sand layer: (a) The peak horizontal displacement of the column top; (b) The peak vertical displacement of the foundation top on the right side; (c) The peak reinforcement strain at the bottom of the column on the left side; (d) The peak compressive concrete strain at the bottom of the column on the right side

* * *

Due to the small number of tested samples, it is difficult to conclude what thickness of the limestone sand layer would be most effective, *i.e.* which allows the greatest reduction of strain/stress of the structure. Furthermore, it should be noted that the sand layers are slightly compacted and that the effect of compaction on the layer aseismic efficiency was not investigated. Also, a major problem of this substrate should be mentioned related to the possible

calcification of wet compacted sand, *i.e.* to the reduction of deformation properties and stiffening of the substrate over time. This could have a significant effect on reducing the aseismic efficiency of the substrate over time. The efficiency of such seismic isolation and durability over time could probably be improved by mixing sand with expanded glass beads, light metal beads, recycled rubber beads, etc., which should be the subject of separate research. Such composite seismic isolation layers should be as thin as possible due to the issue of rationality.

### 2.8.2 Stone pebble aseismic layer – *ASL-2*, and stone pebble layer with sliding geogrid and geomembrane layers – *ASL-3*

## Introduction

#### A. Research presented in papers [II, III, IV, and V]

Extensive and systematic research presented in these papers is focused on finding the most efficient stone pebble aseismic layer *ASL-2*, and research of the effect of external factors on its efficiency. The effect of the following parameters was investigated:

**(i) Pebble layer parameters:**

- thickness (0.30 m and 0.60 m)
- fraction (4-8 mm, 8-16 mm, and 16-32 mm)
- moisture (10% and 60%)
- compaction (*MS* = 10 MPa, *MS* = 30 MPa, and *MS* = 60 MPa)

**(ii) Model (structural) parameters:**

a. Stiffness

- rigid ($T = 0$) – $M_0$
- very stiff ($T = 0.05$ s) – $M_1$
- stiff ($T = 0.30$ s) – $M_2$
- medium-stiff ($T = 0.60$ s) – $M_3$
- soft ($T = 1.40$ s) – $M_4$

b. Foundation size

- small foundation – *SF*
- large foundation – *LF*

c. The vertical contact stress below the foundation

- 0.04 MPa
- 0.10 MPa

- 0.20 MPa

**(iii) Earthquake parameters:**

a. Earthquake type

- Artificial accelerogram – *AA*
- Accelerogram Petrovac – *AP*
- Accelerogram Ston – *AS*
- Accelerogram Banja Luka – *ABL*

b. Peak ground acceleration

- one-time, with lower value (structural stress in the elastic region)
- incremental until structure collapse

c. Repeating earthquakes

- incremental scaling *PGA* until structure collapse

*ASL-2* isolation layer with the following characteristics was selected as optimal (approximately the most efficient, most economical and easiest to construct): the pebble fraction $\Phi_b$ = 16-32 mm, the pebble layer compaction *MS* = 30 MPa, and the pebble moisture *h* = 10%.

It was concluded that the highest efficiency of this seismic isolation is for the very stiff $M_1$ and stiff $M_2$ structural models, so only they will be considered further (the medium-stiff $M_3$ and $M_4$ models based on *ASL-2* resulted in a small efficiency or is even detrimental).

Also, compared to a smaller foundation, a larger foundation resulted with a smaller isolation efficiency, which is due to the reduced rocking effect, *i.e.* lower dissipation of earthquake energy. As the tested seismic isolations are intended for application in rigid structures with low rocking impact, and especially because it is on the side of greater safety, models $M_1$ and $M_2$ with a larger foundation and an optimal pebble layer *ASL-2* will be considered further.

**B. Research presented in papers [VI, VII]**

The research presented in these papers is focused on finding the optimal *ASL-3* isolation layer, which is composite containing combinations of stone pebbles with different types and positions of sliding elements/materials (geogrid, geomembrane over limestone sand layer). A total of ten different composite aseismic layers were considered. The conclusions from the research related to the *ASL-2* layer were applied, *i.e.* only models with a larger foundation and the optimal pebble layer were considered. Equal excitations were also adopted.

It was concluded that the most optimal composite seismic isolation *ASL-3* is the one composed of *ASL-2* with a higher tensile strength geogrid at the layer top. Furthermore, it was concluded

that the highest efficiency of this seismic isolation is for the very stiff structural model $M_1$ and the stiff structural model $M_2$. Therefore, only the $M_1$ and $M_2$ models on the optimal composite isolation will be considered further.

### C. The most important research results

In order to emphasize the most important research results, which are crucial for assessing the efficiency of the considered seismic isolations and the possibility of their application in practice, they are presented only for the substrates shown in Figure 2.13. The results for all applied accelerograms (*AA*, *AP*, *AS*, and *ABL*) are presented, in order to see the effect of the earthquake type on the behaviour of each tested model. The test results are presented separately for the rigid model $M_0$, and separately for the deformable models $M_1$ and $M_2$.

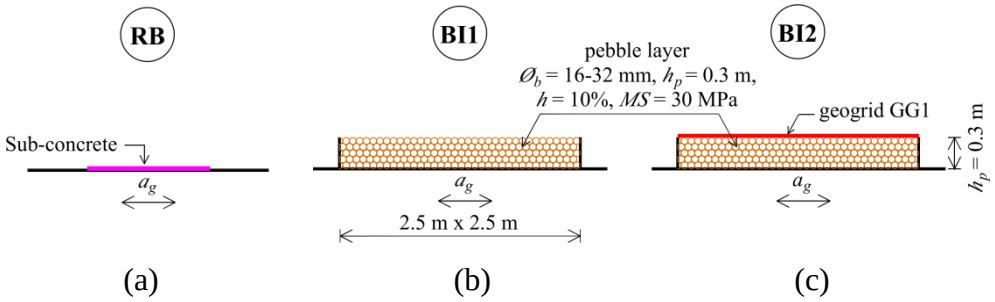


*Figure 2.13* Tested substrates for which part of the results is presented: (a) Rigid base *RB*; (b) Stone pebble isolation layer *BI1*; (c) Stone pebble and geogrid isolation layer *BI2*

#### C.1 Research results for the rigid structural model – $M_0$

The peak acceleration $a_m$ of the $M_0$ model for all excitations applied depending on the substrate type (*RB*, *BI1*, and *BI2*) and *PGA* level (0.2 g, 0.4 g, and 0.6 g) is presented on Figure 2.14. The mean value of the results and the result envelope were also drawn for each substrate. It is noticeable that the peak $a_m$ values significantly depend on the type of applied excitation (*AA*, *AP*, *AS*, and *ABL*) and the substrate type (*RB*, *BI1*, and *BI2*).

For all substrate types, the *ABL* excitation was the most favourable, and on average *AA* was the most unfavourable, followed by *AP* and *AS* excitations. It is noticeable that with the increase in *PGA*, the measured $a_m$ generally increases, but not proportionally. Also, it can be noted that the $a_m$ on the *RB* are higher than on the *BI1* isolation and especially on the *BI2* isolation.

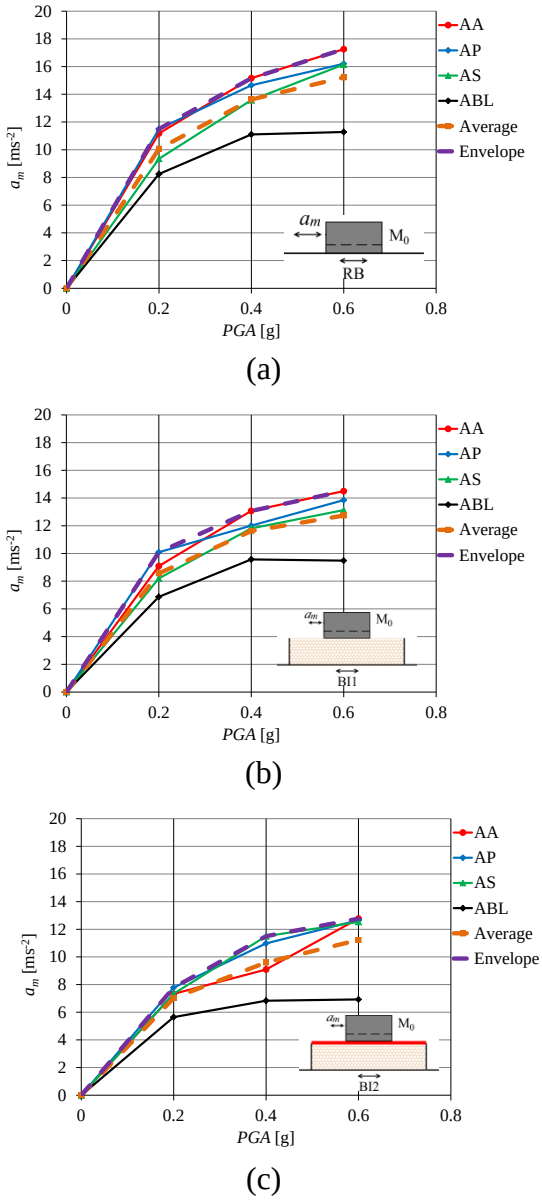


*Figure 2.14* The peak acceleration $a_m$ of the $M_0$: (a) $M_0$ on *RB*; (b) $M_0$ on *BI1*; (c) $M_0$ on *BI2*

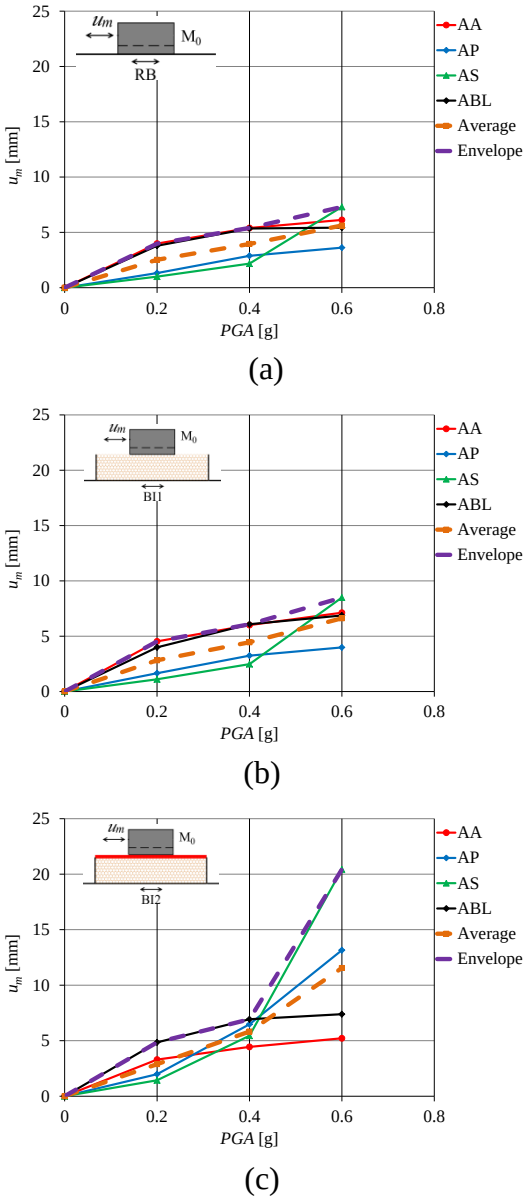


*Figure 2.15* The peak displacement $u_m$ of the $M_0$: (a) $M_0$ on *RB*; (b) $M_0$ on *BI1*; (c) $M_0$ on *BI2*

The peak displacement $u_m$ of the $M_0$ model for all excitations applied depending on the substrate type (*RB*, *BI1*, and *BI2*) and *PGA* level (0.2 g, 0.4 g, and 0.6 g) is presented on Figure 2.15. The mean value of the results and the result envelope were also drawn for each substrate. Previously stated conclusions regarding acceleration apply for displacements also. The peak $u_m$ values significantly depend on the excitation type applied, *PGA* level, and the substrate type. Impact-type earthquakes *AS* and *ABL*, especially at high *PGA* level, resulted in large displacements, *i.e.* they were the most unfavourable. The unfavourable effect of impact-type earthquakes on rigid model is explained by the fact of the dominant influence of shear force in relation to the bending.

The peak acceleration $a_m$ envelope of all excitation applied for $M_0$ based on *RB*, *BI1*, and *BI2* substrates is shown in Figure 2.16. For *PGA* = 0.6 g, the $a_m$ ratio is *RB*:*BI1*:*BI2* = 1:1.19:1.36,

and, for *PGA* = 0.2 g, this ratio is RB:BI1:BI2 = 1:1.14:1.48. In terms of the $a_m$, the *BI1* isolation is approximately 19% and the *BI2* isolation is approximately 36% more favourable than the conventional *RB*.

The peak displacement $u_m$ envelope of all excitation applied for $M_0$ based on *RB*, *BI1*, and *BI2* substrates is shown in Figure 2.17. For *PGA* = 0.6 g, the $u_m$ ratio is RB:BI1:BI2 = 1:1.14:2.80. Therefore, *BI1* isolation results in approximately 14% and BI2 isolation with approximately 280% larger $u_m$ than the *RB*. It is obvious, and what was to be expected, that soft substrate (especially *BI2* with a sliding layer on the layer top) resulted in larger model displacement than a rigid base. For PGA ≤ 0.4 g (lower values of earthquake acceleration), the displacements for *BI1* and *BI2* are only slightly larger than for the *RB*.

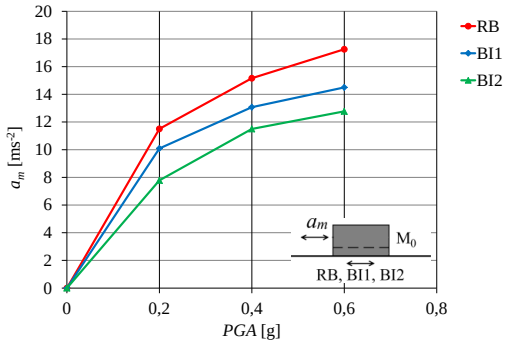


*Figure 2.16* The peak acceleration $a_m$ envelope of all excitation applied on the $M_0$ based on *RB*, *BI1*, and *BI2*

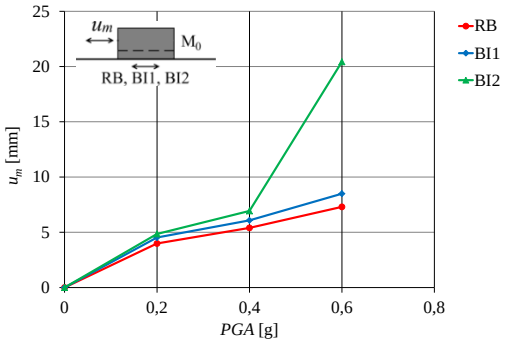


*Figure 2.17* The peak displacement $u_m$ envelope of all excitation applied on the $M_0$ based on *RB*, *BI1*, and *BI2*

### C.2 Research results for the $M_1$ and $M_2$ structural models

Due to the large volume of experimental tests, testing of $M_1$ and $M_2$ models was performed for a one-time base excitation with *PGA* = 0.3 g for *AA*, *AP*, *AS*, and *ABL*, while model testing with successive increase in *PGA* until structure collapse was performed only for the *AA* excitation (successive increase of *PGA* by 0.05 g). Here it is necessary to emphasize that the displacement and strain state of the model at a one-time excitation with *PGA* = 0.3 g is more favourable than the displacement and strain state for the same excitation and *PGA* when the model is previously exposed to a series of excitations with lower levels of *PGA* = n × 0.05 g (n = 1 to 5). For the previous reason, these two states are different.

The peak acceleration $a_m$ of the $M_1$ based on *RB*, *BI1*, and *BI2* is presented in Figure 2.18. It is noticeable that with the increase in *PGA*, the $a_m$ generally increases, but not proportionally. Also, it can be noted that the $a_m$ for the same structural model on the *RB* are higher than on the *BI1*, and especially on the *BI2*.

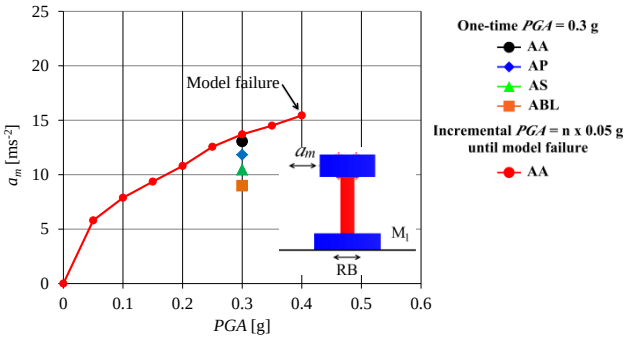


(a)

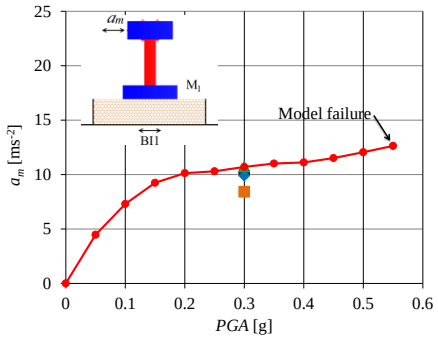


(b)

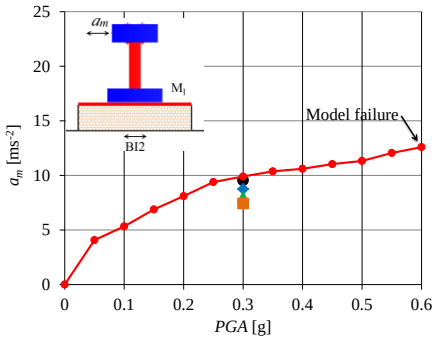


(c)

*Figure 2.18* The peak acceleration $a_m$ of the $M_1$: (a) $M_1$ on *RB*; (b) $M_1$ on *BI1*; (c) $M_1$ on *BI2*

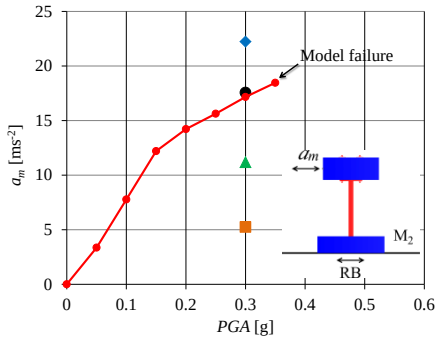


(a)

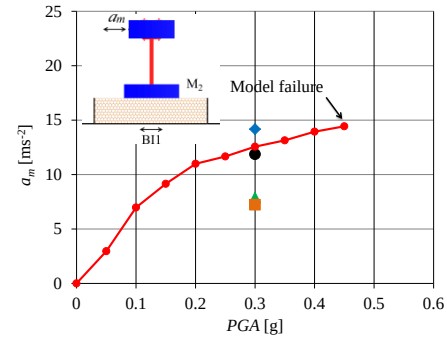


(b)

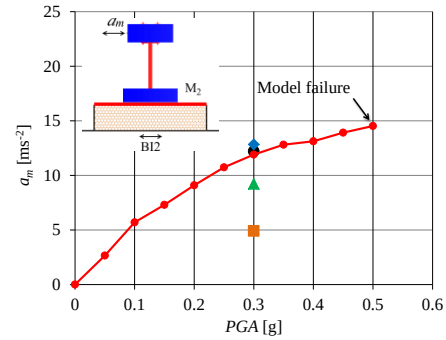


(c)

*Figure 2.19* The peak acceleration $a_m$ of the $M_2$: (a) $M_2$ on *RB*; (b) $M_2$ on *BI1*; (c) $M_2$ on *BI2*

The $a_m$ of the $M_2$ based on *RB*, *BI1*, and *BI2* is presented in Figure 2.19, and the analogous statements apply as for the $M_1$ model shown in Figure 2.18.

The $a_m$ of the $M_1$ and $M_2$ based on *RB*, *BI1*, and *BI2* is presented in Figure 2.20. The $M_1$ (Figure 2.20a) based on the *RB* collapsed at *PGA* = 0.4 g, based on *BI1* isolation collapsed at *PGA* = 0.55 g, and based on *BI2* collapsed at *PGA* = 0.6 g. At the aforementioned *PGA*, $a_m$ was 15.44 ms$^{-2}$ for *RB*, 12.63 ms$^{-2}$ for *BI1*, and 12.59 ms$^{-2}$ for *BI2*, respectively. It is obvious that the *BI1* and especially *BI2* seismic isolations are more favourable than the classical foundation on a rigid base. Similarly, the above conclusions apply to the $M_2$ (Figure 2.20b). Collapse of the $M_2$ based on the *RB* occurred at *PGA* = 0.35 g, based on *BI1* collapsed at *PGA* = 0.45 g, and based on *BI2* collapsed at *PGA* = 0.50 g. At the aforementioned *PGA*, $a_m$ was 18.46 ms$^{-2}$ for *RB*, 14.43 ms$^{-2}$

for *BI1*, and 14.52 ms$^{-2}$ for *BI2*, respectively. Thus, it can be stated that the *BI1* and especially *BI2* are more favourable than the classical foundation on a *RB*.

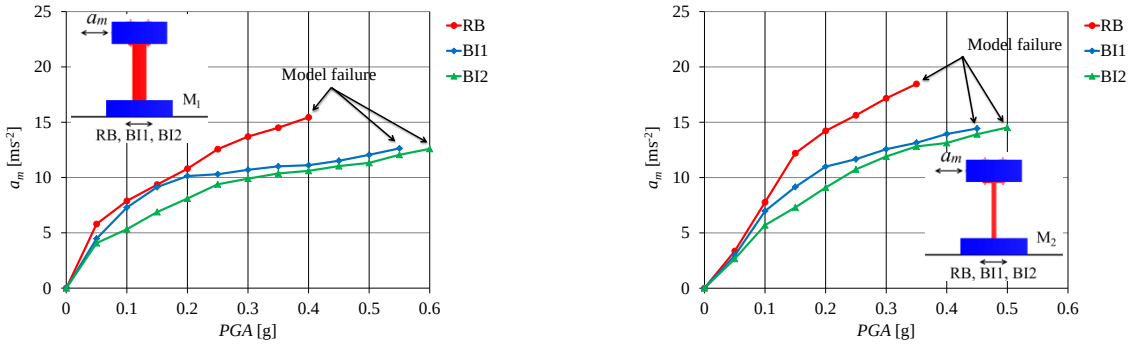


*Figure 2.20* The peak acceleration $a_m$ of model based on *RB*, *BI1*, and *BI2*: (a) $M_1$; (b) $M_2$

The $u_m$ of the $M_1$ is presented on Figure 2.21. For $PGA \leq 0.4$ g, when the $M_1$ collapsed on the *RB*, models based on seismic isolation had slightly smaller displacements (especially the $M_1$) than the corresponding model on the *RB*, which is favourable. Smaller displacements of the $M_1$ and $M_2$ based on seismic isolations than of the $M_0$ displacement on the same substrate are explained by the reduced influence of shear force (slip of the model foundation along the seismic isolation top) in the $M_1$ and $M_2$ in relation to the $M_0$.

The $u_m$ of the $M_2$ is presented on Figure 2.22. It can be noted that until the collapse of the model on the *RB*, the displacements of the $M_2$ based on the *BI1* and *BI2* were also somewhat smaller than on the *RB*, which is also favourable.

The $u_m$ of the $M_1$ and $M_2$ on the *RB*, *BI1*, and *BI2* for all excitations applied are presented in Figure 2.23. On this Figure is more clearly visible what is referred to Figures 2.21 and 2.22. Thus, it can be noted that even the displacements (and not only the accelerations) of the $M_1$ and $M_2$ on the *BI1* and *BI2* are more favourable than in the case of the *RB*.

The most adequate indicator of the seismic isolation efficiency is the ratio of strain in the structure on isolation in relation to the structure without seismic isolation. The peak strain $\varepsilon_m$ at the bottom of the $M_1$ column is presented in Figure 2.24, and of the $M_2$ is presented in Figure 2.25. It can be noted that the shape of these diagrams is similar to the diagrams of the $a_m$ presented in Figures 2.18 and 2.19. That is, the seismic isolations efficiency in relation to the *RB* is equally manifested through $\varepsilon_m$ and $a_m$ values.

The $\varepsilon_m$ values of $M_1$ and $M_2$ based on *RB*, *BI1*, and *BI2* are presented in Figure 2.26. It can be stated that the seismic isolation efficiency through the reduction of strains in $M_1$ and $M_2$ is analogous to the efficiency through the reduction of accelerations (Figure 2.20).

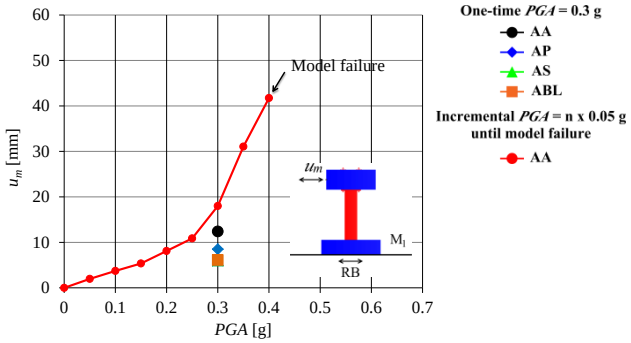


(a)

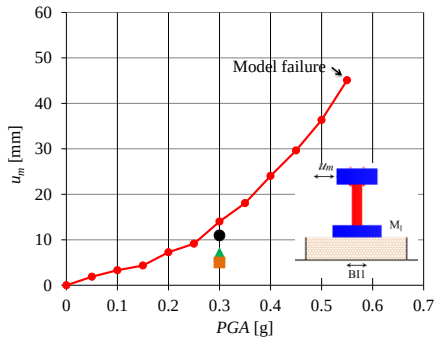


(b)

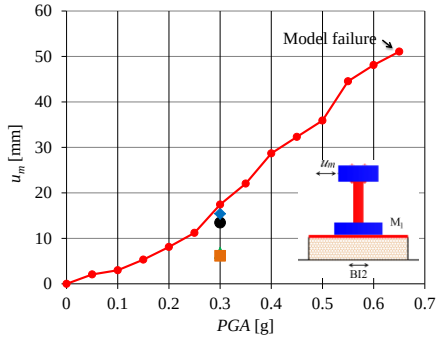


(c)

*Figure 2.21* The peak displacement $u_m$ of the $M_1$: (a) $M_1$ on *RB*; (b) $M_1$ on *BI1*; (c) $M_1$ on *BI2*

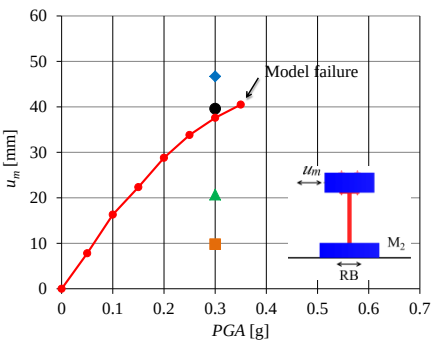


(a)

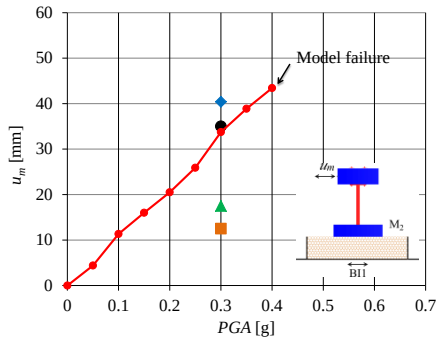


(b)

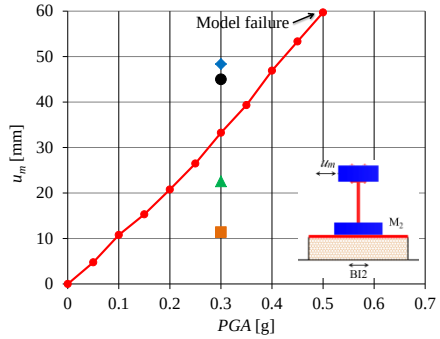


(c)

*Figure 2.22* The peak displacement $u_m$ of the $M_2$: (a) $M_2$ on *RB*; (b) $M_2$ on *BI1*; (c) $M_2$ on *BI2*

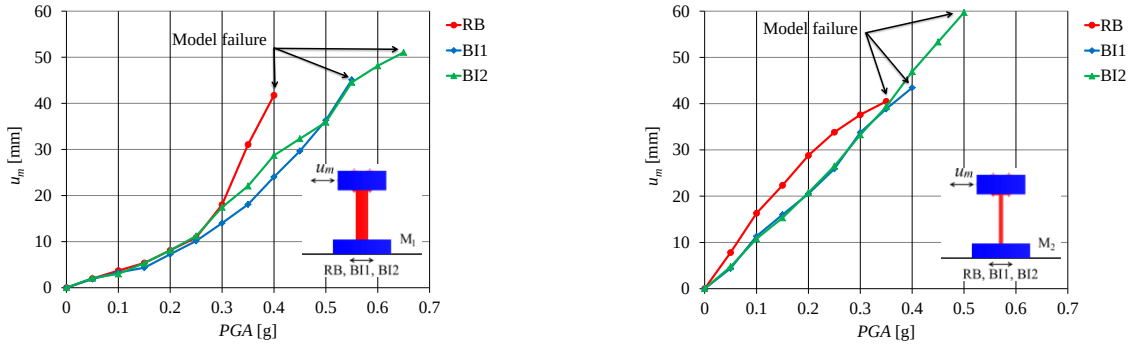


(a) (b)

*Figure 2.23* The peak displacement $u_m$ of model based on *RB*, *BI1*, and *BI2*: (a) $M_1$; (b) $M_2$

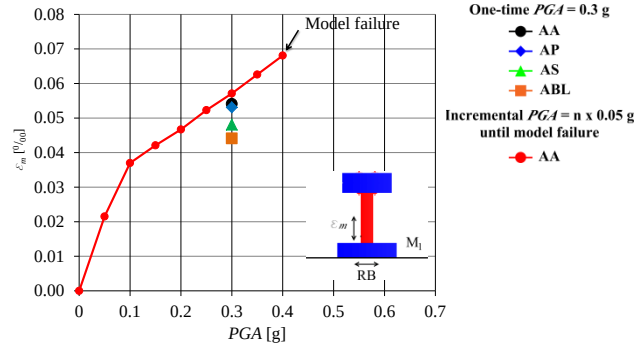


(a) (a)

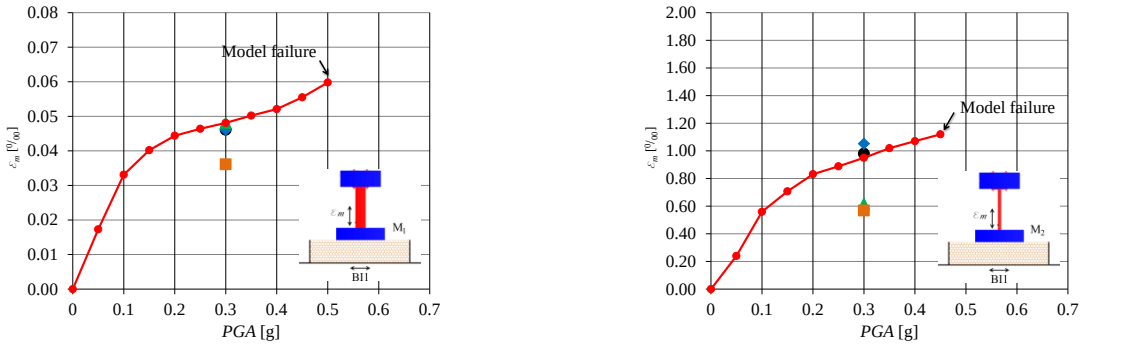


(b) (b)

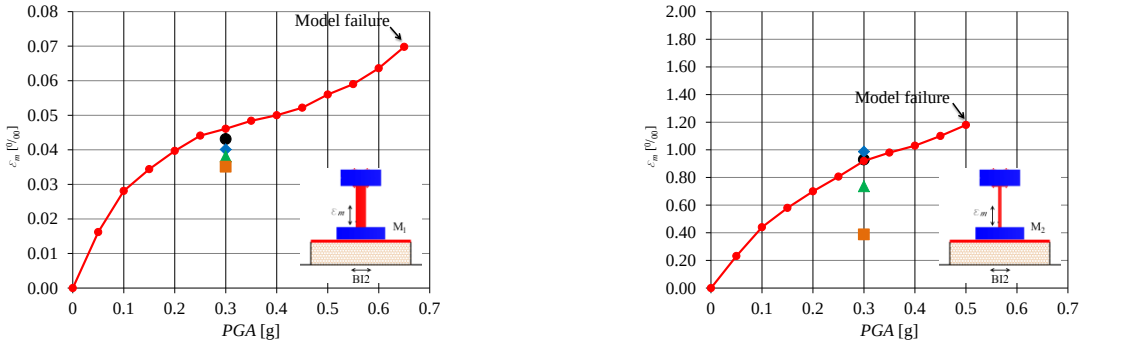


(c) (c)

*Figure 2.24* The peak strain $\varepsilon_m$ at the bottom of the $M_1$ column

*Figure 2.25* The peak strain $\varepsilon_m$ at the bottom of the $M_2$ column

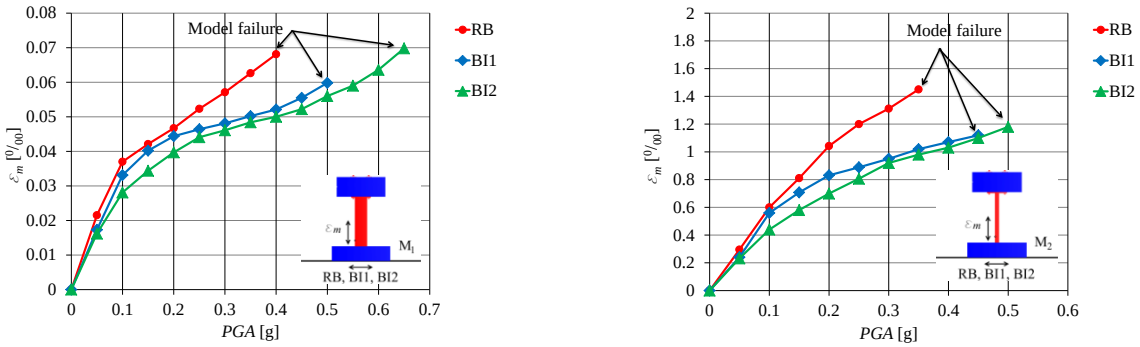


(a) (b)

*Figure 2.26* The peak strain $\varepsilon_m$ of model based on *RB*, *BI1*, and *BI2*: (a) $M_1$; (b) $M_2$

* * *

Based on quite extensive experimental studies of the behaviour of structural models of different stiffness on seismic isolation *ASL-2* and *ASL-3*, with respect to the rigid base without seismic isolation, it can be concluded that they significantly reduce seismic forces and strains in very stiff $M_1$ and stiff $M_2$ structural models. Furthermore, *ASL-3* is significantly more efficient than *ASL-2*, and somewhat more expensive. In relation to the *RB* without seismic isolation, the average efficiency of the *ASL-2* through the reduction of acceleration and strain in the tested models is 13%, and the average efficiency of the *ASL-3* is 25%. The mean efficiency value for the $M_1$ and $M_2$ for the "average" excitation applied is given. At the same time, the isolation efficiency for the $M_1$ model is higher than for the $M_2$ model. The seismic isolations efficiency depended significantly on the type of applied accelerogram. The efficiency is the lowest for the so-called impact-type earthquakes, which are of short duration and short predominant period, which fail to rock the structure more strongly and which bring little energy into the structure. Fortunately, however, such earthquakes cause significantly lower inertial forces and strains in the structure than earthquakes of longer duration and longer predominant period.

## 2.9 Main conclusions of the experimental research

Based on the conducted experimental research of the structural models' behaviour without seismic isolation – *RB* on the *ASL-1* limestone sand aseismic layer, on the *ASL-2* stone pebble aseismic layer, and on the composed *ASL-3* stone pebble layer with different sliding layers of geogrid, geomembrane over limestone sand layer, exposed to four different earthquake accelerograms, the main conclusions below can be drawn.

### 2.9.1 Limestone sand aseismic layer – *ASL-1*

Brief research has confirmed that the use of a thin limestone sand layer (thickness 2 cm and 10 cm), in relation to the *RB* without seismic isolation, reduces inertial (seismic) force and stress in the considered structural model for lower *PGA* levels and at model collapse. These reductions were approximately 10% for lower *PGA* levels, whereas the *ASL-1*-based models had a higher ultimate load-bearing capacity of approximately 14%. It should be noted that the seismic isolations were slightly compacted and had similar efficiencies (a 10 cm thick layer was slightly more efficient).

Due to the effect of sand calcification over the time, as well as due to compaction and moisture, the long-term seismic efficiency of such a layer is questionable. In this regard, further extensive research into the efficiency of this seismic isolation is needed.

### 2.9.2 Stone pebble aseismic layer – *ASL-2*, and stone pebble layer with sliding geogrid and geomembrane layers – *ASL-3*

Relatively extensive research has confirmed that the use of these seismic isolation layers in relation to the *RB* without seismic isolation reduces inertial/seismic force in the considered structural models, both for lower *PGA* levels and in the case of model testing until collapse. It was found that these seismic isolations are sufficiently effective for very stiff and stiff structural models $M_1$ and $M_2$, while for softer models they are not efficient or even detrimental. It was also found that the efficiency of these seismic isolations is lower for the case of structural models with larger foundation ground plan dimensions. Therefore, when evaluating the efficiency of these seismic isolations, conservative values of earthquake force and strain reduction were considered (structural models with a larger foundation), with low rocking effect.

*ASL-2* isolation layer with the following characteristics was selected as optimal (approximately the most efficient, most economical and easiest to construct): the pebble fraction $\Phi_b$ = 16-32 mm, the pebble layer compaction *MS* = 30 MPa and the pebble moisture *h* = 10%.

The most optimal *ASL-3* composite seismic isolation is the one composed of an optimal 0.30 m thick stone pebble layer *ASL-2* with a higher tensile strength geogrid at the layer top. The *ASL-3* layer is slightly more expensive than the *ASL-2* layer, equally simple and quick to construct, but significantly more efficient in reducing seismic force and strain in the structural models.

In relation to the *RB* without seismic isolation, the $M_1$ and $M_2$ based on the *ASL-2* seismic isolation layer had an average reduction in seismic force and strain/stress by approximately 13% at lower *PGA* levels and approximately 25% at model failure.

In relation to the models based on the *ASL-2*, the $M_1$ and $M_2$ based on the *ASL-3* had an average reduction in seismic force and strain/stress by approximately 10% at lower *PGA* levels and approximately 25% at model failure.

In relation to the *RB* without seismic isolation, the $M_1$ and $M_2$ based on the *ASL-3* had an average reduction in seismic force and strain/stress by approximately 25% at lower *PGA* levels and approximately 34% at model failure.

Based on the above, the *ASL-3* is considered more optimal than the *ASL-2*.

It is important to highlight that the seismic isolations efficiency depended significantly on the type of applied accelerogram. Seismic isolation efficiency was higher for *AA* and *AP* excitation than for *AS* and *ABL*. This behaviour is explained by the fact that *AA* and *AP* are long-lasting earthquakes that bring high energy into the system and produce more pronounced rocking of the model. Namely, beside the sliding mechanism, the reduction or earthquake forces in this isolation concept is achieved by reduced rocking stiffness, taking the advantages of rocking isolation concept. The low efficiency of seismic isolation for *AS* and *ABL* accelerograms should be seen in the context that they cause low stresses in the tested models, which diminishes the fact of less efficient seismic isolation for such excitations. Owing the limitations of the performed research (relatively simple building models, just four building models, only four base excitations applied, and uniaxial base excitation), the obtained conclusions should be strengthened by further research.

Due to the above statement, further experimental researches on this topic are needed (preferably on real structures or models with realistic material and a slightly reduced geometry).

# 3. NUMERICAL MODELLING

## 3.1 Introduction

One of the planned research objectives was the development of a numerical model for nonlinear dynamic analysis of planar structures with seismic base isolation using stone pebble layer. Compared to the total duration of all research conducted, the research time in the field of numerical modelling was significantly shorter than the time devoted to experimental research on the efficiency of seismic base isolation using natural materials under the foundation. Nevertheless, the planned goal was achieved in this area as well, in accordance with the research methodology in Section 1.4.2. The developed numerical model is described in more detail in the paper by Banović *et al.* [B.12], also referred as [VIII], and will be presented here synthesized and abbreviated.

Section 3.2 briefly describes the stress state at the pebble layer top, as a guideline for the development of appropriate constitutive models for reliable modelling of the pebble layer behaviour, as well as the foundation-pebble layer coupling surface behaviour. Section 3.3 presents a developed numerical model for the simulation of planar structures made of different materials, which are based on a stone pebble aseismic layer. Section 3.4 summarizes the results of the necessary experimental tests performed to define several basic parameters of the constitutive models for stone pebble layer and the foundation-pebble coupling surface. The verification of the developed numerical model on the results of some shake-table tests is presented in Section 3.5. Finally, conclusions regarding the developed numerical model are presented in Section 3.6.

## 3.2 Description of the stress state under the foundation at the pebble layer top

Generally, the vertical force $N$, the transverse force $Q$ and the bending moment $M$ are transmitted below foundation to the substrate (Figure 3.1). The distribution of vertical normal $\sigma_v$ and shear $\tau$ stress below foundation depends on the moment $M$ and force $N$ ratio, *i.e.* on the eccentricity $e$ of the force $N$ in relation to the middle of the foundation of length $B$ ($e = M/N$). If $e$ is inside the foundation plan core, the foundation–pebble coupling surface is under pressure along its entire length. With increasing $e$, there is a lifting of the foundation from the substrate, a significant increase in vertical normal stress, as well as an increase in shear stress due to the reduction of the foundation active area to transfer the shear to the ground. Namely, shear stress can be transmitted to the substrate only on the foundation surface with vertical compressive stress.

This low-cost seismic isolation is designed for low-rise buildings, whose foundations are buried shallow in the stiff soil. Therefore, the horizontal normal stress $\sigma_h$ in the pebble layer is small. Because of the relatively low level of $\sigma_h$ in relation to $\sigma_v$, its influence on the ultimate bearing capacity of the seismic isolation layer is ignored here, which is on the side of greater safety.

Stone pebbles are an extremely incoherent material, with a fairly high compressive strength and without any tensile strength. Also, the pebble layer is anisotropic, *i.e.* approximately orthotropic, with significantly different strength and deformation in the vertical and horizontal directions.

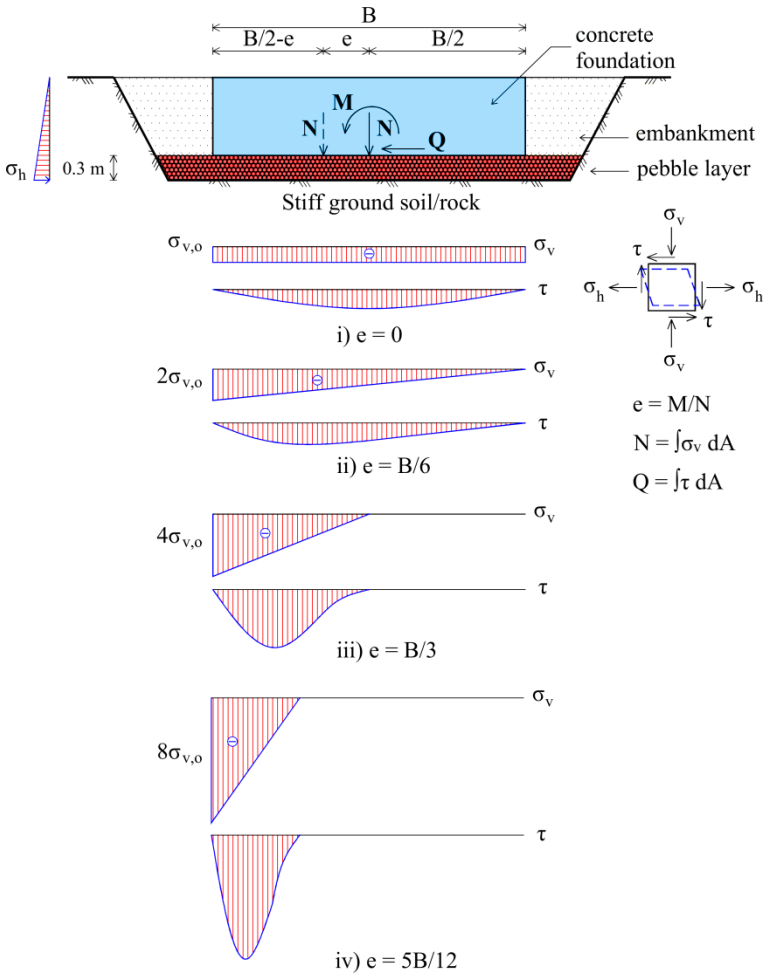


*Figure 3.1.* The distribution scheme of normal and shear stress below the foundation

## 3.3 Numerical model

The presented numerical model for dynamic analysis of planar structures with seismic isolation consists of the basic numerical model for dynamic analysis of such structures without seismic isolation, developed by Radnić *et al.* [R.2], and later improved by (Baloević *et al.* [B.1, B.2, B.3], Radnić *et al.* [R.3, R.4], and Smilović *et al.* [S.3, S.4, S.5]), in which the developed constitutive models for simulating the pebble layer and the foundation-pebble layer contact surface behaviour are coupled.

### 3.3.1 Basic numerical model

The basic numerical model, developed by Radnić *et al.* [R.2], and later improved by (Baloević *et al.* [B.1, B.2, B.3], Radnić *et al.* [R.3, R.4], and Smilović *et al.* [S.3, S.4, S.5]), is based on the *FEM* for the spatial discretization of the structure (the observed system remains a continuum in all phases of deformation), and the finite difference method for temporal discretization. The model will be briefly described, because it belongs to the classic models of such purpose, which are reliable and proven.

Basic 8-node "serendipity" 2D elements were used to discretize the structure and seismic isolation layer, and 6-node 2D contact elements for contact surface simulation. An updated Lagrangian formulation was adopted for geometric nonlinear analysis. To solve the system of nonlinear equations, Newton-Raphson initial and tangential stiffness methods can be used. The convergence criterion of the iterative procedure is defined as a function of the increase in displacement increment. Implicit, explicit, or implicit-explicit Newmark's algorithm, developed in iterative form by Hughes *et al.* [H.3] is used for the solution of the dynamic equilibrium equation. Constitutive models for reinforced concrete, steel, masonry and cohesive soil are defined.

The constitutive model for concrete is based on elastoplastic behaviour in pressure and elastobrittle behaviour in tension. Furthermore, linear unloading behavior is assumed. The yield criterion in compression is defined as a function of stress and the crushing criterion as a function of strain. The opening and closing of cracks in the tension, which were modeled as fixed, orthogonal and smeared, was simulated. The tensile and shear stiffness of cracked concrete was modeled. The reinforcement was simulated with 1D element, inside the concrete 2D element, with an elastoplastic constitutive model. Full compatibility of concrete and reinforcement displacements was assumed.

The constitutive model for structural steel is also based on the elastoplastic model, with defined yield criteria (stress function) and the failure criterion (strain function). Linear behavior was adopted during unloading.

A macro model of masonry was adopted. It is possible to use an isotropic or anisotropic model of masonry behavior. The effect of biaxial compressive stresses on the limit bearing capacity of masonry has not been modeled. The behavior of masonry (cracks, crushing, etc.) is simulated analogously to the simulation of concrete behavior.

The constitutive model for coherent soil is not particularly developed. It is possible to use a masonry or concrete model behavior, with corresponding material parameters.

### 3.3.2 Developed constitutive model for stone pebble layer

Proposed orthotropic constitutive model for stone pebble layer (main direction of anisotropy is *v*-vertical and *h*-horizontal) is presented on Figure 3.2, with the adopted normal stress-normal strain relation (Figure 3.2a), the shear stress-shear strain relation (Figure 3.2b), and the shear stress-normal stress relation (Figure 3.2c). Symbols in the Figure denote the following: $\sigma_v$, $\sigma_h$ normal vertical and horizontal stress; $\varepsilon_v$, $\varepsilon_h$ normal strains; $f_v$, $f_h$ compressive strengths; $E_v$, $E_h$ modulus of elasticity; $\varepsilon_{e,v}$, $\varepsilon_{e,h}$ yield strains; $\varepsilon_{u,v}$, $\varepsilon_{u,h}$ limit compressive strains; $G$ shear modulus.

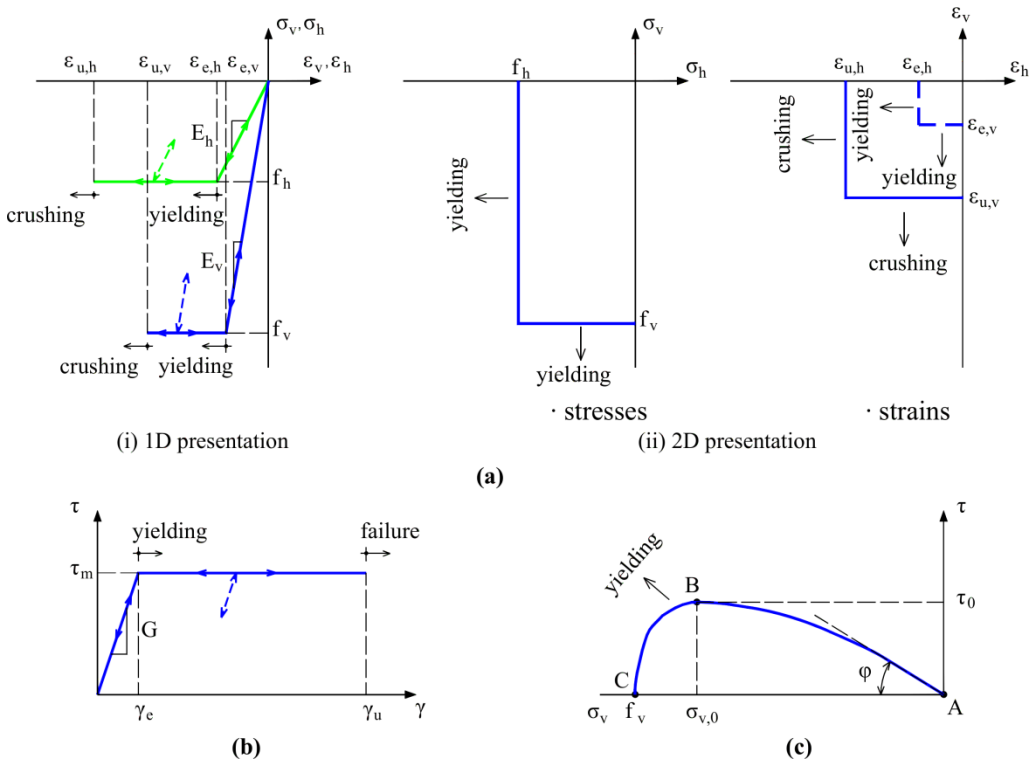


*Figure 3.2.* Proposed constitutive model for stone pebble layer: (a) Normal stress-normal strain relation; (b) Shear stress-shear strain relation; (c) Shear strength-normal stress relation

The orthotropic coefficient $c_0$ is defined by:

$$c_0 = E_h/E_v = f_h/f_v \tag{3.1}$$

where $v_h$ and $v_v$ are Poisson's ratios for the horizontal and vertical directions, respectively.

The shear modulus of pebbles $G$ is defined by:

$$G = 1/[(1+v_h)/E_h + (1+v_v)/E_v] \tag{3.2}$$

Thus, the normal stress-normal strain relation is defined by a simple elastoplastic model, with a linear unloading behaviour, analogous to that for the masonry. The shear stress-shear strain relation is also defined by a simple elastoplastic model, with a linear unloading behaviour. The shear strength-normal stress relation is shown in Figure 3.2c, and is defined by a cubic parabola passing through points A, B and C. The tangent of the curve at point B is horizontal, and at point

A an angle of internal friction $\varphi$. Some parameters of this curve are assumed and need to be determined experimentally. The shear bearing capacity criterion is satisfied if the ratio $\tau$-$\sigma_v$ is such that it is below the assumed curve. Otherwise, the current shear stress $\tau$ is reduced to the curve for the current $\sigma_v$ and a further iterative procedure is performed with $G$ = 0 (plastic yielding). The shear failure criterion in that point is defined when $\gamma > \gamma_u$.

### 3.3.3 Developed constitutive model for foundation-pebble layer contact behaviour

To simulate the foundation-pebble layer coupling surface, a 2D six-node contact finite elements were used. Figure 3.3 presents proposed constitutive model for simulating the foundation-pebble contact behavior. Symbols in the Figure denote the following (the prefix $_c$ denotes contact): $\sigma_{v,c}$, $\varepsilon_{v,c}$ normal stress and normal strain; $f_{v,c}$ compressive strength; $E_c$ modulus of elasticity; $\varepsilon_{u,c}$ limit compressive strain; $\tau_{m,c}$ the current shear strength; $\gamma_{u,c}$ limit shear strain; $G_c$ shear modulus; $\tau_{0,c}$ peak shear strength; $\varphi_c$ angle of internal friction. Basically, analogous solutions are used as in Figure 3.2 for the pebble layer, where there is only one normal compressive stress perpendicular to the contact surface. The possibility of tension transmission at the foundation-pebble layer coupling surface is excluded. The constitutive model parameters are taken as the "weaker link" at the joint, which is the pebble layer. Other features of the constitutive model at the contact are analogous to the constitutive model within the pebble layer.

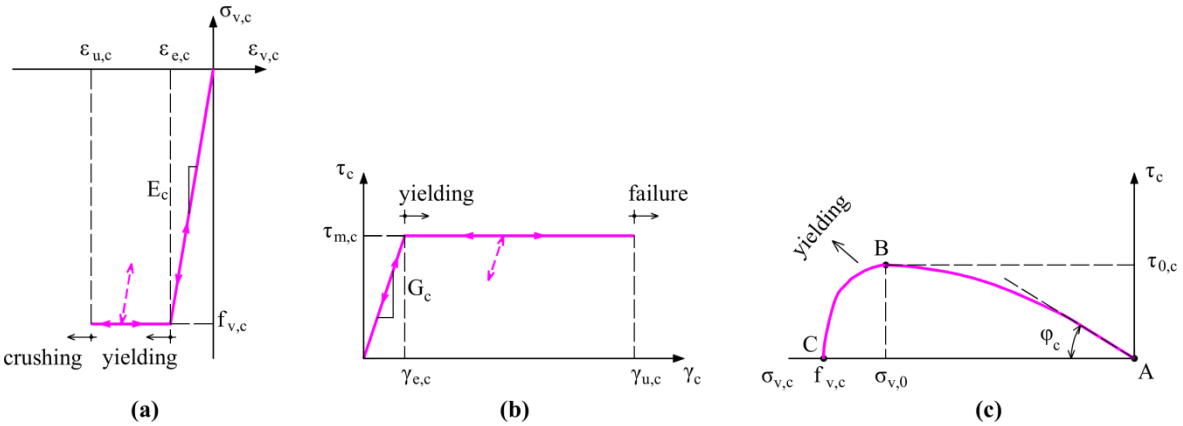


*Figure 3.3.* Proposed constitutive model for foundation-pebble layer contact behaviour: (a) Normal stress–normal strain relation; (b) Shear stress–shear strain relation; (c) Shear strength–normal stress relation

## 3.4 Experimental tests for determining the parameters of the pebble layer and foundation-pebble layer coupling surface constitutive models

Using a large-scale direct shear test (Figure 3.4), the shear strength, angle of internal friction and modulus of elasticity of the pebble layer in the vertical direction was determined. Assuming the isotropic behaviour of the pebbles in the rigid box (prevented lateral deformation) and the known vertical stress, the Poisson's ratio for the horizontal direction was determined, followed by the modulus of elasticity for the horizontal direction and the Poisson's ratio for the vertical direction.

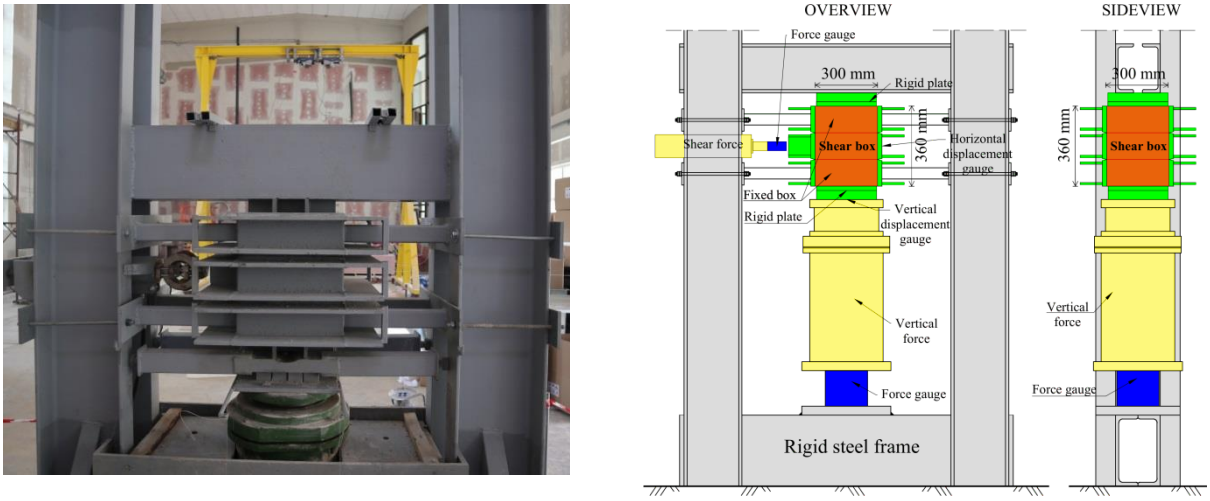


(a) (b)

*Figure 3.4.* Equipment for large-scale direct shear test: (a) Photography; (b) Basic data

Shear stress-normal stress relation and frictional angle $\varphi$ derived from direct shear tests are shown in Figure 3.5. For low levels of vertical normal stress, it was found to be $\varphi = 48^{\circ}$, which is close to the value experimentally determined by Indraratna *et al.* [I.1] for similar material.

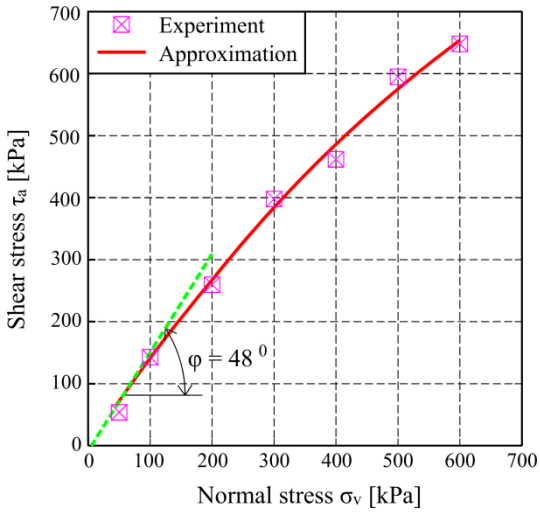


*Figure 3.5.* Shear stress–normal stress relation and angle $\varphi$ derived from direct shear tests

The friction angle $\varphi_c$ of the pebble layer subjected to different vertical stresses against a smooth prefabricated foundation interface (used in the experimental tests of models $M_0$, $M_1$, $M_2$, $M_3$, and $M_4$), an experimental test was performed according to Figure 3.6a. Based on the experimental results, $\varphi_c = 27^{\circ}$ was adopted. Clearly, there is a large difference between $\varphi_c$ and friction angle within the pebble layer.

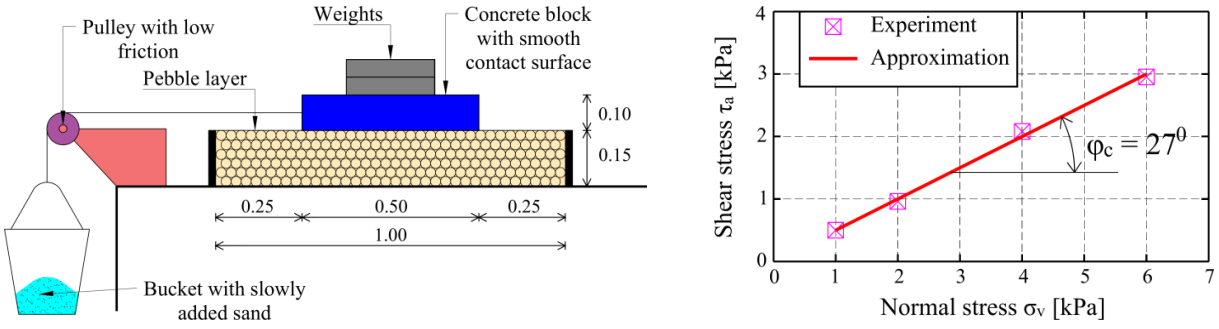


(a) (b)

*Figure 3.6.* Experimental test for determining foundation-pebble layer coupling surface constitutive model parameters: (a) Rigid concrete block with smooth contact surface designed to slide against the pebble layer; (b) Normal stress-shear stress relation

## 3.5 Verification of the developed numerical model

The basic numerical model, which is updated by the developed constitutive models according to Sections 3.3.2 and 3.3.3, was verified on several shake-table tests of structural models $M_1$ and $M_2$ with a larger foundation on the optimal stone pebble aseismic layer ($h_p$ = 0.3 m, $\phi_b$=16-32 mm, *MS* = 30 MPa and $h$ = 10%), according to Table 3.1.

*Table 3.1.* Numerically simulated experimental tests

| Excitation | Model $M_1$ | Model $M_2$ | |
|---|---|---|---|
| AA | + | + | *One-time base excitation with PGA = 0.3 g* |
| AP | + | + | |
| AS | + | + | |
| ABL | + | + | |
| AA | + | + | *Successive application of AA excitation until model collapse* |

Finite element discretization of tested models is presented in Figure 3.7, and the parameters of steel, stone pebbles, and contact element constitutive models are presented in Table 3.2.

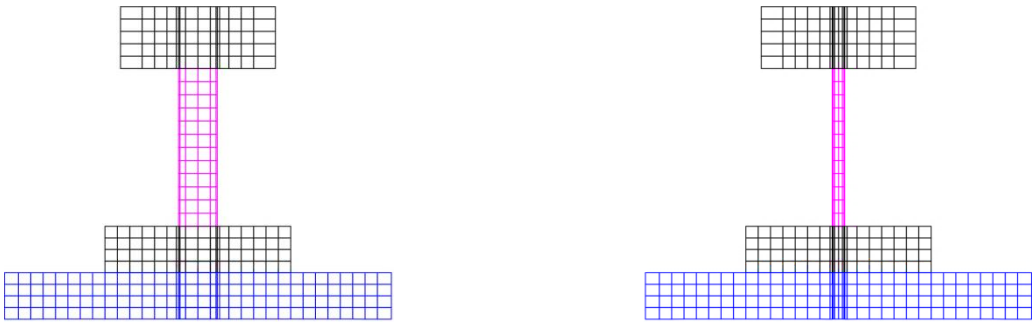

(a) (b)

*Figure 3.7.* Finite element spatial discretization: (a) $M_1$; (b) $M_2$

*Table 3.2* The parameters of steel, stone pebbles, and contact element constitutive models

| *Steel* | | | | | | | | | | | |
|---|---|---|---|---|---|---|---|---|---|---|---|
| $E$ (GPa) | | $f_{c,\,steel}$ (MPa) | | $f_{t,\,steel}$ (MPa) | | $v_{steel}$ | | $\varepsilon_{steel}$ [‰] | | | |
| 200 | | 520 | | 520 | | 0.3 | | 20 | | | |
| *Stone pebbles* | | | | | | | | | | | |
| $E_v$ (MPa) | $E_h$ (MPa) | $f_v$ (MPa) | $f_h$ (MPa) | $\tau_m$ (MPa) | $v_v$ | $v_h$ | $\varepsilon_{u,v}$ [‰] | $\varepsilon_{u,h}$ [‰] | $G$ (MPa) | $\gamma_u$ [‰] | $\varphi$ [$^0$] |
| 270 | 135 | 6.0 | 3.0 | 1.8 | 0.24 | 0.48 | 20 | 40 | 64.3 | 100 | 48 |
| *Contact element: foundation-pebble layer coupling surface* | | | | | | | | | | | |
| $E_c$ (MPa) | | $f_{v,c}$ (MPa) | | $\tau_{m,c}$ (MPa) | | $v_c$ | $\varepsilon_{u,c}$ [‰] | | $G_c$ (MPa) | $\gamma_{u,c}$ [‰] | $\varphi_c$ [$^0$] |
| 270 | | 6.0 | | 1.01 | | 0.24 | 20 | | 36.17 | 177 | 27 |

A comparison of some experimental and numerical results is shown in Figures 3.8 and 3.9, and on Table 3.3.

*Table 3.3* Comparison of some peak values of experimentally determined and numerically obtained results for one-time base excitation ($PGA$ = 0.3 g)

| | AA | | | AP | | | AS | | | ABL | | |
|---|---|---|---|---|---|---|---|---|---|---|---|---|
| Model $M_1$ | Exp. | Num. | Rel. error [%] | Exp. | Num. | Rel. error [%] | Exp. | Num. | Rel. error [%] | Exp. | Num. | Rel. error [%] |
| $a$ [ms$^{-2}$] | 10.18 | 11.17 | 9.7 | 9.90 | 10.74 | 8.4 | 10.73 | 12.34 | 15 | 8.41 | 9.96 | 18.4 |
| $\varepsilon_1$ [‰] | 0.040 | 0.043 | 7.5 | 0.040 | 0.042 | 5.0 | 0.042 | 0.047 | 11.9 | 0.030 | 0.035 | 16.7 |
| $u_2$ [mm] | 7.95 | 7.52 | 5.7 | 5.20 | 4.81 | 7.5 | 7.00 | 5.97 | 17.2 | 5.00 | 4.42 | 13.1 |
| Model $M_2$ | | | | | | | | | | | | |
| $a$ [ms$^{-2}$] | 11.86 | 13.17 | 10.0 | 14.17 | 15.89 | 12.1 | 7.89 | 8.86 | 10.9 | 7.22 | 9.24 | 14.1 |
| $\varepsilon_1$ [‰] | 0.870 | 0.962 | 11.1 | 1.020 | 1.121 | 9.9 | 0.587 | 0.660 | 12.4 | 0.537 | 0.606 | 12.8 |
| $u_2$ [mm] | 33.75 | 30.7 | 9.4 | 40.4 | 37.1 | 8.2 | 17.5 | 15.1 | 15.9 | 12.5 | 10.41 | 16.7 |

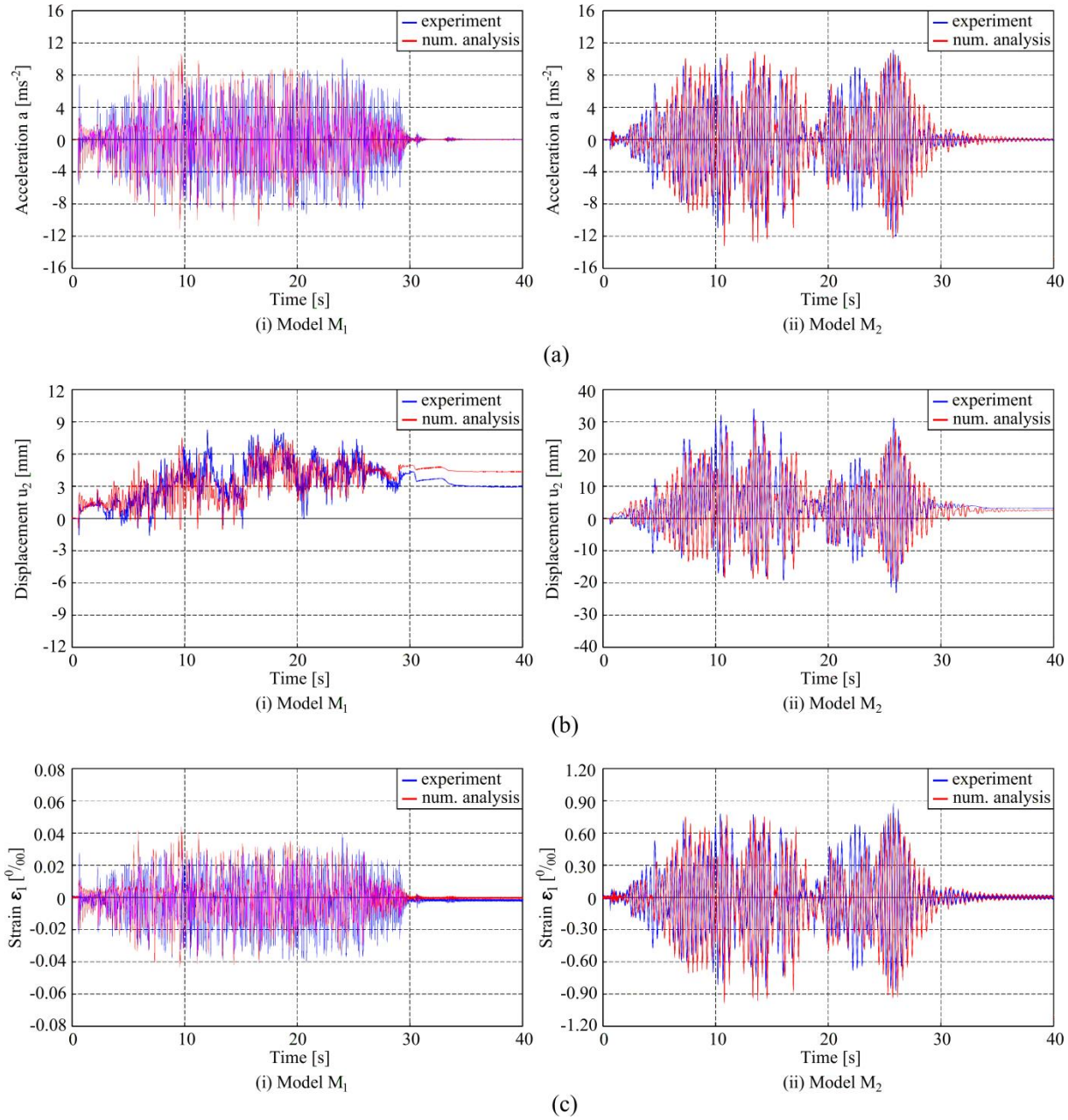


*Figure 3.8.* Comparison of experimentally determined and numerically obtained results for applied *AA* accelerogram (*PGA* = 0.3 g): (a) Horizontal acceleration $a$ of the mass at the column top; (b) Horizontal displacement $u_2$ of the mass at the column top; (c) Vertical strain $\varepsilon_1$ on the right bottom side of the steel column

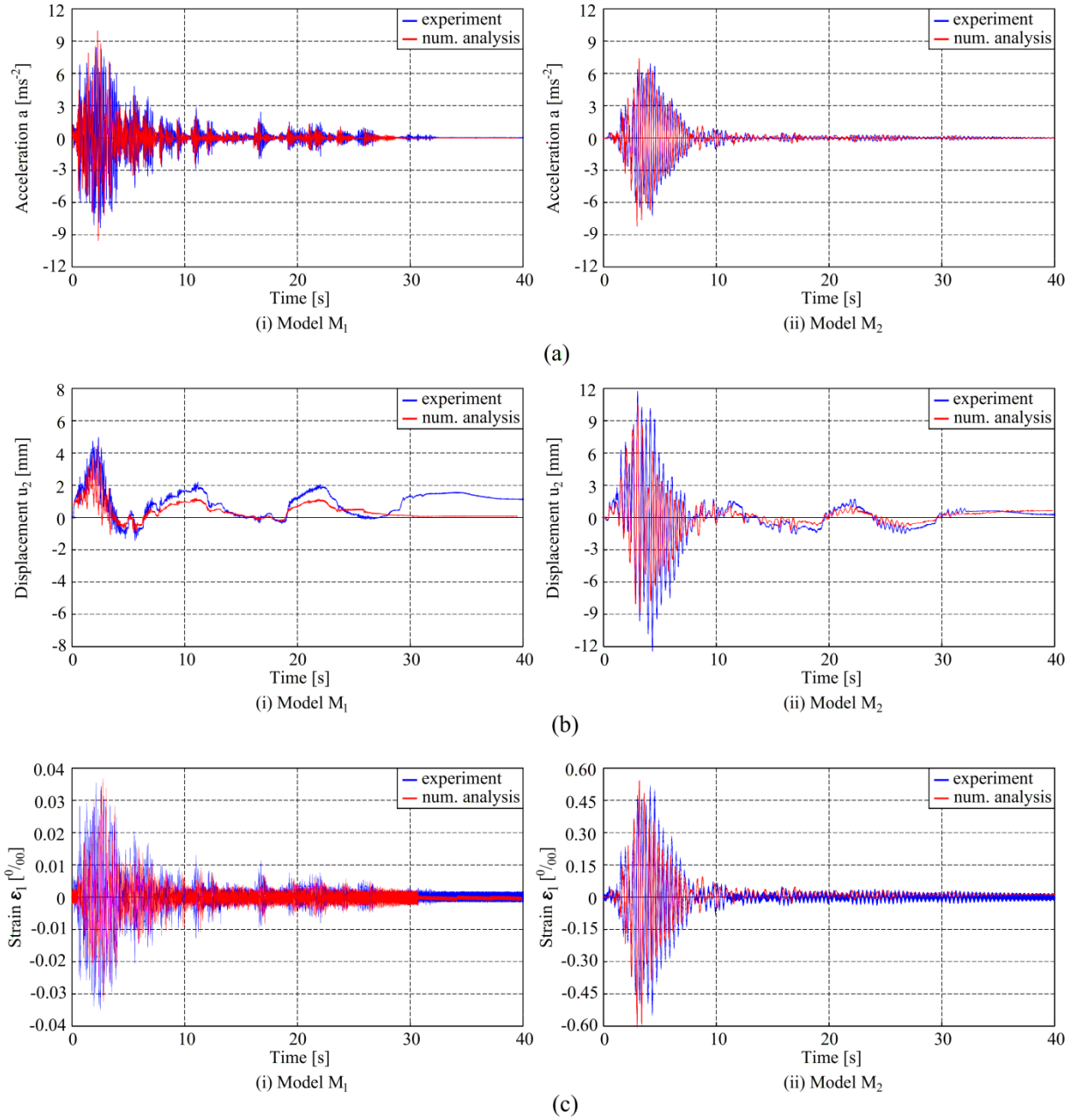


*Figure 3.9.* Comparison of experimentally determined and numerically obtained results for applied *ABL* accelerogram (*PGA* = 0.3 g): (a) Horizontal acceleration $a$ of the mass at the column top; (b) Horizontal displacement $u_2$ of the mass at the column top; (c) Vertical strain $\varepsilon_1$ on the right bottom side of the steel column

The largest deviations of the numerical results in relation to the experimental results were up to approximately 18.4% (refers to all performed numerical tests for one-time base excitation with *PGA* = 0.3 g). Furthermore, the average deviation from the experimental values is approximately 11.6%.

The deviations of the experimental and numerical values of the ultimate load-bearing capacity (*PGA* at failure) of the $M_1$ and $M_2$ under the action of an *AA* are on average 10% and 13%,

respectively. The above can be considered acceptable, given the limitations of the numerical model, the relatively rough spatial discretization of the tested samples and the high nonlinearity in the model (especially close to collapse).

## 3.6 Conclusion

With the development of constitutive models for stone pebble layer and the foundation-pebble layer coupling surface, the basic numerical model was updated to perform dynamic analysis of the planar structures with seismic base isolation using a stone pebble layer. The model is simple, based on a small number of parameters and is intended for practical applications. Some basic parameters of the model were determined using a large-scale direct shear test, and a sliding test between concrete block with smooth contact surface and the pebble layer top.

The updated numerical model was verified on several shake-table tests of structural models $M_1$ and $M_2$ based on the stone pebble layer, for different excitations and levels of acceleration. A relatively small deviation of displacement, acceleration and strain determined using the experimental model and calculated using the presented numerical model (up to 18.4%) was found, which can be considered acceptable. Further verification of the presented numerical model on more complex structures and other excitations, as well as on the results of other numerical models, is required.

Also, improvements of the pebble layer constitutive model are needed, especially in the part of simulating the shear strength-normal stress relation. In this regard, as well as for the purpose of determining the vertical compressive strength of pebbles at lower horizontal compressive stress, it is necessary to conduct further experimental tests to more precisely define the required parameters of the improved model.

# 4. GENERAL CONCLUSION

The performed experimental research is mostly related to the seismic efficiency of the stone pebble aseismic layer – *ASL-2* and on stone pebbles with sliding geogrid and geomembrane layer – *ASL-3*, and to a small extent to the seismic efficiency of the limestone sand aseismic layer – *ASL-1*. As part of all the conducted experimental research, over 500 shake-table tests were performed for different dynamic excitations and different models. As part of numerical research, a numerical model for nonlinear dynamic analysis of planar structures isolated with *ASL-2* was developed and tested.

## 4.1 Experimental research

### 4.1.1 *ASL-1* aseismic layer efficiency

In brief experimental studies, it has been found that a layer of limestone sand 2 cm and 10 cm thick, in relation to the *RB* without seismic isolation, can reduce seismic force and strain/stress on the considered simple concrete cantilever column model by approximately 10% for lower *PGA* values, and approximately 14% at model failure. Due to the effect of sand calcification over time, the long-term seismic efficiency of such a layer is questionable. In this regard, further extensive research into the efficiency of this seismic isolation is needed. Research needs to be extended to more appropriate structural models, to the effect of several different earthquakes, and to improve the efficiency of such seismic isolation in combination with other materials (glass, metal, and rubber balls, etc.).

### 4.1.2 *ASL-2* and *ASL-3* aseismic layers efficiency

These reliable seismic base isolations enable a significant reduction of seismic force and strain/ stress in very stiff $M_1$ and stiff $M_2$ structural models with a fundamental period of oscillation up to approximately $T$ = 0.3 s - 0.4 s. Optimal *ASL-2* layer has the following characteristics: $h_p$ = 0.3 m, $\Phi_b$ = 16 - 32 mm, $MS$ = 30 MPa and $h$ = 10%. When selecting the optimal aseismic layer, the effect of seismic efficiency, rationality and simplicity of construction was considered.

The most optimal *ASL-3* composite seismic isolation is the one composed of an optimal *ASL-2* layer with a higher tensile strength geogrid at the layer top.

In relation to the *RB* without seismic isolation, the $M_1$ and $M_2$ based on the *ASL-2* had an average reduction in seismic force and strain/stress by approximately 13% at lower *PGA* levels and approximately 25% at model failure.

In relation to the models based on the *ASL-2*, the $M_1$ and $M_2$ based on the *ASL-3* had an average reduction in seismic force and strain/stress by approximately 10% at lower *PGA* levels and approximately 25% at model failure.

In relation to the *RB* without seismic isolation, the $M_1$ and $M_2$ based on the *ASL-3* had an average reduction in seismic force and strain/stress by approximately 25% at lower *PGA* levels and approximately 34% at model failure.

In relation to the *RB* without seismic isolation, the *ASL-2* and *ASL-3* did not result in major model displacements, which is also favourable.

The above conclusions were reached on the basis of systematically performed extensive experimental research using a shake-table, examining the effect of a large number of parameters (model stiffness, ground plan dimensions of the model foundation, four types of accelerograms, numerous pebble layer parameters, numerous composite aseismic layer parameters, etc.).

It is important to highlight that the seismic isolations efficiency depended significantly on the type of applied accelerogram. The most unfavourable state of acceleration, displacement and strain/stress was caused by earthquakes of long duration and with a longer predominant period (which bring more earthquake input energy into system and produce more pronounced rocking of the model – excitations *AA* and *AP*). However, for such earthquakes, the highest *ASL-2* and *ASL-3* efficiency was observed in relation to the *RB*.

Impact-type earthquakes, with short duration and small predominant period (*AS* and ABL), which produce the greatest shear force effect, caused lower strain/stress in the structure. In their action, the *ASL-2* and *ASL-3* were less effective.

## 4.2 Numerical research

With the development of new constitutive models for stone pebble layer and the foundation-pebble layer coupling surface, the previously developed basic numerical model was updated to perform dynamic analysis of the planar structures with seismic base isolation using a stone pebble layer. The developed material constitutive models are simple and are based on a small number of parameters. Some parameters of the pebble layer constitutive model were determined by performed experimental tests (large-scale direct shear test, etc.). A good agreement was observed between the numerical and experimental values of the measured quantities, both for lower *PGA* levels and for structural collapse at higher *PGA* levels. The largest deviations of the numerical results in relation to the experimental results were up to approximately 18.4%, which can be considered acceptable. The basic idea was to develop a simple and sufficiently reliable

numerical model for engineering applications, which will be based on a smaller number of parameters.

## 4.3 Research limitations

The performed experimental research has certain limitations, which need to be mentioned:

- relative simple structural models,
- just five different models,
- only four different base excitations applied, and
- only uniaxial base excitation of the shake-table.

Owing the above limitations, the obtained conclusions should be strengthened by further research on this topic with more realistic structural models and with a larger number of considered earthquakes.

Further verification of the created numerical model on the results of other experimental tests is needed, but also improvement of the developed constitutive models. For this purpose, additional experimental tests will be required to determine some model parameters.

## 4.4 Practical application

According to current knowledge, based on extensive research over the past four years, it is considered that the *ASL-2* and especially *ASL-3* have great potential for practical application on very stiff and stiff buildings and bridges ($T$ < 0.3 s - 0.4 s) based on solid ground. This seismic isolation is very rational and easy to implement. The funds spent on isolation will be significantly lower than the savings on the load-bearing structure due to the reduction of seismic forces. Furthermore, the application of this seismic isolation can significantly increase the building seismic resistance.

The developed numerical model for nonlinear dynamic analysis of planar structures with presented seismic base isolation can be very useful in seismic analysis of structures in practice.

## 4.5 Originality

The originality of the conducted research is contained firstly in careful selection and composition of natural materials for the purpose of creating efficient and rational seismic base isolation layers. Furthermore, several innovations are presented in conducted systematic and complex experimental studies that analysed a large number of different parameters that affect the

efficiency of aseismic layers, as well as in a number of conclusions reached. Finally, an original numerical model for nonlinear dynamic analysis of planar structures with presented seismic isolation was also developed and verified.

# 5. REFERENCES

[A.1] S. Ahmad, F. Ghani, R. Adil, Seismic friction base isolation performance using demolished waste in masonry housing, Construction and Building Materials, Vol. 23(1), 146–152, 2009.

[A.2] N. Ambraseys, P. Smit, R. Sigbjörnsson, P. Suhadolc, M. Margaris, Internet-Site for European Strong-Motion Data, www.isesd.hi.is/ESD_Local/frameset.htm, EVR1-CT-1999-40008, European Commission, Directorate-General XII, Environmental and Climate Programme, Brussels, Belgium, 2001.

[A.3] A. Amendola, G. Carpentieri, L. Feo, F. Fraternali, Bending dominated response of layered mechanical metamaterials alternating pentamode lattices and confinement plates, Vol. 157, Composite Structures, 71-77, 2016.

[A.4] A. Amendola, C. J. Smith, R. Goodall, F. Auricchio, L. Feo, G. Benzoni, F. Fraternali, Experimental response of additively manufactured metallic pentamode materials confined between stiffening plates, Composite Structures, Vol. 142, 254-262, 2016.

[A.5] I. Anastasopoulos, M. Loli, T. Georgarakos, V. Drosos, Shaking Table Testing of Rocking-Isolated Bridge Pier on Sand, Journal of Earthquake Engineering, Vol. 17(1), 1-32, 2012.

[A.6] I. Anastasopoulos, R. Kourkoulis, F. Gelagoti, E. Papadopoulos, Rocking response of SDOF systems on shallow improved sand: An experimental study, Soil Dynamics and Earthquake Engineering, Vol. 40, 15-33, 2012.

[A.7] M. G. Arab, E. Kavazanjian Jr., Time-domain analysis of frictional base isolation using geosynthetics, Proceedings of 9th International Conference on Geosynthetics, Vol. 2, 695–698, 2010.

[A.8] A. M. Avossa, G. Pianese, Damping effects on the seismic response of base-isolated structures with LRB devices, Ingegneria Sismica, Vol. 34(2), 3-30, 2017.

[A.9] B. Azinović, V. Kilar, D. Koren, The seismic response of low-energy buildings founded on a thermal insulation layer –a parametric study, Engineering Structures, Vol. 81, 398-411, 2014.

[A.10] B. Azinović, V. Kilar, D. Koren, Energy-efficient solution for the foundation of passive houses in earthquake-prone regions, Engineering Structures, Vol. 112, 133-145, 2016.

[A.11] W. Azzam, M. Ayeldeen, M. El Siragy, Improving the structural stability during earthquakes using in-filled trench with EPS geofoam-numerical study, Arabian Journal of Geosciences, Vol. 11(14), 395, 2018.

[B.1] G. Baloević, J. Radnić, N. Grgić, Numerical model for dynamic analysis of masonry-infilled steel and concrete frames, Materialwissenschaft und Werkstofftechnik, Vol. 50(5), 519-532, 2019.

[B.2] G. Baloević, J. Radnić, N. Grgić, D. Matešan, M. Smilović, Numerical model for nonlinear analysis of composite concrete-steel-masonry bridges, Coupled Systems Mechanics, Vol. 5(1), 1-20, 2016.

[B.3] G. Baloević, J. Radnić, D. Matešan, N. Grgić, I. Banović, Comparison of Developed Numerical Macro and Micro Masonry Models for Static and Dynamic Analysis of Masonry-infilled Steel Frames, Latin American Journal of Solids and Structures, Vol. 13(12), 2251-2265, 2016.

[B.4] S. Bandyopadhyay, A. Sengupta, G. R. Reddy, Performance of sand and shredded rubber tire mixture as a natural base isolator for earthquake protection, Earthquake Engineering and Engineering Vibration, Vol. 14(4), 683–693, 2015.

[B.5] I. Banović, J. Radnić, N. Grgić, Shake table study on the efficiency of seismic base isolation using natural stone pebbles, Advances in Materials Science and Engineering, Article ID 1012527, 20 pages, 2018.

[B.6] I. Banović I., Radnić J., Grgić N., Geotechnical seismic isolation system based on sliding mechanism using stone pebble layer: shake-table experiments, Shock and Vibration, Article ID 9346232, 26 pages, 2019.

[B.7] I. Banović, J. Radnić, N. Grgić, Foundation size effect on the efficiency of seismic base isolation using a layer of stone pebbles, Earthquakes and Structures, Vol. 19(2), 103-117, 2020.

[B.8] I. Banović, J. Radnić, N. Grgić N., Effect of structural stiffness on the efficiency of seismic base isolation using layers of stone pebbles, Ingegneria Sismica, 37(2): 66-91, 2020.

[B.9] I. Banović, J. Radnić, N. Grgić, Effectiveness of several low-cost composite seismic base isolations: A shake table study, submitted to WoS journal, 2020.

[B.10] I. Banović, J. Radnić, N. Grgić, Effect of geogrid on the efficiency of seismic base isolation using natural stone pebbles: A shake table study, submitted to WoS journal, 2020.

[B.11] I. Banović, J. Radnić, N. Grgić, D. Matešan, The use of limestone sand for the seismic base isolation of structures, Advances in Civil Engineering, Article ID 9734283, 12 pages, 2018.

[B.12] I. Banović, J. Radnić, N. Grgić, Numerical model for dynamic analysis of structures with seismic base isolation using a layer of stone pebbles, submitted to WoS journal, 2020.

[B.13] L. Briançon, H. Girard, J. P. Gourc, A new procedure for measuring geosynthetic friction with an inclined plane, Geotextiles and Geomembranes, Vol. 29(5), 472–482, 2011.

[B.14] L. Briançon, H. Girard, D. Poulain, Slope stability of lining systems-experimental modeling of friction at geosynthetic interfaces, Geotextiles and Geomembranes, Vol. 20(3), 147–172, 2002.

[B.15] S. Brunet, J. C. de la Llera, E. Kausel, Non-linear modeling of seismic isolation systems made of recycled tire-rubber, Soil Dynamics and Earthquake Engineering, Vol. 85, 134–145, 2016.

[C.1] P. M. Calvi, G. M. Calvi, Historical development of friction-based seismic isolation systems, Soil Dynamics and Earthquake Engineering, Vol. 106, 14-30, 2018.

[C.2] P. M. Calvi, M. Moratti, G. M. Calvi, Seismic isolation devices based on sliding between surfaces with variable friction coefficient, Earthquake Spectra, Vol. 32(4), 2291-2315, 2016.

[C.3] L. Carbone, J. P. Gourc, P. Carrubba, P. Pavanello, N. Moraci, Dry friction behaviour of a geosynthetic interface using inclined plane and shaking table tests, Geotextiles and Geomembranes, Vol. 43(4), 293–306, 2015.

[C.4] L. Carbone, P. Pavanello, P. Carrubba, J. P. Gourc, N. Moraci, L. Briançon, M. Scotto, Geosynthetic interface shear strength under static and seismic loading conditions, Proceedings of 10th International Conference on Geosynthetics, Berlin, Germany, 21–25 September 2014.

[C.5] G. Cardile, D. Gioffrè, N. Moraci, L. S. Calvarano, Modelling interference between the geogrid bearing members under pullout loading conditions, Geotextiles and Geomembranes, Vol. 45, 169–177, 2017.

[C.6] G. Cardile, N. Moraci, L. S. Calvarano, Geogrid pullout behaviour according to the experimental evaluation of the active length, Geosynthetics International, Vol. 23 (3), 194–205, 2016.

[C.7] B. Carpani, A survey of ancient geotechnical engineering techniques in sub foundation preparation, 9th International Conference on Structural Analysis of Historical Constructions, Mexico City, Mexico, 2014.

[C.8] B. Carpani, Base isolation from a historical perspective, 16th World Conference on Earthquake, Paper N° 4934, Santiago, Chile, 2017.

[C.9] P. Castaldo, M. Ripani, Optimal design of single concave sliding bearings for isolated structures considering intermediate isolation degrees, Ingegneria Sismica, Vol. 34 (5), 5-24, 2017.

[C.10] C. M. Chang, B. F. Spencer, Active base isolation of buildings subjected to seismic excitations, Earthquake Engineering and Structural Dynamics, Vol. 39, 1493–1512, 2010.

[C.11] X. Chen, X. Xia, X. Zhang, J. Gao, Seismic performance and design of bridge piers with rocking isolation, Structural Engineering and Mechanics, Vol. 73(4), 447-454, 2020.

[C.12] Y. L. Chung, L. J. Du, H. H. Pan, Performance evaluation of a rocking steel column base equipped with asymmetrical resistance friction damper, Earthquakes and Structures, Vol. 17(1), 49-61, 2019.

[D.1] A. De, T. F. Zimmie, Estimation of dynamic interfacial properties of geosynthetics, Geosynthetics International, Vol. 5(1–2), 17–39, 1998.

[D.2] D. De Domenico, G. Ricciardi, S. Infanti, G. Benzoni, Frictional heating in double curved surface sliders and its effects on the hysteretic behavior: an experimental study, Frontiers in Built Environment, Vol. 5(74), 2019.

[D.3] B. S. Deviprasad, G. R. Dodagoudar, Seismic response of bridge pier supported on rocking shallow foundation, Geomechanics and Engineering, Vol. 21(1), 73-84, 2020.

[D.4] J. S. Dhanya, A. Boominathan, B. Subhadeep, Performance of geo-base isolation system with geogrid reinforcement, International Journal of Geomechanics, Vol. 19(7), 2019.

[D.5] J. S. Dhanya, A. Boominathan, B. Subhadeep, Response of low-rise building with geotechnical seismic isolation system, Soil Dynamics and Earthquake Engineering, Vol. 136, 2020.

[D.6] I. Doudoumis, P. Papadopoulos, T. Papaliangas, Low-cost base isolation system on artificial soil layers with low shearing resistance, Proceedings of the 12th European Conference on Earthquake Engineering, London, UK, 2002.

[E.1] M. Eatherton, X. Ma , H. Krawinkler, D. Mar, S. Billington, J. F. Hajjar, G. G. Deierlein, Design concepts for controlled rocking of self-centering steel-braced frames, Journal of Structural Engineering, Vol. 140(11), 04014082, 2014.

[E.2] EN 1998-1:2004. Eurocode 8: Design of structures for earthquake resistance- Part 1: General rules, seismic actions and rules for buildings, Brussels: European Committee for Standardization, 2004.

[F.1] F. Fabbrocino, A. Amendola, G. Benzoni, F. Fraternali, Seismic application of pentamode lattices, Ingegneria Sismica, Vol. 1, 62-71, 2016.

[F.2] R. Feng, Y. Chen, G. Cui, Dynamic response of post-tensioned rocking wall-moment frames under near-fault ground excitation, Earthquakes and Structures, Vol. 15(3), 243-251, 2018.

[F.3] D. Forcellini, Assessment on geotechnical seismic isolation (GSI) on bridge configurations, Innovative Infrastructure Solutions, Vol. 2(1), 9 pages, 2017.

[F.4] D. Forcellini, Assessment of Geotechnical Seismic Isolation (GSI) as a Mitigation Technique for Seismic Hazard Events, Geosciences, Vol. 10, 222, 2020.

[F.5] F. Fraternali, A. Amendola, G. Benzoni, Innovative seismic isolation devices based on lattice materials: A review, Ingegneria Sismica, Vol. 4(4), 93-113, 2018.

[G.1] N. Grgić, Experimental testing and numerical modeling of slender reinforced concrete columns under seismic conditions, PhD thesis, University of Split, 2014.

[G.2] N. Grgić, J. Radnić, D. Matešan, I. Banović, Stirrups effect on the behavior of concrete columns during an earthquake, Materialwissenschaft und Werkstofftechnik, Vol. 48 (5), 406-419, 2017.

[G.3] N. Grgić, J. Radnić, D. Matešan, A. Buzov, Effect of mass on the behavior of concrete columns under seismic load, Materialwissenschaft und Werkstofftechnik, Vol. 47 (5/6), 483-493, 2016.

[H.1] H. A. Hadad, A. Calabrese, S. Strano, G. Serino, A base isolation system for developing countries using discarded tyres filled with elastomeric recycled materials, Journal of Earthquake Engineering, Vol. 21(2), 246-266, 2017.

[H.2] E. Hernández, A. Palermo, G. Granello, G. Chiaro, L. Banasiak, Eco-rubber seismic-isolation foundation systems: a sustainable solution for the New Zealand context, Structural Engineering International, 1-9, 2020.

[H.3] T. J. R. Hughes, K. S. Pister, R. L. Taylor, Implicit-explicit finite elements in nonlinear transient analysis, Computer Methods in Applied Mechanics and Engineering, Vol. 17–18, 159–182, 1979.

[H.4] H. H. Hung, K. Y. Liu, K. C. Chang, Rocking behavior of bridge piers with spread footings under cyclic loading and earthquake excitation, Earthquakes and Structures, Vol. 7, 1001-1024, 2014.

[I.1] B. Indraratna, T. Ngo, C. Rujikiatkamjorn, Behavior of geogrid-reinforced ballast under various levels of fouling, Geotextiles and Geomembranes, Vol. 29(3), 313-322, 2011.

[K.1] V. Kalpakcı, A. T. Bonab, M. Y. Özkan, Z. Gülerce, Experimental evaluation of geomembrane/geotextile interface as base isolating system, Geosynthetics International, Vol. 25(1), 1-11, 2018.

[K.2] X. Karatzia, G. Mylonakis, G. Bouckovalas, Seismic Isolation of Surface Foundations Exploiting the Properties of Natural Liquefiable Soil, Soil Dynamics and Earthquake Engineering, Vol. 121, 233-251, 2019.

[K.3] X. Karatzia, G. Mylonakis, Geotechnical seismic isolation using eps geofoam around piles, 6th International Conference on Computational Methods in Structural Dynamics and Earthquake Engineering, Rhodes Island, Greece, 2017.

[K.4] J. Kelly, Aseismic base isolation: review and bibliography, Soil Dynamics and Earthquake Engineering, Vol. 5(4), 202-216, 1986.

[K.5] J. Kelly, Natural Rubber Isolation Systems for Earthquake Protection of Low-Cost Buildings, Report No. UCB/EERC-95-12, Earthquake Engineering Research Center, University of California, Berkeley, California, 1996

[K.6] J. Kelly, W. Taniwangsa, Experimental and Analytical Studies of Base Isolation Applications for Low-Cost Housing, Report No. UCB/EERC-96-04, Earthquake Engineering Research Center, University of California, Berkeley, California, 1996.

[K.7] D. Koren, V. Kilar, Seismic vulnerability of reinforced concrete building structures founded on an XPS layer, Earthquakes and Structures, Vol. 10(4), 939 -963, 2016.

[K.8] S. Kulukčija, M. Humo, Survey of historic foundation engineering, Baština, Sarajevo, 2009.

[K.9] S. Kulukčija, M. Humo, E. Mandžić, K. Mandžić, M. Selimović, Existing historical foundation system of two old bridges from the Ottoman period in Bosnia and Herzegovina, Third International Congress on Construction History, Cottbus, Germany, 2009.

[K.10] A. Kuvat, E. Sadoglu, Dynamic properties of sand-bitumen mixtures as a geotechnical seismic isolation material, Soil Dynamics and Earthquake Engineering, 132, 106043, 2020.

[L.1] G. Lomiento, N. Bonessio, G. Benzoni, Concave sliding isolator's performance under multi-directional excitation, Ingegneria Sismica, Vol. 30, 17-32, 2013.

[M.1] N. Makris, Seismic isolation: early history, Earthquake Engineering and Structural Dynamics, Vol. 48 (2), 269-283, 2018.

[M.2] N. Makris, A half-century of rocking isolation, Earthquakes and Structures, Vol. 7(6), 1187-1221, 2014.

[M.3] S. A. Masoud, M. M. M. H. Seyed, J. Alireza, Effect of soil reinforcement on rocking isolation potential of high-rise bridge foundations, Soil Dynamics and Earthquake Engineering, Vol, 115, 142-155, 2018.

[M.4] E. Mavronicola, P. Komodromos, D. C. Charmpis, Numerical investigation of potential usage of rubber–soil mixtures as a distributed seismic isolation approach, Proceedings of the 10th International Conference on Computational Structures Technology, Valencia, Spain, September 14–17, 2010.

[M.5] T. A. Morgan, S. A. Mahin, The use of base isolation systems to achieve complex seismic performance objectives, PEER Report No. 2011/06, Pacific Earthquake Engineering Research Center, University of California, Berkeley, CA, USA, 2011.

[M.6] C. Murillo, L. Thorel, B. Caicedo, Ground vibration isolation with geofoam barriers: centrifuge modelling, Geotextiles and Geomembranes, Vol. 27(6), 423-434, 2009.

[N.1] F. Naiem, J. M. Kelly, Design of seismic isolated structures: From Theory to Practice, John Willey & Sons, Inc., 1999.

[N.2] R. P. Nanda, P. Agarwal, M. Shrikhande, Suitable friction sliding materials for base isolation of masonry buildings, Shock and Vibration, Vol. 19 (6), 1327-1339, 2012.

[N.3] R. P. Nanda, M. Shrikhande, P. Agarwal, Effect of ground motion characteristics on the pure friction isolation system, Earthquakes and Structures, Vol. 3(2), 169–180, 2012.

[N.4] R. P. Nanda, M. Shrikhande, P. Agarwal, Low-cost base-isolation system for seismic protection of rural buildings, Practice Periodical on Structural Design and Construction, Vol. 21(1), 2015.

[N.5] R. P. Nanda, P. Agarwal, M. Shrikhande, Base isolation by geosynthetic for brick masonry buildings, Journal of Vibration and Control, Vol. 18(6), 903–910, 2012.

[N.6] R. P. Nanda, P. Agarwal, M. Shrikhande, Frictional base isolation by geotextiles for brick masonry buildings, Geosynthetics International, Vol. 17(1), 48–55, 2010.

[N.7] P. Narjabadifam, M. Chavoshi, Modern aseismic applications of geosynthetic materials, International Journal of Science and Engineering Applications, Vol. 7, 034, 2018.

[O.1] OECD, Costs of Inaction of Environmental Policy Challenges, Report ENV/EPOC(2007)17/REV2, 2008.

[P.1] A. Panjamani, M. D. Ramegowda, R. Divyesh, Low cost damping scheme for low to medium rise buildings using rubber soil mixtures, Japanese Geotechnical Society Special Publication, 2015.

[P.2] S. J. Patil, G. R. Reddy, R. Shivshankar, R. Babu, B. R. Jayalekshmi, B. Kumar, Natural base isolation of structures having raft foundations, International Journal of Emerging Technology and Advanced Engineering, Vol. 2(8), 23-38, 2012.

[P.3] S. J. Patil, G. R. Reddy, R. Shivshankar, R. Babu, B. R. Jayalekshmi, B. Kumar, Seismic base isolation for structures using river sand, Earthquakes and Structures, Vol. 10(4), 829-847, 2016.

[P.4] P. Pavanello, P. Carrubba, Methodological aspects in the experimental measurement of the interface friction between geosynthetics, Procedia Engineering, Vol. 158, 260–265, 2016.

[P.5] P. Pavanello, P. Carrubba, N. Moraci, Dynamic friction and the seismic performance of geosynthetic interfaces, Geotextiles and Geomembranes, Vol. 46(6), 715-725, 2018.

[P.6] P. Pavanello, P. Carrubba, N. Moraci, The determination of interface friction by means of vibrating table tests, Geotextiles and Geomembranes, Vol. 46(6), 830-835, 2018.

[P.7] A. Pecker, J. H. Prevost, L. Dormieux, Analysis of pore pressure generation and dissipation in cohesionless materials during seismic loading, Journal of Earthquake Engineering, Vol. 5(4), 441-464, 2001.

[P.8] A. Pecker, Aseismic foundation design process, lessons learned from two major projects: the Vasco de Gama and the Rion Antirion bridges, Proceedings of the ACI International Conference on Seismic Bridge Design and Retrofit, La Jolla, CA, USA, 2003.

[P.9] G. Petrone, T. Ferrentino, G. Alfano, Influence of PGA/PGV ratio on the seismic reliability of base-isolated system with FPS, Ingegneria Sismica, Vol. 34(3), 39-62, 2017.

[P.10] G. A. Pistolas, K. Pitilakis, A. Anastasiadis, A numerical investigation on the seismic isolation potential of rubber/soil mixtures, Earthquake Engineering and Engineering Vibration, Vol. 19, 683–704, 2020.

[P.11] K. Pitilakis, S. Karapetrou, K. Tsagdi, Numerical investigation of the seismic response of RC buildings on soil replaced with rubber–sand mixtures, Soil Dynamics and Earthquake Engineering, Vol. 79, 237–252, 2015.

[P.12] J. Przewłócki, I. Dardzinska, J. Swinianski, Review of historical buildings' foundations, Géotechnique, Vol. 55, 363-372, 2005.

[Q.1] M. Qamaruddin, S. Ahmad, Seismic response of pure-friction base isolation masonry building with restricted base sliding, Journal of Engineering Research, Vol. 4(1), 82–94, 2007.

[R.1] J. Radnić, N. Grgić, D. Matešan, G. Baloević, Shake table testing of reinforced concrete columns with different layout size of foundation, Materialwissenschaft und Werkstofftechnik, Vol. 46(4-5), 348–367, 2015.

[R.2] J. Radnić, A. Harapin, D. Matešan, B. Trogrlić, M. Smilović, N. Grgić, G. Baloević, Numerical Model for Analysis of Masonry Structures, Gradjevinar, Vol. 63(6), 529-546, 2011.

[R.3] J. Radnić, R. Markić, N. Grgić, M. Glibić, I. Banović, Comparison of numerical models for nonlinear static analysis of planar concrete frames based on 1D and 2D finite elements, Materialwissenschaft und Werkstofftechnik, Vol. 47(5-6), 369-581, 2016.

[R.4] J. Radnić, D. Matešan, A. Harapin, M. Smilović, N. Grgić, Numerical model for static and dynamic analysis of masonry structures, Mechanics and Properties of Composed Materials and Structures, Advanced Structured Materials, 1–33, Springer-Verlag, Berlin, Germany, 2012.

[R.5] K. M. Ravi, G. Gourav, Sustainable application of waste tire chips and geogrid for improving load carrying capacity of granular soils, Journal of Cleaner Production, Vol. 200, 542-551, 2018.

[S.1] N. I. Sarand, A. Jalali, Seismic response evaluation of concentrically rocking zipper braced frames, Structural Engineering and Mechanics, Vol. 73(3), 303-317, 2020.

[S.2] SIMQKE (SIMulation of earthQuaKE ground motions), http://gelfi.unibs.it/software/simqke/simqke_gr.htm, 1976.

[S.3] M. Smilović Zulim, J. Radnić, Anisotropy Effect of Masonry on the Behaviour and Bearing Capacity of Masonry Walls, Advances in Materials Science and Engineering, 5676901, 2020.

[S.4] M. Smilović Zulim, J. Radnić, N. Grgić, G. Baloević, Effect of anisotropy of masonry on the behaviour of unreinforced and confined masonry walls under ground motion, Engineering Design Applications, Heidelberger, Springer, Cham, 173-183, 2018.

[S.5] M. Smilović Zulim, J. Radnić, A. Harapin, Shear effect on seismic behaviour of masonry walls, Materialwissenschaft und Werkstofftechnik, Vol. 50(5), 565-579, 2019.

[S.6] L. Sorrentino, R. Masiani, L. D. Decanini, Overturning of rocking rigid bodies under transient ground motions, Structural Engineering and Mechanics, Vol. 22(3), 293-310, 2006.

[S.7] L. Sorrentino, R. Masiani, M. C. Griffith, The vertical spanning strip wall as a coupled rocking rigid body assembly, Structural Engineering and Mechanics, Vol. 29(4), 433-453, 2008.

[S.8] J. Stanton, C. Roeder, Advantages and Limitations of Seismic Isolation, Earthquake Spectra, Vol. 7, 301-323, 1991.

[S.9] J. S. Steenfelt, B. Foged, A. H. Augustesen, Izmit Bay bridge-geotechnical challenges and innovative solutions, International Journal of Bridge Engineering (IJBE), Vol. 3(3), 53–68, 2015.

[T.1] L. Tashkov, K. Manova, L. Krstevska, M. Garevski, Evaluation of efficiency of ALSC floating-sliding base-isolation system based on shake table test and floor response spectra, Bulletin of Earthquake Engineering, Vol. 8, 995-1018, 2010.

[T.2] F. M. Tehrani, A. Hasani, Behaviour of Iranian low rise buildings on sliding base to earthquake excitation, Proceedings of the 11th World Conference on Earthquake Engineering, Paper 1433, Acapulco, Mexico, 1996.

[T.3] M. D. Titirla, K. Katakalos, G. Zuccaro, F. Fabbrocino, On the mechanical modeling of an innovative energy dissipation device, Ingegneria Sismica, Vol. 34(2), 126-137, 2017.

[T.4] H. H. Tsang, Geotechnical seismic isolation, Earthquake Engineering: New Research, 55–87, Nova Science Publishers Inc., New York, NY, USA, 2009.

[T.5] H. H. Tsang, Seismic isolation by rubber-soil mixtures for developing countries, Earthquake Engineering and Structural Dynamics, Vol. 37(2): 283–303, 2008.

[T.6] H. H. Tsang, K. Pitilakis, Mechanism of geotechnical seismic isolation system: Analytical modeling, Soil Dynamics and Earthquake Engineering, Vol. 122, 171-184, 2019.

[T.7] H. H. Tsang, S. H. Lo, X. Xu, M. Neaz Sheikh, Seismic isolation for low-to-medium-rise buildings using granulated rubber-soil mixtures: numerical study, Earthquake Engineering and Structural Dynamics, Vol. 41(14), 2009–2024, 2012.

[T.8] A. Tsatsis, I. Anastasopoulos, Performance of rocking systems on shallow improved sand: shaking table testing, Frontiers in Built Environment, Vol.1, 1-9, 2015.

[T.9] A. Tsiavos, N. A. Alexander, A. Diambra, E. Ibraim, P. J. Vardanega, A. Gonzalez-Buelga, A. Sextos, A sand-rubber deformable granular layer as a low-cost seismic isolation strategy in developing countries: experimental investigation, Soil Dynamics and Earthquake Engineering, 125, 2019.

[T.10] A. Tsiavos, A. Sextos, A. Stavridis, M. Dietz, L. Dihoru, N. A. Alexander, Large-scale experimental investigation of a low-cost PVC 'sand-wich' (PVC-s) seismic isolation for developing countries, Earthquake Spectra, 2020.

[T.11] A. Tsiavos, N. A. Alexander, A. Sextos, Numerical investigation of the sliding response of flexible structures founded on a deformable granular layer, 2nd International Conference on Earthquake Engineering and Post Disaster Reconstruction Planning, Bhaktapur, Nepal, 2019.

[T.12] A. Tsiavos, P. Haladij, A. Sextos, N. A. Alexander, Analytical investigation of the effect of a deformable sliding layer on the dynamic response of seismically isolated structures, Structures, Vol. 27, 2426-2436, 2020.

[W.1] J. Wang, J. X. He, Q. S. Yang, N. Yang, Study on mechanical behaviors of column foot joint in traditional timber structure, Structural Engineering and Mechanics, Vol. 66(1), 1-14, 2018.

[W.2] G. P. Warn, K. L. Ryan, A review of seismic isolation for buildings: historical development and research needs, Buildings, Vol. 2(3), 300-325, 2012.

[W.3] Y. Wasti, Z. B. Özdüzgün, Geomembrane-geotextile interface shear properties as determined by inclined board and direct shear box tests, Geotextiles and Geomembranes, Vol. 19, 45–57, 2001.

[X.1] H. Xiao, J. W. Butterworth, T. Larkin, Low-technology techniques for seismic isolation, Proceedings of the NZSEE Conference, Rototua, New Zealand, 2004.

[X.2] W. Xiong, Y. Li, Seismic isolation using granulated tire-soil mixtures for less-developed regions: experimental validation, Earthquake Engineering and Structural Dynamics, Vol. 42(14), 2187-2193, 2013.

[X.3] W. Xiong, M. R. Yan, Y. Z. Li, Geotechnical seismic isolation system - further experimental study, Applied Mechanics and Materials, Vol. 580-583, 1490-1493, 2014.

[X.4] R. Xu, B. Fatahi, Influence of geotextile arrangement on seismic performance of mid-rise buildings subjected to MCE shaking, Geotextiles and Geomembranes, Vol. 46(4), 511-528, 2018.

[Y.1] M. K. Yegian, M. Catan, Soil isolation for seismic protection using a smooth synthetic liner, Journal of Geotechnical & Geoenvironmental Engineering, Vol. 130(11), 1131–1139, 2004.

[Y.2] M. K. Yegian, U. Kadakal, Geosynthetic interface behavior under dynamic loading, Geosynthetics International, Vol. 5(1–2), 1–16, 1998.

[Y.3] M. K. Yegian, U. Kadakal, Foundation isolation for seismic protection using a smooth synthetic liner, Journal of Geotechnical and Geoenvironmental Engineering, Vol. 130(11), 1121–1130, 2004.

[Y.4] M. K. Yegian, A. M. Lahlaf, Dynamic interface shear strength properties of geomembranes and geotextiles, International Journal of Geotechnical Engineering, Vol. 118(5), 760–779, 1992.

[Y.5] M. K. Yegian, A. M. Lahlaf, Geomembranes as base isolation, Geotechnical Fabrics Report, Vol. 10(6), 17-21, 1992.

[Z.1] G. H. Zhang, Study on the Suitability of Seismic Isolation Technologies for Rural Buildings, Applied Mechanics and Materials, Vol. 353-356, 2221-2227, 2013.

[Z.2] X. Zhao, Q. Zhang, Q. Zhang, J. He, Numerical study on seismic isolation effect of gravel cushion, Proceedings of the 7th International Conference on Discrete Element Methods, Vol. 188, 1055-1063, Dalian, China, 2016.

[Z.3] M. Ziegler, Application of geogrid reinforced constructions: history, recent and future developments, Procedia Engineering, Vol. 172, 42-51, 2017.

[Z.4] M. Zorn, Natural Disasters and Less Developed Countries: Nature, Tourism and Ethnicity as Drivers of (De)Marginalization, Perspectives on Geographical Marginality, Vol 3. Springer, Cham, 2018.

# CURRICULUM VITAE

Ivan Banović, mag. ing. aedif. was born on June 27, 1989 in Split, Croatia. He attended elementary school "Bijaći" in Kaštel Novi and High School of Civil Engineering and Geodesy in Split. In the academic year 2008/2009 he enrolled in undergraduate studies, and 2011/2012 in graduate studies of Civil Engineering at University of Split, Faculty of Civil Engineering, Architecture and Geodesy. He graduated in July 2014 with the topic: „A part of the passenger terminal extension structure at Split Airport“, under supervision of Prof. Jure Radnić, PhD and acquired the professional title of Master of Civil Engineering. Ivan Banović has won several awards for outstanding results achieved during his studies.

From 2015 to 2018, he was employed at the Faculty of Civil Engineering, Architecture and Geodesy, Chair for Concrete Structures and Bridges, as an expert associate. Since 2018, he is employed at the same institution as a doctoral student (assistant) within the project "Young researchers' career development project – training of doctoral students" of the Croatian Science Foundation funded by the European Union from the European Social Fund. Since the beginning of his work at the Faculty, he has been involved in the scientific research and professional activities of the Chair.

He enrolled in the postgraduate doctoral study of Civil Engineering at the same Faculty in 2015. In addition, he is a collaborator (doctoral student) on the research project "Seismic base isolation of a building by using natural materials - shake table testing and numerical modelling" -HRZZ IP 2016-06-5325, in the period from 2017.-2021., under supervision of Prof. Jure Radnić, PhD.

Ivan Banović is the co-author of 9 scientific papers cited in WoS CC, SCI and SCI Expanded databases, 2 abstracts published in conference proceedings with international peer-review and one scientific paper in the conference proceedings. He has presented at domestic and international conferences. As an associate designer, he participated in the development of 30 professional projects. He is fluent in English.

He is married and father of two children.

# APPENDIX

List of appended papers:

| No. | Paper Title | JCR Rank* |
|---|---|---|
| [I] | **Banović I.**, Radnić J., Grgić N., Matešan D., *The use of limestone sand for the seismic base isolation of structures*, Advances in Civil Engineering, Article ID 9734283, 12 pages, 2018., doi:10.1155/2018/9734283 | Q3 |
| [II] | **Banović I.**, Radnić J., Grgić N., *Geotechnical seismic isolation system based on sliding mechanism using stone pebble layer: shake-table experiments*, Shock and Vibration, Article ID 9346232, 26 pages, 2019., doi:10.1155/2019/9346232 | Q2 |
| [III] | **Banović I.**, Radnić J., Grgić N., *Shake table study on the efficiency of seismic base isolation using natural stone pebbles*, Advances in Materials Science and Engineering, Article ID 1012527, 20 pages, 2018., doi:10.1155/2018/1012527 | Q3 |
| [IV] | **Banović I.**, Radnić J., Grgić N., *Effect of structural stiffness on the efficiency of seismic base isolation using layers of stone pebbles*, Ingegneria Sismica, Vol. 37 (2), 66-91, 2020. | Q2 |
| [V] | **Banović I.**, Radnić J., Grgić N., *Foundation size effect on the efficiency of seismic base isolation using a layer of stone pebbles*, Earthquakes and Structures, Vol. 19 (2), 103-117, 2020., doi:10.12989/eas.2020.19.2.103 | Q3 |
| [VI] | **Banović I.**, Radnić J., Grgić N., *Effectiveness of several low-cost composite seismic base isolations: A shake table study*, 2020., submitted for publication to WoS journal | |
| [VII] | **Banović I.**, Radnić J., Grgić N., *Effect of geogrid on the efficiency of seismic base isolation using natural stone pebbles: A shake table study*, 2020., submitted for publication to WoS journal | |
| [VIII] | **Banović I.**, Radnić J., Grgić N., *Numerical model for dynamic analysis of structures with seismic base isolation using a layer of stone pebbles*, 2020., submitted for publication to WoS journal | |

*****Quartiles are determined for the year of the paper submission or the paper publication, according to the more favourable classification for the candidate

# PAPER I

Hindawi
Advances in Civil Engineering
Volume 2018, Article ID 9734283, 12 pages
https://doi.org/10.1155/2018/9734283

*Research Article*

# The Use of Limestone Sand for the Seismic Base Isolation of Structures

**Ivan Banović, Jure Radnić, Nikola Grgić, and Domagoj Matešan**

*Faculty of Civil Engineering, Architecture and Geodesy, University of Split, Matice Hrvatske 15, 21000 Split, Croatia*

Correspondence should be addressed to Nikola Grgić; nikola.grgic@gradst.hr

Received 19 March 2018; Revised 11 June 2018; Accepted 27 June 2018; Published 1 August 2018

Academic Editor: Evangelos J. Sapountzakis



The possibility of the use of a layer of natural material under foundations for seismic base isolation was investigated. The dissipation of seismic energy of a low-cost natural material with adequate thickness, bearing capacity, and lateral and vertical stiffness, which can serve as an optimal solution for seismic base isolation under the foundations of many structures, was tested. This paper presents the results of a brief experimental study to determine the effectiveness of ordinary limestone sand under the foundation of a cantilever concrete column to increase its seismic resistance. The behavior of small-scale columns with three substrates below the foundation (rigid base, the thin layer of limestone sand, and the thick layer of limestone sand) was investigated by the shake table. The column was exposed to a set of horizontal base accelerations until structure collapse. It was concluded that a layer of limestone sand of appropriate thickness and compressibility can serve as the means a seismic base isolation. The nonlinear numerical model for the dynamic analysis of planar concrete structures coupled with soil is briefly presented and verified by the performed experimental tests.

## 1. Introduction

Earthquakes typically occur when stresses within the earth's crust exceed the strength of the rock, thus causing rock breakage and slip along a fault. The released energy is carried as seismic waves that travel outward in all directions from the initial point of rupture or focus. The seismic waves are reflected and refracted in the earth's crust and at the surface, thereby losing energy with distance as they travel away from the focus. High-frequency seismic waves yield rapid expansion of ground vibrations, whereas low-frequency waves yield a less-rapid expansion and cause ground motions similar to those of sea waves [1, 2].

The frequency of seismic waves is very important in determining the nature of the damage to buildings. An earthquake has dominant frequencies that depend on its power, type of fault rupture, distance from the epicenter, geological conditions, and soil characteristics. The dominant natural frequency of vibration of a structure depends on the overall structural characteristics and the soil-structure interaction. If the dominant frequency of earthquake ground shaking is close to the dominant natural frequency of vibration of the structure, then the amplification of waves (resonance) can increase the amount of damage to the structure. Rigid structures are most vulnerable to strong, high-frequency seismic waves. High-frequency waves are strongest near the epicenter but rapidly dissipate as they move outward. High-rise and most deformable structures are the most vulnerable to strong, long duration, low-frequency waves. Low-frequency waves, which dissipate much more slowly than high-frequency waves, may cause damage at great distances from the epicenter [1, 2].

In traditional design and calculation of new structures, as well in renovation of existing, the concept in which the seismic ground acceleration is directly applied to the structure is adopted. Thereby, appropriate codes for seismic analysis of structures are used. To achieve a sufficient level of safety of structures, such an approach often results in buildings of high cost.

In recent decades, the technique increasingly used was seismic base isolation, by which the incoming earthquake ground motion (acceleration) is attenuated before its

transfer to the structure. Seismic isolation is a technique that has been used around the world to protect building structures, nonstructural components, and the contents of buildings from the damaging effects of earthquake ground shaking. In the base isolation technique approach, the structure is essentially decoupled from the earthquake ground motion by providing separate isolation devices between the structure and the base. The main concept of base isolation is to shift the fundamental period of the structure out of the range of the dominant frequencies of expected earthquakes to reduce the seismic forces on the structure. The consequence of using this concept is the increase of the structure displacements, which must be controlled and limited.

All of the base isolation systems have certain features in common; for example, they exhibit flexibility and have a high energy absorbing capacity. These base isolation systems are mainly categorized into three types: (i) passive base isolation techniques, (ii) hybrid base isolation techniques with semiactive devices, and (iii) hybrid base isolation techniques with passive energy dissipaters. These systems are not considered here. Some detailed information on modern techniques of hybrid passive and active seismic isolation can be found in [3, 4]. A review of the literature on the theoretical aspects of seismic isolation is given in [5]. The theoretical underpinning of seismic base isolation, which has been firmly established, and the technology that has been verified by extensive experimental work over the past decades are given in [6]. The limits of the applicability of equivalent linear analysis in response to ground motions that can lead to large displacements were investigated in [7]. The "almost lifted structure concept" base isolation system, which was investigated on a two-component shaking table at the Institute of Earthquake Engineering and Engineering Seismology (IZIIS) facility, is shown in [8]. To investigate possible improvements on the design of isolated structures, an extensive research program was conducted at the Pacific Earthquake Engineering Research Center (PEER) [9]. The application of passive seismic isolation for buildings that was primarily practiced in the United States is discussed in [10]. The analysis of an innovative earthquake protection method by placing rubber-soil mixtures (RSMs) around the foundation of structures to absorb seismic energy based on shaking table experimental tests is presented in [11] and based on parametric numerical study in [12].

The devices used in practice are of different complexities, efficiencies, and costs. Unfortunately, the use of such devices is sometimes not economical. In particular, the cost of the used devices sometimes exceeds the savings enabled by the reduction of seismic forces of the structure. A small number of embedded devices have been tested on actual strong earthquakes, while a large number of these devices had not yet been exposed to a strong earthquake, and their actual effectiveness is unknown. Unfortunately, to date, no such device has a life span equal to or greater than the life of a structure, free from the effects of environment and fire and free from maintenance.

For the purpose of broad practical application, such systems of seismic base isolation which are sufficiently efficient, economical, simply to fabricate, safe from the effects of the environment and fire, and easy to maintain are preferred. It is believed that one such solution for many buildings is a layer of adequate natural material placed under the foundation with adequate thickness, bearing capacity, and shear and vertical stiffness, along with the ability to dissipate earthquake energy. Such materials should retain their main mechanical properties over the projected life of the building.

Figure 1 shows a stiff building based directly on rigid ground (a) and based indirectly through a layer of natural material that acts as a seismic isolator (b). As dynamic interaction of the soil-structure coupled system occurs during an earthquake, it is reasonable to expect that the foundation of a building, according to Figure 1(b), can provide higher safety and bearing capacity of the building during an earthquake with higher dominant frequencies. First, in any case, the type of expected ground motions for use in the analysis on respective location must be determined; that is, the dominant frequencies of expected earthquakes, ground motion intensity, and spectral shape are crucial [13]. Next, the optimal natural material for the layer under the foundation acting as a seismic isolator should be determined. Currently, to the author's knowledge, there are very few studies related to the use of natural materials for seismic base isolation of buildings [14–16].

This paper presents the results of a brief experimental study to determine the effectiveness of limestone sand under the foundation of a cantilever concrete column to increase its seismic resistance. The main purpose of this paper is to confirm that the application of one common natural material under the foundation of the cantilever concrete column can increase its bearing capacity and safety during an earthquake. Namely, even decades ago, many restorers of historical buildings suspected that use of a layer of natural stone material under foundation was used not only to increase the soil's bearing capacity but also to help reduce the earthquake forces on the building. This was a motive to check whether a layer of sand below the foundation of the building could reduce earthquake forces.

As the tested structure is fairly soft, the greater efficiency of this approach for seismic base isolation is expected for stiff structures.

## 2. Shake Table Testing of Cantilever Concrete Columns with a Foundation on Different Substrates

The behavior of small-scale cantilever concrete columns with three different substrates below the foundation (Figure 2) was experimentally investigated using a shake table at the University of Split, Croatia. The foundation of the column is placed on a shake table according to each of the following conditions: (i) fixed to the shake table (column C1), (ii) over a 20 mm thick layer of limestone sand (column C2), and (iii) over a 100 mm thick layer of limestone sand (column C3). The column is 1080 mm in height (slenderness approximately 75), with a square cross section of 100 mm × 100 mm. The column is rigidly constrained at the foundation with

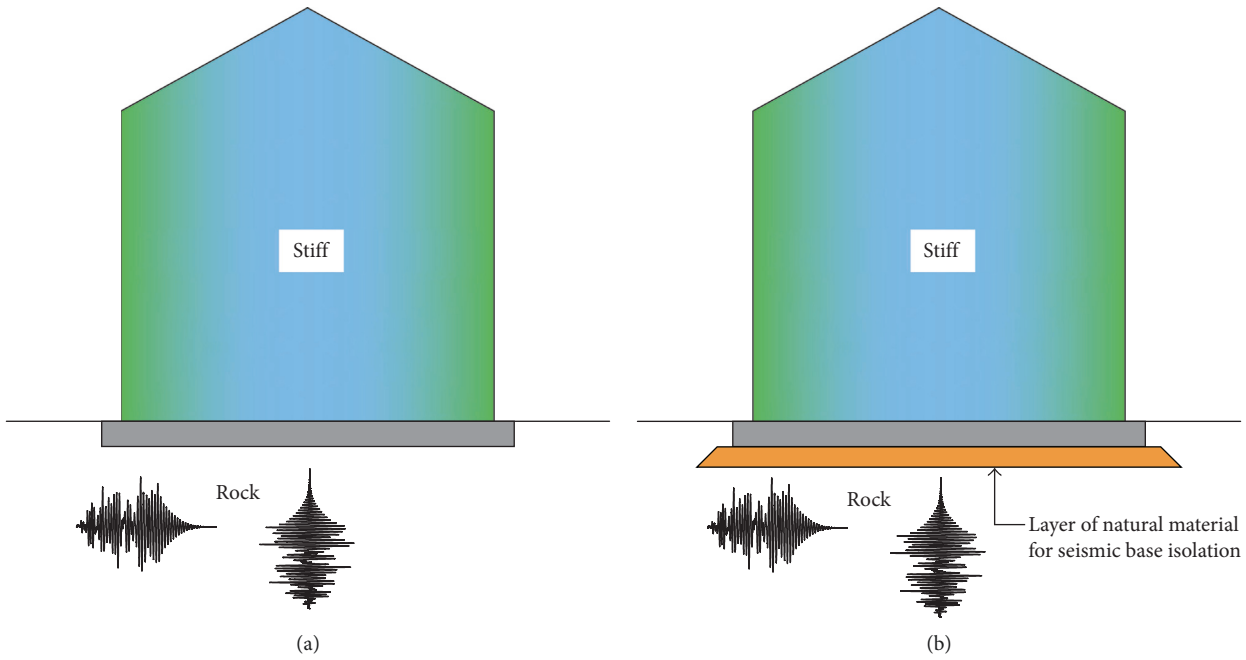


Figure 1: Two variants of foundations of stiff buildings on rigid soil.

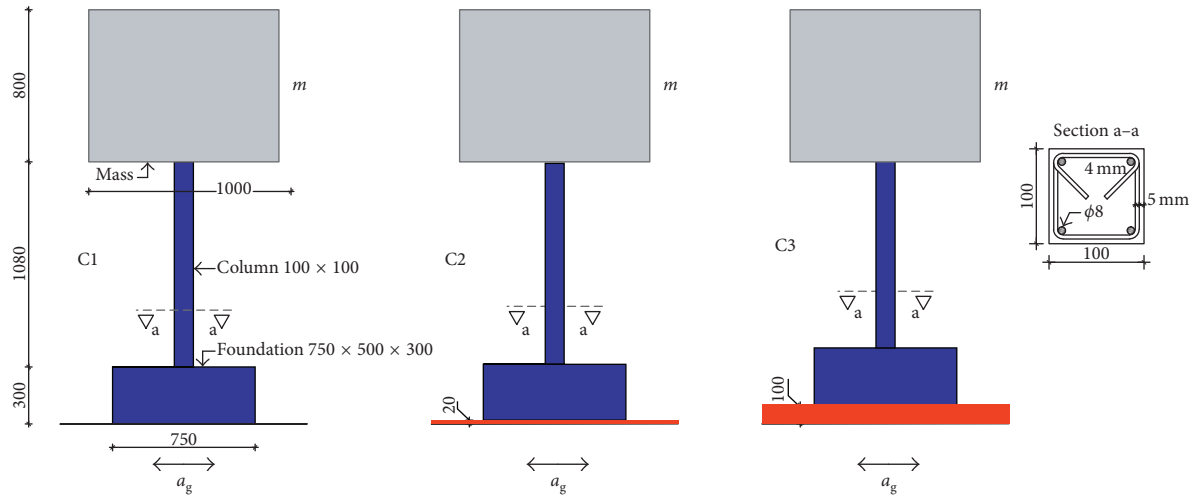


Figure 2: Basic data of the tested column.

a length of 750 mm, a width of 500 mm, and a height of 300 mm. A mass of 2 tons is placed on the top of the column, comprised of a concrete block of size of 1000 mm × 1000 mm × 800 mm. The center of mass coincides with the axis of the column; that is, the column was a centrically loaded due to gravity load.

The column and foundation were made of concrete with limestone aggregate, with a maximal grain size of 8 mm. The compressive strength of the concrete was 37.2 MPa and Young's modulus was 33.2 GPa. The flexural tensile strength of concrete was 3.9 MPa. The column was reinforced with vertical bars 4Φ8 mm (As = 201.1 mm$^2$, i.e., 2% of the concrete cross-sectional area) and Φ4.2 mm stirrups at a spacing of 50 mm. The ultimate strength of the steel was 653 MPa, and Young's modulus was 205 GPa. The foundation was reinforced with longitudinal bars 4Φ10 mm in the upper and bottom zones and with stirrups at a spacing of 100 mm. Only slightly compacted dry limestone sand below the foundation of columns C2 and C3, with a grain size in the range of 0–4 mm, was used as the seismic isolator.

The tested structures were exposed to a set of repeated horizontal base accelerations of artificial accelerograms created to match the elastic response spectra according to EN 1998 (EC 8) for type 1 and soil type A (Figure 3). Herein, $T$ is the natural period of the elastic single degree-of-freedom system, and $S_a$ is the spectral acceleration. Artificial accelerograms were obtained by the software SIMQKE, generated as a superposition of sinus functions

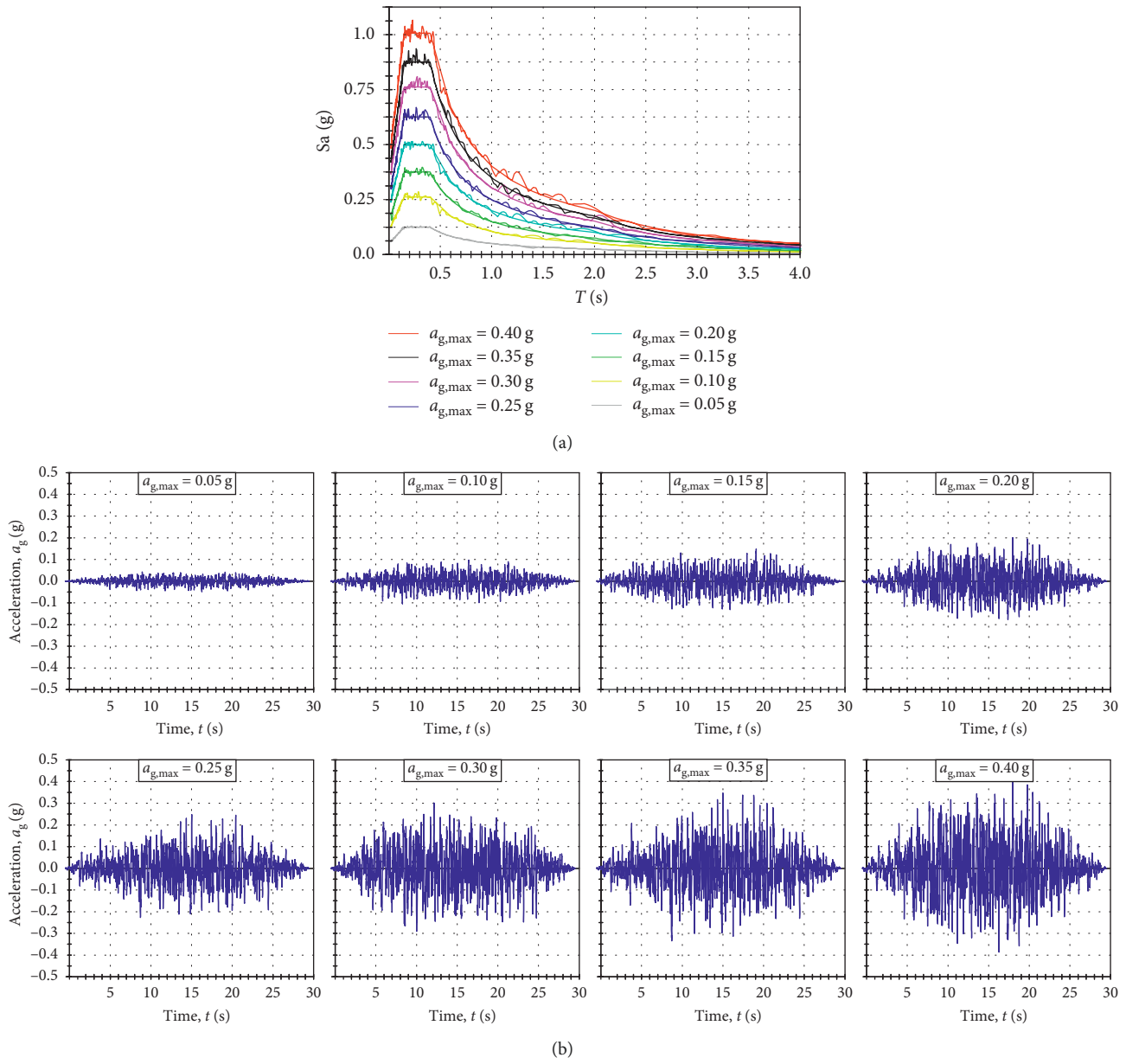


Figure 3: Applied horizontal base accelerations. (a) Elastic response spectra. (b) Artificial accelerograms.

[17]. The maximum acceleration for the first excitation was $a_{g,max} = 0.05$ g and, for the subsequent excitations, was successively increased by 0.05 g.

Characteristic displacements, accelerations, and strains of the structure (Figure 4) were measured for each excitation. Note that the measured tensile concrete strains may contain the impact of the eventual formed concrete cracks in the measuring zone and that the strains of the steel rebar can be determined by the position of cracks in the concrete in the measuring zone. The measured values for some applied excitations are presented hereinafter, and a detailed presentation of the equipment used in the study can be found in [18, 19].

Horizontal displacement of the top of the column is presented in Figure 5. Column C1 already had a significant irreversible displacement of the top of approximately 10 mm after excitation with $a_{g,max} = 0.2$ g. At $a_{g,max} = 0.3$ g, the top of column C1 had an irreversible displacement of approximately 55 mm. The tops of columns C2 and C3 had a small irreversible displacement at this excitation. At $a_{g,max} = 0.3$ g, the top of column C2 had an irreversible displacement of approximately 20 mm, and the top of the column C3 of about 6 mm. Column C1 collapsed under excitation with $a_{g,max} = 0.35$ g. The top of column C3 had a greater displacement at $a_{g,max} = 0.35$ g than that at the top of column C2. At the excitation with $a_{g,max} = 0.4$ g, columns C2 and C3 collapsed.

Vertical displacement of the top of the foundation is shown in Figure 6. Column C1 was fixed to the surface of the shake table, and its foundation had no vertical movement.

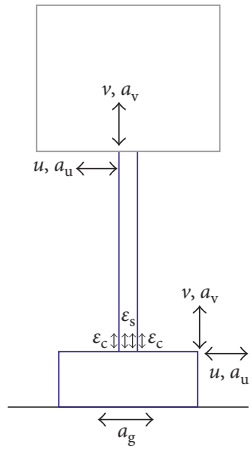


$u$: horizontal displacement
$v$: vertical displacement
$a_u$: horizontal acceleration
$a_v$: vertical acceleration
$\varepsilon_c$: concrete strain
$\varepsilon_s$: reinforcement strain
$a_g$: shake table acceleration

Figure 4: Measured values.

As a result of compaction of the limestone sand below the foundation, after excitations with higher accelerations, foundations of columns C2 and C3 had a permanent settlement. The column C3 with the thick layer of sand had a significantly greater settlement. After compaction of the limestone sand under the foundation of column C3 under repeated excitations, vertical displacement of foundation was consolidated. The foundation of column C3 had a greater uplifting than the foundation of column C2.

The reinforcement strain at the bottom of the column on its left side for some excitations is shown in Figure 7. At the excitation with $a_{g,max} = 0.2$ g, column C2 had a high tensile strain in the reinforcement (approximately 8‰), which caused yielding of the steel rebar. At the end of this excitation, the tensile strain in the reinforcement remained irreversible for approximately 4‰. During this excitation, no irreversible tensile strain in columns C1 and C3 occurred. At $a_{g,max} = 0.3$ g, column C1 had irreversible tensile strain in the reinforcement of approximately 2.5‰, while irreversible strain in the reinforcement of column C3 did not occur. At $a_{g,max} = 0.35$ g, column C2 had a high tensile strain in the reinforcement (approximately 22.0‰), which remained irreversible for approximately 6.0‰ at the end of the excitation. At $a_{g,max} = 0.35$ g, column C1 collapsed, with irreversible tensile strain in reinforcement of approximately 2.0‰ only. Columns C2 and C3 collapsed under excitation with $a_{g,max} = 0.4$ g. Thus, the irreversible tensile strain in the reinforcement of the column C2 was approximately 7.5‰ and that in the reinforcement of the column C3 was only approximately 1.0‰. It is obvious that the tensile strain in the reinforcement on the left side of column C3 was lower than the tensile strain in the same reinforcement of columns C1 and C2.

Reinforcement strain at the bottom of the column on its right side for some excitations is shown in Figure 8. At $a_{g,max} = 0.2$ g, the irreversible tensile strain in the reinforcement of column C1 was approximately 3.0‰ and that of column C2 was approximately 2.0‰. Irreversible strain in the reinforcement of column C3 did not occur. At the excitation with $a_{g,max} = 0.3$ g, the tensile strain in the reinforcement of column C2 reached 15.0‰, with irreversible tensile strain of approximately 5.0‰ at the end of the excitation. Small irreversible tensile strain in the reinforcement of column C1 occurred at the end of this excitation. At $a_{g,max} = 0.35$ g, column C1 collapsed with irreversible tensile strain in reinforcement of only approximately 2.0‰. At the excitation with $a_{g,max} = 0.4$ g, the irreversible tensile strain in the reinforcement of the column C3 was about approximately 4.0‰, while maximal compression strain in the reinforcement of the column C2 was approximately −9.0‰.

The concrete strain at the bottom of the column at its left side is shown in Figure 9. Only concrete compressive strain is discussed below. At $a_{g,max} = 0.2$ g, the compressive strain in the concrete of column C2 was close to −4.0‰; that is, the concrete was close to being crushed. The compressive strain in the concrete of columns C1 and C3 was smaller.

The concrete strain at the bottom of the column at its right side is shown in Figure 10. The compressive strain is discussed below. At $a_{g,max} = 0.2$ g, the compressive strain in the concrete of column C1 was close to −2.5‰ and that for columns C2 and C3 were smaller. At $a_{g,max} = 0.3$ g, the compressive strain in the concrete of column C1 was over −5.0‰ and failure of the strain gauge occurred. The concrete of this column was very close to being crushed. At $a_{g,max} = 0.3$ g, the concrete of column C3 reached a compressive strain of approximately −3.0‰.

Horizontal acceleration of the column top ($a_u$) is shown in Figure 11. The maximal horizontal accelerations of the top of all the columns were approximately equal. The valorization of the above values should be carefully done because the higher acceleration value does not mean at the same time greater stress in the structure. Namely, the strain sizes shown in Figures 7–10 are more relevant for describing the stress levels in the construction.

The first period of free oscillation of the columns ($T_1$) after the end of each successive base excitation was experimentally determined, at the maximum base acceleration $a_{g,max}$, as shown in Figure 12(a), and the stiffness value of each column was calculated according to the following simplified expression as shown Figure 12(b):

$$k = m\frac{4\pi^2}{T^2}. \quad (1)$$

The columns had almost equal values of $T_1$ which were approximately $T_1 = 0.64$ s before starting the test, from which it follows that the layer of limestone sand below the foundation had no practical effect on the initial dynamic characteristics of the coupled system. After the first base excitation with $a_{g,max} = 0.05$ g, an almost equal decrease in stiffness of all the columns occurred due to the appearance of plastic strains, which resulted in an increase of $T_1$. The stiffness of the columns decreased after the end of each successive base excitation, and $T_1$ increased. Before the

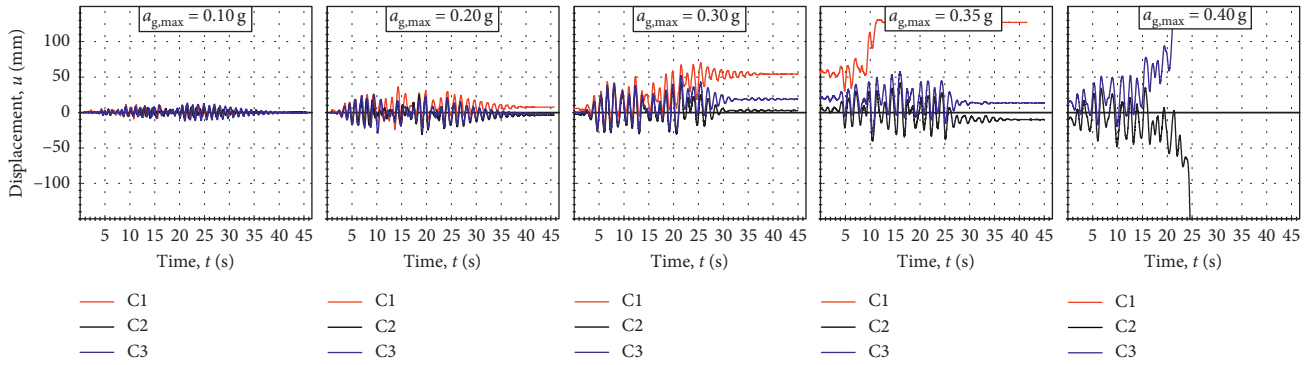


Figure 5: Horizontal displacement of the top of the column.

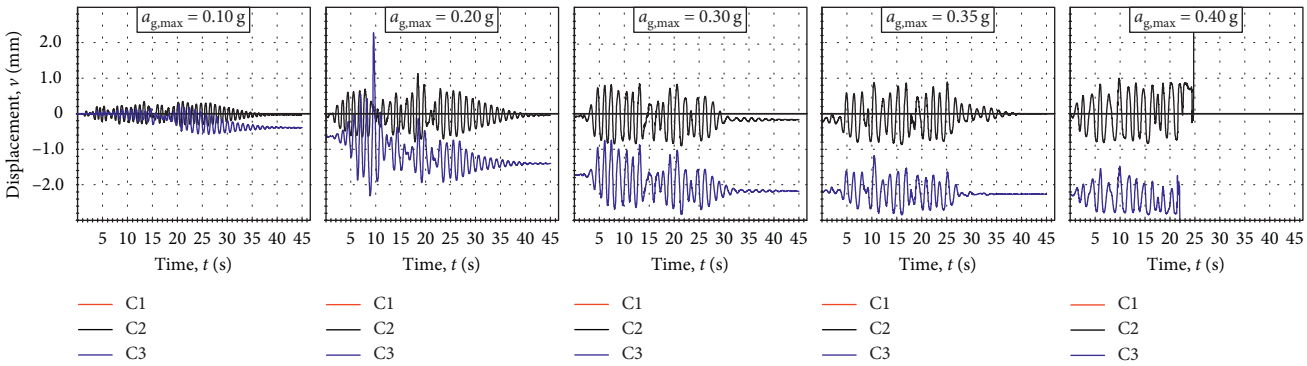


Figure 6: Vertical displacement of the top of the foundation on the left edge.

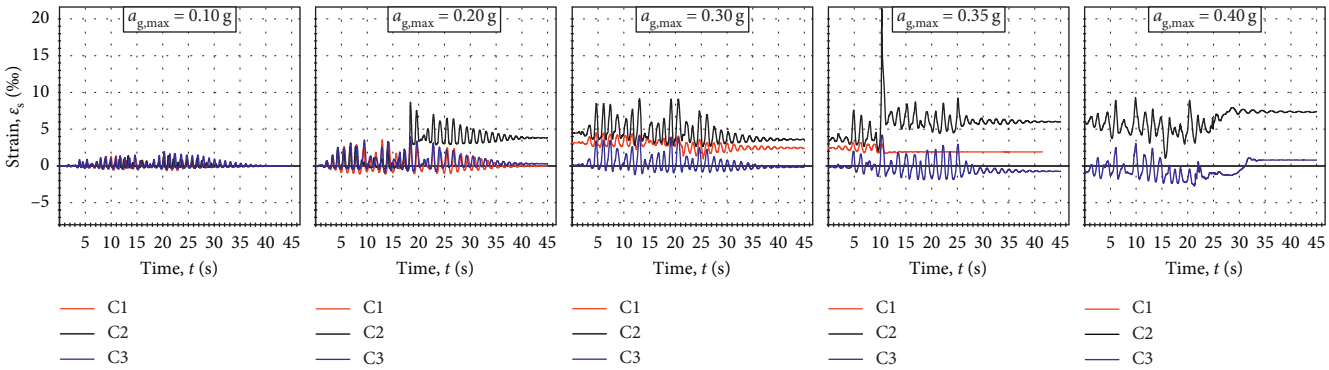


Figure 7: Reinforcement strain at the bottom of the column on the left side.

collapse of the columns, $T_1$ was approximately two times higher than before the application of the first base excitation. Thus, column C1 had a slightly higher decrease in stiffness up to $a_{g,max} = 0.3$ g, whereas columns C2 and C3 had approximately equal decreases in stiffness.

The tested columns clearly exhibited different behaviors under the applied excitations and exhibited different mechanisms of the collapse. The column C1 collapsed under excitation with $a_{g,max} = 0.35$ g; that is, it had the lowest bearing capacity. Columns C2 and C3 collapsed under excitation with $a_{g,max} = 0.4$ g, with column C3 having the most favorable behavior during the previous excitations. Namely, the column C3 had a minimum reinforcement and concrete strain/stress (Figures 7–10) and maximum remaining stiffness (Figure 12).

Because of the small number of experiments in the presented study, it is not possible to make more precise conclusions regarding the thickness of the sand layer that could achieve the highest ultimate bearing capacity of the column. Extensive research studies on this problem based on the shake table are planned, which would include variation of the type of structure (rigid, stiff, and soft), the natural

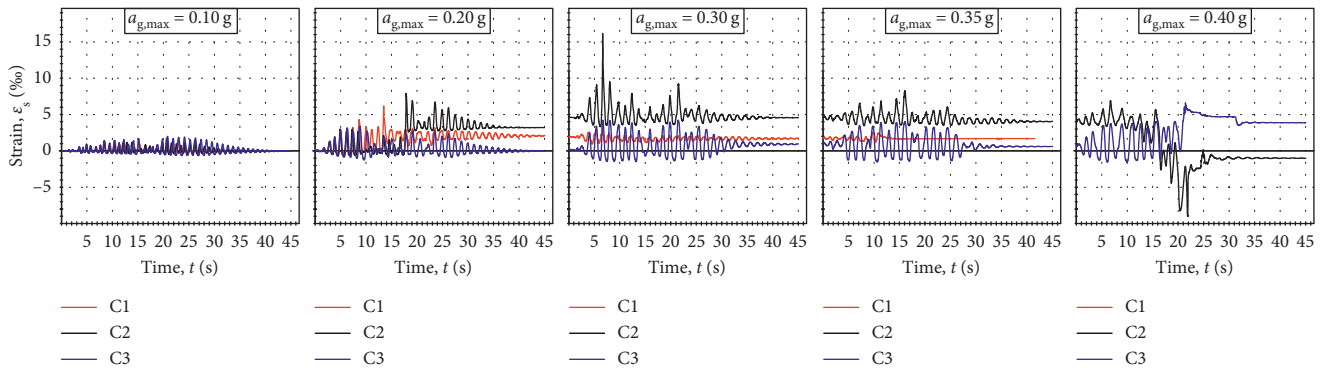


Figure 8: Reinforcement strain at the bottom of the column on the right side.

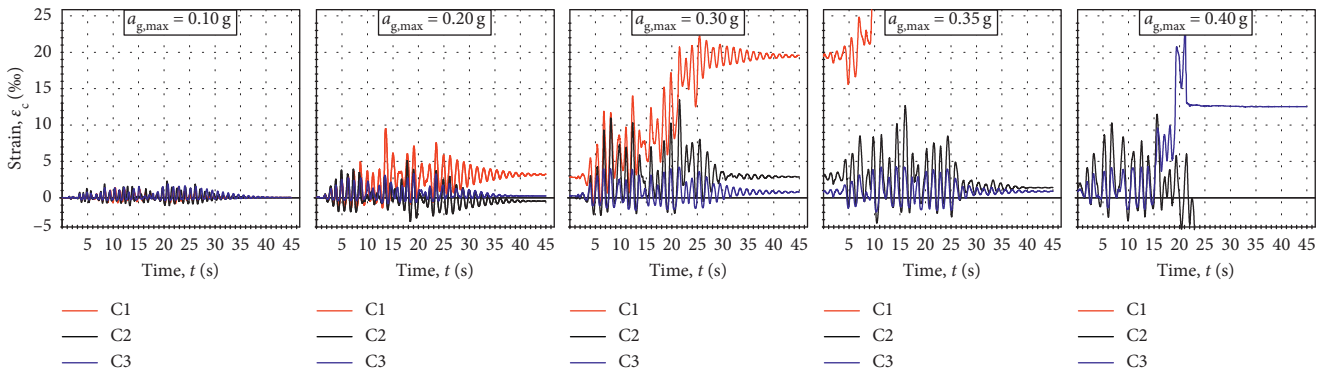


Figure 9: Concrete strain at the bottom of the column on the left side.

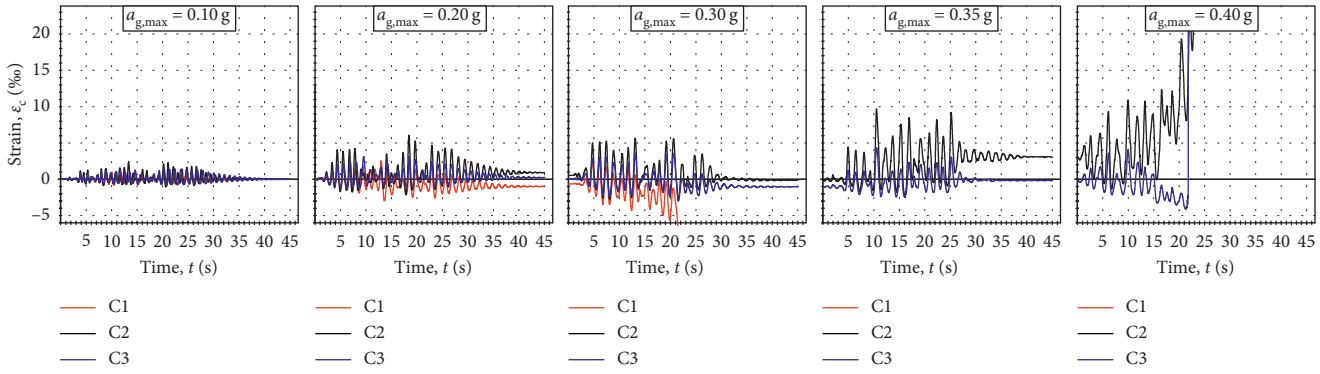


Figure 10: Concrete strain at the bottom of the column on the right side.

materials under the foundation (limestone sand, stone pebbles, etc.), the thickness and compaction of the layer, and the dominant frequencies of the base excitation.

## 3. Numerical Modeling of the Performed Experimental Test

The results of the performed experimental test presented in Section 2 can be simulated using a previously developed numerical model for static and dynamic analysis of planar concrete structures [19–23]. The model is briefly described hereinafter.

The adopted numerical model is quite simple, but it can simulate the primary material and geometric nonlinear effects of the concrete structures in contact with the ground. The model is primarily intended for practical use. The graphical interpretation of the adopted model is shown in Figure 13.

The model is based on the finite element method for spatial discretization of the soil-foundation-structure coupled system and on the finite difference method for the time integration of the equations of motion. Basic 8-node serendipity finite elements are used. 6-node planar and 2-node bar elements are adopted for contact elements (Figure 13(a)).

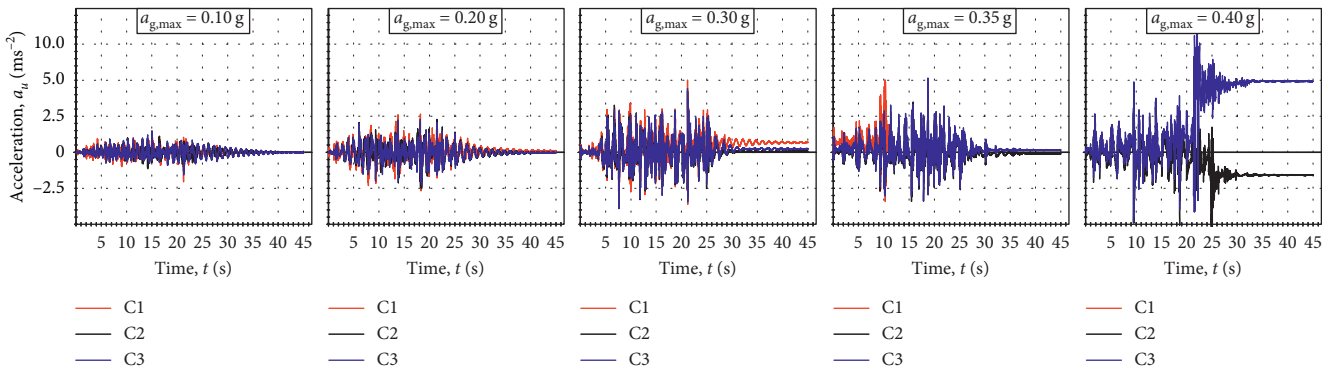


Figure 11: Horizontal acceleration of the column top.

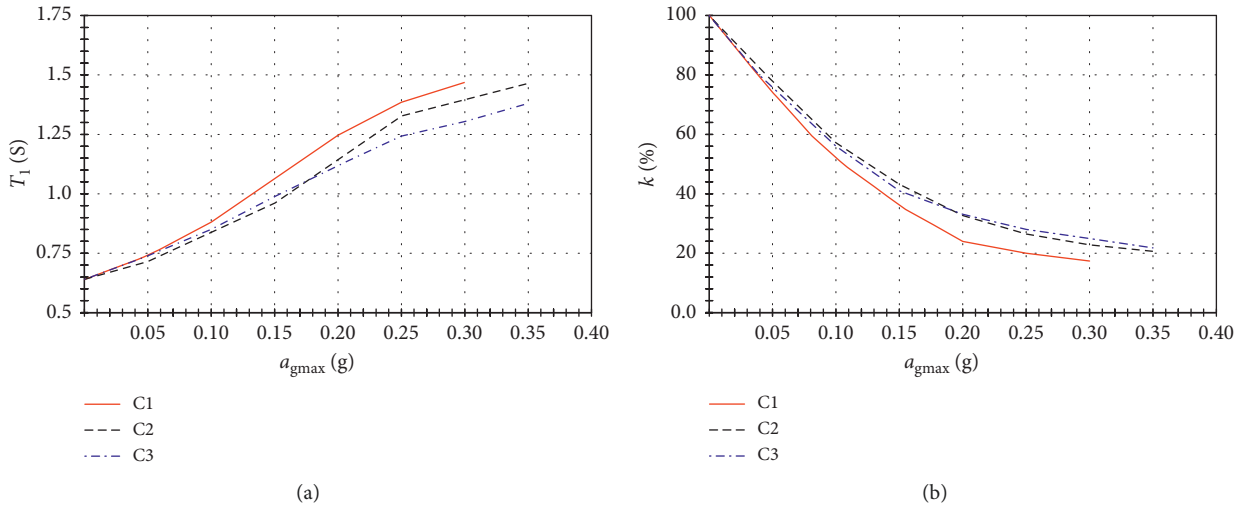


Figure 12: (a) First period of free oscillation of the columns determined after the end of each base excitation. (b) Normalized stiffness of the columns after the end of each successive base excitation.

To include the effects of large displacements, updated Lagrange formulation is used. Convergence criterion of incremental-iterative procedure is given as a function of current displacements' increment in relation to total displacements.

Biaxial failure of planar steel structures is modeled by the influence of normal stresses only. A classical elastic-plastic model for steel is used, with linear behavior in unloading (Figure 13(b)). Biaxial failure of planar steel structures is modeled by the effect of normal stresses only. Same behavior of steel in tension and compression is adopted. The von Mises yield criterion is used for steel yielding. The failure criterion of steel is defined as a function of principal strains, in an analogous way as a steel yielding.

The behavior of concrete in compression is described using an elastic-plastic theory (Figure 13(b)). The behavior of concrete in tension is described using an elastic-brittle model, including the modeling of cracks after the stresses reaching the maximal tensile concrete strength. The smeared crack model with fixed orthogonal cracks is adopted. The tensile stiffness of concrete between the cracks is simulated using a gradual reduction of the stiffness after the tensile stresses reaching the tensile strength of the concrete. The shear stiffness of the cracked concrete is simulated using gradual reduction of the shear modulus of the concrete as a function of the concrete strain perpendicular to the crack plane. Opening and closing of the cracks are also modeled.

The reinforcement is simulated using a one-dimensional curved bar element, within the basic concrete element. The full compatibility of the displacements between the concrete and the reinforcement is assumed. The behavior of the reinforcement steel is described by the polygonal stress-strain curve, with a linear behavior in unloading (Figure 13(b)). The influence of fatigue on the mechanical properties of concrete and steel related to the cyclic loading is not simulated. The simulation of the strain rate effects on the mechanical properties of concrete and steel due to the dynamic loading is enabled. Soil is simulated using a constitutive model of concrete, with adjustment of the associated material parameters. The constitutive model of the contact elements is described by the normal stress-normal strain polygonal curve and by the shear stress-shear strain polygonal curve (Figure 13(c)). The simulation of penetration,

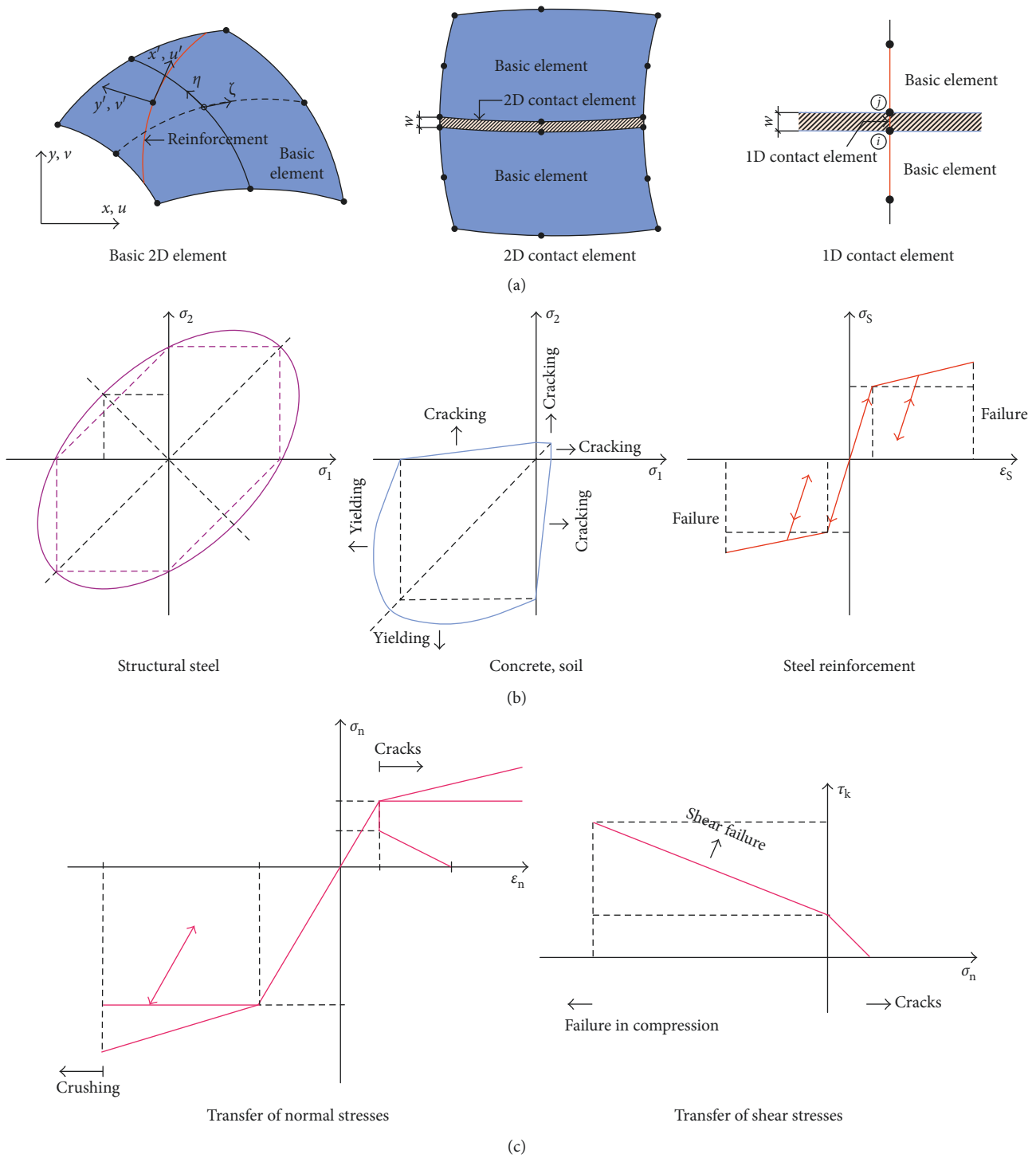


FIGURE 13: The graphical interpretation of the adopted model. (a) Adopted finite elements for a spatial discretization. (b) Adopted constitutive material models. (c) Constitutive models for contact elements.

separation, and sliding on the contact surface between the foundation and the soil is modeled.

Spatial discretization of tested column C3 is presented in Figure 14(a), and the shake table test model is shown in Figure 14(b). A comparison of some of the experimentally determined and numerically obtained results for column C3 is presented in Figure 15.

Generally, a relatively good agreement between the experimental and the numerical results was observed. During the excitations with lower levels of acceleration and a lower level of nonlinearity in the system, the best agreement between the experimental and numerical results was recorded. With an increase in the number of successive base excitations and an increase in the amplitude of the


(a) (b)

Figure 14: Tested column C3. (a) Spatial discretization. (b) Shake table test model.

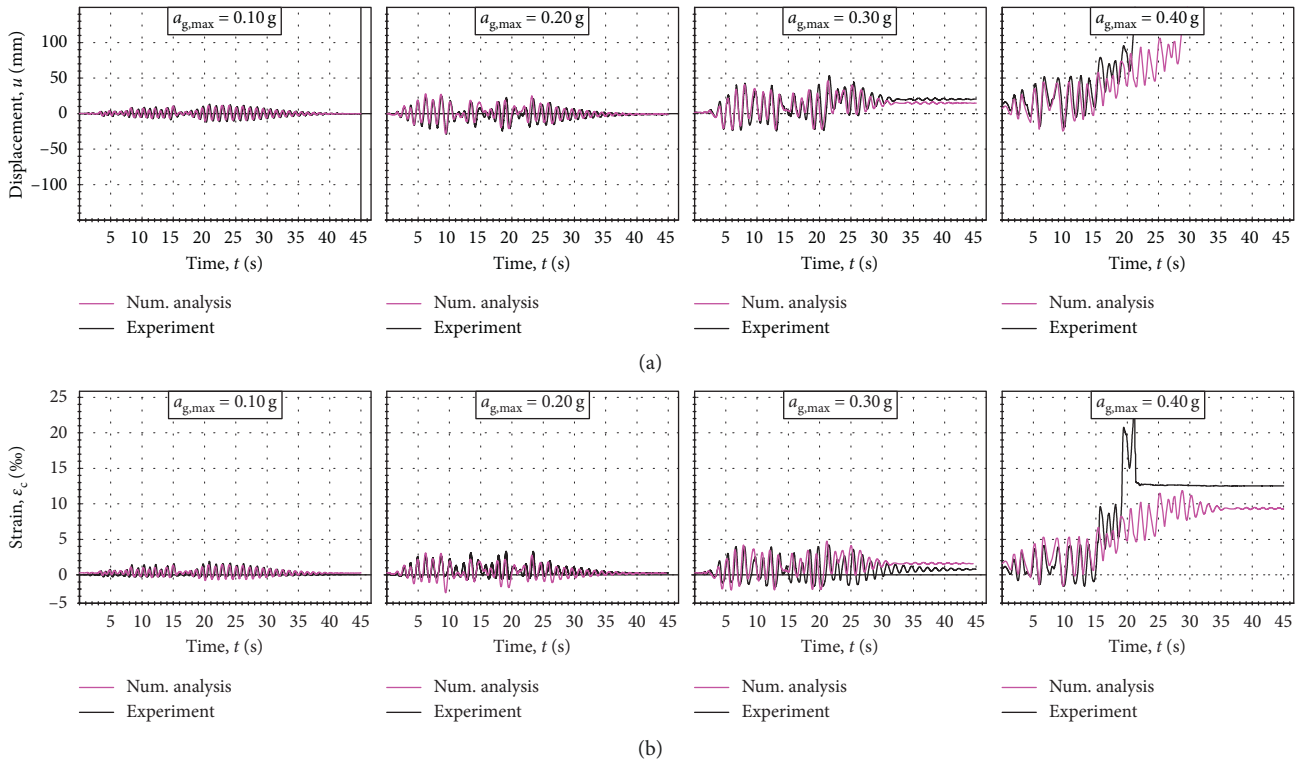


Figure 15: Comparison of some experimentally determined and numerically obtained results. (a) Horizontal displacement of the top of column C3. (b) Concrete strain at the bottom of column C3 on the left side.

Table 1: Comparison of some maximum values of experimental and numerical results.

| | $a_{g,max} = 0.1$ g | | $a_{g,max} = 0.2$ g | | $a_{g,max} = 0.3$ g | | $a_{g,max} = 0.4$ g | |
|---|---|---|---|---|---|---|---|---|
| | Experimental | Numerical | Experimental | Numerical | Experimental | Numerical | Experimental | Numerical |
| *Column C1* | | | | | | | | |
| $u$ (mm) | 11.02 | 11.29 | 36.20 | 38.01 | 70.31 | 72.30 | — | — |
| $v$ (mm) | — | — | — | — | — | — | — | — |
| $\varepsilon_s$-left side (‰) | 1.69 | 1.77 | 3.56 | 3.42 | 4.48 | 4.53 | — | — |
| $\varepsilon_c$-right side (‰) | −0.92 | −0.94 | −2.53 | −2.62 | −5.52 | −5.47 | — | — |
| $a_u$ (ms$^{-2}$) | 2.01 | 1.98 | 2.52 | 2.61 | 5.06 | 4.99 | — | — |
| *Column C2* | | | | | | | | |
| $u$ (mm) | 10.05 | 10.45 | 31.11 | 30.98 | 43.12 | 42.98 | 76.31 | 73.42 |
| $v$ (mm) | 0.34 | 0.35 | 1.13 | 1.21 | 0.82 | 0.79 | 1.08 | 1.06 |
| $\varepsilon_s$-left side (‰) | 1.38 | 1.45 | 8.65 | 8.77 | 9.06 | 8.99 | 9.24 | 9.35 |
| $\varepsilon_c$-right side (‰) | −1.05 | −1.16 | −2.12 | −2.08 | −3.15 | −3.26 | −1.35 | −1.29 |
| $a_u$ (ms$^{-2}$) | 1.12 | 1.18 | 2.51 | 2.42 | 3.28 | 3.48 | 5.06 | 4.99 |
| *Column C3* | | | | | | | | |
| $u$ (mm) | 13.06 | 13.51 | 29.12 | 28.55 | 52.22 | 49.11 | 96.57 | 105.2 |
| $v$ (mm) | 0.58 | 0.63 | 2.27 | 2.12 | 2.84 | 2.95 | 2.84 | 2.96 |
| $\varepsilon_s$-left side (‰) | 1.94 | 1.88 | 4.00 | 3.95 | 4.08 | 3.98 | 3.00 | 2.95 |
| $\varepsilon_c$-right side (‰) | −0.82 | −0.86 | −1.22 | −1.32 | −3.05 | −3.11 | −4.15 | −4.00 |
| $a_u$ (ms$^{-2}$) | 1.51 | 1.62 | 2.25 | 2.02 | 4.42 | 4.51 | 12.54 | 11.28 |

acceleration, significant nonlinearities (including plastic deformation) in the system were found to occur, which result in certain disagreements between the experimental and numerical results. Disagreements are the consequences of the shortcomings of the constitutive models, the spatial and temporal discretization, the convergence criteria, and some other influential parameters. Numerical simulations are also made for columns C1 and C2. A comparison of some maximum experimentally determined and numerically obtained results for columns C1, C2, and C3 are presented in Table 1. Generally, a relatively good agreement between the experimental and the numerical results was observed.

## 4. Conclusions

Unfortunately, to date, no devices exist for seismic isolation of structures that can comply with the numerous requirements that must be satisfied for their wide application in practice. The placement of a layer of appropriate natural materials under the foundation can be an optimal solution for seismic base isolation for many structures, especially in less-developed parts of the world [14–16]. Such materials should retain all of their mechanical characteristics over the projected life of the building.

The results of experimental research presented in this paper shows that the application of a layer of classical stone sand below the foundation can serve as a means of high-quality seismic isolation for rigid construction. In the performed small-scale shake table tests, a cantilever concrete column with a fixed foundation on the shake table had lower ultimate bearing capacity than the same column with the layers of limestone sand below its foundation. Therefore, the layer of limestone sand below the foundation increases the safety of the column under earthquake loading. Herein, it is necessary to adopt the appropriate thickness and compaction of this layer. In the performed tests, the 100 mm thick layer of limestone sand was more efficient than the 20 mm thick layer. Namely, the C3 column based on the 100 mm thick layer of limestone sand, for maximum base acceleration, had the lowest strain/stress in the structure and the highest residual stiffness, that is, the highest safety. Here, note that the layers were slightly compacted. For the layers made of the same material, its thickness and compactness have a great influence on the seismic response of the structure. Because of the small number of experiments in the present study, it is not possible to make more precise conclusions regarding the reliable effects of the sand layer below the foundation on the decrease in the seismic forces in the structure. Therefore, more extensive experimental studies of seismic base isolation using different natural materials below a foundation of different types of structures are planned.

The presented numerical model for static and dynamic analysis of planar concrete structures coupled with soil, which can simulate the primary nonlinear effects of the system, was verified based on the results of previously performed experimental shake table tests. Good agreement of numerical and experimental results confirms that the presented numerical model may find use in practical application. However, further verification of the model is required.

## Data Availability

All data underlying the findings of the study are presented in this article.

## Conflicts of Interest

The authors declare that there are no conflicts of interest regarding the publication of this paper.

## Acknowledgments

The research and publication of this paper was funded by authors.

## References

[1] G. E. Christenson, "Earthquake Ground Shaking in Utah," in *Utah Geological Survey Public Information Series*, Utah Geological Survey, Salt lake city, UT, USA, 1994.

[2] A. K. Chopra, *Dynamics of Structures: Theory and Applications to Earthquake Engineering*, Pearson Prentice Hall, Upper Saddle River, NJ, USA, 2007.

[3] C. M. Chang and B. F. Spencer, "Active base isolation of buildings subjected to seismic excitations," *Earthquake Engineering and Structural Dynamics*, vol. 39, no. 13, pp. 1493–1512, 2010.

[4] M. Eatherton, X. Ma, H. Krawinkler et al., "Design concepts for controlled rocking of self-centering steel-braced frames," *Journal of Structural Engineering*, vol. 140, no. 11, article 04014082, 2014.

[5] J. M. Kelly, "Aseismic base isolation: review and bibliography," *Soil Dynamics and Earthquake Engineering*, vol. 5, no. 4, pp. 202–216, 1986.

[6] F. Naiem and J. M. Kelly, *Design of Seismic Isolated Structures: From Theory to Practice*, John Willey & Sons, Inc., Hoboken, NJ, USA, 1999.

[7] J. Stanton and C. Roeder, "Advantages and limitations of seismic isolation," *Earthquake Spectra*, vol. 7, no. 2, pp. 301–323, 1991.

[8] L. Tashkov, K. Manova, L. Krstevska, and M. Garevski, "Evaluation of efficiency of ALSC floating-sliding base-isolation system based on shake table test and floor response spectra," *Bulletin of Earthquake Engineering*, vol. 8, no. 4, pp. 995–1018, 2010.

[9] T.A. Morgan and S.A. Mahin, "The use of base isolation systems to achieve complex seismic performance objectives," PEER Report No. 2011/06, Pacific Earthquake Engineering Research Center, University of California, Berkeley, CA, USA, 2011.

[10] G. P. Warn and K. L. Ryan, "A review of seismic isolation for buildings: historical development and research needs," *Buildings*, vol. 2, no. 3, pp. 300–325, 2012.

[11] W. Xiong and Y. Li, "Seismic isolation using granulated tire–soil mixtures for less-developed regions: experimental validation," *Earthquake Engineering and Structural Dynamics*, vol. 42, pp. 2187–2193, 2013.

[12] H. H. Tsang, S. H. Lo, X. Xu, and S. M. Neaz, "Seismic isolation for low-to-medium-rise buildings using granulated rubber–soil mixtures: numerical study," *Earthquake Engineering and Structural Dynamics*, vol. 41, no. 14, pp. 2009–2024, 2013.

[13] C. Haselton, J. Baker, A. Lied, and G. Deierlein, "Accounting for ground-motion spectral shape characteristics in structural collapse assessment through an adjustment for epsilon," *Journal of Structural Engineering*, vol. 137, no. 3, pp. 332–344, 2011.

[14] M. K. Yegian and U. Kadakkal, "Foundation isolation for seismic protection using a smooth synthetic liner," *Journal of Geotechnical and Geo-Environmental Engineering*, vol. 130, no. 11, pp. 1121–1130, 2004.

[15] S. J. Patil, G. R. Reddy, R. Shivshankar, R. Babu, B. R. Jayalekshmi, and B. Kumar, "Natural base isolation of structures having raft foundations," *International Journal of Emerging Technology and Advanced Engineering*, vol. 2, no. 8, pp. 23–38, 2012.

[16] S. J. Patil, G. R. Reddy, R. Shivshankar et al., "Seismic base isolation for structures using river sand," *Earthquakes and Structures*, vol. 10, no. 4, pp. 829–847, 2016.

[17] http://dicata.ing.unibs.it/gelfi/software/simqke.

[18] J. Radnić, N. Grgić, D. Matešan, and G. Baloević, "Shake table testing of reinforced concrete columns with different layout size of foundation," *Material Science and Engineering Technology*, vol. 46, no. 4-5, pp. 348–367, 2015.

[19] N. Grgić, *Experimental testing and numerical modeling of slender reinforced concrete columns under seismic conditions*, Ph.D. thesis, University of Split, Split, Croatia, 2014.

[20] J. Radnić, A. Harapin, D. Matešan et al., "Numerical model for analysis of masonry structures," *Gradjevinar*, vol. 63, no. 6, pp. 529–546, 2011.

[21] N. Grgić, J. Radnić, D. Matešan, and A. Buzov, "Effect of mass on the behavior of concrete columns under seismic load," *Material Science and Engineering Technology*, vol. 47, no. 5-6, pp. 483–493, 2016.

[22] N. Grgić, J. Radnić, D. Matešan, and I. Banović, "Stirrups effect on the behavior of concrete columns during an earthquake," *Material Science and Engineering Technology*, vol. 48, no. 5, pp. 406–419, 2017.

[23] G. Baloević, J. Radnić, D. Matešan, N. Grgić, and I. Banović, "Comparison of developed numerical macro and micro masonry models for static and dynamic analysis of masonry-infilled steel frames," *Latin American Journal of Solids and Structures*, vol. 13, no. 12, pp. 2251–2265, 2016.

# PAPER II

Hindawi
Shock and Vibration
Volume 2019, Article ID 9346232, 26 pages
https://doi.org/10.1155/2019/9346232

*Research Article*

# Geotechnical Seismic Isolation System Based on Sliding Mechanism Using Stone Pebble Layer: Shake-Table Experiments

**Ivan Banović, Jure Radnić, and Nikola Grgić**

*University of Split, Faculty of Civil Engineering, Architecture and Geodesy, Matice Hrvatske 15, 21000 Split, Croatia*

Correspondence should be addressed to Ivan Banović; ivan.banovic@gradst.hr

Received 21 December 2018; Revised 7 March 2019; Accepted 12 March 2019; Published 27 March 2019

Academic Editor: Yuri S. Karinski



Using a shake-table, the effects of several stone pebble layer parameters (the layer thickness, the fraction of pebbles, the pebble compaction, the pebble moisture, the vertical contact stress below the foundation, and the effect of repeated excitations) on layer aseismic efficiency were investigated. For each considered parameter, a model of a rigid building on an aseismic layer was exposed to four different accelerograms, with three levels of peak ground acceleration (PGA), while all other layer parameters were kept constant. For each test, the characteristic displacements and accelerations were measured. Based on the test results, the main conclusions regarding the effect of the considered parameters on the effectiveness of the adopted aseismic layer are given.

## 1. Introduction

In recent decades, intensive research has been carried out to reduce earthquake forces on buildings, bridges, and other structures to make them safer and more rational in seismically active areas. For this purpose, different approaches and principles of reducing seismic forces have been used, and they have resulted in different solutions in terms of efficiency, rationality, complexity, reliability, durability, and other important characteristics. The basic principle of seismic isolation is to "soften" the structure, i.e., to reduce the structure's stiffness and increase the free oscillation period to minimize earthquake/inertial forces in the structure during earthquake.

For the purpose of practical application, simplicity of realization, and rationality, the possibility of applying the so-called low-cost and low-tech seismic base isolation for small and medium-sized economically developed countries is investigated. The possibility of using natural materials for seismic base isolation is of great importance. There are indications that ancient builders used natural materials (sand, stone, wood beams, etc.) for the purpose not only of increasing the soil bearing capacity but also for reducing earthquake forces on buildings. In this seismic isolation approach, dissipation of earthquake energy is achieved primarily by reducing friction under the foundation and its horizontal sliding on the substrate. It is expected that this type of seismic isolation can be useful in the case of rigid and medium-rigid low- to mid-rise buildings, where the effect of earthquake vertical component is not significant. Unfortunately, research in seismic base isolation is still at the beginning. Currently, there are very few studies related to this topic. Some are briefly described below.

The origin and early development of seismic isolation were presented by Makris [1]. Patil et al. [2] performed experiments and analytical work on a structural model with isolated footing using river sand and found encouraging results. Radnić et al. [3] and Banović et al. [4] found by shake-table study that a layer of limestone sand of appropriate thickness and compressibility can serve as seismic base isolation material. Experimental studies with dune sand and lightweight expanded clay as sliding layers in adobe buildings in Iran can be found in [5]. Zhao et al. [6] performed numerical simulation of the isolation layer consisting of gravel using a discrete element method. The isolation effect of the cushion is shown to increase with the increase of layer thickness and decrease with the increase of base pressure. Gravel and sand cushions have been used in some bridges such as the Rio–Antirio Bridge [7] in Greece, the Vasco de Gama Bridge [8] in Portugal, and the Izmit Bay

Bridge [9] in Turkey. Anastasopoulos et al. [10] studied the seismic performance of a rocking-isolated bridge pier on surface foundations resting on sand. A series of reduced-scale shake-table tests were conducted, comparing the performance of a rocking-isolated system to that of a pier founded on a conventionally designed foundation. Development of seismic isolation technologies applicable to rural buildings under current rural economic conditions of China is presented by Zhang [11]. Doudoumis et al. [12] examined the concept of interposing an artificial soil layer between the superstructure and the foundation soil. Yegian et al. [13, 14] proposed smooth synthetic liners underneath the foundation of structures or between soil layers for dissipating seismic energy through sliding. Many numerical and experimental studies have been performed dealing with rubber-soil mixtures (RSM) for seismic base isolation of structures. Tsang et al. [15] proposed RSM around the foundation of structures for absorbing seismic energy and exerting a function similar to that of a cushion. Further work dealing with RSM can be found in [16–19]. Experimental studies based on shake-table tests by providing geotextiles and a smooth marble frictional base isolation system at the plinth level of a brick masonry building were performed by Nanda et al. [20–23]. Some papers dealing pure-friction base isolation systems can be found in [24–26].

Banović et al. [27] performed an experimental shake-table study to investigate the possibility of using a layer of natural stone pebbles below the foundation for seismic base isolation of buildings. Models of stiff and medium-stiff buildings were tested with the model on different layers of pebbles and on the rigid base with the possibility of foundation uplifting. Four different horizontal accelerograms were applied. To exclude the influence of construction material nonlinearity on conclusions regarding the efficiency of this seismic base isolation concept, the tested model stress remained in the elastic area. The research results are very encouraging. Namely, depending on the type of applied excitation and some other parameters, compared to the rigid base case, a pebble layer reduced the strain/stress in the model up to 53%. For most applied excitations, compared to the rigid base case, the pebble layer reduced the horizontal displacement of the mass centre at the column top. However, firm conclusions require further research.

The base isolation concept in [27] can be categorised as a "Geotechnical Seismic Isolation (GSI) system," as defined initially by Tsang [28] and also adopted by Brunet et al. [29] and Forcellini [30]. Namely, the dissipation of earthquake energy and the reduction of earthquake forces on the building in this concept are dominated by the sliding mechanism of the foundation on seismic isolation and between pebbles sublayers. Another way to describe mechanism of this isolation concept is the "distributed seismic isolation system," which has been discussed by Tsang [31] and Mavronicola et al. [32].

This paper presents the results of a further research segment related to the concept of seismic base isolation using a layer of natural stone pebbles below the foundation presented in [27]. Namely, the research results of six different parameters related to the effectiveness of the adopted aseismic layer are presented. For simplicity, a rigid building model was adopted. This should have no impact on the conclusions made for cases of "softer" structure. Namely, as stated above, this concept is primarily intended for stiff and medium-stiff low- to mid-rise buildings, where maximum vertical stress below the foundation is adapted to the bearing capacity of the stone pebble layer. The effect of the following parameters was investigated: the layer thickness, the fraction of pebbles, the pebble compaction, the pebble moisture, the vertical contact stress below the foundation, and the effect of repeated excitations. For each considered parameter, the model of a rigid building on an aseismic layer was exposed to four different accelerograms with three levels of peak ground acceleration: PGA (0.2 g, 0.4 g, and 0.6 g). The effects of all parameters were evaluated based on the analysis of measured horizontal acceleration and displacement in the characteristic model points. For each considered parameter, all other layer parameters were kept constant. Since tests in this paper are conducted on the same small-scale model in order to investigate a relative effect of several parameters (parametric analysis), it is believed that conclusions obtained are representative for a real structure as well. The main conclusions of the research are presented at the end of the paper.

## 2. Tested Models

The basic data regarding the adopted building model and aseismic layer are shown in Figure 1. As stated above and for simplicity, a rigid building model was adopted. This should not have an impact on the conclusions because this aseismic concept is primarily intended for stiff buildings, and in addition, research has been carried out to investigate the relative effect of several parameters on layer aseismic efficiency. The building is approximated by a rigid concrete block with mass $m = 2000$ kg and dimensions of $1.0\,\text{m} \times 2.0\,\text{m} \times 0.4\,\text{m}$. The concrete block is formed in height by prefabricated elements, rigidly coupled with prestressed bolts. The block has a reduced area in contact with the aseismic layer in order to achieve the desired contact stress under the foundation of the building.

An aseismic pebble layer with height $h_p$ is formed within a frame with a plan size of $2.5\,\text{m} \times 2.5\,\text{m}$ and fixed to the shake-table. The purpose of this study was to determine the effect of several adopted aseismic layer parameters (layer thickness, fraction of pebbles, pebble compaction, pebble moisture, vertical contact stress below the foundation, and the effect of repeated excitation) on the displacement and acceleration of the rigid structure model. The model was exposed to four different accelerograms, with three levels of PGA (0.2 g, 0.4 g, and 0.6 g).

## 3. Analysed Stone Pebble Layer Parameters

*3.1. Aseismic Layer Thickness.* In the conducted tests, the following two layer thicknesses were used: $h_p = 0.3$ m and $h_p = 0.6$ m, along with other constant parameters (Figure 2). Namely, in the event of proven effectiveness of this seismic base isolation concept, the intention was to form a relatively

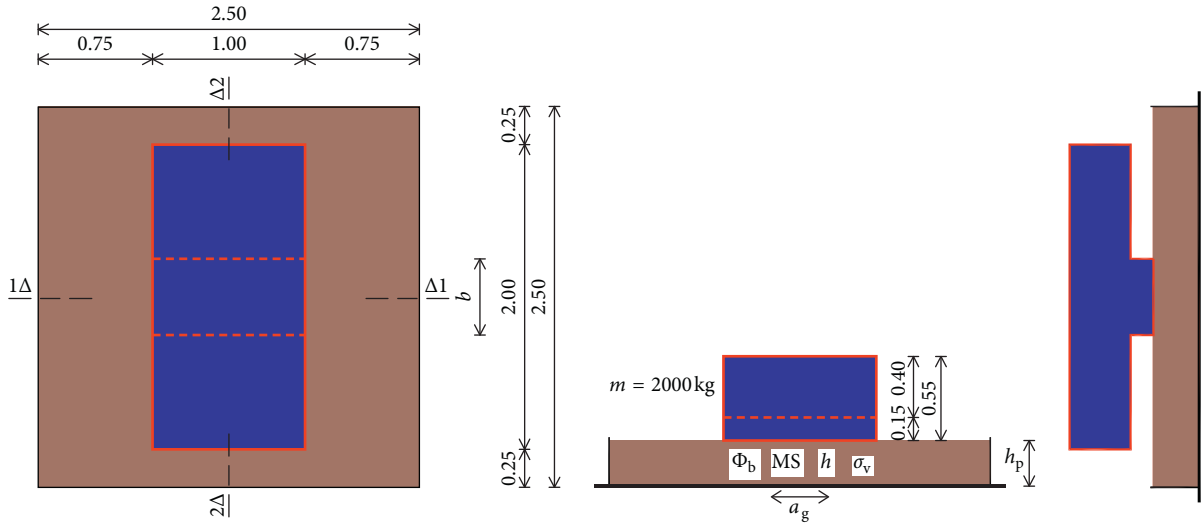


Variable parameters:

(1) $h_p$ = 0.3 m; 0.6 m (the aseismic layer thickness)

(2) $\Phi_b$ = 4–8 mm; 8–16 m; 16–32 m (the pebble fraction)

(3) MS = 10 MPa; 30 MPa; 60 MPa (the pebble fraction)

(4) $h$ = 10%; 60%; (the pebble moisture)

(5) $\sigma_v$ = 0.04 MPa; 0.10 MPa; 0.20 MPa ($b$ = 0.5 m; 0.2 m; 0.1 m;) (the vertical contact stress below foundation)

Figure 1: Adopted model of rigid building and aseismic layer. (a) Layout of model. (b) Section 1-1. (c) Section 2-2.

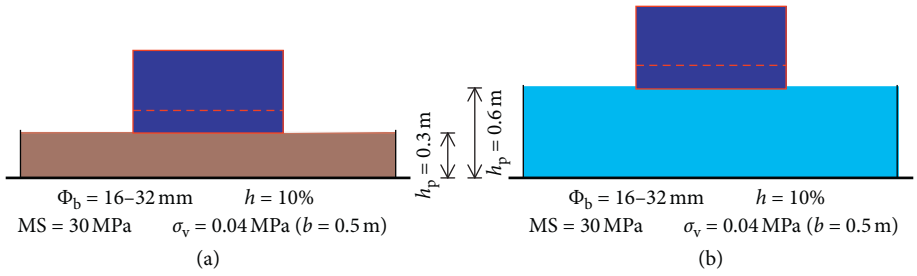


Figure 2: Analysed thickness of the aseismic layer. (a) $h_p$ = 0.3 m. (b) $h_p$ = 0.6 m.

thin layer of stone pebbles below the building foundation in practice. To reduce the possible excavation and the amount of stone pebbles, from the aspect of rationality and speed of construction, it is desirable for the aseismic layer to be as thin as possible. It is assumed that aseismic layer thickness should not have greater impact on layer horizontal shear stiffness. The thicker layer would probably provide lower resistance than the thin layer to horizontal foundation displacement (lower friction) and larger vertical displacement (smaller flexural stiffness) upon rotation of the foundation. The use of a thicker aseismic layer also means raising the centre of the building mass above the top of the indigenous soil. This results in higher inertial force (acceleration) in the structure. The assumption is that a thin layer would be optimal for low buildings (approx. 1–3 floors), and a thicker layer would be optimal for slightly taller buildings (approx. 4–6 floors). An additional advantage of thin stone pebble layers, compared to thicker layers, is that they are easier to make and compact.

*3.2. Pebble Fraction.* The effect of three fractions of stone pebbles (Figure 3) was investigated: $\Phi_b$ = 4–8 mm (i.e., small pebbles), $\Phi_b$ = 8–16 mm (i.e., medium pebbles), and $\Phi_b$ = 16–32 mm (i.e., large pebbles). In fact, standardly separated pebble fractions in the exploitation of river gravel are used. It is expected that the pebbles of one fraction provide less friction between the foundation and the top of the aseismic layer. Therefore, no fractions with large differences in pebble grain size were used. Additionally, dust-free pebbles were used. The average compressive strength of the pebbles was approximately 80 MPa. The compressive strength of the pebbles did not affect the test results due to the small stresses in the aseismic layer. The larger pebbles are generally slightly cheaper than smaller pebbles.

*3.3. Pebble Layer Compaction.* The compaction of the formed pebble layer was determined by measuring the compaction modulus (MS) at the top of the layer. The layers

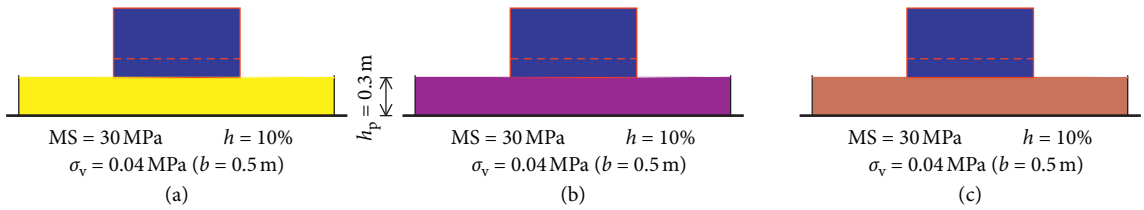


Figure 3: Analysed pebble fractions. (a) $\Phi_b = 4$–$8$ mm. (b) $\Phi_b = 8$–$16$ mm. (c) $\Phi_b = 16$–$32$ mm.

were formed in 0.10 m thick sublayers, with dynamic compaction using the shake-table and static compaction to the expected MS. Three MS values were studied (Figure 4): MS = 10 MPa, MS = 30 MPa, and MS = 60 MPa. It should be noted that there were variations of approximately 8% in the previously stated MS values for some base excitations and that the compaction was not completely uniform over the entire surface of the aseismic layer.

*3.4. Pebble Moisture.* Although it is expected that pebble layers below the buildings are dominantly dry, it is possible that a smaller or larger part of the aseismic layer becomes wet. Assuming that pebble moisture has a certain effect on the friction between them, and thus on friction between the foundation bottom and aseismic layer top, the effects of two pebble moisture contents were analysed (Figure 5): $h = 10\%$ (i.e., dry pebbles) and $h = 60\%$ (i.e., wet pebbles). It should be noted that there were variations of approximately 10% within the previously stated $h$ in the preparation of the aseismic layer. Additionally, it should be noted that pebble moisture was not completely uniform over the entire surface of the aseismic layer.

*3.5. Vertical Contact Stress below the Foundation.* Considering the possible application of the proposed concept of seismic base isolation to lower buildings, depending on the foundation ground plan, relatively low vertical contact stress on top of the aseismic layer is expected. As already mentioned, maximum vertical stress below the foundation should be lower than the bearing capacity of the stone pebble layer. Three levels of contact stress due to gravity load were varied: $\sigma_v = 0.04$ MPa, $\sigma_v = 0.10$ MPa, and $\sigma_v = 0.20$ MPa. Equal vertical stress under the foundation can be realized in different ways: for example, with a different building height (weight) or the same building height (weight) and different foundation surface. A model with equal height (weight) and foundation different surface (Figure 6) was adopted, to achieve equal size and position of the tested model inertia force.

*3.6. Effect of Repeated Excitation on Aseismic Layer Efficiency.* In reality, it is likely that similar earthquakes of moderate or high strength occur several times during the lifetime of a building. To investigate the effect of such a possibility on the behaviour and efficiency of the aseismic layer, as well as on the overall model displacements, tests were performed on the same model with six consecutive equal excitations, without updating the pebble layer. The accelerogram of the Ston earthquake and the artificial accelerogram with PGA = 0.6 g are applied, which generate the highest model accelerations and displacements (Section 4). All parameters of the aseismic layer are kept constant.

## 4. Applied Base Excitations

Applied dynamic horizontal base excitations and their spectral values are presented in Figure 7. The N-S accelerogram of the B. Luka earthquake (BiH, 1982): ABL [33] and the N-S accelerogram of the Ston earthquake (Croatia, 1996): AS [33] are characterized by short impact action with short predominant period. These excitations have small spectral velocity and displacement, i.e., they do not bring high earthquake input energy into the structure. The N-S accelerogram of the Petrovac earthquake (Montenegro, 1979): AP [33] and the artificial accelerogram: AA [34] characterize long-lasting action with pronounced accelerations (especially AA) and longer predominant periods (especially AP). An artificial accelerogram is created to match the elastic response spectra according to EC8 [34], for type 1 and soil type A. These excitations have higher spectral velocities and displacements, i.e., they bring higher earthquake input energy into the structure. The adopted excitations cover quite a wide spectrum of potential earthquake types. Each tested sample is exposed to sets of three successive base excitations (Figure 7(a)) with PGA = 0.2 g, PGA = 0.4 g, and PGA = 0.6 g, where PGA = $a_{g,max}$. After each set of three successive base excitations, the pebble layer and the model were updated for the next set of excitations. This approach, in which accumulation of displacements from previous excitations and eventual degradation of the pebble layer occurs, is possible in practice and is interesting in terms of monitoring the possible foundation eccentricity in relation to the aseismic layer. According to the seismic situation in Croatia, PGA = 0.2 g represents weak earthquakes, PGA = 0.4 g represents moderately strong earthquakes, and PGA = 0.6 g represents strong earthquakes.

## 5. Measured Quantities and Measuring Equipment

The behaviour of the tested rigid model during base excitation is best described by displacements and accelerations. The following values were measured on each tested sample (Figure 8): horizontal displacements $u_1$ and $u_2$, vertical displacements $v_1$ and $v_2$ (rotation of the foundation), and horizontal acceleration of the mass centre $a$.

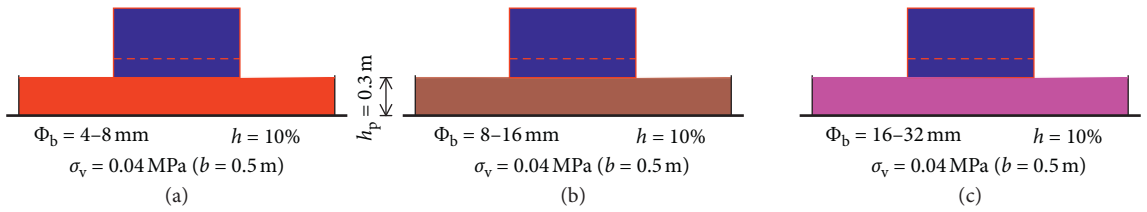


Figure 4: Analysed pebble layer compaction. (a) MS = 10 MPa. (b) MS = 30 MPa. (c) MS = 60 MPa.

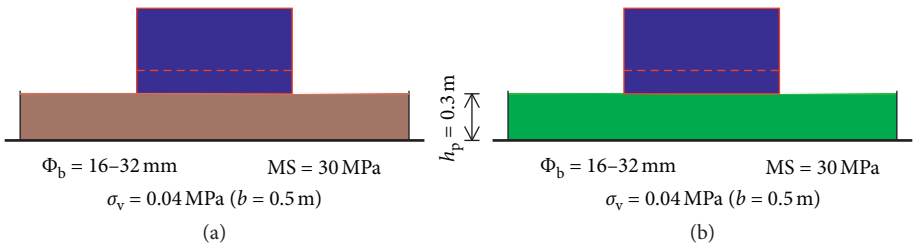


Figure 5: Analysed pebble layer moisture. (a) $h$ = 10%. (b) $h$ = 60%.

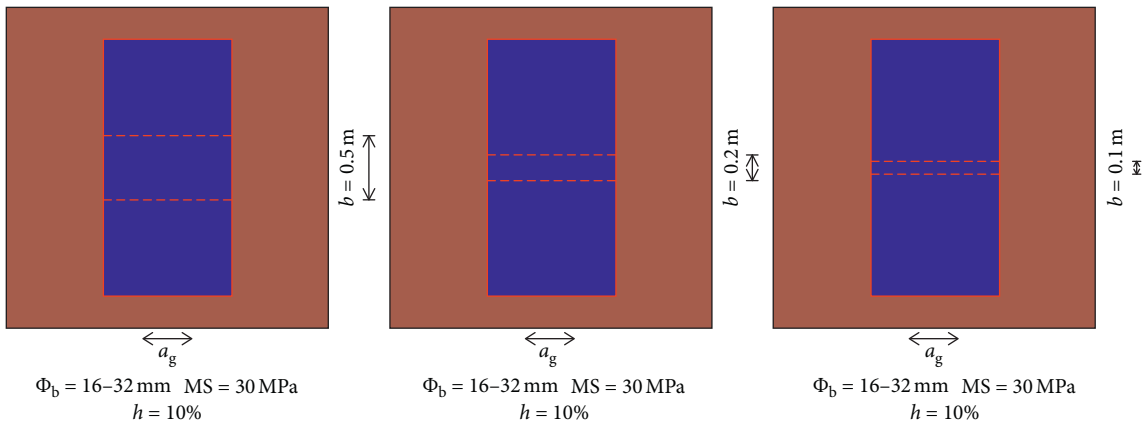


Figure 6: Analysed vertical contact stress below the foundation. (a) $\sigma_v$ = 0.04 MPa. (b) $\sigma_v$ = 0.10 MPa. (c) $\sigma_v$ = 0.20 MPa.

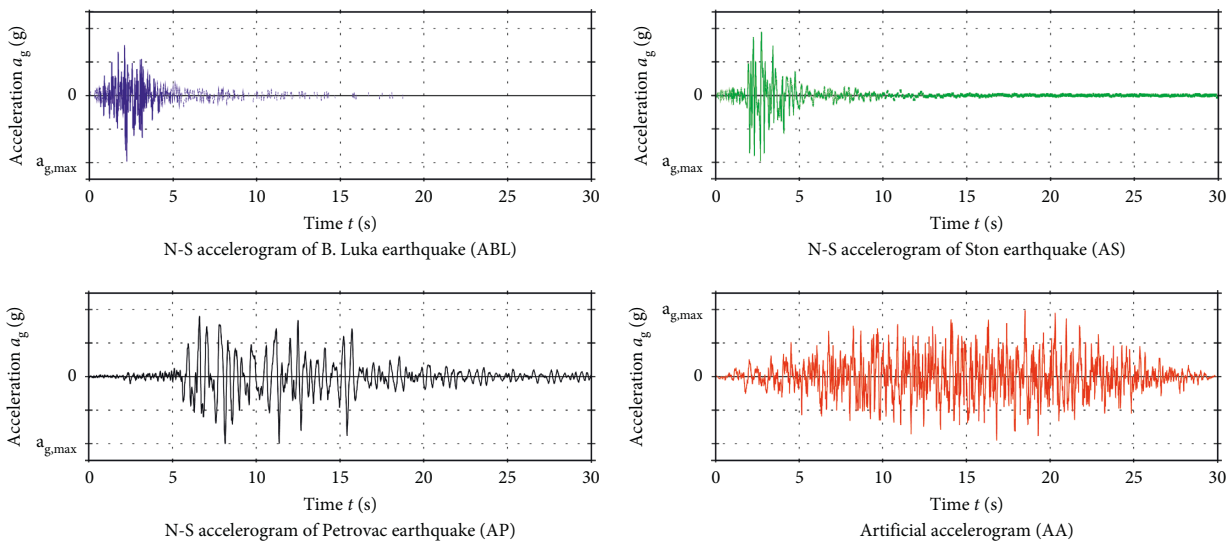


(a)

Figure 7: Continued.

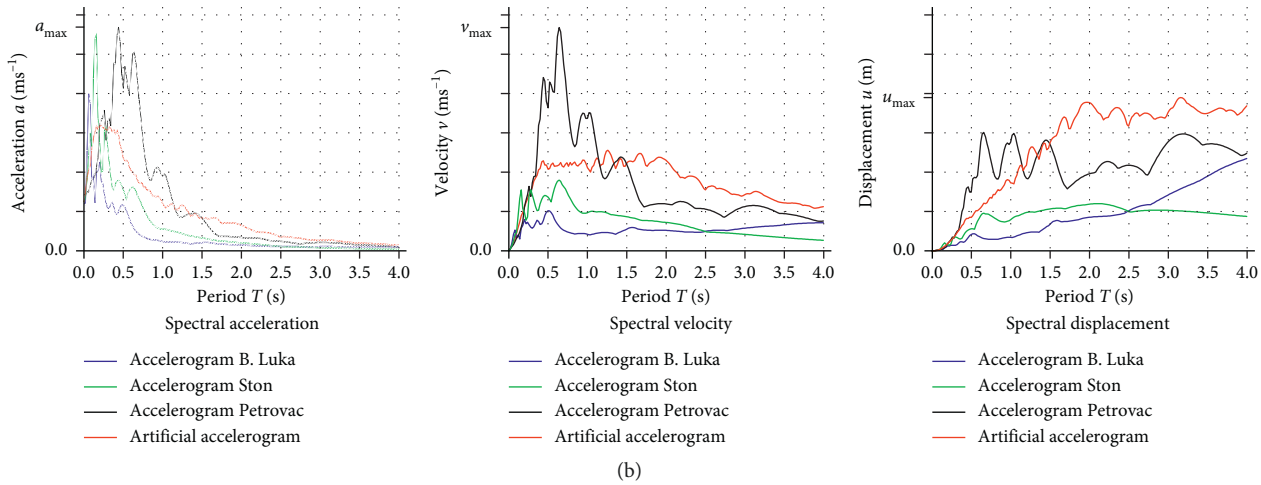


(b)

Figure 7: Acceleration time history and elastic response spectra of the applied excitations. (a) Applied horizontal base excitations. (b) Elastic response spectra of applied excitations.

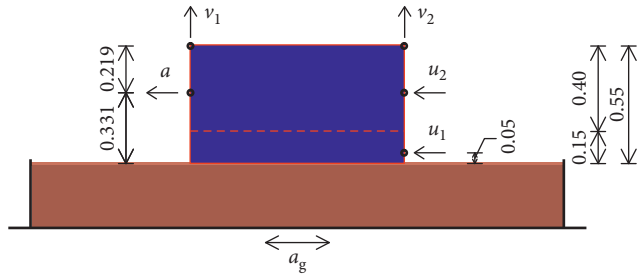


Figure 8: Measured quantities.

A uniaxial shake-table at the University of Split, Faculty of Civil Engineering, Architecture and Geodesy (Croatia), was used to test the models. Data acquisition from sensors during the shake-table test was ensured using the Quantum-X MX 840A (HBM) high-speed data acquisition system. The displacements were measured using analogue displacement sensors, type PB-25-S10-N0S-10C (Uni Measure). The accelerations were measured by a piezoelectric low-frequency accelerometer type 4610 (MS). The sampling rate during the shake-table test was 200 Hz. A video camera was used for test monitoring.

## 6. Experimental Results

Only some obtained results are given hereafter. For each analysed parameter of the pebble layer, the results are shown separately for each applied accelerogram. The results are shown separately for the first lowest acceleration (PGA = 0.2 g) and for the last successive acceleration (PGA = 0.6 g). When evaluating the accuracy of the obtained results, it should be noted that there are possible minor deviations of the measured values of displacements and accelerations. Namely, the accuracy of the measured values affects a large number of parameters. Some parameters will be briefly commented upon below.

The analysed layer is an anisotropic medium, formed in sublayers with static and dynamic compaction, as a classical embankment. It is likely that in many reconstructions, in order to study various parameters, theoretically equal aseismic layers will not always be the same in reality. The behaviour of the adopted layer of unbound material is nonlinear even with low values of acceleration, with the possibility of occurrence and intensity of different nonlinearities in different places in a theoretically equal aseismic layer. When installing the model, it is possible that it was not always perfectly mounted considering the centre of the shake-table, as well as that the aseismic layer was not completely horizontal. The impact on measured results may also have the accuracy of repeated application of the same shake-table excitation, as well as the precision of the measuring equipment and the accuracy of the measurement. With regard to the previous years of experience in experimental testing, it can be assumed that the impact of the abovementioned possibilities was small. It can be comprehensively stated that the difference in declared values of the measured quantities and their real values is within acceptable limits and that the difference does not have any major influence on the conclusions. Hereafter, the results are presented separately for each considered pebble layer parameter, with the effect of the excitation type and PGA.

*6.1. Effect of Aseismic Layer Thickness.* Some photos of the experimental setup before testing are shown in Figure 9, in

(a) (b)

Figure 9: Photos of experimental setup before testing. (a) Pebble layer $h_p = 0.3$ m. (b) Pebble layer $h_p = 0.6$ m.

accordance with Section 3.1. The effect of aseismic layer thickness on horizontal displacement $u_2$ is shown in Figure 10, and peak $u_2$ values are shown in Figure 11. It is noticeable that, independently of the pebble layer thickness, the results significantly depend on the type of applied excitation and PGA.

The time-history displacement curves for $h_p = 0.3$ m and $h_p = 0.6$ m are approximately affine, especially for PGA = 0.2 g (where low nonlinearity in the layers is present). After the excitations with PGA = 0.2 g, small permanent $u_2$ remained. The largest permanent $u_2$ was produced by ABL and AA. For excitations with PGA = 0.6 g, permanent $u_2$ was significantly higher (especially for AS, which is the result of the foundation slipping at the pebble layer top).

For PGA = 0.2 g, the largest $u_2$ was produced by AA (approx. 3.4 mm). For PGA = 0.6 g, the largest $u_2$ was produced by AS (approx. 15.5 mm), while the same excitation for PGA = 0.2 g produced the lowest $u_2$. This is explained by the fact that the AS is characterized by a short impact action, with a more pronounced shear impact compared to bending. For the smallest PGA, there was no block sliding on the aseismic layer, and at the largest PGA, slipping was significantly larger than for other excitations. The effect of the adopted aseismic layer thickness on $u_2$ is not particularly pronounced, except for excitations AS and AP at PGA = 0.6 g. In this case, $u_2$ is partly higher for $h_p = 0.3$ m and partly for $h_p = 0.6$ m. For PGA = 0.6 g and excitations AS and AP, the thick layer had significantly higher maximum and permanent $u_2$ than the thin layer. The effect of aseismic layer thickness on layer efficiency depends on the type of applied excitation and PGA.

The effect of aseismic layer thicknesses on horizontal acceleration $a$ is shown in Figure 12, and peak acceleration values are shown in Figure 13. As with $u_2$, acceleration $a$ significantly depends on the excitation type and the PGA. The time-history acceleration curves for $h_p = 0.3$ m and $h_p = 0.6$ m are almost affine. Compared to the excitations with PGA = 0.2 g, excitations with PGA = 0.6 g produced significantly higher $a$, but not proportionally with applied base accelerations. It is obvious that increasing PGA increased the nonlinearity in the aseismic layer. For PGA = 0.2 g, the highest $a$ was produced by AP (approx. 10.1 ms$^{-2}$). For PGA = 0.6 g, the highest $a$ was equal for AS, AP, and AA. The effect of adopted aseismic layer thickness on peak acceleration values is relatively small. For some excitations, the highest $a$ was for a thin layer, and for others, it was for a thicker layer. The highest $a$ is related to foundation slipping at the pebble layer top.

In conducted tests, the maximum accelerations and displacements were produced by AS with PGA = 0.6 g and for layer thickness 0.6 m. Based on the aforementioned results, it can be stated that the aseismic layer with $h_p = 0.3$ m showed slightly better behaviour from the aspect of displacement and acceleration. As a thinner aseismic layer requires less excavation below the foundation, less pebbles, and simpler and faster construction, a layer thickness of 0.3 m is more optimal than 0.6 m.

*6.2. Effect of the Pebble Fraction.* The effect of pebble fraction on horizontal displacement $u_2$ is shown in Figure 14, and peak $u_2$ values are shown in Figure 15. It is noticeable that, independent of pebble layer thickness, the results significantly depend on the type of applied excitation and PGA. The global overview of the effect of excitation type and PGA on $u_2$ is considered in Section 6.1 and will not be repeated hereafter.

The time-history displacement curves for all considered fractions are approximately affine, especially for PGA = 0.2 g. The small pebble fraction ($\Phi_b = 4$–$8$ mm) for excitation ABL with PGA = 0.2 g and PGA = 0.6 g produced the smallest $u_2$, whereas AS with PGA = 0.6 g and AP with PGA = 0.2 g produced the largest $u_2$. The medium pebble fraction ($\Phi_b = 8$–$16$ mm), for AS with PGA = 0.2 g and for AP with PGA = 0.6 g produced the largest $u_2$. The large pebble fraction ($\Phi_b = 16$–$32$ mm) had the lowest $u_2$ for AS with PGA = 0.2 g and PGA = 0.6 g and for AP at PGA = 0.6 g. The maximum $u_2$ values of the large pebble fraction were for ABL and AA with PGA = 0.2 g and PGA = 0.6 g.

It is noticeable that the pebble fraction has a complex effect on the size of the model displacement, and no unique law exists. Namely, the maximum $u_2$ values for each adopted pebble fraction depend on the type of applied excitation and PGA. However, all the adopted pebble fractions resulted in similar average model displacements.

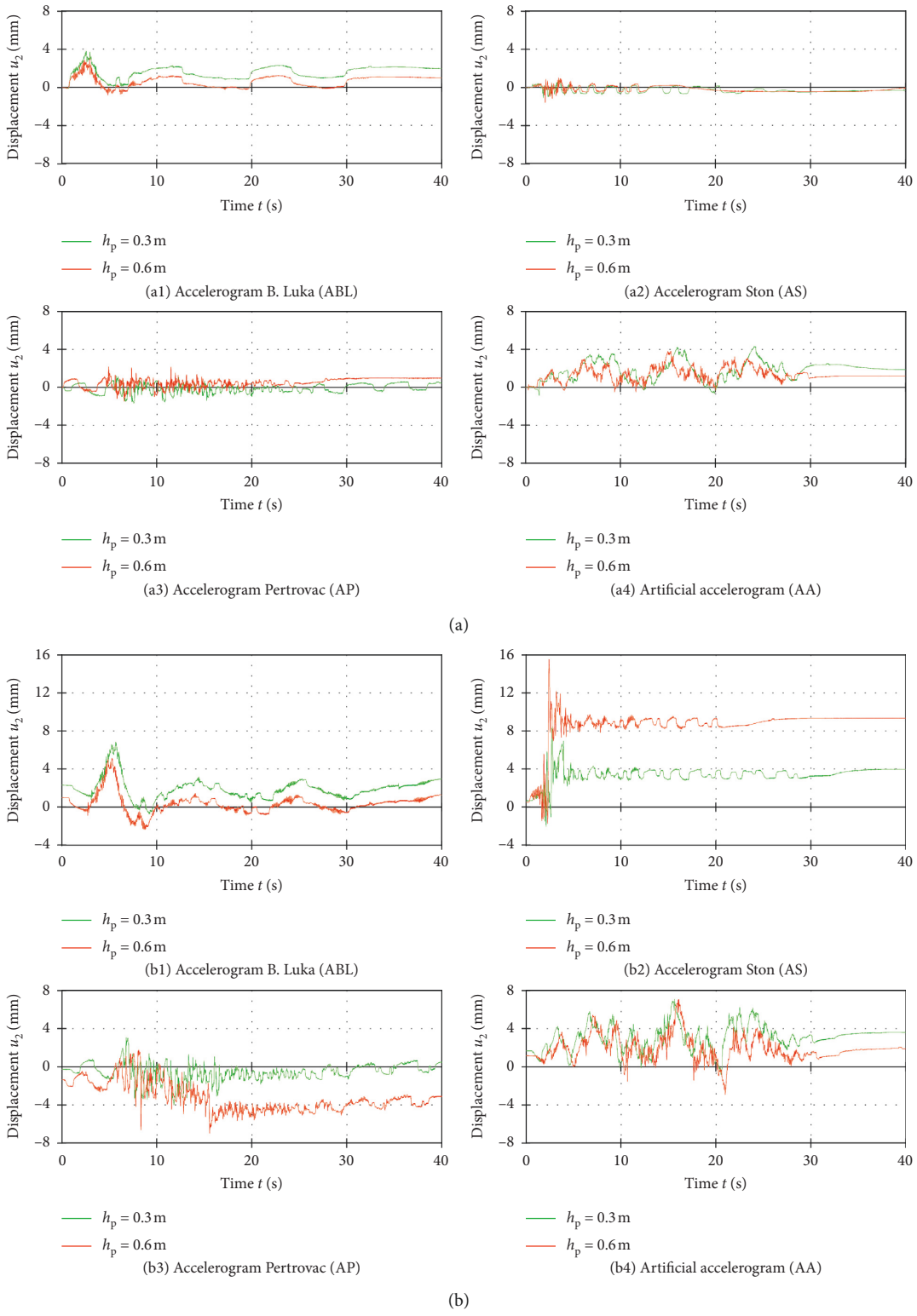


Figure 10: The effect of aseismic layer thickness on horizontal displacement $u_2$. (a) PGA = 0.2 g. (b) PGA = 0.6 g.

The effect of $\Phi_b$ on horizontal acceleration $a$ is shown in Figure 16, and peak acceleration values are shown in Figure 17. Obviously, the discussed $\Phi_b$ also has an impact on model acceleration, but this impact is significantly lower than that for the previously considered model displacements. Namely, the time-history acceleration curves for some $\Phi_b$ are even more affine, and the difference in peak accelerations is significantly lower. It can be stated that all considered $\Phi_b$ generate similar inertial forces in the model for the same excitation and equal PGA. The highest/lowest

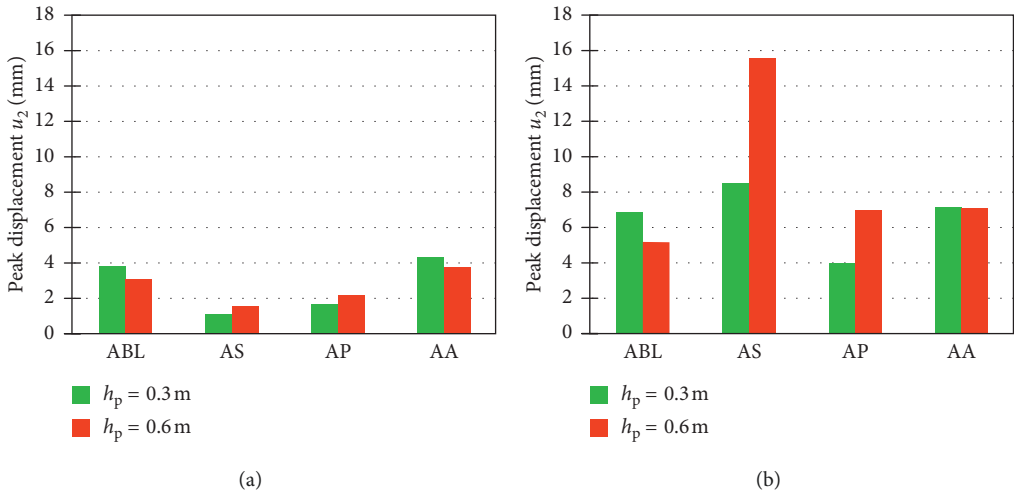


Figure 11: The effect of aseismic layer thickness on peak horizontal displacement $u_2$. (a) PGA = 0.2 g. (b) PGA = 0.6 g.

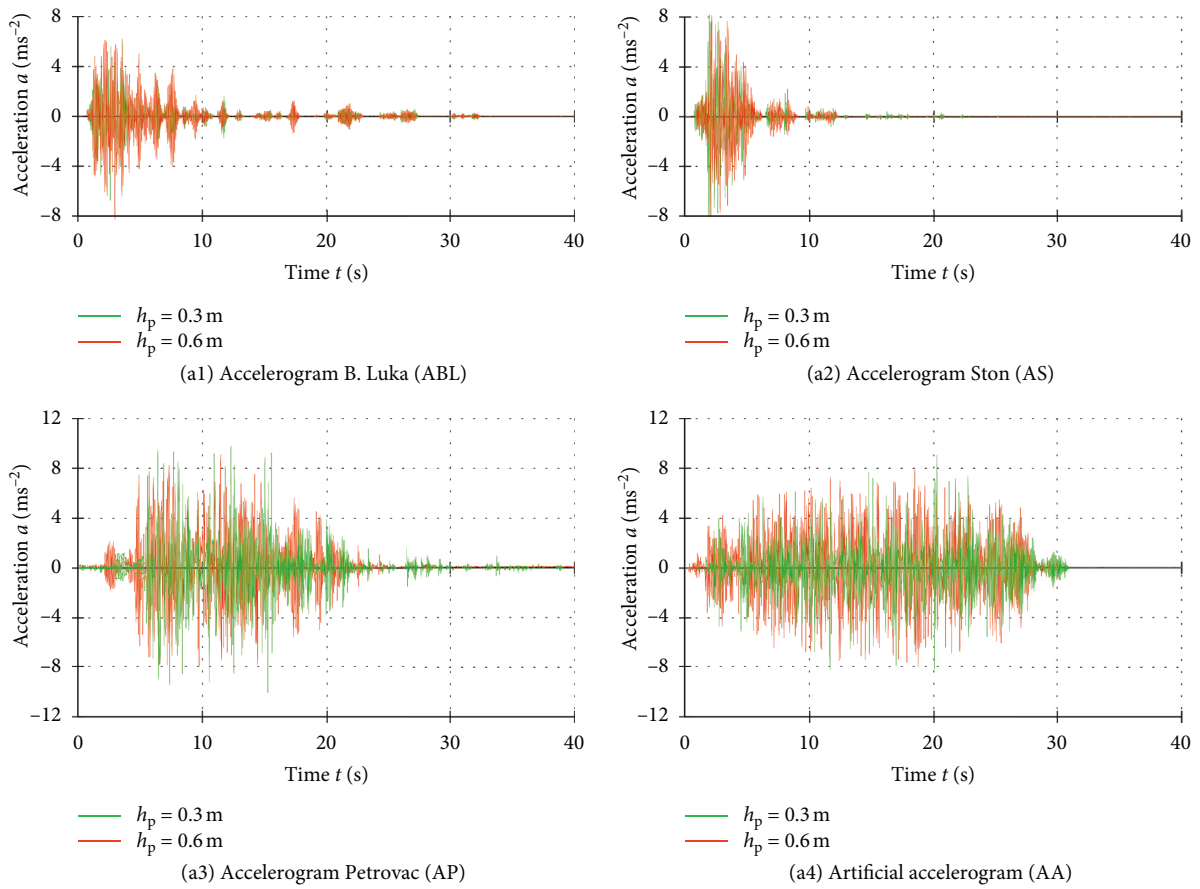


Figure 12: Continued.

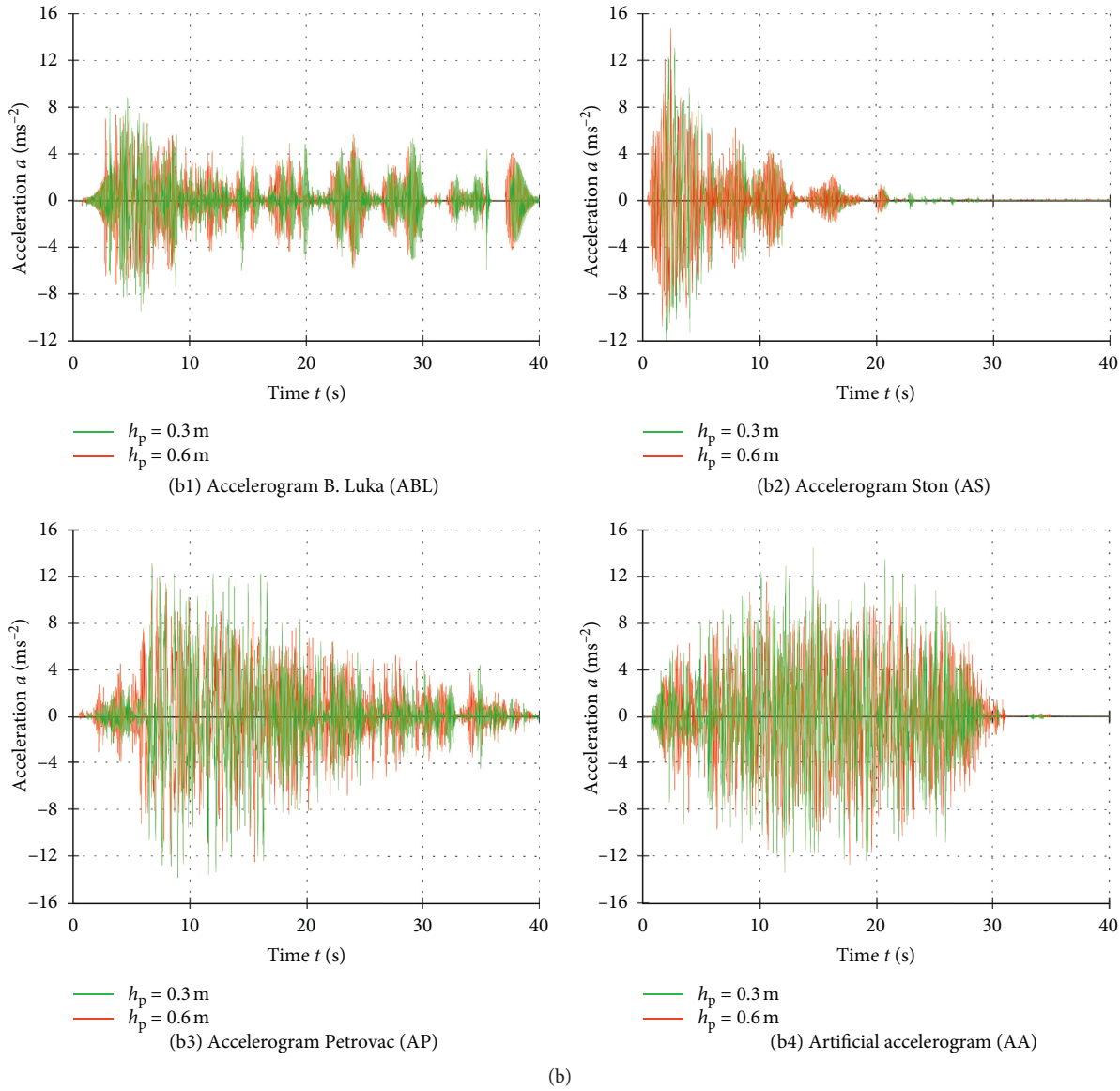


Figure 12: The effect of aseismic layer thicknesses on horizontal acceleration $a$. (a) PGA = 0.2 g. (b) PGA = 0.6 g.

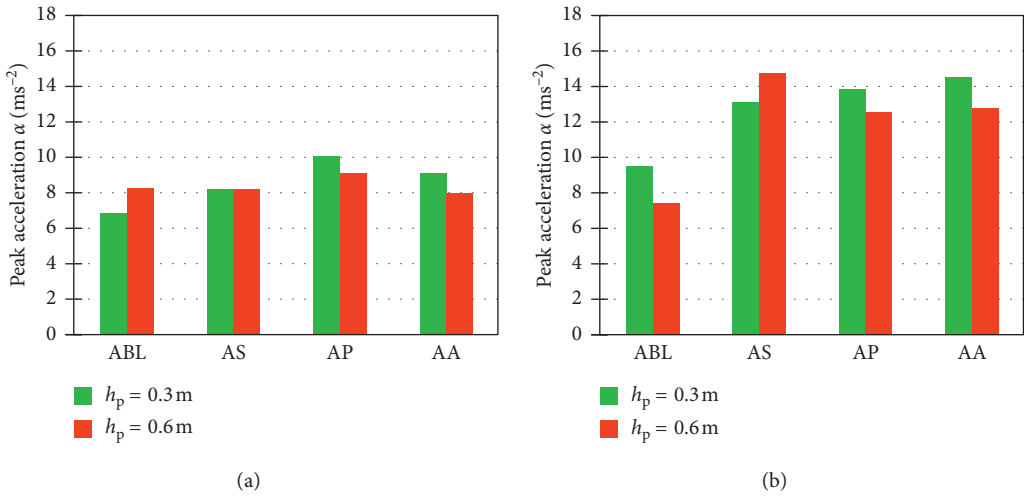


Figure 13: The effect of aseismic layer thicknesses on peak horizontal acceleration $a$. (a) PGA = 0.2 g. (b) PGA = 0.6 g.

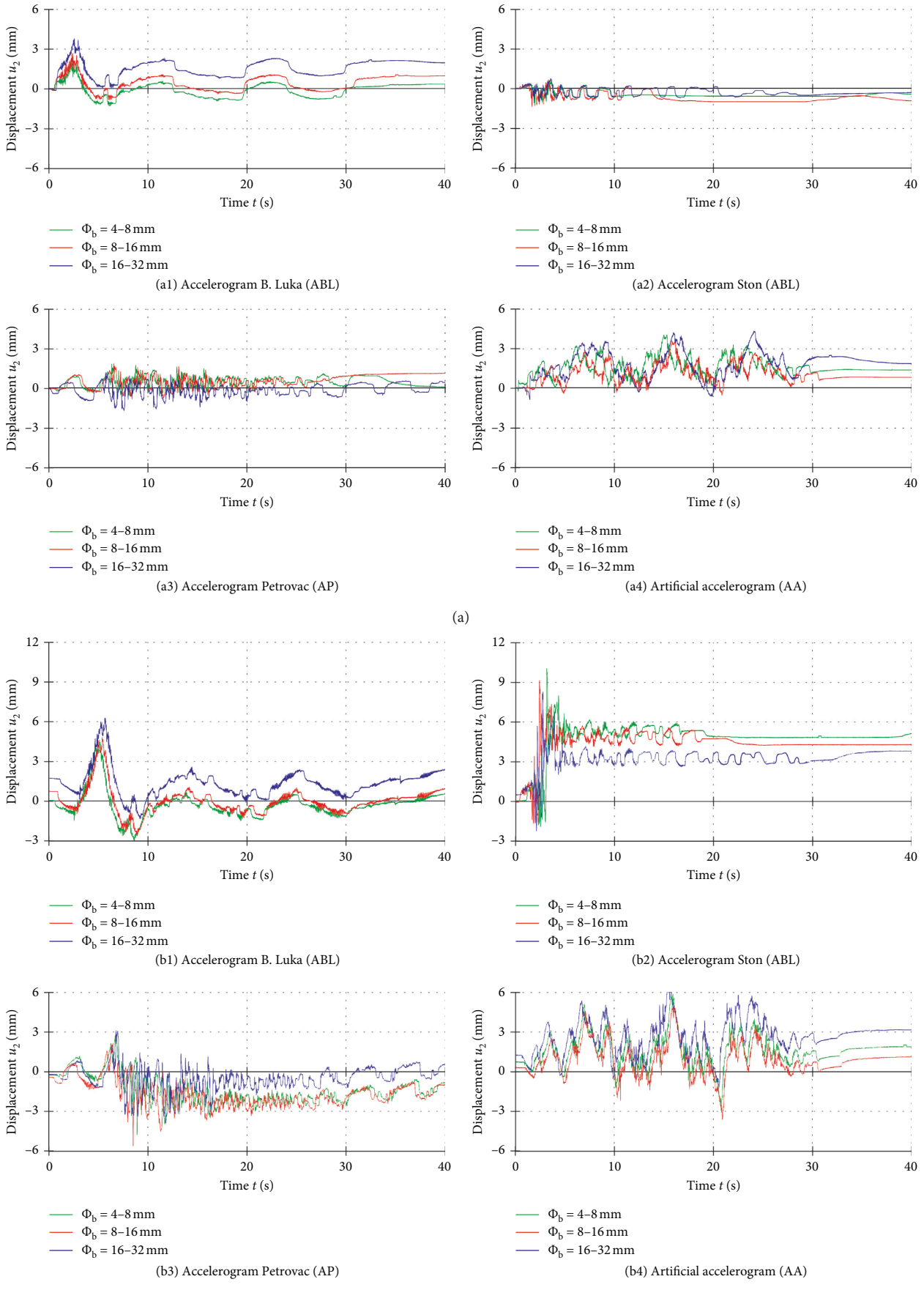


FIGURE 14: The effect of pebble fraction on horizontal displacement $u_2$. (a) PGA = 0.2 g. (b) PGA = 0.6 g.

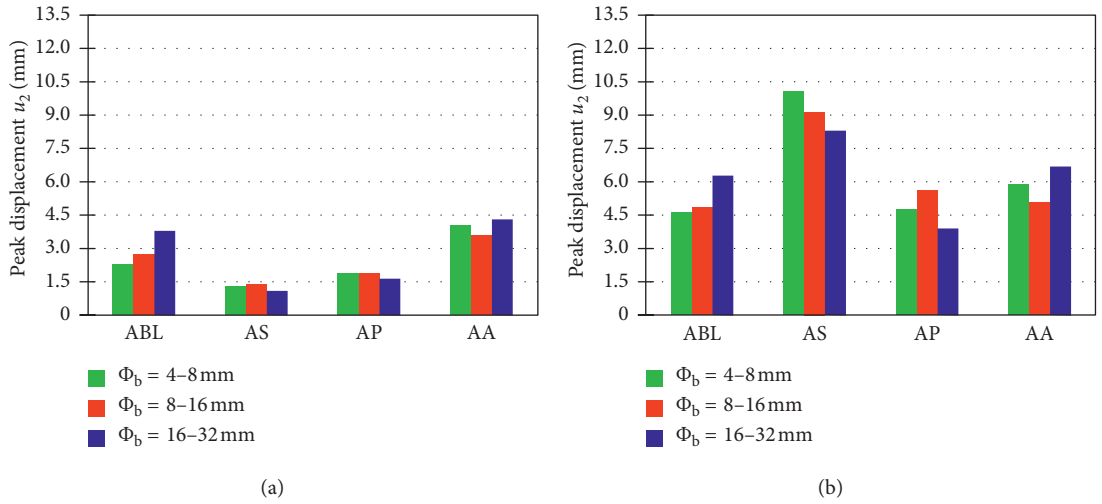


Figure 15: The effect of pebble fraction on peak horizontal displacement $u_2$. (a) PGA = 0.2 g. (b) PGA = 0.6 g.

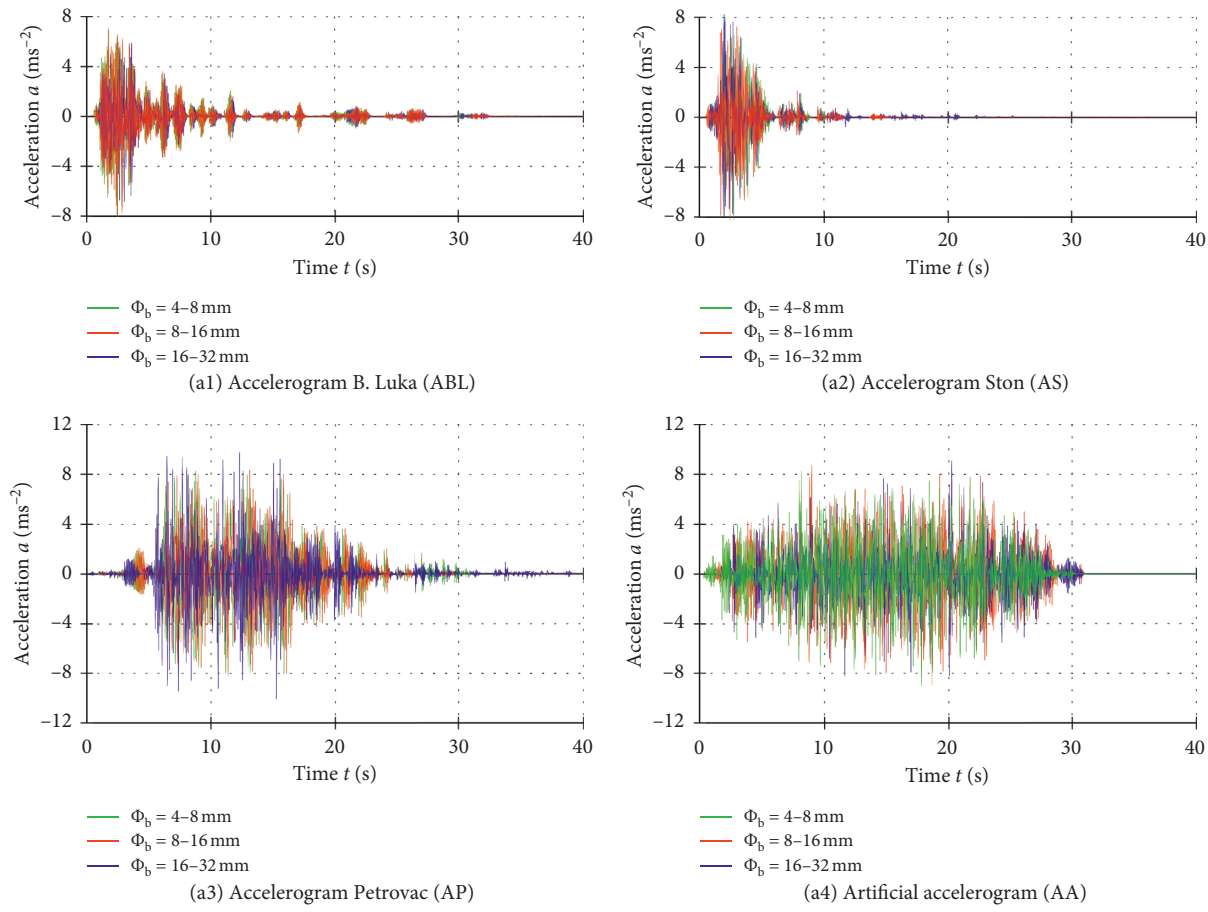


Figure 16: Continued.

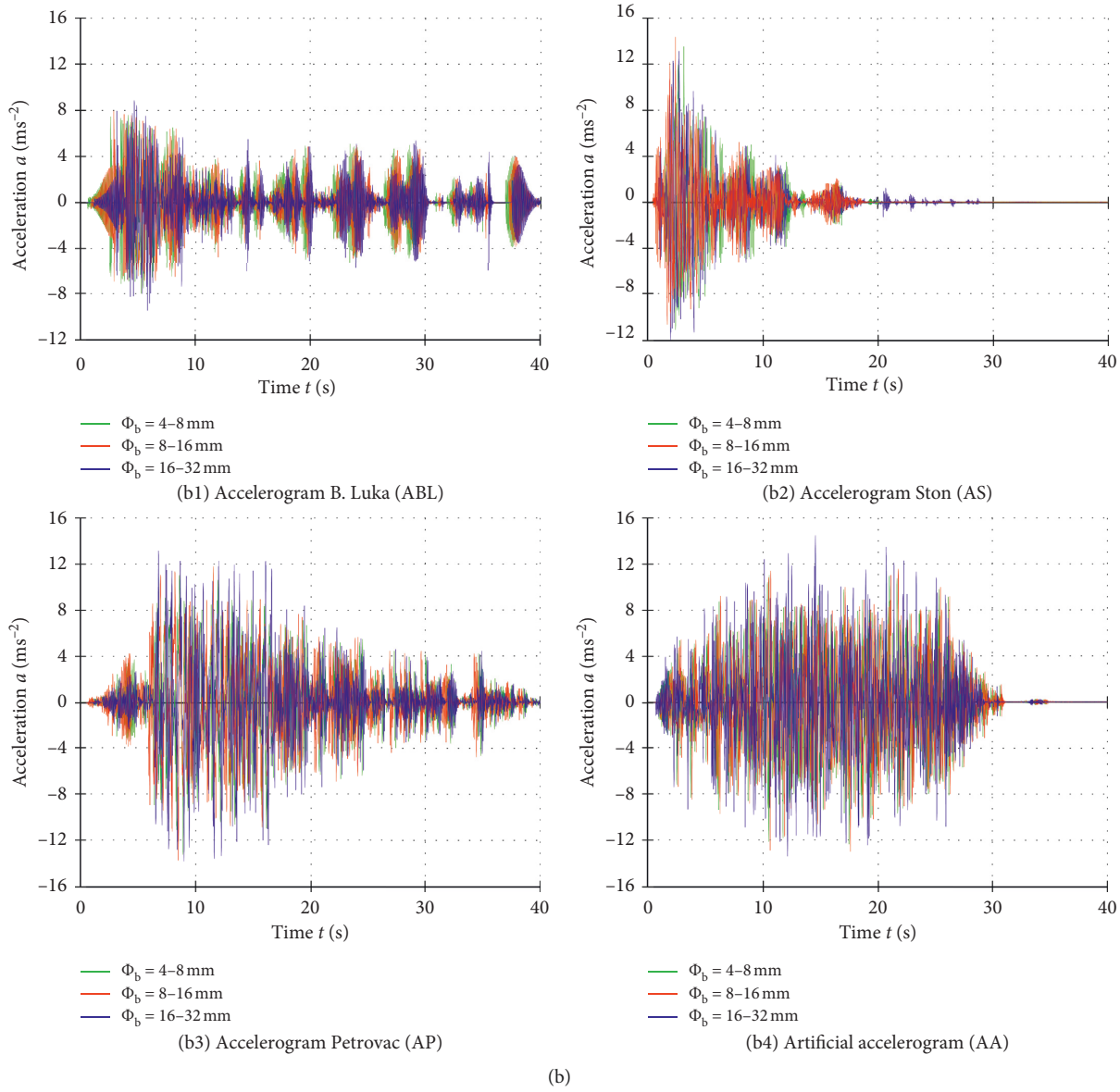


Figure 16: The effect of pebble fraction on horizontal acceleration $a$. (a) PGA = 0.2 g. (b) PGA = 0.6 g.

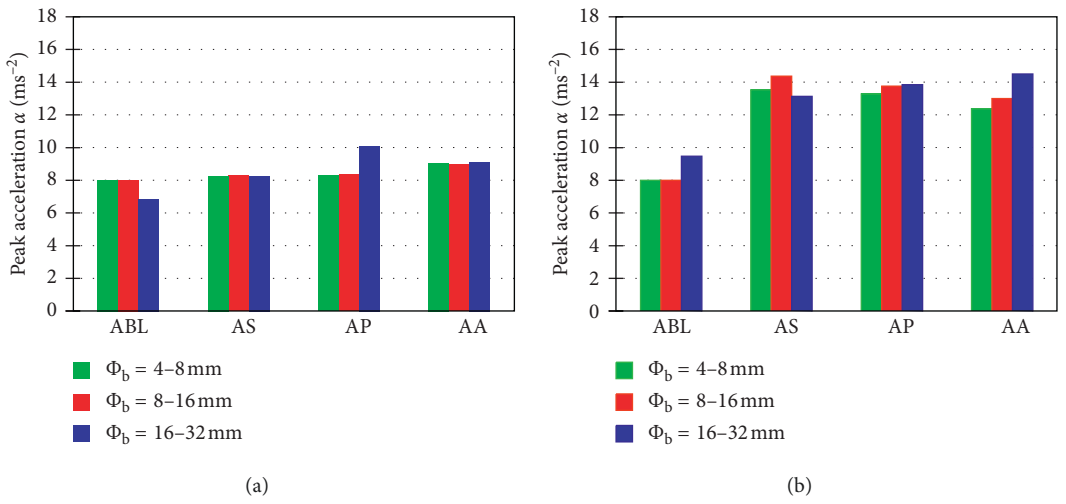


Figure 17: The effect of pebble fraction on peak horizontal acceleration $a$. (a) PGA = 0.2 g. (b) PGA = 0.6 g.

maximum $a$ values for a particular fraction depend on the type of excitation and PGA. Based on the aforementioned results, for $u_2$ and $a$, it can be stated that all considered pebble fractions result in similar displacement and rigid model acceleration. As larger pebble factions are regularly cheaper than smaller fractions, $\Phi_b = 16–32$ mm can be considered more favourable than other pebble factions.

*6.3. Effect of Pebble Layer Compaction.* The time-history $u_2$ curves for adopted test samples are shown in Figure 18, and peak $u_2$ values are shown in Figure 19. The time-history displacement curves are approximately affine for all considered compaction modules. For different compaction modules (MS), excitations with PGA = 0.6 g resulted in a greater difference in maximum $u_2$ (Figure 19) than with PGA = 0.2 g. The largest difference is for AS. The largest $u_2$ values were for the smallest MS (10 MPa), whereas the smallest value was for the highest MS (60 MPa). This was expected because a high MS reduces the aseismic layer bending and shear stiffness.

Horizontal acceleration $a$ is shown in Figure 20, and peak $a$ values are shown in Figure 21. The shape of the time-history acceleration curve depends primarily on the type of excitation and is very similar for all adopted MS values. The maximum $a$ values generally increase with increasing MS, which is expected because a higher MS results in a stiffer substrate.

Based on the aforementioned results, it can be concluded that a smaller MS results in a larger displacement and smaller acceleration of the rigid building. Consequently, it can be stated that lower MS is optimal, with limited maximum displacement, as it reduces construction costs for the aseismic layer. However, a certain level of compactness is necessary for the substrate under the foundation to have sufficient bearing capacity for all relevant structural loads and to minimize pebble layer settlement from long-term load.

*6.4. Effect of Pebble Moisture.* To shorten the paper, only maximum values of displacements $u_2$ and accelerations $a$ are presented. For PGA = 0.2 g, the maximum $u_2$ (Figure 22) slightly depends on pebble moisture, whereas the $u_2$ values were mostly higher for $h = 10\%$ moisture than for $h = 60\%$ moisture. For PGA = 0.6 g, the aseismic layer showed similar behaviour. For ABL and AA excitations, the dry pebble layer ($h = 10\%$) had larger maximum displacement $u_2$, whereas for AS and AP excitations, the wet pebble layer ($h = 60\%$) had the larger maximum displacement.

For PGA = 0.2 g, based on the average values of displacement $u_2$, it can be stated that the dry pebble layer case resulted in larger average displacement $u_2$. At PGA = 0.6 g, both pebble moisture cases resulted in similar maximum displacement $u_2$. In general, the pebble moisture has no major influence on the aseismic layer efficiency.

The average maximum $a$ (Figure 23) for all excitations is higher for dry pebbles. Thus, compared to the wet pebble layer, higher inertial forces are generated for dry pebbles. Based on the aforementioned results, it can be stated that pebble moisture has no major impact on the rigid building model displacement and acceleration. The average acceleration $a$ for all considered excitations was only slightly higher for dry pebbles. Thus, in the case of applying the proposed concept of seismic base isolation, pebble moisture factor would not be relevant to the effectiveness of the considered aseismic concept.

*6.5. Effect of Vertical Contact Stress below the Foundation.* The time-history $u_2$ curves are shown in Figure 24, with peak $u_2$ values shown in Figure 25. At low PGA (0.2 g), the largest $u_2$ was produced by ABL and AA for low contact stress ($\sigma_v = 0.04$ MPa), whereas for excitations AS and AP, the largest $u_2$ was for medium contact stress ($\sigma_v = 0.10$ MPa). At high PGA (0.6 g), the largest $u_2$ for all excitations was for $\sigma_v = 0.10$ MPa. It is obvious that the level of contact stress from gravitational load has a significant impact on the rigid model displacement size, but the behaviour of that effect is complex. However, it can be stated that for the majority of different excitations, the displacements $u_2$ will be larger for high gravitational contact stress.

The effect of vertical contact stress below the foundation on acceleration $a$ is shown on Figure 26, and the peak values of $a$ are shown in Figure 27. At PGA = 0.2 g, the highest $a$ was for $\sigma_v = 0.04$ MPa, followed by $\sigma_v = 0.10$ MPa, and the minimum was for $\sigma_v = 0.20$ MPa. At PGA = 0.6 g, the highest $a$ value depends on excitation type. For $\sigma_v = 0.04$ MPa, the highest $a$ was produced by ABL and AA, whereas for $\sigma_v = 0.20$ MPa, the highest $a$ was produced by AS and AP. Like $u_2$, the effect of contact stress level on acceleration $a$ is ambiguous. For low PGA, it is expected that the low levels of contact stress will produce higher acceleration (lower aseismic layer efficiency). For high PGA, high levels of contact stress produce higher acceleration.

*6.6. Effect of Repeated Excitation on Aseismic Layer Efficiency.* The effect of repeated excitation AS with PGA = 0.6 g on displacement $u_2$ is shown in Figure 28. The increase in overall $u_2$ after the action of each excitation is evident, due to the permanent displacement from the previous excitation. However, the relative displacement for each repeated excitation was approximately equal. With respect to the initial state, the maximum $u_2$ after the first excitation was approximately 14 mm, whereas after the last (sixth) it was approximately 45 mm (i.e., approx. 3.5 times larger). The effect of repeated excitation AA with PGA = 0.6 g on displacement $u_2$ is shown in Figure 29. Compared to the AS case, the model behaviour is analogous, only overall and relative displacement $u_2$ is far smaller for AA. The reason is that AS is a short impact excitation with a more pronounced shear-force effect on the model causing large foundation slipping at the pebble layer top. Excitation AA exerts a longer oscillatory effect with greater bending impact.

The effect of repeated excitation AS with PGA = 0.6 g on acceleration $a$ is shown in Figure 30. It is noticeable that the time-history acceleration curves are affine,

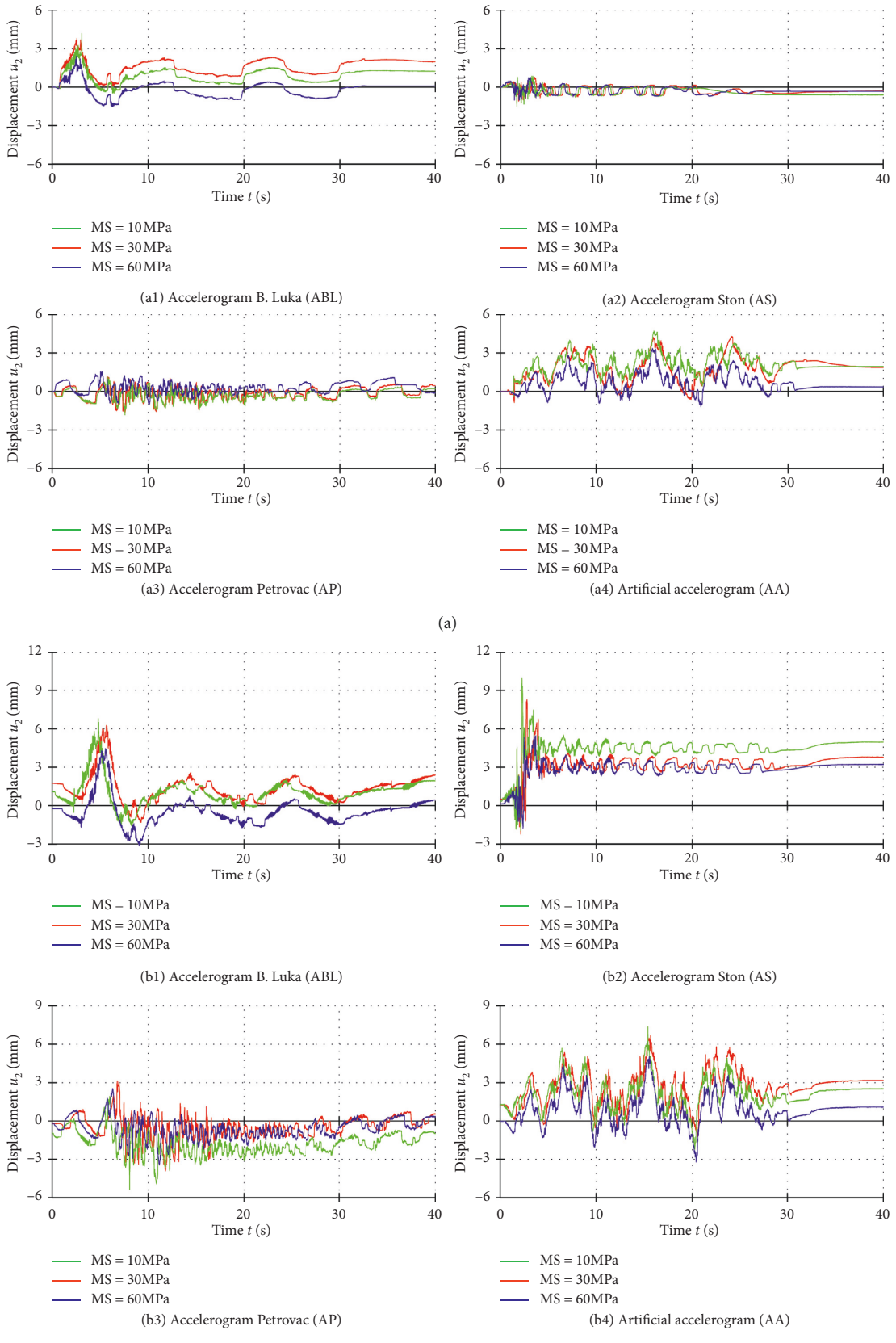


Figure 18: The effect of pebble layer compaction on horizontal displacement $u_2$. (a) PGA = 0.2 g. (b) PGA = 0.6 g.

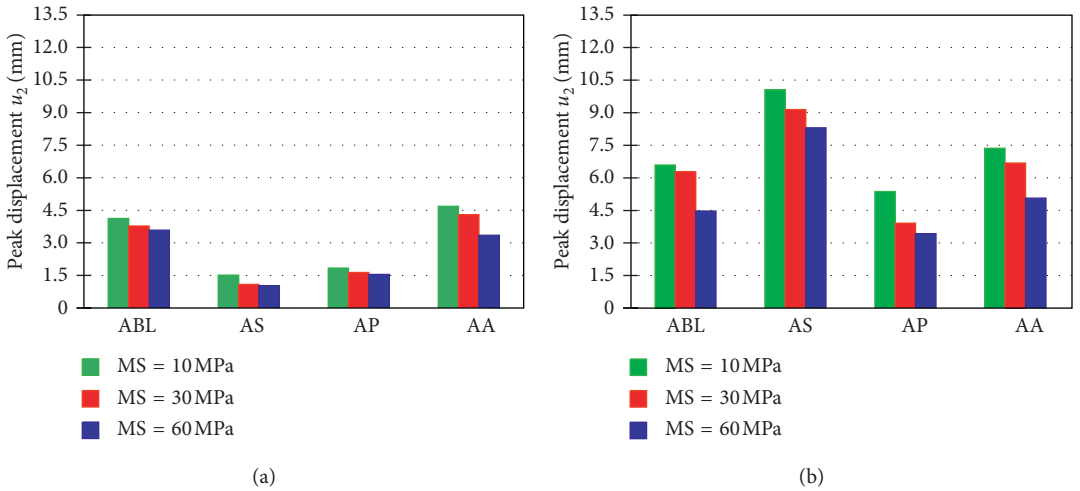


Figure 19: The effect of pebble layer compaction on peak horizontal displacement $u_2$. (a) PGA = 0.2 g. (b) PGA = 0.6 g.

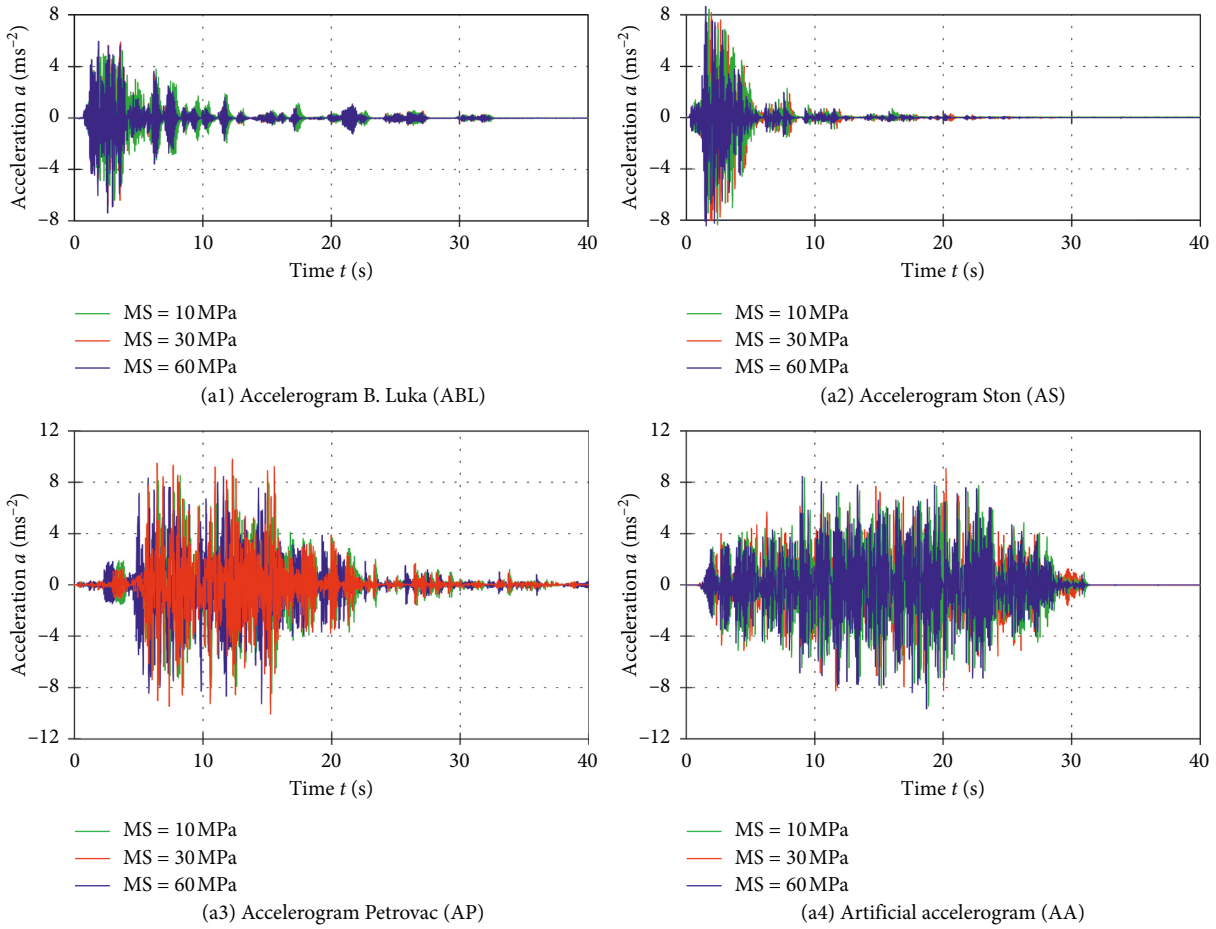


(a)

Figure 20: Continued.

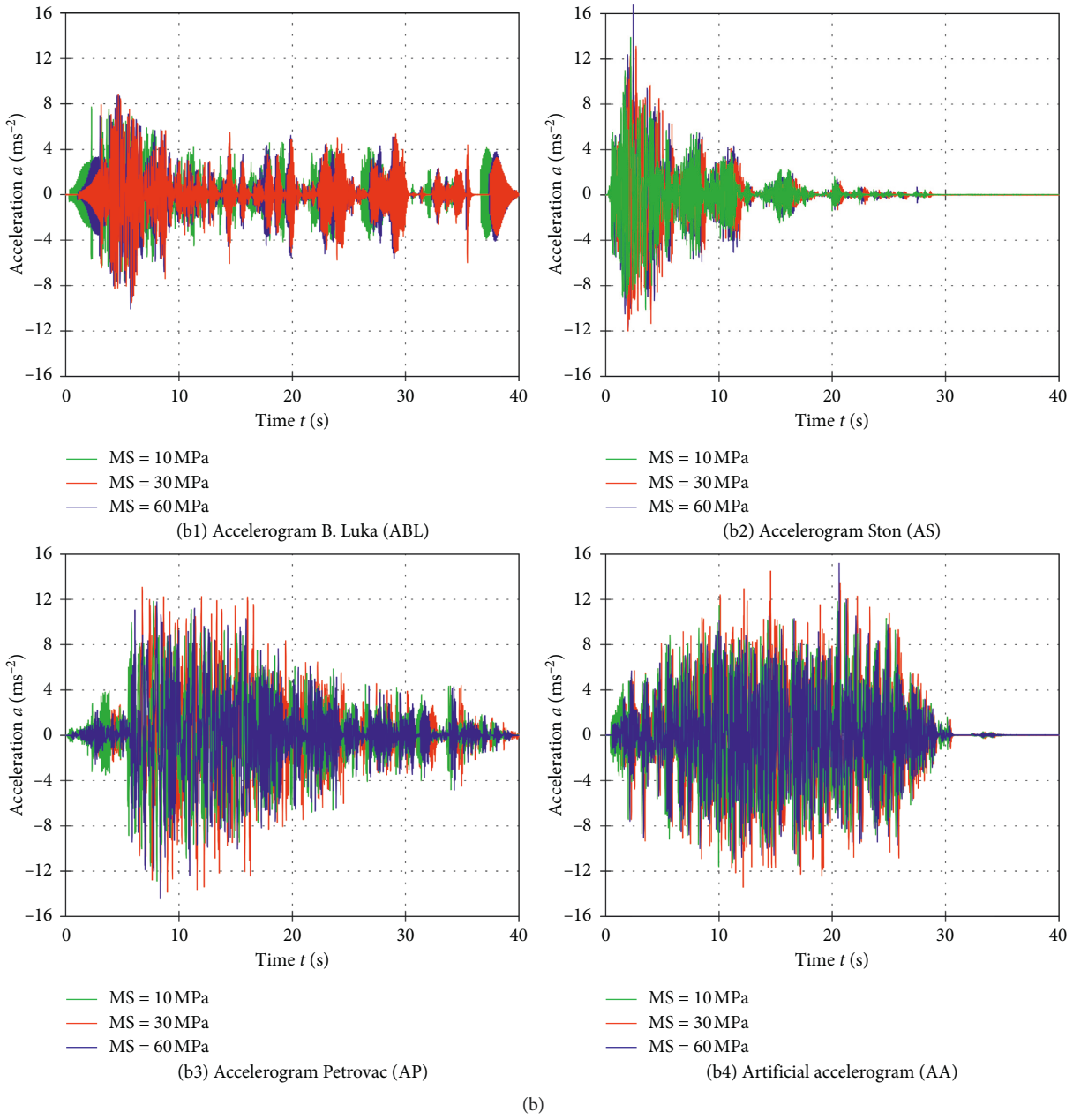


Figure 20: The effect of pebble layer compaction on horizontal acceleration $a$. (a) PGA = 0.2 g. (b) PGA = 0.6 g.

wherein each successive excitation increases the peak acceleration.

At the first excitation, the maximum $a$ was approximately 14.8 ms$^{-2}$, and at the sixth, it was approximately 18 ms$^{-2}$, i.e., an increase of approximately 20%.

The effect of repeated excitation AA with PGA = 0.6 g on $a$ is shown in Figure 31. Obviously, these diagrams are analogous to those in Figure 30, except that here, the largest $a$ increase was only approximately 6%.

It is notable that a large number of strong earthquake repetitions can result in large permanent horizontal displacement and reduce aseismic layer efficiency (increase acceleration). The influence of six equal consecutive strong earthquakes on aseismic layer efficiency was tested, and this can occur very rarely in reality. For that unlikely event, at the end of the most unfavourable considered excitation, the initial displacement increased by approximately 3.5 times and initial maximum acceleration by approximately 20%.

For eliminating the displacement effect, it is necessary that the aseismic layer is sufficiently wider than the foundation. Regarding the reduction of the initial aseismic layer efficiency, it is within acceptable limits even in the case of a large number of strong earthquake repetitions.

The cause of the aforementioned unfavourable aseismic layer behaviour is successive foundation slipping on the pebble layer top and successive foundation penetration into the aseismic layer.

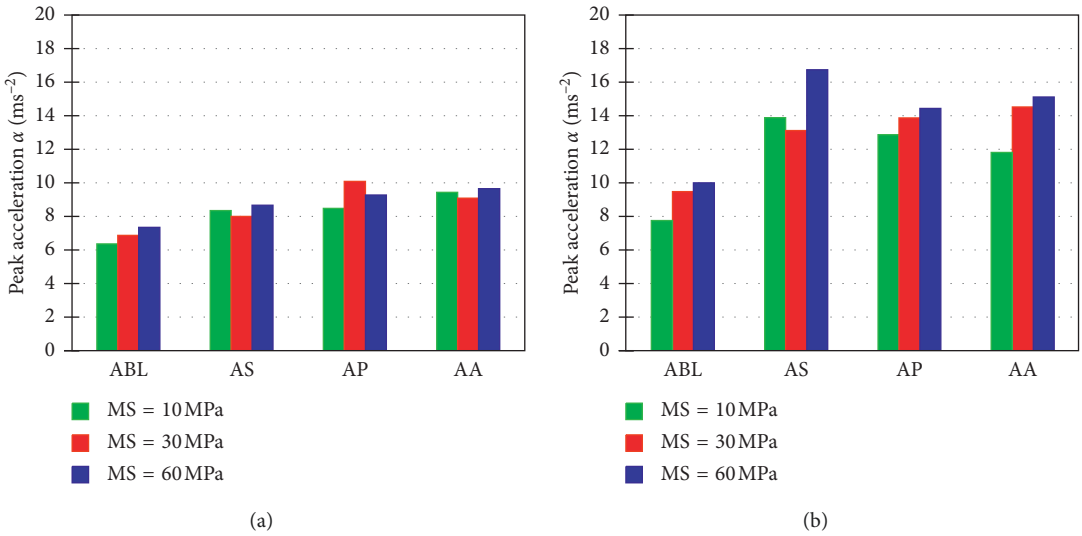


Figure 21: The effect of pebble layer compaction on peak horizontal acceleration $a$. (a) PGA = 0.2 g. (b) PGA = 0.6 g.

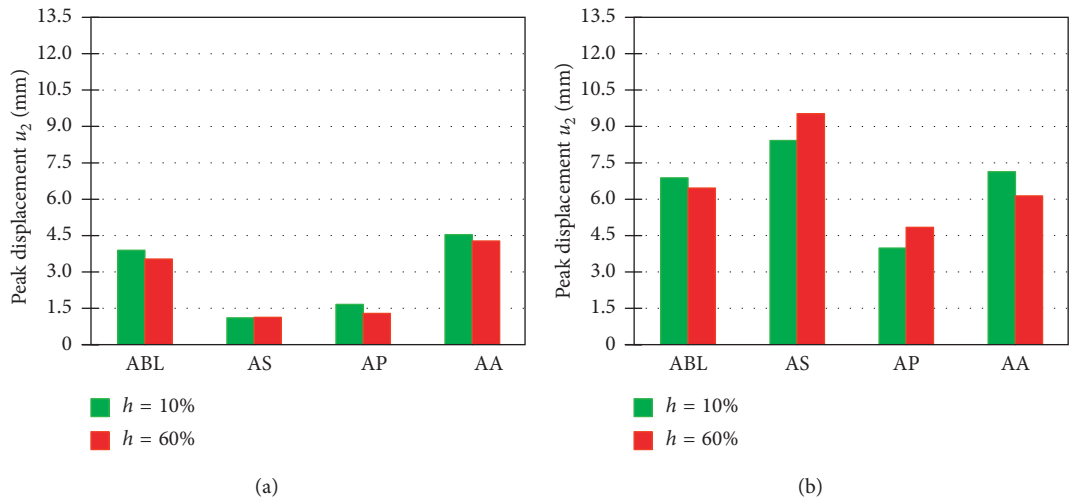


Figure 22: The effect of pebble layer moisture on peak horizontal displacement $u_2$. (a) PGA = 0.2 g. (b) PGA = 0.6 g.

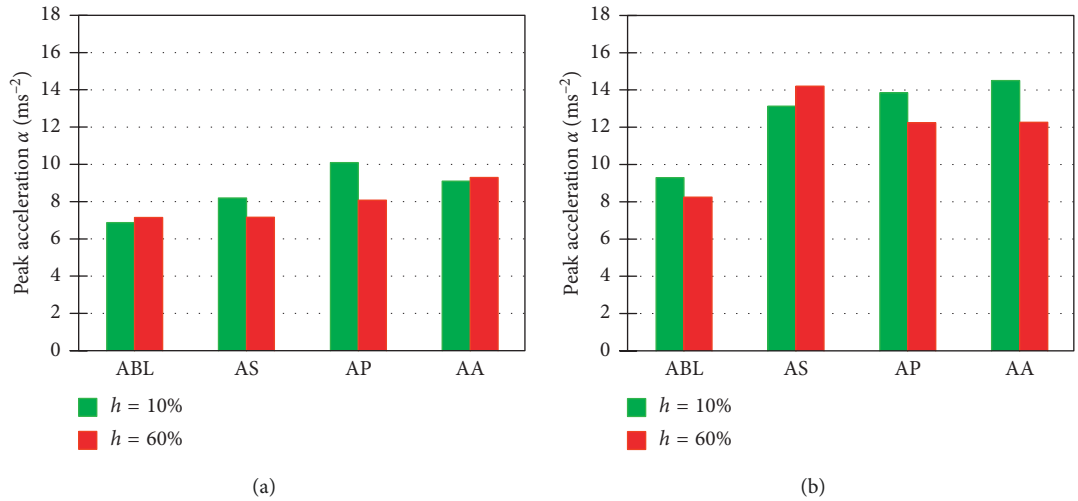


Figure 23: The effect of pebble layer moisture on peak horizontal acceleration $a$. (a) PGA = 0.2 g. (b) PGA = 0.6 g.

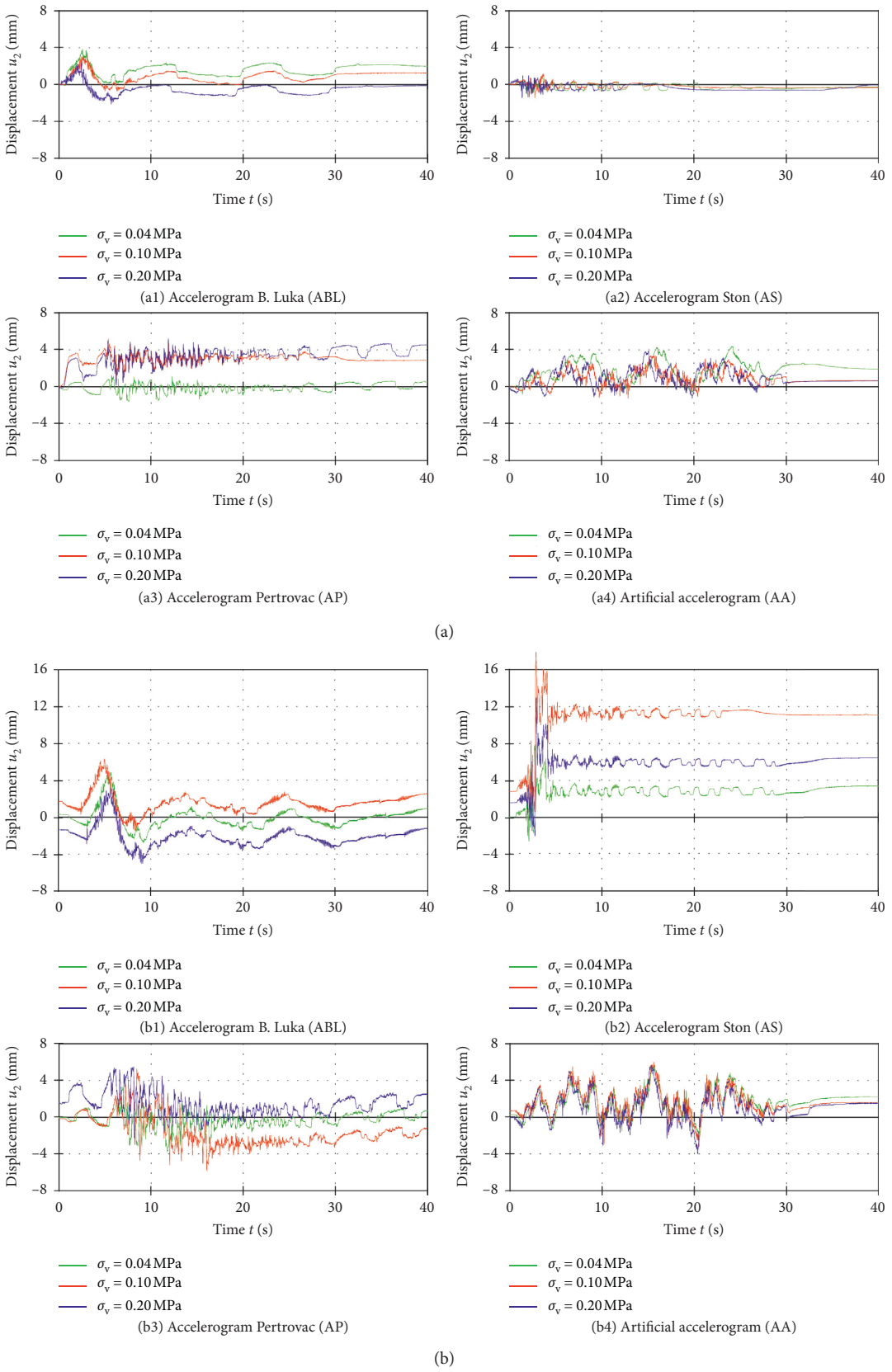


Figure 24: The effect of vertical contact stress below the foundation on horizontal displacement $u_2$. (a) PGA = 0.2 g. (b) PGA = 0.6 g.

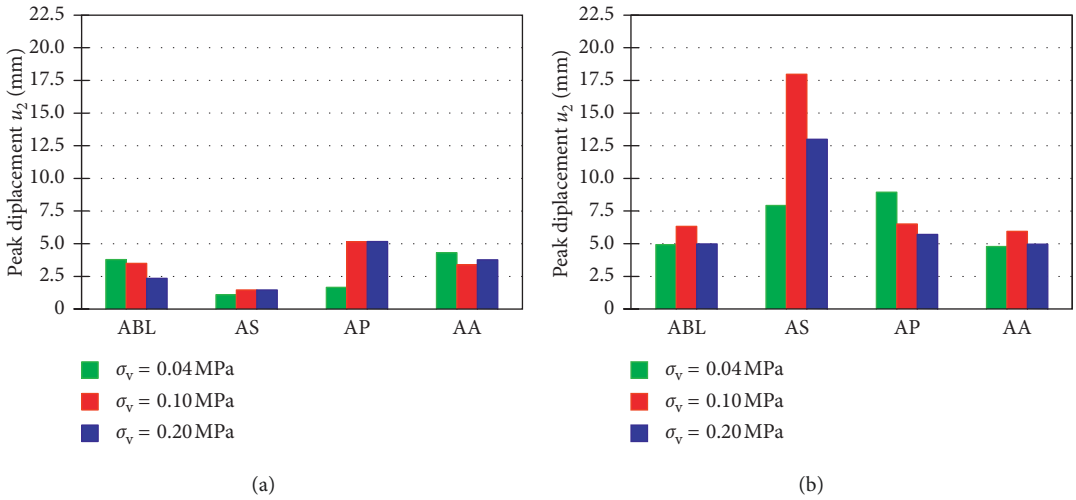


Figure 25: The effect of vertical contact stress below the foundation on peak horizontal displacement $u_2$. (a) PGA = 0.2 g. (b) PGA = 0.6 g.

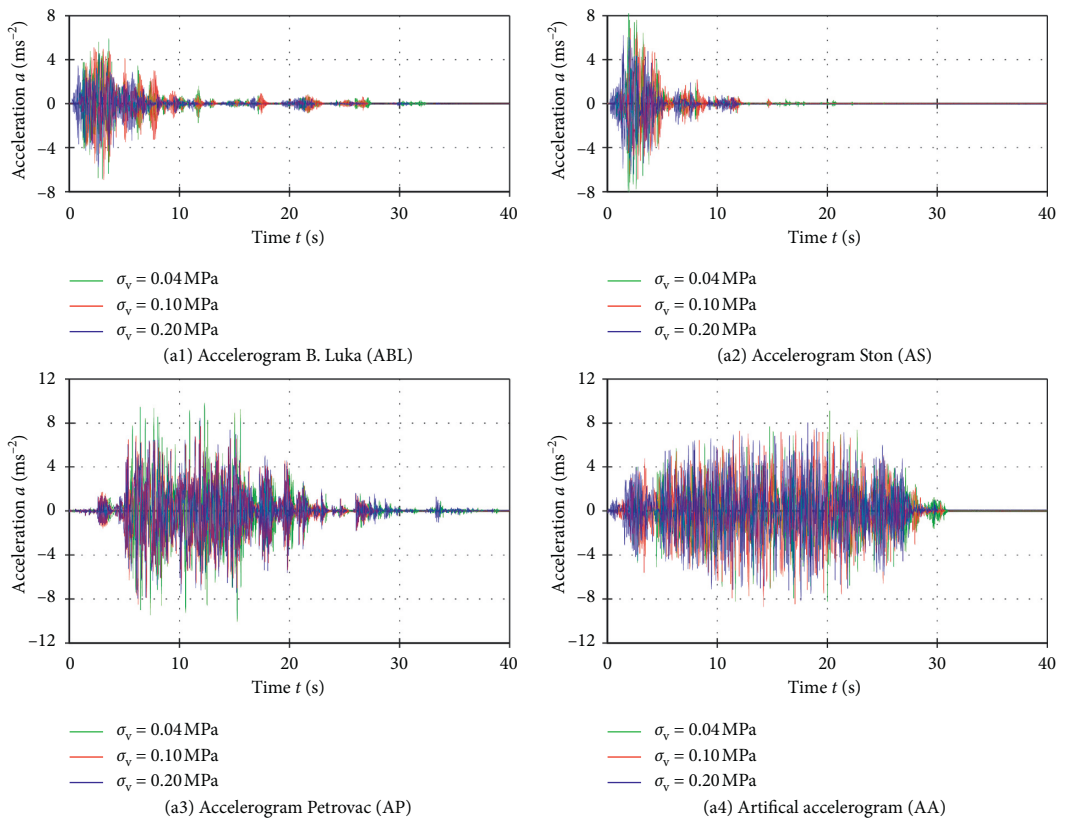


(a)

Figure 26: Continued.

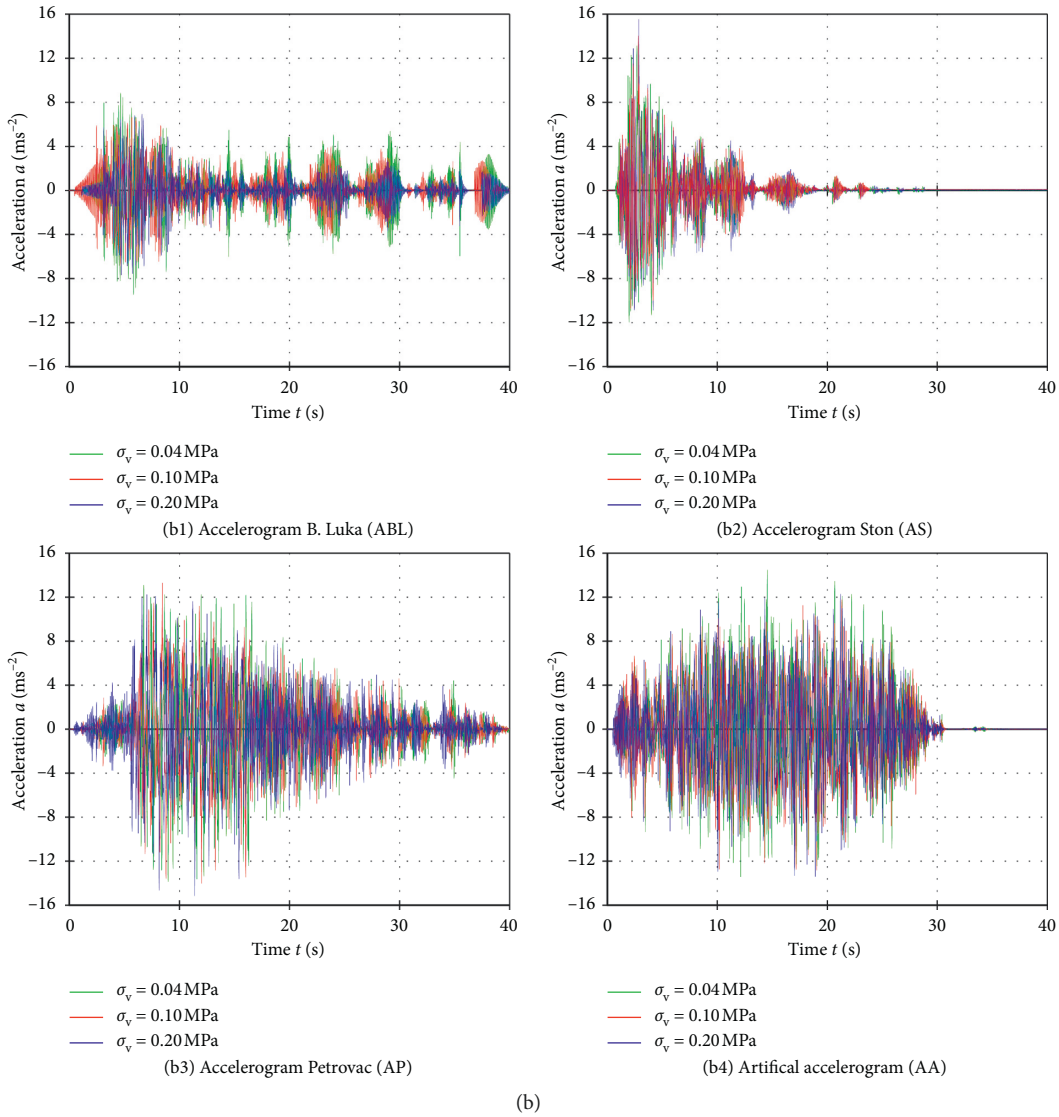


Figure 26: The effect of vertical contact stress below the foundation on horizontal acceleration $a$. (a) PGA = 0.2 g. (b) PGA = 0.6 g.

The effects of repeated excitation AS with PGA = 0.6 g on vertical displacements $v_1$ and $v_2$ are shown in Figure 32. It is notable that the permanent total displacement (settlement) $v_1 = 9.1$ mm and $v_2 = 13.3$ mm remained after the sixth repetition. Different $v_1$ and $v_2$ indicate that a steady angle of rigid model rotation (tilt) has occurred. In the successive repetition of the excitation, substrate compaction and vertical displacement reduction occurred. As the largest vertical displacement is approximately 4.3% of the aseismic layer thickness, this effect can be practically ignored. The effect of repeated excitation AA on vertical displacements $v_1$ and $v_2$ is significantly smaller (Figure 33).

## 7. Conclusions

Previous research [27] has suggested that a natural stone pebble layer below the foundation can significantly reduce strain/stresses of stiff and medium-stiff building models under earthquake load. Namely, depending on the type of applied excitation and some other parameters, compared to the rigid base case, a pebble layer reduced the strain/stress in the MSB model from 28% to 53% and in the MSSB model from 8% to 47%.

However, the practical application of this concept requires further research. This paper presents experimental study results regarding the effect of several stone pebble layer parameters on layer aseismic efficiency. The main conclusions are outlined below:

(i) Generally, aseismic layer efficiency and the effects of all observed layer parameters are significantly dependent on the type of applied excitation and PGA.

(ii) Regarding the effect of aseismic layer thickness ($h_p = 0.3$ m and $h_p = 0.6$ m), thinner layers had more favourable response for some excitations, whereas for others it was opposite. The aseismic layer is considered more efficient if the generated

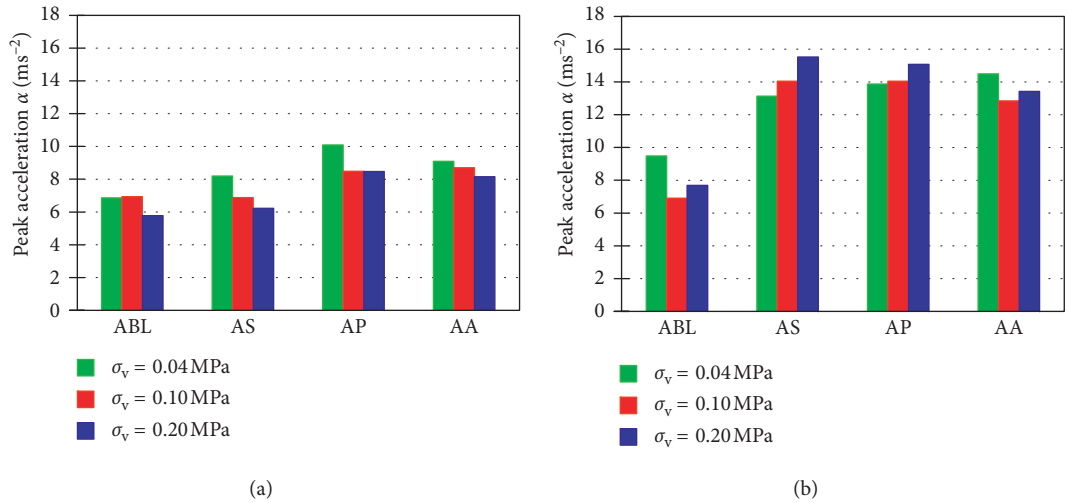


Figure 27: The effect of vertical contact stress below the foundation on peak horizontal acceleration $a$. (a) PGA = 0.2 g. (b) PGA = 0.6 g.

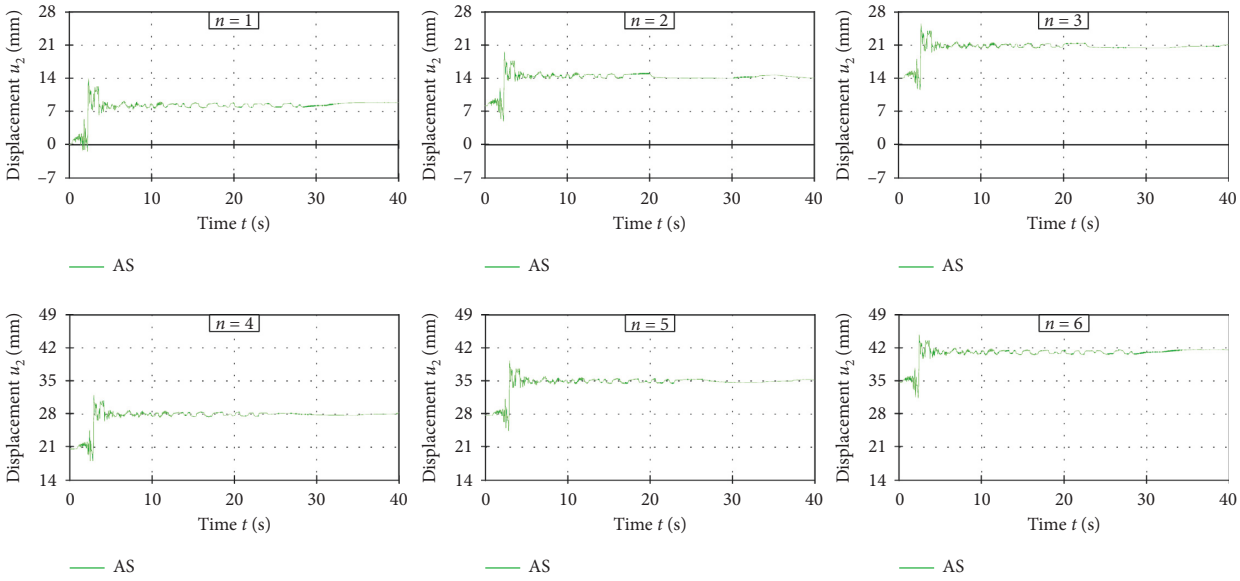


Figure 28: Horizontal displacement $u_2$ for repeated excitation AS.

accelerations (inertial forces) are lower and the displacements have acceptable values. As the aseismic effectiveness of the considered layers was almost equal, for rationality and faster construction, a thinner layer is considered more favourable.

(iii) In terms of the effect of the considered pebble fraction ($\Phi_b$ = 4–8 mm, $\Phi_b$ = 8–16 mm, and $\Phi_b$ = 16–32 mm), different pebble fractions result in similar model displacements and accelerations, i.e., have the same efficiency. The fraction $\Phi_b$ = 16–32 mm is considered optimal because it is cheaper than smaller fractions.

(iv) Regarding the effect of the pebble layer compaction modulus (MS = 10 MPa, MS = 30 MPa, and MS = 60 MPa), a lower MS results in smaller model accelerations and larger displacements. The test results show that different MS values do not result in significant differences in model displacements and accelerations. Therefore, a lower compaction modulus can be considered more favourable, if the structure displacements are within acceptable limits. A certain level of compactness is necessary for the substrate under the foundation to have sufficient bearing capacity for all relevant structural loads and limited displacements in the case of earthquake load.

(v) In terms of the effect of pebble moisture ($h$ = 10% and $h$ = 60%), slightly higher inertial forces are generated for dry pebbles, whereas the model displacements are similar. It can be stated that pebble moisture has no major impact on the pebble layer aseismic efficiency but may be relevant to

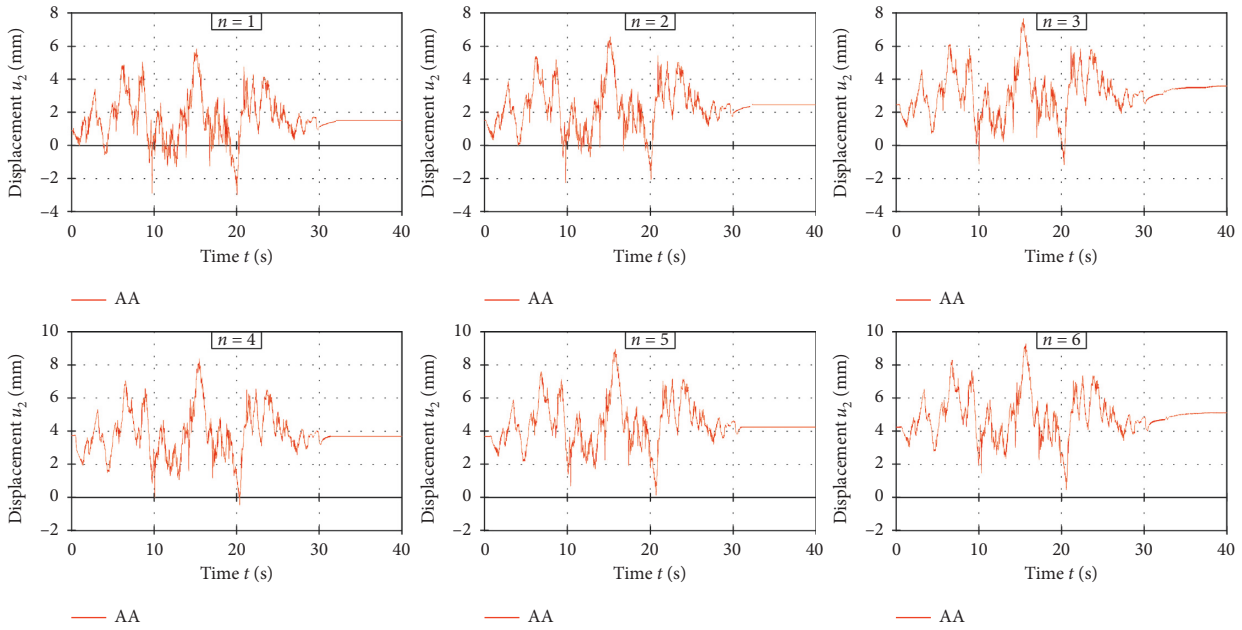


Figure 29: Horizontal displacement $u_2$ for repeated excitation AA.

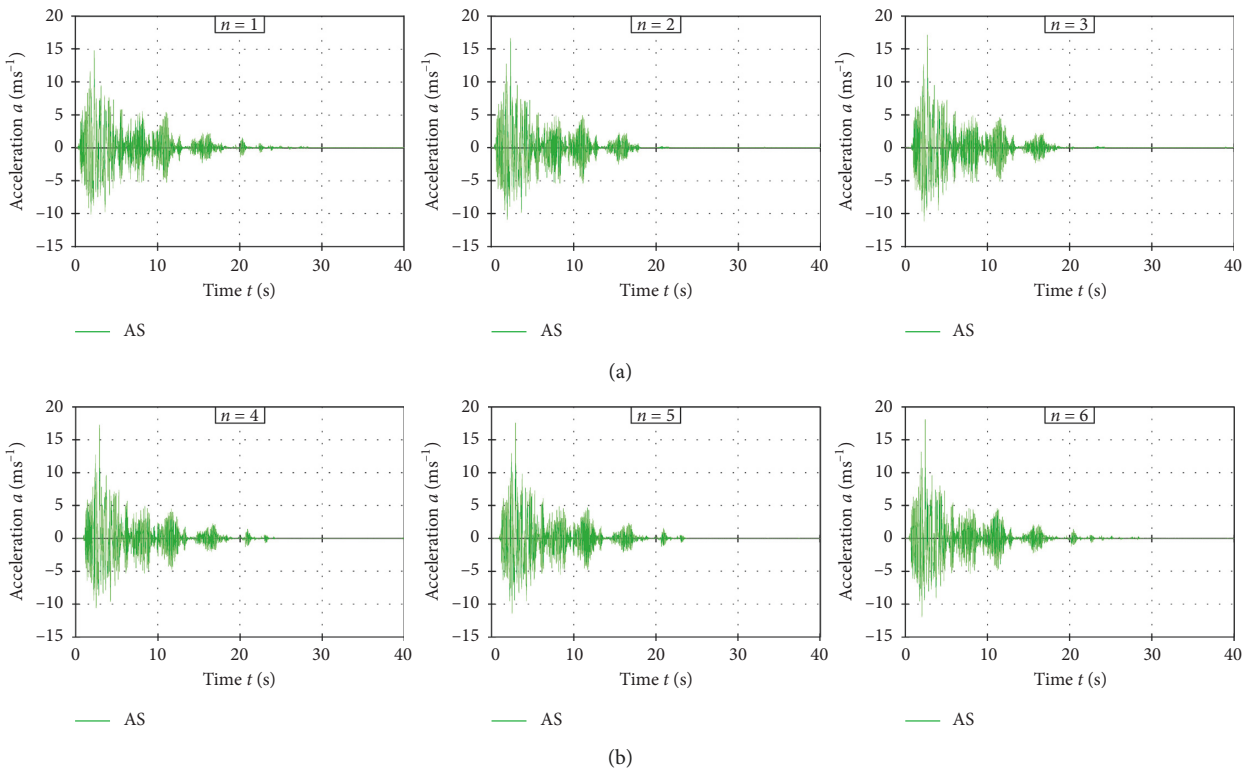


Figure 30: Horizontal acceleration $a$ for repeated excitation AS.

more easily achieving the required layer compaction modulus.

(vi) Regarding the effect of gravitational load contact stress level ($\sigma_v = 0.04$ MPa, $\sigma_v = 0.10$ MPa, and $\sigma_v = 0.20$ MPa), it cannot be precisely defined even for the same excitation. The probable reason is the inconsistency of the declared initial compaction modulus on the entire surface of the aseismic layer, as well as the change of compactness during each excitation. For low PGA values, it can be expected that low levels of contact stress produce higher accelerations (lower aseismic layer efficiency). For high PGA, high levels of contact stress produce higher accelerations.

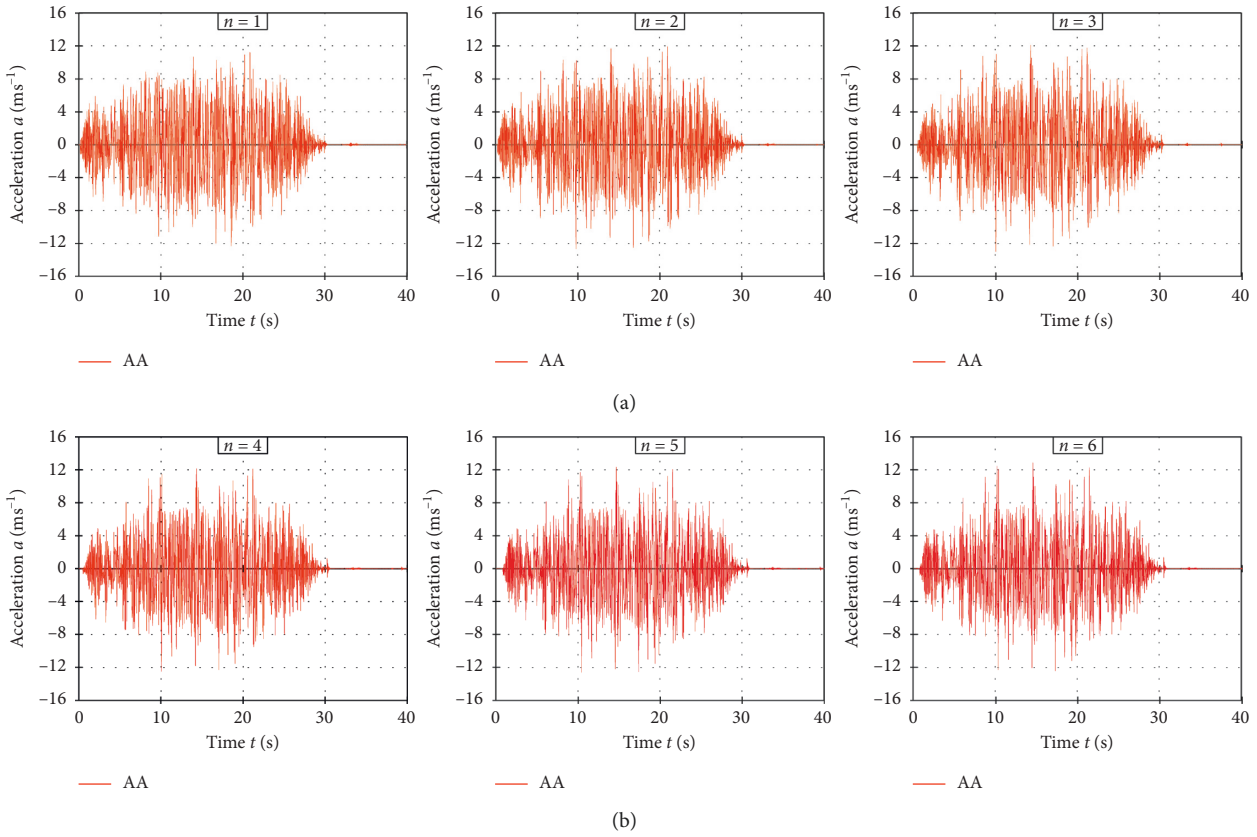


Figure 31: Horizontal acceleration $a$ for repeated excitation AA.

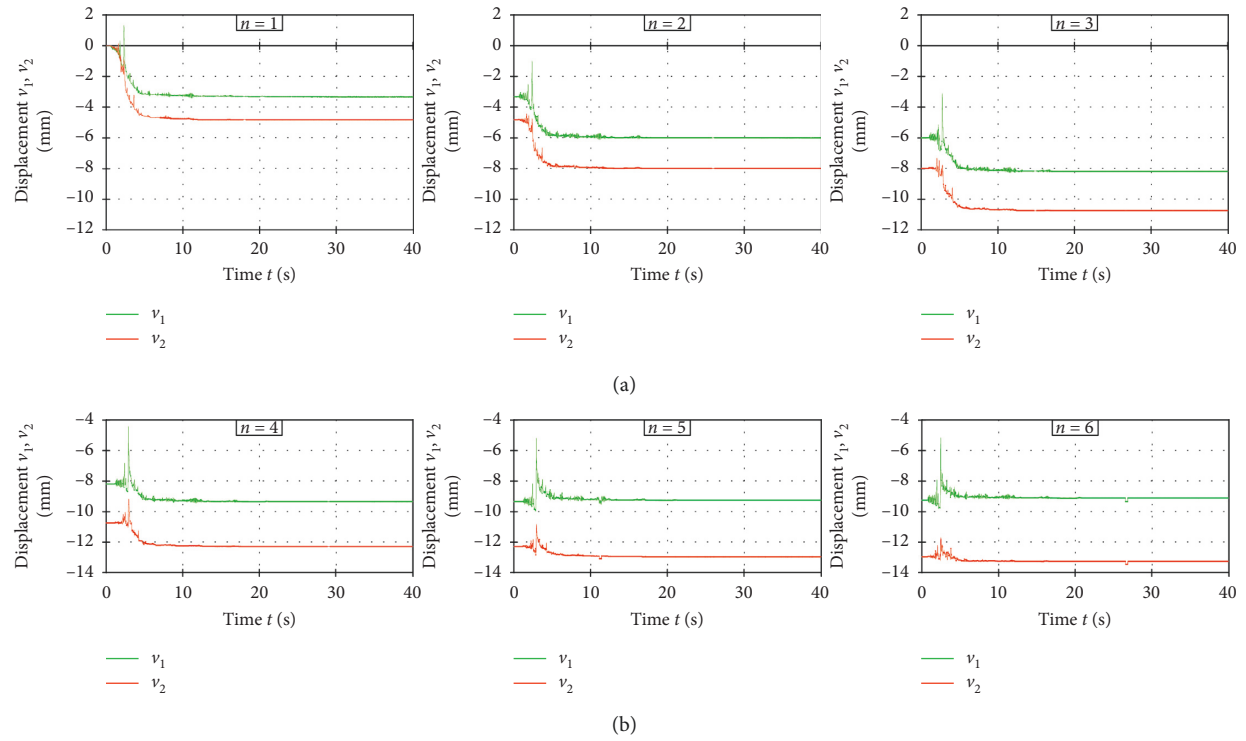


Figure 32: Vertical displacements $v_1$ and $v_2$ for repeated excitation AS.

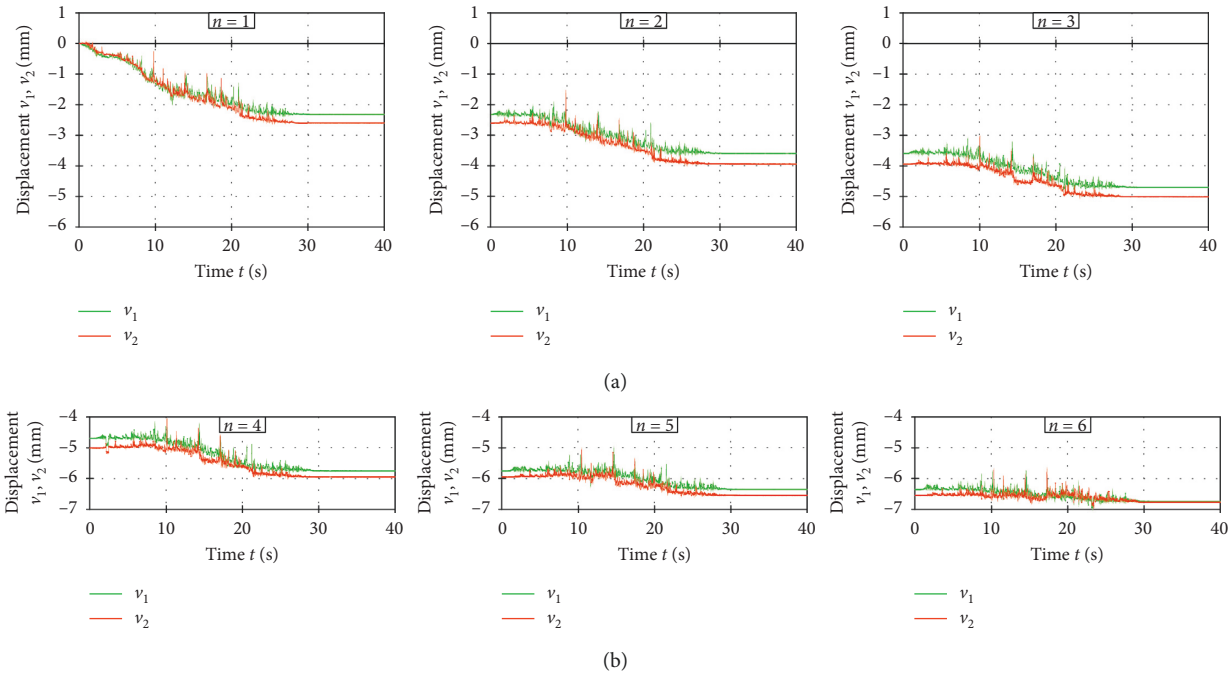


Figure 33: Vertical displacements $v_1$ and $v_2$ for repeated excitation AA.

(vii) For the effect of successive strong earthquake repetition (six consecutive repeats of two different types of earthquakes with PGA = 0.6 g), the conducted tests have shown that large permanent horizontal building displacement can occur (up to 3.5 times the initial displacement) and increase the initial building horizontal acceleration (up to 20%), i.e., reduction of aseismic layer efficiency. The impact of accumulated horizontal displacements can be annulled by an adequate extension of the aseismic layer in relation to the foundation. Aseismic layer efficiency reduction can be considered acceptable, even in the case of large strong earthquake repetitions. Vertical settlement and building tilt can occur in strong earthquake repetition, but this impact can be practically neglected.

## Abbreviations

$a$: Horizontal acceleration of the mass centre
$a_g$: Ground (shake-table) acceleration
$a_{g,max}$: Peak ground (shake-table) acceleration
$b$: Width of the model foundation
$h$: Pebble layer moisture
$h_p$: Pebble layer thickness
MS: Compaction modulus of the pebble layer
$u$: Displacement
$u_1$: Horizontal displacement of the model foundation
$u_2$: Horizontal displacement of the mass centre
$v$: Velocity
$v_1$: Vertical displacement of the model on left side
$v_2$: Vertical displacement of the model on right side
$\sigma_v$: Vertical contact stress on top of the aseismic layer
$\Phi_b$: Pebble fraction.

## Data Availability

All data underlying the findings of the study are presented in this paper.

## Conflicts of Interest

The authors declare that there are no conflicts of interest regarding the publication of this paper.

## Acknowledgments

This work was fully supported by the Croatian Science Foundation under the project "Seismic base isolation of a building by using natural materials: shake-table testing and numerical modelling" (IP-06-2016-5325). The work of doctoral student Ivan Banović was fully supported by the "Young researchers' career development project: training of doctoral students" of the Croatian Science Foundation funded by the European Union from the European Social Fund. The authors are grateful for the support.

## References

[1] N. Makris, "Seismic isolation: early history," *Earthquake Engineering & Structural Dynamics*, vol. 48, no. 2, pp. 269–283, 2018.

[2] S. J. Patil, G. R. Reddy, R. Shivshankar, R. Babu, B. R. Jayalekshmi, and B. Kumar, "Seismic base isolation for structures using river sand," *Earthquakes and Structures*, vol. 10, no. 4, pp. 829–847, 2016.

[3] J. Radnić, N. Grgić, D. Matešan, and G. Baloević, "Shake table testing of reinforced concrete columns with different layout size of foundation," *Materialwissenschaft und Werkstofftechnik*, vol. 46, no. 4-5, pp. 348–367, 2015.

[4] I. Banović, J. Radnić, N. Grgić, and D. Matešan, "The use of limestone sand for the seismic base isolation of structures," *Advances in Civil Engineering*, vol. 2018, Article ID 9734283, 12 pages, 2018.

[5] F. M. Tehrani and A. Hasani, "Behaviour of Iranian low rise buildings on sliding base to earthquake excitation," in *Proceedings of the 11th World Conference on Earthquake Engineering,* Paper 1433, Acapulco, Mexico, June 1996.

[6] X. Zhao, Q. Zhang, Q. Zhang, and J. He, "Numerical study on seismic isolation effect of gravel cushion," in *Proceedings of the 7th International Conference on Discrete Element Methods*, vol. 188, pp. 1055–1063, Dalian, China, August 2016.

[7] A. Pecker, J. H. Prevost, and L. Dormieux, "Analysis of pore pressure generation and dissipation in cohesionless materials during seismic loading," *Journal of Earthquake Engineering*, vol. 5, no. 4, pp. 441–464, 2001.

[8] A. Pecker, "Aseismic foundation design process, lessons learned from two major projects: the Vasco de Gama and the Rion Antirion bridges," in *Proceedings of the ACI International Conference on Seismic Bridge Design and Retrofit*, La Jolla, CA, USA, 2003.

[9] J. S. Steenfelt, B. Foged, and A. H. Augustesen, "Izmit Bay Bridge-geotechnical challenges and innovative solutions," *International Journal of Bridge Engineering (IJBE)*, vol. 3, no. 3, pp. 53–68, 2015.

[10] I. Anastasopoulos, M. Loli, T. Georgarakos, and V. Drosos, "Shaking table testing of rocking-isolated bridge pier on sand," *Journal of Earthquake Engineering*, vol. 17, no. 1, pp. 1–32, 2012.

[11] G. H. Zhang, "Study on the suitability of seismic isolation technologies for rural buildings," *Applied Mechanics and Materials*, vol. 353-356, pp. 2221–2227, 2013.

[12] I. Doudoumis, P. Papadopoulos, and T. Papaliangas, "Low-cost base isolation system on artificial soil layers with low shearing resistance," in *Proceedings of the 12th European Conference on Earthquake Engineering*, London, UK, September 2002.

[13] M. K. Yegian and U. Kadakal, "Foundation isolation for seismic protection using a smooth synthetic liner," *Journal of Geotechnical and Geoenvironmental Engineering*, vol. 130, no. 11, pp. 1121–1130, 2004.

[14] M. K. Yegian and M. Catan, "Soil isolation for seismic protection using a smooth synthetic liner," *Journal of Geotechnical and Geoenvironmental Engineering*, vol. 130, no. 11, pp. 1131–1139, 2004.

[15] H.-H. Tsang, S. H. Lo, X. Xu, and M. Neaz Sheikh, "Seismic isolation for low-to-medium-rise buildings using granulated rubber-soil mixtures: numerical study," *Earthquake Engineering & Structural Dynamics*, vol. 41, no. 14, pp. 2009–2024, 2012.

[16] K. Pitilakis, S. Karapetrou, and K. Tsagdi, "Numerical investigation of the seismic response of RC buildings on soil replaced with rubber-sand mixtures," *Soil Dynamics and Earthquake Engineering*, vol. 79, pp. 237–252, 2015.

[17] W. Xiong and Y. Li, "Seismic isolation using granulated tire-soil mixtures for less-developed regions: experimental validation," *Earthquake Engineering & Structural Dynamics*, vol. 42, 2013.

[18] A. Panjamani, M. Devarahalli Ramegowda, and R. Divyesh, "Low cost damping scheme for low to medium rise buildings using rubber soil mixtures," *Japanese Geotechnical Society Special Publication*, vol. 3, no. 2, pp. 24–28, 2015.

[19] S. Bandyopadhyay, A. Sengupta, and G. R. Reddy, "Performance of sand and shredded rubber tire mixture as a natural base isolator for earthquake protection," *Earthquake Engineering and Engineering Vibration*, vol. 14, no. 4, pp. 683–693, 2015.

[20] R. P. Nanda, P. Agarwal, and M. Shrikhande, "Suitable friction sliding materials for base isolation of masonry buildings," *Shock and Vibration*, vol. 19, no. 6, pp. 1327–1339, 2012.

[21] R. P. Nanda, P. Agarwal, and M. Shrikhande, "Base isolation by geosynthetic for brick masonry buildings," *Journal of Vibration and Control*, vol. 18, no. 6, pp. 903–910, 2012.

[22] R. P. Nanda, M. Shrikhande, and P. Agarwal, "Effect of ground motion characteristics on the pure friction isolation system," *Earthquakes and Structures*, vol. 3, no. 2, pp. 169–180, 2012.

[23] R. P. Nanda, M. Shrikhande, and P. Agarwal, "Low-cost base-isolation system for seismic protection of rural buildings," *Practice Periodical on Structural Design and Construction*, vol. 21, no. 1, article 04015001, 2015.

[24] H. Xiao, J. W. Butterworth, and T. Larkin, "Low-technology techniques for seismic isolation," in *Proceedings of the NZSEE Conference*, Rototua, New Zealand, 2004.

[25] M. Qamaruddin and S. Ahmad, "Seismic response of pure-friction base isolated masonry building with restricted base-sliding," *Journal of Engineering Research [TJER]*, vol. 4, no. 1, pp. 82–94, 2007.

[26] S. Ahmad, F. Ghani, and M. Raghib Adil, "Seismic friction base isolation performance using demolished waste in masonry housing," *Construction and Building Materials*, vol. 23, no. 1, pp. 146–152, 2009.

[27] I. Banović, J. Radnić, and N. Grgić, "Shake table study on the efficiency of seismic base isolation using natural stone pebbles," *Advances in Materials Science and Engineering*, vol. 2018, Article ID 1012527, 20 pages, 2018.

[28] H. H. Tsang, "Geotechnical seismic isolation," in *Earthquake Engineering: New Research*, pp. 55–87, Nova Science Publishers Inc., New York, NY, USA, 2009.

[29] S. Brunet, J. C. de la Llera, and E. Kausel, "Non-linear modeling of seismic isolation systems made of recycled tire-rubber," *Soil Dynamics and Earthquake Engineering*, vol. 85, pp. 134–145, 2016.

[30] D. Forcellini, "Assessment on geotechnical seismic isolation (GSI) on bridge configurations," *Innovative Infrastructure Solutions*, vol. 2, no. 1, p. 9, 2017.

[31] H.-H. Tsang, "Seismic isolation by rubber-soil mixtures for developing countries," *Earthquake Engineering & Structural Dynamics*, vol. 37, no. 2, pp. 283–303, 2008.

[32] E. Mavronicola, P. Komodromos, and D. C. Charmpis, "Numerical investigation of potential usage of rubber–soil mixtures as a distributed seismic isolation approach," in *Proceedings of the 10th International Conference on Computational Structures Technology*, Valencia, Spain, September 2010.

[33] N. Ambraseys, P. Smit, R. Sigbjörnsson, P. Suhadolc, and M. Margaris, *EVR1-CT-1999-40008, European Commission, Directorate-General XII*, Environmental and Climate Programme, Brussels, Belgium, 2001, http://www.isesd.hi.is/ESD_Local/frameset.htm.

[34] EN 1998-1:2004, *Eurocode 8: Design of Structures for Earthquake Resistance-Part 1: General Rules, Seismic Actions and Rules for Buildings*, European Committee for Standardization, Brussels, Belgium, 2004.

# PAPER III

Hindawi
Advances in Materials Science and Engineering
Volume 2018, Article ID 1012527, 20 pages
https://doi.org/10.1155/2018/1012527

*Research Article*

# Shake Table Study on the Efficiency of Seismic Base Isolation Using Natural Stone Pebbles

**Ivan Banović, Jure Radnić, and Nikola Grgić**

*University of Split, Faculty of Civil Engineering, Architecture and Geodesy, Matice Hrvatske 15, 21000 Split, Croatia*

Correspondence should be addressed to Ivan Banović; ivan.banovic@gradst.hr

Received 6 September 2018; Accepted 21 October 2018; Published 20 December 2018

Academic Editor: Georgios I. Giannopoulos



The results of a shake table study of the efficiency of a seismic base isolation using a layer of natural stone pebbles are presented. Models of stiff and medium-stiff buildings were tested. Case studies were conducted with the foundation of model on the rigid base and on four different layers of pebbles (thin and thick layer with small and large pebbles). Four different horizontal accelerograms were applied, and the characteristic displacements, accelerations, and strains were measured. Strains/stresses of the tested models remained in the elastic area. It was concluded that the effectiveness of the stone pebble layer under the foundation, i.e., the reduction in the seismic forces and stresses in the structure compared to the classical solution of foundation, significantly depends on the type of the applied excitation and depends relatively little on the layer thickness and pebble fraction. The results of the study showed that a layer of pebbles can significantly reduce the peak acceleration and strains/stresses of the model, with acceptable displacements. Further research is expected to confirm the effectiveness of this low-cost and low-tech seismic base isolation and to pave the way to its practical application.

## 1. Introduction

Modern science in recent decades has explored numerous solutions to reduce the seismic forces on buildings, aiming to improve safety during earthquakes and to provide more rational solutions. Some of these aseismic solutions are quite simple and rational (e.g., different variants of elastomeric bearings) and have found applications in the construction of bridges and important buildings. Unfortunately, a large number of the devices for reducing the seismic forces on structures and for controlling their displacements in the earthquake remain complex and expensive, and their practical application remains rare. To enable widespread application of a solution for seismic isolation, especially in less-developed countries, it should be simple and based on low technology.

Solutions involving the application of a layer of appropriate materials under the foundation to reduce seismic forces on buildings, which are expected to be efficient and rational for use in the so-called low-cost buildings, are the starting point of our study. Such a low-cost and low-technology method could be widely used in seismic isolation of low-rise buildings around the world. The research results of one such seismic isolation method are presented in this paper.

There are indications that in ancient history, builders used layers of different materials to increase the seismic resistance of buildings. Contemporary researchers are exploring this ancient approach to find the appropriate solutions that enable replacement of sophisticated devices for seismic isolation in many buildings with simple methods. Currently, to the author's knowledge, there are very few studies related to the use of natural materials for seismic base isolation of buildings.

A concept of interposing an artificial soil layer between the superstructure and the foundation soil was examined by Doudoumis et al. [1]. Extended investigation of utilization of a smooth synthetic liner placed within the soil deposit can be found in [2, 3]. Xiao et al. [4] tested five potential isolation materials to characterize their frictional features by both semidynamic and shake table experiments. The materials were sand, lighting ridge pebble, polypropylene sheet, PVC sheet, and polythene membrane. A series of numerical simulations and a parametric study on seismic base isolation using rubber-soil mixtures can be found in [5]. Radnić et al.

[6, 7] found from shake table tests that a thin layer of plain sand under the foundation can reduce seismic forces to a cantilever concrete column by over 10%. Xiong and Li [8] analyzed seismic base isolation using rubber-soil mixtures (RMSs) based on shake table tests and a parametric numerical study in [9]. The effectiveness of utilizing a rubber-sand mixture (RSM) in the foundation soil of different moment-resisting frame (MRF) typologies was assessed through numerical simulations in [10]. The results highlighted the beneficial effects of the use of RSM as a foundation layer on the structures' response under dynamic loading, particularly for the mid- and high-rise buildings, leading to a reduction in the base shear and maximum interstory drift up to 40% and 30%, respectively, in comparison with the clean sand profile. Panjamani et al. [11] obtained similar results in terms of acceleration and interstory drift reduction; at different floor levels with the use of RSM, the reduction can be approximately 40 to 50%. Bandyopadhyay et al. [12] found from shake table tests that a composite consisting of sand and 50% shredded rubber tire placed under the foundation was most promising as a low-cost effective base isolator. Patil et al. [13] found encouraging results regarding the efficiency of seismic base isolation using river sand based on experimental and analytical work. Nanda et al. [14–17] conducted experimental studies based on shake table tests by providing geotextiles and a smooth marble frictional base isolation system at the plinth level of a brick masonry building. A 65% reduction in absolute response acceleration at the roof level was obtained in comparison with the response of the fixed base structure. Further work on pure-friction base isolation systems can be found in [18, 19].

This paper presents the results of a shake table study regarding the efficiency of seismic base isolation using natural stone pebbles below the foundation for the reduction in seismic forces on structures, with the aim that such a solution finds practical application in the construction of low-cost buildings and smaller bridges in seismically active regions. Testing was performed on stiff and medium-stiff buildings. Four different accelerograms were applied, and stresses of the models remained in the elastic area. First, a model with the foundation directly on a rigid base (shake table) was tested, and then a model with a layer of stone pebbles under the foundation (the layer thickness and fraction of the pebbles are varied) was tested. Characteristic displacements, accelerations, and strains were measured. Some study results are presented and discussed, and the main conclusions of the research are given at the end of the paper. However, further research on some important effects that were not considered in this study is required to achieve even more reliable conclusions regarding the efficiency and rationality of the considered concept of seismic isolation.

## 2. Layer of Natural Stone Pebbles below the Foundation

Stone pebbles are natural material created from larger pieces of stone under the long-lasting action of rivers and sea. In this process, the sharp parts of stone were rounded, and the weak parts of stone have fallen off as a result only solid, smooth, rounded pieces of stone (stone pebbles) remain. In this study, stone pebbles from a riverbed were used. The pebbles are mainly of limestone and partly of granite. In the conducted tests, the following two fractions of pebbles were used (Figure 1): 4–8 mm (i.e., small pebbles) and 16–32 mm (i.e., large pebbles). The average compressive strength of the pebbles was approximately 80 MPa, and the humidity was approximately 10%. It is assumed that the thickness of the pebble layer of approximately 0.3 to 1.0 m could be effective in terms of reducing the seismic forces to the building, while being a rational approach. A thicker layer is probably more efficient but requires deeper excavation and a taller embankment, i.e., higher costs. In the conducted tests, the following two layer thicknesses were used (Figure 2): $d = 0.3$ m (thin layer) and $d = 0.6$ m (thick layer). Layers are formed within a frame with a plan size of 2.5 m × 2.5 m, which was fixed to the shake table. The deformation conditions of the layer within the frame are sought to be similar to those that the layer would have under the foundation of a real building. Although a reduced model of the building was used, the layer thickness was used in real size because the reduced building model has the same dynamic characteristics (periods of free oscillations) as that of the target full-scale building. The layers were formed in sub-layers with a thickness of 0.10 m, with static compaction and dynamic compaction using the shake table. The average compaction module at the top of the layer was approximately MS = 30 MPa.

## 3. Adopted Building Models

Seismic forces on the structure significantly depend on their dynamic characteristics, i.e., on the structure stiffness and the weight. The dynamic characteristics of the building are well described by its periods and forms of free oscillations. According to [20], for type 1 and type of ground soil A, spectral acceleration $S_e$ for a elastic single-degree-of-freedom (SDOF) system of a cantilever column with mass on its top is defined according to the fundamental free oscillation period $T$ (Figure 3). Real buildings have a wide stiffness range, from very stiff to very soft, i.e., a wide spectrum of $T$.

Instead of a small-scale model of a real building, which results in a series of problems and doubts, a model (cantilever column with a mass on top—SDOF) that has the same fundamental period $T$ as a real building is adopted in this study. Thus, this model well represents the dynamic characteristics of the real building. Two models of buildings shown in Figure 4 were tested: the MSB model with $T = 0.05$ s which represents stiff buildings and the MSSB model with $T = 0.6$ s which represents medium-stiff buildings (Figure 3). The adopted models include a foundation because the behavior of real buildings in the earthquake depends significantly on their foundations, i.e., on the soil-structure interaction. The calculation of the seismic forces based on an SDOF system starts from the assumption that there is no displacements and rotations of the column bottom, i.e., there is no displacement and rotation of the foundation. This study takes these effects into consideration.

(a) (b)

Figure 1: Used fractions of pebbles. (a) 4–8 mm. (b) 16–32 mm.

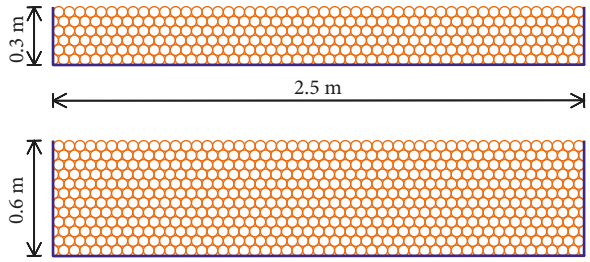


Figure 2: Used thicknesses of pebble layer.

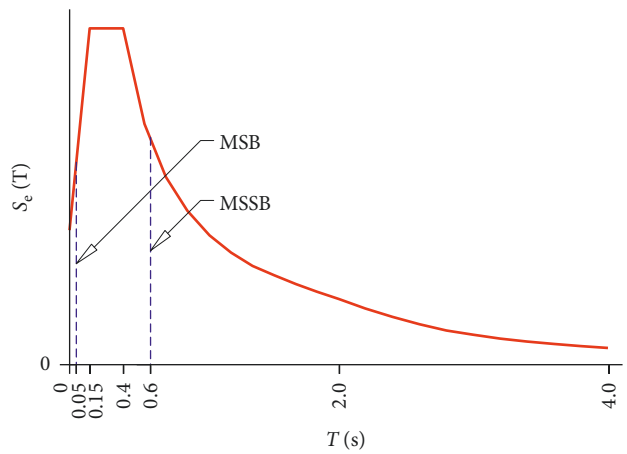


Figure 3: Seismic response spectra according to [20], for type 1 and type of ground soil A.

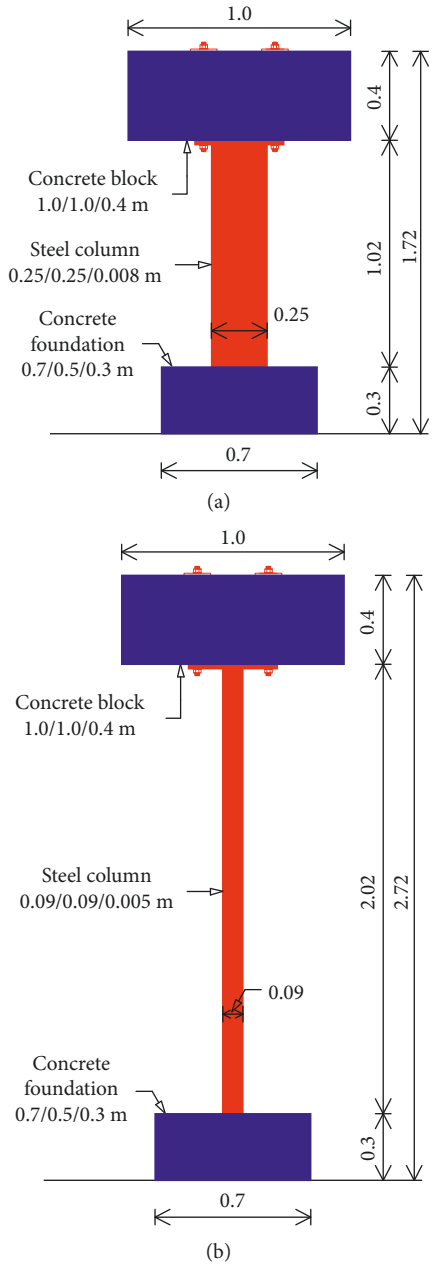


Figure 4: Considered building models. (a) MSB ($T$ = 0.05 s). (b) MSSB ($T$ = 0.60 s).

The same foundation and mass on the top of the column were adopted in both models, with different column heights and dimensions of its cross section. The foundation and mass at the top of the column ($m$ = 1000 kg) are made from concrete (cube strength of 46 MPa), and the column is a square steel tube with uniaxial tensile strength of 355 MPa. The foundation is highly reinforced and is practically rigid. In the conducted experimental tests, relatively small plan dimensions of the foundation were adopted. However, they are the same in the case of the foundation supported on the rigid base and on the pebble layers. In further research, it is planned to vary the different plan dimensions of the foundation. In the adopted steel columns, stresses remained in the elastic area for all performed tests. Namely, the starting point was that for all tests, nonlinearity does not appear in the whole structure (column and foundation), i.e., all nonlinearity and dissipation of seismic energy are realized in the pebble layer and in the layer-foundation coupling surface. Thus, the intention was to exclude the influence of nonlinearity in the construction material, i.e., the dissipation of seismic energy in the form of plastification and damage of the construction material, on the results regarding the aseismic efficiency of the tested pebble layer.

## 4. Tested Samples

Ten different samples were experimentally tested (Figure 5) under four different types of dynamic excitation produced by the shake table. The first tested MSB and MSSB models were supported on a rigid base $P_r$ (Figure 5(a)). A concrete layer was placed and fixed on the top of the shake table to simulate the usual subconcrete under foundation of a real building. This situation approximates the real buildings with a classic foundation without seismic base isolation. The horizontal displacement of the foundation in relation to the base (shake table) is prevented, while the rocking and uplifting of the foundation is allowed. Next, MSB and MSSB models supported on different layers of pebble ($P_{p1}$ to $P_{p4}$) were tested (Figure 5(b)). The layer thickness $d$ (0.3 m and 0.6 m) and the pebble fraction $\Phi$ (4 to 8 mm and 16 to 32 mm) were varied. The pebble layer was returned to its initial condition after each test, i.e., recompaction to the required compaction module and leveling of the layer top. The same shake table acceleration was adopted for the model supported on a rigid base and on a pebble layer. It is assumed that the real earthquake acceleration at the top of the natural solid ground in both cases is the same.

## 5. Dynamic Excitations

The models of buildings with considered variants of foundation support (Figure 5) were exposed to horizontal accelerations of the shake table in the direction of larger dimension of the foundation, using the accelerograms shown in Figure 6. The maximum acceleration $a_{g,max}$ of the accelerogram is scaled to 0.3 g and 0.2 g for the MSB and MSSB model, respectively. An artificial accelerogram (AA), as shown in Figure 6(a), is created to match the elastic response spectra according to [20]. The horizontal component N-S of the Petrovac earthquake (Montenegro) [21] is shown in Figure 6(b) (AP), the horizontal component N-S of the Ston earthquake (Croatia) [21] is shown in Figure 6(c) (AS), and the horizontal component N-S of the Banja Luka earthquake (BiH) [21] is shown in Figure 6(d) (ABL). Elastic response spectra of the adopted accelerograms are shown in Figure 7. It is difficult to predict which applied accelerogram will be most unfavorable for each tested sample in Figure 5 because of the possible occurrence of nonlinearities in the system. The adopted accelerograms cover a wide spectrum of potential earthquake types. Namely, the artificial accelerogram (AA) is characterized by the long-lasting action, moderate predominant period, large spectral displacements, and high earthquake input energy in structure. Compared to AA, accelerogram Petrovac (AP) has similar characteristics, slightly shorter duration and longer predominant period. The Ston accelerogram (AS) and B. Luka accelerogram (ABL) are characterized by a short impact action with a short predominant period. Namely, AS and ABL represent the so-called impact earthquakes.

## 6. Measured Values

The following values were measured on each tested sample (Figure 8): horizontal displacement of the mass center at the column top ($u_1$), horizontal displacement at the foundation top ($u_2$), vertical displacement at the right edge ($v_1$) and at the left edge ($v_2$) of the foundation, vertical strain on the bottom of the steel column at the right side ($\varepsilon_1$) and at the left side ($\varepsilon_2$), and horizontal acceleration of the mass center at the column top (a).

## 7. Testing and Measuring Equipment

Tests were performed using a shake table at the University of Split, Faculty of Civil Engineering, Architecture and Geodesy (Croatia). Data collection from all sensors was performed using the Quantum-x mx 840A system (HBM). The displacements were measured using analog displacement sensors, type PB-25-S10-N0S-10C (Uni Measure). The strains were measured using strain gauges, type 6/120 LY11 (HBM). The accelerations were measured by a piezo-electric low frequency accelerometer type 4610 (MS). Some photos of experimental setup before testing are shown in Figure 9.

## 8. Experimental Results

The test results are shown in a graphic form to ensure that the presentation is concise and clear, even with reduced size of the drawings. The results are separately shown for some of the measured values, for the models MSB and MSSB. Each of the drawings shows the measured values separately at each applied accelerogram, for all five considered substrate types: $P_r$—rigid base; $P_{p1}$—pebble layer ($d$ = 0.3 m, $\Phi$ = 16 to 32 mm); $P_{p2}$—pebble layer ($d$ = 0.6 m, $\Phi$ = 16 to 32 mm); $P_{p3}$—pebble layer ($d$ = 0.3 m, $\Phi$ = 4 to 8 mm); and $P_{p4}$—pebble layer ($d$ = 0.6 m, $\Phi$ = 4 to 8 mm); see Figure 5.

In order to investigate the impact of some possible negative factors on the conclusions of the study, preliminary research has been carried out. Namely, in order to investigate the impact of subsequent earthquakes on the efficiency of the considered seismic base isolation, the tested structure was exposed to a set of six repeated base accelerations, without updating the pebble layer. Testing was performed with AA and AS, for MSB on layer $P_{p1}$ (Figure 5) and MSSB on layer $P_{p4}$. Compared to the first excitation, repeated excitations produced up to 8.6% higher strain/stress on the bottom of the steel column and up to 196% larger irreversible horizontal displacement at the foundation top. This can be considered acceptable because it is unlikely that some buildings would be exposed to a large number of medium to severe earthquakes that would cause building displacements in the same direction. To prevent a possible similar scenario, the problem can be solved so that the width of the aseismic layer is sufficiently wider than the foundation.

Tests with repeated high base accelerations that could cause nonlinearities in the model were not performed. The pebble layer efficiency for repeated base accelerations is explained by the fact that the layer of stone pebbles of the same grain size is very difficult to compact. Also, the influence of compaction of $P_{p1}$ and $P_{p4}$ layers was also tested with AA and AS. The average compaction module at the top of the layers was MS = 30 MPa and MS = 60 MPa, respectively. The maximum strain/stress on the bottom of the

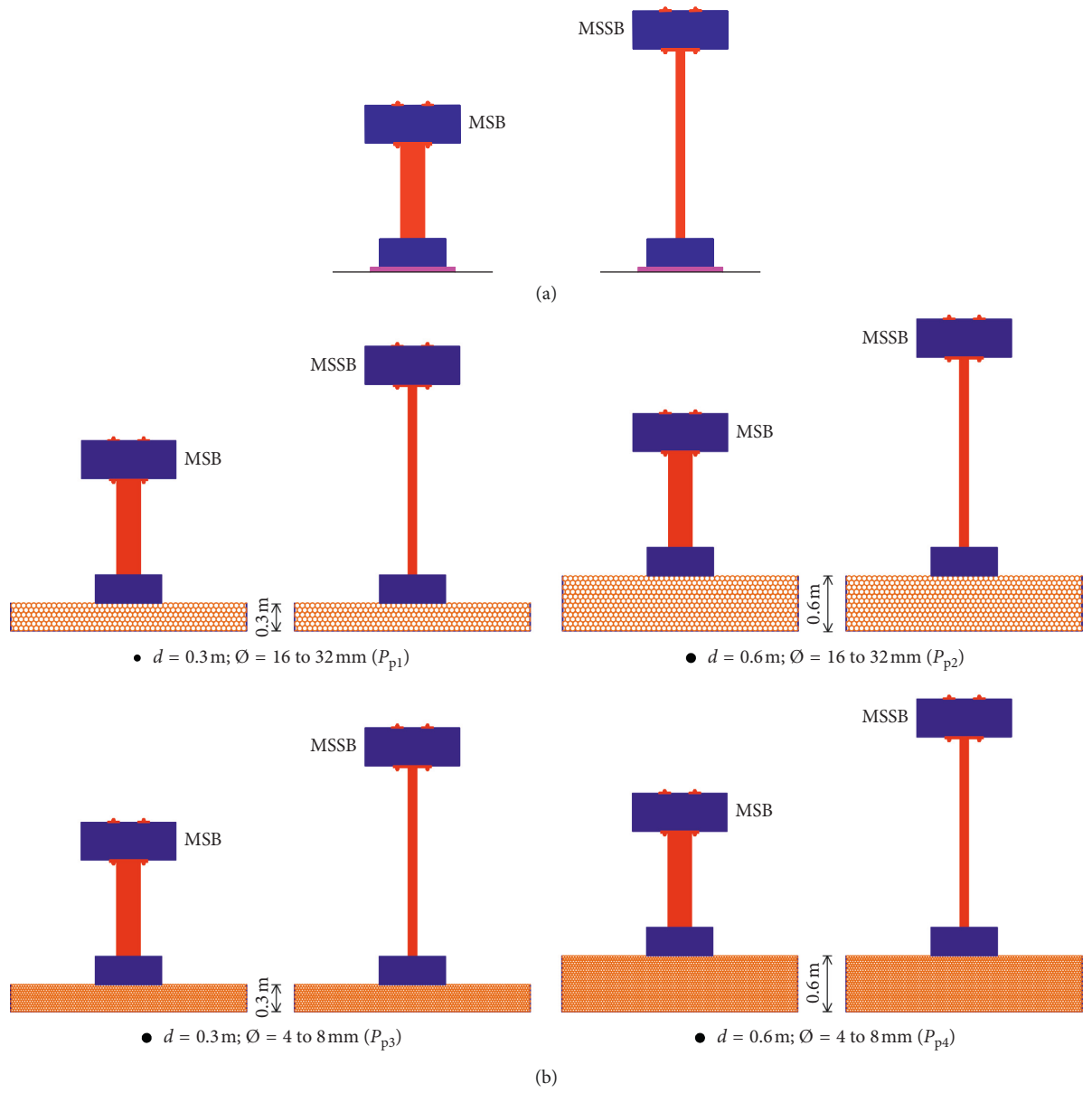


Figure 5: Tested samples. (a) Rigid base ($P_r$). (b) Pebble layers.

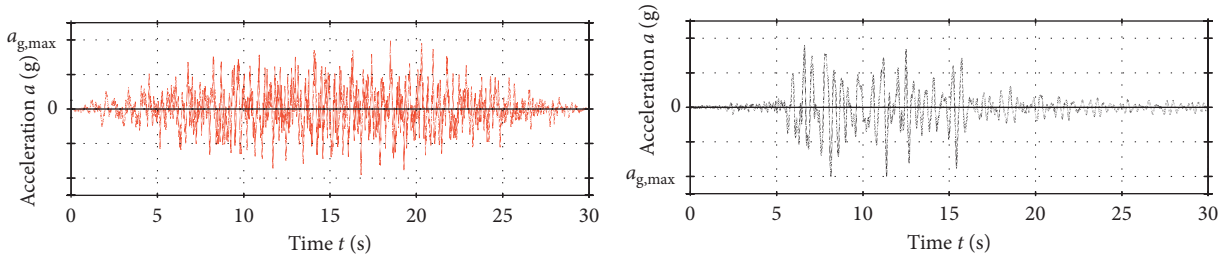


Figure 6: Continued.

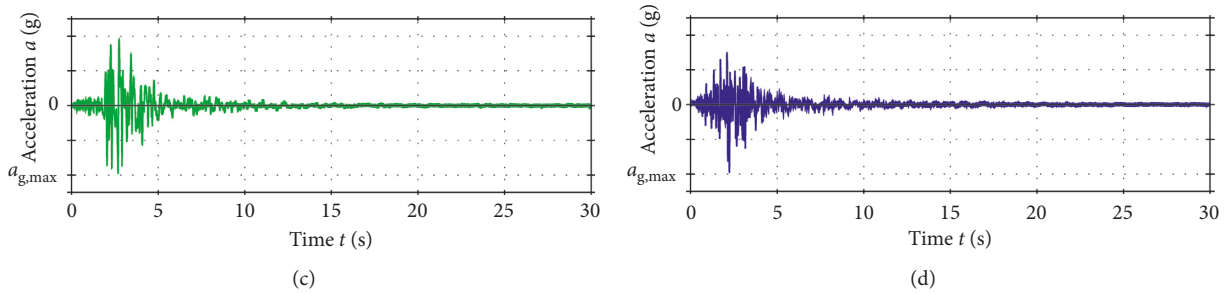


Figure 6: Applied horizontal base accelerations ($a_{g,max}$ scaled to 0.2 g for MSSB and 0.3 g for MSB). (a) Artificial accelerogram (AA). (b) N-S accelerogram of Petrovac earthquake (AP). (c) N-S accelerogram of Ston earthquake (AS). (d) N-S accelerogram of B. Luka earthquake (ABL).

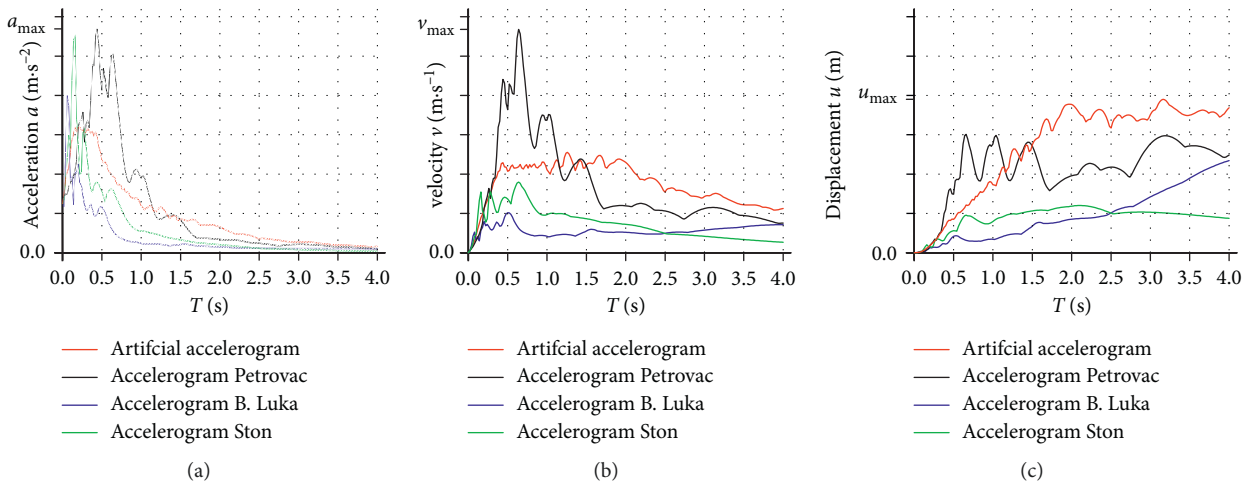


Figure 7: Elastic response spectra for applied accelerograms. (a) Spectral acceleration. (b) Spectral velocity. (c) Spectral displacement.

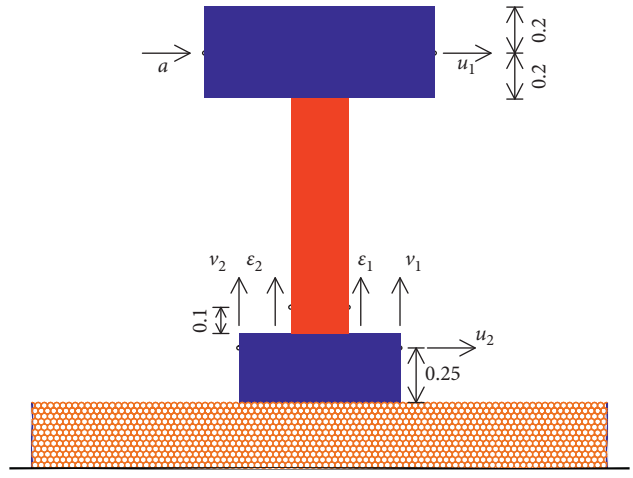


Figure 8: Measured values.

steel column for MS = 60 MPa was 4.9% higher than for MS = 30 MPa. This can be considered acceptable.

Foregoing suggests that the proposed seismic base isolation can be effective throughout the lifetime of the building and it is not necessary to renew.

*8.1. Model of Stiff Building MSB.* Horizontal acceleration of the mass center at the column top (a) is shown in Figure 10. It is found that the rigid base produced maximum acceleration for all considered accelerograms and that the maximum accelerations for the pebble layer were similar. Compared to the rigid base, thin layer with large pebbles produced the lowest reduction in acceleration. For $a_{g,max} = 3.0\,m{\cdot}s^{-2}$, the highest acceleration on the rigid base was produced by AA (approx. $11.6\,m{\cdot}s^{-2}$), whereas the lowest was produced by ABL (approx. $5.8\,m{\cdot}s^{-2}$). The maximum acceleration with a pebble layer

(a) (b)

Figure 9: Photos of experimental setup before testing. (a) MSB on rigid base. (b) MSB on layer $P_{p2}$.

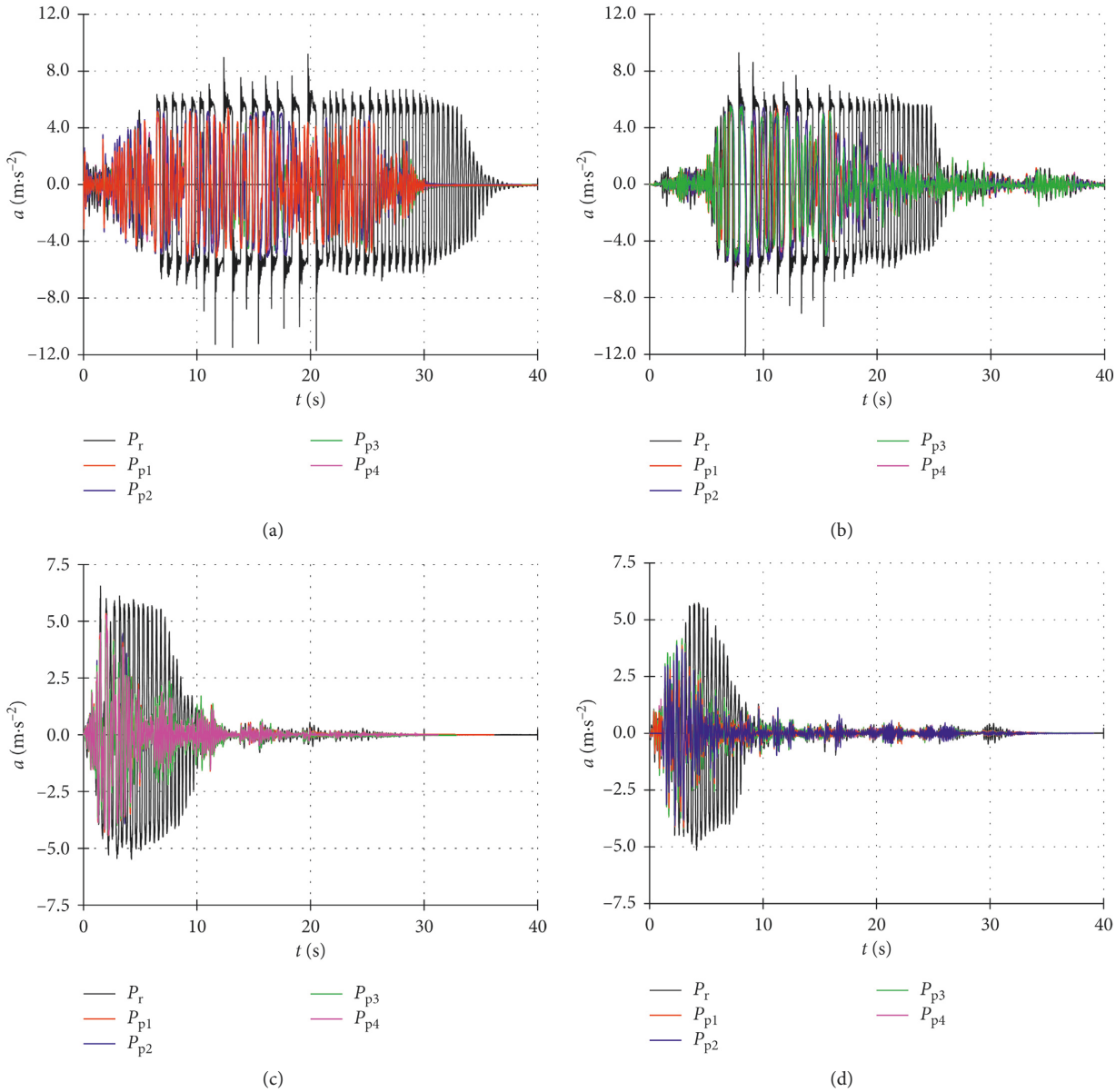


Figure 10: Horizontal acceleration of the mass center at the column top (a) for MSB. (a) Artificial accelerogram (AA). (b) Accelerogram Petrovac (AP). (c) Accelerogram Ston (AS). (d) Accelerogram B. Luka (ABL).

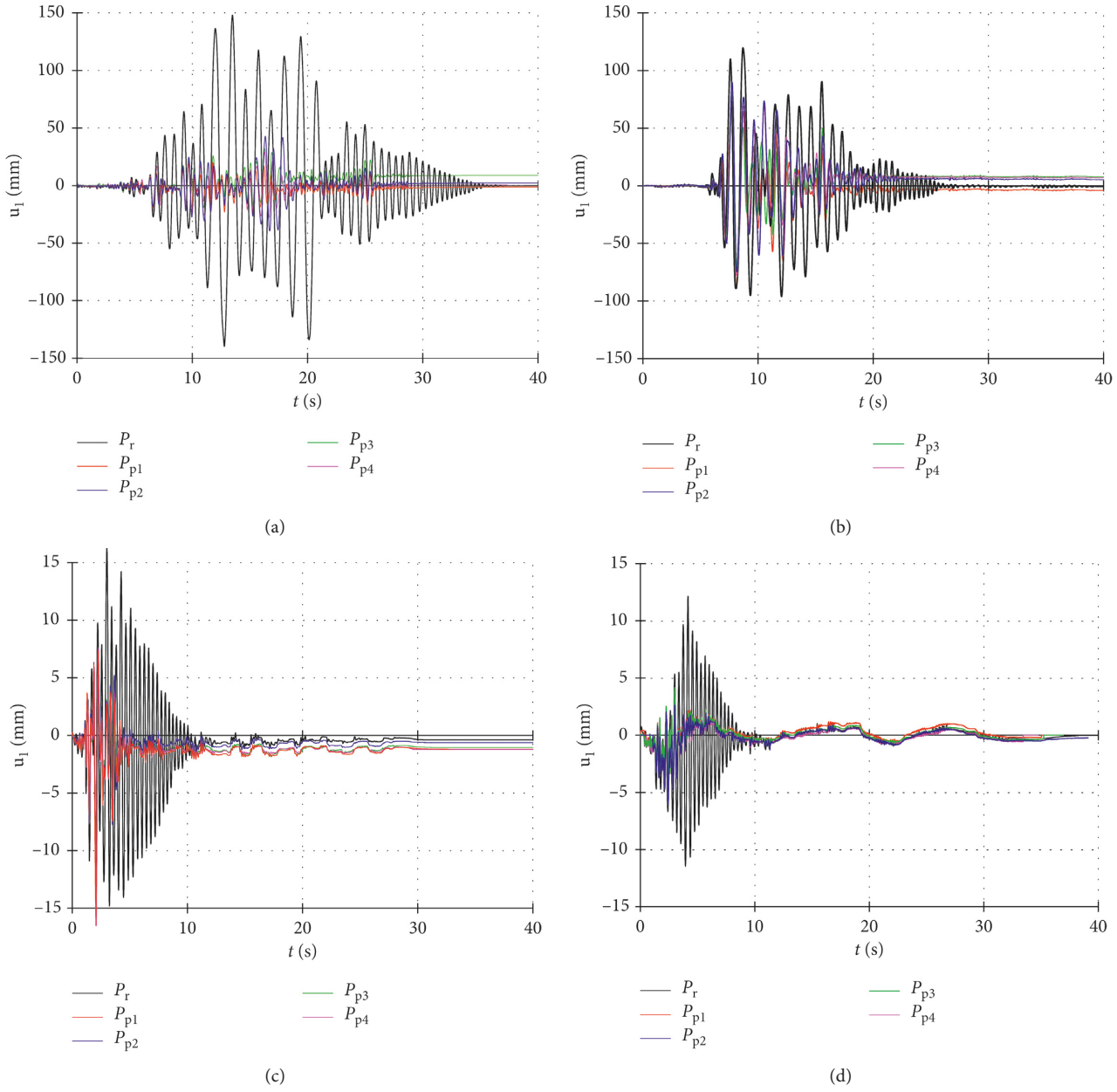


Figure 11: Horizontal displacement of the mass center at the column top ($u_1$). (a) Artificial accelerogram (AA). (b) Accelerogram Petrovac (AP). (c) Accelerogram Ston (AS). (d) Accelerogram B. Luka (ABL).

for AA and ABL was approx. 5.7 m·s$^{-2}$ and approx. 4.1 m·s$^{-2}$, respectively.

The largest horizontal displacement of the mass center at the column top ($u_1$) for all considered accelerograms was produced with the rigid base, and the maximum displacements on all pebble layers were similar (Figure 11). Compared to the rigid base, the slightest reduction in the displacement was produced using a thin layer with large pebbles. For the rigid base, AA produced the largest displacement of approximately 150 mm, whereas ABL produced the smallest displacement of approximately 12 mm. The largest displacement on the pebble layer was produced by AP (approx. 80 mm), whereas the smallest was produced by ABL (approx. 3.5 mm).

The vertical strain on the right bottom side of the steel column ($\varepsilon_1$) is presented in Figure 12. Note that the model on the rigid base had the maximum strain for all considered accelerograms and that the maximum strain for the model on the pebble layers was similar. Compared to the rigid base, the slightest reduction in strain also produced a thin layer with large pebbles. The largest strain on the rigid base was caused by AP (approx. 0.059‰), whereas the smallest was caused by ABL (approx. 0.018‰). The largest strain on the pebble layer was caused by AP (approx. 0.028‰), whereas the smallest was caused by ABL (approx. 0.018‰). All strains (stresses) were within the elastic area of the steel (≤1.7‰).

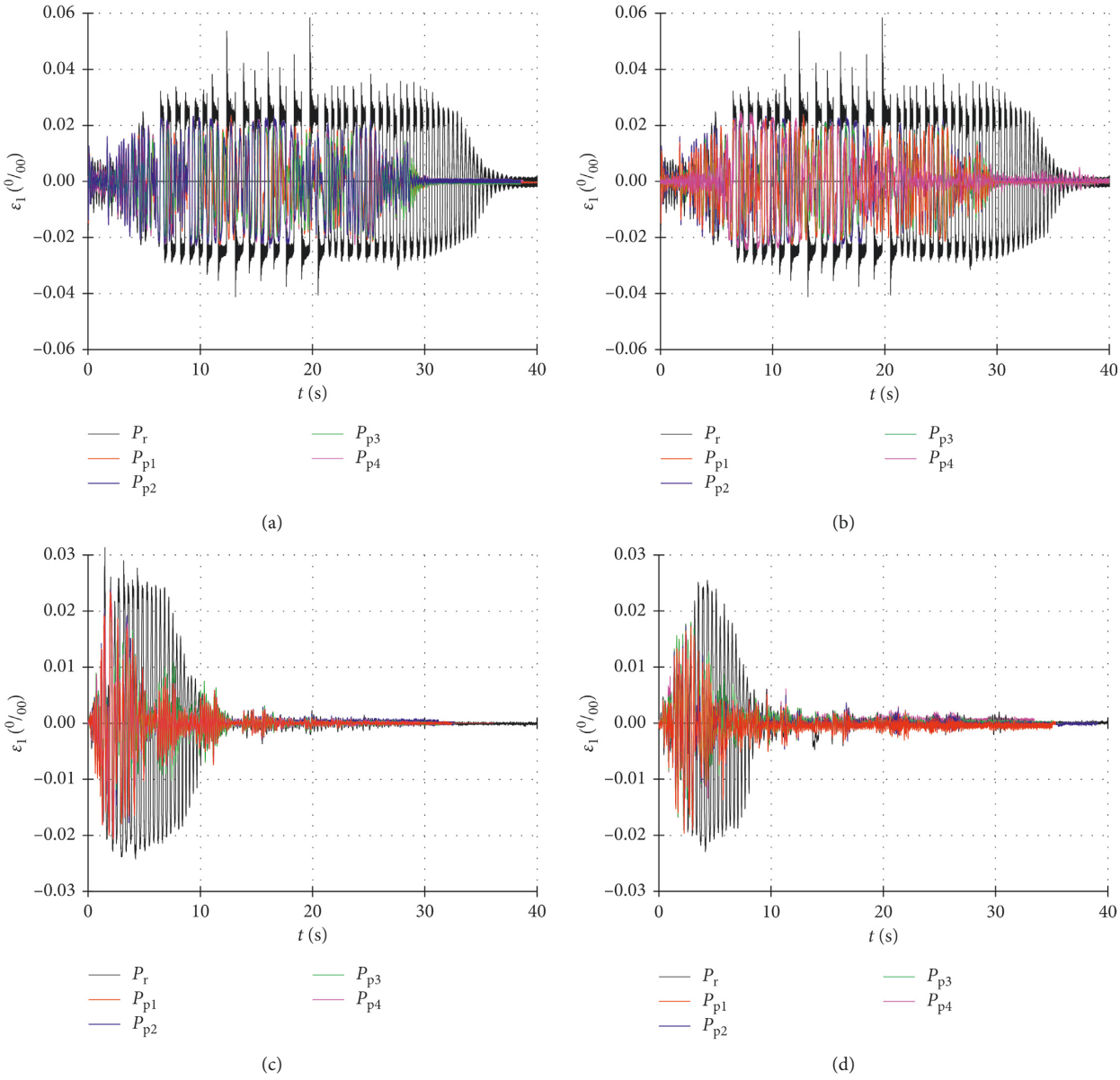


Figure 12: Vertical strain on the right bottom side of the steel column ($\varepsilon_1$) for MSB. (a) Artificial accelerogram (AA). (b) Accelerogram Petrovac (AP). (c) Accelerogram Ston (AS). (d) Accelerogram B. Luka (ABL).

The horizontal displacement at the foundation top ($u_2$) is prevented for a rigid base (Figure 13), i.e., the bottom of the foundation is fixed to the base (shake table). The largest displacement for the pebble layer was produced by AP (approx. 18.5 mm), whereas the smallest was produced by ABL (approx. 1.2 mm). Thicker layers resulted in larger horizontal displacements. The largest permanent displacement for the pebble layer was produced also by AP (approx. 6.0 mm), which is the result of the foundation slipping at the pebble layer top. Thus, the ratio of the largest permanent displacement of the foundation and peak foundation displacement for AP is approximately 6 mm : 18.5 mm or about 1 : 3.

The largest uplifts of the foundation (Figure 14) were produced for models with the rigid base, approximately 64 mm for AA and approximately 4.4 mm for ABL. The largest uplift of the foundation for the pebble layer was produced by AP (approx. 35 mm), whereas the smallest was produced by ABL (approx. 1.8 mm). The largest permanent settlement on the left edge of the foundation of approximately 7 mm was produced by AP (thin layer with large pebbles).

*8.2. Model of Medium-Stiff Building MSSB.* Horizontal acceleration of the mass center at the column top (a) is shown in Figure 15. It can be seen that the rigid base produced maximum acceleration for all applied accelerograms and that the maximum accelerations for the pebble layer were similar (analogous to model MSB). For $a_{g,max} = 2.0\ m{\cdot}s^{-2}$, the

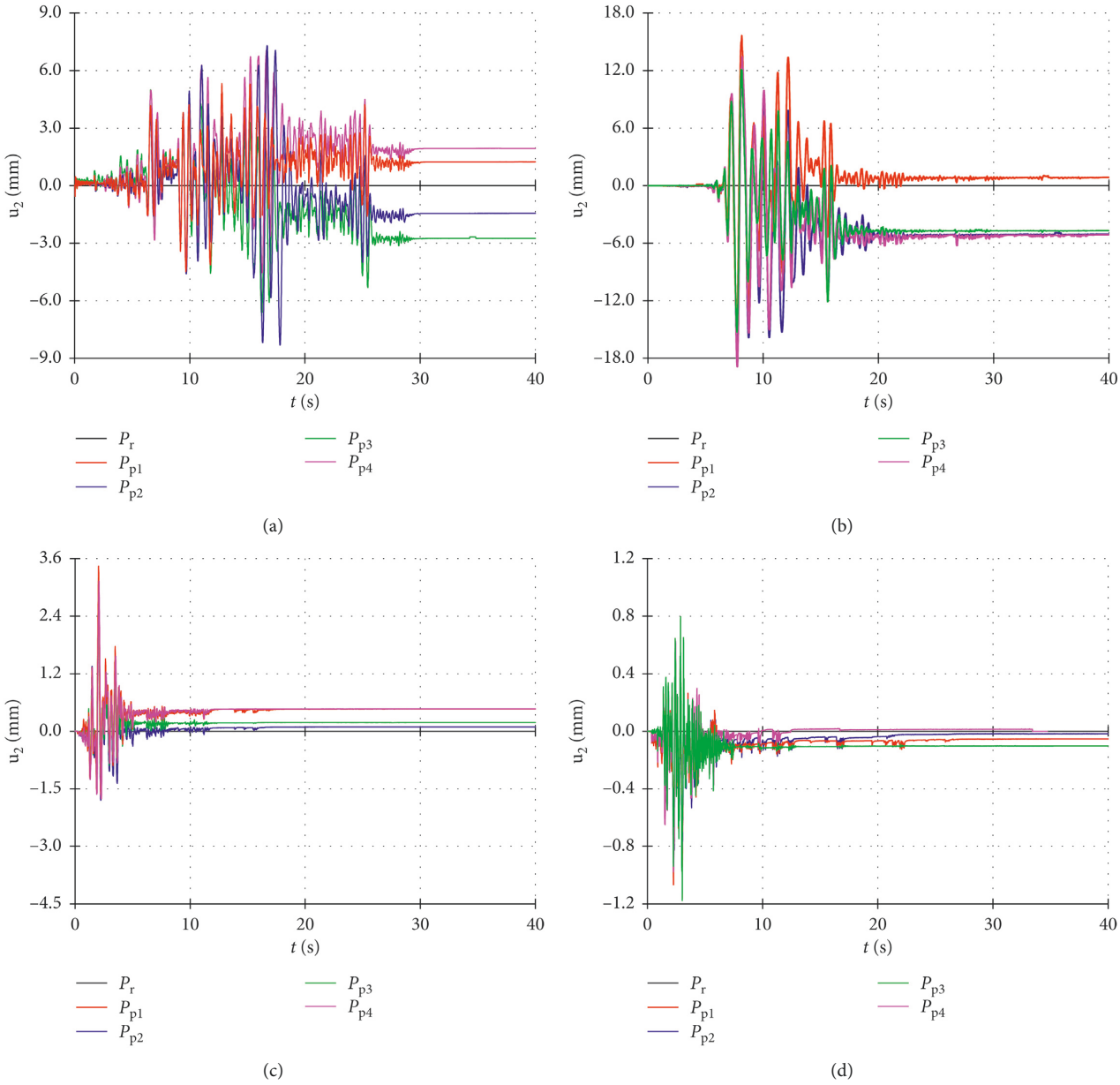


Figure 13: Horizontal displacement at the foundation top ($u_2$) for MSB. (a) Artificial accelerogram (AA). (b) Accelerogram Petrovac (AP). (c) Accelerogram Ston (AS). (d) Accelerogram B. Luka (ABL).

highest acceleration for the model on the rigid base was produced by AA and AP (approx. 7.5 m·s$^{-2}$), whereas the lowest was produced by ABL (approx. 2.8 m·s$^{-2}$). The maximum acceleration with a pebble layer for AA and ABL was approximately 4.4 m·s$^{-2}$ and approximately 2.4 m·s$^{-2}$, respectively.

The largest horizontal displacements of the mass center at the column top ($u_1$) were also for the rigid base case (Figure 16): AA produced the largest displacement of approximately 170 mm, whereas ABL produced the smallest of approximately 21.5 mm. The largest displacement for the model on the pebble layer was produced by AP (approx. 110 mm), whereas the smallest was produced by ABL (approx. 21.5 mm). The largest permanent displacement on the pebble layer was for AA (approx. 25 mm), which is the result of the foundation slipping at the pebble layer top and foundation rotation on the vertically deformable substrate.

The vertical strain on the right bottom side of the steel column ($\varepsilon_1$) is presented in Figure 17. The maximum strain for the rigid base was approximately equal for AA and AP (approx. 0.82‰), i.e., within the elastic steel behavior. The minimum strain was for ABL (approx. 0.33‰). Compared to the MSB model, the MSSB model had significantly greater stresses/strains. For the pebble layer, AA produced maximum strain of approximately 0.45‰.

The largest displacement at the foundation top ($u_2$) for the pebble layer (Figure 18) was produced by AA (approx.

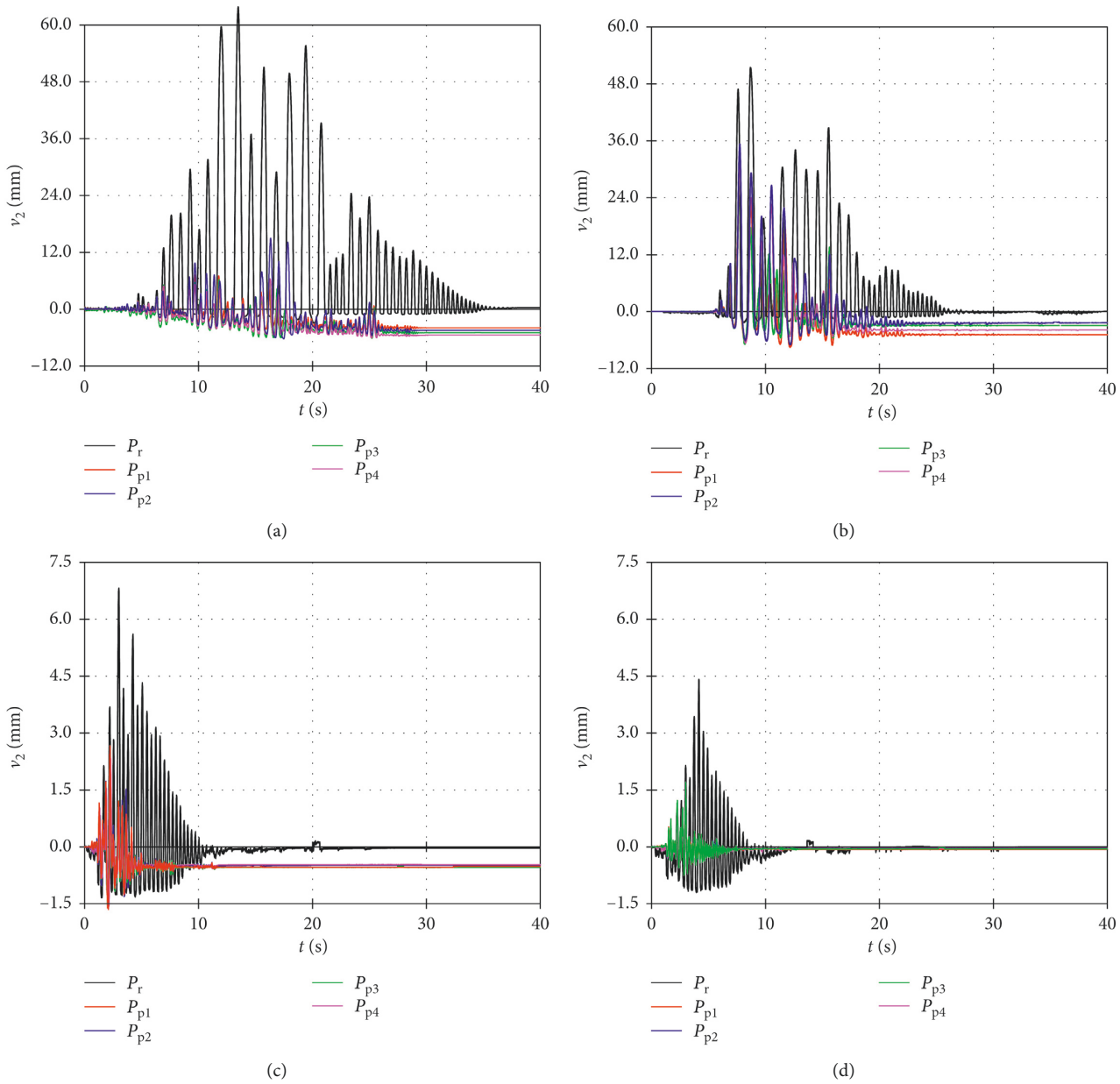


Figure 14: Vertical displacement at the left edge of the foundation ($v_2$) for MSB. (a) Artificial accelerogram (AA). (b) Accelerogram Petrovac (AP). (c) Accelerogram Ston (AS). (d) Accelerogram B. Luka (ABL).

13 mm), whereas the smallest was produced by ABL (approx. 1.6 mm). The largest permanent displacement ($u_2$) for the pebble layer was for AA (approx. 7 mm) with a thick layer of large pebbles, as a result of the foundation sliding on the pebble layer top.

The largest uplift at the left edge of the foundation ($v_2$) for the rigid base (Figure 19) was produced by AA (approx. 37 mm), whereas the smallest was produced by ABL (approx. 1.4 mm). The largest uplift on the pebble layer was produced by AP and AA (approx. 14 mm). The largest permanent settlement on the left edge of the foundation of approximately 5 mm for the pebble layer was for AA (thick layer with large pebbles). The consequence of the different permanent vertical settlement of the left edge and right edge of the foundation is the rotation of the model and the occurrence of an additional permanent horizontal displacement $u_1$.

*8.3. Comparison of Experimental Results for Models MSB and MSSB.* Table 1 presents the maximum values of some of the measured experimental results for building models MSB and MSSB on a rigid base and on the pebble layer as well as the ratio of these values. Note that the efficiency of the pebble layer depends on the stiffness of the building model and the type of accelerogram (earthquake characteristics). The values in Table 1 are shown in Figures 20–23, which provide a better visual insight into the ratio of measured

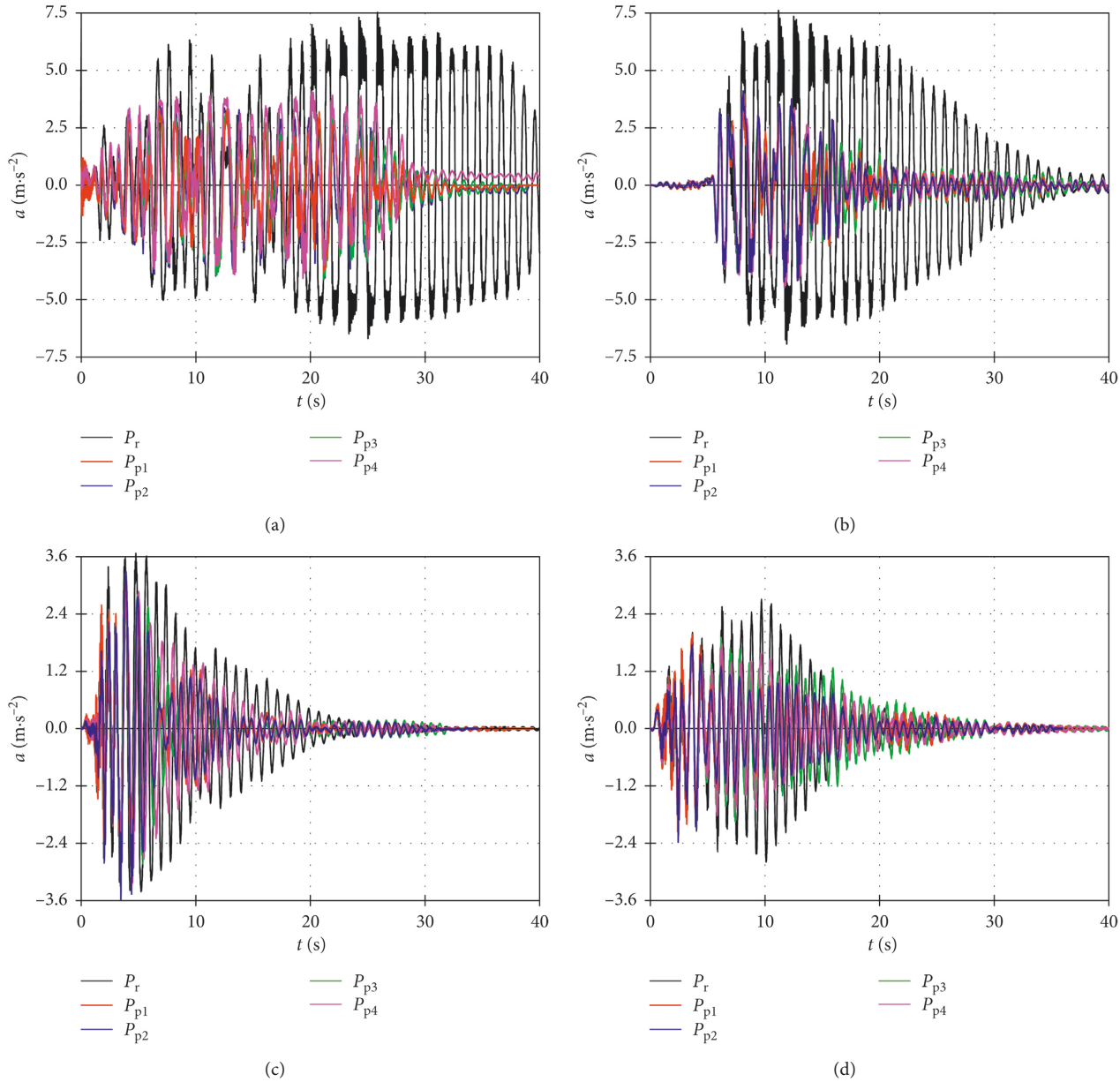


Figure 15: Horizontal acceleration of the mass center at the column top (a) for MSSB. (a) Artificial accelerogram (AA). (b) Accelerogram Petrovac (AP). (c) Accelerogram Ston (AS). (d) Accelerogram B. Luka (ABL).

maximum values on the rigid base and pebble layer, i.e., a better insight into the effectiveness of the pebble layer compared to the rigid base.

*8.3.1. Artificial Accelerogram (AA).* For the MSB model of the stiff building, compared to the rigid base case, the pebble layer reduced the horizontal displacement of the mass center at the column top by 70% and reduced the uplift of foundation by 77%. The horizontal acceleration of the mass center at the column top (inertial forces) was reduced by 50%, and the strains/stresses at the bottom of the steel column were reduced by 47%. There is remarkable similarity between the acceleration of the mass at the column top and the strains at the bottom of the steel column because the strains are the dominant consequence of the inertial force of mass at the column top.

For the MSSB model of the medium-stiff building, compared to the rigid base case, the pebble layer reduced the horizontal displacement of the mass center at the column top by 38% and reduced the uplift of the foundation by 56%. The horizontal acceleration of the mass center at the column top (inertial forces) was reduced by 42%, and the strains/stresses at the bottom of the steel column were reduced by 47%.

The pebble layer efficiency from the aspect of strain reduction at the bottom of the steel column is similar for the

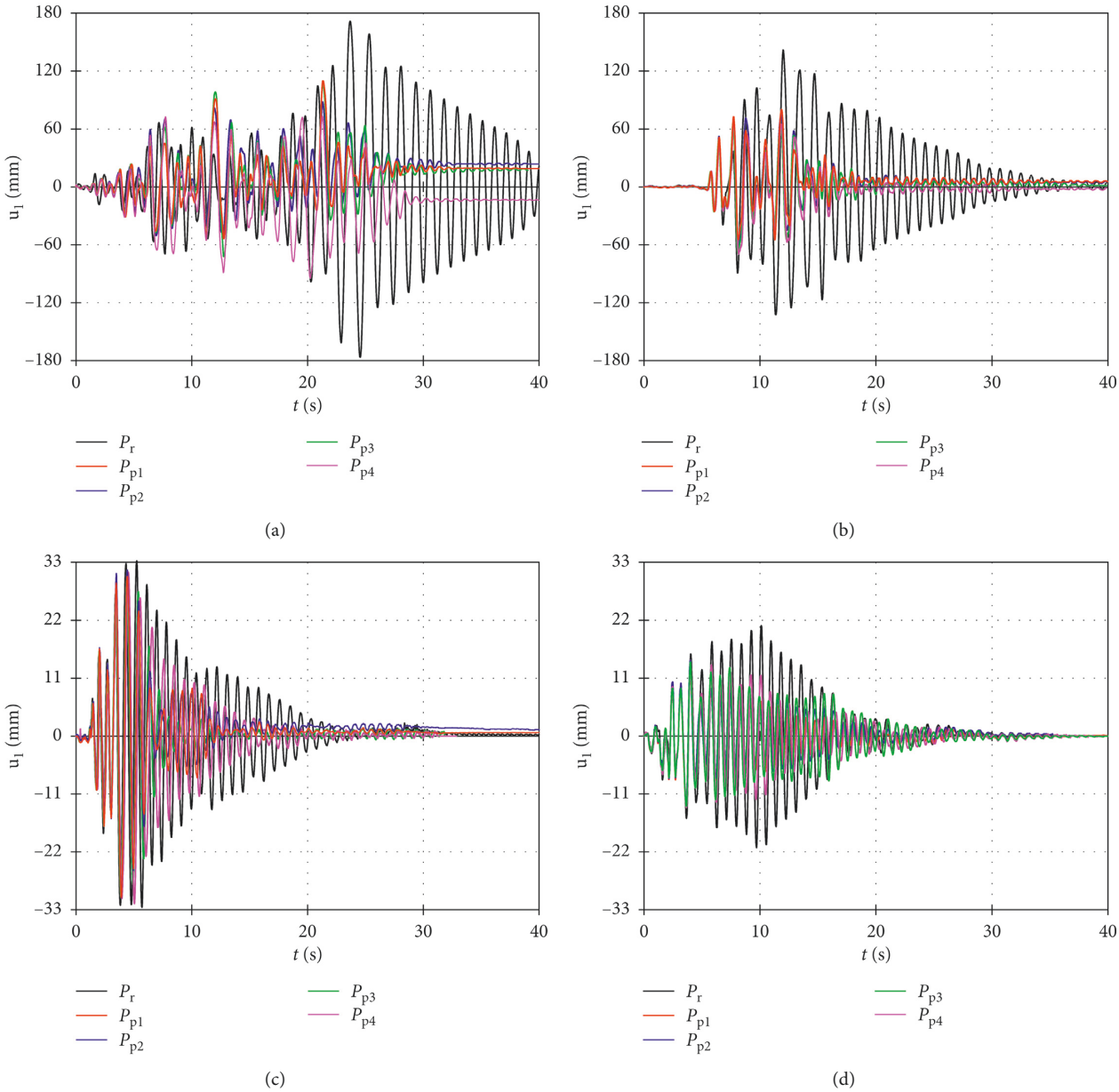


FIGURE 16: Horizontal displacement of the mass center at the column top ($u_1$) for MSSB. (a) Artificial accelerogram (AA). (b) Accelerogram Petrovac (AP). (c) Accelerogram Ston (AS). (d) Accelerogram B. Luka (ABL).

MSB and MSSB models, and from the aspect of displacement reduction, the MSB model is more favorable. The strains at the bottom of the steel column are several times higher for the MSSB model than for the MSB model. Large horizontal displacements of the mass center at the column top are the consequence of the adopted small dimensions of the foundation.

*8.3.2. Accelerogram Petrovac (AP).* For the MSB model of the stiff building, compared to the rigid base case, the pebble layer reduced the horizontal displacement of the mass center at the column top by 29%. The uplift of the foundation was reduced by 31%. The horizontal acceleration of the mass center at the column top and strain at the bottom of the steel column were reduced by 53%.

For the MSSB model of the medium-stiff building, compared to the rigid base case, the pebble layer reduced the horizontal displacement of the mass center at the column top by 44% and the uplift of the foundation by 52%. The horizontal acceleration of the mass center at the column top (inertial forces) was reduced by 41%, and the strains/stresses at the bottom of the steel column were reduced by 47%.

From the aspect of strain/stress reduction at the bottom of the steel column, the efficiency of the pebble layer is similar for the MSB and MSSB models. Moreover, the strain reduction at the bottom of the steel column is similar for AA and AP.

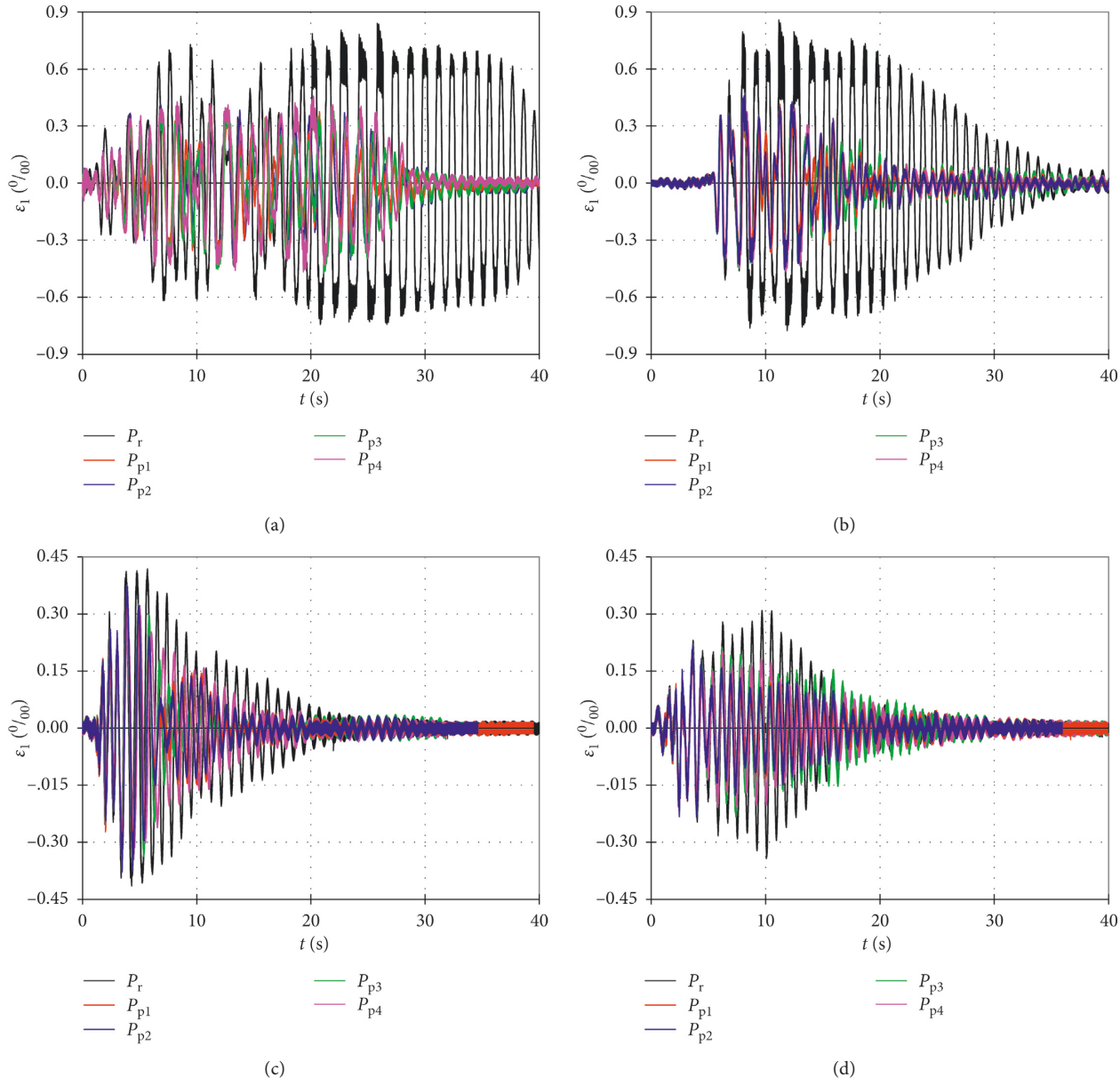


Figure 17: Vertical strain on the right bottom side of the steel column ($\varepsilon_1$) for MSSB. (a) Artificial accelerogram (AA). (b) Accelerogram Petrovac (AP). (c) Accelerogram Ston (AS). (d) Accelerogram B. Luka (ABL).

*8.3.3. Accelerogram Ston (AS).* Compared to AP and AA, AS produced several times smaller horizontal displacements of the mass center at the column top. However, regarding strains/stresses at the bottom of the steel column, no such difference was found. AS develops low values of displacement and stress/strain reduction because that excitation did not produce strong oscillations of the pebble layer. For the MSB model, compared to the rigid base case, the pebble layer reduced the strains at the bottom of the steel column by 26%. For the MSSB model, the reduction was only 8%. Obviously, the pebble layer for AS showed significantly lower efficiency than those for AA and AP and generated strains/stresses in models for AS that were significantly lower.

*8.3.4. Accelerogram B. Luka (ABL).* Generally, the comments in Section 8.3.3 regarding AS are valid. Compared to AS, the efficiency of the pebble layer in terms of strain reduction at the bottom of the steel column is higher for ABL. Compared to the rigid base case, the pebble layer reduced the strain at the bottom of the steel column by 28% and 31% on the MSB and MSSB model, respectively.

## 9. Conclusions

Based on the experimental research results of the behavior of two tested building models with fundamental periods $T$ = 0.05 s (the so-called model of stiff building (MSB)) and $T$ = 0.6 s (the so-called model of medium-stiff building (MSSB))

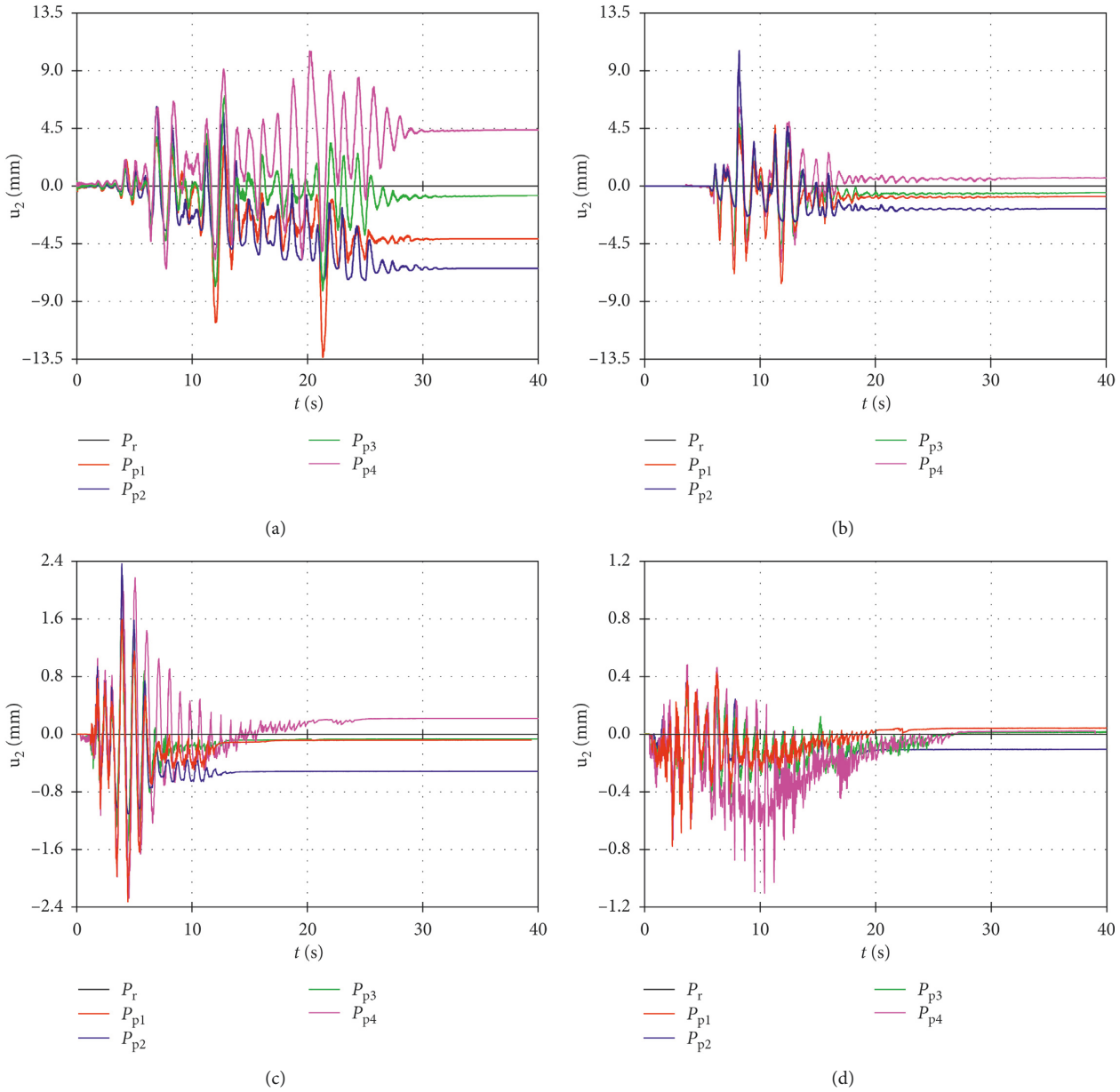


FIGURE 18: Horizontal displacement at the foundation top ($u_2$) for MSSB. (a) Artificial accelerogram (AA). (b) Accelerogram Petrovac (AP). (c) Accelerogram Ston (AS). (d) Accelerogram B. Luka (ABL).

supported on a rigid base and a pebble layer with a thicknesses of 0.3 m (the so-called thin layer) and 0.6 m (the so-called thick layer), with pebble fractions of 4–8 mm (the so-called small pebbles) and 16–32 mm (the so-called large pebbles), exposed to four different horizontal accelerograms (artificial accelerogram—AA, accelerogram Petrovac—AP, accelerogram Ston—AS, and accelerogram B. Luka—ABL) with model stresses in the elastic area, the following conclusions can be drawn:

(i) In relation to the behavior of the building models with the foundation on a rigid base, the use of a natural stone pebble layer under the foundation resulted in a much more favorable response to seismic base accelerations.

(ii) The strain/stress reduction in the column above the foundation for AA, AP, AS, and ABL was 47%, 53%, 26%, and 28% for the MSB model and 47%, 47%, 8%, and 31%, respectively, for the MSSB model. Note that all stresses were in the elastic area, without material nonlinearity of the structure.

(iii) The reduction in the horizontal displacement of the mass center at the column top for AA, AP, AS, and ABL was 70%, 29%, 0%, and 46% for MSB and 38%, 44%, 5%, and 31%, respectively, for MSSB.

(iv) The efficiency of the pebble layer for MSSB was almost equal as that for MSB.

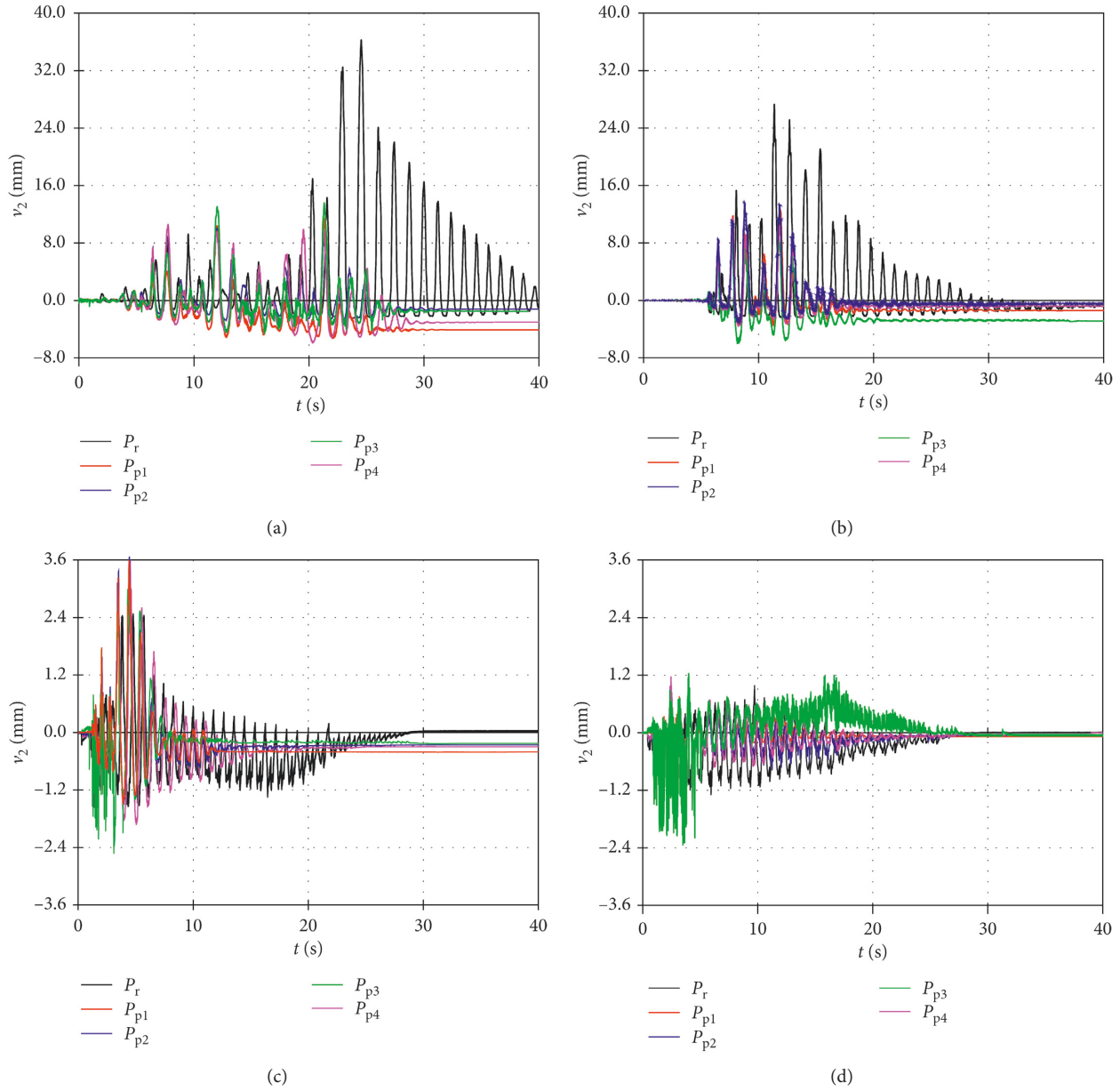


Figure 19: Foundation vertical displacement at the left edge ($v_2$) for MSSB. (a) Artificial accelerogram (AA). (b) Accelerogram Petrovac (AP). (c) Accelerogram Ston (AS). (d) Accelerogram B. Luka (ABL).

(v) The pebble layer efficiency in the performed tests was relatively independent of the thickness (0.3 m and 0.6 m) and the pebble fraction (4–8 mm and 16–32 mm).

(vi) According to the tests results, a small permanent horizontal displacement and vertical settlement (rotation) of the foundation on a real building on the considered pebble layer is expected.

(vii) Based on the results of the conducted experimental research, it can be expected that a stone pebble layer below the foundation of a real building is a sufficiently efficient low-technology seismic base isolation method, which is particularly useful for low-cost buildings in less-developed countries. However, firm conclusions require further research.

(viii) Although the above conclusions are based on the results of tests on small-scale models, we believe that they are also applicable to buildings in practice. This is explained by the fact that small-scale models had a fundamental free oscillation period as full-scale buildings and that only relative effects of the considered parameters were tested on small-scale models.

(ix) It should be noted that the proposed concept of seismic base isolation would not be efficient in

Table 1: Maximum values of some measured experimental results and their ratios.

| Applied excitation | Building model | Horizontal displacement of the block center | | | Vertical uplift of the foundation | | | Acceleration of the block center | | | Strain at the bottom of the column | | |
|---|---|---|---|---|---|---|---|---|---|---|---|---|---|
| | | $u_1$ (mm) | $u_1^*$ (mm) | $u_1^*/u_1$ | $v_1, v_2$ (mm) | $v_1^*, v_2^*$ (mm) | $(v_1^*, v_2^*)/(v_1, v_2)$ | $a$ (m·s$^{-2}$) | $a^*$ (m·s$^{-2}$) | $a^*/a$ | $\varepsilon_1, \varepsilon_2$ (‰) | $\varepsilon_1^*, \varepsilon_2^*$ (‰) | $(\varepsilon_1^*, \varepsilon_2^*)/(\varepsilon_1, \varepsilon_2)$ |
| Artificial | MSB | 150 | 45 | 0.30 | 64 | 15 | 0.23 | 11.6 | 5.5 | 0.47 | 0.055 | 0.029 | 0.53 |
| Accelerogram | MSSB | 173 | 107 | 0.62 | 39 | 17 | 0.44 | 7.6 | 4.4 | 0.58 | 0.850 | 0.460 | 0.53 |
| Accelerogram | MSB | 120 | 85 | 0.71 | 51 | 35 | 0.69 | 12.1 | 5.7 | 0.47 | 0.058 | 0.027 | 0.47 |
| Petrovac | MSSB | 142 | 80 | 0.56 | 28 | 13.5 | 0.48 | 7.6 | 4.5 | 0.59 | 0.870 | 0.460 | 0.53 |
| Accelerogram | MSB | 16.2 | 16.5 | 1.02 | 6.8 | 5.5 | 0.81 | 6.5 | 5.2 | 0.80 | 0.031 | 0.023 | 0.74 |
| Ston | MSSB | 33.6 | 32 | 0.95 | 3.2 | 3.7 | 1.16 | 3.7 | 3.7 | 1.00 | 0.415 | 0.380 | 0.92 |
| Accelerogram | MSB | 12 | 6.5 | 0.54 | 4.4 | 1.7 | 0.39 | 5.8 | 4.1 | 0.71 | 0.025 | 0.018 | 0.72 |
| B. Luka | MSSB | 21 | 14.5 | 0.69 | 1.4 | 2.3 | 1.64 | 2.8 | 2.4 | 0.86 | 0.320 | 0.220 | 0.69 |

$u_1$, $v_1$, $v_2$, $a$, $\varepsilon_1$, and $\varepsilon_2$ are the maximum values for the rigid base. $u_1^*$, $v_1^*$, $v_2^*$, $a^*$, $\varepsilon_1^*$, and $\varepsilon_2^*$ are the maximum values for the pebble layer.

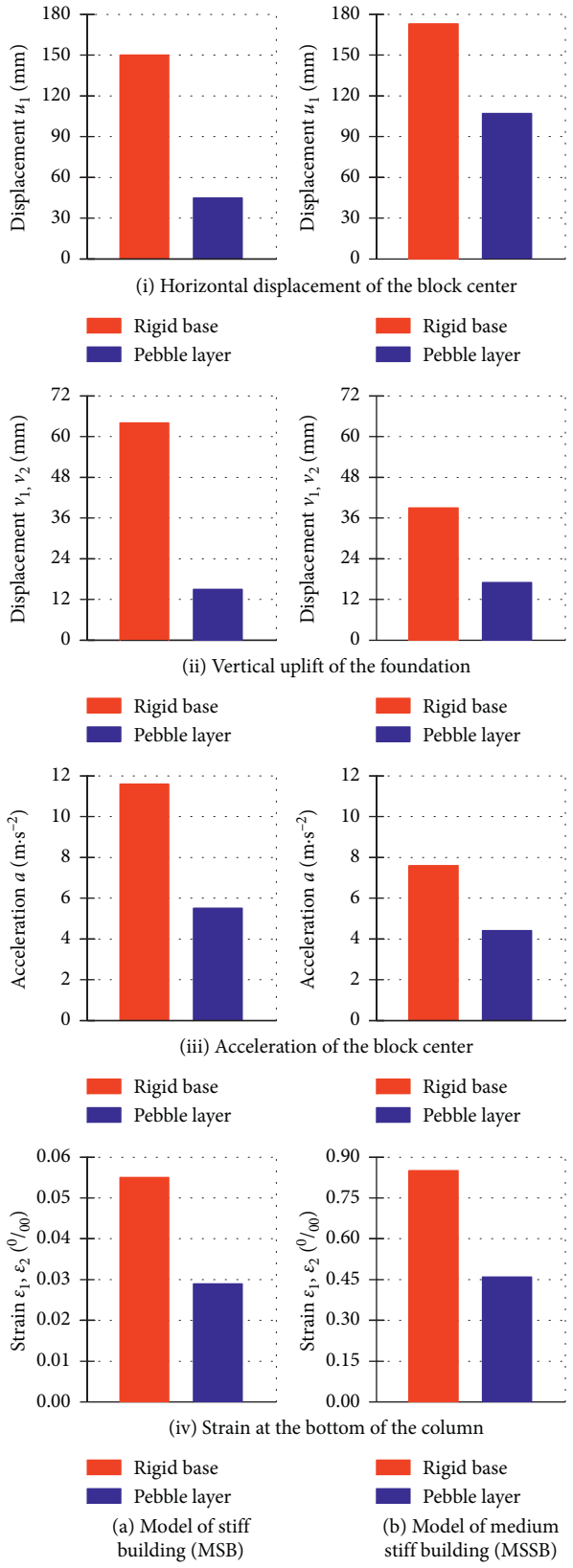


Figure 20: Some maximum measured values for an artificial accelerogram (AA). (a) Model of stiff building (MSB). (b) Model of medium stiff building (MSSB).

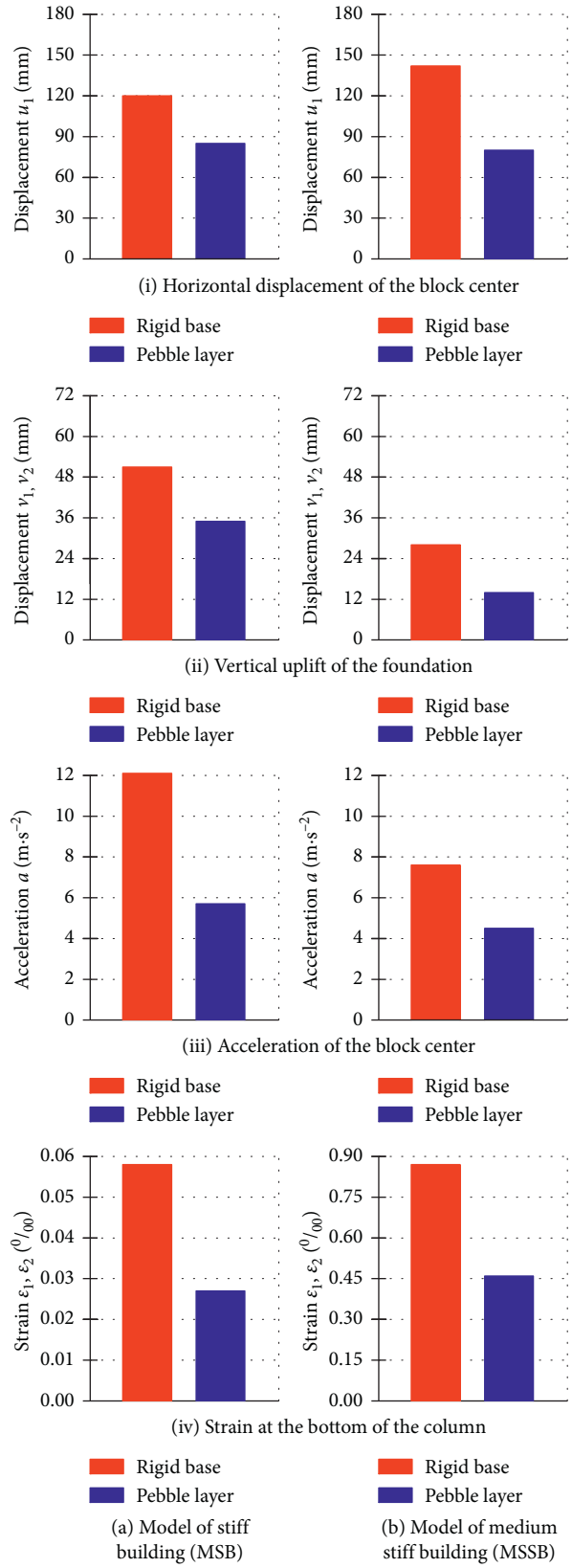


Figure 21: Some maximum measured values for the accelerogram Petrovac (AP). (a) Model of stiff building (MSB). (b) Model of medium stiff building (MSSB).

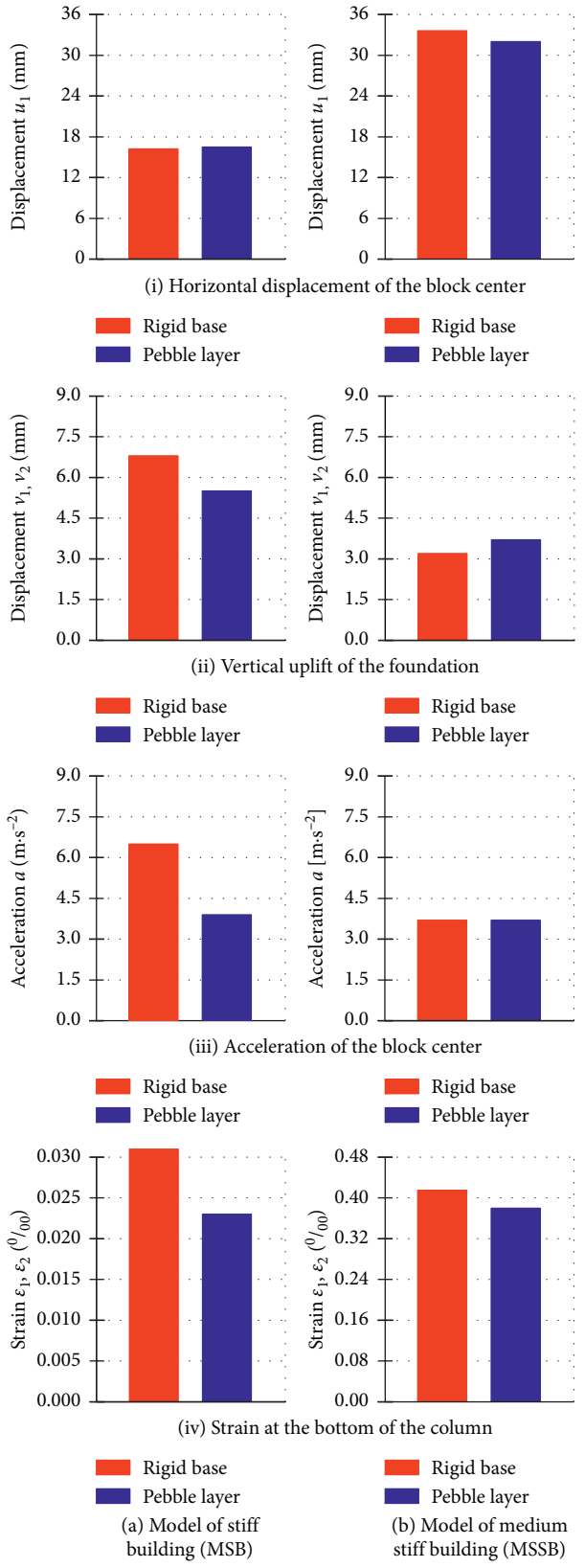


Figure 22: Some maximum measured values for the accelerogram Ston (AA). (a) Model of stiff building (MSB). (b) Model of medium stiff building (MSSB).

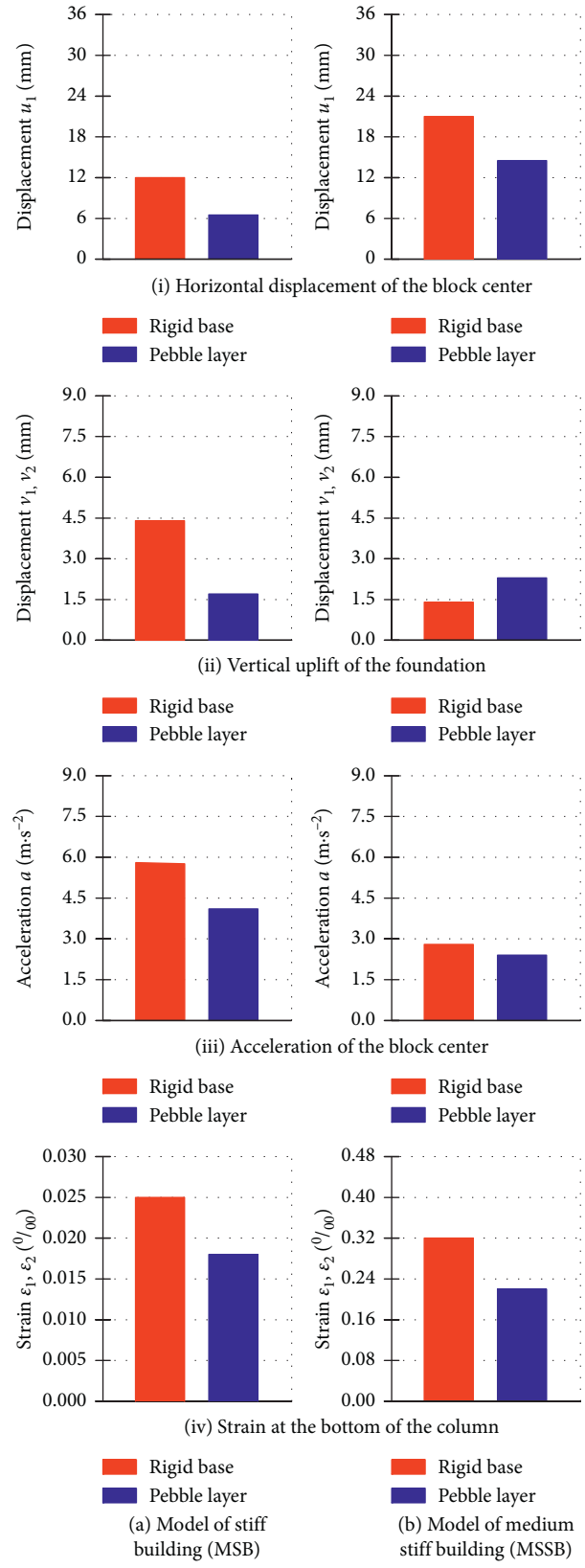


Figure 23: Some maximum measured values for the accelerogram B. Luka (ABL). (a) Model of stiff building (MSB). (b) Model of medium stiff building (MSSB).

earthquakes where the vertical acceleration component is dominant in relation to the horizontal component.

## Data Availability

The data used to support the findings of this study are included within the article.

## Conflicts of Interest

The authors declare that there are no conflicts of interest regarding the publication of this paper.

## Acknowledgments

This work has been fully supported by the Croatian Science Foundation under the project "*Seismic base isolation of a building by using natural materials – shake table testing and numerical modelling*" (IP-06-2016–5325). The work of doctoral student Ivan Banović has been fully supported by the "*Young researchers' career development project – training of doctoral students*" of the Croatian Science Foundation funded by the European Union from the European Social Fund. The authors are grateful for the support.

## References

[1] I. Doudoumis, P. Papadopoulos, and T. Papaliangas, "Low-cost base isolation system on artificial soil layers with low shearing resistance," in *Proceedings of the 12th European Conference on Earthquake Engineering*, London, UK, September 2002.

[2] M. K. Yegian and U. Kadakkal, "Foundation isolation for seismic protection using a smooth synthetic liner," *Journal of Geotechnical and Geo-Environmental Engineering*, vol. 130, no. 11, pp. 1121–1130, 2004.

[3] M. K. Yegian and M. Catan, "Soil isolation for seismic protection using a smooth synthetic liner," *Journal of Geotechnical and Geo-Environmental Engineering*, vol. 130, no. 11, pp. 1131–1139, 2004.

[4] H. Xiao, J. W. Butterworth, and T. Larkin, "Low-technology techniques for seismic isolation," in *Proceedings of NZSEE Conference*, New Zealand, 2004.

[5] H. H. Tsang, "Seismic isolation by rubber–soil mixtures for developing countries," *Earthquake Engineering & Structural Dynamics*, vol. 37, no. 2, pp. 283–303, 2008.

[6] J. Radnić, N. Grgić, D. Matešan, and G. Baloević, "Shake table testing of reinforced concrete columns with different layout size of foundation," *Materialwissenschaft und Werkstofftechnik*, vol. 46, no. 4-5, pp. 348–367, 2015.

[7] I. Banović, J. Radnić, N. Grgić, and D. Matešan, "The use of limestone sand for the seismic base isolation of structures," *Advances in Civil Engineering*, vol. 2018, Article ID 9734283, 12 pages, 2018.

[8] W. Xiong and Y. Li, "Seismic isolation using granulated tire–soil mixtures for less-developed regions: experimental validation," *Earthquake Engineering & Structural Dynamics*, vol. 42, pp. 2187–2193, 2013.

[9] H. H. Tsang, S. H. Lo, X. Xu, and S. M. Neaz, "Seismic isolation for low-to-medium-rise buildings using granulated rubber–soil mixtures: numerical study," *Earthquake Engineering & Structural Dynamics*, vol. 41, no. 14, pp. 2009–2024, 2012.

[10] K. Pitilakis, S. Karapetrou, and K. Tsagdi, "Numerical investigation of the seismic response of RC buildings on soil replaced with rubber–sand mixtures," *Soil Dynamics & Earthquake Engineering*, vol. 79, pp. 237–252, 2015.

[11] A. Panjamani, M. D. Ramegowda, and R. Divyesh, "Low cost damping scheme for low to medium rise buildings using rubber soil mixtures," *Japanese Geotechnical Society Special Publication*, vol. 3, no. 2, pp. 24–28, 2015.

[12] S. Bandyopadhyay, A. Sengupta, and G. R. Reddy, "Performance of sand and shredded rubber tire mixture as a natural base isolator for earthquake protection," *Earthquake Engineering & Engineering Vibration*, vol. 14, no. 4, pp. 683–693, 2015.

[13] S. J. Patil, G. R. Reddy, R. Shivshankar, R. Babu, B. R. Jayalekshmi, and B. Kumar, "Seismic base isolation for structures using river sand," *Earthquakes and Structures*, vol. 10, no. 4, pp. 829–847, 2016.

[14] R. P. Nanda, P. Agarwal, and M. Shrikhande, "Frictional base isolation by geotextiles for brick masonry buildings," *Geosynthetics International*, vol. 17, no. 1, pp. 48–55, 2010.

[15] R. P. Nanda, P. Agarwal, and M. Shrikhande, "Base isolation by geosynthetic for brick masonry buildings," *Journal of Vibration and Control*, vol. 18, no. 6, pp. 903–910, 2012.

[16] R. P. Nanda, M. Shrikhande, and P. Agarwal, "Effect of ground motion characteristics on the pure friction isolation system," *Earthquakes and Structures*, vol. 3, no. 2, pp. 169–180, 2012.

[17] R. P. Nanda, M. Shrikhande, and P. Agarwal, "Low-cost base-isolation system for seismic protection of rural buildings," *Practice Periodical on Structural Design and Construction*, vol. 21, no. 1, 2015.

[18] M. Qamaruddin and S. Ahmad, "Seismic response of pure-friction base isolation masonry building with restricted base sliding," *Journal of Engineering Research*, vol. 4, no. 1, pp. 82–94, 2007.

[19] S. Ahmad, F. Ghani, and R. Adil, "Seismic friction base isolation performance using demolished waste in masonry housing," *Construction and Building Materials*, vol. 23, no. 1, pp. 146–152, 2009.

[20] EN 1998-1:2004, *Eurocode 8: Design of Structures for Earthquake Resistance. Part 1: General Rules, Seismic Actions and Rules for Buildings*, European Committee for Standardization, Brussels, Belgium, 2004.

[21] N. Ambraseys, P. Smit, R. Sigbjörnsson, P. Suhadolc, and M. Margaris, *Internet-Site for European Strong-Motion Data, EVR1-CT-1999-40008*, European Commission, Directorate-General XII, Environmental and Climate Programme, Brussels, Belgium, 2001, http://www.isesd.hi.is/ESD_Local/frameset.htm.

# PAPER IV

ingegneria sismica
International Journal of Earthquake Engineering
Anno XXXVII – Num.2 - 2020

# EFFECT OF STRUCTURAL STIFFNESS ON THE EFFICIENCY OF SEISMIC BASE ISOLATION USING LAYERS OF STONE PEBBLES

*Ivan Banović*[1], *Jure Radnić*[1], *Nikola Grgić*[1]

[1]University of Split, Faculty of Civil Engineering, Architecture and Geodesy, Split, Croatia

SUMMARY: *The effect of structural stiffness on the efficiency of seismic base isolation using layers of stone pebbles is experimentally investigated by shake-table. The efficiency of the adopted layers is tested on four models with different stiffness, under four different earthquake accelerograms. A part of the study was carried out for one-time accelerations of the shake-table with strains in elastic range, and another part, for the most unfavourable accelerogram, was carried out by successive increase in the acceleration to the collapse of the model. It is concluded that efficiency of the considered seismic isolations systems decreased with decrease of model stiffness and that this concept shows great potential in increase of structural seismic resistance.*

KEYWORDS: *seismic base isolation, stone pebble layer, effect of structural stiffness, shake-table testing*

## 1 Introduction

The development of seismic isolation with a layer of natural and combined widely available materials underlying the foundations of lower buildings in seismic zones of small and medium-sized economically developed countries has increasingly intensified in recent years. One of the main limitations of conventional seismic isolation is significant up-front cost [Tsiavos *et al.* 2019]. Owing to the low economic power, application of conventional seismic isolation techniques is limited in these areas. Therefore, an alternative, simple, low-cost, environmentally friendly, and efficient system for these regions is needed.

Unfortunately, such reliable seismic isolation, which dissipates seismic energy predominantly through slipping (exceeding of friction) within the aseismic layer and on the layer-foundation coupling surface, has not yet been found. Below are some experimental and numerical studies that investigate acceptable low-cost and low-tech seismic isolation.

In ancient times, it was not uncommon for builders to interpose sand, gravel or clay bedding between the ground and foundations [Carpani, 2017]. Carpani [2014] also presented a number of technological achievements in the ancient world and provided significant insight into the geotechnical skills of architects and builders in the ancient world. Kelly [1996a] and Kelly and Taniwangsa [1996] described the development of seismic isolators for low-cost buildings. A review of aspects of the development, theory, and application of base isolation can be found in the literature [Kelly, 1996b] [Naeim and Kelly, 1999] [Warn and Ryan, 2012] [Calvi and Calvi, 2018] [Makris, 2018]. Tehrani and Hasani [1996] concluded from experimental studies that dune sand and lightweight expanded clay may be good materials for creating sliding layers in adobe buildings in Iran. Patil *et al.* [2016] isolated a structural model using river sand and found encouraging results. Zhao *et al.* [2016] numerically

Corresponding author: Ivan Banović, University of Split, Faculty of Civil Engineering, Architecture and Geodesy, Croatia.
Email: ivan.banovic@gradst.hr

simulated a gravel isolation layer. The acceleration reduction is shown to increase with the increase in layer thickness and to decrease with the increase in base pressure. Seismic performance of a rocking-isolated bridge pier on surface foundations resting on sand by shake-table tests was studied by Anastasopoulos *et al.* [2012]. The rocking-isolated system is proven to be remarkably resistant to cumulative cyclic loading.

Some of the world's biggest bridges like the Rio–Antirio Bridge [Pecker *et al*., 2001] in Greece, the Vasco de Gama Bridge [Pecker *et al*., 2003] in Portugal, and the Izmit Bay Bridge [Steenfelt *et al.*, 2015] in Turkey have pylons founded on caisson-cushion-pile composite foundation. In a search for the simplest seismic isolation from natural materials, Radnić *et al.* [2015] and Banović *et al.* [2018a] experimentally confirmed that even a thin layer of limestone sand under the foundation can reduce earthquake-induced stresses in the concrete column by approximately 10 %. Karatzia *et al.* [2019] proposed a design method for the seismic protection of structures on liquefied ground using shallow (instead of deep) foundations. The proposed geotechnical approach exploits the presence of natural liquefiable soil as a natural base isolation system that de-amplifies the seismic ground motion and hence reduces the seismic demand on the superstructure. Many researchers investigated pure-friction base isolation systems [Xiao *et al.*, 2004] [Lomiento *et al*., 2013] [Calvi *et al.*, 2016] [Castaldo and Ripani, 2017] [De Domenico, 2019]. In recent years, innovative seismic isolation devices based on lattice materials are developed [Amendola *et al.*, 2016a, 2016b] [Fabbrocino *et al.*, 2016] [Fraternali *et. al.*, 2018].

There are some studies involving smooth synthetic liners and geomembranes/geotextiles for dissipating seismic energy through sliding [Doudoumis *et al.*, 2002] [Yegian and Kadakal, 2004] [Yegian and Catan, 2004] [Kalpakcı *et al.*, 2018]. Tsang [2008] proposed rubber-soil mixtures (RSM) around the foundations of structures for absorbing seismic energy and exerting a function similar to that of a cushion. Furthermore, Tsang [2008] proposed that the aforementioned seismic isolation methods involving geotechnics could be collectively termed "*Geotechnical Seismic Isolation (GSI)*", in contrast to the commonly used "*Structural Seismic Isolation*". Namely, the dissipation of earthquake energy and the reduction of earthquake forces on the building in this concept are dominated by the sliding mechanism of the foundation for seismic isolation and between soil sublayers. Another way to describe the mechanism of this isolation concept is the "distributed seismic isolation system," which has been discussed by Tsang [2008] and Mavronicola *et al.* [2010]. The concept of GSI has gained a lot of momentum in the past few years. Current GSI efforts are mainly focused on soil replacement by rubber-soil mixtures [Tsang, 2009] [Tsang *et al.*, 2012] [Xiong and Li, 2013] [Xiong *et al.*, 2014] [Bandyopadhyay *et al.*, 2015] [Panjamani *et al.*, 2015] [Brunet *et al.*, 2016] [Forcellini, 2017] [Hadad *et al.*, 2017] [Tsiavos *et al.* 2019] or geofoam [Murillo *et al.*, 2009] [Azinović *et al.*, 2014, 2016] [Koren and Kilar, 2016] [Karatzia and Mylonakis, 2017] [Azzam *et al.*, 2018]. Relatively fewer works concern the sliding mechanism [Banović *et al*., 2018b, 2019].

Banović *et al.* [2018b] experimentally tested models of stiff and medium-stiff structures (free-standing steel column with concrete foundation and mass at the column top) and confirmed that a layer of natural stone pebbles can greatly reduce the inertial forces and strains/stresses in the tested models. For such a solution, Banović *et al.* [2019] experimentally investigated the optimum properties of an aseismic layer (the layer thickness, the fraction of pebbles, the pebble compaction, the pebble moisture, the vertical contact stress below the foundation, and the effect of repeated excitations). They concluded that the results of the

research are very encouraging but that further research is needed in order to make possible the practical application of such a solution.
This paper presents the results of a further research segment related to the potential application of seismic base isolation presented in Banović *et al.* [2018b]. Namely, this paper presents research results related to the efficiency of the adopted seismic isolation depending of the stiffness of the structure model: very stiff structure ($M_1$), stiff structure ($M_2$), medium-stiff structure ($M_3$) and soft structure ($M_4$). Thus, the research has expanded to include the possibility of applying this concept in a very wide stiffness range of potential buildings. Experiments were carried out on the free-standing models as in Banović *et al.* [2018b], with four characteristic earthquake accelerograms. A part of the study was carried out for the lower maximum acceleration of the shake-table (up to 0.3 g) with the stresses of the model in the elastic range (Section 7), and part of the study for the most unfavorable accelerogram was carried out by incremental base acceleration tests to the collapse of the model (Section 8). The most important conclusions of the research are presented in Section 9.

## 2 Aseismic layers

Two thicknesses of the aseismic layer were considered: $h_p$ = 0.3 m and $h_p$ = 0.6 m (Figure 1). In accordance with the results of the study [Banović *et al.*, 2019], the following characteristics of the pebble layer were adopted as optimal: the pebble fraction $\Phi_b$ = 16-32, the pebble layer compaction *MS* = 30 MPa and the pebble moisture *h* = 10 %. Layers are formed within a rigid frame with a plan size of 2.5 m × 2.5 m and fixed to the shake-table. Aseismic layers are reconstructed to the predicted compactness and moisture, with the alignment of the top, after the completion of the application of each base excitation. Although a simple structural model was used, the layer thickness was used in real size. This concept is logical because adopted structure model has the same dynamic characteristics (stiffness and periods of free oscillations) as that of the target full-scale structure.

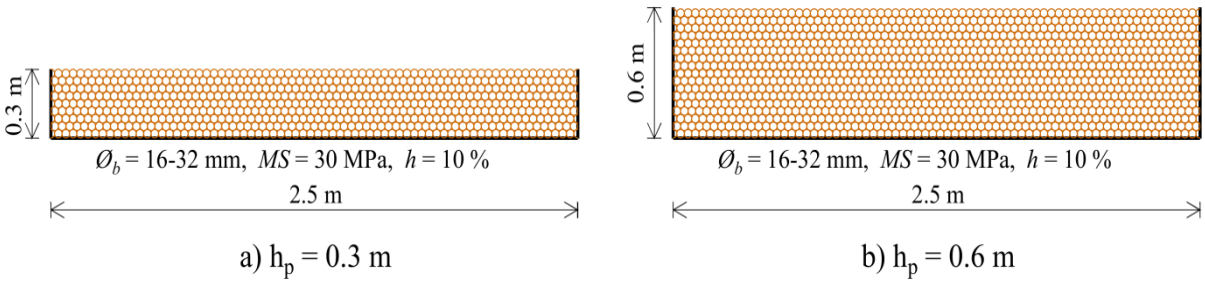


Figure 1 - *Adopted aseismic layers*

## 3 Analyzed structure models

As mentioned above, four structure models, $M_1$, $M_2$, $M_3$ and $M_4$, are tested, which are free-standing steel columns with concrete foundation and mass on the column top (Figure 2). The columns are made of a square hollow hot-rolled steel tubes (S355), wherein the period of vibration (T) of $M_1$ is T = 0.05 s, that of $M_2$ is T = 0.30 s, that of $M_3$ is T = 0.60 s, and that of $M_4$ is T = 1.40 s. Vibration period of models are calculated for linear system and verified on shake-table. Main objective was to investigate effect of different structural stiffness on the efficiency of seismic base isolation using layer of stone pebbles. Model $M_1$ represents a very

stiff structure, $M_2$ a stiff structure, $M_3$ a medium-stiff structure and $M_4$ a soft structure. The models include a foundation for incorporating the effect of soil-foundation-structure interaction on structure behaviour. A mass of m = 1000 kg was adopted at the column top, formed from a concrete block of 1 m x 1 m x 0.4 m that was rigidly coupled with the column. The adopted square hollow cross-section dimensions of the steel column are such that the stresses during the tests presented in Section 7 remain elastic. The intention was to exclude the influence of nonlinearity in the construction material, *i.e.*, all nonlinearities and dissipation of seismic energy are realized in the pebble layer and in the layer-foundation coupling surface. In this way, the efficiency of seismic isolation is most clearly demonstrated. All the samples were first tested for the case of classical support on a rigid base without seismic isolation (a thin concrete layer fixed on the shake-table that simulates the usual sub-concrete under the foundation of a real building). For this support case, the horizontal displacement of the foundation in relation to the base (shake-table) is prevented, while the rocking and uplifting of the foundation are allowed. This support case is more realistic than the fixed base support case. In the fixed base support case, structures are analysed with the assumption that there is no displacement and rotation of the foundation in relation to the base. Also, compared to the fixed base, rigid base support case produces lower seismic forces on the model, which gives more conservative seismic base isolation efficiency. Subsequently, the samples were tested on the considered aseismic layers.
Some testing results for incremental base acceleration tests until considered models collapsed are presented in Section 8.

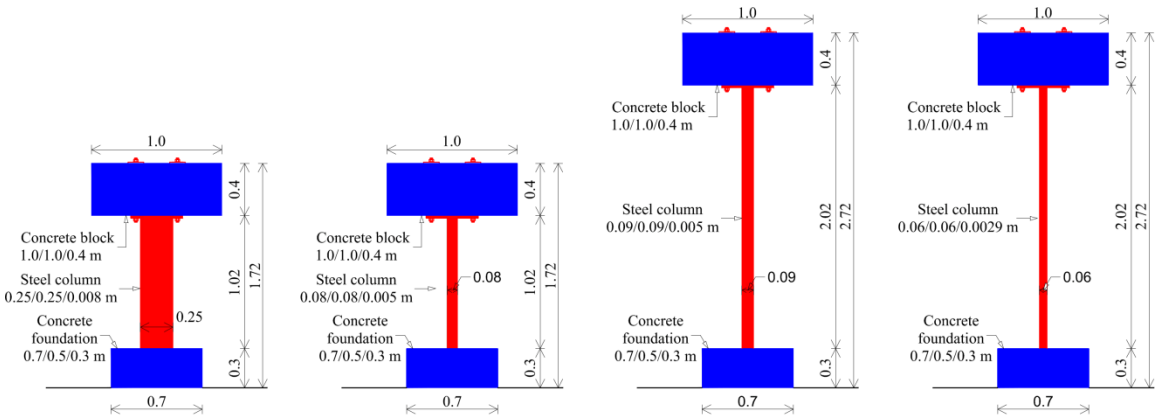


Figure 2 - *Adopted structure models*

## 4 Dynamic base excitations

Choosing adequate accelerograms for the analysis of different structures is not an easy task. It is well known that the seismic wave propagation is influenced by: the characteristics of the earthquake excitation (magnitude, type of fault breaking and source-site distance) and, the local response in function of very complex interactions between seismic waves and local conditions, generally known as "site effects" [Zuccaro *et al.*, 2018].
In this study, four accelerograms for dynamic base excitation were adopted, and the uniaxial horizontal acceleration and spectral values are presented in Figure 3. An artificial accelerogram, AA, was created to match elastic response spectrum according to EC 8 [2004]

for earthquake type 1 and soil type A, and the N-S accelerogram of the Petrovac earthquake (Montenegro, 1979), AP [Ambraseys *et al.*, 2001], represents long-lasting earthquakes with a relatively longer predominant period. Artificial accelerogram (AA) was generated using SIMQKE software (1976), as a superposition of sine functions. The N-S accelerogram of the Ston earthquake (Croatia, 1996), AS [Ambraseys *et al.*, 2001], and the N-S accelerogram of the B. Luka earthquake (BiH, 1981), ABL [Ambraseys *et al.*, 2001], represent short impact earthquakes with a short predominant period. Accelerograms AA and AP bring high earthquake input energy into the structure and have a greater structure bending effect, whereas accelerograms AS and ABL have a more pronounced effect of the shear force. The intention was not to find the most unfavourable excitation for the considered models but to choose excitations that cover a wide spectrum of potential earthquake types. Within the research presented in Section 7, all the excitations were applied once with $a_{g,max}$ = 0.3 g for $M_1$ and $M_2$ and with $a_{g,max}$ = 0.2 g for $M_3$ and $M_4$. Within the research presented in Section 8, each tested sample was exposed to incremental base acceleration tests by scaling the peak ground acceleration (PGA) for $\Delta a_{g,max}$ = 0.05 g until the structure collapsed.
The main characteristic of the four ground motions used are presented in Table 1. It should be noted that all the ground motions presented are scaled to the same acceleration values.

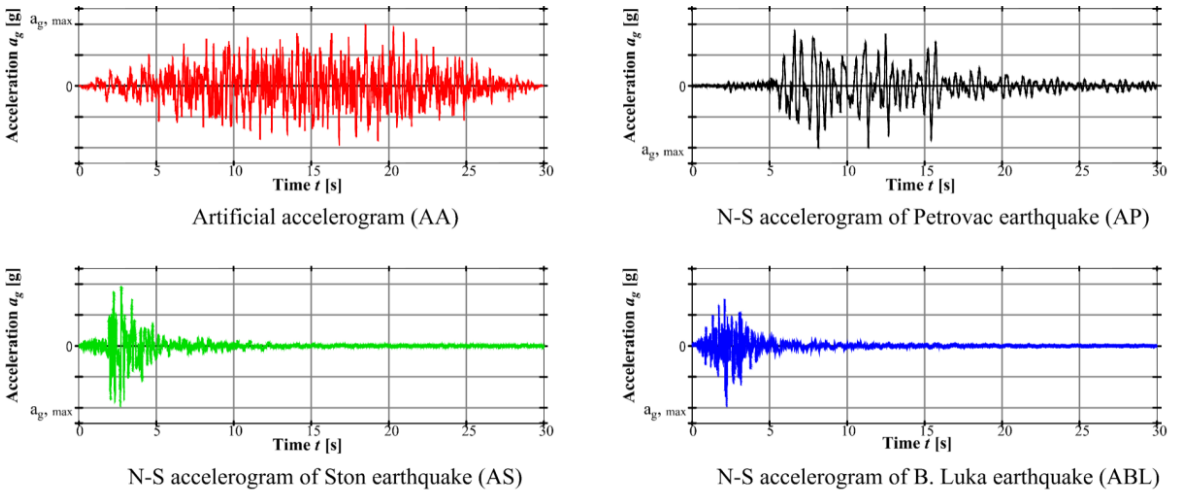


Figure 3 - *Adopted dynamic excitations*

Table 1 - *Main characteristics of ground motions used*

| No. | Event | Station and instrument | Magnitude (Mw) | Epicentre distance (km) | Fault distance (km) | PGA (g) |
|---|---|---|---|---|---|---|
| 1 | Petrovac, Montenegro - AP (15.04.1979. 06:19:41 UTC) | Petrovac-Hotel Oliva, SMA-1 | 6.9 | 25 | 3 | 0.454 |
| 2 | Ston, Croatia - AS (05.09.1996. 20:44:17 UTC) | Ston-Salt Plant, SMA-1 | 6.0 | 16 | 15 | 0.653 |
| 3 | Banja Luka, BiH - ABL (13.08.1981. 02:58:12 UTC) | Banja Luka-Material Testing Institute, SMA-1 | 5.7 | 7 | 4 | 0.442 |
| 4 | Artificial accelerogram - AA | Generated as superposition of sine functions (SIMQKE software, 1976) | | | | |

## 5 Measured quantities

The following quantities were measured on each tested sample (Figure 4): horizontal acceleration of the mass centre at the column top $a$, horizontal displacement at the foundation top $u_1$, horizontal displacement of the mass centre at the column top $u_2$, vertical displacements at the right edge $v_1$ and at the left edge $v_2$ of the foundation, and vertical strains on the bottom of the steel column at the right side $\varepsilon_1$ and at the left side $\varepsilon_2$.

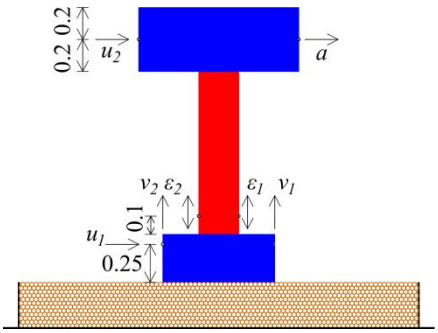


Figure 4 - *Measured quantities*

## 6 Instrumentation

A uniaxial shake-table at the University of Split, Faculty of Civil Engineering, Architecture and Geodesy (Croatia), was used to test the models. The shake-table had a layout size of 4 m × 4 m, maximum capacity was 20 000 kg, a maximum displacement of ±150 mm, a maximum acceleration of up to 5 g, and frequencies ranging from 0-20 Hz. The shake-table is controlled via acceleration, and the acceleration function can be arbitrary. Weight of test samples, shake-table displacement (acceleration) and the oscillation frequency are mutually

dependent. A Hottinger Baldwin Messtechnik GmbH (HBM) QuantumX high-speed data acquisition system with 16 channels was used. Analogue displacement sensors of type PB-25-S10-N0S-10C (Uni Measure) were used for measuring displacement. The accelerations were measured by a piezoelectric low-frequency accelerometer type 4610 (MS). The sampling rate during the tests was 200 Hz. A video camera (Canon EOS M5) was used to monitor and record the tests.

## 7 Some test results for one-time base excitation application with elastic stresses in models

First, the behavior of models $M_1$-$M_4$ on a rigid base and on the two pebble layers with one-time application of AA, AS, ABL and AP was investigated. Excitations were applied with $a_{g,max}$ = 0.3 g for $M_1$ and $M_2$ and $a_{g,max}$ = 0.2 g for $M_3$ and $M_4$. Only some obtained results are given hereafter, separately for all the tested models.

### 7.1 Time-history presentation of some measured test results

The time histories for some of the measured quantities ($\varepsilon_1$, $a$, $u_1$, $u_2$, and $v_1$) are presented in Figures 5-16. Figures 5-8 refer to accelerogram AA, Figures 9 and 10 refer to accelerogram AP, Figures 11-14 refer to accelerogram AS, and Figures 15 and 16 refer to accelerogram ABL. A relatively wide range of experimental results has been presented for possible calibration of numerical models. The obtained results are briefly commented on below, after presentation of all Figures.
The maximum values of the considered quantities are commented in Section 7.2.

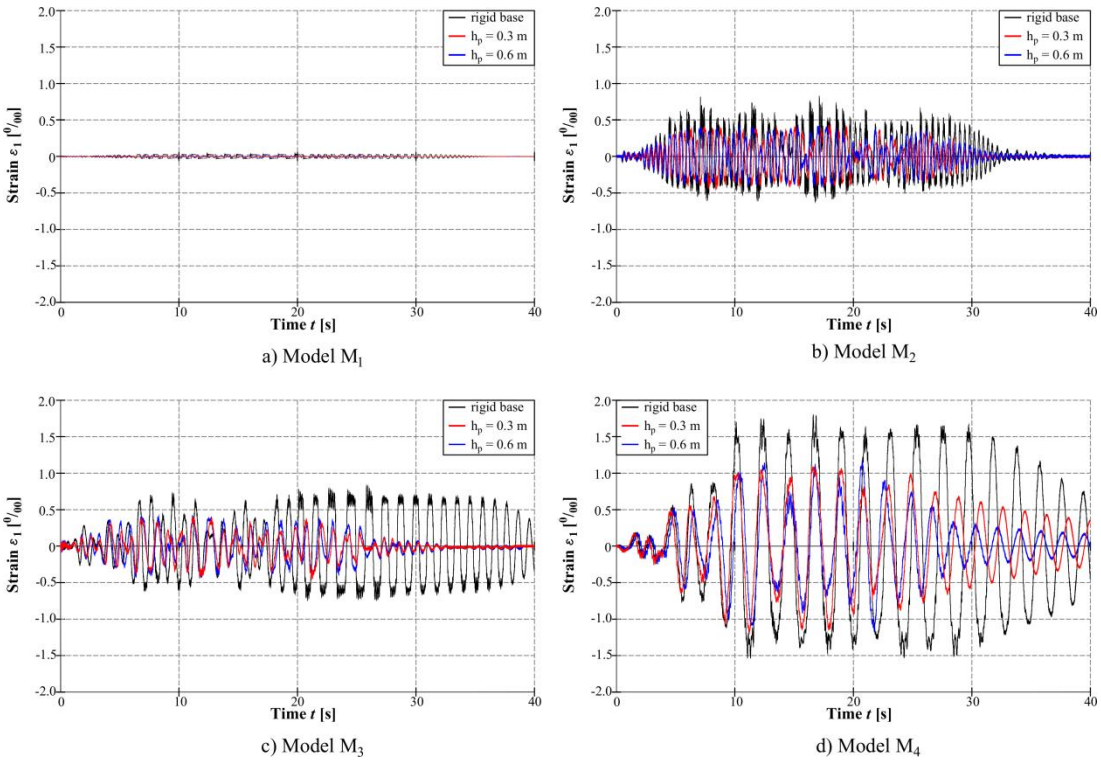


Figure 5- *Vertical strain on the right bottom side of the steel column $\varepsilon_1$ for accelerogram AA*

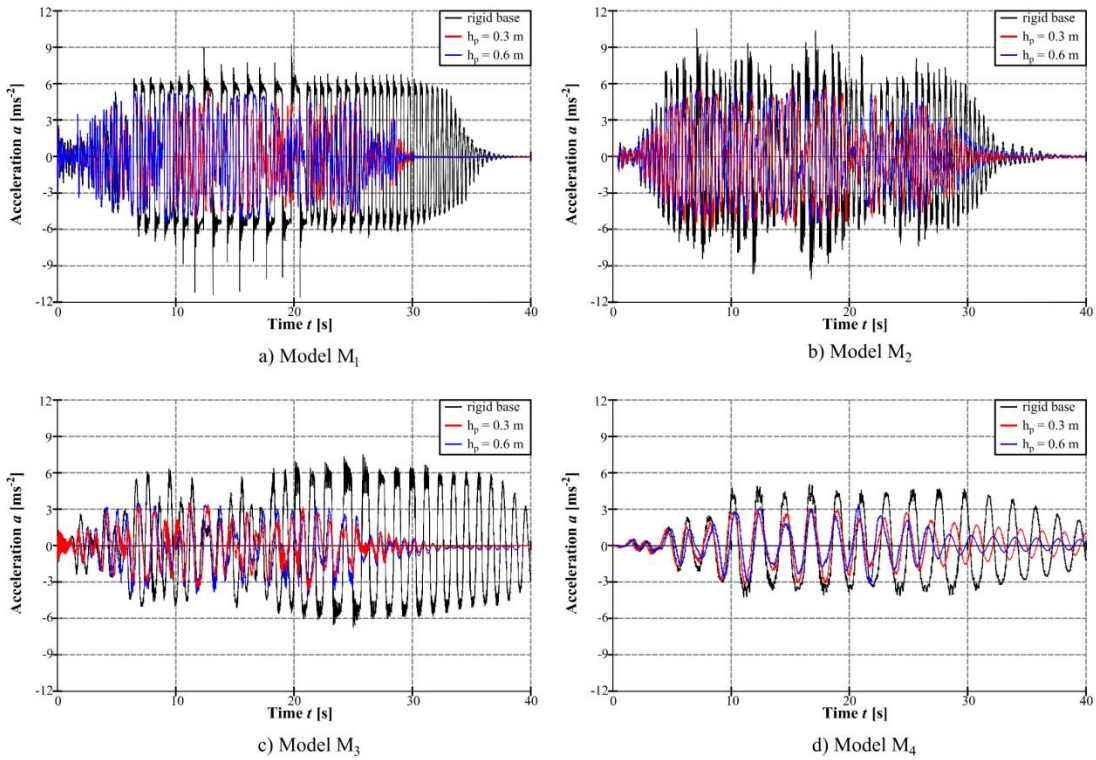


Figure 6 - *Horizontal acceleration of the mass centre at the column top a for accelerogram AA*

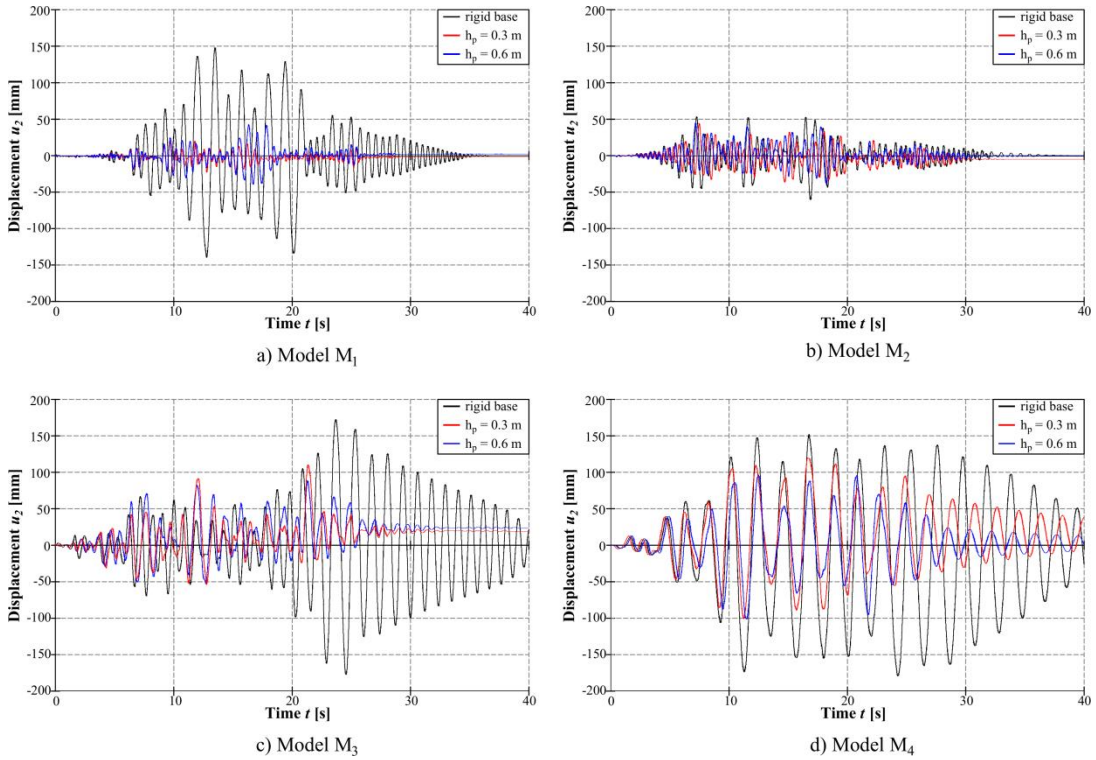


Figure 7 - *Horizontal displacement of the mass centre at the column top $u_2$ for accelerogram AA*

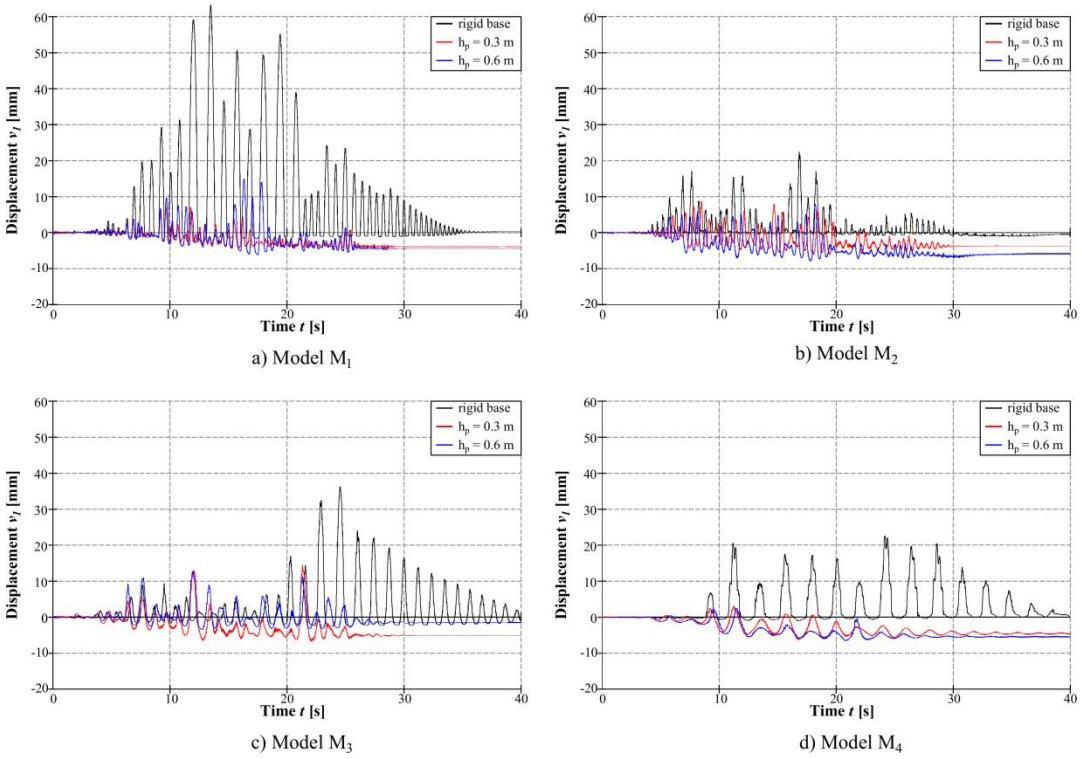


Figure 8 - *Vertical displacement at the left edge of the foundation $v_1$ for accelerogram AA*

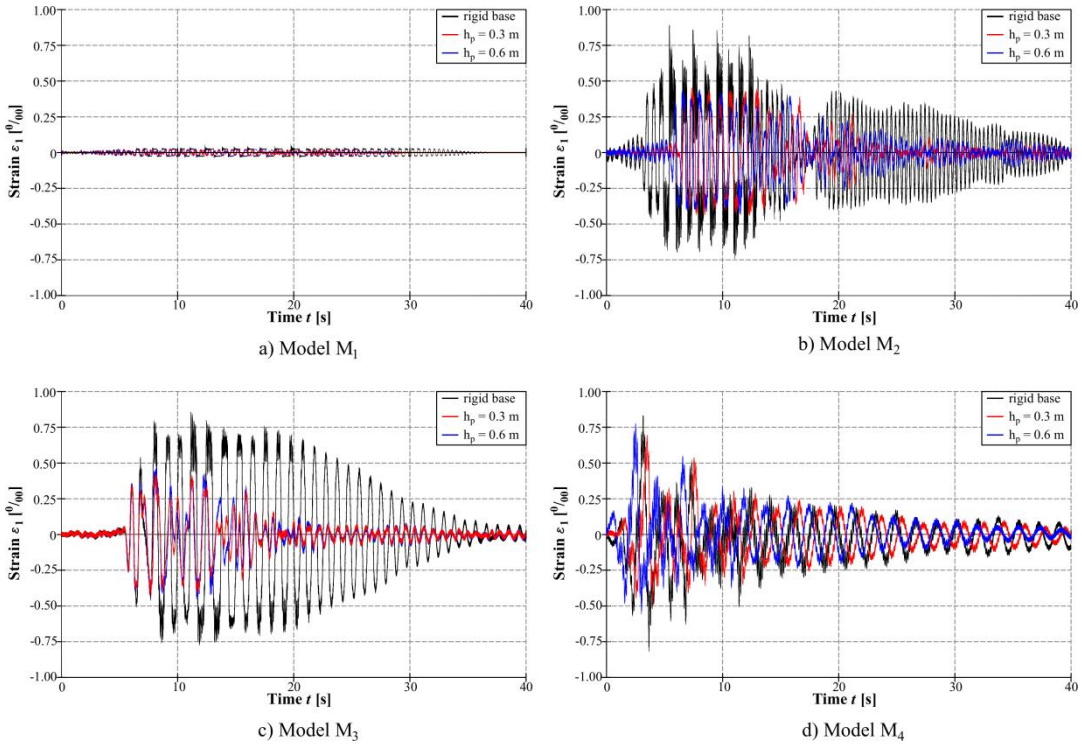


Figure 9 - *Vertical strain on the right bottom side of the steel column $\varepsilon_1$ for accelerogram AP*

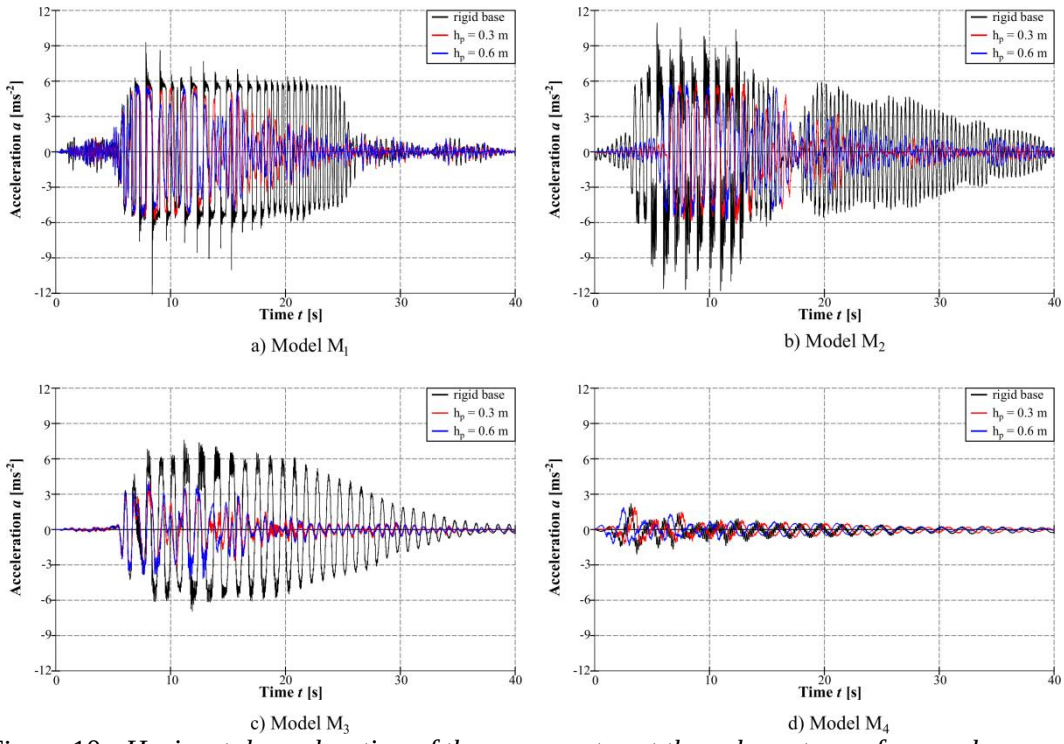


a) Model $M_1$ b) Model $M_2$

c) Model $M_3$ d) Model $M_4$

Figure 10 - *Horizontal acceleration of the mass centre at the column top a for accelerogram AP*

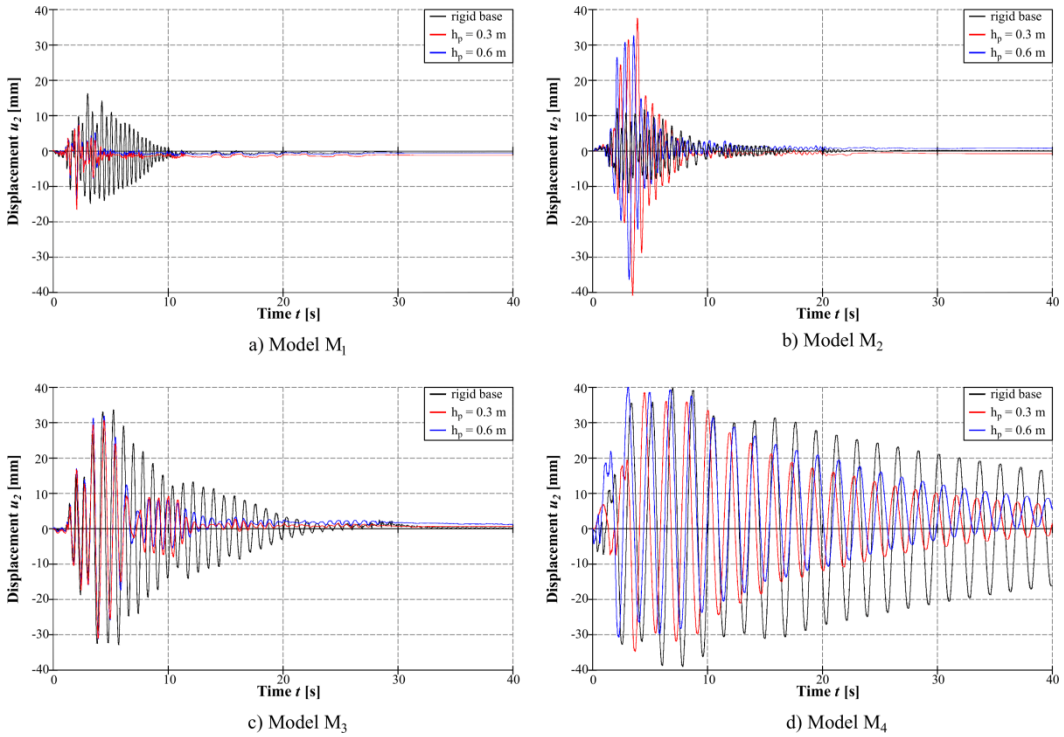


a) Model $M_1$ b) Model $M_2$

c) Model $M_3$ d) Model $M_4$

Figure 11 - *Horizontal displacement of the mass centre at the column top $u_2$ for accelerogram AS*

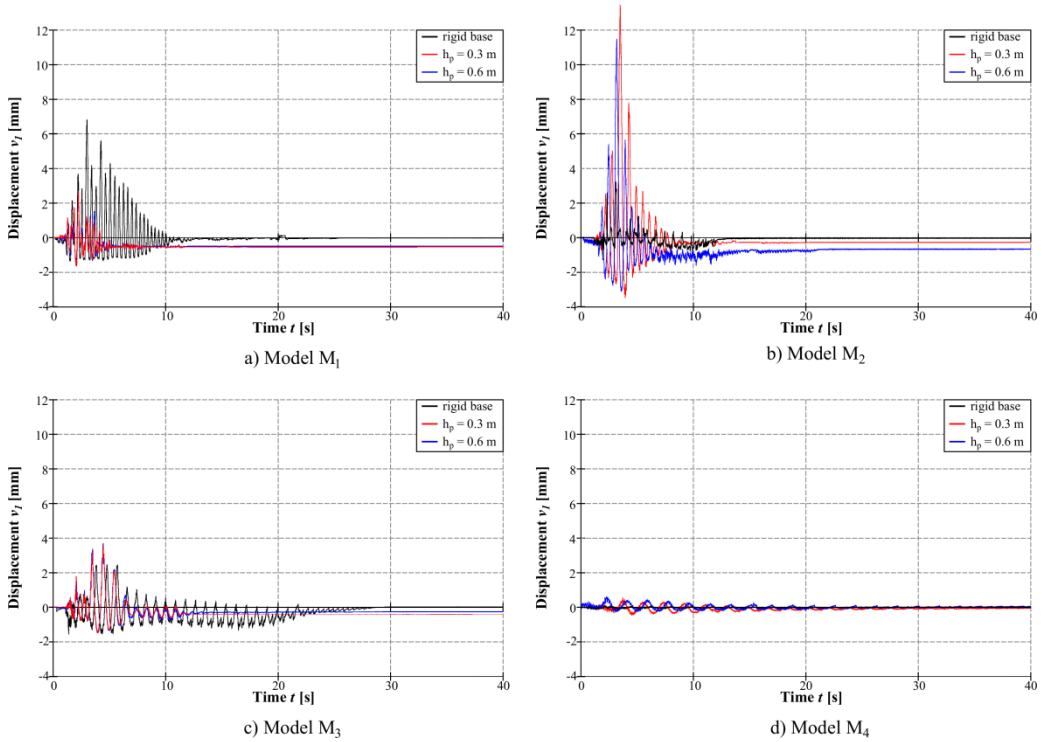


a) Model $M_1$ b) Model $M_2$

c) Model $M_3$ d) Model $M_4$

Figure 12 - *Vertical displacement at the left edge of the foundation $v_1$ for accelerogram AS*

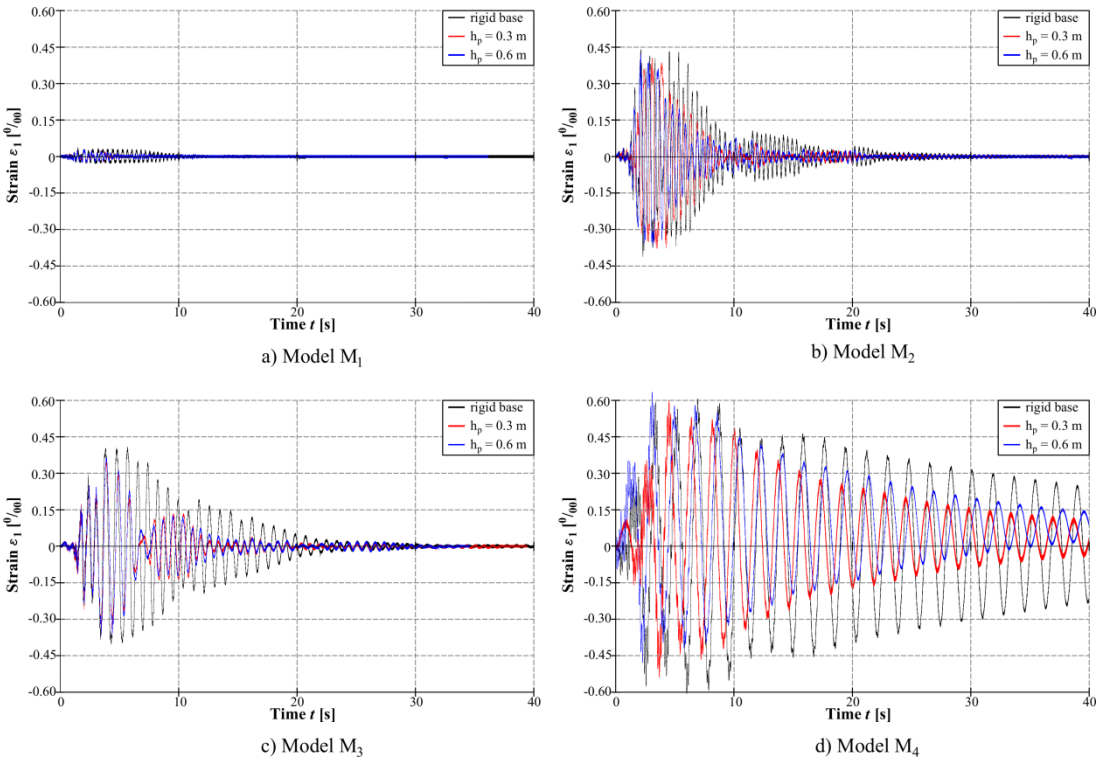


a) Model $M_1$ b) Model $M_2$

c) Model $M_3$ d) Model $M_4$

Figure 13 - *Vertical strain on the right bottom side of the steel column $\varepsilon_1$ for accelerogram AS*

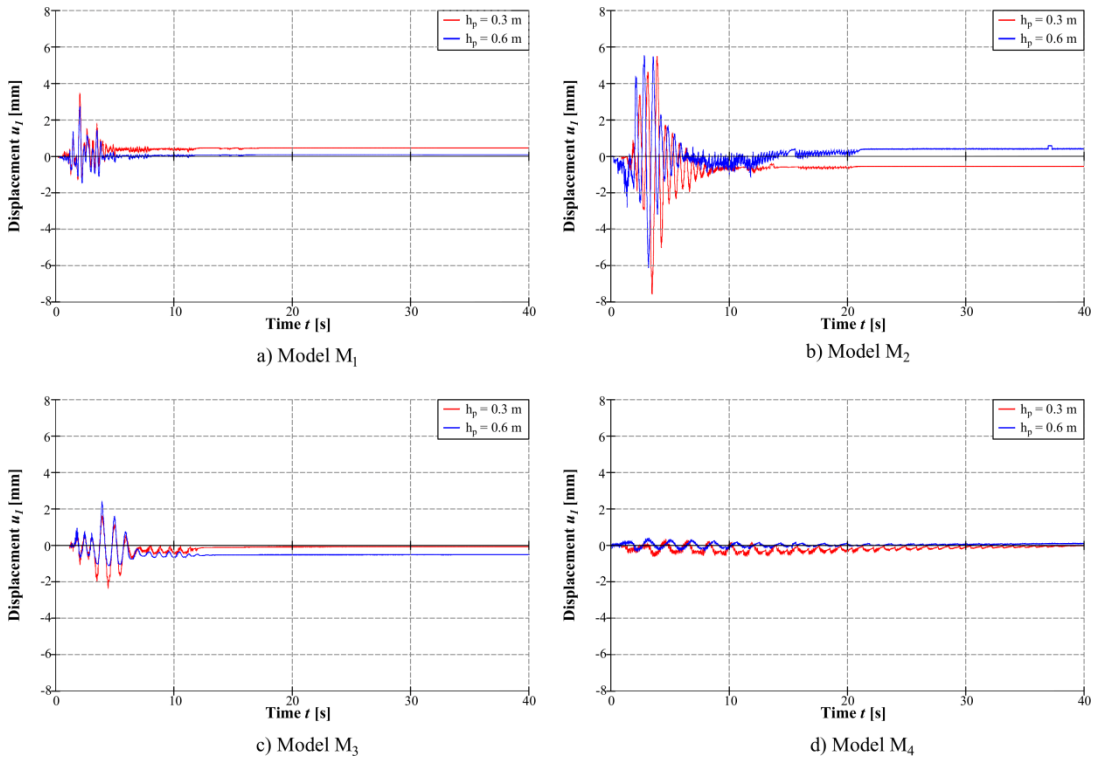


Figure 14 - *Horizontal displacement at the foundation top $u_1$ for accelerogram AS*

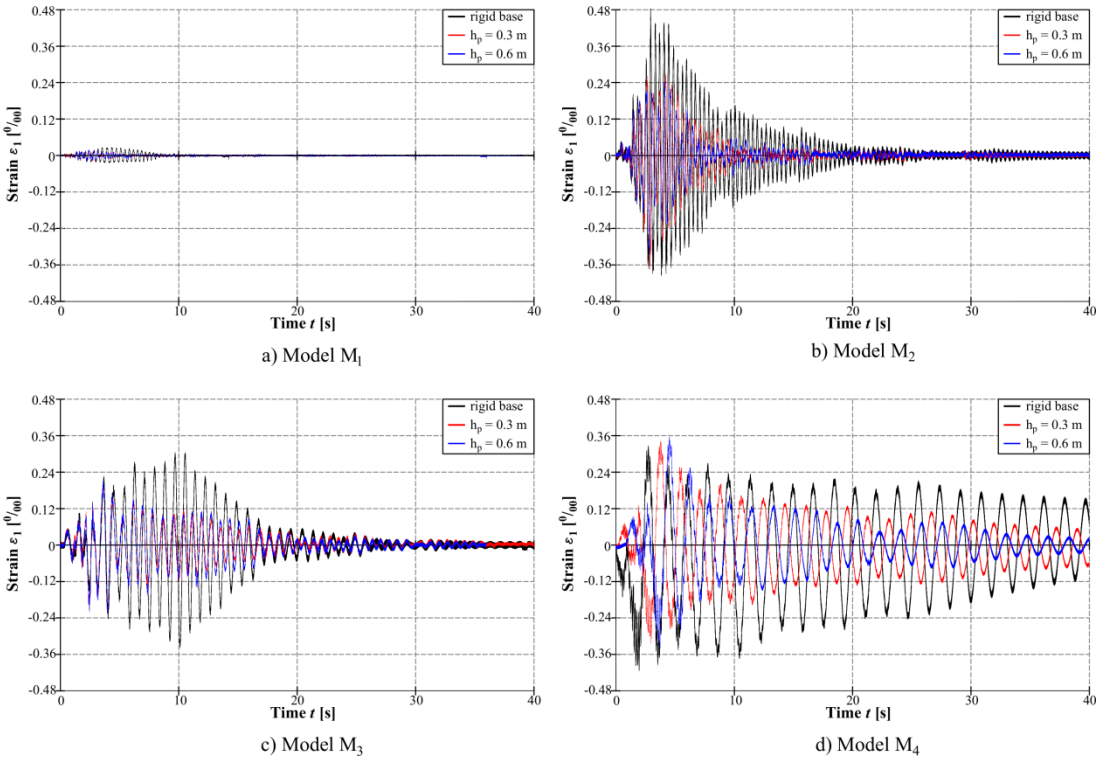


Figure 15 - *Vertical strain on the right bottom side of the steel column $\varepsilon_1$ for accelerogram ABL*

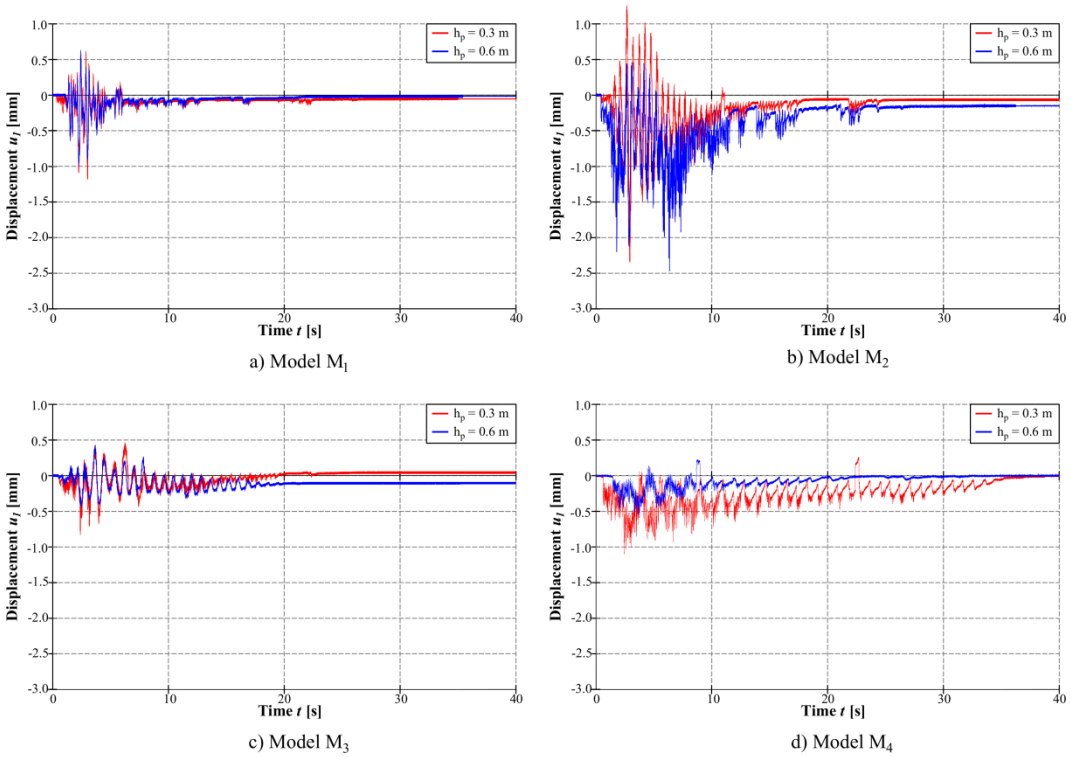


Figure 16 - *Horizontal displacement at the foundation top $u_1$ for accelerogram ABL*

Each of the previous Figures shows the measured values separately for each applied accelerogram, for the four considered models and all the considered substrate types: rigid base and pebble layer with $h_p$ = 0.3 m and $h_p$ = 0.6 m. As the comparison of the maximum values of measured quantities will be presented in Section 7.2, only a brief discussion of the principal relationships between the measured values is presented below.

The changes in the considered quantities in time were primarily dependent on the type of accelerogram and model stiffness, as well as the deformability of the substrate.

For almost all the cases considered, the difference in the measured results for the layers of pebbles $h_p$ = 0.3 m and $h_p$ = 0.6 m (for the same excitation and model) was small. This confirms that the aseismic layer with $h_p$ = 0.3 m is more optimal due to lower material consumption and faster construction.

For almost all the considered models and excitations, measured quantities for aseismic substrate cases were more favourable than in the case of a rigid base. Namely, in the case of a model support on aseismic layer, the strain values $\varepsilon_1$ and $\varepsilon_2$ (which remained elastic), the acceleration $a$, the horizontal displacement $u_2$ and the vertical displacement $v_1$ were lower. Thus, the results of the study showed that for all considered models $M_1$-$M_4$, a more favourable state of strain/stress, acceleration, and displacement is achieved when the models are supported on aseismic layers rather than on a rigid base. The greatest efficiency of the aseismic layer was for $M_1$, and the smallest was for $M_4$, i.e., the isolation efficiency is greater as the structural stiffness increases.

The main concept of base isolation is to shift the fundamental period of the structure out of the range of the dominant frequencies of expected earthquakes, to reduce the seismic forces on the structure [Banović *et al.*, 2018a]. Since models $M_1$ (T = 0.05 s) and $M_2$ (T=0.3 s) have

low period values, isolation proven to be effective because the fundamental period of the structure was shifted out of the range of the dominant frequencies of applied earthquakes. On the other hand, the model $M_3$ (T = 0.6 s) and especially the model $M_4$ (T = 1.4 s) already have high vibration period, and low seismic isolation efficiency is expected because dominant frequencies of applied earthquakes are lower.
For all tested models, artificial accelerogram (AA) was most unfavorable, with high earthquake input energy into structure. This primarily refers to the most important quantities: strain / stress and displacement.
The largest strain values for all models and excitations remained elastic, *i.e.* there was no irreversible strain. Given the highest rigidity and resistance, the $M_1$ was by far the least deformable model. The biggest displacements were with the $M_4$ model.
The most unfavorable state of strain and displacement was in the case of the foundation support on a rigid base, due to the greatest influence of rocking. Rocking is particularly pronounced for small-scale models and higher than that of full-scale models. The influence of foundation size on the behavior of the considered models and the efficiency of the considered aseismic layer is planned in a future study.

## 7.2 Comparison of the maximum measured values of some quantities for all the applied excitations

Figure 17 presents the peak values of some experimental results for the $M_1$ model, Figure 18 presents those for the $M_2$ model, Figure 19 presents those for the $M_3$ model, and Figure 20 presents those for the $M_4$ model. $\varepsilon_{1,2}$ refers to a larger (less favourable) value of $\varepsilon_1$ and $\varepsilon_2$, whereas $v_{1,2}$ refers to a larger (less favourable) value of $v_1$ and $v_2$, respectively.
For a very rigid model $M_1$ (Figure 17), it is clear that the most unfavorable accelerograms were AA and AP. The values of acceleration $a$, strains $\varepsilon_1$ and $\varepsilon_2$, and displacements $u_2$, $v_1$, and $v_2$ were in principle significantly lower for the aseismic layer case than for the rigid base case. Small differences in the results for layers with $h_p$ = 0.3 m and $h_p$ = 0.6 m are evident. Sliding of the $M_1$ model on the substrate (displacement $u_1$), which is prevented for the rigid base case, was the highest for accelerogram AP. The largest vertical displacements $v_{1,2}$ (rotation) were for a rigid base case for the AA and AP accelerograms. The lower effect of the AS and ABL accelerograms on the models, in relation to the AA and AP accelerograms, is explained by the fact that they are characterized by a short impact action with a short predominant period (so-called impact earthquakes) and that they do not bring high earthquake input energy into the structure.
The results for the $M_2$ (Figure 18), $M_3$ (Figure 19) and $M_4$ (Figure 20) models are analogous to the results for the $M_1$ model presented in Figure 17. The efficiency of seismic isolation (decreases in $\varepsilon_{1,2}$, $a$, and $u_2$) is greater as the structural stiffness increases.

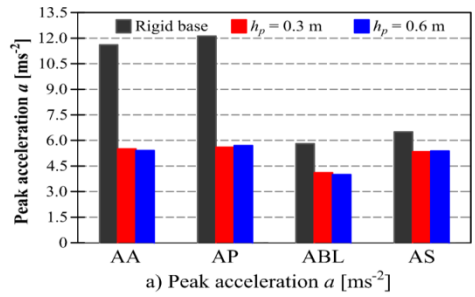

a) Peak acceleration $a$ [ms$^{-2}$]

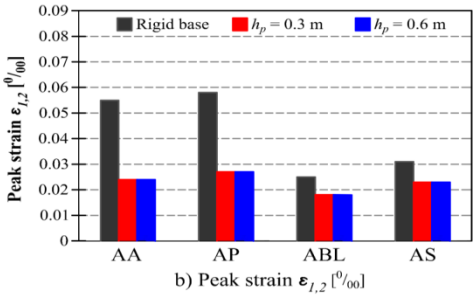

b) Peak strain $\varepsilon_{1,2}$ [$^0/_{00}$]

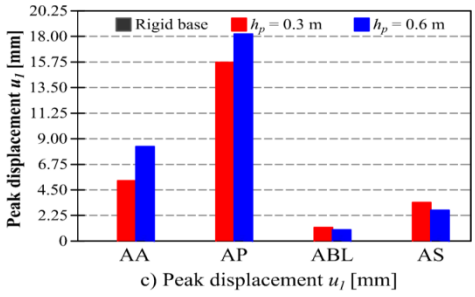

c) Peak displacement $u_1$ [mm]

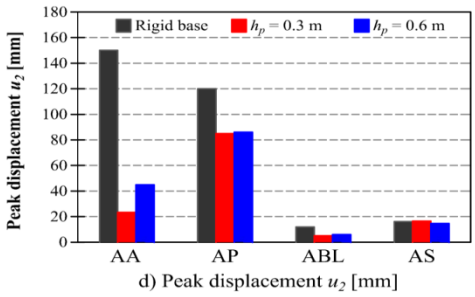

d) Peak displacement $u_2$ [mm]

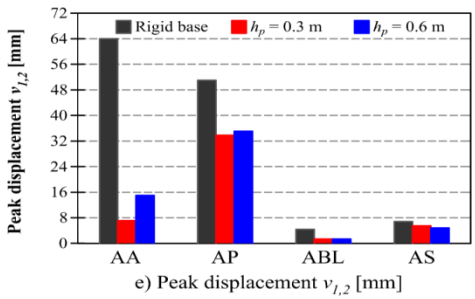

e) Peak displacement $v_{1,2}$ [mm]

Figure 17 - *Peak values of some experimental results for the $M_1$ model*

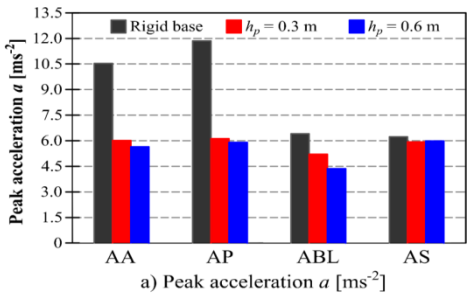

a) Peak acceleration $a$ [ms$^{-2}$]

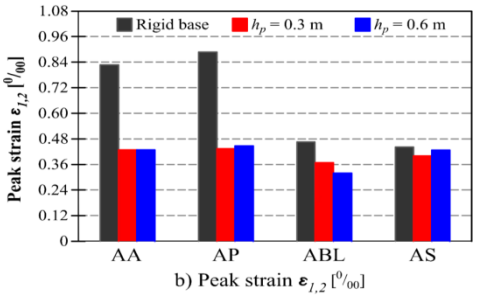

b) Peak strain $\varepsilon_{1,2}$ [$^0/_{00}$]

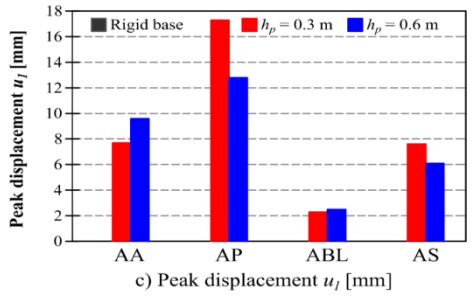

c) Peak displacement $u_1$ [mm]

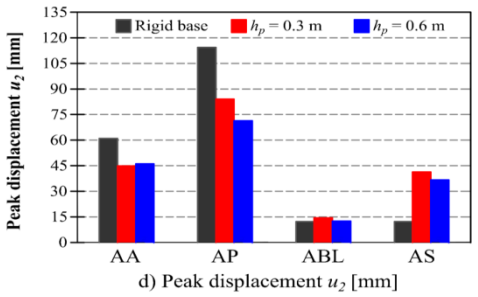

d) Peak displacement $u_2$ [mm]

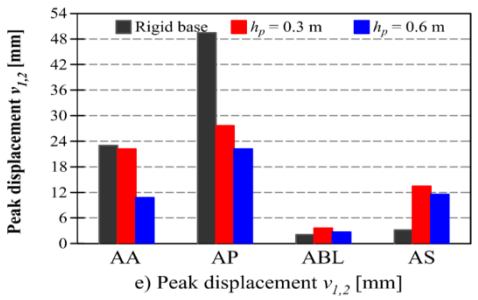

e) Peak displacement $v_{1,2}$ [mm]

Figure 18 - *Peak values of some experimental results for the $M_2$ model*

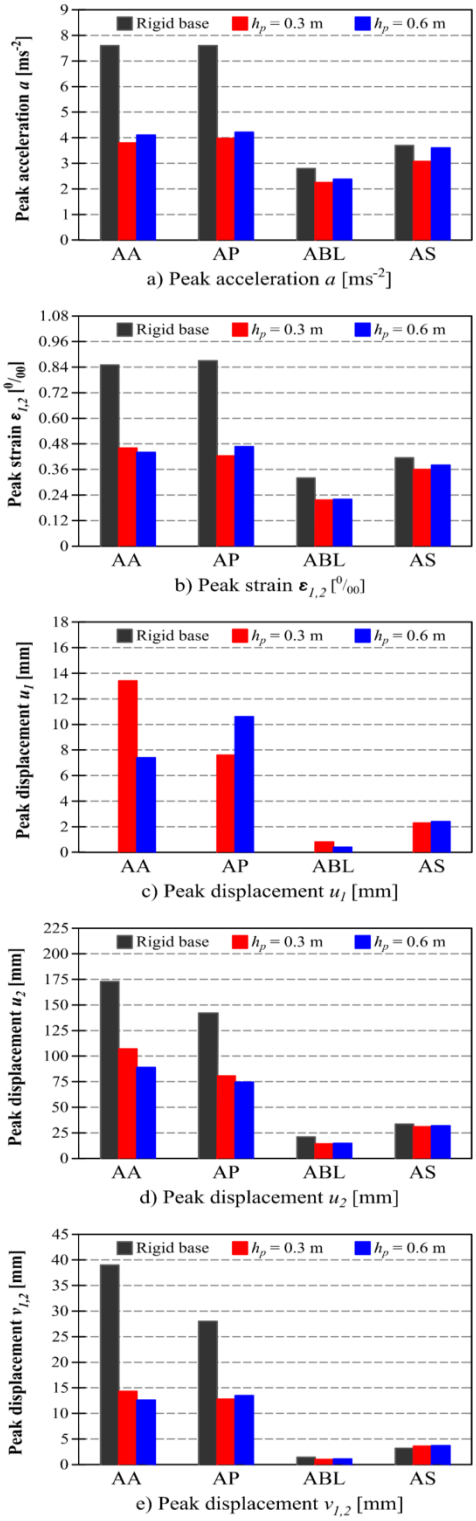


Figure 19 - *Peak values of some experimental results for the $M_3$ model*

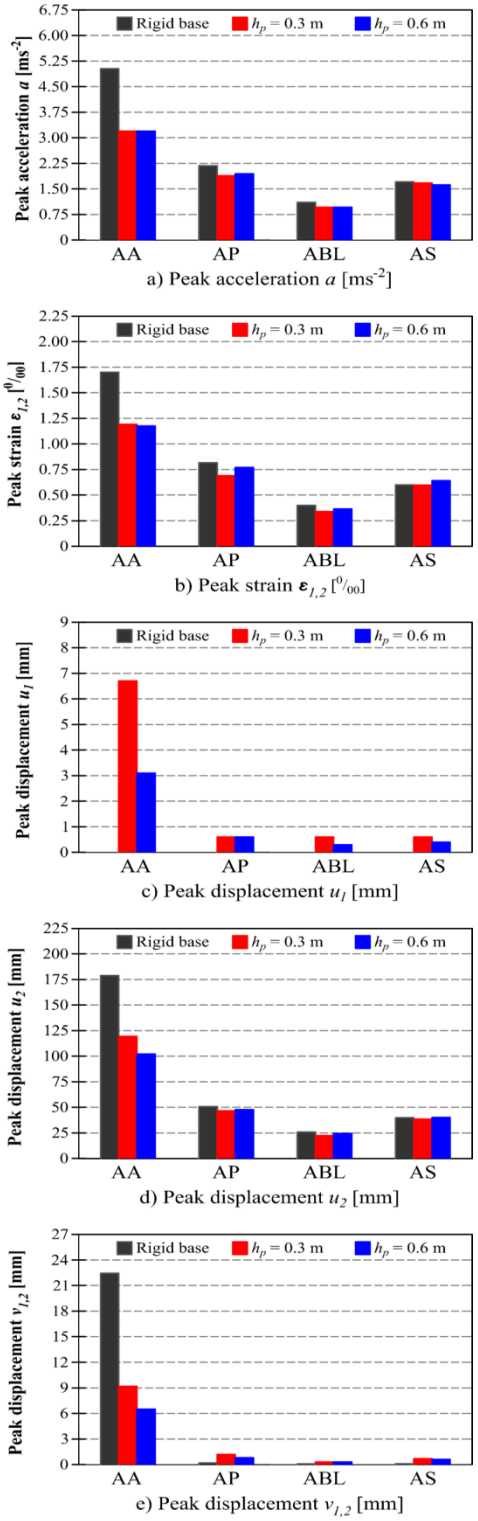


Figure 20 - *Peak values of some experimental results for the $M_4$ model*

## 7.3 Seismic isolation efficiency for all the models and applied excitations

The seismic isolation efficiency for one-time base excitation is defined by the seismic isolation efficiency coefficients *c*. The seismic isolation efficiency coefficients *c* are calculated according to Equation (1),

$$c = \frac{\mathrm{q}_{(\text{base isolation})}}{\mathrm{q}_{(\text{rigid base})}} \tag{1}$$

where $\mathrm{q}_{(\text{base isolation})}$ is the highest quantity value for the model based on the aseismic layer (larger value of $h_p$ = 0.3 m and $h_p$ = 0.6 m), and $\mathrm{q}_{(\text{rigid base})}$ is the highest quantity value for the model supported on a rigid base. Efficiency coefficients *c* are calculated for acceleration *a*, strain $\varepsilon_{1,2}$, displacement $u_2$ and displacement $v_{1,2}$. Hence, if the coefficient *c* is less than 1.0, the corresponding parameters are smaller (more favourable) for the pebble layer (BI)-based models than for the rigid base (RB)-based models. Otherwise, the corresponding parameters are higher (less favourable) for the BI-based models than for the other models. The values of these coefficients are presented in Table 2. The coefficients of seismic isolation efficiency, irrespective of the stiffness of the model, are generally more favorable for long-lasting earthquakes that bring more energy into the system (AA and AP) than for short impact earthquakes (AS and ABL). In addition, it is important to note that short impact accelerograms caused significantly lower acceleration and strain in the models, which diminishes the fact of less efficient seismic isolation for such excitations. In addition, almost independently of the excitation type, the efficiency of seismic isolation typically declined with a decrease in the stiffness of the model. The seismic isolation efficiency for the soft structure model ($M_4$) is still respectable for the AA and AP excitations. Thus, the coefficient $c_a$ values for the models $M_1$:$M_2$:$M_3$:$M_4$ at excitation AA are 0.47:0.57:0.54:0.64; at excitation AP, they are 0.47:0.52:0.56:0.89; and for ABL, they are 0.71:0.81:0.85:0.86.

Table 2 - *Some coefficients of seismic isolation efficiency*

| Coefficient | Accelerogram | Model | | | |
|---|---|---|---|---|---|
| | | $M_1$ | $M_2$ | $M_3$ | $M_4$ |
| $c_a$ (acceleration *a*) | AA | 0.47 | 0.57 | 0.54 | 0.64 |
| | AP | 0.47 | 0.52 | 0.56 | 0.89 |
| | AS | 0.83 | 0.96 | 0.97 | 0.98 |
| | ABL | 0.71 | 0.81 | 0.85 | 0.86 |
| $c_{\varepsilon 1,2}$ (strain $\varepsilon_{1,2}$) | AA | 0.44 | 0.52 | 0.54 | 0.67 |
| | AP | 0.47 | 0.50 | 0.54 | 0.94 |
| | AS | 0.74 | 0.97 | 0.92 | 1.07 |
| | ABL | 0.72 | 0.79 | 0.69 | 0.91 |
| $c_{u2}$ (displacement $u_2$) | AA | 0.30 | 0.75 | 0.62 | 0.67 |
| | AP | 0.72 | 0.73 | 0.57 | 0.94 |
| | AS | 1.02 | 3.38 | 0.95 | 1.01 |
| | ABL | 0.50 | 1.18 | 0.70 | 0.94 |
| $c_{v1,2}$ (displacement $v_{1,2}$) | AA | 0.23 | 0.96 | 0.37 | 0.41 |
| | AP | 0.69 | 0.56 | 0.48 | 5.26 |
| | AS | 0.81 | 4.16 | 1.15 | 5.23 |
| | ABL | 0.69 | 0.56 | 0.48 | 2.89 |

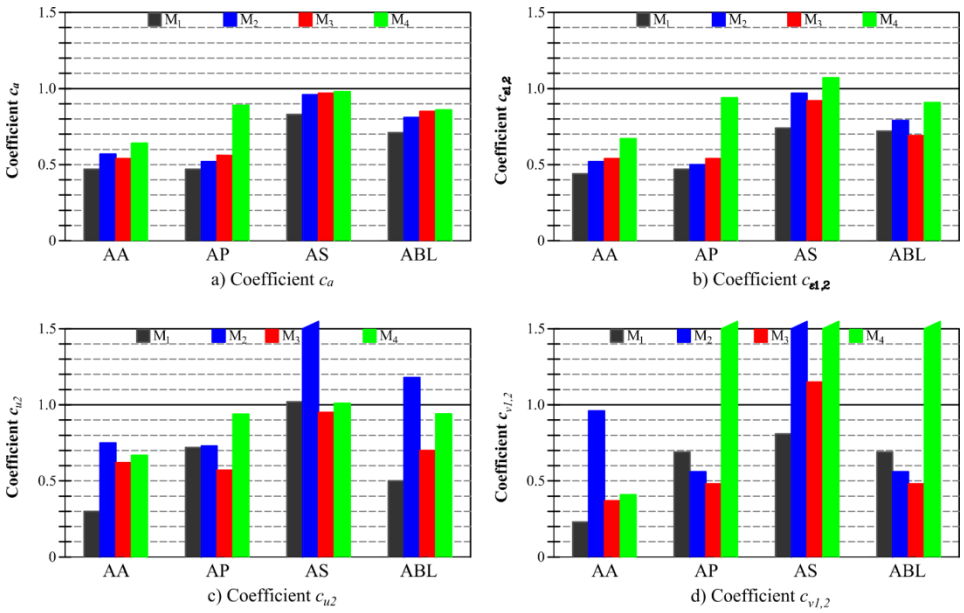


Figure 21 - *Coefficients of seismic isolation efficiency displayed by accelerograms*

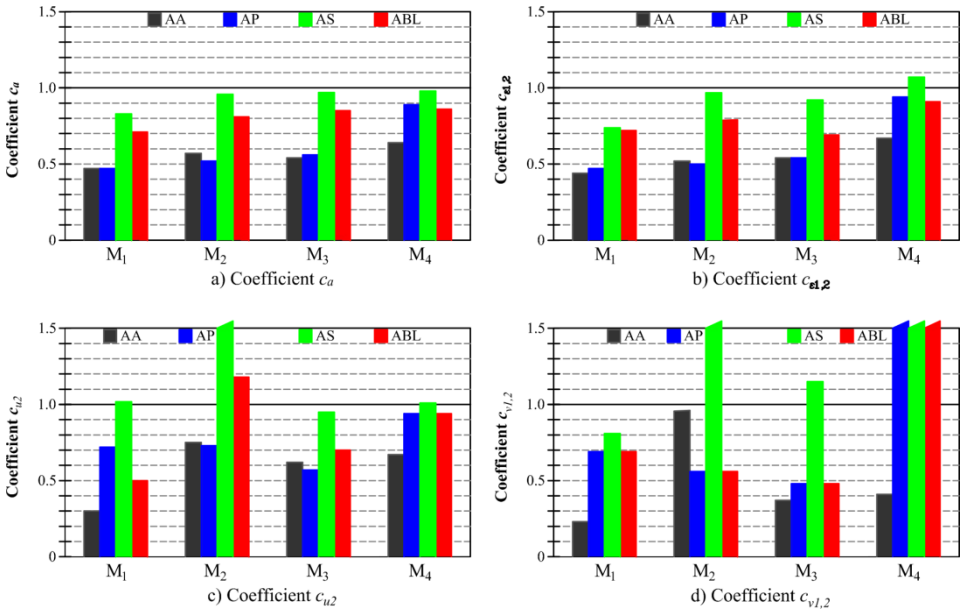


Figure 22 - *Coefficients of seismic isolation efficiency displayed by models*

The coefficient $c_{\varepsilon 1,2}$ values for the models $M_1$:$M_2$:$M_3$:$M_4$ at excitation AA are 0.44:0.52:0.54:0.67; at excitation AP, they are 0.47:0.50:0.54:0.94; and for ABL, they are 0.72:0.79:0.69:0.91. Sliding of the model on the pebble layer (displacement $u_1$) and consequently displacement $u_2$ as well as the $v_{1,2}$ displacements are significantly higher for accelerograms AS and ABL. Thus, the values of the coefficient $c_{u2}$ for the $M_1$:$M_2$:$M_3$:$M_4$ models at excitation AA are 0.30:0.75:0.62:0.67; for ABL, they are 0.50:1.18:0.70:0.94; and for AS, they are 1.02:3.38:0.95:1.01. The coefficient $c_{v1,2}$ values for the $M_1$:$M_2$:$M_3$:$M_4$ models at excitation AA are 0.23:0.96:0.37:0.41; and for AS, they are 0.81:4.16:1.15:5.23.

## 8 Some testing results for incremental base acceleration tests until model collapse

The $M_1$-$M_4$ models were tested on a rigid base and on aseismic layers with $h_p$ = 0.3 m and $h_p$ = 0.6 m. Each tested sample was exposed to a set of incremental base acceleration tests by scaling the peak ground acceleration (PGA) for $\Delta a_{g,max}$ = 0.05 g until the structure collapsed. Structure collapse was defined as failure of steel column or when model loses stability. The aim was to determine how much the bearing capacity of the model supported on the aseismic layer exceeds the bearing capacity of the same model on a rigid base. The acceleration $a_{g,max}$, at which the model collapsed, is shown in Table 3. The ratio of acceleration $a_{g,max}$ at which the model collapsed on seismic isolation (lower value for $h_p$ = 0.3 m and $h_p$ = 0.6 m) and acceleration $a_{g,max}$ at which the model collapsed on a rigid base was 1.50:1.25:1.25:1.20 for models $M_1$, $M_2$, $M_3$ and $M_4$. It can be noted that the seismic isolation efficiency is significant and that the efficiency decreases with the decrease in the stiffness of the model. Photos of some models after collapse are shown in Figure 23, and some results for the $M_2$ model are shown in Figure 24.

Table 3 - *$a_{g,max}$ (g) at model collapse*

| Model | Rigid base | Aseismic pebble layer | |
|---|---|---|---|
| | | $h_p$ = 0.3 m | $h_p$ = 0.6 m |
| $M_1$ | 0.50 | 0.75 | 0.80 |
| $M_2$ | 0.40 | 0.50 | 0.55 |
| $M_3$ | 0.40 | 0.55 | 0.50 |
| $M_4$ | 0.25 | 0.35 | 0.35 |

*a) $M_1$ on the rigid base*

*b) $M_2$ on the rigid base*

*c) $M_2$ on layer $h_p$ = 0.3 m*

*d) $M_2$ on layer $h_p$ = 0.6 m*

*e) $M_3$ on layer $h_p$ = 0.3 m*

*f) $M_4$ on layer $h_p$ = 0.3 m*

Figure 23 - *Photos of some models after collapse*

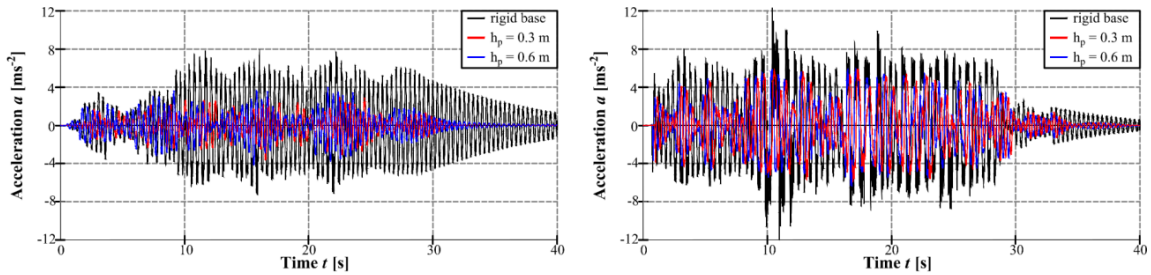


a.1) $a_{g,max}$ = 0.1 g a.2) $a_{g,max}$ = 0.35 g

a) Acceleration $a$ of $M_2$ model for accelerogram AA

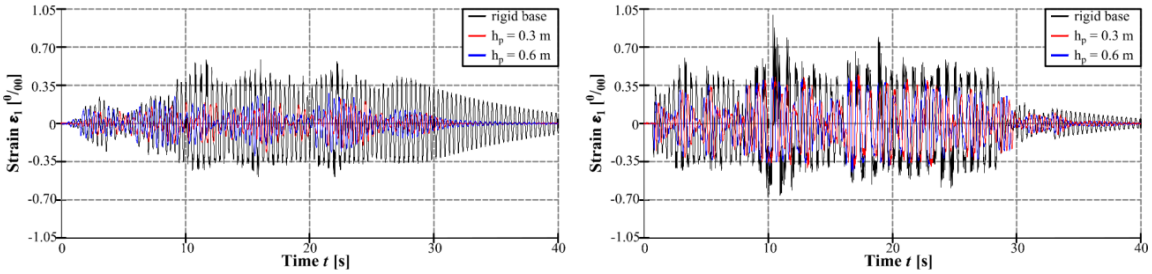


b.1) $a_{g,max}$ = 0.1 g b.2) $a_{g,max}$ = 0.35 g

b) Strain $\varepsilon_1$ of $M_2$ model for accelerogram AA

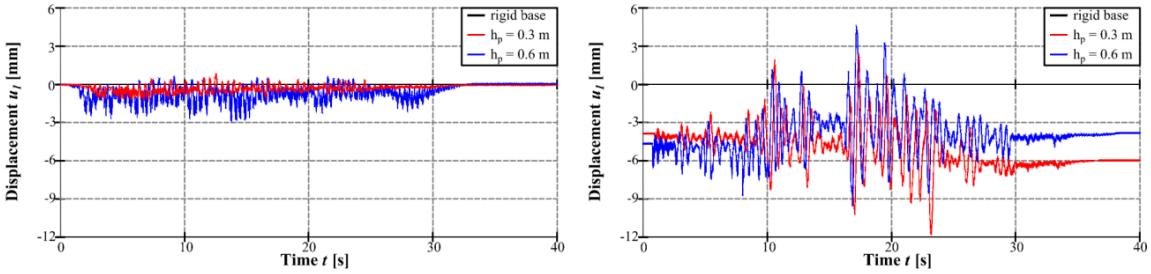


c.1) $a_{g,max}$ = 0.1 g c.2) $a_{g,max}$ = 0.35 g

c) Displacement $u_1$ of $M_2$ model for accelerogram AA

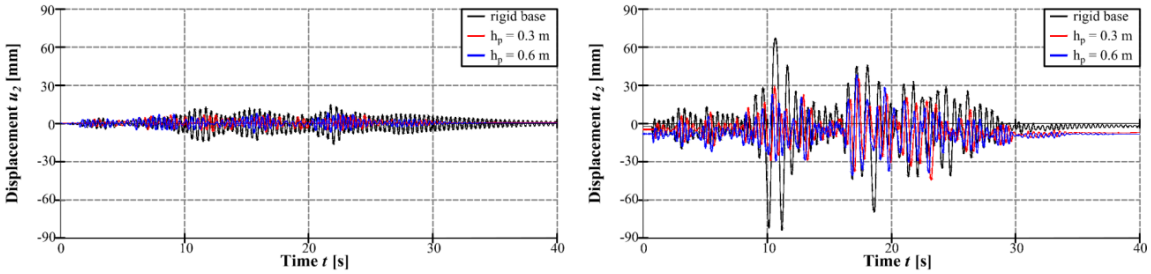


d.1) $a_{g,max}$ = 0.1 g d.1) $a_{g,max}$ = 0.1 g

d) Displacement $u_2$ of $M_2$ model for accelerogram AA

Figure 24 - *Some results for the $M_2$ model*

## 9 Conclusions

Based on the research results of the effect of structural stiffness on seismic base isolation efficiency using a layer of stone pebbles, the following main conclusions can be drawn:

- The first part of the study was carried out for the lower maximum acceleration of the shake-table (up to 0.3 g) with the elastic stresses of the model. The highest seismic isolation efficiency was for $M_1$, followed in order by those for $M_2$, $M_3$ and $M_4$. The isolation efficiency is greater as the structural stiffness increases. The seismic isolation efficiency for one-time base excitation is previously defined by the seismic isolation efficiency coefficients *c*. The efficiency of seismic isolation was highly dependent on the type of applied accelerogram, regardless of the tested model. The highest efficiency was for the AA and AP excitations, which are of long duration and long predominant period and which bring high earthquake input energy into the structure. For excitations AS and ABL, which have a short impact effect, the efficiency was lower. It should be emphasized that excitations AS and ABL produced far smaller strain/stress and acceleration of the model than the AA and AP excitations. For the seismic isolation efficiency, the coefficients $c_a$ (horizontal acceleration of the mass centre at the column top *a* ratio) and particularly $c_{\varepsilon 1,2}$ (the ratio of strain at the bottom of the column $\varepsilon$) are most appropriate. Thus, according to the above conclusions, the coefficients $c_a$ for AA were 0.47 ($M_1$), 0.57 ($M_2$), 0.54 ($M_3$), and 0.64 ($M_4$), and those for AS were 0.83 ($M_1$), 0.96 ($M_2$), 0.97 ($M_3$) and 0.98 ($M_4$). The coefficients $c_{\varepsilon 1,2}$ for AA were 0.44 ($M_1$), 0.52 ($M_2$), 0.54 ($M_3$), and 0.64 ($M_4$), and those for AS were 0.74 ($M_1$), 0.97 ($M_2$), 0.92 ($M_3$), and 1.07 ($M_4$). The increase in displacement of the model based on the seismic isolation when compared to the rigid base case was within acceptable limits (predominantly for AS and ABL) or even smaller (for AA and AP).
- In the other part of the study, each tested sample was exposed to a set of incremental base acceleration tests with artificial accelerogram (AA) by scaling the peak ground acceleration (PGA) for $\Delta a_{g,max}$ = 0.05 g until the structure collapsed. The ratios of acceleration $a_{g,max}$ at which the model collapsed on the seismic isolation (lower value for $h_p$ = 0.3 m and $h_p$ = 0.6 m) and acceleration $a_{g,max}$ at which the model collapsed on a rigid base were 1.50:1.25:1.25:1.20 for models $M_1$, $M_2$, $M_3$ and $M_4$. The efficiency of seismic isolation decreased with the decline in the stiffness of the model. It can be concluded that the seismic isolation efficiency for the soft structure model $M_4$ is still respectable.
- Globally, the considered concept of seismic base isolation shows significant potential for reducing earthquake forces and strain/stress in the structures, as well as increased bearing capacity, in comparison with the classical foundation on a rigid base. In addition, the isolation efficiency increases as the structural stiffness increases. However, further research is needed in order to allow the possible practical application of this concept for seismic isolation of buildings. In the ongoing study, the effect of the ground plan dimensions of the model's foundation on the efficiency of the considered seismic isolation will be explored.

## 10 Acknowledgements

This work has been fully supported by the Croatian Science Foundation under the project *"Seismic base isolation of a building by using natural materials - shake table testing and numerical modeling*" [IP-06-2016-5325]. The work of doctoral student Ivan Banović has been fully supported by the *"Young researchers' career development project – training of doctoral students"* of the Croatian Science Foundation funded by the European Union from the European Social Fund. The authors are grateful for the support.

## References

Ambraseys, N., Smit, P., Sigbjornsson, R., Suhadolc, P., Margaris, M. (2001). EVR1-CT-1999-40008, European Commission, Directorate-General XII, Environmental and Climate Programme, Brussels, Belgium

Amendola, A., Carpentieri, G., Feo, L., Fraternali, F. (2016a). Bending dominated response of layered mechanical metamaterials alternating pentamode lattices and confinement plates. Compos. Struct. 157, 71-77.

Amendola, A., Smith, C.J., Goodall, R., Auricchio, F., Feo, L., Benzoni, G., Fraternali, F. (2016b). Experimental response of additively manufactured metallic pentamode materials confined between stiffening plates. Compos. Struct. **142**, 254-262.

Anastasopoulos, I., Loli, M., Georgarakos, T., Drosos, V. (2012). Shaking table testing of rocking-isolated bridge pier on sand. Journal of Earthquake Engineering **17**(1): 1–32.

Azinović, B., Kilar, V., Koren, D. (2014). The seismic response of low-energy buildings founded on a thermal insulation layer – A parametric study. Engineering Structures **81**, 398-411.

Azinović, B., Kilar, V., Koren, D. (2016). Energy-efficient solution for the foundation of passive houses in earthquake-prone regions. Engineering Structures **112**, 133-145.

Azzam, W., Ayeldeen, M., El Siragy, M. (2018). Improving the structural stability during earthquakes using in-filled trench with EPS geofoam—numerical study. Arabian Journal of Geosciences **11**(14):395, doi.org/10.1007/s12517-018-3739-4

Bandyopadhyay, S., Sengupta, A., Reddy, G. R. (2015). Performance of sand and shredded rubber tire mixture as a natural base isolator for earthquake protection. Earthquake Engineering and Engineering Vibration **14**(4): 683–693.

Banović, I., Radnić, J., Grgić, N. (2018b). Shake table study on the efficiency of seismic base isolation using natural stone pebbles. Advances in Materials Science and Engineering **2018**, Article ID 1012527, 20 pages

Banović, I., Radnić, J., Grgić, N., Matešan, D. (2018a). The use of limestone sand for the seismic base isolation of structures. Advances in Civil Engineering **2018**, Article ID 9734283, 12 pages

Banović, I., Radnić, J., Grgić, N. (2019). Geotechnical Seismic Isolation System Based on Sliding Mechanism Using Stone Pebble Layer: Shake-Table Experiments. Shock and Vibration **2019**, Article ID 9346232, 26 pages

Brunet, S., de la Llera, J. C., Kausel, E. (2016). Non-linear modeling of seismic isolation systems made of recycled tire-rubber. Soil Dynamics and Earthquake Engineering **85**, 134–145.

Calvi, P. M. and Calvi, G. M. (2018). "Historical development of friction-based seismic isolation systems. Soil Dynamics and Earthquake Engineering **106**, 14-30.

Calvi, P. M., Moratti, M., Calvi, G. M. (2016). Seismic Isolation Devices Based on Sliding Between Surfaces with Variable Friction Coefficient. Earthquake Spectra **32**(4): 2291-2315.

Carpani, B. (2014). A Survey of ancient geotechnical Engineering techniques in Sub foundation Preparation. 9th International Conference on Structural Analysis of Historical Constructions, Mexico City, Mexico

Carpani, B. (2017). Base isolation from a historical perspective. 16th World Conference on Earthquake, Paper N° 4934, Santiago, Chile

Castaldo, P. and Ripani, M. (2017). Optimal design of single concave sliding bearings for isolated structures considering intermediate isolation degrees. Ingegneria Sismica. 34 (5)

De Domenico, D., Ricciardi, G., Infanti, S., Benzoni G. (2019). Frictional Heating in double curved surface sliders and its effects on the hysteretic behavior: an experimental study. Front. Built Environ. **5**(74)

Doudoumis, I., Papadopoulos, P., Papaliangas, T. (2002). Low-cost base isolation system on artificial soil layers with low shearing resistance. Proceedings of the 12th European Conference on Earthquake Engineering, London, UK

EN 1998-1:2004 (2004). Eurocode 8: Design of Structures for Earthquake Resistance-Part 1: General Rules, Seismic Actions and Rules for Buildings, European Committee for Standardization, Brussels, Belgium

Fabbrocino, F., Amendola, A., Benzoni, G., Fraternali, F. (2016). Seismic application of pentamode lattices. Ingegneria Sismica. **1**:62-71.

Forcellini, D. (2017). Assessment on geotechnical seismic isolation (GSI) on bridge configurations. Innovative Infrastructure Solutions **2**(1), 9 pages

Fraternali, F., Amendola, A., Benzoni, G. (2018). Innovative seismic isolation devices based on lattice materials: A review. Ingegneria Sismica. **4**:93-113.

Hadad, H. A, Calabrese, A., Strano, S., Serino, G. (2017). A Base Isolation System for Developing Countries Using Discarded Tyres Filled with Elastomeric Recycled Materials. Journal of Earthquake Engineering **21**(2): 246-266.

Kalpakcı, V., Bonab, A. T., Özkan, M. Y., Gülerce, Z. (2018). Experimental evaluation of geomembrane/geotextile interface as base isolating system. Geosynthetics International **25**(1): 1-11.

Karatzia, X. and Mylonakis, G. (2017). Geotechnical seismic isolation using eps geofoam around piles. 6th International Conference on Computational Methods in Structural Dynamics and Earthquake Engineering, Rhodes Island, Greece

Karatzia, X., Mylonakis, G., Bouckovalas, G. (2019). Seismic Isolation of Surface Foundations Exploiting the Properties of Natural Liquefiable Soil. Soil Dynamics and Earthquake Engineering **121**, 233-251.

Kelly, J. (1996a). Natural Rubber Isolation Systems for Earthquake Protection of Low-Cost Buildings. Report No. UCB/EERC-95-12, Earthquake Engineering Research Center, University of California, Berkeley, California

Kelly, J. (1996b). Aseismic base isolation: review and bibliography. Soil Dynamics and Earthquake Engineering **5**(4): 202-216.

Kelly, J. and Taniwangsa, W. (1996). Experimental and Analytical Studies of Base Isolation Applications for Low-Cost Housing. Report No. UCB/EERC-96-04, Earthquake Engineering Research Center, University of California, Berkeley, California

Koren, D. and Kilar, V. (2016). Seismic vulnerability of reinforced concrete building structures founded on an XPS layer. Earthquakes and Structures **10**(4): 939 -963.

Lomiento, G., Bonessio, N., Benzoni, G. (2013). Concave sliding isolator's performance under multi-directional excitation. Ingegneria Sismica. **30**:17-32.

Makris, N. (2018). Seismic isolation: early history. Earthquake Engineering & Structural Dynamics **48**(2): 269-283.

Mavronicola, E., Komodromos, P., Charmpis, D. C. (2010). Numerical investigation of potential usage of rubber–soil mixtures as a distributed seismic isolation approach. Proceedings of the 10th International Conference on Computational Structures Technology, Valencia, Spain

Murillo, C., Thorel, L., Caicedo, B. (2009). Ground vibration isolation with geofoam barriers: Centrifuge modelling. Geotextiles and Geomembranes **27**(6): 423-434.

Naeim, F. and Kelly, J. M. (1999). Design of seismic isolated structures: From theory to practice. John Wiley & Sons, Inc., New York.

Panjamani, A., Devarahalli Ramegowda, M., Divyesh, R. (2015). Low cost damping scheme for low to medium rise buildings using rubber soil mixtures. Japanese Geotechnical Society Special Publication **3**(2): 24–28.

Patil, S. J., Reddy, G. R., Shivshankar, R., Babu, R., Jayalekshmi, B. R., Kumar, B. (2016). Seismic base isolation for structures using river sand. Earthquakes and Structures **10**(4): 829-847.

Pecker, A., Prevost, J. H., Dormieux, L. (2001). Analysis of pore pressure generation and dissipation in cohesionless materials during seismic loading. Journal of Earthquake Engineering **5**(4): 441-464.

Pecker, A. (2003). Aseismic foundation design process, lessons learned from two major projects: the Vasco de Gama and the Rion Antirion bridges. Proceedings of the ACI International Conference on Seismic Bridge Design and Retrofit, La Jolla, CA, USA

Radnić, J., Grgić, N., Matešan, D., Baloević, G. (2015). Shake table testing of reinforced concrete columns with different layout size of foundation. Materialwissenschaft und Werkstofftechnik **46**(4-5): 348–367.

Steenfelt, J. S., Foged, B., Augustesen, A. H. (2015). Izmit Bay Bridge-geotechnical challenges and innovative solutions. International Journal of Bridge Engineering (IJBE) **3**(3):53–68.

Tehrani, F. M. and Hasani, A. (1996). Behaviour of Iranian low rise buildings on sliding base to earthquake excitation. Proceedings of the 11th World Conference on Earthquake Engineering, Paper 1433, Acapulco, Mexico

Tsang, H. H. (2008). Seismic isolation by rubber-soil mixtures for developing countries. Earthquake Engineering & Structural Dynamics **37**(2):283–303.

Tsang, H. H. (2009). Geotechnical seismic isolation. Earthquake Engineering: New Research, pp. 55–87, Nova Science Publishers Inc., New York, NY, USA

Tsang, H. H., Lo, S. H., Xu, X., Neaz Sheikh, M. (2012). Seismic isolation for low-to-medium-rise buildings using granulated rubber-soil mixtures: numerical study. Earthquake Engineering & Structural Dynamics **41**(14):2009–2024.

Tsiavos, A., Alexander, N. A., Diambra, A., Ibraim, E., Vardanega, P. J., Gonzalez-Buelga, A., Sextos A. (2019). A sand-rubber deformable granular layer as a low-cost seismic isolation strategy in developing countries: experimental investigation. Soil Dynamics and Earthquake Engineering, **125**.

Warn, G. P. and Ryan, K. L. (2012). A review of seismic isolation for buildings: historical development and research needs. Buildings **2**(3):300-325.

Xiao, H., Butterworth, J. W., Larkin, T. (2004). Low-technology techniques for seismic isolation. Proceedings of the NZSEE Conference, Rototua, New Zealand

Xiong, W. & Li, Y. (2013). Seismic isolation using granulated tire-soil mixtures for less-developed regions: experimental validation. Earthquake Engineering & Structural Dynamics **42**(14):2187-2193.

Xiong, W., Yan, M. R., Li, Y. Z. (2014). Geotechnical Seismic Isolation System - Further Experimental Study. Applied Mechanics and Materials **580-583**:1490-1493.

Yegian, M. K. and Catan, M. (2004). Soil isolation for seismic protection using a smooth synthetic liner. Journal of Geotechnical and Geoenvironmental Engineering **130**(11):1131–1139.

Yegian, M. K. and Kadakal, U. (2004). Foundation isolation for seismic protection using a smooth synthetic liner. Journal of Geotechnical and Geoenvironmental Engineering **130**(11):1121–1130.

Zhao, X., Zhang, Q., Zhang, Q., He, J. (2016). Numerical study on seismic isolation effect of gravel cushion. Proceedings of the 7th International Conference on Discrete Element Methods **188**:1055-1063., Dalian, China

Zuccaro, G., De Gregorio, D., Titirla, M., Modano, M., Rosati, L. (2018). On the simulation of the seismic energy transmission mechanisms. Ingegneria Sismica, **35**(1): 109-130.

ingegneria sismica
International Journal of Earthquake Engineering
Anno XXXVII – Num.2 - 2020

# EFFETTO DELLA RIGIDEZZA STRUTTURALE SULL'EFFICIENZA DI UN SISTEMA DI ISOLAMENTO SISMICO ALLA BASE COMPOSTO DA STRATI DI GHIAIA

*Ivan Banović*[1], *Jure Radnić*[1], *Nikola Grgić*[1]

[1]University of Split, Faculty of Civil Engineering, Architecture and Geodesy, Split, Croatia

SUMMARY: *L'effetto della rigidezza strutturale sull'efficienza dei sistemi di isolamento composti da strati di ghiaia è studiata mediante prove su tavola vibrante. L'efficienza della stratificazione è testata su quattro modelli strutturali, differenti per rigidezza, e con altrettante registrazioni accelerometriche. Nella prima parte di questo lavoro, i quattro accelerogrammi sono utilizzati per condurre prove non distruttive, con controllo delle deformazioni durante le prove. A seguire, analisi dinamiche incrementali sono condotte considerando la serie più sfavorevole, e portando le strutture a collasso. L'efficienza del sistema di isolamento proposto aumenta all'aumentare della rigidezza strutturale e, in conclusione, la metodologia dimostra di poter apportare benefici a strutture in zona sismica..*

KEYWORDS: *seismic base isolation, stone pebble layer, effect of structural stiffness, shake-table testing*

Corresponding author: Ivan Banović, University of Split, Faculty of Civil Engineering, Architecture and Geodesy, Croatia.
Email: ivan.banovic@gradst.hr

# PAPER V

**Earthquakes and Structures**, *Vol. 19, No. 2 (2020)000-000*
DOI: https://doi.org/10.12989/eas.2020.19.2.000 

# Foundation size effect on the efficiency of seismic base isolation using a layer of stone pebbles

Ivan Banović, Jure Radnić and Nikola Grgić*

*University of Split, Faculty of Civil Engineering, Architecture and Geodesy, Matice hrvatske 15, 21000 Split, Republic of Croatia*

*(Received March 25, 2020, Revised May 20, 2020, Accepted June, 10, 2020)*

**Abstract.** The effect of the foundation size on the efficiency of seismic base isolation using a layer of stone pebbles is experimentally investigated. Four scaled models of buildings with different stiffnesses (from very stiff to soft) were tested, each with the so-called small and large foundation, and exposed to four different accelerograms (different predominant periods and durations). Tests were conducted so that the strains in the model remained elastic and afterwards the models were tested until collapse. Each model was tested for the case of the foundation being supported on a rigid base and on an aseismic layer. Compared to the smaller foundation, the larger foundation results in a reduced rocking effect, higher earthquake forces and lower bearing capacity of the tested models, with respectable efficiency (reduced strain/stress, displacement and increase of the ultimate bearing capacity of the model) for the considered seismic base isolation compared to the foundation on a rigid base.

**Keywords:** seismic base isolation; pebble layer; foundation size effect; shake-table study

## 1. Introduction

The application of seismic base isolation by various aseismic devices is becoming increasingly widespread. Unfortunately, some deficiencies (cost, complexity, durability, maintenance during building lifetime, etc.) are the reason why such seismic isolation is not yet widely used. According to Tsang (2009), in the past century, earthquakes have killed an average of over 20,000 people a year throughout the world, with 90% of fatalities occurring in developing countries. This fact indicates that low-cost and low-tech seismic base isolation is necessary. In recent years, simple solutions for seismic base isolation, suitable for less developed countries and simple structures, have been intensively explored. Such solutions, with sufficient efficiency and reliability, should be significantly more rational and easier to apply than the above aseismic devices.

The application of seismic base isolation using natural materials has been utilized throughout history (Przewłócki *et al*. 2005 and Carpani 2017). Historically, builders used layers of gravel, stone, and wood (multi-layered timber grillage) for the seismic base isolation of various buildings and bridges (Kulukčija *et al.* 2009, Kulukčija and Humo 2009). J.A. Calantarients, a medical doctor from England, at the beginning of 20th century proposed separation of the building from its foundation with a layer of sand or talk, as an earthquake resistant design approach (Naeim and Kelly 1999). Modern builders, guided by the experience of their predecessors, tend to find low-cost seismic base isolation. The development of such isolation goes in several directions, using different materials below the foundation including, sand, gravel, stone pebbles, rubber-soil mixtures (RSM), geofoam, and geosynthetics. All of these materials have the same purpose, namely, that seismic energy is dissipated before it transmits into the structure. Some of the most important studies are briefly outlined below.

New experimental and numerical studies on the use of sand and gravel for the seismic base isolation of buildings are increasing. Tehrani and Hasani (1996) performed an experimental study to evaluate the performance of sand and lightweight expanded clay for the seismic base isolation of buildings in Iran. Banović *et al.* (2018a) and Radnić *et al*. (2015) also proved by a shake-table study that layer of limestone sand can serve as a base isolation material. Patil *et al.* (2016) and Anastasopoulos *et al.* (2012) experimentally investigated the performance of river sand for seismic base isolation, while Zhao *et al.* (2016) numerically simulated a gravel isolation layer using a discrete element method. Seismic isolation using gravel has appeared in modern applications in the construction of the Rio-Antirion Bridge in Greece (Pecker *et al.* 2001), Vasco de Gama Bridge in Portugal (Pecker 2003) and the Izmit Bay Bridge in Turkey (Steenfelt *et al.* 2015).

Since it was first proposed by Tsang (2008), the concept of geotechnical seismic isolation (GSI) using a rubber-soil mixture (RMS) around the foundations of structures for absorbing seismic energy has attracted significant research interest. The effectiveness of the GSI system is analysed through numerical (Xiao *et al*. 2004, Mavronicola *et al.* 2010, Tsang *et al.* 2012, Panjamani *et al.* 2015, Bandyopadhyay *et al.* 2015, Brunet *et al.* 2016, Forcellini 2017, Tsiavos *et al.* 2019, Tsang and Pitilakis 2019) and experimental (Xiong and Li 2013, Xiong *et al.* 2014) studies. Other GSI research efforts are on soil replacement by geofoam (Murillo *et al.* 2009, Azinović *et al.* 2014, Azinović *et al.* 2016, Koren and Kilar 2016, Hadad *et al.* 2017, Karatzia *et al.* 2017, Azzam *et al.* 2018). The

*Corresponding author, Ph.D. Assistant Professor
E-mail: nikola.grgic@gradst.hr


 ISSN: 2092-7614 (Print), 2092-7622 (Online)

application of smooth synthetic liners and geomembranes/geotextiles for dissipating seismic energy through sliding has also been proposed (Doudoumis *et al.* 2002, Yegian and Catan 2004, Yegian and Kadakal 2004, Nanda *et al.* 2012a, Nanda *et al*. 2012b, Kalpakci *et al.* 2018). The concept of rocking isolation as seismic protection strategy is studied by many researchers (Makris 2014, Chung *et al.* 2019, Feng *et al*. 2018, Wang *et al.* 2018).

Banović *et al.* (2018b, 2019) experimentally investigated the effectiveness of seismic base isolation using a layer of natural stone pebbles. First, a shake-table study on the efficiency of seismic base isolation using natural stone pebbles was performed (Banović *et al.* 2018b), with very encouraging research results. The models of stiff and medium-stiff buildings (a free-standing steel column with a concrete foundation and mass at the column top) were tested. Case studies were conducted on a model founded on the rigid base and on different layers of pebbles. Four different horizontal accelerograms were applied. The strains/stresses of the tested models remained in the elastic region. The results of the study showed that a layer of pebbles can significantly reduce the peak acceleration and strains/stresses of the model, with acceptable displacements.

After the very encouraging research results of the first study (Banović *et al.* 2018b), Banović *et al.* (2019) experimentally investigated the optimum properties of an aseismic stone pebble layer (the layer thickness, the fraction of pebbles, the pebble compaction, the pebble moisture, the vertical contact stress below the foundation, and the effect of repeated excitations).

This paper presents the results of further research related to the possibility of applying seismic base isolation using a layer of stone pebbles below the foundation, as previously shown in Banović *et al.* (2018b, 2019). The effect of the foundation size (ground plan dimensions), i.e., the foundation rotational stiffness, on the efficiency of the seismic isolation was investigated. The results of the tests are compared for two ground plan dimensions (stiffness) of the foundation, namely, the so-called small foundation (SF) and so-called large foundation (LF). Experimental tests on scaled models of buildings with four different stiffnesses (period of free oscillation) were performed. Increasing the rotational stiffness of the foundation eliminates the beneficial effect of rocking and therefore reduces the efficiency of seismic isolation. However, it was concluded that even in the case of a building where very low foundation rotation is possible, considered seismic isolation still exhibits considerable efficiency for low-rise very stiff and stiff buildings based on stiff soil.

## 2. Considered building models with foundation

The considered building models ($M_1$, $M_2$, $M_3$, and $M_4$) of different stiffnesses (periods of free oscillation $T$) with two types of foundations (SF and LF) are shown in Fig. 1. SF denotes a small foundation with dimensions of 0.7 x 0.5 x 0.3 m (m=260 kg), and LF denotes a large foundation with dimensions of 1.2 x 0.7 x 0.3 m (m=630 kg). Thus, the foundations (concrete with cube strength 46 MPa) are of equal height and different layout dimensions. The smaller foundation represents real buildings with a high rocking effect, while the large foundation represents those with a low rocking effect. The building models (Banović *et al*. 2018b) are free-standing steel columns (steel S355) with a concrete block (cube strength 46 MPa) of mass m=1000 kg at the column top. It should be noted that the complete oscillating mass is a sum of masses (block, column and foundation). Further, the structural response in the case of earthquake is governed by oscillating mass, column's stiffness, soil-structure-interaction and the stiffness and capacity of the column-foundation joint connection.

Models $M_1$ and $M_2$ have a column height of 1.02 m and models $M_3$ and $M_4$ have a column height of 2.02 m. The square hollow cross sections of the columns are different for the $M_1$-$M_4$ models, according to Fig. 1. Building models included in research represent a very wide stiffness range of potential buildings for possible application of this seismic isolation concept: $M_1$ – very stiff structure ($T$=0.05 s), $M_2$ – stiff structure ($T$=0.30 s), $M_3$ – medium-stiff structure ($T$=0.60 s) and $M_4$ – soft structure ($T$=1.40 s). Vibration period of models are calculated for linear system, without foundation and with rigid column-foundation joint connection. Vibration periods are verified on shake-table and are valid for rigid base case.

All samples were first tested for the case where the foundation is supported on a rigid base (allowing the foundation lifting, while the horizontal displacement of the foundation in relation to the shake-table is prevented). Fig. 1f reveals how the lifting was enabled and horizontal displacement prevented, simultaneously. Also, compared to the fixed base support case, this support case produces usually lower seismic forces on the model, which gives more conservative seismic base isolation efficiency.

After that, models were tested with the foundation on a pebble layer with the following characteristics: thickness $h_p$=0.3 m, fraction $\Phi_b$=16-32 mm, compaction $MS$=30 MPa and humidity $v$=10%, all analogous to the study in Banović *et al*. (2019). For the models based on pebble layer, sliding between the foundation and the stone pebbles in not prevented.

First part of the study was performed for one-time base acceleration so that the strains in the model remained elastic ($a_{g,\,max}$=0.3 g for $M_1$ and $M_2$ and with $a_{g,\,max}$=0.2 g for $M_3$ and $M_4$), and afterwards for the most unfavourable accelerogram the models were tested until collapse.

## 3. Base accelerations

Adopted base accelerations are presented in Fig. 2 (Banović *et al.* 2018b, 2019). The artificial accelerogram (AA) and accelerogram Petrovac (AP) (Ambraseys *et al.* 2001) represent long-lasting earthquakes with long predominant periods, while Ston (AS) and Banja Luka (ABL) (Ambraseys *et al.* 2001) accelerograms represent short-duration earthquakes with short predominant periods (impact earthquakes). The AA was created to match the elastic response spectrum according to EC 8 (2004) for

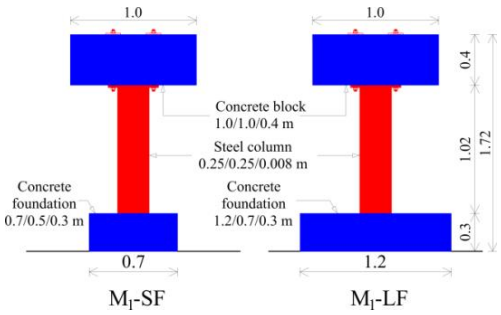


(a) Model $M_1$ (T = 0.05 s)

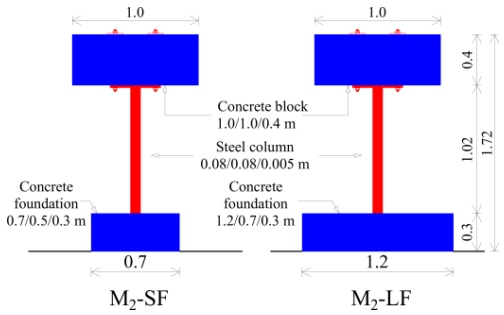


(b) Model $M_2$ (T = 0.30 s)

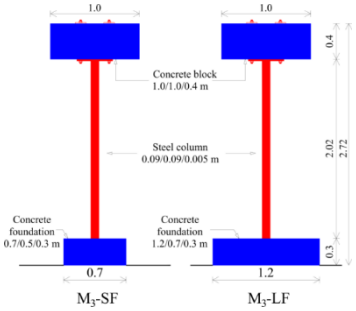


(c) Model $M_3$ (T = 0.60 s)

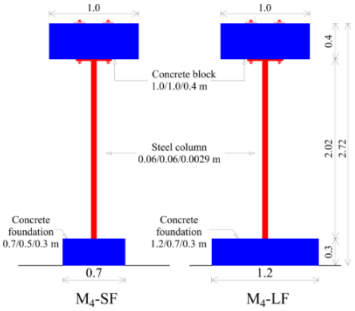


(d) Model $M_4$ (T = 1.40 s)

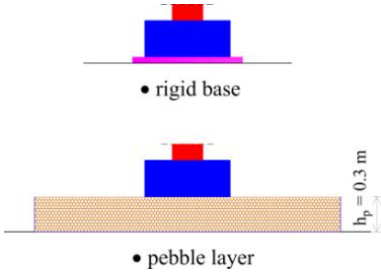


(e) Foundation support variants

(f) Foundation on rigid base: prevented horizontal displacement and enabled uplifting

Fig. 1 Considered building models

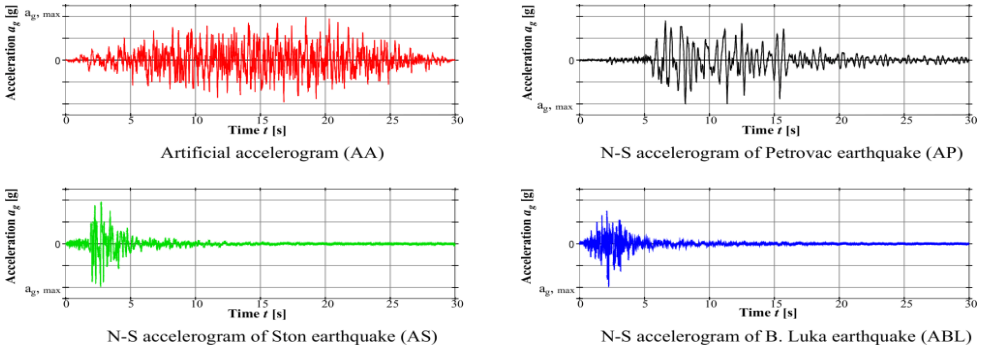


(a) Adopted horizontal base excitations

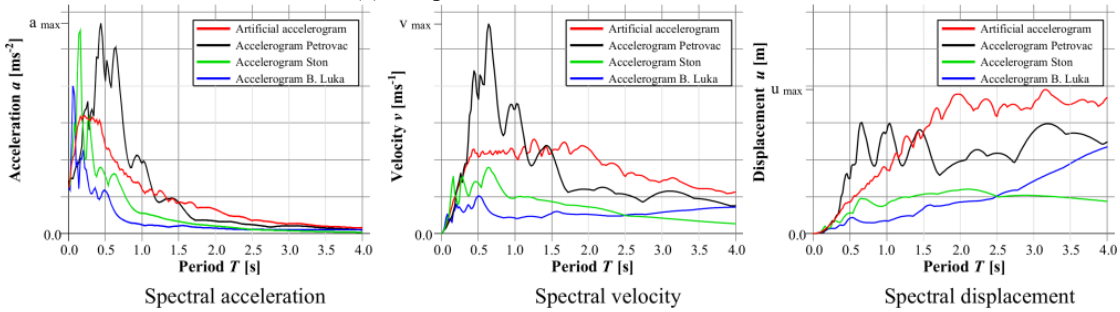


(b) Elastic response spectra of adopted excitations

Fig. 2 Basic information on applied base excitations (Banović *et al.* 2018b, 2019)

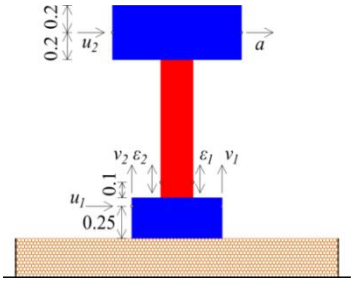

Fig. 3 Measured quantities

earthquake type 1 and soil type A. The AA and AP generate large displacements of the structure and bring high seismic energy with a strong bending effect, while AS and ABL have a more pronounced shear force effect.

## 4. Measured quantities and instrumentation

The following quantities were measured on each tested model (Fig. 3): the horizontal acceleration of the mass centre at the column top $a$, horizontal displacements $u_1$ (foundation top) and $u_2$ (mass centre at the column top), vertical displacements of the foundation $v_1$ (at the right edge) and $v_2$ (at the left edge), and vertical strains on the bottom of the steel column $\varepsilon_1$ (at the right side) and $\varepsilon_2$ (at the left side).

The uniaxial shake-table from the University of Split, Faculty of Civil Engineering, Architecture and Geodesy (Croatia) was used for model testing. A Quantum-x mx 840A (Hottinger Baldwin Messtechnik-HBM) high-speed data acquisition system was used for data collection and processing. The strains were measured using strain gauges, type 6/120 LY11 (HBM). A piezo-electric low-frequency accelerometer type 4610 (MS) measured the accelerations, and the displacements were measured using analogue displacement sensors, type PB-25-S10-N0S-10C (Uni Measure). The adopted sampling rate during the tests was 200 Hz. For test monitoring, a video camera (Canon EOS M5) was used.

## 5. Small-scale models

It is well known that a reduced model 1: $n$ of a real structure (prototype), where $n$ is the factor of its reduction, cannot fully describe the actual behaviour of the real structure in an earthquake. The inconsistencies increase as the levels of reduction and nonlinearities in the structure increase. Reduced models can be reliable when investigating the relative effect of a parameter on the behaviour of the actual structure, i.e., when performing a parametric analysis. Caution should be present when assessing the behaviour, local effects and degree of safety of a real structure based on reduced model testing.

A brief theoretical overview of the expected differences in the test results with different foundation sizes is discussed below. As the larger foundation is 1.2 m long and 0.7 m wide and the smaller foundation is 0.7 m long and 0.5 m wide, the ratio of the area, resistance moment and inertia torque of the larger to smaller foundations are 1.71, 4.11 and 7.05, respectively. Therefore, a larger foundation will have significantly smaller rotation angles. The consequence is that less of a rocking effect is observed, i.e., less influence of the nonlinearity on the contact of foundation and substrate. Due to the larger surface area and lower contact stresses, it is possible that the horizontal displacements of the larger foundation relative to the base may be larger than those of the small foundation. It is expected that the smaller effect of rocking on a larger foundation will be present for the case of a rigid base, as well as for the case of the foundation support being on a layer of stone pebbles.

Smaller dimensions of the foundation result in a lower structural stiffness, higher foundation rocking effect and smaller earthquake forces in the structure, which is convenient. However, in such cases, the collapse of the structure can often occur due to overturning, without exhausting the load-bearing capacity of the structure. The essence of earthquake engineering, including in particular the seismic isolation concept, is basically to achieve an acceptable compromise for the structure displacements (stiffness) and stresses/strains (resistance) relation.

The adopted large foundation corresponds to lower and stiffer real buildings where the rocking effect during an earthquake is small or negligible, while the small foundation corresponds to higher real buildings with lower ground plans and greater bending influence. The efficiency of the considered seismic isolation is expected to be lower (more conservative) for models with larger foundation than for models with smaller foundation. The present research was conducted to further determine the conservative efficiency of considered seismic isolation for the most unfavourable expected conditions and possible applications in practice.

## 6. Test results for one-time base accelerations ($a_{g,max}$=0.3 g for $M_1$ and $M_2$ and with $a_{g,max}$=0.2 g for $M_3$ and $M_4$)

### *6.1 Peak values of the measured quantities*

The peak values of the measured quantities are presented on Figs. 4 - 7. $\varepsilon_{1,2}$ refers to a larger (less favourable) value of $\varepsilon_1$ and $\varepsilon_2$, whereas $v_{1,2}$ refers to a larger (less favourable) value of $v_1$ and $v_2$, respectively. It can be seen from Figs. 4 - 7 that the effect of the size of the foundation on the peak values of $a$, $\varepsilon_{1,2}$, $u_{1,2}$, $v_{1,2}$ depends on the stiffness of the model ($M_1$, $M_2$, $M_3$ and $M_4$), the type of excitation (AA, AP, AS, ABL) and the type of substrate (RB, BI).

Authors are aware that there is a lot of data and variables in the manuscript. Unfortunately, due to limited space, it is not possible to explain and comment on all the results in detail. By careful analysis of presented Figs. 4 - 7., it can be concluded that a larger foundation (LF), compared to a smaller foundation (SF) results in the following:

- Higher acceleration $a$ for all models and all excitations. The exceptions where the $M_3$ and $M_4$

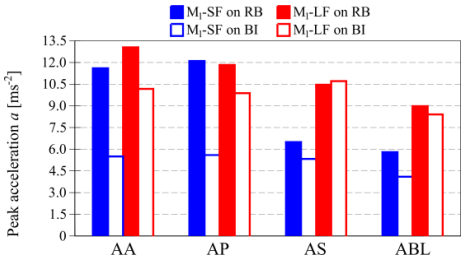


(a) Peak acceleration $a$ [ms$^{-2}$]

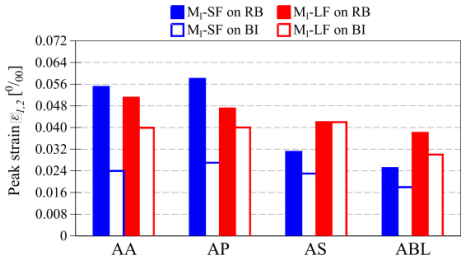


(b) Peak strain $\varepsilon_{1,2}$ [$^{0}/_{00}$]

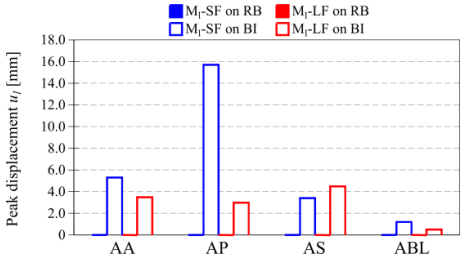


(c) Peak displacement $u_1$ [mm]

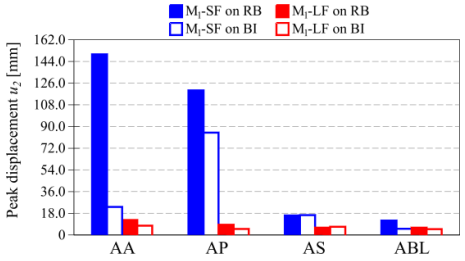


(d) Peak displacement $u_2$ [mm]

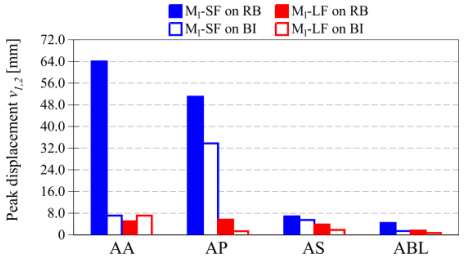


(e) Peak displacement $v_{1,2}$ [mm]

Fig. 4 Peak values of the results for the $M_1$ model

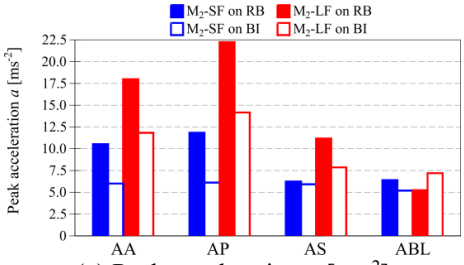


(a) Peak acceleration $a$ [ms$^{-2}$]

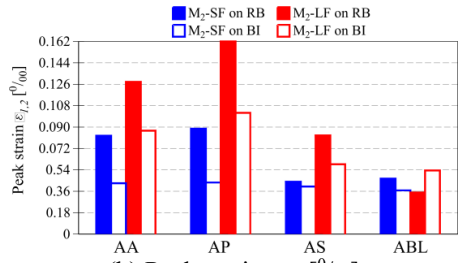


(b) Peak strain $\varepsilon_{1,2}$ [$^{0}/_{00}$]

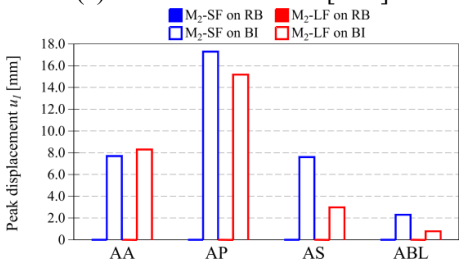


(c) Peak displacement $u_1$ [mm]

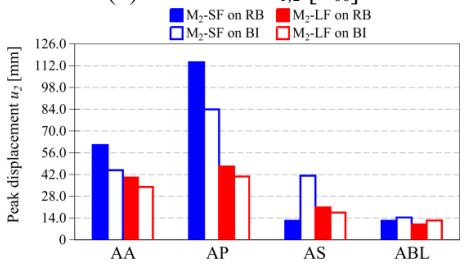


(d) Peak displacement $u_2$ [mm]

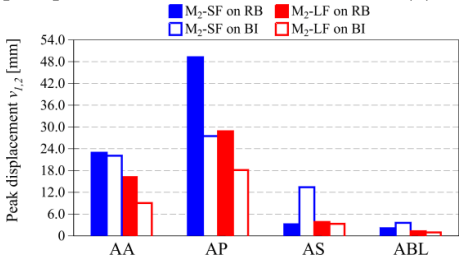


(e) Peak displacement $v_{1,2}$ [mm]

Fig. 5. Peak values of the results for the $M_2$ model

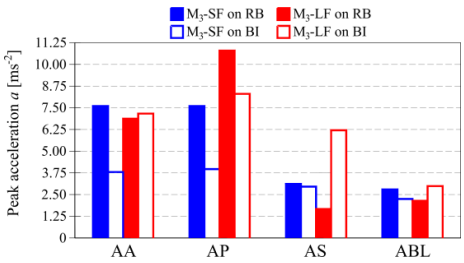


(a) Peak acceleration $a$ [ms$^{-2}$]

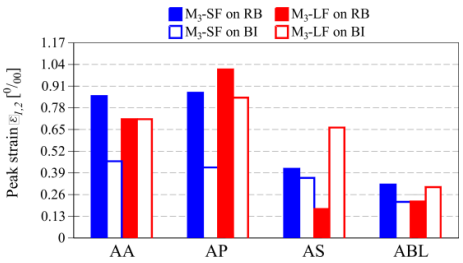


(b) Peak strain $\varepsilon_{1,2}$ [$^0/_{00}$]

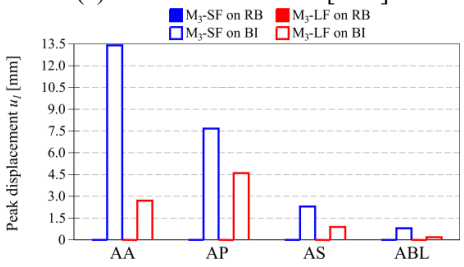


(c) Peak displacement $u_1$ [mm]

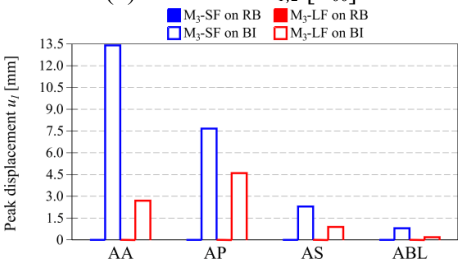


(d) Peak displacement $u_2$ [mm]

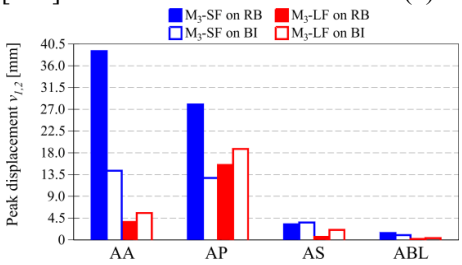


(e) Peak displacement $v_{1,2}$ [mm]

Fig. 6 Peak values of the results for the $M_3$ model

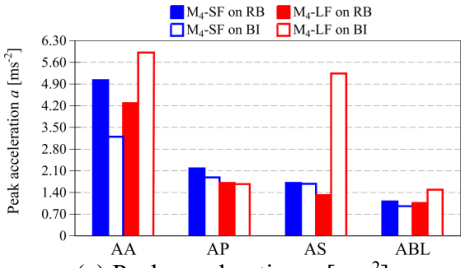


(a) Peak acceleration $a$ [ms$^{-2}$]

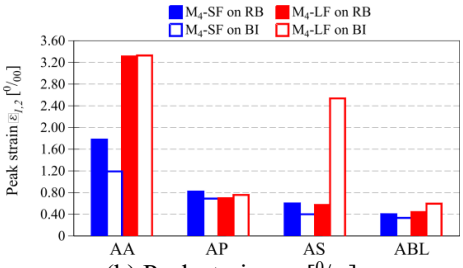


(b) Peak strain $\varepsilon_{1,2}$ [$^0/_{00}$]

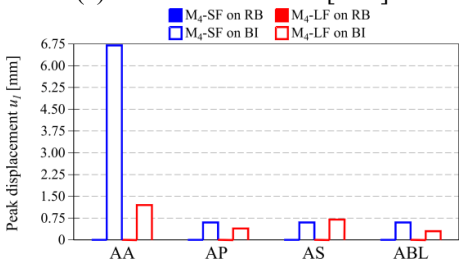


(c) Peak displacement $u_1$ [mm]

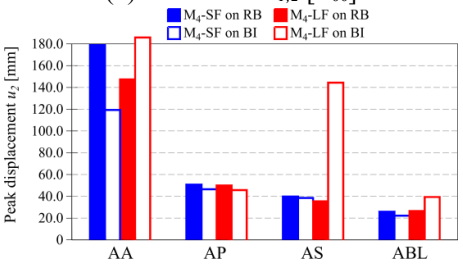


(d) Peak displacement $v_{1,2}$ [mm]

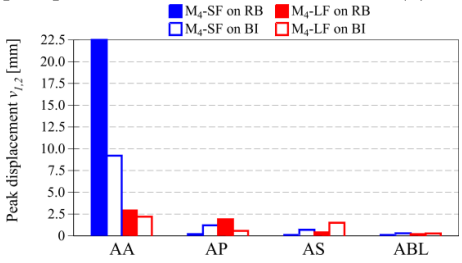


(e) Peak displacement $v_{1,2}$ [mm]

Fig. 7 Peak values of the results for the $M_4$ model

models based on RB. Higher accelerations may not always result in greater displacements and strains.

• Predominantly larger strains $\varepsilon_{1,2}$ were obtained for model $M_4$ at AA and AS excitations. For AA excitation, steel yielding at the bottom of the column occurred (the start of the plastic deformation for steel S355 occurred at 1.7 $^0/_{00}$).

• Significantly smaller displacements $u_1$ were obtained for almost all the models and excitations.

• Significantly smaller $u_2$ displacements were obtained for almost all the models and excitations. The larger displacements were only found for model $M_4$ at AA and AS excitations, where steel yielding at the bottom of the column occurred.

• Significantly smaller vertical displacements of foundation $v_{1,2}$ for almost all models and excitations.

The increased layout size of the foundation results in an increased rotational stiffness and reduced foundation rotation angle. Thus, the effect of rocking decreases and indirectly increases the rigidity of the model. This results in slightly higher earthquake accelerations (forces) but smaller horizontal and vertical displacements. Additionally, strains at the bottom of the column increase, especially for the $M_4$ model with the lowest stiffness. For this model, a larger foundation significantly contributes to the increase in the column restraint in the base.

The AA and AP excitations were generally significantly less favourable than the AS and ABL excitations. The exception is the $M_4$ model, where the AS excitation was less favourable than the AP excitation.

One of the key indicators of the aseismic layer efficiency, relative to the rigid base, is the measured strains $\varepsilon_{1,2}$ at the bottom of the column. The analysis of Figs. 4-7. shows that $\varepsilon_{1,2}$ values for $M_3$ and $M_4$ models with a larger foundation (LF) are larger for the foundation on base isolation (BI) than for the foundation on rigid base (RB). This result confirms the assumption at the beginning of the study for the considered concept of seismic isolation that it is likely to be favourable only for very rigid and rigid lower structures based on stiff ground.

### *6.2 Time-history presentation of the results*

Only some of the time histories of the measured quantities are presented in Figs. 8 - 15. The time histories are presented to show changes in the considered quantity depending on the model type, foundation size, earthquake type, and substrate type. Additionally, the results are presented for the purpose of possible numerical simulation the performed experimental tests.

Fig. 8 presents the vertical strain on the right bottom side of the steel column $\varepsilon_1$ for accelerogram AA. It can be seen that the smallest strains are recorded from the very stiff model $M_1$ and the largest strains are recorded from the soft model $M_4$. Additionally, for the $M_4$ model, there was an increase in the strain for the large foundation (LF) with base isolation (BI), compared to that of small foundation (SF) with base isolation (BI) and a significant plastic (irreversible) strain.

Fig. 9 presents the horizontal displacement of the mass

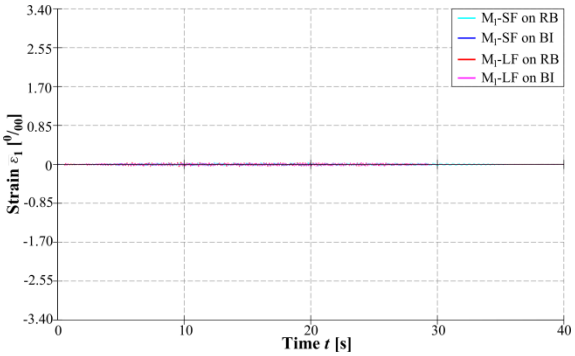


(a) Model $M_1$

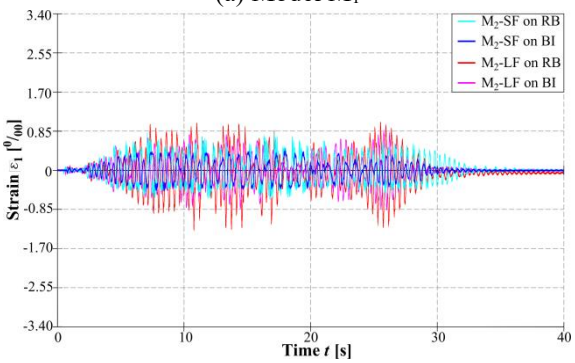


(b) Model $M_2$

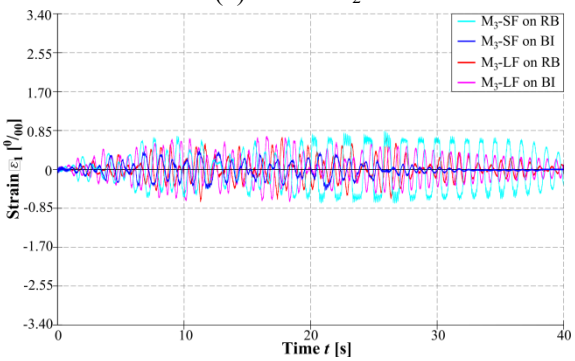


(c) Model $M_3$

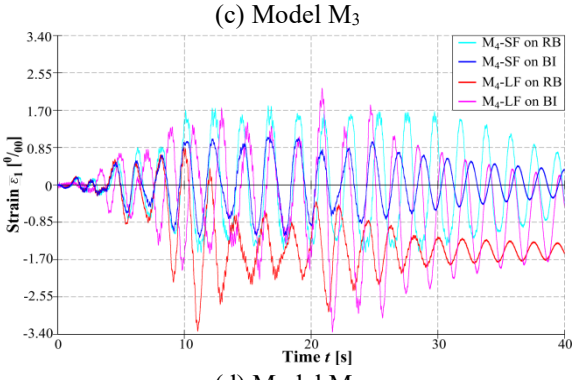


(d) Model $M_4$

Fig. 8 Vertical strain on the right bottom side of the steel column $\varepsilon_1$ for accelerogram AA

centre at the column top $u_2$ for accelerogram AA. The displacements are largest for the softer models ($M_3$ and $M_4$). For models $M_1$, $M_2$, and $M_3$ with a larger foundation (LF), the displacements are significantly smaller than those for the models with a small foundation (SF), and the displacements are elastic (reversible). For $M_4$ with a large

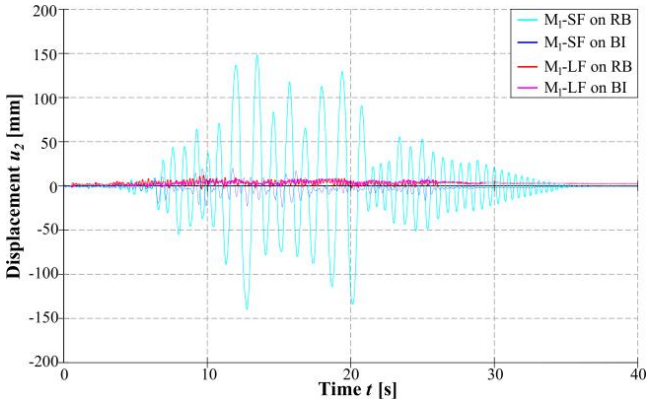


(a) Model $M_1$

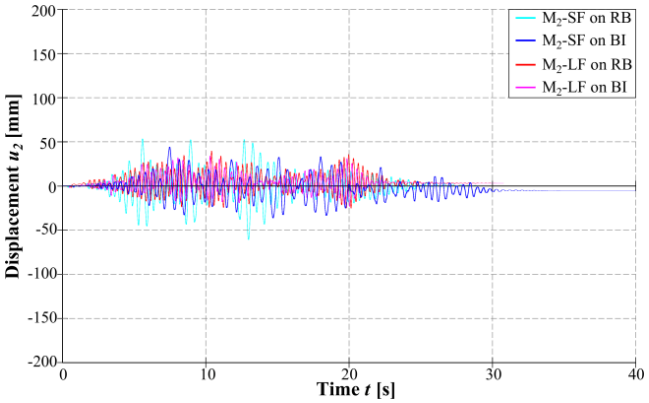


(b) Model $M_2$

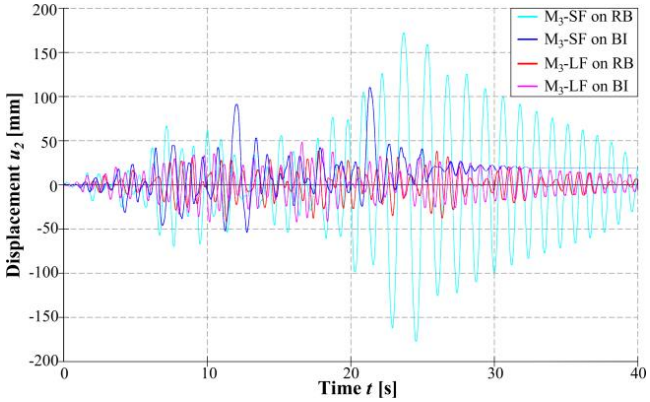


(c) Model $M_3$

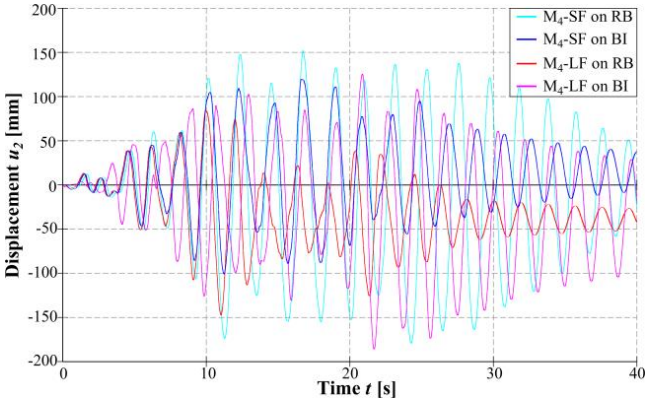


(d) Model $M_4$

Fig. 9 Horizontal displacement of the mass centre at the column top $u_2$ for accelerogram AA

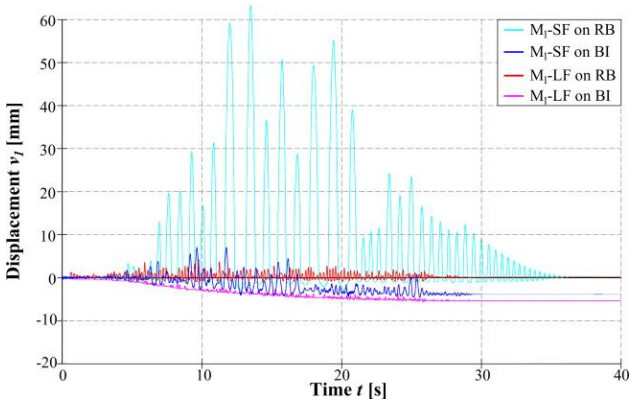


(a) Model $M_1$

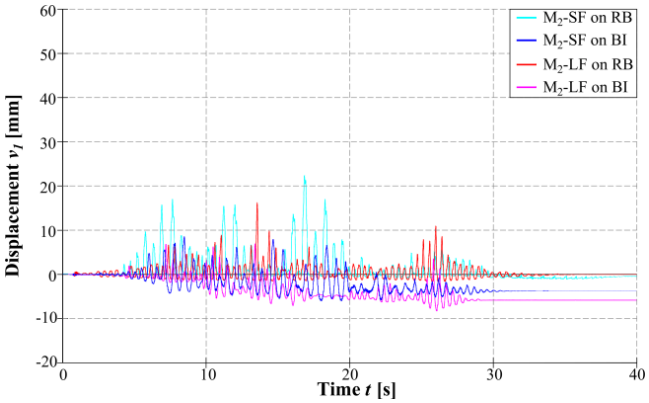


(b) Model $M_2$

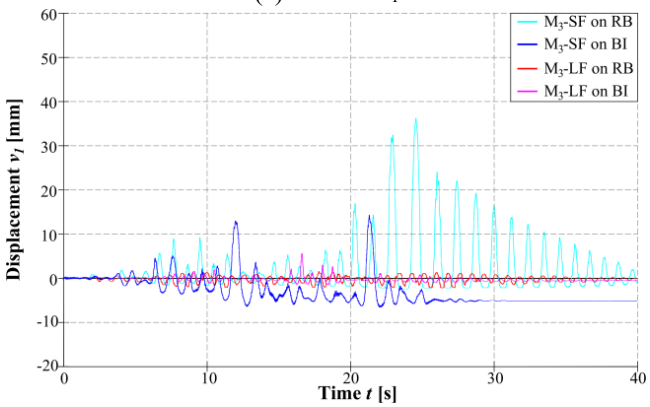


(c) Model $M_3$

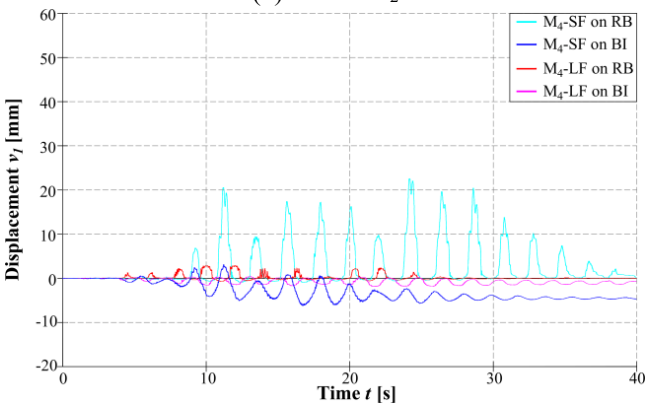


(d) Model $M_4$

Fig. 10 Vertical displacement at the left edge of the foundation $v_1$ for accelerogram AA

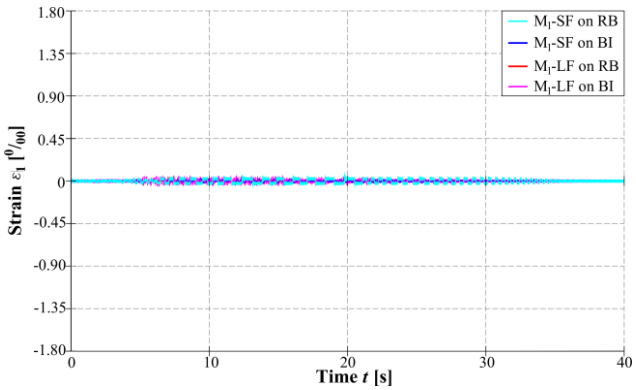


(a) Model $M_1$

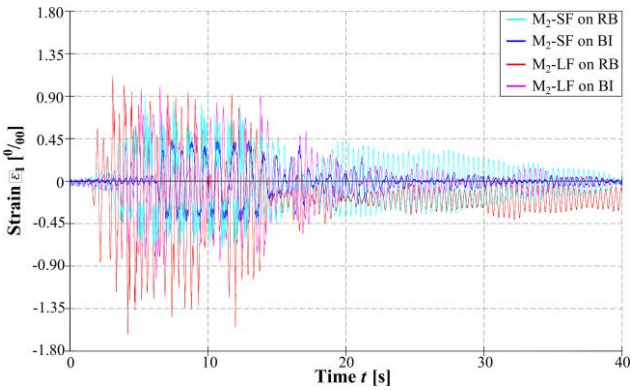


(b) Model $M_2$

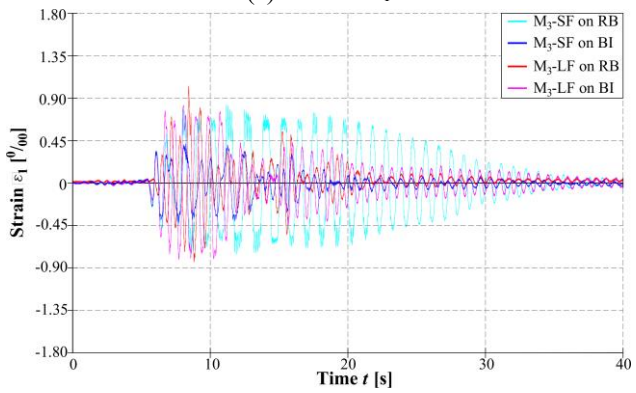


(c) Model $M_3$

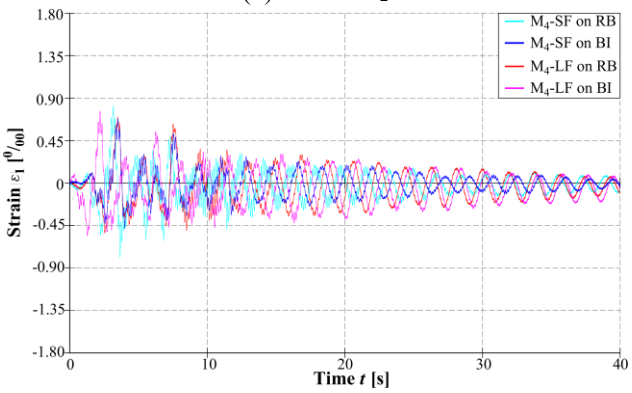


(d) Model $M_4$

Fig. 11 Vertical strain on the right bottom side of the steel column $\varepsilon_1$ for accelerogram AP

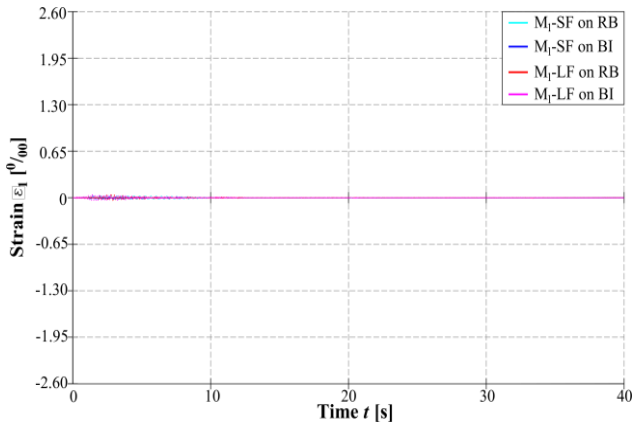


(a) Model $M_1$

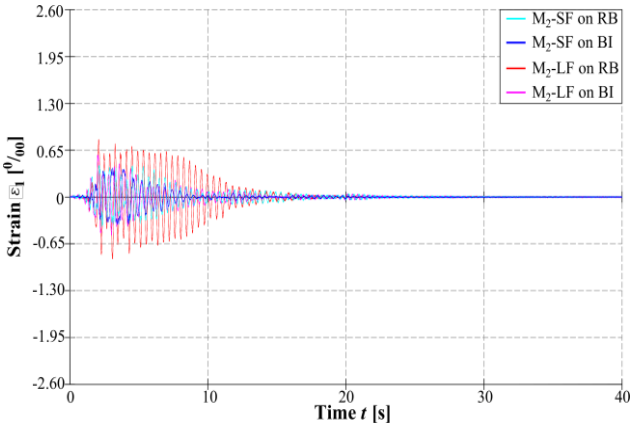


(b) Model $M_2$

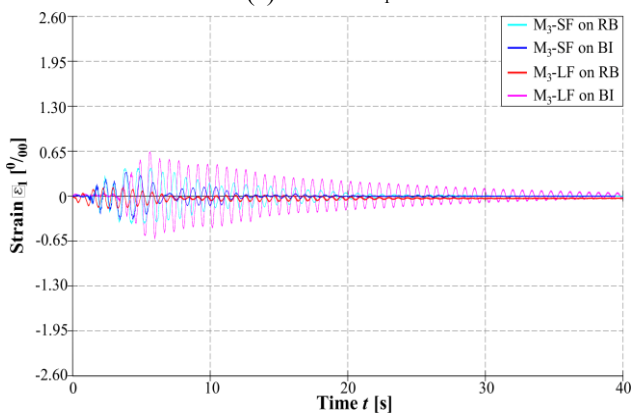


(c) Model $M_3$

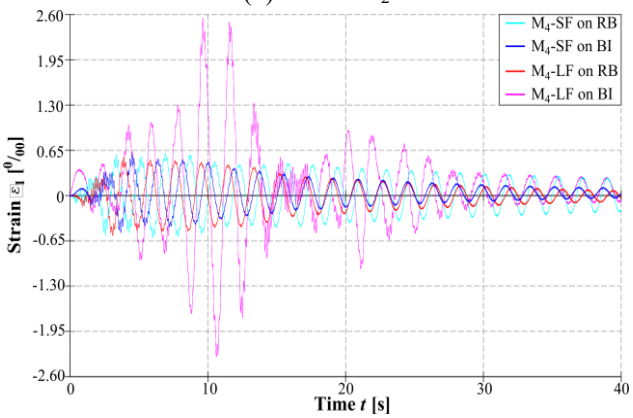


(d) Model $M_4$

Fig. 12 Vertical strain on the right bottom side of the steel column $\varepsilon_1$ for accelerogram AS

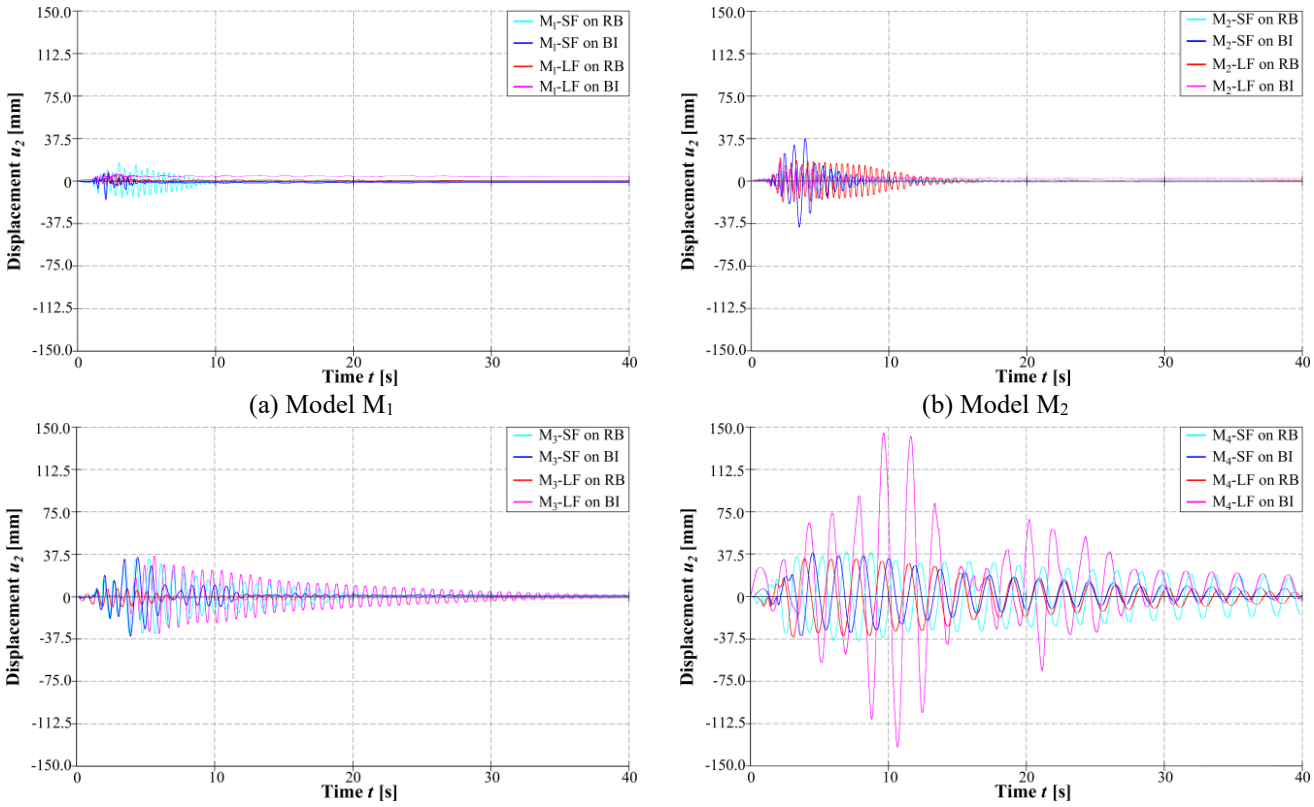


(a) Model $M_1$ (b) Model $M_2$

(c) Model $M_3$ (d) Model $M_4$

Fig. 13 Horizontal displacement of the mass centre at the column top $u_2$ for accelerogram AS

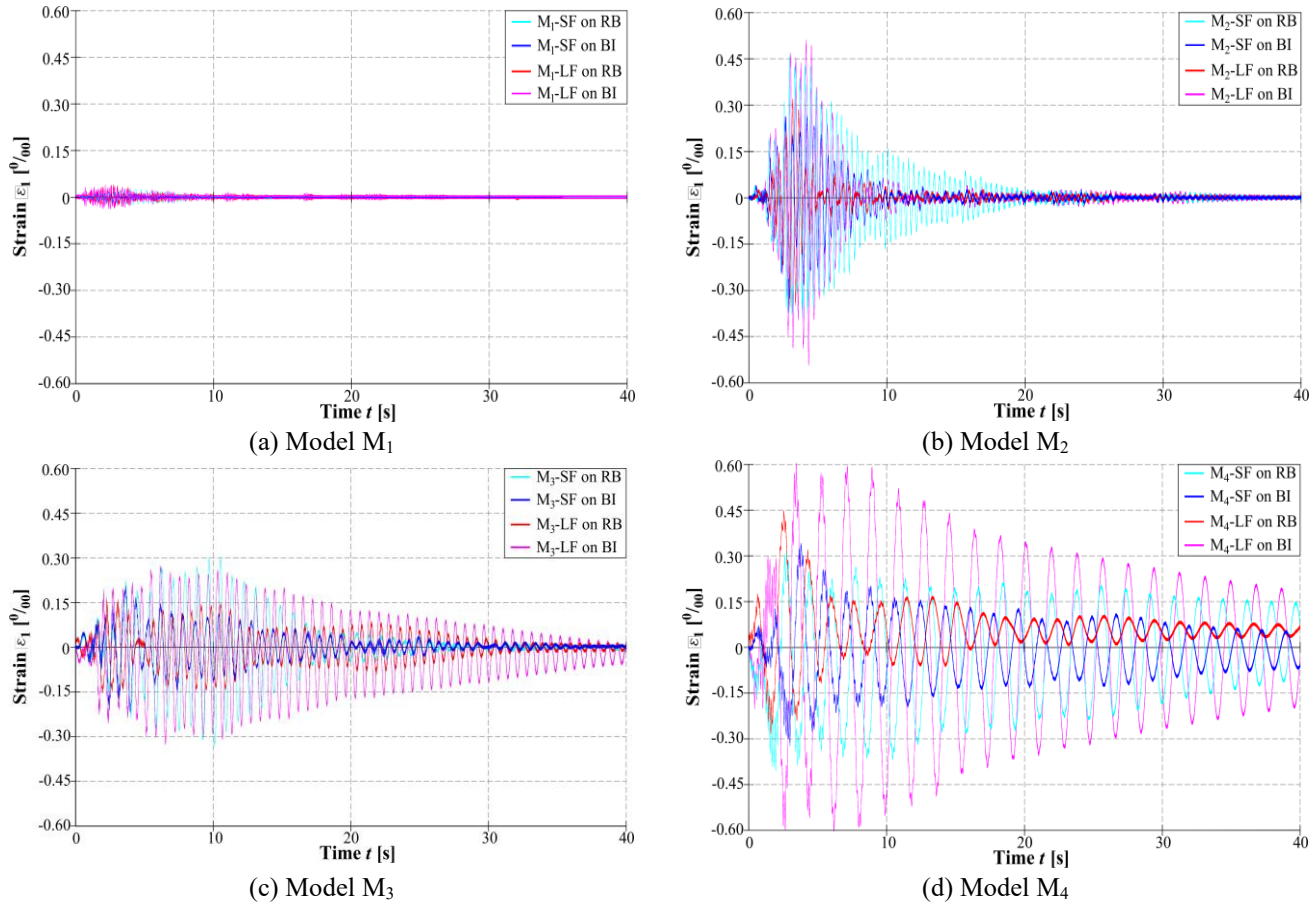


(a) Model $M_1$ (b) Model $M_2$

(c) Model $M_3$ (d) Model $M_4$

Fig. 14 Vertical strain on the right bottom side of the steel column $\varepsilon_1$ for accelerogram ABL

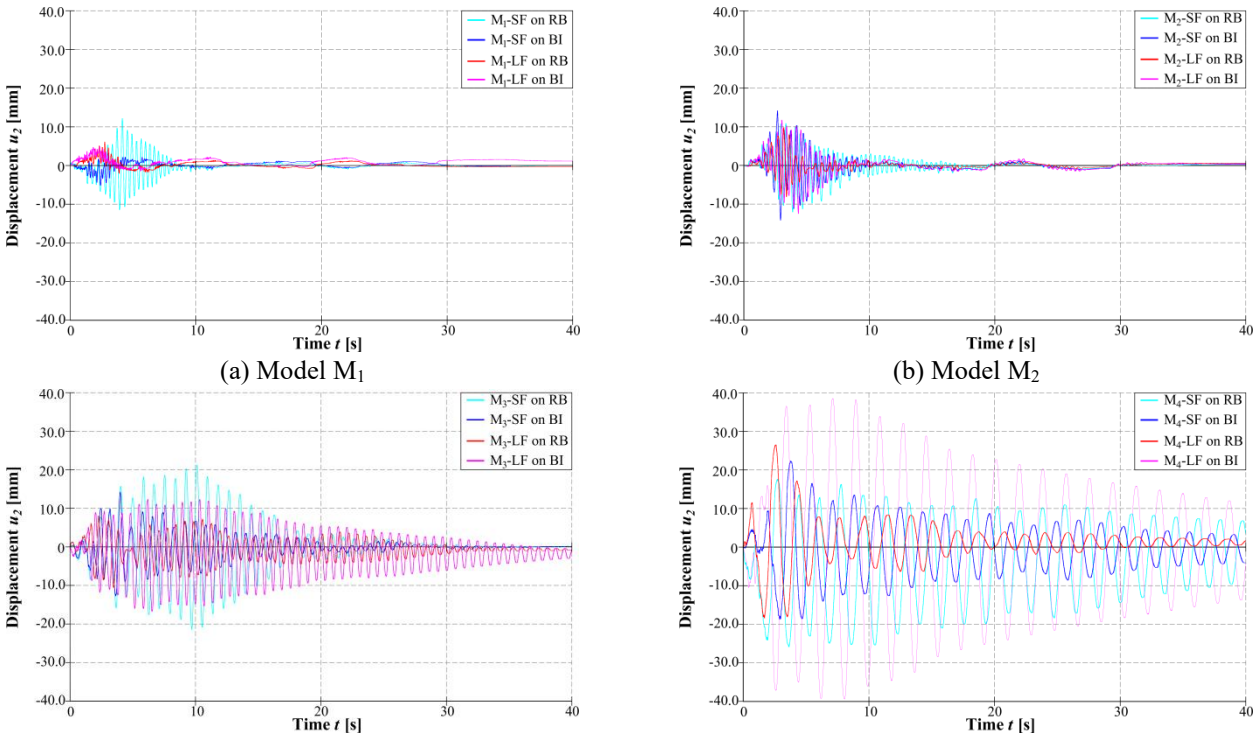


(a) Model $M_1$ (b) Model $M_2$

(c) Model $M_3$ (d) Model $M_4$

Fig. 15 Horizontal displacement of the mass centre at the column top $u_2$ for accelerogram ABL

Table 1 Coefficients of seismic isolation efficiency

| Coefficient | Excitation | Model | | | | | | | |
|---|---|---|---|---|---|---|---|---|---|
| | | $M_1$ | | $M_2$ | | $M_3$ | | $M_4$ | |
| | | $M_1$-SF | $M_1$-LF | $M_2$-SF | $M_2$-LF | $M_3$-SF | $M_3$-LF | $M_4$-SF | $M_4$-LF |
| $c_a$ | AA | 0.47 | 0.78 | 0.57 | 0.68 | 0.50 | 1.04 | 0.64 | 1.38 |
| | AP | 0.46 | 0.84 | 0.52 | 0.64 | 0.52 | 0.77 | 0.87 | 0.98 |
| | AS | 0.82 | 1.03 | 0.95 | 0.66 | 0.83 | 3.72 | 0.98 | 3.98 |
| | ABL | 0.71 | 0.94 | 0.81 | 1.38 | 0.80 | 1.40 | 0.86 | 1.41 |
| $c_{\varepsilon 1,2}$ | AA | 0.44 | 0.78 | 0.52 | 0.68 | 0.54 | 1.00 | 0.67 | 1.01 |
| | AP | 0.47 | 0.85 | 0.49 | 0.63 | 0.49 | 0.84 | 0.84 | 1.09 |
| | AS | 0.74 | 1.00 | 0.91 | 0.71 | 0.87 | 3.83 | 1.00 | 4.44 |
| | ABL | 0.72 | 0.89 | 0.79 | 1.53 | 0.68 | 1.39 | 0.85 | 1.37 |
| $c_{u2}$ | AA | 0.16 | 0.64 | 0.73 | 0.85 | 0.62 | 1.16 | 0.67 | 1.26 |
| | AP | 0.71 | 0.61 | 0.73 | 0.87 | 0.57 | 0.99 | 0.92 | 0.92 |
| | AS | 1.02 | 1.16 | 3.38 | 0.85 | 0.92 | 3.88 | 0.97 | 4.10 |
| | ABL | 0.43 | 0.82 | 1.18 | 1.27 | 0.68 | 1.39 | 0.86 | 1.49 |
| $c_{v1,2}$ | AA | 0.11 | 1.44 | 0.96 | 0.56 | 0.37 | 1.51 | 0.41 | 0.75 |
| | AP | 0.66 | 0.30 | 0.56 | 0.63 | 0.46 | 1.21 | 5.26 | 0.30 |
| | AS | 0.81 | 0.49 | 4.16 | 0.89 | 1.13 | 3.45 | 5.23 | 4.03 |
| | ABL | 0.66 | 0.30 | 0.56 | 0.63 | 0.46 | 1.21 | 2.89 | 1.48 |

foundation (LF), compared to the small foundation (SF), the displacements are larger and irreversible.

Comparing Figs. 11 and 8, it can be concluded that for models $M_1$, $M_2$ and $M_3$, the strain $\varepsilon_1$ is approximately the same for AA and AP excitations. The authors explain this behaviour that probably AA led to the resonant motion of the $M_4$ model. Namely, the AA excitation contains a wide range of frequencies and is often the most unfavourable excitation. It should be noted that the excitation AP also causes high strains in the model $M_4$.

The vertical strain on the right bottom side of steel column $\varepsilon_1$ for accelerogram AS (Fig. 12) has higher values for all models with a large foundation (LF), particularly for the $M_4$ model, compared to values for models with a small foundation.

The horizontal displacement of the mass centre at the column top $u_2$ for accelerogram AS (Fig. 13), compared to the SF case, is slightly smaller for the LF case for models $M_1$, $M_2$, and $M_3$ and significantly larger for model $M_4$. All the displacements are reversible.

For the ABL excitation, the vertical strain $\varepsilon_1$ (Fig. 14) and the horizontal displacement $u_2$ (Fig. 15) are also largest for the $M_4$ model, with a LF resulting in a significantly larger $\varepsilon_1$ and $u_2$ than those with a SF. For the other models, the values of these quantities are approximately equal for the LF and SF models.

### 6.3 Seismic isolation efficiency

Table 1 presents the efficiency of the considered seismic isolation for one-time base excitation ($a_{g,max}$=0.3 g for $M_1$ and $M_2$ and with $a_{g,max}$=0.2 g for $M_3$ and $M_4$), depending on the model type, foundation size, earthquake type, and substrate type. The seismic isolation efficiency coefficients $c_a$, $c_{\varepsilon 1,2}$, $c_{u2}$ and $c_{v1,2}$ are defined as the ratio of the highest value of the considered model parameter (acceleration, strain, displacement) on the aseismic layer ($h_p$=0.3 m) and the model supported on a rigid base. The $c_{\varepsilon 1,2}$ and $c_{v1,2}$ tags refer to the larger values of $\varepsilon_1$ and $\varepsilon_2$ ($v_1$ and $v_2$), respectively. Thus, if the coefficients are less than 1.0, the corresponding parameters are smaller (more favourable) for the pebble layer (BI)-based models than for the rigid base (RB)-based models. Otherwise, the corresponding parameters are higher (less favourable) for the BI-based models (values in the rectangle in Table 1) than for the other models.

When evaluating the importance of the considered coefficients, it should be noted that the accelerograms of the longer duration and longer predominant period AA and AP give significantly higher strains (stresses) and displacements than those of the short period, impact AS and ABL accelerograms. Namely, these coefficients represent relative relationships, regardless of the level of strain and displacement for each excitation. Further, irrespective on the foundation size and structural stiffness, seismic isolation efficiency was higher for AA and AP excitation than for AS and ABL. This behaviour is explained by the fact that AA and AP are long-lasting earthquakes that bring high energy into the system and produce more pronounced rocking of the model. Namely, beside the sliding mechanism, the reduction or earthquake forces in this isolation concept is achieved by reduced rocking stiffness, taking the advantages of rocking isolation concept.

The most important coefficients are those related to the strains (stresses) at the bottom of the column and to the displacements. Higher model accelerations do not necessarily result in larger strains; therefore the strain coefficient more accurately describes the real state in the structure than the acceleration coefficient.

The larger foundation (LF) models generally have a less favourable strain state and a more favourable displacement state than those of the small foundation (SF) models. It is also evident that with decreasing stiffness in the model (increasing its period of free oscillations), the efficiency of the considered seismic isolation decreases. For example, the ratio of the coefficient $c_{\varepsilon 1,2}$ for models with a larger foundation, namely, $M_1$-LF, $M_2$-LF, $M_3$-LF, and $M_4$-LF are 0.78, 0.68, 1.00, and 1.01 for excitation AA; 0.85, 0.63, 0.84, and 1.09 for excitation AS; 0.85, 0.63, 0.84, and 1.09 for excitation AP; and 0.89, 1.53, 1.39, and 1.37 for ABL excitation. Thus, even for the most conservative case of a building with virtually no foundation rotation, the considered seismic isolation with earthquake stresses in the elastic region results in a significant reduction of the strains (stresses) in the construction of very stiff ($M_1$) and stiff ($M_2$) buildings but also somewhat reduce the strains for softer buildings ($M_3$ and $M_4$) for some earthquake loading conditions.

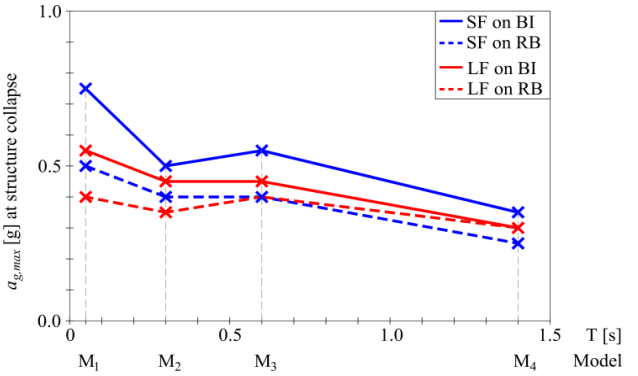


Fig. 16 Acceleration $a_{g,\,max}$ [g] of accelerogram AA at which the structure collapsed

The ratio of the coefficients $c_{u2}$ for the models $M_1$-LF, $M_2$-LF, $M_3$-LF, and $M_4$-LF are 0.64, 0.85, 1.16, and 1.26 for the AA excitation; 0.61, 0.87, 0.99, and 0.92 for the AP excitation; 1.16, 0.85, 3.88, and 4.10 for the AS excitation; and 0.82, 1.27, 1.39, and 1.49 for the ABL excitation. Thus, the presented seismic base isolation is also favourable in terms of the horizontal displacements for the $M_1$ and $M_2$ models. As seen in Figs. 6 and 7., the impact accelerogram of AS excitation is proven to be very unfavourable for softer models $M_3$ and $M_4$ with a large foundation, which can be explained by the large influence of the shear force.

## 7. Test results for a successive increase in the base acceleration until structure collapsed

The acceleration $a_{g,\,max}$ for AA excitation (mainly the most unfavourable excitation) at which the tested model collapsed or lost stability, is shown in Fig. 16.

The purpose of this test was to determine how much the bearing capacity of the model supported by the 0.3 m thick aseismic layer exceeds the bearing capacity of the same model supported by a rigid base, separately for the small foundation (SF) case and large foundation (LF) case. The ratios (coefficients) for models with a small foundation (SF) for $M_1$-SF, $M_2$-SF, $M_3$-SF, and $M_4$-SF were 1.50, 1.25, 1.38, and 1.40, and for models with a large foundation (LF) for $M_1$-LF, $M_2$-LF, $M_3$-LF, and $M_4$-LF were 1.38, 1.29, 1.19, and 1.00. The accuracy of the results on Fig. 16 would be higher if $\Delta a_{g,\,max}$ was less than 0.05 g. From the above results, it can be concluded that with the increase in the ground dimensions of the foundation, the limit state efficiency of the considered seismic isolation decreases. Additionally, it can be noted that as the period of free oscillations of the model increases (decrease in stiffness), the limit state efficiency of the considered seismic isolation

decreases. Thus, the ratio of acceleration $a_{g,\,max}$ at which the model collapsed for seismic isolation (BI) and $a_{g,\,max}$ at which the model collapsed for a rigid base (RB) for the $M_3$-LF medium-stiff model is 1.13, and for the $M_4$-LF soft model, the ratio is only 1.0.

## 8. Conclusions

The following conclusions can be made based on the research results of the effect of the ground plan dimension of the foundation on the seismic base isolation efficiency using a layer of stone pebbles for building models with four different stiffnesses (from very rigid $M_1$ to soft $M_4$) exposed to the acceleration of four different types of earthquakes (AA and AP of longer duration and longer predominant period, and AS and ABL with short duration and impact type).

For the case of the one-time base acceleration of the adopted excitations with $a_{g,\,max}$=0.2 g ($M_1$ and $M_2$ model) or $a_{g,\,max}$=0.2 g ($M_3$ and $M_4$ model), which causes only elastic strains/stresses in the model column (except for the $M_4$ model at AA excitation), the following general conclusions apply:

- Compared to models with smaller foundations, models with larger foundations result in higher accelerations, larger column strains (especially for the soft $M_4$ model), significantly smaller foundation and column top displacements, and significantly smaller vertical foundation displacements (settlement and uplifting).
- The reason for the foregoing is a significant increase in rotational stiffness at a larger foundation and a decrease in the foundation rotation, i.e., a decrease in the effect of rocking. This results in an indirect increase in the stiffness of the entire model and the generation of higher earthquake accelerations (forces) in the model.
- As the size of the foundation increases, the efficiency of the seismic base isolation with the layer of stone pebbles decreases. The seismic isolation efficiency coefficient is defined as the ratio of the highest value of the considered quantity for the model parameter on the aseismic layer and for the model supported by a rigid base. Thus, the ratio of the coefficient of strain (stress) at the bottom of column $c_{\varepsilon 1,2}$ for models with larger foundations, namely, $M_1$-LF, $M_2$-LF, $M_3$-LF, and $M_4$-LF were 0.78, 0.68, 1.00, and 1.01 for excitation AA, 0.85, 0.63, 0.84, and 1.09 for excitation AS; 0.85, 0.63, 0.84, and 1.09 for excitation AP; and 0.89, 1.53, 1.39, and 1.37 for excitation ABL. Thus, even for the most unfavourable condition with very little foundation rotation, the considered seismic isolation results in a significant reduction in the strains at the bottom of the column in very stiff ($M_1$) and stiff ($M_2$) building models. The ratio of the displacement coefficients of the column top $c_{u2}$ for models with a larger foundation for $M_1$-LF, $M_2$-LF, $M_3$-LF, and $M_4$-LF are 0.64, 0.85, 1.16, and 1.26 for the AA excitation; 0.61, 0.87, 0.99, and 0.92 for the AP excitation; 1.16, 0.85, 3.88, and 4.10 for the AS excitation; and 0.82, 1.27, 1.39, and 1.49 for the ABL excitation. It follows that the considered seismic base isolation also results in a smaller column top displacement $u_2$ for all the models subjected to AA and AP excitations. It can be concluded that the seismic base isolation has proven to be sufficiently effective for models of very stiff ($M_1$) and stiff ($M_2$) buildings with all the accelerograms applied.
- The difference in response of investigated models under accelerograms with long predominant periods (AA, AP) and the ones with short predominant periods (AS, ABL) is observed. Irrespective on the foundation size and structural stiffness, seismic isolation efficiency was higher for AA and AP excitation than for AS and ABL. This behaviour is explained by the fact that AA and AP are long-lasting earthquakes that bring high energy into the system and produce more pronounced rocking of the model. Namely, beside the sliding mechanism, the reduction or earthquake forces in this isolation concept is achieved by reduced rocking stiffness, taking the advantages of rocking isolation concept. The low efficiency of seismic isolation for AS and ABL accelerograms should be seen in the context that they cause low stresses in the tested models, which diminishes the fact of less efficient seismic isolation for such excitations.

Every model was exposed to a set of repeated artificial accelerogram (AA) (the most unfavourable excitation) by scaling the peak ground acceleration (PGA) until the structure collapsed or lost stability. The ratios of the acceleration $a_{g,max}$ (load-bearing capacity) of the considered models for the foundation supported on the stone pebble layer and the foundation supported on a rigid base for the small foundation case (SF) for $M_1$-SF, $M_2$-SF, $M_3$-SF, and $M_4$-SF were 1.50, 1.25, 1.38, and 1.40, and for the large foundation (LF) case, for $M_1$-LF, $M_2$-LF, $M_3$-LF, and $M_4$-LF the ratios were 1.38, 1.29, 1.13, and 1.00. Obviously, as the size of the foundation increases, the limit state efficiency of the seismic isolation decreases when reaching the model load-bearing capacity or losing stability. Additionally, reducing the stiffness of the model (the column), with the same foundation, reduces the limit state efficiency of the seismic isolation. Thus, the ratio of the acceleration $a_{g,\,max}$ at which the model collapses for seismic isolation and $a_{g,\,max}$ at which the model collapses for a rigid base for the $M_3$-LF medium-stiff model is 1.13, and for the $M_4$-LF soft model is only 1.0. Therefore, the research carried out to the collapse condition of the considered models confirms that the seismic isolation limit state efficiency decreases with the increase in the model foundation and with the decrease in the column stiffness. However, for very stiff ($M_1$) and stiff ($M_2$) models supported on the large foundation with low rocking effect, seismic isolation with a thin layer of stone pebbles can significantly increase load-bearing capacity of models (up to approximately 38%), depending on the type of earthquake.

The conducted research has confirmed the conclusions of the previous studies (Banović *et al*. 2018b, 2019) on the efficiency of the considered seismic isolation, which with new studies is reduced and restricted mainly to very stiff and stiff buildings on stiff soil (with a free oscillation period up to approximately 0.3 s - 0.4 s). Owing the limitations of

the performed research (relative simple building models, just four building models, only four base excitations applied, and uniaxial base excitation), the obtained conclusions should be strengthened by further research. Due to the above statement, further experimental research on this topic (preferably on real structures or models with realistic material and a slightly reduced geometry) and research using numerical models are needed.

## Acknowledgments

This work has been fully supported by the Croatian Science Foundation under the project *"Seismic base isolation of a building by using natural materials - shake table testing and numerical modelling*" [IP-06-2016-5325]. The work of doctoral student Ivan Banović has been fully supported by the *"Young researchers' career development project – training of doctoral students"* of the Croatian Science Foundation funded by the European Union from the European Social Fund. The authors are grateful for the support.

## References

Ambraseys, N., Smit, P., Sigbjornsson, R., Suhadolc, P. and Margaris, M. (2001), EVR1-CT-1999-40008, European Commission, Directorate-General XII, Environmental and Climate Programme, Brussels, Belgium

Anastasopoulos, I., Loli, M., Georgarakos, T. and Drosos, V. (2012), "Shaking table testing of rocking-isolated bridge pier on sand", *J. Earthq. Eng.*, **17**(1), 1-32. https://doi.org/10.1016/j.soildyn.2012.04.006.

Azinović, B., Kilar, V. and Koren, D. (2014), "The seismic response of low-energy buildings founded on a thermal insulation layer –a parametric study", *Eng. Struct.*, **81**, 398-411. https://doi.org/10.1016/j.engstruct.2014.10.015.

Azinović, B., Kilar, V. and Koren, D. (2016), "Energy-efficient solution for the foundation of passive houses in earthquake-prone regions", *Eng. Struct.*, **112**, 133-145. https://doi.org/10.1016/j.engstruct.2016.01.015.

Azzam, W., Ayeldeen, M. and El Siragy, M. (2018), "Improving the structural stability during earthquakes using in-filled trench with EPS geofoam—numerical study", *Arab. J. Geosci.*, **11**(14), 395. https://doi.org/10.1007/s12517-018-3739-4.

Bandyopadhyay, S., Sengupta, A. and Reddy, G.R. (2015), "Performance of sand and shredded rubber tire mixture as a natural base isolator for earthquake protection", *Earthq. Eng. Eng. Vib.*, **14**(4), 683-693. https://doi.org/10.1007/s11803-015-0053-y.

Banović, I., Radnić, J. and Grgić, N. (2018b), "Shake table study on the efficiency of seismic base isolation using natural stone pebbles", *Advan. Mater. Sci. Eng.*, 1012527, https://doi.org/10.1155/2018/1012527.

Banović, I., Radnić, J. and Grgić, N. (2019), "Geotechnical seismic isolation system based on sliding mechanism using stone pebble layer: shake-table experiments", *Shock Vib.*, 9346232, https://doi.org/10.1155/2019/9346232.

Banović, I., Radnić, J., Grgić, N. and Matešan, D. (2018a), "The use of limestone sand for the seismic base isolation of structures", *Advan. Civil Eng.*, https://doi.org/10.1155/2018/9734283.

Brunet, S., de la Llera, J.C. and Kausel, E. (2016), "Non-linear modeling of seismic isolation systems made of recycled tire-rubber", *Soil Dyn. Earthq. Eng.*, **85**, 134-145. https://doi.org/10.1016/j.soildyn.2016.03.019.

Carpani, B. (2017). Base isolation from a historical perspective. 16th World Conference on Earthquake, Paper N° 4934, Santiago, Chile

Chung Y.L., Du L.J. and Pan H.H. (2019), "Performance evaluation of a rocking steel column base equipped with asymmetrical resistance friction damper", *Earthq. Struct.*, **17**(1), 49-61. https://doi.org/10.12989/eas.2019.17.1.049.

Doudoumis, I., Papadopoulos, P. and Papaliangas, T. (2002), "Low-cost base isolation system on artificial soil layers with low shearing resistance", Proceedings of the 12th European Conference on Earthquake Engineering, London, U.K.

Eurocode (2004) EN 1998-1:2004 Eurocode 8: Design of structures for earthquake resistance-Part 1: general rules, seismic actions and rules for buildings, European Committee for Standardization (CEN), Brussels, Belgium

Feng, R., Chen, Y. and Cui, G. (2018), "Dynamic response of post-tensioned rocking wall-moment frames under near-fault ground excitation", *Earthq. Struct.*, **15**(3), 243-251. https://doi.org/10.12989/eas.2018.15.3.243.

Forcellini, D. (2017), "Assessment on geotechnical seismic isolation (GSI) on bridge configurations", *Innovat. Infrastruct. Solution*., **2**(1), https://doi.org/10.1007/s41062-017-0057-8.

Hadad, H.A, Calabrese, A., Strano, S. and Serino, G. (2017), "A base isolation system for developing countries using discarded tyres filled with elastomeric recycled materials", *J. Earthq. Eng.*, **21**(2), 246-266. https://doi.org/10.1080/13632469.2016.1172371.

Kalpakcı, V., Bonab, A.T., Özkan, M.Y. and Gülerce, Z. (2018), "Experimental evaluation of geomembrane/geotextile interface as base isolating system", *Geosynth. Int.*, **25**(1), 1-11. https://doi.org/10.1680/jgein.17.00025.

Karatzia, X. and Mylonakis, G. (2017), "Geotechnical seismic isolation using eps geofoam around piles", *The 6th International Conference on Computational Methods in Structural Dynamics and Earthquake Engineering*, Rhodes Island, Greece.

Koren, D. and Kilar, V. (2016), "Seismic vulnerability of reinforced concrete building structures founded on an XPS layer", *Earthq. Struct.*, **10**(4), 939-963. https://doi.org/10.12989/eas.2016.10.4.939.

Kulukčija S. and Humo M. (2009), "Survey of historic foundation engineering", Baština, Sarajevo.

Kulukčija S., Humo M., Mandžić E., Mandžić K., and Selimović M. (2009), "Existing historical foundation system of two old bridges from the Ottoman period in Bosnia and Herzegovina", *The Third International Congress on Construction History*, Cottbus, Germany.

Makris, N. (2014), "A half-century of rocking isolation", *Earthq. Struct.*, **7**(6), 1187-1221. https://doi.org/10.12989/eas.2014.7.6.1187.

Mavronicola, E., Komodromos, P. and Charmpis, D.C. (2010), "Numerical investigation of potential usage of rubber–soil mixtures as a distributed seismic isolation approach", *The Proceedings of the 10th International Conference on Computational Structures Technology*, Valencia, Spain.

Murillo, C., Thorel, L. and Caicedo, B. (2009), "Ground vibration isolation with geofoam barriers: centrifuge modelling", *Geotext. Geomembranes*, **27**(6), 423-434. https://doi.org/10.1016/j.geotexmem.2009.03.006.

Naeim, F. and Kelly, J.M. (1999), "Design of seismic isolated structures: From theory to practice", John Wiley & Sons, Inc., New York.

Nanda, R.P., Agarwal, P., and Shrikhande, M. (2012a), "Base isolation by geosynthetic for brick masonry buildings", *J. Vib.*

*Control*, **18**(6), 903-910. https://doi.org/10.1177/1077546311412411.

Nanda, R.P., Shrikhande, M. and Agarwal, P. (2012b), "Effect of ground motion characteristics on the pure friction isolation system", *Earthq. Struct.*, **3**(2), 169-180. https://doi.org/10.12989/eas.2012.3.2.169.

Panjamani, A., Devarahalli Ramegowda, M. and Divyesh, R. (2015), "Low cost damping scheme for low to medium rise buildings using rubber soil mixtures", *Japan. Geotech. Soc. Spec. Publications*, **3**(2), 24-28. https://doi.org/10.3208/jgssp.v03.i05.

Patil, S.J., Reddy, G.R., Shivshankar, R., Babu, R., Jayalekshmi, B.R. and Kumar, B. (2016), "Seismic base isolation for structures using river sand", *Earthq. Struct.*, **10**(4), 829-847. https://doi.org/10.12989/eas.2016.10.4.829.

Pecker, A. (2003), "A seismic foundation design process, lessons learned from two major projects: the Vasco de Gama and the Rion Antirion bridges", *The Proceedings of the ACI International Conference on Seismic Bridge Design and Retrofit*, La Jolla, U.S.A.

Pecker, A., Prevost, J.H. and Dormieux, L. (2001), "Analysis of pore pressure generation and dissipation in cohesionless materials during seismic loading", *J. Earthq. Eng.*, **5**(4), 441-464. https://doi.org/10.1080/13632460109350401.

Przewłócki, J., Dardzinska, I. and Swinianski, J. (2005), "Review of historical buildings' foundations", *Géotechnique*, **55**, 363-372. https://doi.org/10.1680/geot.2005.55.5.363.

Radnić, J., Grgić, N., Matešan, D. and Baloević, G. (2015), "Shake table testing of reinforced concrete columns with different layout size of foundation", *Materialwissenschaft und Werkstofftechnik*, **46**(4-5), 348-367. https://doi.org/10.1002/mawe.201500410.

Steenfelt, J.S, Foged, B. and Augustesen, A.H. (2015), "Izmit Bay bridge-geotechnical challenges and innovative solutions", *Int. J. Bridge Eng*., *(IJBE)* **3**(3), 53-68.

Tehrani, F.M. and Hasani, A. (1996), "Behaviour of Iranian low rise buildings on sliding base to earthquake excitation", *The Proceedings of the 11th World Conference on Earthquake Engineering*, Acapulco, Mexico.

Tsang, H.H. (2008), "Seismic isolation by rubber-soil mixtures for developing countries", *Earthq. Eng. Struct. Dyn.*, **37**(2), 283-303. https://doi.org/10.1002/eqe.756.

Tsang, H.H. (2009), "Geotechnical seismic isolation", *Earthq. Eng.: New Res., New York, U.S.A. Nova Science Publishers Inc*., 55-87.

Tsang, H.H. and Pitilakis, K. (2019), "Mechanism of geotechnical seismic isolation system: analytical modeling", *Soil Dyn. Earthq. Eng.*, **122**, 171-184. https://doi.org/10.1016/j.soildyn.2019.03.037.

Tsang, H.H., Lo, S.H., Xu, X. and Neaz Sheikh, M. (2012), "Seismic isolation for low-to-medium-rise buildings using granulated rubber-soil mixtures: numerical study", *Earthq. Eng. Struct. Dyn.*, **41**(14), 2009-2024. https://doi.org/10.1002/eqe.2171.

Tsiavos, A., Alexander N.A., Diambra A., Ibraim E., Vardanega P. J., Gonzalez-Buelga A. and Sextos A. (2019), "A sand-rubber deformable granular layer as a low-cost seismic isolation strategy in developing countries: experimental investigation", *Soil Dyn. Earthq. Eng.*, **125** https://doi.org/10.1016/j.soildyn.2019.105731.

Wang J., He J.X., Yang Q.S. and Yang, N. (2018), "Study on mechanical behaviors of column foot joint in traditional timber structure", *Struct. Eng. Mech.*, **66**(1), 1-14. https://doi.org/10.12989/sem.2018.66.1.001.

Xiao, H., Butterworth, J.W. and Larkin, T. (2004), "Low-technology techniques for seismic isolation", *The Proceedings of the NZSEE Conference*, Rototua, New Zealand.

Xiong, W. and Li, Y. (2013), "Seismic isolation using granulated tire-soil mixtures for less-developed regions: experimental validation", *Earthq. Eng. Struct. Dyn.*, **42**(14), 2187-2193. https://doi.org/10.1002/eqe.2315.

Xiong, W., Yan, M.R., and Li, Y.Z. (2014), "Geotechnical seismic isolation system - further experimental study", *Appl. Mech. Mater.*, **580-583**, 1490-1493. https://doi.org/10.4028/www.scientific.net/AMM.580-583.1490.

Yegian, M. K. and Catan, M. (2004), "Soil isolation for seismic protection using a smooth synthetic liner", *J. Geotech. Geoenviron. Eng.*, **130**(11), 1131-1139. https://doi.org/10.1061/(ASCE)10900241(2004)130:11(1131).

Yegian, M.K. and Kadakal, U. (2004), "Foundation isolation for seismic protection using a smooth synthetic liner", *J. Geotech. Geoenviron. Eng*., **130**(11), 1121-1130. https://doi.org/10.1061/(ASCE)10900241(2004)130:11(1121).

Zhao, X., Zhang, Q., Zhang, Q. and He, J. (2016), "Numerical study on seismic isolation effect of gravel cushion", *The Proceedings of the 7th International Conference on Discrete Element Methods*, **188**, 1055-1063., Dalian, China.

# PAPER VI

# Effectiveness of several low-cost composite seismic base isolations: A shake table study

Ivan Banović[1*], Jure Radnić[1], Nikola Grgić[1]

[1]*University of Split, Faculty of Civil Engineering, Architecture and Geodesy, Matice hrvatske 15, 21000 Split, Republic of Croatia*

**Abstract.** This paper presents the findings of an experimental investigation of the efficiency of several low-cost frictional composite seismic base isolations on a rigid building model. A total of eleven different aseismic layers were considered. One layer was made of stone pebbles only, whereas the remaining ten layers were composites containing combinations of stone pebbles with different types and positions of "sliding" elements/materials (geogrid, geomembrane, and limestone sand layers). All the samples were exposed to four earthquake accelerograms of different durations and predominant periods, with three levels of peak ground acceleration (PGA): 0.2, 0.4, and 0.6 g. The test results confirm that the composite aseismic layers relative to the stone pebble layer could significantly reduce the inertial/earthquake forces of the building model, depending on the type of earthquake and PGA. The need for further research on this issue in various building models is highlighted.

**Keywords:** low-cost seismic base isolation; geogrid; geomembrane; pebble layer; shake table test

## 1. Introduction

The use of low-cost seismic base isolation has attracted much attention in the past few years. The need for this type of seismic base isolation arises from the fact that most earthquake victims live in impoverished parts of the world. It is not viable to use expensive forms of seismic isolation in such regions due to low economic power; therefore, it is essential to use low-cost alternatives. Low-cost seismic base isolation can be defined as a technological approach that involves the use of a continuous layer of low-modulus materials below the building foundation to mitigate the earthquake hazards on low-rise buildings constructed on rigid soil. In this seismic isolation approach, dissipation of earthquake energy is primarily achieved by reducing the friction under the foundation and its horizontal sliding on the substrate and sliding between the low-modulus material sub-layers (Banović *et al.* 2018a, Banović *et al*. 2019, Tsang and Pitilakis 2019). Earthquake energy can also be dissipated by reducing the rocking stiffness (Tsang and Pitilakis 2019), taking the advantages of rocking isolation, which is a well-known seismic isolation technique (Sorrentino *et al.* 2006, Sorrentino *et al.* 2008, Hung *et al.* 2014, Makris 2014, Tsatsis and Anastasopoulos 2015, Feng *et al.* 2018, Wang *et al.* 2018, Xu and Fatahi 2018, Chung *et al.* 2019, Chen *et al.* 2020, Deviprasad and Dodagoudar 2020, Sarand and Jalali 2020). Researchers have used various types of low-modulus material, such as sand (Tehrani and Hasani 1996, Anastasopoulos *et al.* 2012a, b, Radnić *et al.* 2015, Patil *et al.* 2016, Banović *et al.* 2018b), gravel (Pecker *et al.* 2001, Pecker 2003, Steengelt *et al.* 2015, Zhao *et al.* 2016), stone pebbles (Banović *et al.* 2018b, Banović *et al.* 2019), rubber-soil mixtures (Tsang 2008, Tsang 2009, Mavronicola *et al.* 2010, Tsang *et al.* 2012, Xiong and Li 2013, Bandyopadhyay *et al.* 2015, Panjamani *et al.* 2015, Xiong *et al.* 2015, Brunet *et al.* 2016, Forcellini 2017, Tsiavos *et al.* 2019a, b, Hernández *et al.* 2020), and geofoam (Murillo *et al.* 2009, Azinović *et al.* 2014, Azinović *et al.* 2016, Koren and Kilar 2016, Hadad *et al.* 2017, Karatzia *et al.* 2017, Azzam *et al.* 2018). The base isolation concept was categorized by Tsang (2008) as a "geotechnical seismic isolation (GSI) system" and also adopted by Brunet *et al.* (2016), Forcellini (2017), and Banović *et al.* (2019).

Geosynthetics have been commonly used in several civil engineering applications within the last few decades. Their standard applications include soil drainage, filtration, separation, waterproofing, and reinforcement. Owing to low friction, geosynthetic-soil and geosynthetic-geosynthetic dynamic-interface shear properties play significant roles. Several researchers have studied this issue under static, pull-out, and dynamic loading conditions (De and Zimmie 1998, Wasti and Özdüzgün 2001, Briançon *et al.* 2002, Briançon *et al.* 2011, Carbone *et al.* 2014, Cardile *et al.* 2014, Carbone *et al.* 2015, Cardile *et al.* 2015, Pavanello and Carrubba 2016, Pavanello *et al.* 2018a, b).

In addition to standard civil engineering applications, scholars have recognized the potential of geosynthetics as low-cost seismic isolation materials (Yegian and Lahlaf 1992, Yegian and Kadakal 1998, Yegian and Catan 2004, Yegian and Kadakal 2004, Arab and Kavazanjian 2010,

* Corresponding author, Ph.D. candidate
E-mail: ivan.banovic@gradst.hr

Nanda *et al.* 2012a, b, Kalpakci *et al.* 2018). These scholars performed experimental tests on various smooth synthetic liners, geomembranes, and geotextile layers, and they reported that the system effectively dissipates seismic energy through the sliding and reduction of forces transferred to the structure. Based on the results of these tests, the authors decided to apply geosynthetics in this study to enhance the efficiency of a seismic base isolation consisting of a stone pebble layer.

(Banović *et al.* 2018b, Banović *et al.* 2019, Banović *et al.* 2020a, Banović *et al.* 2020b) experimentally investigated the effectiveness of a low-cost seismic base isolation using a thin layer of natural stone pebbles (river gravel). The study results confirmed a significant decrease in the strains and stresses in the considered building models, as well as in the accelerations relative to the case with a rigid base foundation. Generally, such seismic isolations from cheap natural materials could reduce the strains and stresses in the considered building models by up to 50%, depending on the building stiffness and earthquake type. However, further rigorous investigations are required to apply this low-cost seismic base isolation generally in practice.

This paper presents the results of a shake table study on the effectiveness of several low-cost composite aseismic layers below the foundations of buildings. The aseismic layers were formed using natural stone pebbles, similar to (Banović *et al.* 2018b, Banović *et al.* 2019), with combinations of different elements/materials for additional reduction of layer shear stiffness. The isolations were made of a pebble layer with different geogrid combinations at the top and middle of the layer. In addition, a stone pebble layer with a high-density polyethylene (HDPE) geomembrane over a thin layer of limestone sand on the top of the pebble layer was tested. The initial assumption was that such a simple and low-cost composite seismic isolation could further reduce the earthquake/inertial forces relative to the seismic isolation from only the stone pebbles, with an acceptable increase in structural displacements. As already stated, the dissipation of earthquake energy and the reduction of earthquake forces on a building in the seismic base isolation approach using only a stone pebble layer is dominated by the sliding mechanism of the foundation on the seismic isolation and between the pebble sublayers (Banović *et al.* 2018b, Banović *et al.* 2019). The additional dissipation of seismic energy in a composite seismic isolation occurs through the additional sliding between the foundation, new elements/materials (geosynthetics), and pebble layer. It is expected that the efficiency of composite seismic isolation will increase in relation to the seismic isolation from stone pebbles only. The results of the shake table tests on a rigid building model confirmed the initial assumptions. The main conclusions of this study are presented in Section 7.

## 2. Composite seismic base isolation layers

The considered composite seismic isolations are shown in Fig. 1. A total of eleven different isolations were tested (B1 to B11), nine with a 0.3 m (P30) pebble layer thickness, and two with a 0.6 m (P60) pebble layer thickness. Isolation B1 was formed only from the pebble layer, as reported by (Banović *et al.* 2018b, Banović *et al.* 2019), whereas Isolations B2 and B3, including one geogrid with a higher tensile strength (GG1) and a lower tensile strength (GG2), were formed at the layer top. Isolations B4 and B5 were formed with the addition of two geogrids, GG1 and GG2, respectively, on the pebble layer top. The B6 and B7 isolations had GG1 and GG2 geogrids, respectively, at the top and middle of the pebble layer. The B8 isolation had a GG1 geogrid above a 3 cm thick limestone sand layer (S), and the B9 isolation had an HDPE geomembrane (GM) above the same sand layer. Isolation B10 with $h_p$ = 0.6 m (P60) had a GG1 geogrid at the top, and isolation B11 with $h_p$ = 0.6 m had an GM above the limestone sand layer (S). All the seismic isolations were formed within a rigid frame with a plan size of 2.5 m × 2.5 m, and the isolations were fixed to the shake table (Banović *et al.* 2018b, Banović *et al.* 2019).

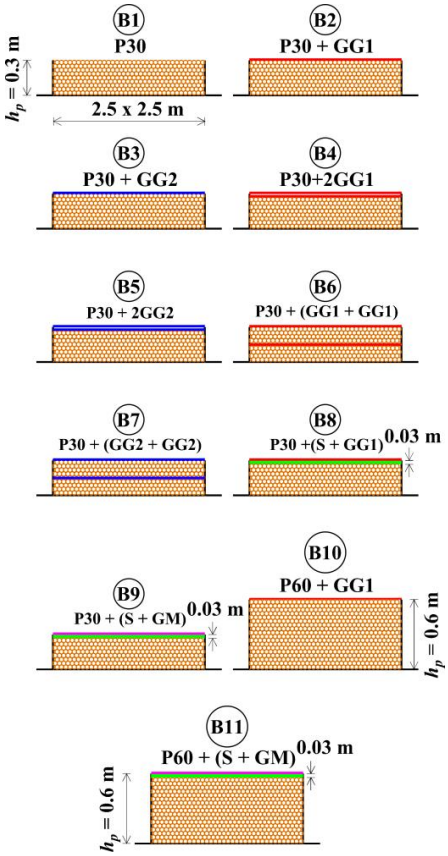


Fig. 1 Composite seismic base isolations considered in this study

The adopted materials/elements for the construction of the considered seismic base isolations are displayed in Fig. 2. The following characteristics of the pebble layer were adopted for all the tested samples, as optimal for practical applications (Banović *et al.* 2019): pebble fraction $\Phi_b$ = 16-32 mm, pebble layer compaction *MS* = 30 MPa, and pebble moisture *h* = 10%.

The adopted geogrids were made of stretched, monolithic polyester flat bars with welded junctions. Geogrid GG1 was type Secugrid 120/40 R6, and geogrid

GG2 was type Secugrid 40/20 R6; both were produced by Naue, Germany. Basic data for the adopted geogrids are presented in Table 1. The adopted geomembrane was a 2 mm thick CARBOFOL HDPE 406 with smooth surfaces produced by Naue, Germany. Basic data for the adopted geomembrane are presented in Table 2. The limestone sand layer (S) was 3 cm thick and compacted at MS = 30 MPa.

(a) Stone pebbles

(b) Limestone sand

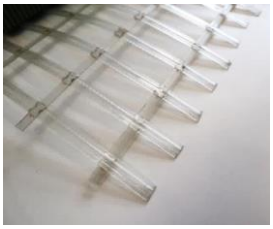

(c) Geogrid GG1 (120/40 R6)

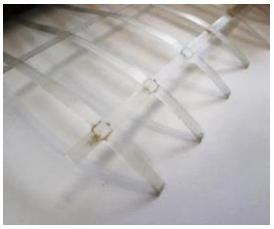

(d) Geogrid GG2 (40/20 R6)

(e) Geomembrane HDPE 406

Fig. 2 Adopted materials/elements for the aseismic layer

Table 1 Basic data for the adopted geogrids

| Property | Test method | Unit | 40/20 R6 | 120/40 R6 |
|---|---|---|---|---|
| Raw material | - | - | Polyester, transparent | |
| Mass per unit area | EN ISO 9864 | g/m$^2$ | 285 | 580 |
| Max. tensile strength, md/cmd* | EN ISO 10319 | kN/m | ≥ 40 / ≥ 20 | ≥ 120 / ≥ 40 |
| Elongation at nominal strength, md/cmd* | EN ISO 10319 | % | ≤ 7 / ≤ 7 | |
| Aperture size, md/cmd* | - | mm × mm | 73 × 31 | 71 × 28 |

*md = machine direction, cmd = cross machine direction

Table 2 Basic data for the adopted geomembrane

| Property | Test method | Unit | Value |
|---|---|---|---|
| Thickness | ASTM D5199 | mm | 2 |
| Density | ASTM D1505/ ASTM D792 | g/cm$^3$ | 0.942 |
| Tensile strength at break | ASTM D6693 | kN/m | 56 |
| Elongation at break | ASTM D6693 | % | 700 |
| Tear resistance | ASTM D1004 | N | 260 |
| Puncture resistance | ASTM D4833 | N | 640 |

## 3. Tested building model

A model of a rigid building with mass m = 2000 kg (Fig. 3a) was used, as in a previous study (Banović *et al.* 2019). This model was adopted to compare the performance of a previously tested seismic base isolation formed only of a stone pebble layer (B1) and composite seismic base isolation layers comprising stone pebbles, geogrids, GM, and limestone sand layer (B2 to B11). The aim was to experimentally determine whether the addition of such typical elements and materials to the underlying aseismic layer consisting of only stone pebbles would further increase its aseismic efficiency. The selected rigid building model should not influence the conclusions because previous research has been conducted to determine the relative influence of several parameters on the layer aseismic efficiency. Additionally, seismic isolation is primarily intended and potentially useful for only lower (rigid) buildings resting on solid ground. The model had a reduced area in contact with the aseismic layer to achieve the expected contact stress below the foundations of the lower building. The shake table setup of the model on Layer B11 ready for testing is depicted in Fig. 3b.

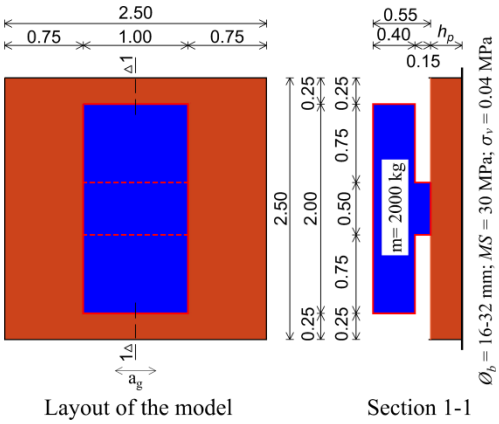


(a) Basic model data

(b) Shake table setup on isolation layer B11

Fig. 3 Adopted model of the rigid building (Banović *et al.* 2019)

## 4. Applied base accelerations

The adopted earthquake accelerograms (Ambraseys *et al.* 2001) and their spectral values are presented in Fig. 4.

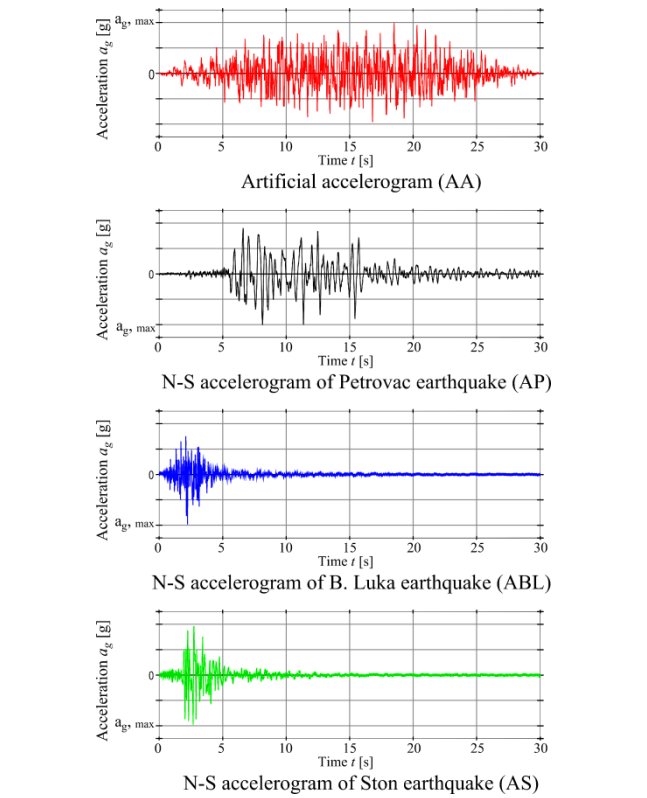


(a) Adopted horizontal accelerograms

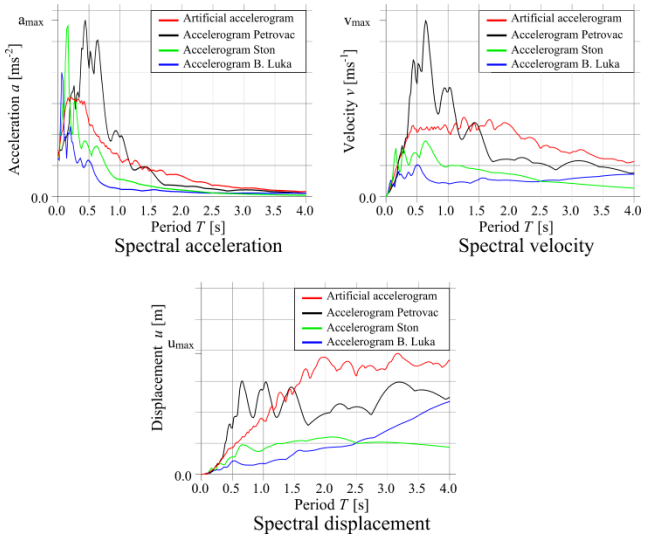


(b) Elastic response spectra of the adopted accelerograms

Fig. 4 Adopted earthquake accelerograms and their spectral values (Banović *et al.* 2018b, Banović *et al.*2019)

The accelerograms simulated quite a wide range of different earthquake types in practice. The artificial accelerogram (AA) and accelerogram Petrovac (AP, Montenegro 1979, orientation N-S) represented earthquakes of longer duration and with relatively longer predominant periods, which generated more seismic energy in the structure. In contrast, accelerogram Ston (AS, Croatia 1996, orientation N-S) and accelerogram Banja Luka (ABL, BiH 1982, orientation N-S) characterized the so-called impact earthquakes of short duration and short predominant period, with a significant effect of shear force. An artificial accelerogram was generated using the software, SIMQKE (1976), as a superposition of sine functions. This was created to match the elastic response spectra according to EC8 (2004) for Type 1 and Soil Type A. The test samples were exposed to sets of three successive base excitations with PGA = 0.2, 0.4, and 0.6 g. After being subjected to each set of the three successive base excitations, the pebble layer and the model were updated for the next set of excitations. This approach, similar to that of a previous study (Banović *et al.* 2019) in which displacements accumulated from previous excitations and the pebble layer eventually degraded, can be applied in practice and is interesting in terms of monitoring the probable foundation eccentricity with the aseismic layer.

## 5. Instrumentation and measured quantities

All the considered models were tested on a shake table located at the Seismic Testing Centre at the Faculty of Civil Engineering, Architecture and Geodesy, University of Split, Croatia. The shake table (Fig. 3b) was uniaxial with a layout size of 4 m × 4 m, and its maximum capacity was 20 000 kg. The shake table had a maximum displacement of ±150 mm, a maximum acceleration of up to 5 g, and frequencies ranging from 0-20 Hz. The characteristic accelerations $a$, horizontal displacements $u_1$ and $u_2$, and vertical displacements, $v_1$ and $v_2$, were measured (Fig. 5). Data acquisition was achieved using an (Hottinger Baldwin Messtechnik-HBM) Quantum-X mx 840A high-speed data acquisition system with 16 channels. The displacements were measured using analog displacement sensors of type PB-25-S10-N0S-10C (Uni Measure), whereas piezo-electric low-frequency accelerometer of type 4610 (Measurement Specialties) were used to measure the accelerations. The sampling rate during the shake table tests was 200 Hz. For the test recording, a video camera (Canon EOS M5) was used.

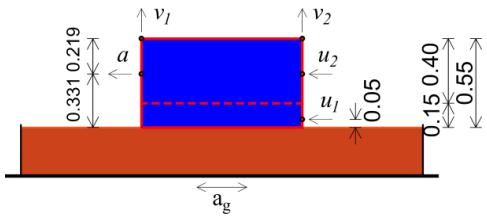


Fig. 5 Measured acceleration $a$ and displacements $u$ and $v$

The horizontal acceleration of mass center $a$ is an essential indicator of model behavior because higher accelerations of the rigid model indicate higher inertial (earthquake) forces. If the acceleration of the model based on composite seismic isolations B2 to B11 is smaller than that of the pebble layer B1, then the composite seismic isolation will be considered more efficient. However, in actual buildings, higher acceleration may not always result in higher strains and stresses in the structure.

## 6. Experimental test results and discussion

The peak values of the measured quantities $a_{max}$, $u_{1max}$,

$u_{2max}$, and $v_{1max}$ are shown in Figs. 6-9, separately for all the applied excitations (AA, AP, ABL, and AS) and all the successive base excitations (PGA = 0.2, 0.4, and 0.6 g). Only some of the obtained results are presented subsequently. The measured quantities for the considered seismic isolations significantly depend on the type of applied earthquake and the PGA level. In all the graphs, the featured curve for Isolation B1 is highlighted to provide a clear insight into the relationship of the measured values for this seismic isolation with the composite seismic isolations considered in this study (B2 to B11). It is noticeable that with the increase in PGA, the measured size generally increases, but not proportionally. However, in a few cases, the measured values for PGA = 0.6 g were lower than those for PGA = 0.4 g.

The peak acceleration values $a_{max}$ (Fig. 6) for the AA and ABL excitations were measured for Isolation B1 (except for the ABL excitation and B5 isolation at PGA = 0.2 g). Seismic Isolations B2 and B10 at PGA = 0.2 g, B4 and B2 at PGA = 0.4 g, and B10 and B11 at PGA = 0.6 g, were most effective for the AA excitation. For the ABL excitation, the most effective isolations were B3, B6, and B11 at PGA = 0.2 g, B3 and B8 at PGA = 0.4 g, and B2 and B10 at PGA = 0.6 g.

For the AP and AS excitations, the composite seismic isolations generally had a lower $a_{max}$ than the B1 isolation (Fig. 6). The exceptions were B8 and B9 for the AP excitation at PGA = 0.4 g, B5 and B8 for the AP excitation at PGA = 0.6 g, B8, B9, and B11 for the AS excitation at PGA = 0.2 g, and B7, B8, and B11 for the AS excitation at PGA = 0.6 g. Seismic isolations B8, B9, and B11 had a layer of limestone sand above the pebbles, which did not perform satisfactorily. B5 and B9 at PGA = 0.2 g, B4 and B10 at PGA = 0.4 g, and B10 and B11 at PGA = 0.6 g were most effective for the AP excitation. B10 and B5 at PGA = 0.2 g, B6 and B10 at PGA = 0.4 g, and B4 and B10 at PGA = 0.6 g were most efficient for the AS excitation.

Based on the analysis of Fig. 6 and the above statements, it is difficult to precisely determine which of the considered composite seismic isolations are generally the most favorable, that is, which leads to the lowest acceleration of the model. In general, the following can be concluded:

- The limestone sand layer (S) at the pebble layer top did not have a positive effect on decreasing the inertial forces of the model.
- The impact of the geogrid strength (GG1 or GG2) was insignificant. On the average, geogrid GG1 was more favorable.
- The influence of the geogrid number (1 or 2) at the top of the pebble layer was also insignificant. On the average, two geogrids were more favorable than one geogrid.
- The use of combined geogrids in the middle and at the top of the pebble layer (B6 and B7) did not prove to be more favorable than the use of both grids at the top of the pebble layer (B4 and B5).
- Isolations B2 and B10 showed similar efficiency, with a slightly higher efficiency by B10. Thus, the 0.6 m thick layer of pebbles was slightly more effective than that of the 0.3 m thickness.
- The use of GM on Isolations B9 and B11 did not result in a higher reduction in acceleration compared with Isolation B1. In some cases, these isolations were less efficient than B1.

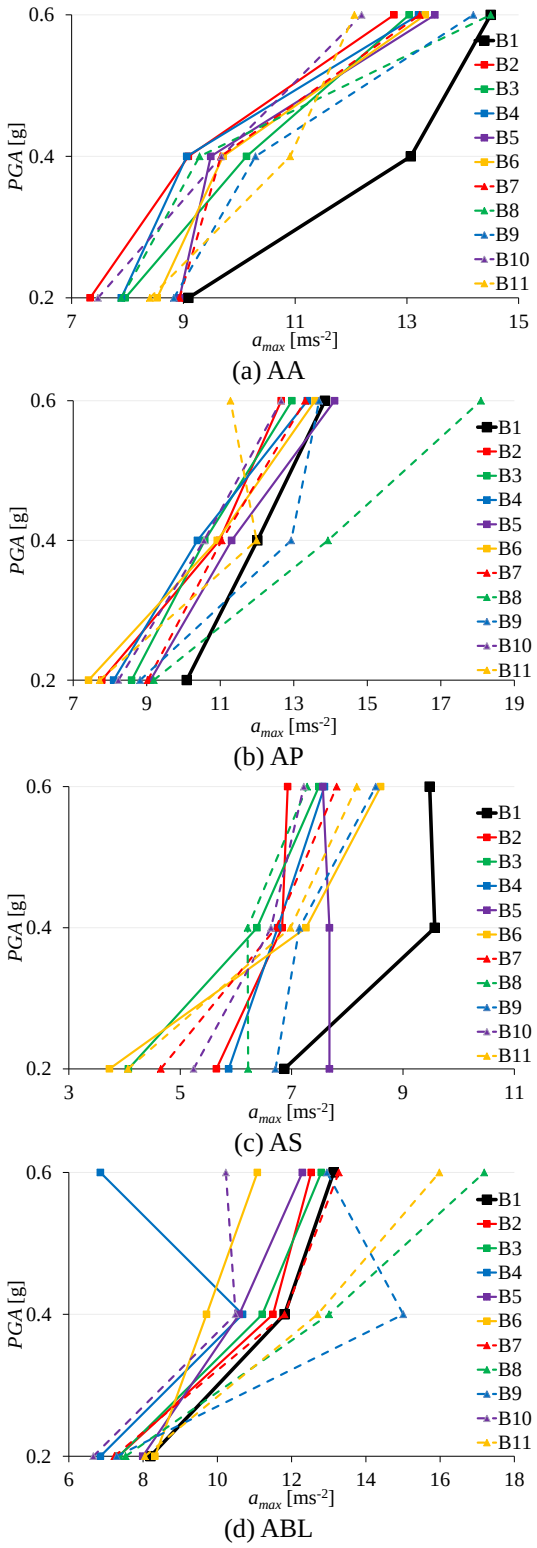


Fig. 6 Peak horizontal acceleration of the mass center $a_{max}$

The horizontal displacement of the model foundation $u_1$ (Fig. 7) was due to model sliding along the seismic isolation

top, the horizontal displacement of the seismic isolation top relative to the shake table top, and probably a smaller part of the rotation of the model relative to the shake table. For the AA and ABL excitations, the displacement $u_1$ of Isolation B1 was higher than that of composite seismic isolations (except for B11 at PGA = 0.6 g). For these excitations, the inertial (earthquake) forces were lower for the B1 isolation than for the composite isolations. In this case, Isolations B5 and B8 for the ABL excitation, and Isolation B2 for the AA excitation, had the smallest displacements. The displacements $u_1$ for the AA and ABL excitations were relatively small and ranged up to approximately 7 mm.

For the AP and AS excitations, the displacement $u_1$ for B1 was significantly smaller than that for the horizontally softer composite seismic isolation (B2 to B11). For the composite layers, the displacement $u_1$ significantly increased at PGA = 0.6 g, where the rigid model slipped along the isolation layer top. The largest displacements $u_1$ occurred for Isolations B4, B11, and particularly B9 for AP excitation, whereas for excitation AS, the largest displacements $u_1$ occurred for Isolations B10, B11, and particularly B4, respectively. The slip in the model was significantly contributed by the limestone sand layer at Isolations B9 and B11, two geogrids at the layer top of Isolation B4, and the increased depth of the pebbles for Isolations B10 and B11. The largest displacements $u_1$ occurred for the AS excitation.

The horizontal displacements of the model mass center $u_2$ (Fig. 8) were significantly affected by the horizontal displacement of the model foundation $u_1$ (Fig. 7). The effect of the foundation rotation was greater for $u_2$ than for $u_1$. The $u_2$ displacements for the AP and AS excitations were significantly higher than those for the AA and ABL excitations. For the composite base isolations (some isolations of the AA and ABL excitations were exceptions), the displacements $u_2$ were larger than those for Isolation B1, especially for the AP and AS excitations. For the AS excitation, the $u_2$ displacements were largest (up to approximately 43 mm for B4) and slightly smaller for the AP excitation (up to approximately 24 mm for B9). The larger $u_2$ displacements for almost all the composite seismic isolations relative to B1 occurred due to their lower horizontal stiffnesses.

The vertical displacement of the rigid model $v_1$ (Fig. 9) occurred as a result of the vertical deformation of the stone pebble layer and the rotation of the model. For almost all the excitations, the displacement $v_1$ for Isolation B1 was smaller than that for the composite seismic isolations. The probable cause was the slightly higher vertical stiffness of B1. The increased vertical displacements for B10 at AP and AS excitations, and B11 isolation at the AP excitation, were likely due to the greater depth of the pebble layer in these isolations.

The displacements $v_2$, which were not shown here, were almost compatible with $v_1$. It is difficult to evaluate the displacement magnitudes $u_1$, $u_2$, $v_1$, and $v_2$ in the context of actual buildings because a simple reduced model of a rigid building was used in this study.

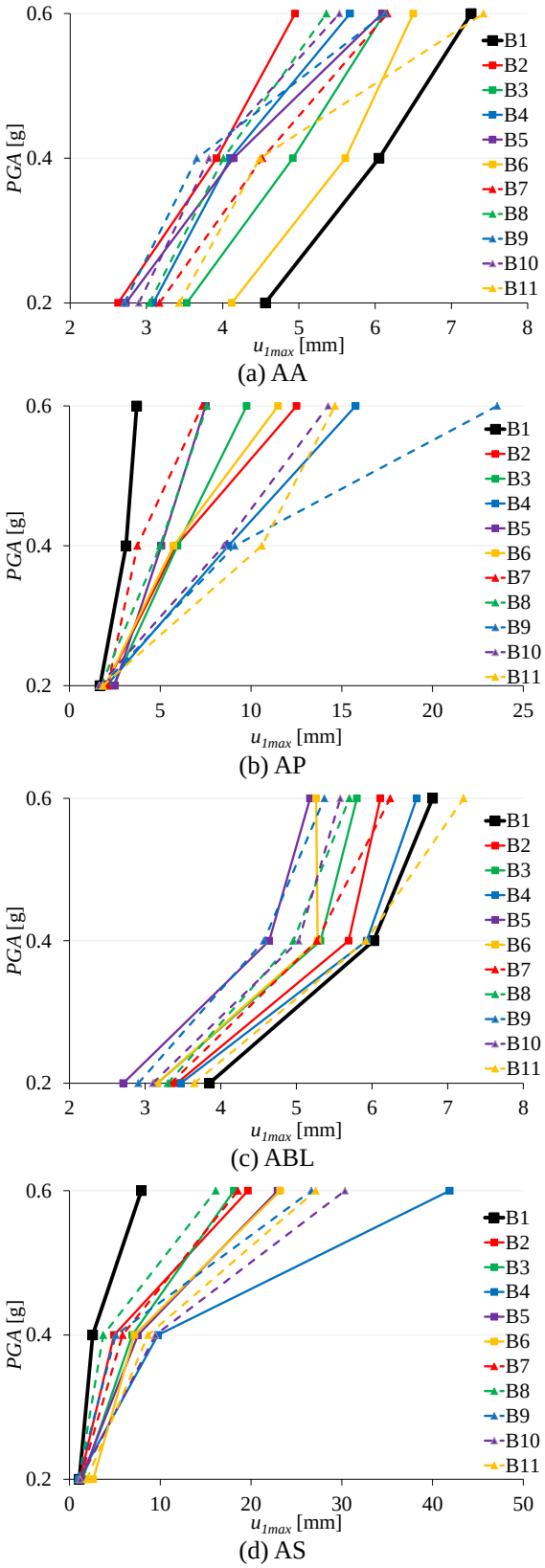


Fig. 7 Peak horizontal displacement of the model foundation $u_{1max}$

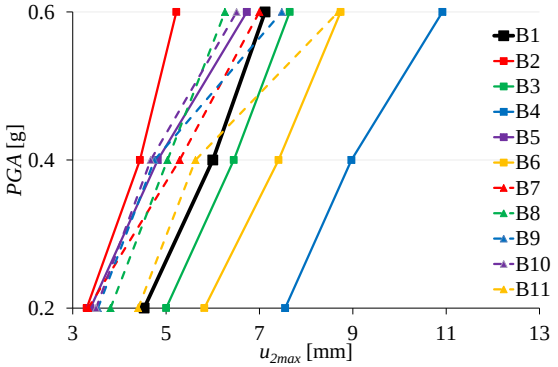


(a) AA

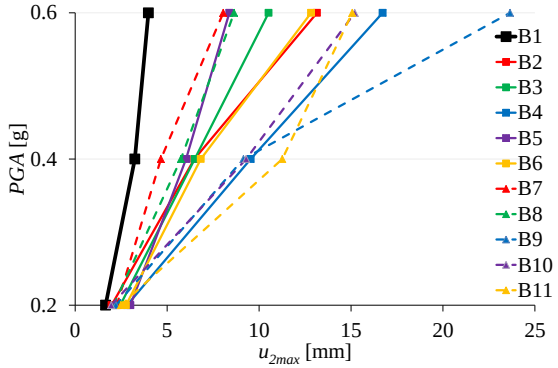


(b) AP

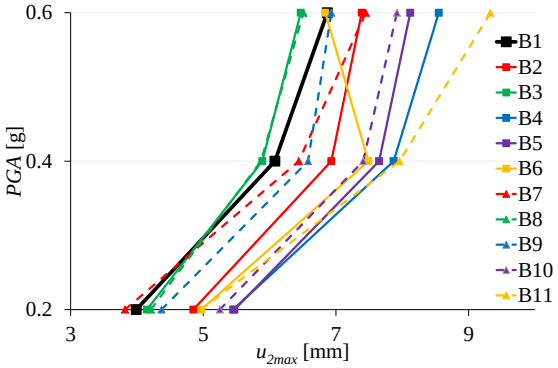


(c) ABL

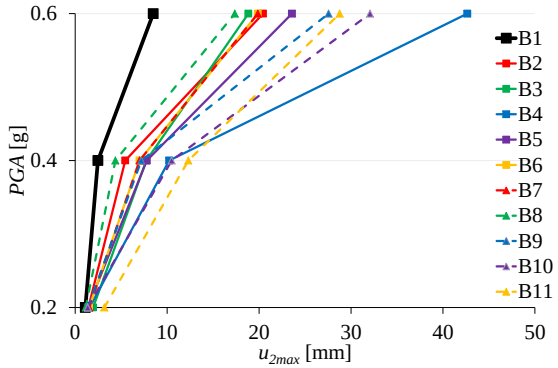


(d) AS

Fig. 8 Peak horizontal displacements of the model mass center $u_{2max}$

Figs. 6-9. show the measured peak values of $a$, $u_1$, $u_2$, and $v_1$ for all the considered isolations. Let us label with BC = B2 to B11 for the average composite seismic isolation, as the mean value of all the considered composite isolations. The ratios mentioned above represent the seismic isolation efficiency coefficients of the BC isolations in relation to the B1 isolation. The efficiency coefficients are shown separately for each excitation and averaged for all the applied excitations (Figs. 10-13).

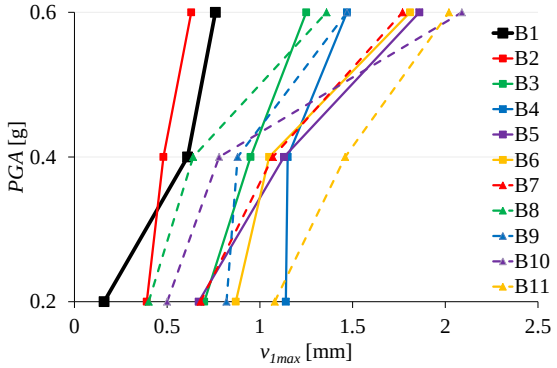


(a) AA

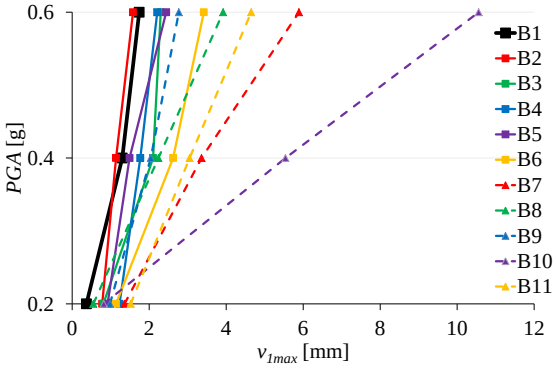


(b) AP

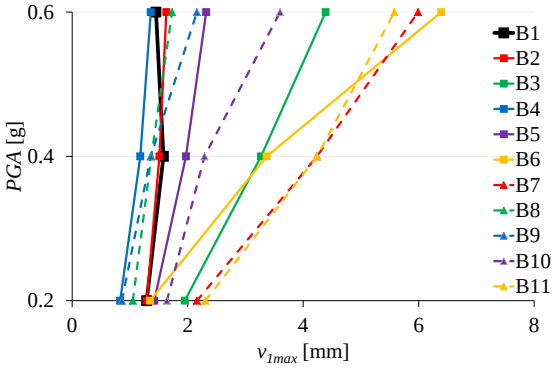


(c) ABL

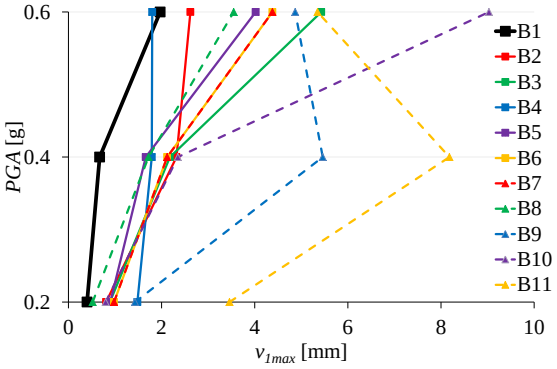


(d) AS

Fig. 9 Peak vertical displacement of the rigid model $v_{1max}$

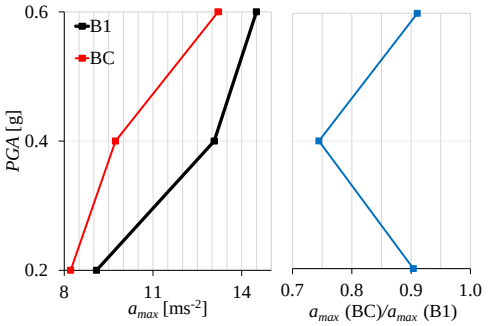


• AA

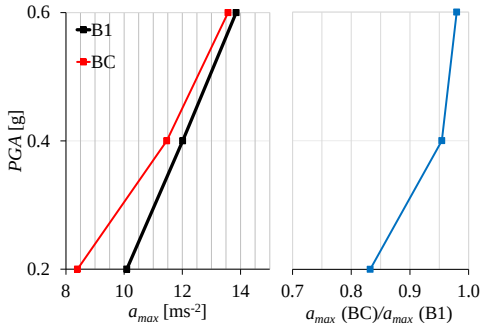


• AP

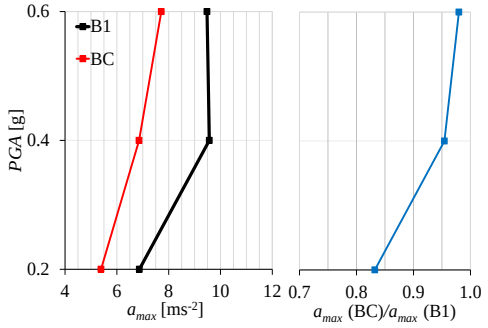


• ABL

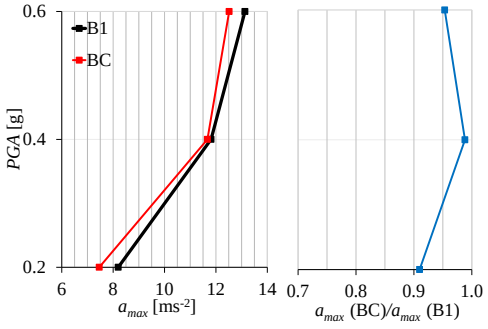


• AS

(a) Ratios for the individual accelerograms

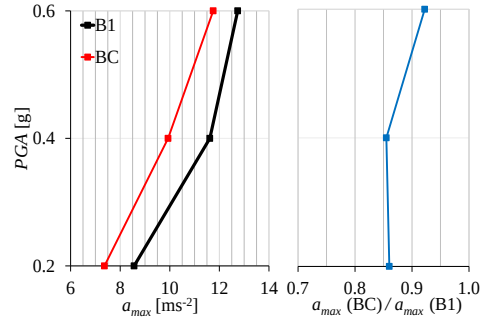


(b) Ratios for the average accelerogram

Fig. 10 Relationship between the peak accelerations $a_{max}$ (BC) and $a_{max}$ (B1)

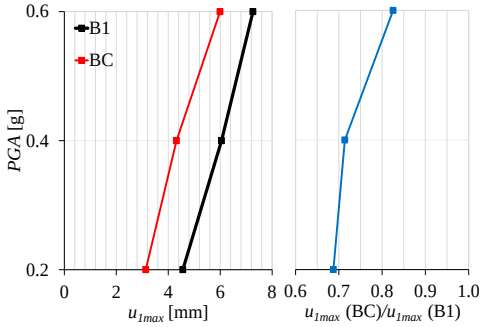


• AA

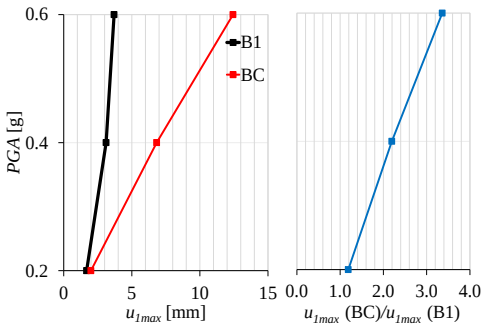


• AP

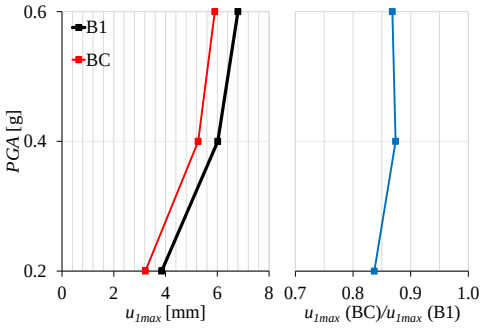


• ABL

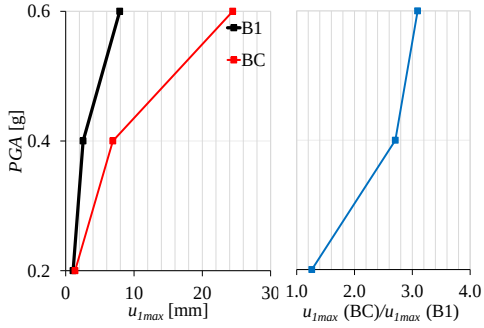


• AS

(a) Ratios for the individual accelerograms

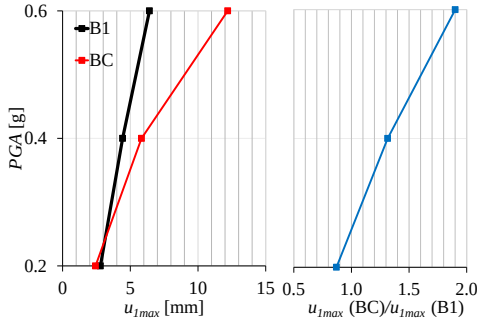


(b) Ratios for the average accelerogram

Fig. 11 Relationship between the peak displacements $u_{1max}$ (BC) and $u_{1max}$ (B1)

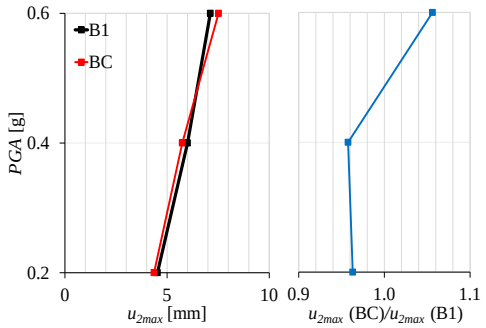


• AA

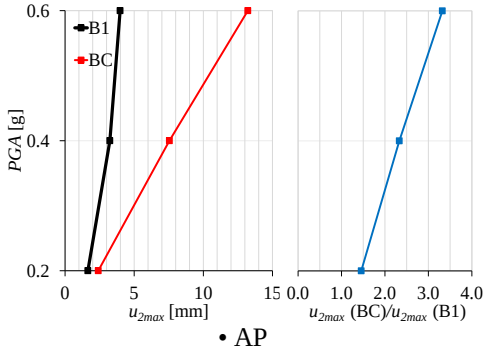


• AP

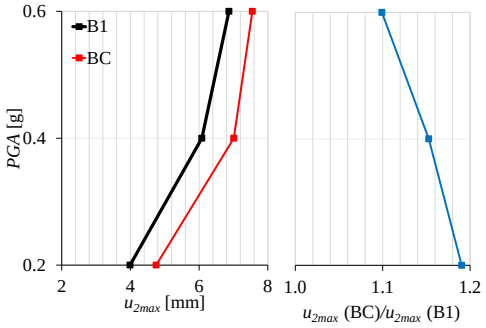


• ABL

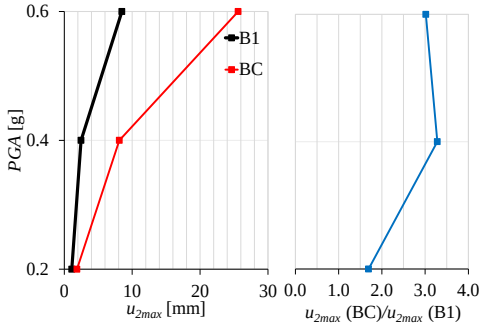


• AS

(a) Ratios for the individual accelerograms

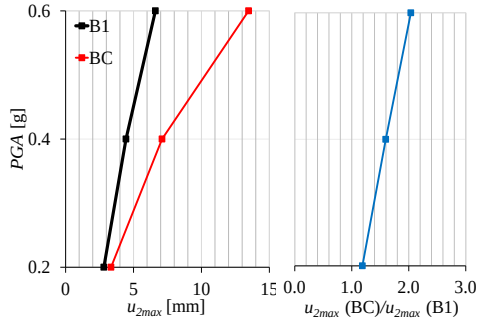


(b) Ratios for the average accelerogram

Fig. 12 Relationship between the peak displacements $u_{2max}$ (BC) and $u_{2max}$ (B1)

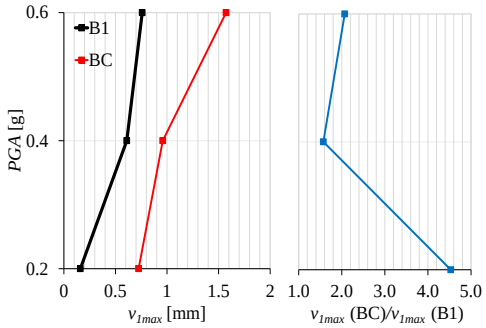


• AA

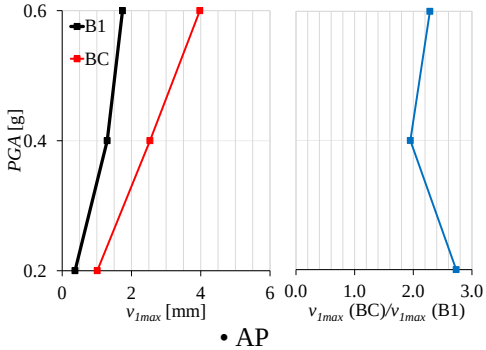


• AP

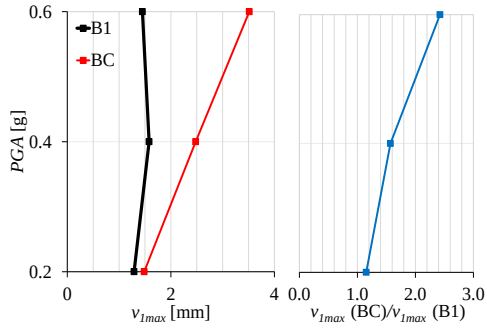


• ABL

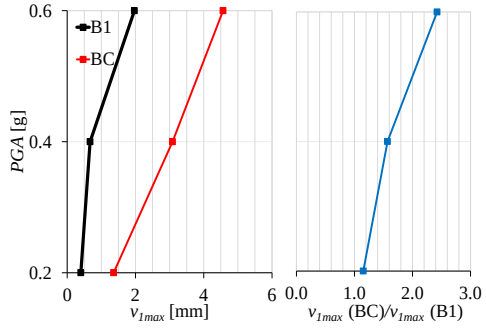


• AS

(a) Ratios for the individual accelerograms

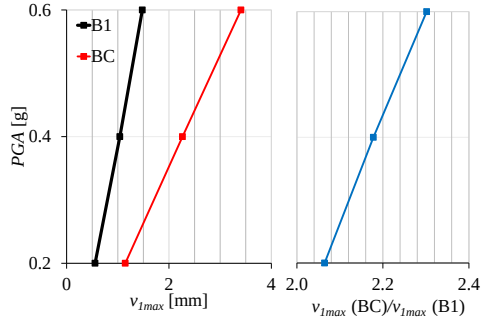


(b) Ratios for the average accelerogram

Fig. 13 Relationship between the peak displacements $v_{1max}$ (BC) and $v_{1max}$ (B1)

The $a_{max}$ values of the average isolation BC denoted as $a_{max}$ (BC), and the $a_{max}$ values for the isolation B1 denoted as $a_{max}$ (B1), are shown in Fig. 10. The relationships for the individual accelerograms and average accelerogram are shown in Figs. 10a and 10b, respectively.

It can be noticed that the efficiency coefficient of the acceleration $c_a$ = $a_{max}$ (BC)/$a_{max}$ (B1) for the individual accelerograms (Fig. 10a) ranges from 0.72-0.99, depending on the accelerogram type and PGA level. Additionally, the BC isolation efficiency was the lowest for the AS excitation. Fig. 10b shows that the $c_a$ coefficient for the average accelerogram values range from 0.85-0.92, and the BC isolation efficiency decreases with increasing PGA.

Similarly, for the coefficient $c_a$ (Fig. 10), the coefficients $c_{u1}$ = $u_{1max}$ (BC)/$u_{1max}$ (B1), $c_{u2}$ = $u_{2max}$ (BC)/$u_{2max}$ (B1), and $c_{v1}$ = $v_{1max}$ (BC)/$v_{1max}$ (B1) were considered, as shown in Figs. 11-13. The analysis of Figs. 11-13. suggests that generally, the displacements of the model on the average composite BC isolation are significantly larger (less favorable) than those on B1. These results are logical and expected because the BC isolations had lower horizontal stiffnesses than B1.

Similar to Figs. 10-13., Figs. 14-17. are presented as the ratio of the peak measured quantities of the average composite isolations B2 and B10 in relation to B1. In other words, the seismic isolation efficiency coefficients $c_a$ = $a_{max}$ (B2, B10)/$a_{max}$ (B1), $c_{u1}$ = $u_{1max}$ (B2, B10)/$u_{1max}$ (B1), $c_{u2}$ = $u_{2max}$ (B2, B10)/$u_{2max}$ (B1), and $c_{v1}$ = $v_{1max}$ (B2, B10)/$v_{1max}$ (B1), are determined.

Comparing the values in Figs. 14-17. with the corresponding values in Figs. 10-13., the peak accelerations for the average isolation B2 and B10 were significantly lower (had significantly higher efficiency) than those for the average composite isolation BC. It can also be concluded that the measured peak displacements of the rigid building model for average composite isolation B2 and B10 were smaller than those for the average composite isolation BC.

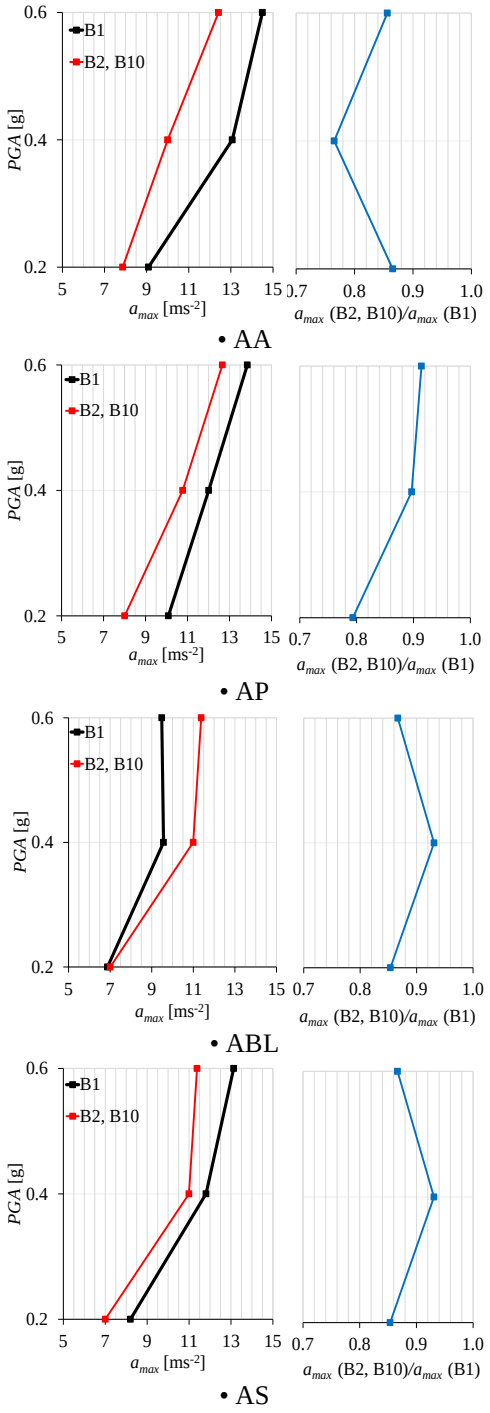


(a) Ratios for the individual accelerograms

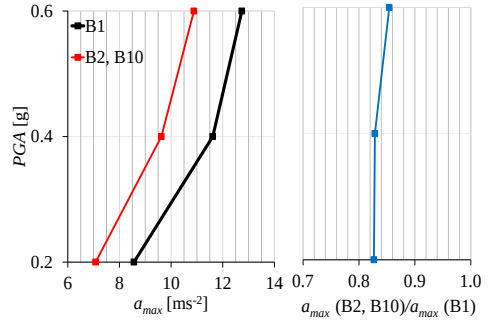


(b) Ratios for the average accelerogram

Fig. 14 Relationship of the peak accelerations $a_{max}$ (B2, B10) and $a_{max}$ (B1)

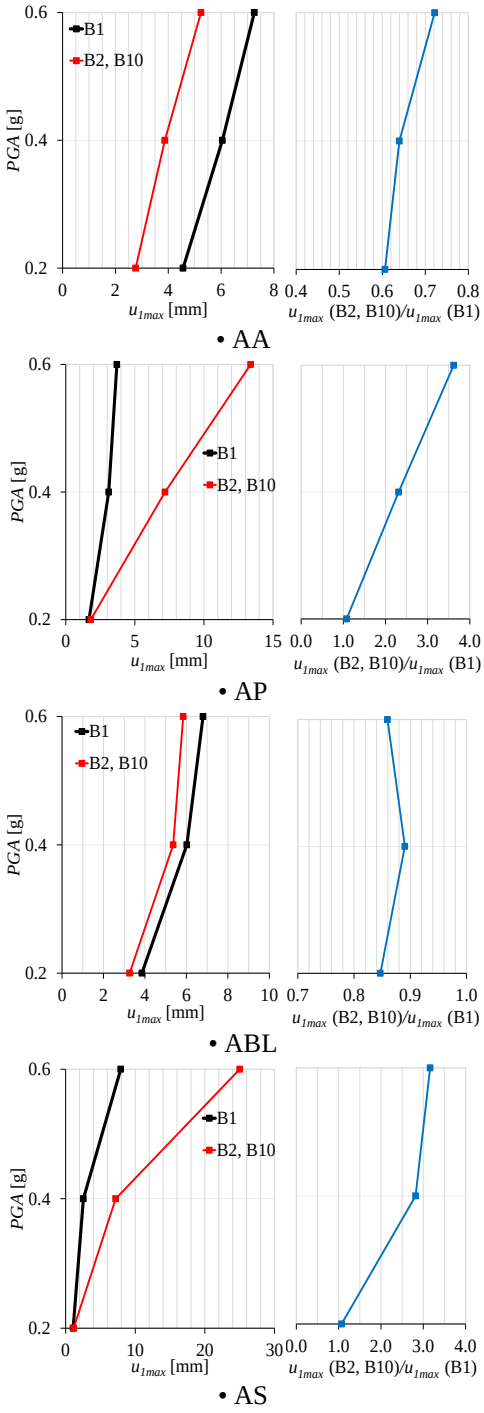


(a) Ratios for the individual accelerograms

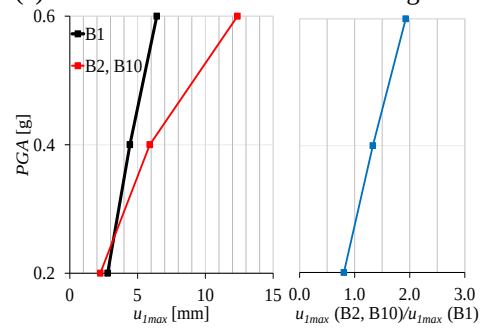


(b) Ratios for the average accelerogram

Fig. 15 Relationship between the peak displacements $u_{1max}$ (B2, B10) and $u_{1max}$ (B1)

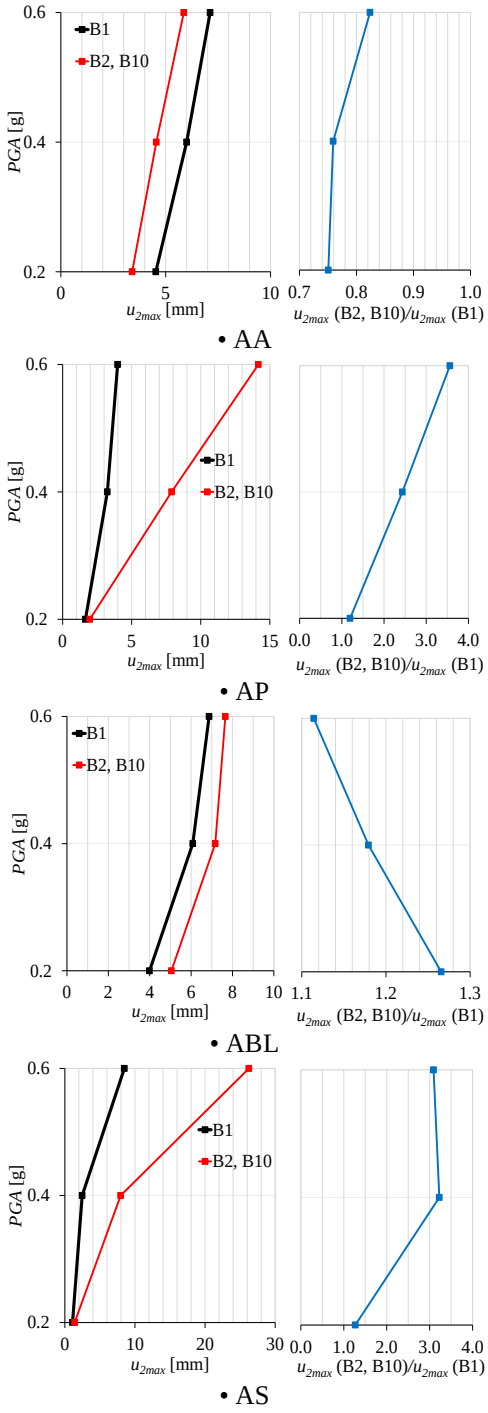


(a) Ratios for the individual accelerograms

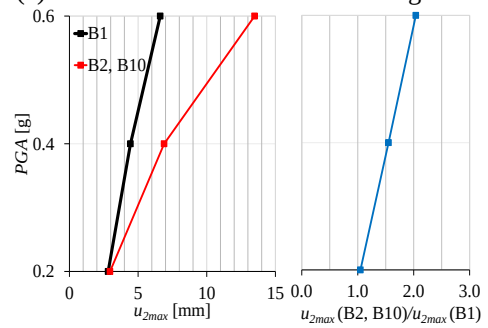


(b) Ratios for the average accelerogram

Fig. 16 Relationship between the peak displacements $u_{2max}$ (B2, B10) and $u_{2max}$ (B1)

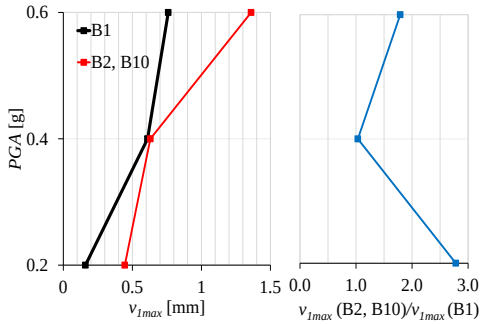


• AA

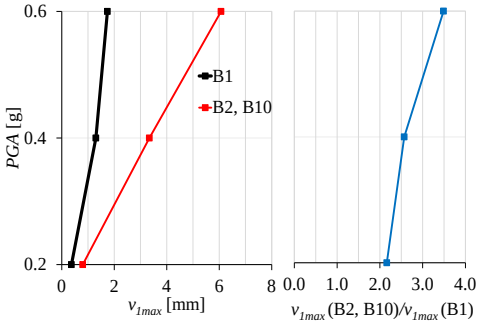


• AP

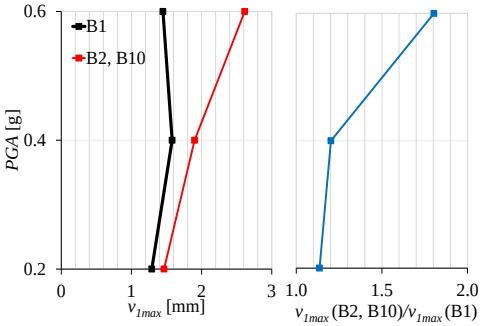


• ABL

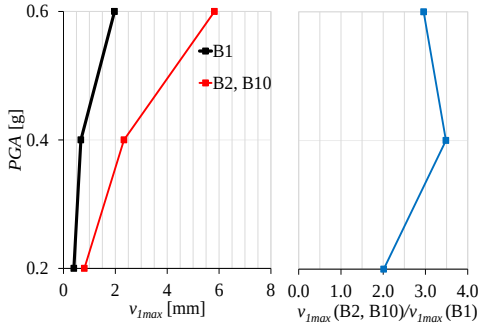


• AS

(a) Ratios for the individual accelerograms

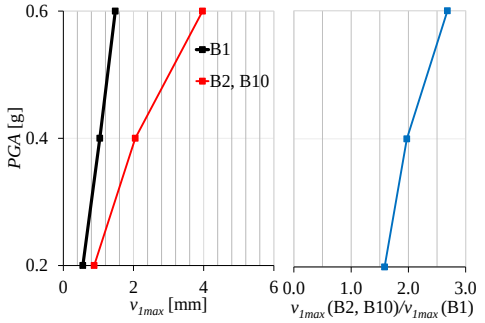


(b) Ratios for the average accelerogram

Fig. 17 Relationship between the peak displacements $v_{1max}$ (B2, B10) and $v_{1max}$ (B1)

Because of the possible calibration of the numerical model for the dynamic analysis of buildings with the considered seismic isolation, several time histories of the experimental tests with Isolations B1, B2, and B10 at the AA excitation with PGA = 0.4 g are presented (Figs. 18 to 21).

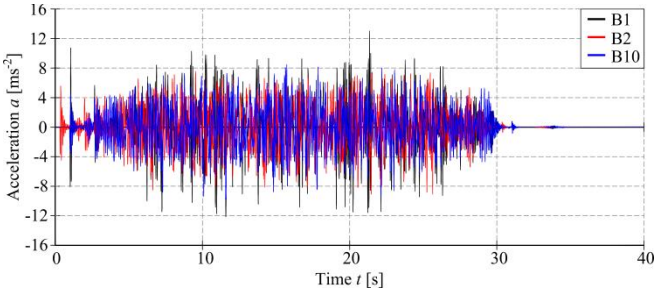


Fig. 18 Horizontal acceleration of the model mass center $a$ for the AA excitation with PGA = 0.4 g

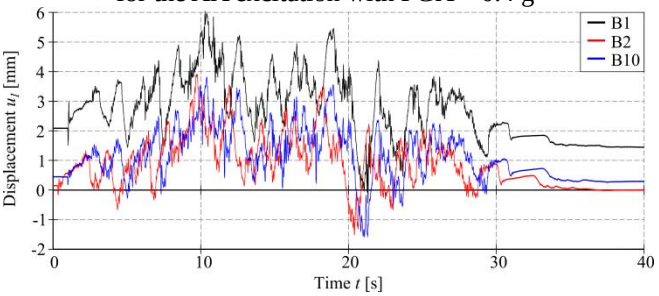


Fig. 19 Horizontal displacement of the model foundation $u_1$ for the AA excitation with PGA = 0.4 g

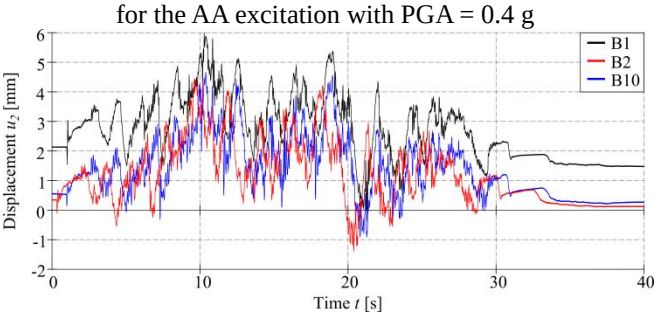


Fig. 20 Horizontal displacement of the model mass center $u_1$ for the AA excitation with PGA = 0.4 g

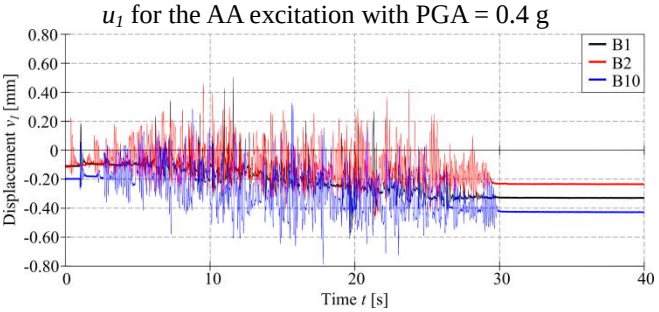


Fig. 21 Vertical displacement of the model $v_1$ for the AA excitation with PGA = 0.4 g

## 7. Conclusions

Based on the results of this experimental study in which the effectiveness (reduction of the inertial forces acting on a building model) of 10 composite seismic isolations (BC = B2 to B11) formed from different combinations of stone pebbles with geogrid, geomembrane, and limestone sand

layers were investigated in relation to the efficiency of the seismic isolation from only the pebble layer (B1), the following conclusions can be drawn:

• All the considered seismic isolations are logical and easy to use, but composite isolations are, on the average, slightly more expensive and time-consuming to construct.

• The efficiency of the considered seismic isolations was significantly dependent on the type of applied earthquake and PGA level.

• The ratio of the peak model acceleration $a_{max}$ (inertial forces) for the average composite isolation BC and the peak model acceleration $a_{max}$ for B1, $a_{max}$ (BC)/$a_{max}$ (B1), was as follows:

-For the AA excitation, 0.90 at PGA = 0.2 g, 0.74 at PGA = 0.4 g, and 0.91 at PGA = 0.6 g.
-For the AP excitation, 0.83 at PGA = 0.2 g, 0.95 at PGA = 0.4 g, and 0.98 at PGA = 0.6 g.
-For the ABL excitation, 0.78 at PGA = 0.2 g, 0.72 at PGA = 0.4 g, and 0.81 at PGA = 0.6 g.
-For the AS excitation, 0.91 at PGA = 0.2 g, 0.99 at PGA = 0.4 g, and 0.95 at PGA = 0.6 g.
-Averaged values for all the excitations: 0.86 at PGA = 0.2 g, 0.85 at PGA = 0.4 g, and 0.92 at PGA = 0.6 g.
-Averaged values over all the excitations and PGA levels was 0.88.

• Previous results indicated that the average composite isolation BC had a significantly higher efficiency than the B1 isolation. The efficiency deviations for the composite seismic isolations were very significant, that is, the B1 isolation was more effective than several composite isolations for specific excitations and PGA levels.

• It is difficult to determine which of the considered composite seismic isolations were generally the most favorable exactly. The limestone sand layer (S) at the top of the pebble layer did not perform favorably, and the strength of the geogrids (GG1 and GG2) and their respective numbers (1 and 2) in the pebble layer were insignificant. In addition, two geogrids at the pebble layer top proved to be more efficient than a combination of geogrids in the middle and at the top of the pebble layer. The thin and thick pebble layers showed similar efficiency, but the thicker geogrid layer (B10) was more efficient than the thin pebble layer. The use of GM was ineffective and acted unfavorably in some cases.

• Model displacements were significantly higher for the composite isolations than for B1 pebble isolation, which was unfavorable. Because the reduced rigid building model was used in this study, it was not possible to determine whether these displacements were excessive in practice.

• If the rationality, simplicity, and construction time of the considered composite isolations are taken into account in addition to their theoretical efficiency, the most straightforward and most practical applications are those with one geogrid at the pebble layer top (B2 and B10 isolations).

• The ratio of the peak model acceleration $a_{max}$ for these seismic isolations and $a_{max}$ for B1, $a_{max}$ (B2, B10)/$a_{\max}$ (B1), was as follows:

-For the AA excitation, 0.87 at PGA = 0.2 g, 0.77 at PGA = 0.4 g, and 0.86 at PGA = 0.6 g.
-For the AP excitation, 0.79 at PGA = 0.2 g, 0.90 at PGA = 0.4 g, and 0.91 at PGA = 0.6 g.
-For the ABL excitation, 0.79 at PGA = 0.2 g, 0.70 at PGA = 0.4 g, and 0.75 at PGA = 0.6 g.
-For the AS excitation, 0.85 at PGA = 0.2 g, 0.93 at PGA = 0.4 g, and 0.87 at PGA = 0.6 g.
-Averaged values over all the excitations, 0.83 at PGA = 0.2 g, 0.83 at PGA = 0.4 g, and 0.85 at PGA = 0.6 g.
-Averaged value over all excitations and PGA levels was 0.84.

• Thus, the maximum acceleration of the rigid building model based on B2 and B10 isolation averaged over all the excitations, and PGA levels were 16% lower than that based solely on the B1 isolation from stone pebbles.

• Higher acceleration (inertial force) in an actual structure may not always lead to higher strains and stresses. Therefore, further related research is required on more realistic models of buildings with several different stiffnesses, only with the most optimal composite seismic base isolations B2 and B10.

## Acknowledgments

This work has been fully supported by the Croatian Science Foundation under the project *"Seismic base isolation of a building by using natural materials - shake table testing and numerical modelling*" [IP-06-2016-5325]. The work of doctoral student Ivan Banović has been fully supported by the *"Young researchers' career development project – training of doctoral students"* of the Croatian Science Foundation funded by the European Union from the European Social Fund. The authors are grateful for the support.

## References

Ambraseys, N., Smit, P., Sigbjornsson, R., Suhadolc, P., and Margaris, M. (2001), EVR1-CT-1999-40008, European Commission, Directorate-General XII, Environmental and Climate Programme, Brussels, Belgium

Anastasopoulos, I., Kourkoulis, R., Gelagoti, F., and Papadopoulos, E. (2012b), "Rocking response of SDOF systems on shallow improved sand: An experimental study", *Soil Dynamics and Earthquake Engineering*, **40**, 15-33. https://doi.org/10.1016/j.soildyn.2012.04.006.

Anastasopoulos, I., Loli, M., Georgarakos, T., and Drosos, V. (2012a), "Shaking table testing of rocking-isolated bridge pier on sand", *Journal of Earthquake Engineering*, **17**(1), 1–32. https://doi.org/10.1080/13632469.2012.705225

Arab, M. G., and Kavazanjian Jr., E. (2010), "Time-domain analysis of frictional base isolation using geosynthetics", Proceedings of 9th International Conference on Geosynthetics, **2**, 695–698.

Azinović, B., Kilar, V., and Koren, D. (2014), "The seismic response of low-energy buildings founded on a thermal insulation layer–a parametric study", *Engineering Structures*, **81**, 398-411. https://doi.org/10.1016/j.engstruct.2014.10.015

Azinović, B., Kilar, V., and Koren, D. (2016), "Energy-efficient solution for the foundation of passive houses in earthquake-prone regions", *Engineering Structures*, **112**, 133-145. https://doi.org/10.1016/j.engstruct.2016.01.015

Azzam, W., Ayeldeen, M., and El Siragy, M. (2018), "Improving the structural stability during earthquakes using in-filled trench with EPS geofoam—numerical study", *Arabian Journal of Geosciences*, **11**(14), 395. https://doi.org/10.1007/s12517-018-3739-4

Bandyopadhyay, S., Sengupta, A., and Reddy, G. R. (2015), "Performance of sand and shredded rubber tire mixture as a natural base isolator for earthquake protection", *Earthquake Engineering and Engineering Vibration*, **14**(4), 683–693. https://doi.org/10.1007/s11803-015-0053-y

Banović, I., Radnić, J., and Grgić, N. (2018a), "Shake table study on the efficiency of seismic base isolation using natural stone pebbles", *Advances in Materials Science and Engineering*, Article ID 1012527, 20 pages https://doi.org/10.1155/2018/1012527

Banović, I., Radnić, J., and Grgić, N. (2019), "Geotechnical seismic isolation system based on sliding mechanism using stone pebble layer: shake-table experiments", *Shock and Vibration*, Article ID 9346232, 26 pages https://doi.org/10.1155/2019/9346232

Banović, I., Radnić, J., Grgić, N., and Matešan, D. (2018b), "The use of limestone sand for the seismic base isolation of structures", *Advances in Civil Engineering*, Article ID 9734283, 12 pages https://doi.org/10.1155/2018/9734283

Banović, I., Radnić, J., and Grgić, N. (2020a), "Effect of structural stiffness on the efficiency of seismic base isolation using layers of stone pebbles", *Ingegneria Sismica*, 37(2), 66-91.

Banović, I., Radnić, J., and Grgić, N. (2020b), "Foundation size effect on the efficiency of seismic base isolation using a layer of stone pebbles", *Earthquakes and Structures*, 19(2), 103-117. https://dx.doi.org/10.12989/eas.2020.19.2.103

Briançon, L., Girard, H., and Gourc, J. P. (2011), "A new procedure for measuring geosynthetic friction with an inclined plane", *Geotextiles and Geomembranes*, **29**(5), 472–482. https://doi.org/10.1016/j.geotexmem.2011.04.002

Briançon, L., Girard, H., and Poulain, D. (2002), "Slope stability of lining systems-experimental modeling of friction at geosynthetic interfaces", *Geotextiles and Geomembranes*, **20**(3), 147–172. https://doi.org/10.1016/S0266-1144(02)00009-2

Brunet, S., de la Llera, J. C., and Kausel, E. (2016), "Non-linear modeling of seismic isolation systems made of recycled tire-rubber", *Soil Dynamics and Earthquake Engineering*, **85**, 134–145. https://doi.org/10.1016/j.soildyn.2016.03.019

Carbone, L., Gourc, J.P., Carrubba, P., Pavanello, P., and Moraci, N. (2015), "Dry friction behaviour of a geosynthetic interface using inclined plane and shaking table tests", *Geotextiles and Geomembranes*, **43**(4), 293–306. https://doi.org/10.1016/j.geotexmem.2015.05.002

Carbone, L., Pavanello, P., Carrubba, P., Gourc, J. P., Moraci, N., Briançon, L., and Scotto, M. (2014), "Geosynthetic interface shear strength under static and seismic loading conditions", Proceedings of 10th International Conference on Geosynthetics, Berlin, Germany, 21–25 September.

Cardile, G., Gioffrè, D., Moraci, N., and Calvarano, L. S. (2017), "Modelling interference between the geogrid bearing members under pullout loading conditions", *Geotextiles and Geomembranes*, **45**, 169–177. https://doi.org/10.1016/j.geotexmem.2017.01.008

Cardile, G., Moraci, N., and Calvarano, L. S. (2016), "Geogrid pullout behaviour according to the experimental evaluation of the active length", *Geosynthetics International*, **23** (3), 194–205. https://doi.org/10.1680/jgein.15.00042

Chen, X., Xia, X., Zhang, X., and Gao, J. (2020), "Seismic performance and design of bridge piers with rocking isolation", *Structural Engineering and Mechanics*, **73**(4), 447-454. https://doi.org/10.12989/sem.2020.73.4.447

Chung, Y. L., Du, L. J., and Pan, H. H. (2019), "Performance evaluation of a rocking steel column base equipped with asymmetrical resistance friction damper", *Earthquakes and Structures*, **17**(1), 49-61. https://doi.org/10.12989/eas.2019.17.1.049

De, A., and Zimmie, T.F. (1998), "Estimation of dynamic interfacial properties of geosynthetics", *Geosynthetics International*, **5**(1–2), 17–39. https://doi.org/10.1680/gein.5.0112

Deviprasad, B. S., and Dodagoudar, G. R. (2020), "Seismic response of bridge pier supported on rocking shallow foundation", *Geomechanics and Engineering*, **21**(1), 73-84. https://doi.org/10.12989/gae.2020.21.1.073

Eurocode 1998-1:2004 (2004), Design of structures for earthquake resistance-Part 1: general rules, seismic actions and rules for buildings, European Committee for Standardization (CEN), Brussels, Belgium

Feng, R., Chen, Y., and Cui, G. (2018), "Dynamic response of post-tensioned rocking wall-moment frames under near-fault ground excitation", *Earthquakes and Structures*, **15**(3), 243-251 https://doi.org/10.12989/eas.2018.15.3.243

Forcellini, D. (2017), "Assessment on geotechnical seismic isolation (GSI) on bridge configurations", *Innovative Infrastructure Solutions*, 2(1), 9 pages https://doi.org/10.1007/s41062-017-0057-8

Hadad, H. A, Calabrese, A., Strano, S., and Serino, G. (2017), "A base isolation system for developing countries using discarded tyres filled with elastomeric recycled materials", *Journal of Earthquake Engineering*, **21**(2), 246-266. https://doi.org/10.1080/13632469.2016.1172371

Hernández, E., Palermo, A., Granello, G., Chiaro, G., Banasiak, L. (2020), "Eco-rubber seismic-isolation foundation systems: a sustainable solution for the New Zealand context", *Structural Engineering International*, 1-9. https://doi.org/10.1080/10168664.2019.1702487

Hung, H. H., Liu, K. Y., and Chang, K. C. (2014), "Rocking behavior of bridge piers with spread footings under cyclic loading and earthquake excitation", *Earthquakes and Structures*, **7**, 1001-1024. https://doi.org/10.12989/eas.2014.7.6.1001

Kalpakcı, V., Bonab, A. T., Özkan, M. Y., and Gülerce, Z. (2018), "Experimental evaluation of geomembrane/geotextile interface as base isolating system", *Geosynthetics International*, **25**(1), 1-11. https://doi.org/10.1680/jgein.17.00025

Karatzia, X., and Mylonakis, G. (2017), "Geotechnical seismic isolation using eps geofoam around piles", 6th International Conference on Computational Methods in Structural Dynamics and Earthquake Engineering, Rhodes Island, Greece

Koren, D., and Kilar, V. (2016), „Seismic vulnerability of reinforced concrete building structures founded on an XPS layer", *Earthquakes and Structures*, **10**(4), 939-963. https://doi.org/10.12989/eas.2016.10.4.939

Makris, N. (2014), "A half-century of rocking isolation", *Earthquakes and Structures*, **7**(6), 1187-1221. https://doi.org/10.12989/eas.2014.7.6.1187

Mavronicola, E., Komodromos, P., and Charmpis, D. C. (2010), "Numerical investigation of potential usage of rubber–soil mixtures as a distributed seismic isolation approach", Proceedings of the 10th International Conference on Computational Structures Technology, Valencia, Spain.

Murillo, C., Thorel, L., and Caicedo, B. (2009), "Ground vibration isolation with geofoam barriers: centrifuge modelling", *Geotextiles and Geomembranes*, **27**(6), 423-434. https://doi.org/10.1016/j.geotexmem.2009.03.006

Nanda, R. P., Agarwal, P., and Shrikhande, M. (2012a), "Base isolation by geosynthetic for brick masonry buildings", *Journal of Vibration and Control*, **18**(6), 903–910. https://doi.org/10.1177/1077546311412411

Nanda, R. P., Shrikhande, M., and Agarwal, P. (2012b), "Effect of

ground motion characteristics on the pure friction isolation system", *Earthquakes and Structures*, **3**(2), 169–180. https://doi.org/10.12989/eas.2012.3.2.169

Panjamani, A., Devarahalli Ramegowda, M., and Divyesh, R. (2015), "Low cost damping scheme for low to medium rise buildings using rubber soil mixtures", *Japanese Geotechnical Society Special Publication*, **3**(2), 24–28. https://doi.org/10.3208/jgssp.v03.i05

Patil, S. J., Reddy, G. R., Shivshankar, R., Babu, R., Jayalekshmi, B. R., and Kumar, B. (2016), "Seismic base isolation for structures using river sand", *Earthquakes and Structures*, **10**(4), 829-847. https://doi.org/10.12989/eas.2016.10.4.829

Pavanello, P., and Carrubba, P. (2016), "Methodological aspects in the experimental measurement of the interface friction between geosynthetics", *Procedia Engineering*, **158**, 260–265. https://doi.org/10.1016/j.proeng.2016.08.439

Pavanello, P., Carrubba, P., and Moraci, N. (2018a), "The determination of interface friction by means of vibrating table tests", *Geotextiles and Geomembranes*, **46**(6), 830-835. https://doi.org/10.1016/j.geotexmem.2018.06.006.

Pavanello, P., Carrubba, P., and Moraci, N. (2018b), "Dynamic friction and the seismic performance of geosynthetic interfaces", *Geotextiles and Geomembranes*, **46**(6), 715-725. https://doi.org/10.1016/j.geotexmem.2018.06.005

Pecker, A. (2003), "Aseismic foundation design process, lessons learned from two major projects: the Vasco de Gama and the Rion Antirion bridges", Proceedings of the ACI International Conference on Seismic Bridge Design and Retrofit, La Jolla, CA, USA.

Pecker, A., Prevost, J. H., and Dormieux, L. (2001), "Analysis of pore pressure generation and dissipation in cohesionless materials during seismic loading", *Journal of Earthquake Engineering*, **5**(4), 441-464. https://doi.org/10.1080/13632460109350401

Radnić, J., Grgić, N., Matešan, D., and Baloević, G. (2015), "Shake table testing of reinforced concrete columns with different layout size of foundation", *Materialwissenschaft und Werkstofftechnik*, **46**(4-5), 348–367. https://doi.org/10.1002/mawe.201500410

Sarand, N. I., and Jalali, A. (2020), "Seismic response evaluation of concentrically rocking zipper braced frames", *Structural Engineering and Mechanics*, **73**(3), 303-317. https://doi.org/10.12989/sem.2020.73.3.303

SIMQKE (1976) (SIMulation of earthQuaKE ground motions), http://gelfi.unibs.it/software/simqke/simqke_gr.htm

Sorrentino, L., Masiani, R., and Decanini, L. D. (2006), "Overturning of rocking rigid bodies under transient ground motions", *Structural Engineering and Mechanics*, **22**(3), 293-310. https://doi.org/10.12989/sem.2006.22.3.293

Sorrentino, L., Masiani, R., and Griffith, M. C. (2008), "The vertical spanning strip wall as a coupled rocking rigid body assembly", *Structural Engineering and Mechanics*, **29**(4), 433-453. https://doi.org/10.12989/sem.2008.29.4.433

Steenfelt, J. S, Foged, B., and Augustesen, A. H. (2015), "Izmit Bay bridge-geotechnical challenges and innovative solutions", *International Journal of Bridge Engineering (IJBE)*, **3**(3), 53–68.

Tehrani, F. M. and Hasani, A. (1996), "Behaviour of Iranian low rise buildings on sliding base to earthquake excitation", in Proceedings of the 11th World Conference on Earthquake Engineering, Paper 1433, Acapulco, Mexico.

Tsang, H. H. (2008), "Seismic isolation by rubber-soil mixtures for developing countries", *Earthquake Engineering and Structural Dynamics*, **37**(2), 283–303. https://doi.org/10.1002/eqe.756

Tsang, H. H. (2009), "Geotechnical Seismic Isolation", Earthquake engineering: new research, New York, U.S. Nova Science Publishers Inc., 55–87.

Tsang, H. H., and Pitilakis, K. (2019), "Mechanism of geotechnical seismic isolation system: analytical modeling", *Soil Dynamics and Earthquake Engineering*, **122**, 171-184. https://doi.org/10.1016/j.soildyn.2019.03.037

Tsang, H. H., Lo, S. H., Xu, X., and Neaz Sheikh, M. (2012), "Seismic isolation for low-to-medium-rise buildings using granulated rubber-soil mixtures: numerical study", *Earthquake Engineering and Structural Dynamics*, **41**(14), 2009–2024. https://doi.org/10.1002/eqe.2171

Tsatsis, A. and Anastasopoulos, I. (2015), "Performance of rocking systems on shallow improved sand: shaking table testing", *Frontiers in Built Environment*, **1**, 1-9. https://doi.org/10.3389/fbuil.2015.00009

Tsiavos, A., Alexander, N. A., and Sextos, A. (2019a), "Numerical investigation of the sliding response of flexible structures founded on a deformable granular layer", 2nd International Conference on Earthquake Engineering and Post Disaster Reconstruction Planning, Bhaktapur, Nepal.

Tsiavos, A., Alexander, N. A., Diambra, A., Ibraim, E., Vardanega, P. J., Gonzalez-Buelga, A., and Sextos A. (2019b), "A sand-rubber deformable granular layer as a low-cost seismic isolation strategy in developing countries: experimental investigation", *Soil Dynamics and Earthquake Engineering*, **125**, https://doi.org/10.1016/j.soildyn.2019.105731

Wang, J., He, J. X., Yang, Q. S., and Yang, N. (2018), "Study on mechanical behaviors of column foot joint in traditional timber structure", *Structural Engineering and Mechanics*, **66**(1), 1-14. https://doi.org/10.12989/sem.2018.66.1.001

Wasti, Y., and Özdüzgün, Z. B. (2001), "Geomembrane-geotextile interface shear properties as determined by inclined board and direct shear box tests", *Geotextiles and Geomembranes*, **19**, 45–57. https://doi.org/10.1016/S0266-1144(00)00002-9

Xiong, W. and Li, Y. (2013), "Seismic isolation using granulated tire-soil mixtures for less-developed regions: experimental validation", *Earthquake Engineering and Structural Dynamics*, **42**(14), 2187-2193. https://doi.org/10.1002/eqe.2315

Xiong, W., Yan, M. R., and Li, Y. Z. (2014), "Geotechnical seismic isolation system - further experimental study", *Applied Mechanics and Materials*, **580-583**, 1490-1493. https://doi.org/10.4028/www.scientific.net/AMM.580-583.1490

Xu, R. and Fatahi, B. (2018), "Influence of geotextile arrangement on seismic performance of mid-rise buildings subjected to MCE shaking“, *Geotextiles and Geomembranes*, **46**(4), 511-528. https://doi.org/10.1016/j.geotexmem.2018.04.004

Yegian, M. K., and Kadakal, U. (2004), "Foundation isolation for seismic protection using a smooth synthetic liner", *Journal of Geotechnical and Geoenvironmental Engineering*, **130**(11), 1121–1130. https://doi.org/10.1061/(ASCE)10900241(2004)130:11(1121)

Yegian, M. K., and Catan, M. (2004), "Soil isolation for seismic protection using a smooth synthetic liner", *Journal of Geotechnical & Geoenvironmental Engineering*, **130**(11), 1131–1139. https://doi.org/10.1061/(ASCE)10900241(2004)130:11(1131)

Yegian, M. K., and Kadakal, U. (1998), "Geosynthetic interface behavior under dynamic loading", *Geosynthetics International*, **5**(1–2), 1–16. https://doi.org/10.1680/gein.5.0111

Yegian, M. K., and Lahlaf, A.M. (1992), "Dynamic interface shear strength properties of geomembranes and geotextiles", *International Journal of Geotechnical Engineering*, **118**(5), 760–779. https://doi.org/10.1061/(ASCE)07339410(1992)118:5(760)

Zhao, X., Zhang, Q., Zhang, Q., and He, J. (2016), "Numerical study on seismic isolation effect of gravel cushion", Proceedings of the 7th International Conference on Discrete Element Methods, **188**, 1055-1063, Dalian, China

# PAPER VII

# Effect of geogrid on the efficiency of seismic base isolation using natural stone pebbles: A shake table study

Ivan Banović[1*], Jure Radnić[1], Nikola Grgić[1]

[1]*University of Split, Faculty of Civil Engineering, Architecture and Geodesy, Matice hrvatske 15, 21000 Split, Republic of Croatia*

**Abstract.** The effect of geogrid on the efficiency of seismic base isolation using a layer of stone pebbles is experimentally investigated in this study. Four different foundation support cases (rigid base, thin layer of stone pebble, thin layer of stone pebble with geogrid at the layer top, and thick layer of stone pebble with geogrid at the layer top) were tested on four models of different stiffnesses. The models were exposed to the action of four different accelerograms. The efficiency of the seismic isolation with strains in the models in the elastic range and until their collapse was tested. Test results confirmed that the geogrid significantly improved the seismic isolation performance of the stone pebble layer.

**Keywords:** low-cost seismic isolation; stone pebble; geogrid; isolation efficiency; shake table study

## 1. Introduction

Areas of high seismicity where severe earthquakes may occur are often located in less developed countries. Owing to the low economic power and low requirements for the construction of seismically resilient structures, the consequences of mild earthquakes in such regions can be catastrophic. To increase the seismic resistance of buildings, one of the primary goals is to develop cheap, environmentally friendly, and efficient seismic isolation that is applicable to the abovementioned areas. In recent years, studies have been intensified to develop such seismic isolation, which is based on creating an appropriate aseismic layer under the foundation of a building. The dissipation of earthquake energy in this seismic isolation approach is achieved by three dominant effects: sliding of the foundation on the layer top due to reduced friction, as well as sliding between particles in the aseismic layer and by reduced rocking stiffness (Banović *et al.* 2018a, Banović *et al.* 2019, Tsang and Pitilakis 2019). Some studies pertaining to this topic are summarised below.

The concept of seismic base isolation has been known throughout history, as builders utilised a layer of natural material below a structure's foundation for earthquake hazard mitigation (Przewłócki *et al*. 2005, Kulukčija *et al.* 2009, Kulukčija and Humo 2009, Carpani 2014, Carpani 2017). The development, theory, and application of base isolation have been presented by many scholars (Kelly 1996a, Warn and Ryan 2012, Makris 2014, Calvi and Calvi 2018, Makris 2018). Meanwhile, the development of seismic isolators for low-cost buildings has been presented by Kelly (1996b) and Kelly and Taniwangsa (1996).

The use of sand and gravel for seismic base isolation has garnered significant attention in the past decades. Tehrani and Hasani (1996) reported the suitability of dune sand for creating sliding layers in adobe buildings in Iran. Furthermore, Radnić *et al.* (2015) and Banović *et al.* (2018b) presented seismic performances of small-scale cantilever concrete columns isolated with a limestone sand layer. Shake table test results demonstrated that the layer of limestone sand below the foundation increased the safety of the column under earthquake loading. Patil *et al.* (2016) investigated the possibility of using river sand for seismic base isolation. They reported encouraging results based on experimental and analytical studies of a structural model with isolated footing. Anastasopoulos *et al.* (2012a) reported the seismic performance of a rocking-isolated bridge pier on surface foundations resting on sand. The rocking-isolated pier was effectively protected, surviving all seismic excitations without structural damage, at the expense of increased foundation settlement due to a low static factor of safety $FS_v$. Rocking isolation is a well-known alternative seismic design philosophy for large, slender structures, with an intentionally under designed foundation to promote rocking and limit the inertia transmitted to the structure (Sorrentino *et al.* 2006, Sorrentino *et al.* 2008, Hung *et al.* 2014, Makris 2014, Tsatsis and Anastasopoulos 2015, Feng *et al*. 2018, Wang *et al.* 2018, Xu and Fatahi 2018, Chung *et al.* 2019, Chen *et al.* 2020). In this context, Anastasopoulos *et al.* (2012b) presented an experimental study on the rocking response of single-degree-of-freedom systems on shallow improved

* Corresponding author, Ph.D. candidate
E-mail: ivan.banovic@gradst.hr

sand. In this study, shallow soil improvement was considered as an alternative to prevent unforeseen inadequate $FS_v$. Furthermore, Masoud *et al.* (2018) investigated the effect of soil reinforcement on the rocking isolation potential of high-rise bridge foundations. For shallow soil improvement, geogrid and geocell were used as reinforcement elements at different depth ratios. They reported that using a geocell at depth ratios of less than 0.25 effectively reduced settlements.

Zhao *et al.* (2016) recognised that a cushion comprising gravel can be used as an isolation layer to reduce the seismic response of an upper structure. Based on a numerical analysis, they concluded that the isolation effect of the cushion increased with the layer thickness and decreased with the increase in the base pressure. Furthermore, a rocking-isolated pier founded on gravel cushion was applied on the Rio–Antirion Bridge (Pecker *et al*. 2001) in Greece, the Vasco de Gama Bridge (Pecker *et al*. 2003) in Portugal, and the Izmit Bay Bridge (Steenfelt *et al.* 2015) in Turkey.

Karatzia *et al.* (2019) discovered that natural liquefiable soil may serve as natural seismic isolation. They proposed that geotechnical isolation exploits the presence of natural liquefiable soil after a partial remediation of the surface ground as a natural base isolation system that deamplifies the seismic ground motion and hence reduces the seismic demand on the superstructure.

The concept of using rubber–soil mixtures (RSM) as a low-cost seismic isolation strategy for earthquake hazard migration in developing countries has been proposed by Tsang (2008, 2009). He reported that this seismic isolation strategy can reduce substantially not only the horizontal, but also the vertical ground motion acceleration response of structures subjected to earthquakes. In addition, he proposed that seismic isolation methods involving geotechnics should be collectively termed as a "geotechnical seismic isolation (GSI) system". This term has been adopted by other scholars (Brunet *et al.* 2016, Forcellini 2017, and Banović *et al.* 2019).

Following his pioneering research, the application of RSMs as a low-cost alternative for seismic isolation has garnered significant attention in the last decade. In particular, the performance of the GSI system has been studied in a number of numerical and experimental studies (Mavronicola *et al.* 2010, Tsang *et al.* 2012, Xiong and Li 2013, Bandyopadhyay *et al.* 2015, Panjamani *et al.* 2015, Pitilakis *et al.* 2015, Xiong *et al.* 2015, Brunet *et al.* 2016, Forcellini 2017, Raki and Gourav 2018, Tsang and Pitilakis 2019, Tsiavos *et al.* 2019a, Tsiavos *et al.* 2019b, Hernández *et al*. 2020).

Hadad *et al.* (2017) investigated the performance of economic base isolators using tyres filled with elastomeric recycled materials for application in developing countries, where the application of conventional elastomeric rubber bearings due to economic reasons is limited.

Additionally, scholars have proposed geofoam as a potential low-cost seismic isolation material, because passive houses are often founded on a thermal insulation layer, which is placed under the building's RC foundation slab (Murillo *et al.* 2009, Azinović *et al.* 2014, Azinović *et al.* 2016, Koren and Kilar 2016, Karatzia *et al.* 2017, Azzam *et al.* 2018). Doudoumis *et al.* (2002) studied the concept of interposing an artificial soil layer between the superstructure and the natural foundation soil of the buildings. The proposed soil layer has a low shearing resistance, which allows the slipping of the building under the action of strong seismic motions.

Geosynthetics have a wide range of applications in various fields of civil engineering, among others, they have been proposed as base isolation material. Within this context, geosynthetic interface behaviour under dynamic loading was an interesting topic for many researchers (Yegian and Lahlaf 1992a, Yegian and Lahlaf 1992b, De and Zimmie 1998, Yegian and Kadakal 1998, Wasti and Özdüzgün 2001, Briançon *et al.* 2002, Arab and Kavazanjian 2010, Briançon *et al.* 2011, Nanda *et al.* 2012a, Nanda *et al.* 2012b, Carbone *et al.* 2014, Cardile *et al.* 2014, Carbone *et al.* 2015, Cardile *et al.* 2015, Pavanello and Carrubba 2016, Ziegler 2017, Kalpakci *et al.* 2018, Narjabadifam and Chavoshi 2018, Pavanello *et al.* 2018a, Pavanello *et al.* 2018b).

In particular, Yegian and Lahlaf (1992a) investigated the concept of using two sheets of smooth high-density polyethylene geomembrane as base isolation in earthquake hazard mitigation. Yegian and Kadakal (2004) proposed smooth synthetic materials placed underneath foundations of structures, which can serve as seismic protection by absorbing energy through sliding. They concluded based on cyclic and shake table tests that a high strength, nonwoven geotextile placed over an ultrahigh molecular weight polyethylene, UHMWPE (geotextile/UHMWPE) constitutes a liner that is well suited for this application. Furthermore, Yegian and Catan (2004) reported that UHMWPE placed within a soil profile can dissipate seismic energy transmitted to the overlying soil layer and structure. More recently, Kalpakci *et al.* (2018) used a shaking table test setup to evaluate the effect of the geomembrane/geotextile interface on the seismic response of small-to-moderate height structures. They tested a UHMWPE geomembrane, based on the study of Yegian and Kadakal (2004).

An extensive shake table study to investigate the possibility of using a layer of stone pebbles for the seismic isolation of lower buildings has been performed at the Seismic Testing Centre at the Faculty of Civil Engineering, Architecture, and Geodesy, University of Split, Croatia (Banović *et al.* 2018a, 2019, 2020a, 2020b, and 2020c). The dissipation of earthquake energy within such a layer depends on the shape of the pebbles and the smoothness of their surface. These characteristics result in a slight friction between the pebbles as they move during the earthquake. Nonetheless, such a substrate can absorb a relatively high vertical contact stress below the foundation of the building. The conducted experimental studies confirmed that the seismic isolation from the stone pebble layer can significantly reduce the acceleration (seismic force) and strain of the tested building models, especially those of higher stiffness. The efficiency of seismic isolation depended significantly on the stiffness of the tested model, the ground plan dimensions of the foundation, and the type

of earthquake accelerogram applied. It is concluded that such a seismic isolation offers significant potential for practical applications in low-rise rigid buildings on rigid soil; however, for further research is necessitated.

Banović *et al.* (2020c) experimentally investigated the efficiency of composite seismic isolations composed of stone pebbles with geogrids, geomembranes, and a layer of limestone sand. The effectiveness of 10 different composite seismic isolation layers was tested and compared to that of a stone pebble layer. A simple model of a rigid building exposed to four different accelerograms was used. The test result confirmed that the average tested composite seismic isolation can further reduce the inertial forces of the rigid building model relative to the stone pebble layer. In addition, the stone pebble layer isolation was more effective than several composite isolations for specific excitations and peak ground acceleration (PGA) levels.

The results of a study initiated by Banović *et al.* (2020c) are presented herein. The efficiency of two composite seismic isolations with the best performance and the efficiency of the stone pebble layer isolation relative to a rigid base were investigated in detail. Furthermore, the ratios of the efficiency of the two composite seismic isolations to each other and to the efficiency of the stone pebble isolation were presented. Four building models with different stiffnesses (from extremely stiff to soft) were tested on four different substrates exposed to the acceleration of four different earthquake accelerograms. A 0.30-m-thick pebble layer with a geogrid at the layer top and a 0.60-m-thick pebble layer with an equal geogrid at the layer top were adopted as the optimal composite seismic isolation, among 10 tested isolations in a previous study. All models were tested such that the strains in the model remained elastic. For the most unfavourable excitation, the models were tested with successive increases in the PGA until the model collapsed. Based on the measured acceleration and strain of the model, it was concluded that the considered composite seismic isolations have significantly higher efficiency (reduced inertial force and strain) relative to the pebble layer seismic isolation.

## 2. Tested substrates below the model foundation

The considered substrates below the foundations of the tested building models are shown in Fig. 1. RB denotes a rigid substrate without base isolation (subconcrete fixed to the shake table), BI1 the seismic isolation of a 0.3-m-thick stone pebble layer, BI2 the composite seismic isolation of a 0.3-m-thick stone pebble layer with a geogrid on the layer top, and BI3 the composite seismic isolation of a 0.6-m-thick stone pebble layer with a geogrid on the layer top. According to the results of a previous study (Banović *et al.* 2020c), composite seismic isolations BI2 and BI3 yielded the most favourable performances. All seismic isolations were formed within a 2.5 m × 2.5 m rigid box that was fixed to the shake table. Stone pebbles have optimal properties, as demonstrated in a previous study (Banović *et al.* 2019): the pebble fraction $\Phi_b$ = 16–32 mm (Fig. 2a), layer compaction *MS* = 30 MPa, and pebble moisture *h* = 10%. The basic data of the adopted geogrid (Fig. 2b) are presented in Table 1.

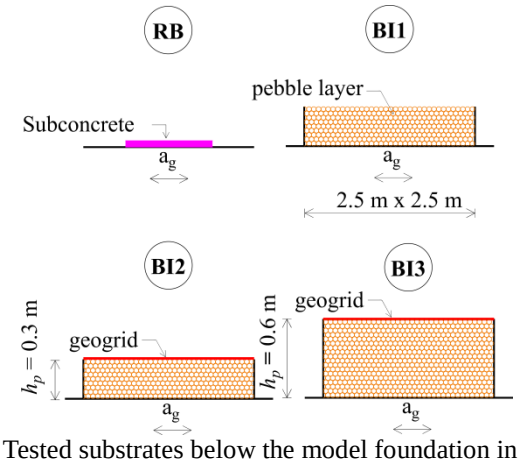


Fig. 1 Tested substrates below the model foundation in this study

(a) Stone pebbles (b) Geogrid 120/40 R6

Fig. 2 Stone pebbles and geogrid utilised in this study

Table 1 Basic data for the geogrid utilised

| Property | Test method | Unit | 120/40 R6 |
|---|---|---|---|
| Raw material | - | - | Polyester, transparent |
| Mass per unit area | EN ISO 9864 | g/m$^2$ | 580 |
| Max. tensile strength, md/cmd* | EN ISO 10319 | kN/m | ≥ 120 / ≥ 40 |
| Elongation at nominal strength, md/cmd* | EN ISO 10319 | % | ≤ 7 / ≤ 7 |
| Aperture size, md/cmd* | - | mm × mm | 71 × 28 |

* md = machine direction, cmd = cross machine direction

## 3. Tested models of buildings

Simple models of buildings according to Fig. 3 were adopted, formed from a concrete foundation (cube strength of 46 MPa), a steel column with hot-rolled a hollow cross section (steel S355), and a concrete block (cube strength of 46 MPa) at the column top, representing the mass of the building. The $M_1$ model represents an extremely stiff building, $M_2$ a stiff building, $M_3$ a medium-stiff building, and $M_4$ a soft building. Namely, the stiffness of the columns (cross-section) and the mass at the top of the column were selected such that the first period of free oscillations of the column ($T_1$) was 0.05, 0.30, 0.60, and 1.40 s, for $M_1$, $M_2$, $M_3$, and $M_4$, respectively. The model has a foundation measuring 1.2 m × 0.7 m × 0.3 m, which minimised the beneficial effect of rocking isolation to simulate the actual

behaviour of the foundations of lower buildings in an earthquake. For the RB support case, the horizontal displacement of the foundation in relation to the base (shake table) was prevented, whereas the rocking and uplifting of the foundation were allowed. The concrete block at the top of the column measured 1.0 m × 1.0 m × 0.4 m, with a mass m = 1000 kg. In this study, the effect of soil–foundation–structure interaction on building behaviour was essential and hence included. These four models encompassed a wide range of building stiffness, which was used to test the effectiveness of the aforementioned base isolations.

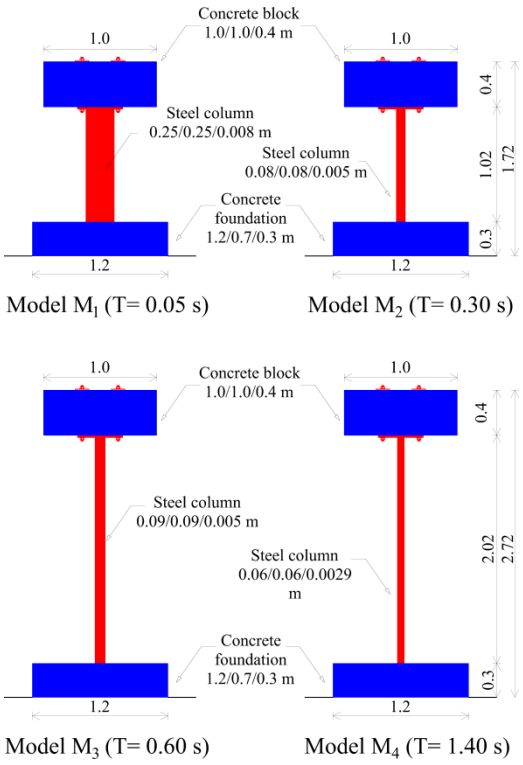


Fig. 3 Tested building models

## 4. Applied base accelerograms

All tested models were exposed to the horizontal acceleration of the four earthquake accelerograms (Fig. 4), as in previous studies (Banović *et al.* 2018a, 2019, and 2020). Two different earthquake accelerogram (Ambraseys *et al.*, 2001) types were utilised. The artificial accelerogram (AA) and accelerogram Petrovac (AP, Montenegro 1979, orientation N–S) represent long-duration earthquakes with long predominant periods, which resulted in a high earthquake energy to the structure. The accelerogram Ston (AS, Croatia 1996, orientation N-S) and the accelerogram Banja Luka (ABL, BiH 1982, orientation N–S) represent short-acting earthquakes with a short predominant period, i.e. the impact earthquakes, with strong shear actions. The artificial accelerogram (AA) is a superposition of sine functions, generated using SIMQKE software (1976). It was created to match the elastic response spectra according to EC8 (2004) for Type 1 and Type A soils.

First, the models were exposed to a one-time base excitation, in which the strain/stress of the model (bottom of the steel column) remained dominant in the elastic range. The maximum base acceleration applied for models $M_1$ and $M_2$ was $a_{g,\,max}$ = 0.3 g, and $a_{g,\,max}$ = 0.2 g for models $M_3$ and $M_4$, where $a_{g,\,max}$ = PGA. Therefore, the effect of energy dissipation (nonlinearity) in the structure was excluded, and the dissipation of earthquake energy occurred only in the substrate below the foundation and on the substrate–foundation coupling surface. This approach clearly demonstrated the efficiency of the seismic isolation.

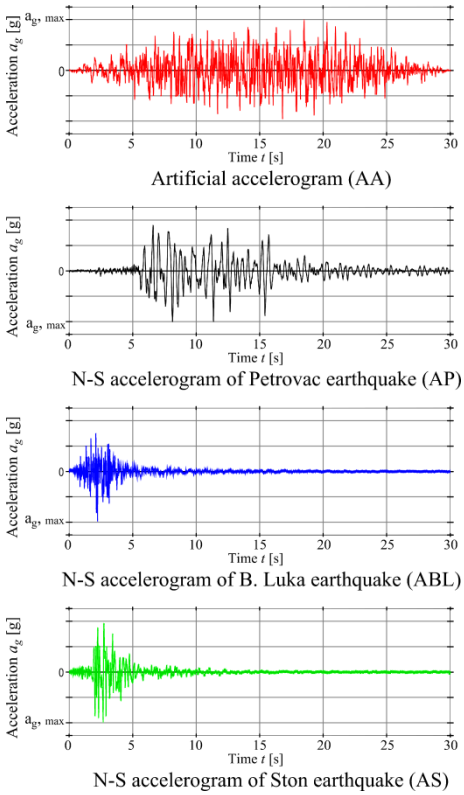


(a) Adopted horizontal accelerograms

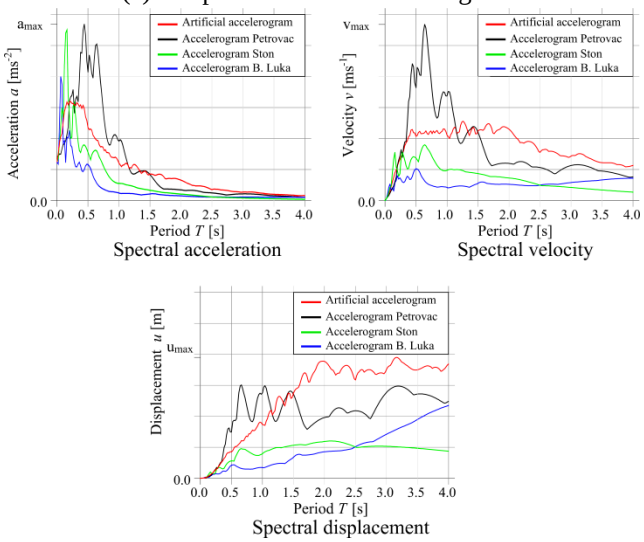


(b) Spectral values of adopted accelerograms

Fig. 4 Adopted accelerograms and their spectral values (Banović *et al.* 2018a, 2019, and 2020)

After each base excitation, the pebble layer (i.e. re-compaction to the required compaction module and

levelling of the layer top) and the model (recentring) were updated for the next excitation.

Following these one-time base excitations, the models were tested with a set of repeated artificial accelerograms by scaling the PGA for $\Delta a_{g,max}$ = 0.05 g until the collapse of the model.

## 5. Measuring equipment and measured quantities

A uniaxial shake table experimental setup shown in Fig. 5a was used for model testing. All tests were performed at the Seismic Testing Centre at the Faculty of Civil Engineering, Architecture, and Geodesy, University of Split, Croatia. The characteristics of the shake table were as follows: layout size of 4 m × 4 m, maximal payload of 20 000 kg, maximum displacement of ±150 mm, maximum acceleration of 5 g, and frequency of 0–20 Hz.

(a) Experimental setup on shake table with model $M_1$ based on BI2 isolation

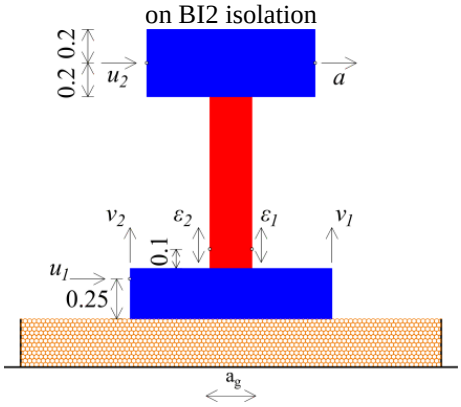


(b) Measured quantities

Fig. 5 Experimental setup and measured quantities

The following quantities were measured (Fig. 5b), as in a previous study (Banović *et al.* 2018a): the horizontal acceleration of the mass centre at the column top $a$, horizontal displacements $u_1$ (foundation top) and $u_2$ (mass centre at the column top), vertical displacements of the foundation $v_1$ (at the right edge) and $v_2$ (at the left edge), and vertical strains on the bottom of the steel column $\varepsilon_1$ (at the right side) and $\varepsilon_2$ (at the left side).

The model behaviour was monitored using sensors, i.e. strain gage of type 6/120 LY11 (Hottinger Baldwin Messtechnik-HBM) for strains; analogue displacement sensors of type PB-25-S10-N0S-10C (Uni Measure) for displacements; and a piezoelectric low-frequency accelerometer-type 4610 (Measurement Specialties) sensor for accelerations. Additionally, a video camera (Canon EOS M5) was used for test monitoring. For data collection and processing, a 16-channel Quantum-x mx 840A (HBM) high-speed data acquisition system (200 Hz sampling rate) was used.

## 6. Experimental results of shake table testing

Owing to the large amount of data, only some test results are presented. Section 6.1 presents the results for a one-time base acceleration, whereas Section 6.2 the results for the successive increase in the acceleration of the AA excitation until model collapse.

### *6.1 Result for one-time base acceleration*

The peak horizontal acceleration of the mass centre at the column top $a$ is presented in Fig. 6 for all applied excitations (AA, AP, ABL, and AS). It is clear that the results depended significantly on the type of applied earthquake and the stiffness of the model. For models $M_1$ and $M_2$, the maximum acceleration was exhibited by rigid substrate RB, whereas the maximum acceleration of composite substrates BI2 and BI3 was smaller than that of the BI1 stone pebble substrate. However, for the $M_3$ model and especially the $M_4$ model, the RB substrate produced the smallest accelerations. It was obvious that the further softening of the substrate below the foundations of already soft buildings was not favourable, i.e. the application of the considered seismic isolations BI1, and in particular BI2 and BI3 was not acceptable for medium stiff ($M_3$) and soft ($M_4$) building models.

The peak vertical strain on the bottom of the steel column $\varepsilon_{1,2}$ is presented in Fig. 7; $\varepsilon_{1,2}$ refers to larger (less favourable) values of $\varepsilon_1$ and $\varepsilon_2$. The measured values of these strains were more plausible for evaluating the efficiency of the considered seismic isolations than the measured acceleration values (Fig. 6). As Figs. 7-8 are compatible, it can be concluded that the measured deformations corresponded approximately to the measured accelerations, i.e. the previous conclusions regarding the efficiency of the considered isolations depending on the stiffness of the model are valid.

The peak horizontal displacement of the mass centre at the column top $u_2$ is presented in Fig. 8. As shown, the displacements $u_2$ for the $M_2$ model and in particular the $M_1$ model are significantly smaller than those for the $M_3$ and $M_4$ models. The displacement $u_2$ depended significantly on the type of applied earthquake. For extremely stiff and stiff models $M_1$ and $M_2$, the largest displacements were primarily exhibited in the RB substrate, and BI1 produced larger displacements than substrates BI2 and BI3.

The peak vertical displacement of the foundation $v_{1,2}$ is presented in Fig. 9, where $v_{1,2}$ refers to larger (less favourable) values of $v_1$ and $v_2$. Furthermore, the largest vertical displacements of the foundation were exhibited in models $M_2$ and $M_3$ under AA and AP excitations.

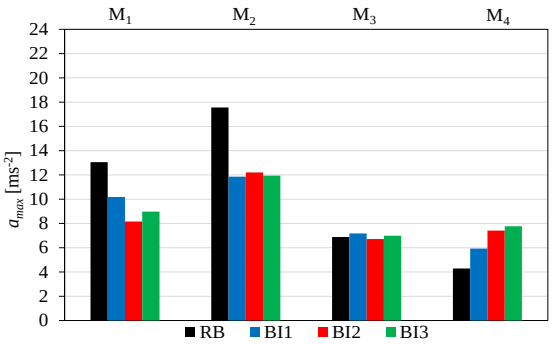


(a) AA

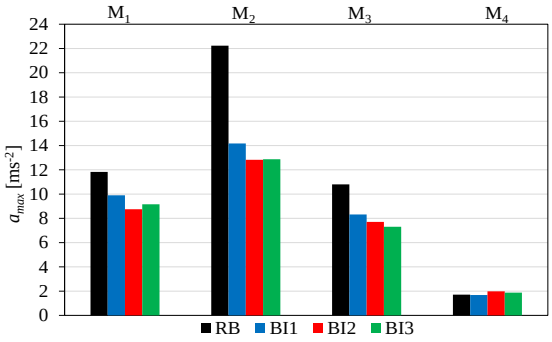


(b) AP

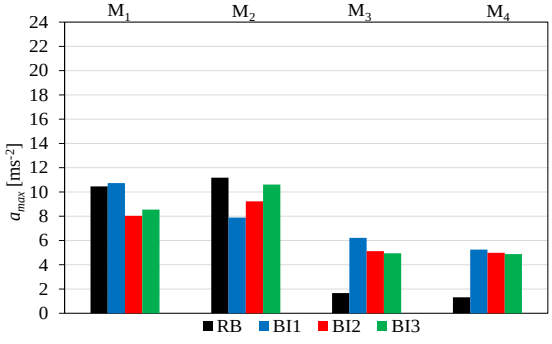


(c) AS

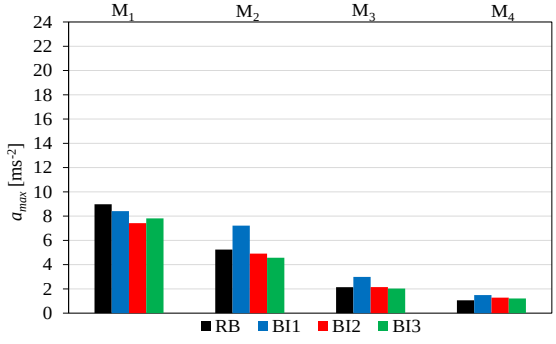


(d) ABL

Fig. 6 Peak horizontal acceleration of the mass centre at the column top $a$

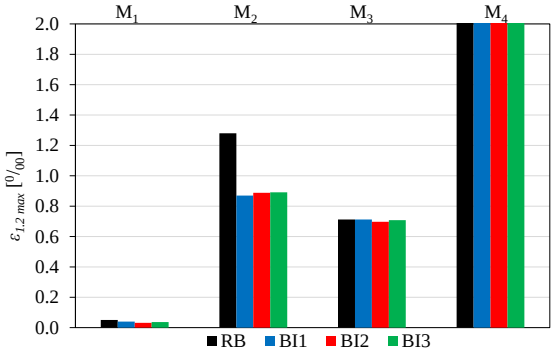


(a) AA

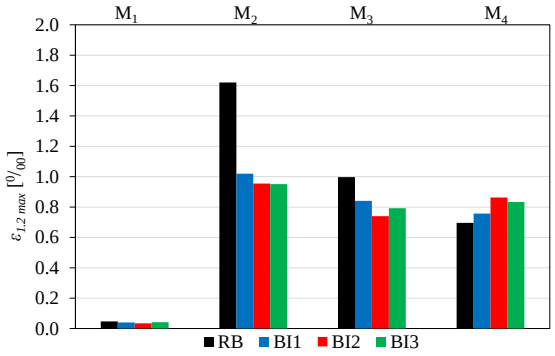


(b) AP

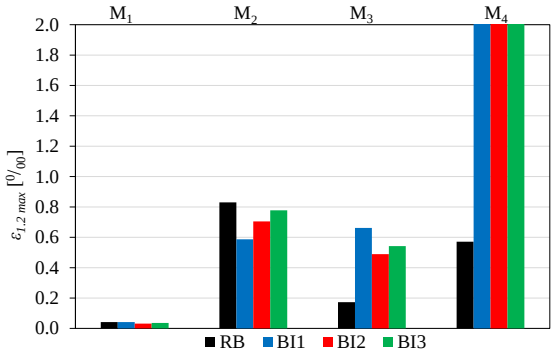


(c) AS

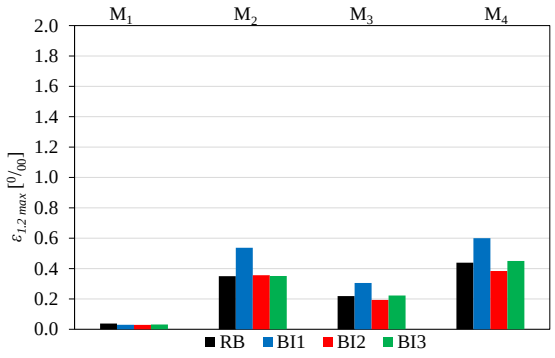


(d) ABL

Fig. 7 Peak vertical strain on bottom of the steel column $\varepsilon_{1,2}$

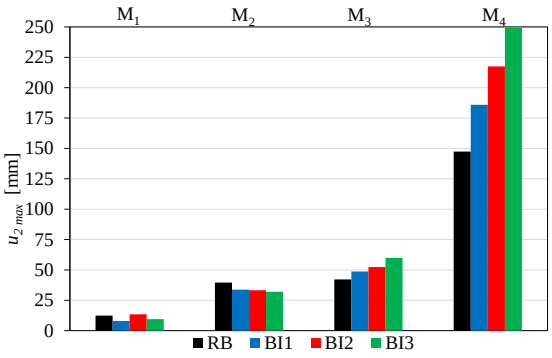


(a) AA

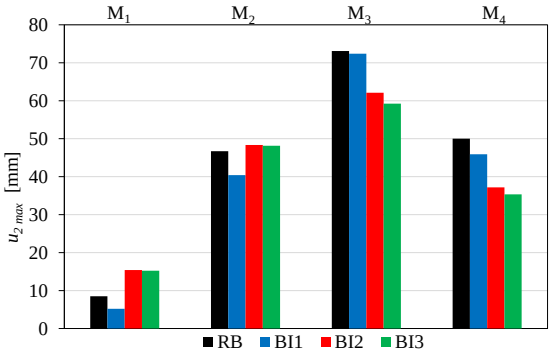


(b) AP

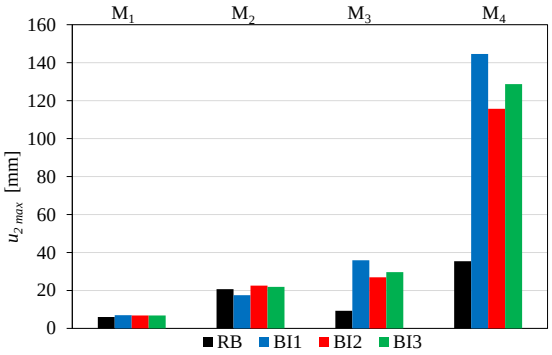


(c) AS

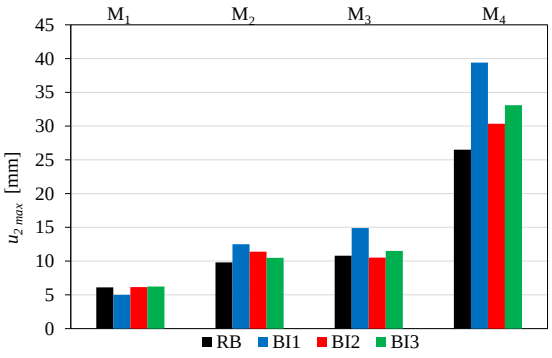


(d) ABL

Fig. 8 Peak horizontal displacement of the mass centre at the column top $u_2$

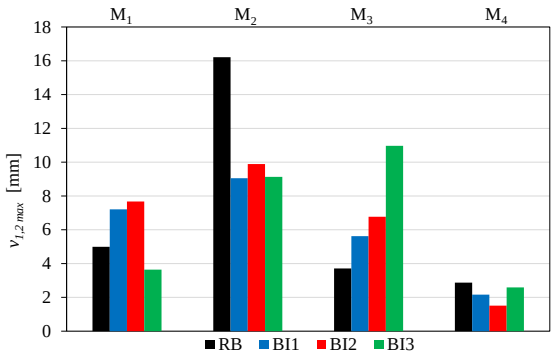


(a) AA

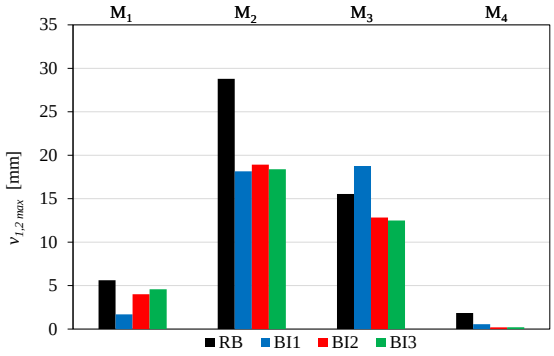


(b) AP

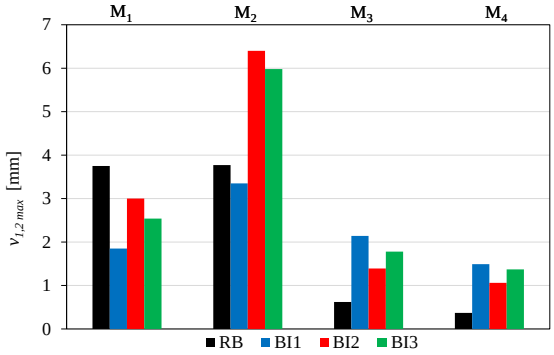


(c) AS

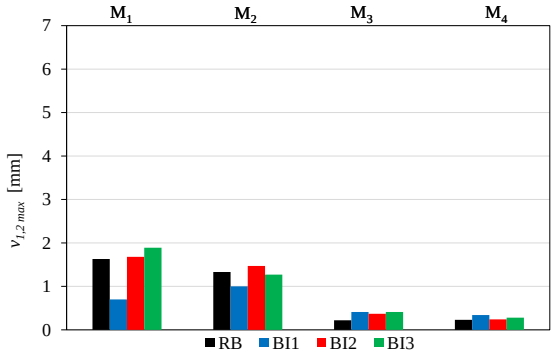


(d) ABL

Fig. 9 Peak vertical displacement of the foundation $v_{1,2}$

If the quotients of the measured peak quantities between seismic isolations and RB, denoted by $c_a$, $c_{\varepsilon 1,2}$, $c_{u2}$, $c_{v1,2}$, respectively, are introduced, they can then be characterised as the seismic isolation efficiency coefficients. Seismic isolation is more efficient (more favourable) than the rigid base if these coefficients have values less than 1.

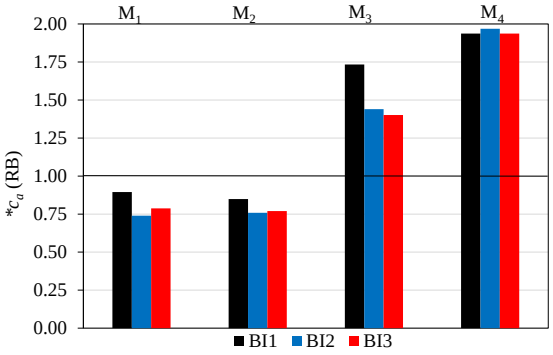


(a) $*c_a$ (RB)

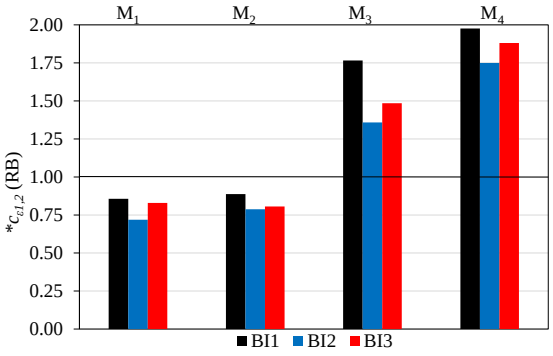


(b) $*c_{\varepsilon 1,\,2}$ (RB)

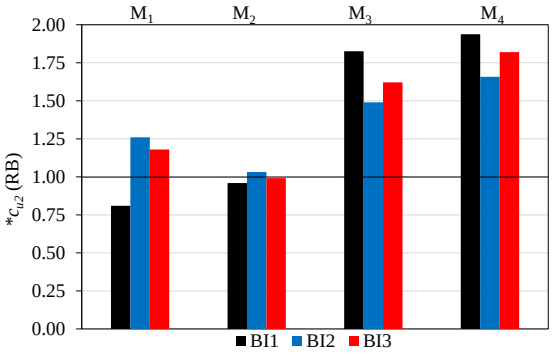


(c) $*c_{u2}$ (RB)

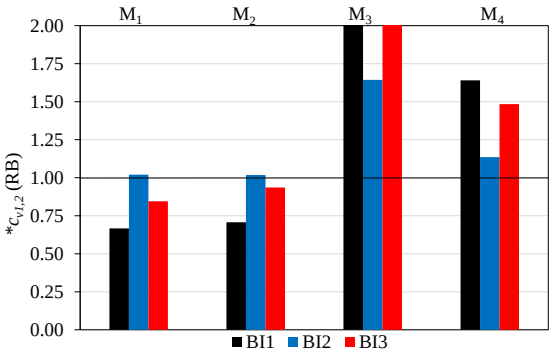


(d) $*c_{v1,\,2}$ (RB)

Fig. 10 Seismic isolation efficiency coefficients of isolations BI1, BI2, and BI3 relative to the rigid base RB for an "average" earthquake

Furthermore, if the mean values of the measured peak quantities for all four applied accelerograms in Figs. 6-9 are used ("average" earthquake), then the mean values of the seismic isolation efficiency coefficients $*c_a$ (RB), $*c_{\varepsilon 1,\,2}$ (RB), $*c_{u2}$ (RB), and $*c_{v1,\,2}$ (RB) can be calculated, as presented in Fig. 10.

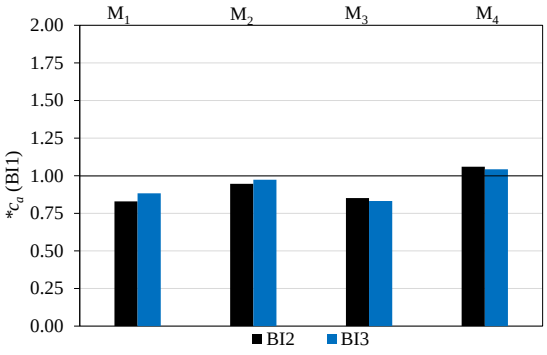


(a) $*c_a$ (BI1)

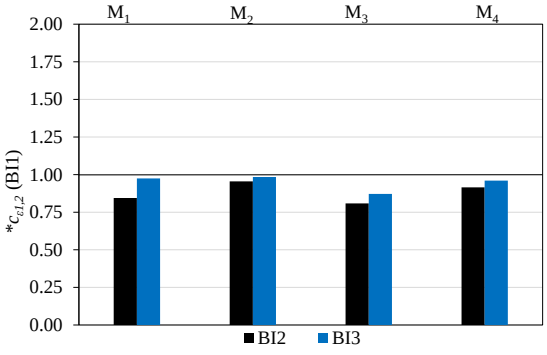


(b) $*c_{\varepsilon 1,\,2}$ (BI1)

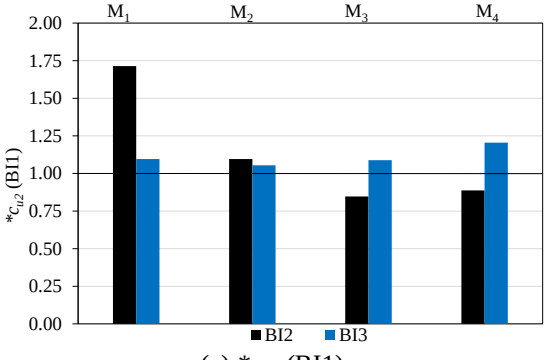


(c) $*c_{u2}$ (BI1)

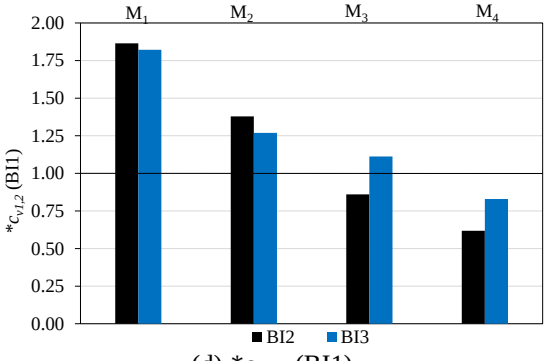


(d) $*c_{v1,\,2}$ (BI1)

Fig. 11 Seismic isolation efficiency coefficients of isolations BI2 and BI3 relative to isolation BI1 for an "average" earthquake

It is observed that the isolation efficiency in terms of inertial force (acceleration), strain, $*c_a$ (RB), and $*c_{\varepsilon 1,\,2}$ (RB) for the extremely stiff and stiff building models ($M_1$ and $M_2$) have values lower than 1 (favourable) for all seismic

isolation substrates. Moreover, the BI2 and BI3 isolations were more efficient that the BI1 isolation. The efficiency of the BI2 and BI3 isolations was similar. Meanwhile, the displacements of the $M_1$ and $M_2$ models (efficiency coefficients per displacement) were more favourable (smaller displacements for seismic isolation compared with the displacements for a rigid base). Substrate BI1 was more favourable than substrates BI2 and BI3, which were equally deformable.

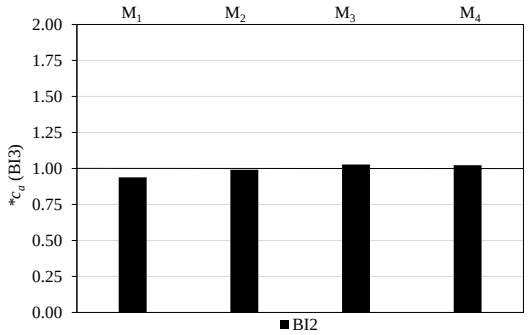


(a) $*c_a$ (BI3)

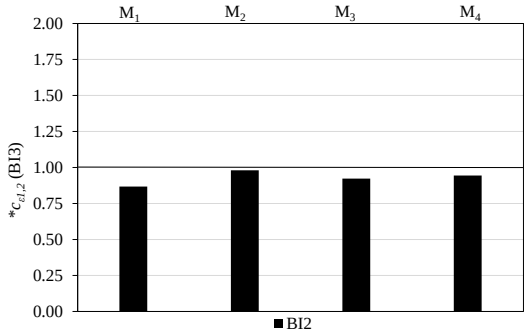


(b) $*c_{\varepsilon 1,\,2}$ (BI3)

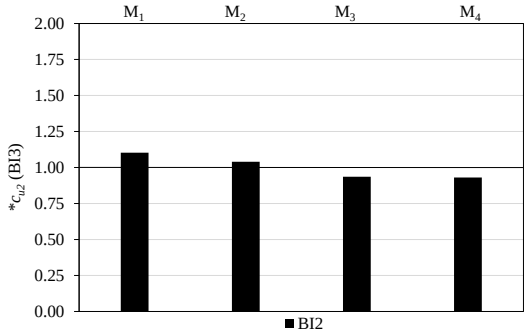


(c) $*c_{u2}$ (BI3)

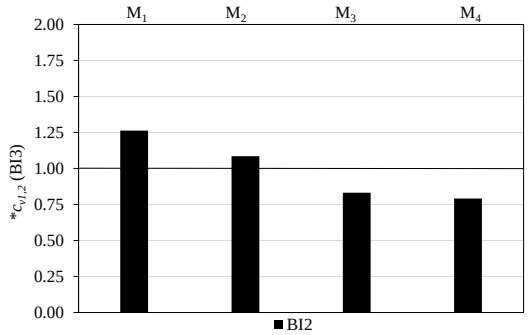


(d) $*c_{v1,\,2}$ (BI3)

Fig. 12 Seismic isolation efficiency coefficients of isolation BI2 relative to isolation BI3 for an "average" earthquake

The seismic isolation efficiency coefficients for softer models $M_3$ and $M_4$ had average values that were significantly higher than 1, i.e. they were unfavourable. As stated above, the seismic isolations considered were not favourable for soft building models.

One of the main objectives of this study is to determine the efficiency of composite seismic isolations BI2 and BI3 relative to seismic isolation BI1. The seismic efficiency coefficients, BI2 relative to BI1 and BI3 relative to BI1, are presented in Fig. 11. These coefficients are denoted by $*c_a$ (BI1), $*c_{\varepsilon 1,\,2}$ (BI1), $*c_{u2}$ (BI1), and $*c_{v1,\,2}$ (BI1). In relation to models $M_1$ and $M_2$, which were the only ones considered, it was observed that isolation BI2 was slightly more favourable than isolation BI3 in terms of reducing the acceleration and strain of the model. In terms of displacement, isolations BI2 and BI3 were less favourable than isolation BI1. Furthermore, isolation BI3 was more favourable than isolation BI2.

If the efficiency of isolation BI2 is compared with that of BI3, then the coefficients $*c_a$ (BI3), $*c_{\varepsilon 1,\,2}$ (BI3), $*c_{u2}$ (BI3), and $*c_{v1,\,2}$ (BI3), shown in Fig. 12, can be obtained, analogously to the previous one. It is evident that for models $M_1$ and $M_2$, isolation BI2 was more favourable than isolation BI3, i.e. the model had a lower inertial force and strain/stress.

To verify the appropriate numerical model for simulating the dynamic responses of buildings with the considered seismic isolation during an earthquake, the time–history of the measured result is presented in Figs. 13–15.

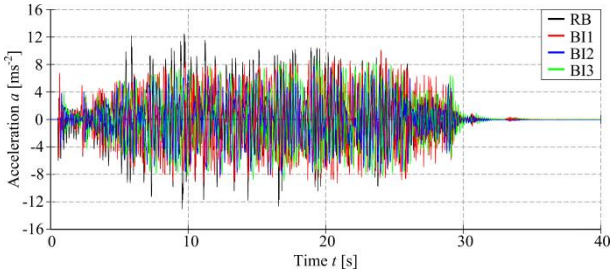


Fig. 13 Horizontal acceleration of the mass centre at the column top $a$ of model $M_1$ for accelerogram AA

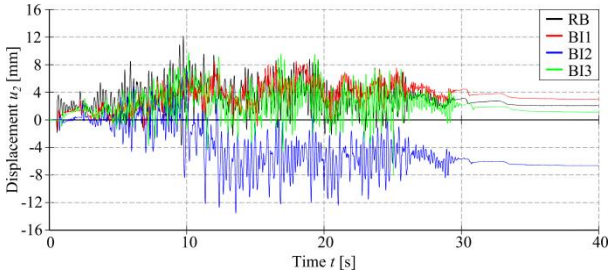


Fig. 14 Horizontal displacement of the mass centre at the column top $u_2$ of model $M_1$ for accelerogram AA

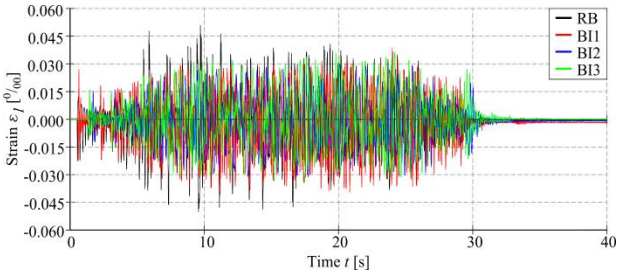


Fig. 15 Vertical strain on the right bottom side of the steel column $\varepsilon_1$ of model $M_1$ for accelerogram AA

### *6.2 Result of successively increasing PGA until model collapse*

For the most unfavourable excitation, i.e. accelerogram AA, the models were tested by successively increasing the PGA until the model collapsed. The $a_{g,\,max}$ acceleration at which the model collapsed is shown in Table 2.

Table 2 $a_{g,\,max}$ (PGA) for AA accelerogram at which the model collapsed

| Model | Foundation support case | | | |
|---|---|---|---|---|
| | RB | BI1 | BI2 | BI3 |
| $M_1$ | 0.40 | 0.55 | 0.65 | 0.60 |
| $M_2$ | 0.35 | 0.45 | 0.50 | 0.50 |
| $M_3$ | 0.40 | 0.45 | 0.50 | 0.45 |
| $M_4$ | 0.30 | 0.30 | 0.30 | 0.30 |

When evaluating the accuracy of the results presented, it is noteworthy that the acceleration increment was 0.05 g. The ratio of acceleration $a_{g,\,max}$ at which the model collapsed on seismic isolations BI2 and BI3 to acceleration $a_{g,\,max}$ at which the model collapsed on seismic isolation BI1, i.e. the ratio of $a_{g,\,max}$ (BI2, BI3)/$a_{g,\,max}$ (BI1) is presented in Fig. 16.

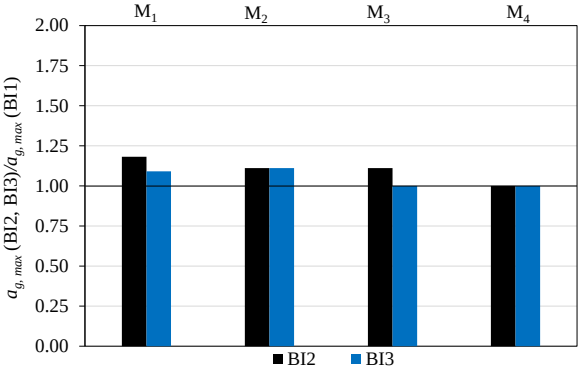


Fig. 16 Relationship of $a_{g,\,max}$ (BI2, BI3)/$a_{g,\,max}$ (BI1) at which the model collapsed

The $a_{g,\,max}$ ratio for substrates RB: BI1: BI2: BI3 at the collapse of model $M_1$ was 1:1.38:1.62:1.5, and at the collapse of model $M_2$ 1:1.29:1.43:1.43.

The $a_{g,\,max}$ ratio for substrates BI2:BI3 at the collapse of model $M_1$ was 1:0.92, and at the collapse of model $M_2$ 1:1.

The high efficiency of all considered seismic isolations in relation to the rigid base support (classical foundation), especially of composite seismic isolations BI2 and BI3, was evident. Seismic isolation BI2 seismic isolation was slightly more favourable than seismic isolation BI3.

## 7. Conclusion

The results of the current study are as follows:

*(i) Tests with the strain of the model remaining in the elastic region*

The efficiency of the considered seismic isolations BI1, BI2, and BI3 with respect to the rigid base RB depended significantly on the stiffness of the model and the type of applied accelerogram. For the extremely stiff $M_1$ and stiff $M_2$ models, the efficiencies of isolations BI1, BI2, and BI3 for all applied excitations were significant, especially those of composite seismic isolations BI2 and BI3, i.e. isolations BI2 and BI3 showed much higher efficiency than the isolation BI1. Meanwhile, BI2, the composite seismic isolation comprising stone pebbles with geogrid on the layer top, was the most effective isolation. This isolation is rational and easy to implement.

The average seismic isolation efficiency coefficient for models $M_1$ and $M_2$, for which this isolation is applicable, was as follows:

- BI2 compared to RB: 0.75;
- BI2 compared to BI1: 0.90;
- BI2 compared to BI3: 0.92.

The displacements of models $M_1$ and $M_2$ on isolation BI1, and in particular on isolations BI2 and BI3, were larger than their displacements on the rigid base RB, which was unfavourable. However, these displacements were considered acceptable with respect to the height of the models considered. It should be emphasised that the horizontal displacements of the model were primarily due to the slip of the model foundation along the seismic isolation top.

The application of seismic isolation BI1, and in particular isolations BI2 and BI3 on medium-stiff ($M_3$) and especially on soft ($M_4$) building models was inefficient. In many cases, especially when the model was based on isolations BI2 and BI3, higher inertial forces and strains occurred in the model than in the case without seismic isolation (RB case).

*(ii) Tests with successively increasing PGA until model collapse*

The ratio of acceleration $a_{g,\,max}$ at which the model collapsed on a rigid base RB to acceleration $a_{g,\,max}$ at which the model collapsed on seismic isolations BI1, BI2, and BI3 (the $a_{g,\,max}$ ratio for substrates RB:BI1:BI2:BI3) was 1.00:1.38:1.62:1.5. For model $M_2$, the ratio was 1:1.29:1.43:1.43. In this test, isolation BI2 proved to be the most effective.

In general, composite seismic isolation BI2 (0.3-m-thick stone pebble layer with geogrid at the layer top) can significantly reduce the inertial forces and strains/stresses of extremely stiff and stiff buildings, compared with classical

foundations without seismic isolation. Tested on four different earthquake accelerograms, this reduction was 25%. However, for the practical application of this seismic isolation, which is highly promising for low-rise rigid buildings resting on solid ground, broader studies on more realistic building models are required.

## Acknowledgments

This work has been fully supported by the Croatian Science Foundation under the project *"Seismic base isolation of a building by using natural materials - shake table testing and numerical modelling*" [IP-06-2016-5325]. The work of doctoral student Ivan Banović has been fully supported by the *"Young researchers' career development project – training of doctoral students"* of the Croatian Science Foundation funded by the European Union from the European Social Fund. The authors are grateful for the support.

## References

Ambraseys, N., Smit, P., Sigbjornsson, R., Suhadolc, P., and Margaris, M. (2001), EVR1-CT-1999-40008, European Commission, Directorate-General XII, Environmental and Climate Programme, Brussels, Belgium

Anastasopoulos, I., Kourkoulis, R., Gelagoti, F., and Papadopoulos, E. (2012b), "Rocking response of SDOF systems on shallow improved sand: An experimental study", *Soil Dynamics and Earthquake Engineering*, **40**, 15-33. https://doi.org/10.1016/j.soildyn.2012.04.006.

Anastasopoulos, I., Loli, M., Georgarakos, T., and Drosos, V. (2012a), "Shaking table testing of rocking-isolated bridge pier on sand", *Journal of Earthquake Engineering*, **17**(1), 1–32. https://doi.org/10.1080/13632469.2012.705225

Arab, M.G., and Kavazanjian Jr., E. (2010), "Time-domain analysis of frictional base isolation using geosynthetics", In: Proc. of 9th International Conference on Geosynthetics, 2, 695–698.

Azinović, B., Kilar, V., and Koren, D. (2014), "The seismic response of low-energy buildings founded on a thermal insulation layer–a parametric study", *Engineering Structures*, **81**, 398-411. https://doi.org/10.1016/j.engstruct.2014.10.015

Azinović, B., Kilar, V., and Koren, D. (2016), "Energy-efficient solution for the foundation of passive houses in earthquake-prone regions", *Engineering Structures*, **112**, 133-145. https://doi.org/10.1016/j.engstruct.2016.01.015

Azzam, W., Ayeldeen, M., and El Siragy, M. (2018), "Improving the structural stability during earthquakes using in-filled trench with EPS geofoam—numerical study", *Arabian Journal of Geosciences*, **11**(14), 395. https://doi.org/10.1007/s12517-018-3739-4

Bandyopadhyay, S., Sengupta, A., and Reddy, G. R. (2015), "Performance of sand and shredded rubber tire mixture as a natural base isolator for earthquake protection", *Earthquake Engineering and Engineering Vibration*, **14**(4), 683–693. https://doi.org/10.1007/s11803-015-0053-y

Banović, I., Radnić, J., and Grgić, N. (2018a), "Shake table study on the efficiency of seismic base isolation using natural stone pebbles", *Advances in Materials Science and Engineering*, Article ID 1012527, 20 pages https://doi.org/10.1155/2018/1012527

Banović, I., Radnić, J., and Grgić, N. (2019), "Geotechnical seismic isolation system based on sliding mechanism using stone pebble layer: shake-table experiments", *Shock and Vibration*, Article ID 9346232, 26 pages https://doi.org/10.1155/2019/9346232

Banović, I., Radnić, J., and Grgić, N. (2020a), "Effect of structural stiffness on the efficiency of seismic base isolation using layers of stone pebbles", *Ingegneria Sismica*, 37(2), 66-91.

Banović, I., Radnić, J., and Grgić, N. (2020b), "Foundation size effect on the efficiency of seismic base isolation using a layer of stone pebbles", *Earthquakes and Structures*, 19(2), 103-117. https://dx.doi.org/10.12989/eas.2020.19.2.103

Banović, I., Radnić, J., and Grgić, N. (2020c), "Effectiveness of several low-cost composite seismic base isolations: A shake table study"

Banović, I., Radnić, J., Grgić, N., and Matešan, D. (2018b), "The use of limestone sand for the seismic base isolation of structures", *Advances in Civil Engineering*, Article ID 9734283, 12 pages https://doi.org/10.1155/2018/9734283

Briançon, L., Girard, H., and Gourc, J. P. (2011), "A new procedure for measuring geosynthetic friction with an inclined plane", *Geotextiles and Geomembranes*, **29**(5), 472–482. https://doi.org/10.1016/j.geotexmem.2011.04.002

Briançon, L., Girard, H., and Poulain, D. (2002), "Slope stability of lining systems - experimental modeling of friction at geosynthetic interfaces", *Geotextiles and Geomembranes*, **20**(3), 147–172. https://doi.org/10.1016/S0266-1144(02)00009-2

Brunet, S., de la Llera, J. C., and Kausel, E. (2016), "Non-linear modeling of seismic isolation systems made of recycled tire-rubber", *Soil Dynamics and Earthquake Engineering*, **85**, 134–145. https://doi.org/10.1016/j.soildyn.2016.03.019

Calvi, P. M., and Calvi, G. M. (2018), "Historical development of friction-based seismic isolation systems", *Soil Dynamics and Earthquake Engineering*, **106**, 14-30. https://doi.org/10.1016/j.soildyn.2017.12.003

Carbone, L., Gourc, J.P., Carrubba, P., Pavanello, P., and Moraci, N. (2015), "Dry friction behaviour of a geosynthetic interface using inclined plane and shaking table tests", *Geotextiles and Geomembranes*, **43**(4), 293–306. https://doi.org/10.1016/j.geotexmem.2015.05.002

Carbone, L., Pavanello, P., Carrubba, P., Gourc, J.P., Moraci, N., Briançon, L., and Scotto, M. (2014), "Geosynthetic interface shear strength under static and seismic loading conditions", In: Proc. of 10th International Conference on Geosynthetics, Berlin, Germany, 21–25 September 2014.

Cardile, G., Gioffrè, D., Moraci, N., and Calvarano, L. S. (2017), "Modelling interference between the geogrid bearing members under pullout loading conditions", *Geotextiles and Geomembranes*, **45**, 169–177. https://doi.org/10.1016/j.geotexmem.2017.01.008

Cardile, G., Moraci, N., and Calvarano, L. S. (2016), "Geogrid pullout behaviour according to the experimental evaluation of the active length", *Geosynthetics International*, **23** (3), 194–205. https://doi.org/10.1680/jgein.15.00042

Carpani, B. (2014), "A survey of ancient geotechnical engineering techniques in sub foundation preparation", in 9th International Conference on Structural Analysis of Historical Constructions, Mexico City, Mexico

Carpani, B. (2017), "Base isolation from a historical perspective", in 16th World Conference on Earthquake, Paper N° 4934, Santiago, Chile

Chen, X., Xia, X., Zhang, X., and Gao, J. (2020), "Seismic performance and design of bridge piers with rocking isolation", *Structural Engineering and Mechanics*, **73**(4), 447-454. https://doi.org/10.12989/sem.2020.73.4.447

Chung, Y. L., Du, L. J., and Pan, H. H. (2019), "Performance evaluation of a rocking steel column base equipped with asymmetrical resistance friction damper", *Earthquakes and Structures*, **17**(1), 49-61.

https://doi.org/10.12989/eas.2019.17.1.049

De, A., and Zimmie, T.F. (1998), "Estimation of dynamic interfacial properties of geosynthetics", *Geosynthetics International*, **5**(1–2), 17–39. https://doi.org/10.1680/gein.5.0112

Doudoumis, I., Papadopoulos, P., and Papaliangas, T. (2002), "Low-cost base isolation system on artificial soil layers with low shearing resistance", in Proceedings of the 12th European Conference on Earthquake Engineering, London, UK

Eurocode (2004) EN 1998-1:2004 Eurocode 8: Design of structures for earthquake resistance-Part 1: general rules, seismic actions and rules for buildings, European Committee for Standardization (CEN), Brussels, Belgium

Feng, R., Chen, Y., and Cui, G. (2018), "Dynamic response of post-tensioned rocking wall-moment frames under near-fault ground excitation", *Earthquakes and Structures*, **15**(3), 243-251 https://doi.org/10.12989/eas.2018.15.3.243

Forcellini, D. (2017), "Assessment on geotechnical seismic isolation (GSI) on bridge configurations", *Innovative Infrastructure Solutions*, 2(1), 9 pages https://doi.org/10.1007/s41062-017-0057-8

Hadad, H. A, Calabrese, A., Strano, S., and Serino, G. (2017), "A base isolation system for developing countries using discarded tyres filled with elastomeric recycled materials", *Journal of Earthquake Engineering*, **21**(2), 246-266. https://doi.org/10.1080/13632469.2016.1172371

Hernández, E., Palermo, A., Granello, G., Chiaro, G., Banasiak, L. (2020), "Eco-rubber seismic-isolation foundation systems: a sustainable solution for the New Zealand context", *Structural Engineering International*, 1-9. https://doi.org/10.1080/10168664.2019.1702487

http://gelfi.unibs.it/software/simqke/simqke_gr.htm

Hung, H. H., Liu, K. Y., and Chang, K. C. (2014), "Rocking behavior of bridge piers with spread footings under cyclic loading and earthquake excitation", *Earthquakes and Structures*, **7**, 1001-1024. https://doi.org/10.12989/eas.2014.7.6.1001

Kalpakcı, V., Bonab, A. T., Özkan, M. Y., and Gülerce, Z. (2018), "Experimental evaluation of geomembrane/geotextile interface as base isolating system", *Geosynthetics International*, **25**(1), 1-11. https://doi.org/10.1680/jgein.17.00025

Karatzia, X., Mylonakis, G., and Bouckovalas, G. (2019), "Seismic Isolation of Surface Foundations Exploiting the Properties of Natural Liquefiable Soil", *Soil Dynamics and Earthquake Engineering*, **121**, 233-251., https://doi.org/10.1016/j.soildyn.2019.03.009

Karatzia, X., and Mylonakis, G. (2017), "Geotechnical seismic isolation using eps geofoam around piles", in 6th International Conference on Computational Methods in Structural Dynamics and Earthquake Engineering, Rhodes Island, Greece

Kelly, J. (1996a), "Aseismic base isolation: review and bibliography", *Soil Dynamics and Earthquake Engineering*, **5**(4), 202-216. https://doi.org/10.1016/0267-7261(86)90006-0

Kelly, J. (1996b), "Natural Rubber Isolation Systems for Earthquake Protection of Low-Cost Buildings," Report No. UCB/EERC-95-12, Earthquake Engineering Research Center, University of California, Berkeley, California.

Kelly, J., and Taniwangsa, W. (1996), "Experimental and Analytical Studies of Base Isolation Applications for Low-Cost Housing", Report No. UCB/EERC-96-04, Earthquake Engineering Research Center, University of California, Berkeley, California.

Koren, D., and Kilar, V. (2016), „Seismic vulnerability of reinforced concrete building structures founded on an XPS layer", *Earthquakes and Structures*, **10**(4), 939-963. https://doi.org/10.12989/eas.2016.10.4.939

Kulukčija, S., and Humo, M. (2009), "Survey of historic foundation engineering", Baština, Sarajevo

Kulukčija, S., Humo, M., Mandžić, E., Mandžić, K., and Selimović, M. (2009), "Existing historical foundation system of two old bridges from the Ottoman period in Bosnia and Herzegovina", in Third International Congress on Construction History, Cottbus, Germany

Makris, N. (2014), "A half-century of rocking isolation", *Earthquakes and Structures*, **7**(6), 1187-1221. https://doi.org/10.12989/eas.2014.7.6.1187

Makris, N. (2018), "Seismic isolation: early history," *Earthquake Engineering and Structural Dynamics*, **48**(2), 269-283, https://doi.org/10.1002/eqe.3124

Masoud, S. A., Seyed, M. M. M. H., and Alireza,J. (2018), "Effect of soil reinforcement on rocking isolation potential of high-rise bridge foundations", *Soil Dynamics and Earthquake Engineering*, **115**, 142-155. https://doi.org/10.1016/j.soildyn.2018.07.035

Mavronicola, E., Komodromos, P., and Charmpis, D. C. (2010), "Numerical investigation of potential usage of rubber–soil mixtures as a distributed seismic isolation approach", in Proceedings of the 10th International Conference on Computational Structures Technology, Valencia, Spain

Murillo, C., Thorel, L., and Caicedo, B. (2009), "Ground vibration isolation with geofoam barriers: centrifuge modelling", *Geotextiles and Geomembranes*, **27**(6), 423-434. https://doi.org/10.1016/j.geotexmem.2009.03.006

Nanda, R. P., Agarwal, P., and Shrikhande, M. (2012a), "Base isolation by geosynthetic for brick masonry buildings", *Journal of Vibration and Control*, **18**(6), 903–910. https://doi.org/10.1177/1077546311412411

Nanda, R.P., Shrikhande, M., and Agarwal, P. (2012b), "Effect of ground motion characteristics on the pure friction isolation system", *Earthquakes and Structures*, **3**(2), 169–180. https://doi.org/10.12989/eas.2012.3.2.169

Narjabadifam, P. and Chavoshi, M. (2018), "Modern aseismic applications of geosynthetic materials", *International Journal of Science and Engineering Applications*, **7**, 034, https://doi.org/038. 10.7753/IJSEA0703.1002.

Panjamani, A., Devarahalli Ramegowda, M., and Divyesh, R. (2015), "Low cost damping scheme for low to medium rise buildings using rubber soil mixtures", *Japanese Geotechnical Society Special Publication*, **3**(2), 24–28. https://doi.org/10.3208/jgssp.v03.i05

Patil, S. J., Reddy, G. R., Shivshankar, R., Babu, R., Jayalekshmi, B. R., and Kumar, B. (2016), "Seismic base isolation for structures using river sand", *Earthquakes and Structures*, 10(4), 829-847. https://doi.org/10.12989/eas.2016.10.4.829

Pavanello, P., and Carrubba, P. (2016), "Methodological aspects in the experimental measurement of the interface friction between geosynthetics", *Procedia Engineering*, **158**, 260–265. https://doi.org/10.1016/j.proeng.2016.08.439

Pavanello, P., Carrubba, P., and Moraci, N. (2018a), "The determination of interface friction by means of vibrating table tests", *Geotextiles and Geomembranes*, **46**(6), 830-835. https://doi.org/10.1016/j.geotexmem.2018.06.006.

Pavanello, P., Carrubba, P., and Moraci, N. (2018b), "Dynamic friction and the seismic performance of geosynthetic interfaces", *Geotextiles and Geomembranes*, **46**(6), 715-725. https://doi.org/10.1016/j.geotexmem.2018.06.005

Pecker, A. (2003), "Aseismic foundation design process, lessons learned from two major projects: the Vasco de Gama and the Rion Antirion bridges", in Proceedings of the ACI International Conference on Seismic Bridge Design and Retrofit, La Jolla, CA, USA

Pecker, A., Prevost, J. H., and Dormieux, L. (2001), "Analysis of pore pressure generation and dissipation in cohesionless materials during seismic loading", *Journal of Earthquake Engineering*, **5**(4), 441-464.

https://doi.org/10.1080/13632460109350401

Pitilakis, K., Karapetrou, S., and Tsagdi, K. (2015), "Numerical investigation of the seismic response of RC buildings on soil replaced with rubber–sand mixtures", *Soil Dynamics and Earthquake Engineering*, **79**, 237–252. https://doi.org/10.1016/j.soildyn.2015.09.018

Przewłócki, J., Dardzinska, I., and Swinianski, J. (2005), "Review of historical buildings' foundations", *Géotechnique*, **55**, 363-372. https://doi.org/10.1680/geot.55.5.363.66017

Radnić, J., Grgić, N., Matešan, D., and Baloević, G. (2015), "Shake table testing of reinforced concrete columns with different layout size of foundation", *Materialwissenschaft und Werkstofftechnik*, **46**(4-5), 348–367. https://doi.org/10.1002/mawe.201500410

Ravi, K. M., and Gourav, G. (2018), "Sustainable application of waste tire chips and geogrid for improving load carrying capacity of granular soils", *Journal of Cleaner Production*, **200**, 542-551. https://doi.org/10.1016/j.jclepro.2018.07.287

Sorrentino, L., Masiani, R., and Decanini, L. D. (2006), "Overturning of rocking rigid bodies under transient ground motions", *Structural Engineering and Mechanics*, **22**(3), 293-310. https://doi.org/10.12989/sem.2006.22.3.293

Sorrentino, L., Masiani, R., and Griffith, M. C. (2008), "The vertical spanning strip wall as a coupled rocking rigid body assembly", *Structural Engineering and Mechanics*, **29**(4), 433-453. https://doi.org/10.12989/sem.2008.29.4.433

Steenfelt, J. S, Foged, B., and Augustesen, A. H. (2015), "Izmit Bay bridge-geotechnical challenges and innovative solutions", *International Journal of Bridge Engineering (IJBE)*, **3**(3), 53–68.

Tehrani, F. M. and Hasani, A. (1996), "Behaviour of Iranian low rise buildings on sliding base to earthquake excitation", in Proceedings of the 11th World Conference on Earthquake Engineering, Paper 1433, Acapulco, Mexico

Tsang, H. H. (2008), "Seismic isolation by rubber-soil mixtures for developing countries", *Earthquake Engineering and Structural Dynamics*, **37**(2), 283–303, https://doi.org/10.1002/eqe.756

Tsang, H. H. (2009), "Geotechnical seismic isolation", Earthquake engineering: new research, New York, U.S. Nova Science Publishers Inc., 55–87.

Tsang, H. H., and Pitilakis, K. (2019), "Mechanism of geotechnical seismic isolation system: analytical modeling", *Soil Dynamics and Earthquake Engineering*, **122**, 171-184, https://doi.org/10.1016/j.soildyn.2019.03.037

Tsang, H. H., Lo, S. H., Xu, X., and Neaz Sheikh, M. (2012), "Seismic isolation for low-to-medium-rise buildings using granulated rubber-soil mixtures: numerical study", *Earthquake Engineering and Structural Dynamics*, **41**(14), 2009–2024, https://doi.org/10.1002/eqe.2171

Tsatsis, A. and Anastasopoulos, I. (2015), "Performance of rocking systems on shallow improved sand: shaking table testing", *Frontiers in Built Environment*, **1**, 1-9, https://doi.org/10.3389/fbuil.2015.00009

Tsiavos, A., Alexander, N. A., and Sextos, A. (2019), "Numerical investigation of the sliding response of flexible structures founded on a deformable granular layer", in 2nd International Conference on Earthquake Engineering and Post Disaster Reconstruction Planning, Bhaktapur, Nepal

Tsiavos, A., Alexander, N. A., Diambra, A., Ibraim, E., Vardanega, P. J., Gonzalez-Buelga, A., and Sextos A. (2019), "A sand-rubber deformable granular layer as a low-cost seismic isolation strategy in developing countries: experimental investigation", *Soil Dynamics and Earthquake Engineering*, **125**, https://doi.org/10.1016/j.soildyn.2019.105731

Wang, J., He, J. X., Yang, Q. S., and Yang, N. (2018), "Study on mechanical behaviors of column foot joint in traditional timber structure", *Structural Engineering and Mechanics*, **66**(1), 1-14. https://doi.org/10.12989/sem.2018.66.1.001

Warn, G. P. and Ryan, K. L. (2012), "A review of seismic isolation for buildings: historical development and research needs", *Buildings*, **2**(3), 300-325, https://doi.org/10.3390/buildings2030300

Wasti, Y., and Özdüzgün, Z. B. (2001), "Geomembrane-geotextile interface shear properties as determined by inclined board and direct shear box tests", *Geotextiles and Geomembranes*, **19**, 45–57. https://doi.org/10.1016/S0266-1144(00)00002-9

Xiong, W. and Li, Y. (2013), "Seismic isolation using granulated tire-soil mixtures for less-developed regions: experimental validation", *Earthquake Engineering and Structural Dynamics*, **42**(14), 2187-2193. https://doi.org/10.1002/eqe.2315

Xiong, W., Yan, M. R., and Li, Y. Z. (2014), "Geotechnical seismic isolation system - further experimental study", *Applied Mechanics and Materials*, **580-583**, 1490-1493. https://doi.org/10.4028/www.scientific.net/AMM.580-583.1490

Xu, R. and Fatahi, B. (2018), "Influence of geotextile arrangement on seismic performance of mid-rise buildings subjected to MCE shaking“, *Geotextiles and Geomembranes*, **46**(4), 511-528. https://doi.org/10.1016/j.geotexmem.2018.04.004

Yegian, M. K., and Kadakal, U. (2004), "Foundation isolation for seismic protection using a smooth synthetic liner", *Journal of Geotechnical and Geoenvironmental Engineering*, **130**(11), 1121–1130. https://doi.org/10.1061/(ASCE)10900241(2004)130:11(1121)

Yegian, M. K., and Catan, M. (2004), "Soil isolation for seismic protection using a smooth synthetic liner", *Journal of Geotechnical & Geoenvironmental Engineering*, **130**(11), 1131–1139, https://doi.org/10.1061/(ASCE)10900241(2004)130:11(1131)

Yegian, M. K., and Kadakal, U. (1998), "Geosynthetic interface behavior under dynamic loading", *Geosynthetics International*, **5**(1–2), 1–16, https://doi.org/10.1680/gein.5.0111

Yegian, M. K., and Lahlaf, A. M. (1992a), "Geomembranes as base isolation", *Geotechnical Fabrics Report*, **10**(6), 17-21.

Yegian, M. K., and Lahlaf, A.M. (1992b), "Dynamic interface shear strength properties of geomembranes and geotextiles", *International Journal of Geotechnical Engineering*, **118**(5), 760–779. https://doi.org/10.1061/(ASCE)07339410(1992)118:5(760)

Zhao, X., Zhang, Q., Zhang, Q., and He, J. (2016), "Numerical study on seismic isolation effect of gravel cushion", in Proceedings of the 7th International Conference on Discrete Element Methods, **188**, 1055-1063, Dalian, China

Ziegler, M. (2017), "Application of geogrid reinforced constructions: history, recent and future developments", Procedia Engineering, 172, 42-51. https://doi.org/10.1016/J.PROENG.2017.02

# PAPER VIII

ingegneria sismica
International Journal of Earthquake Engineering
Under revision

# NUMERICAL MODEL FOR DYNAMIC ANALYSIS OF STRUCTURES WITH SEISMIC BASE ISOLATION USING A LAYER OF STONE PEBBLES

*Ivan Banović*[1], *Jure Radnić*[1], *Nikola Grgić*[1]

[1]University of Split, Faculty of Civil Engineering, Architecture and Geodesy, Split, Croatia

SUMMARY: *This paper presents a developed numerical model for the dynamic analysis of planar structures with seismic base isolation using a layer of stone pebbles. Following a brief presentation of the previously developed numerical model for structural analysis, the developed constitutive model for the stone pebble layer and the constitutive model for simulating the foundation-isolation layer coupling surface are presented. The simple model is based on a relatively small number of parameters, some of which were determined experimentally. The numerical model was verified by simulating the performed shake-table tests of simple structural models based on an aseismic layer of stone pebbles, and good agreement between the experimental and numerical results was observed. Finally, further verification and improvement of the presented numerical model are outlined.*

KEYWORDS: *seismic base isolation, stone pebble layer, numerical model*

## 1 Introduction

An earthquake is one of the deadliest natural disasters, whose time and place of occurrence cannot be predicted. Developing countries are more vulnerable to natural disasters because people live in areas with high risk of natural disasters (unsafe urban areas). Further, the poor construction of buildings makes them prone to damage in the event of a disaster [Zorn, 2017]. In particular, approximately 60,000 people are killed annually in earthquakes worldwide, with approximately 90 % of the deaths occurring in developing countries [OECD, 2008]. For the last 60 years, the application of seismic isolation for earthquake hazard migration has been intensively investigated. Various types of base isolators such as elastomeric bearings, lead rubber bearings, rubber bearings, friction pendulum bearings, and dampers [Kelly, 1996] [Naeim and Kelly, 1999] [Lomiento *et al.*, 2013] [Calvi *et al.*, 2016] [Avossa and Pianese, 2017] [Castaldo and Ripani, 2017] [Petrone *et al.*, 2017] [De Domenico, 2019] have been investigated in detail, and have begun to be used regularly in developed countries. In addition, innovative energy dissipation devices based on lattice metamaterials have been proposed [Amendola *et al.*, 2016a] [Amendola *et al.*, 2016b] [Fabbrocino *et al.*, 2016] [Titirla *et al.*, 2017] [Fraternali *et al.*, 2018]. Owing to conventional base isolator limitations (significant installation cost, highly engineered product, and maintenance during use), their application is limited in low-income regions [Tsiavos *et al.*, 2019a]. Therefore, an alternative, simple, low-cost, environmentally friendly, and efficient system for low-income regions is needed [Banović *et al.* 2020a]. One such solution is a seismic base isolation with a unique, engineered layer below the building foundation for seismic hazard mitigation, known as the

Corresponding author: Ivan Banović, University of Split, Faculty of Civil Engineering, Architecture and Geodesy, Croatia.
Email: ivan.banovic@gradst.hr

geotechnical seismic isolation (GSI) system [Tsang, 2008]. This solution is particularly relevant for developing countries due to its viability and simplicity, with an acceptable reduction of seismic forces on the structure. Some important studies dealing with low-cost seismic isolation are briefly presented below.

The performance of sand and gravel layers for seismic base isolation was tested using shake-table experiments [Teherani and Hasani, 1996] [Anastasopoulos *et al.*, 2012a] [Anastasopoulos *et al.*, 2012b] [Radnić *et. al.*, 2015] [Patil *et al.*, 2016] [Banović *et al.*, 2018a] and numerical studies [Zhao *et al.*, 2016]. More recently, Tsiavos *et al.* [2020a] conducted a large-scale experimental study exploring the beneficial effect of the encapsulation of sand grains between two PVC surfaces on the initiation of sliding and the dissipation of seismic energy between the surfaces. Furthermore, a gravel cushion below a high-rise bridge pier was applied [Pecker *et al.*, 2001] [Pecker *et al.*, 2003] [Steenfelt *et al.*, 2015], with adopted rocking motion as a seismic hazard mitigation technique [Sorrentino *et al.*, 2006] [Sorrentino *et al.*, 2008] [Makris, 2014] [Makris, 2018] [Chung *et al.*, 2019] [Chen *et al.*, 2020].

Tsang [2008] conducted a numerical study on the use of a rubber-soil mixture (RSM) as a low-cost base isolation system, and named it the GSI system. Following this work, numerous researchers have examined the behavior and performance of RSM through several numerical studies [Tsang, 2009] [Mavronicola *et al.*, 2010] [Tsang *et al.*, 2012] [Panjamani *et al.*, 2015] [Bandyopadhyay *et al.*, 2015] [Pitilakis *et al.*, 2015] [Brunet *et al.*, 2016] [Forcellini, 2017] [Tsiavos *et al.*, 2019b] [Tsang and Pitilakis, 2019] [Forcellini, 2020] [Pistolas *et al.*, 2020] [Dhanya *et al.*, 2020] [Hernández *et al.*, 2020] and experimental studies [Xiong and Li, 2013] [Xiong *et al.*, 2014] [Dhanya *et al.*, 2019] [Tsiavos *et al.*, 2019a] [Tsiavos *et al.*, 2020b]. For example, Tsiavos *et al.* [2019a] experimentally tested a sliding layer consisting of a deformable sand-rubber granular mixture as a seismic isolation strategy for low-rise, small-footprint buildings in developing countries. Moreover, Tsang and Pitilakis [2019] developed a simple and efficient lumped-parameter analytical model for analyzing the dynamic soil-foundation-structure interaction of the GSI system.

Kuvat and Sadoglu [2020] proposed asphalt–sand mixtures as an alternative GSI material. The dynamic properties of the geomaterial were investigated by cyclic triaxial experiments. Hadad *et al.* [2017] reported on the seismic performance of kart tires filled with elastomeric recycled materials as base isolators for application in developing countries. The proposed seismic isolators were analyzed via horizontal tests with static and dynamic loadings to determine the horizontal stiffness, hysteretic behavior, and long-term performance. Dhanya *et al.* [2019] proposed the use of geogrid reinforcement to improve the bearing capacity, settlement, and rotational aspects of a shallow foundation resting on a layer of scrap tire–sand mixture under static loading conditions. They reported that the bearing capacity of the layer can be increased up to three times by providing double-layered geogrid reinforcements with a substantial reduction in settlement.

A smooth high-density polyethylene geomembrane as the base isolation material in earthquake hazard mitigation was tested by Yegian and Lahlaf [1992]. Following this work, Yegian and Kadakal [2004] tested various smooth synthetic materials that can serve as seismic protection by absorbing energy through sliding. In particular, Kalpakci *et al.* [2018] tested a UHMWPE geomembrane, based on the study of Yegian and Kadakal [2004]. An artificial soil layer with low shearing resistance, which allows the slipping of the building under the action of strong seismic motions was proposed by Doudoumis *et al.* [2002]. Other interesting applications consist of soil replacement by the thermal insulation layer and

geofoam [Murillo *et al.*, 2009] [Azinović *et al.*, 2014] [Azinović *et al.*, 2016] [Koren and Kilar, 2016] [Karatzia *et al.*, 2017] [Azzam *et al.*, 2018].

This paper's authors published several papers [Banović *et al.*, 2018b] [Banović *et al.*, 2019] [Banović *et al.*, 2020a] [Banović *et al.*, 2020b] on the possibility/efficiency of applying a layer of natural stone pebbles under the building foundation for seismic base isolation. First, they reported the results of a preliminary shake-table study [Banović *et al.*, 2018b], where models of stiff and medium-stiff buildings were exposed to four different seismic excitations. The results of the study showed that a layer of pebbles, compared to the rigid base, can significantly reduce the peak acceleration and strains/stresses of the model, with acceptable displacements. Following this work, they started an extensive shake-table campaign to investigate the possibility of using a layer of stone pebbles for the seismic isolation of low-rise buildings in developing countries.

To determine the optimal pebble layer, Banović *et al.* [2019] conducted a shake-table study on the effects of several layer parameters (the layer thickness, the fraction of pebbles, the pebble compaction, the pebble moisture, the vertical contact stress below the foundation, and the effect of repeated excitations) on the layer aseismic efficiency on the sliding rigid block. The following characteristics of the pebble layer were optimal for practical applications: pebble fraction $\Phi_b$ = 16-32 mm, pebble layer compaction $MS$ = 30 MPa, and pebble moisture $h_m$ = 10 %. Furthermore, they tested the efficiency of the adopted layer on four models with different stiffnesses [Banović *et al.*, 2020a] and foundation sizes [Banović *et al.*, 2020b], under four different earthquake accelerograms. First, they reported that the efficiency of the considered seismic isolation system decreased with a decrease in model stiffness and that this concept shows great potential for increasing the structural seismic resistance. In addition, compared to the smaller foundation, the larger foundation resulted in a reduced rocking effect, higher earthquake forces, and lower bearing capacity of the tested models, with respectable efficiency (reduced strain/stress, displacement, and increase of the ultimate bearing capacity of the model) for the considered seismic base isolation compared to the foundation on a rigid base.

Although much effort has been invested in recent years in the development of suitable seismic base isolation in developing countries, not enough has been done to develop suitable numerical models to simulate seismic isolation. Some numerical models, whether presented as part of experimental studies or independently, can be found in [Mavronicola *et al.*, 2010] [Tsang, 2012] [Pitilakis *et al.*, 2015] [Brunet *et al.*, 2016] [Zhao *et al.*, 2016].

This paper presents and verifies the developed numerical model for dynamic analysis of planar structures with seismic base isolation using a layer of stone pebbles. The model is an extension of the previously developed numerical model for the dynamic analysis of 2D structures without seismic isolation [Radnić *et al.*, 2011] [Radnić *et al.*, 2012] [Baloević *et al.*, 2016a] [Baloević *et al.*, 2016b] [Radnić *et al.*, 2016] [Smilović Zulim *et al.*, 2018] [Baloević *et al.*, 2019] [Smilović Zulim *et al.*, 2019] [Smilović Zulim and Radnić, 2020]. The model is extended with a constitutive material model for simulating the behavior of a stone pebble layer during an earthquake, and modeling the foundation-seismic isolation interaction. The finite element method (FEM) was used for spatial discretization of the structure and isolation layer. In addition to simulating the most important nonlinear effects of individual construction materials (concrete, reinforcement, structural steel, masonry, and pebbles), it is possible to simulate the effect of large displacements and construction of the structure in

stages. The numerical model is simple, based on a small number of parameters, and is primarily intended for practical applications.
The model is verified using shake-table tests of seismically isolated simple models [Banović *et al.*, 2020b] and can be considered reliable. However, further verification is needed.
Section 2 presents a brief overview of the stress state at the top of the aseismic pebble layer below the foundation. The numerical model for the dynamic analysis of 2D structures and the developed constitutive model for the simulation of the aseismic layer are presented in Section 3. Section 4 presents the results of the experimental tests conducted to determine the basic parameters of the constitutive model of the pebble layer. The verification of the presented numerical model using shake-table tests of simple structural models on the aseismic layer is presented in Section 5. Finally, the most important conclusions of the study are presented in Section 6.

## 2 Mechanical properties of the aseismic layer and stress state at the layer top

Full-scale buildings are most often based on a foundation slab, or the walls and columns are based on individual foundations (so-called strip footing or column footing). Accordingly, the aseismic layer can be constructed on the entire ground floor of the building or below its individual vertical load-bearing elements. The distribution scheme of vertical normal stress $\sigma_v$ and shear stress $\tau$ below the foundation slab or individual foundation on the seismic layer in the planar model is shown in Figure 1. In general, the vertical force $N$, bending moment $M$, and shear force $Q$ can be transmitted at the foundation-substrate contact. The distribution of normal and shear stress under the foundation strongly depends on the eccentricity of the vertical force $e$ in relation to the middle of the foundation of length $B$. If $e = 0$, then the foundation is loaded with a centric compressive force $N$, which causes vertical compressive stress at the top of the aseismic layer $\sigma_{v,0}$. As $M$ increases, $e$ increases, and the distribution of normal $\sigma_v$ and shear stress $\tau$ below the foundation changes. The vertical tensile stress as well as shear stress, cannot be transmitted in the part where the foundation is lifted from the substrate. The assumed linear $\sigma_v$ distribution below the foundation is valid only for a rigid foundation with a soft isotropic substrate. The schematically shown $\tau$ stress distribution is in accordance with the possibility of shear transmission as a function of $\sigma_v$.
With the same axial force $N$, the maximum compressive stress below the foundation progressively increases with increasing $e$. For the same force $Q$, the maximum shear stress also increases progressively. External forces on the foundation are in balance with the resultant force from the stress beneath the foundation.
In earthquake action, the horizontal inertial forces resulting in the transverse force $Q$ can reach a high level relative to force $N$, depending on the intensity of the earthquake and the dynamic characteristics of the building. Thus, $M$, resulting from the action of $N$, can cause a very large $e$ so that $N$ and $Q$ can be transmitted over a very small length of the contact surface of the foundation with substrate $b$. In this part of the aseismic layer, very large, normal and shear stresses coexist. For $e = B/2$, the foundation overturns, and the stress in the substrate theoretically tends to infinity. During an earthquake, foundation rocking occurs, that is, alternating lifting and rotation of the foundation. As the depth of the aseismic layer increases, stresses $\sigma_v$ and $\tau$ decrease.
The seismic layer under the foundation can be affected simultaneously by large vertical compressive and horizontal shear stresses, which can increase significantly in relation to the

corresponding compressive and shear strengths of the seismic substrate. Therefore, it is necessary to know the actual stress–strain behavior of the aseismic layer and the bearing capacity at different $\sigma_v$–$\tau$ ratios.

Horizontal normal stress $\sigma_h$ can also occur in the shallow aseismic layer due to lateral soil resistance and friction between the pebbles and the bottom of the foundation. This stress is significantly smaller than the vertical compressive stress $\sigma_v$. The top of the seismic layer is at a very small depth from the top of the surrounding soil, and the lateral soil is regularly significantly deformable. Because of the relatively low level of $\sigma_h$ in relation to $\sigma_v$, its influence on the ultimate bearing capacity of the seismic substrate is ignored here, which is on the side of greater safety.

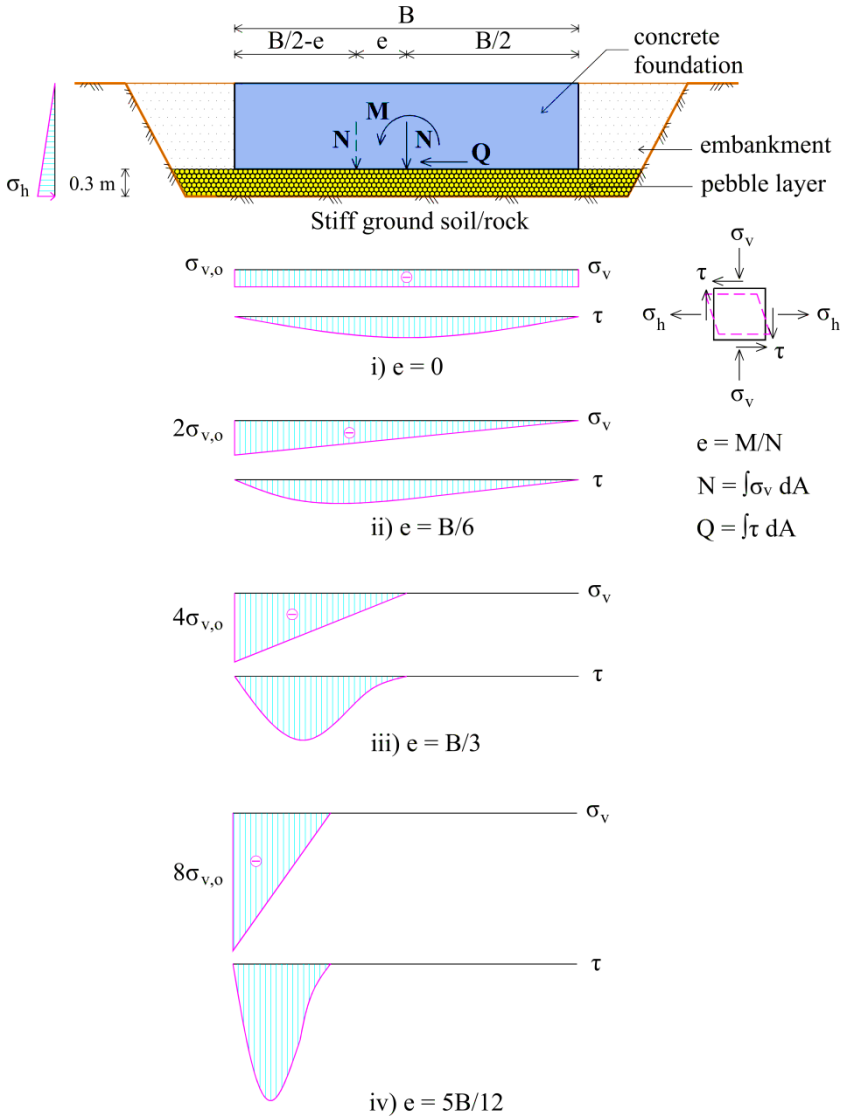


Figure 1 – *Scheme of vertical normal stress and shear-stress distribution below the foundation*

Stone pebbles of fractions 4-8 mm, 8-16 mm, and 16-32 mm [Banović *et al.*, 2019] were tested to determine the optimal layer properties. Based on the performed tests, a fraction of

16-32 mm and a layer thickness of 0.3 m were adopted as optimal (Figure 1). Pebbles are typically granular materials with very complex stress–strain behavior. The behavior of the layer significantly depends on the compaction, which changes under load as well as with the type of applied load. As there is no cohesion between the pebbles, even a well-compacted layer of pebbles has no tensile strength. The pebble layer is anisotropic, with pronounced differences in strength and stiffness/strain in the vertical and horizontal directions. Nevertheless, the strength and modulus of elasticity of the pebble layer in the vertical direction are usually higher than those in the horizontal direction. As with all granular materials, the vertical compressive strength of pebbles is highly dependent on the magnitude of the horizontal lateral pressure. Likewise, the shear strength of the pebble layer strongly depends on the magnitude of the compressive stress. If there is no vertical pressure, the horizontal shear strength of the pebbles disappears.

# 3 Numerical model

As mentioned in Section 1, the complete numerical model for the dynamic analysis of planar structures with seismic base isolation using a layer of pebbles is coupled with a previously developed and well-tested model for the analysis of structures without seismic isolation. Here, we developed a constitutive model for simulating the behavior of the pebble layer and foundation-pebble layer coupling surface. The most important characteristics of the basic numerical model and the adopted constitutive models for materials (reinforced concrete, steel, and masonry) are briefly described in Section 3.1. The developed constitutive model for stone pebbles is presented in Section 3.2, while the developed constitutive model for the simulation of the foundation-isolation layer coupling surface is presented in Section 3.3.

## 3.1 Numerical model for dynamic analysis of planar structures

FEM was used for spatial discretization of the structure and the isolation layer, assuming a state of plane stress. In addition, it is assumed that the observed system remains a continuum in all phases of deformation. Basic 8-node “serendipity” 2D elements were used to discretize the structure and isolation layer. Further, the reinforcement passing through a 2D element is simulated by a 1D element. Contact between basic elements can be simulated with 2D six-node contact finite elements of small thickness. In addition, a 1D bar (two-node) element can simulate possible reinforcement that passes through the contact surface. The sliding, separation, and penetration of the contact surface can be simulated with 2D contact elements. An updated Lagrangian formulation for geometric nonlinear analysis was used. The finite difference method is adopted for temporal discretization, with implicit, explicit, or implicit-explicit Newmark's algorithm, developed in iterative form by Hughes *et al.* [1979] is used for the solution of the dynamic equilibrium equation. Newton-Raphson initial and tangential stiffness methods can be used to solve the system of nonlinear equations. The convergence criterion of the iterative procedure is defined as a function of the increase in displacement increment.

The constitutive model for concrete simulates the nonlinear behavior of concrete in compression and tension. In compression, the elastoplastic behavior with linear unloading behavior is assumed. The yield criterion is defined as a function of stress and the crushing criterion as a function of strain. In tension, elastic behavior is assumed until the uniaxial tensile strength/strain of concrete is reached. Subsequently, the appearance of cracks was

assumed. The opening and closing of cracks, which were modeled as fixed and smeared, was simulated. Further, the tensile and shear stiffness of the cracked concrete were modeled. Within a 2D concrete element, the reinforcement is simulated with a 1D bar element. An elastoplastic stress–strain model of reinforcement steel was adopted, with a linear behavior during unloading. The slippage of reinforcement in relation to concrete has not been simulated.

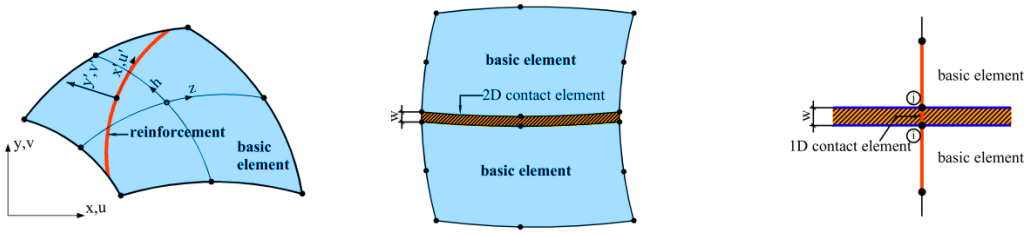


• Basic 2D element • 2D contact element • 1D contact element

Figure 2 - *Adopted finite elements for spatial discretization [Radnić et al., 2012]*

The constitutive model for masonry is analogous to that for concrete. A macro model of masonry was used, in which the complex interactive behavior of masonry elements and mortar in vertical and horizontal joints was modeled with a representative material of equivalent properties. This approach allows the use of larger finite elements, as well as simpler and faster analyses. It is possible to use an isotropic or orthotropic model of masonry behavior. The orthotropic behavior model allows analyses with different load-bearing and stiffness parameters in the vertical and horizontal directions. The effect of biaxial compressive stresses on the limit bearing capacity of masonry has not been modeled.
The behavior of structural steel is simulated by an elastoplastic constitutive model in compression and tension. The yield criterion is defined as a function of stress, and the failure criterion as a function of strain. Linear behavior was adopted during unloading.

## 3.2 The constitutive model for stone pebble layer

The complex behavior of this granular material is described by the simplified constitutive model shown in Figure 3, and is intended for engineering applications in practice. The pebble layer is modeled as a homogeneous orthotropic elastoplastic material, where the main directions of anisotropy are vertical ($v$) and horizontal ($h$).
Figure 3 presents the adopted relation between normal vertical and horizontal stresses and strains, separately for 1D-presentation and 2D-presentation. Symbols in the figure denote the following: $\sigma_v$, $\sigma_h$ normal vertical and horizontal stress; $\varepsilon_v$, $\varepsilon_h$ normal strains; $f_v$, $f_h$ compressive strengths; $E_v$, $E_h$ modulus of elasticity; $\varepsilon_{e,v}$, $\varepsilon_{e,h}$ yield strains; $\varepsilon_{u,v}$, $\varepsilon_{u,h}$ limit compressive strains.
As can be seen from Figure 3, it was assumed that pebbles could only transmit compressive stress. In addition, the influence of lateral pressure on the vertical strength of the pebbles is not included. It should be noted that the possible lateral pressure in a thin layer of pebbles is usually very small. Thus, the linear–elastic behavior in compression is assumed until the compressive strength $f_v$, $f_h$ is attained, that is, the yield strains $\varepsilon_{e,v}$, $\varepsilon_{e,h}$ are attained, respectively. After the yield criterion has been satisfied, an ideal plastic behavior is adopted.

The pebble crushing criterion is defined by the limit compressive strains $\varepsilon_{u,v}$, $\varepsilon_{u,h}$. Linear behavior was adopted during unloading.

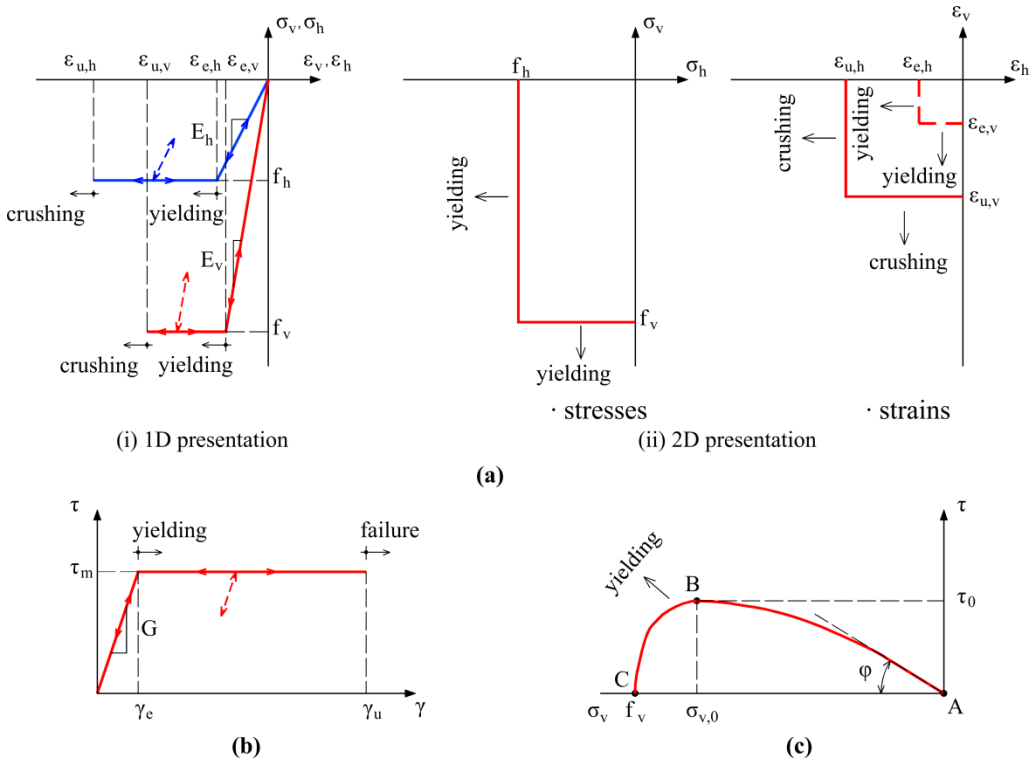


Figure 3 - *Adopted constitutive model for stone pebbles: (a) Normal stress-normal strain relation; (b) Shear stress-shear strain relation; (c) Shear strength-normal stress relation*

As the pebbles were treated as a homogeneous continuum, the opening of the cracks in tension and their closing in compression were monitored. It should be noted that these cracks are fictitious, that is, they simulate the pebble displacement under tension stress. A model of fixed distributed cracks was adopted, which was modeled as for concrete and masonry [Radnić *et al.*, 2012].
Assuming elastic behavior, Equation (1) and Equation (2) apply:

$$\varepsilon_{e,v} = f_v / E_v \tag{1}$$

$$\varepsilon_{e,h} = f_h / E_h \tag{2}$$

The orthotropic coefficient $c_0$ is defined by:

$$c_0 = E_h / E_v = f_h / f_v \tag{3}$$

Wherein valid:

$$E_h \cdot \nu_h = E_v \cdot \nu_v \tag{4}$$

$$c_0 = \nu_v / \nu_h \tag{5}$$

where $\nu_h$ and $\nu_v$ are Poisson's ratios for the horizontal and vertical directions, respectively.
The relationship between shear stress $\tau$ and shear strain $\gamma$ is presented in Figure 3. An elastoplastic relation is also assumed. Symbols in the Figure have the following meaning: $\tau_m$ shear strength, $G$ shear modulus, $\gamma_e = \tau_m / G$ yield shear strain, and $\gamma_u$ limit shear strain. Linear behavior was adopted during unloading. In shear, the yield criterion is also defined as a function of stress, and the crushing criterion as a function of strain, analogously adopted for normal stress.
The shear modulus of pebbles $G$ is defined by:

$$G = 1 / [(1+\nu_h)/E_h + (1+\nu_v)/E_v] \tag{6}$$

Further, the shear stress-normal stress relation for pebbles is also presented in Figure 3. The relation $\tau$-$\sigma_v$ is approximated by a cubic parabola passing through points A, B, and C. Symbols in the Figure have the following meaning: $\varphi$ pebble friction angle, and $\sigma_{v,0}$ vertical compressive stress at which the maximum shear strength of the pebbles $\tau_0$ is achieved. Thus, the tangent to the stress–strain curve at point A is at an angle $\varphi$, while at point B, the tangent of the curve is horizontal. In the lack of experimental data, $\sigma_{v,0} = 0.8 f_v$ and $\tau_0 = 0.3 f_v$ is assumed in this study. Thus, if the ratio $\tau$-$\sigma_v$ is such that it is below the assumed curve, the shear bearing capacity criterion is satisfied. Otherwise, "the current" shear stress $\tau$ is reduced to the curve for "the current" $\sigma_v$ and a further iterative procedure is performed with $G$ = 0 (plastic yielding). The shear failure criterion for that point is defined when $\gamma > \gamma_u$.

## 3.3 Constitutive model for simulation of foundation-pebble layer coupling surface behavior

2D six-node contact finite elements were used to simulate the foundation-pebble layer coupling surface. Contact elements can transmit compressive normal and shear stresses. The constitutive model for these elements is presented in Figure 4. The normal stress–normal strain relation for the contact element $\sigma_{v,c}$- $\varepsilon_{v,c}$ (Figure 4) is identical to that for the pebble layer (Figure 3). Further, the shear stress–shear strain relation (Figure 4) is analogous to that in Figure 3, where the values of $\tau_{m,c}$ , $\gamma_{u,c}$ , $\gamma_{e,c}$ depend on the foundation surface roughness, that is, the foundation construction technology.
In the previously performed experiments [Banović *et al.*, 2018b] [Banović *et al.*, 2020a] [Banović *et al.*, 2020b], the foundation of the model was prefabricated with a smooth bottom surface. Therefore, the above values are lower than those in Figure 3. If the foundation was to be concreted on site, directly at the top of the pebble layer into which the concrete would penetrate, the stated values $\tau_{m,c}$ , $\gamma_{u,c}$ , $\gamma_{e,c}$ would be larger than the corresponding ones within the pebble layer. In this case, the above-mentioned parameters can be adopted for the pebble layer because the thickness of the contact element is very small.
The adopted model of the shear strength of the contact elements is shown in Figure 4. It is analogous to that in Figure 3, that is, following the above stated on the influence of the

foundation surface roughness. In the case of concreting the foundation on site, it can be assumed that $\tau_{0,c}$, $\varphi_c$ are equal to $\tau_0$, $\varphi$, respectively. In the case of a smooth bottom surface of the foundation, $\tau_{0,c}$, $\varphi_c$ has a lower value than $\tau_0$, $\varphi$.

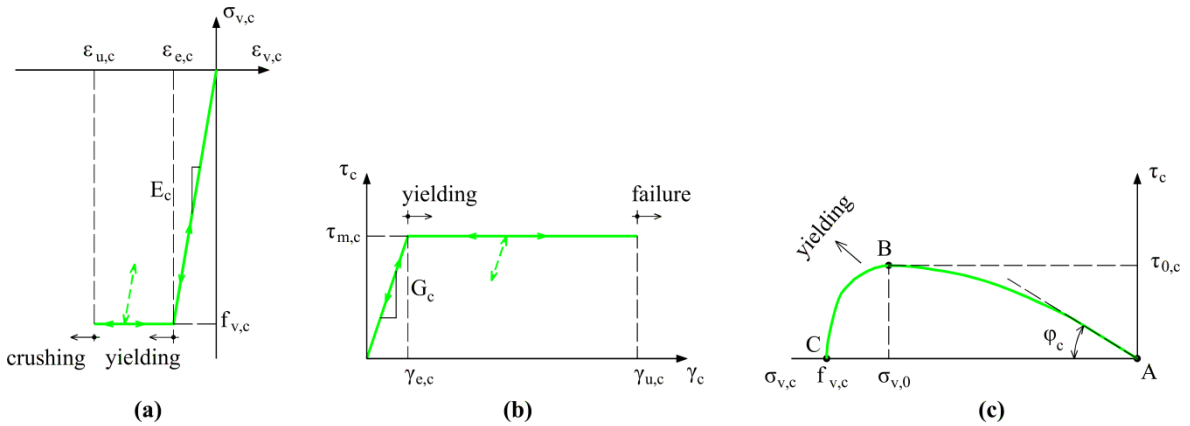


Figure 4 – *Adopted constitutive model for foundation-pebble layer coupling surface: (a) Normal stress–normal strain relation; (b) Shear strength–shear strain relation; (c) Shear stress–normal stress relation*

## 4 Experimental tests for determining the parameters of the pebble layer and foundation-pebble layer coupling surface constitutive models

A limited number of experimental tests to determine the main parameters of the presented constitutive model of pebbles and the constitutive model of the foundation-pebble layer coupling surface were performed. More extensive experimental tests and improvement of the pebble layer constitutive model for the influence of different levels of horizontal stress are planned to continue urgently.

### 4.1 Some parameters of the pebble layer

The shear strength of the pebble layer for constant levels of vertical effective stress was determined using a large-scale direct shear test. For the constant $\sigma_v$ stress state, the shear stress–shear displacement (strain) relation was determined through continuous monitoring of the horizontal shear force until the shear failure of the sample. The shear strength of the sample was determined for a wide $\sigma_v$ spectrum, ranging from 50 kPa to 600 kPa. Based on the normal stress–shear stress relation, the friction angle $\varphi$ of the pebbles was determined.

In addition to the classic direct shear test, the pebbles were tested only for vertical stress, without applying a horizontal force. Testing was performed in a direct shear box, and a normal stress–normal strain curve was derived. The vertical strains of the pebbles were calculated based on the measured vertical displacement. Further, based on the measured horizontal strains of the metal shear box, the horizontal stress of the pebbles was calculated.

Based on these data, the initial modulus of elasticity in the vertical and horizontal directions and Poisson's ratios for the horizontal direction were calculated. In addition, the bulk density of the pebbles was measured.

Basic data on the apparatus used to perform the direct shear test are shown in Figure 5. Two horizontally fixed and middle horizontally movable metal square shear boxes, with internal

dimensions of 300 mm × 300 mm and height of 120 mm, were used. Shear boxes are formed from welded steel sheets and provide extremely small lateral displacements/strains even for very high vertical pebble stresses. It can be concluded that for vertical loading, the pebbles are in a stress–strain state of vertical stress with prevented horizontal strain.
Prior to performing each test, the pebbles were first loaded with a vertical force to ensure compaction MS = 30 MPa. After maintaining a constant vertical force for 15 min, the sample was unloaded and then loaded with vertical force to the level of the considered constant $\sigma_v$. After maintaining the designed stress $\sigma_v$ for 10 min, a horizontal shear force was applied until the shear failure of the pebble sample.

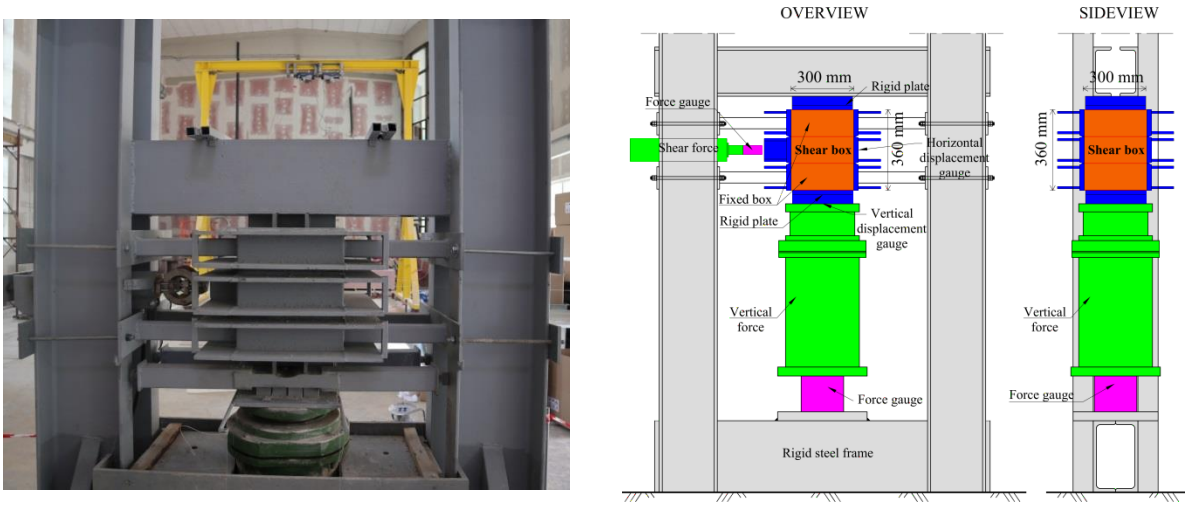


(a) (b)

Figure 5 – *Large-scale direct shear apparatus: (a) Photography of experimental setup, (b) Basic data of the adopted setup*

The measured quantities during the direct shear testing are presented in Figure 6. The vertical force *V*, horizontal force *H*, displacements *v*, *u*, and strain $\varepsilon_1$ were measured.
As stated above, prior direct shear tests, the pebbles were tested only with vertical stress, without applying a horizontal force. Normal stress–normal strain curve derived from that test is presented in Figure 7. The relationship between the vertical stress $\sigma_v$ and the average vertical strain of the pebbles $\varepsilon_v = v/h$ over the entire height of the specimen $h$ = 300 mm for vertical stress is presented in Figure 7. The stress was calculated in relation to the initial shear box area, which remained unchanged with increasing force *V*.
With the exception of the initial part of the diagram, where the "adjustment" at the initial load of the pebbles occurs, the behavior at low vertical compressive stress is almost linear. The average modulus of elasticity of the pebbles in the vertical direction is $E_v$ = 270 MPa. As the normal stress increases, the normal stress–normal strain curve becomes increasingly nonlinear and the tangent modulus of elasticity $E_v$ decreases. However, it should be noted that even under such a low $\sigma_v$ horizontal lateral compressive stress $\sigma_h$ occurs on the pebbles because of the prevented lateral strain of the shear box. Based on the measured lateral strain of the box for $\sigma_v$ = 0.5 MPa, it is estimated that the shear box opposes the approximate horizontal lateral pressure $\sigma_h$ = 0.24 MPa. Thus, in the performed experiments, in addition to the uniaxial pressure, the sample was exposed to a lateral pressure of approximately half the

vertical pressure, which does not correspond to the conditions of the pebble stress according to Figure 1.

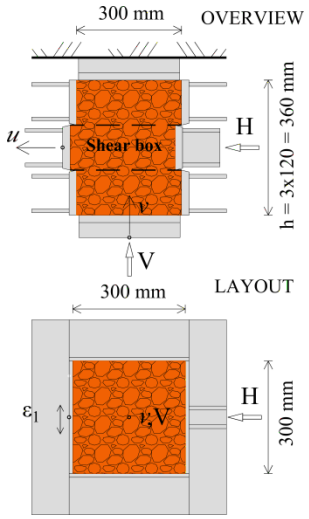


Figure 6 – *Measured quantities during direct shear testing*

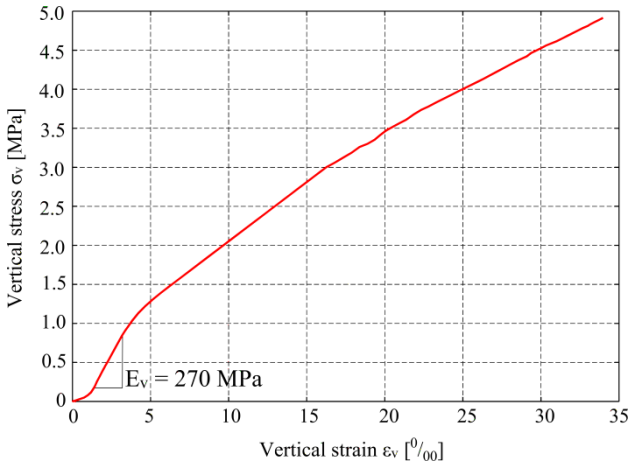


Figure 7 – *Normal stress–normal strain curve due to testing of a stone pebble in shear box subjected to normal stress only (without shear force)*

Assuming that the horizontal strain of the pebbles is completely prevented from the action of normal stress in the shear box and elastic behavior, the following expression yields

$$\varepsilon_h = \sigma_h/E_h - \nu_h \cdot \sigma_v/E_v = 0 \tag{7}$$

and:

$$\nu_h = (\sigma_h \cdot E_v)/(\sigma_v \cdot E_h) \tag{8}$$

Assuming the isotropic elastic behavior of the pebbles in the performed test with prevented lateral strain, from Equation (8) for $\sigma_v = 0.5$ MPa and $\sigma_h = 0.24$ MPa yields

$$\nu_h = \sigma_h/\sigma_v = 0.24/0.50 = 0.48 \tag{9}$$

where $\nu_h$ is very close to the so-called coefficient of resting pressure on the non-deformable vertical wall from the horizontal ground pressure. Assuming the orthotropic coefficient of the real pebble layer according to Figure 1 as $c_o = E_h/E_v = \nu_v/\nu_h = 2$, yields

$$\nu_v = 0.48/2 = 0.24 \tag{10}$$

$$E_h = 270/2 = 135 \text{ MPa} \tag{11}$$

Some results of the direct shear tests are shown hereinafter. The shear stress–horizontal displacement curve due to direct shear testing of stone pebbles subjected to different vertical stresses $\sigma_v$ is presented in Figure 8. If an average shear stress $\tau_a$ is calculated as

$$\tau_a = H/(2A_n) \tag{12}$$

where $H$ is the shear force, $A_n$ is the net cross-sectional area of the pebble sample exposed to the vertical pressure, and if the average shear deformation $\gamma_a$ is expressed as

$$\gamma_a = u/h_1 \tag{13}$$

where $u$ is the horizontal displacement of the middle metal shear box, $h_1$ is its height, and the $\tau_a$-$\gamma_a$ relation shown in Figure 9 is valid.

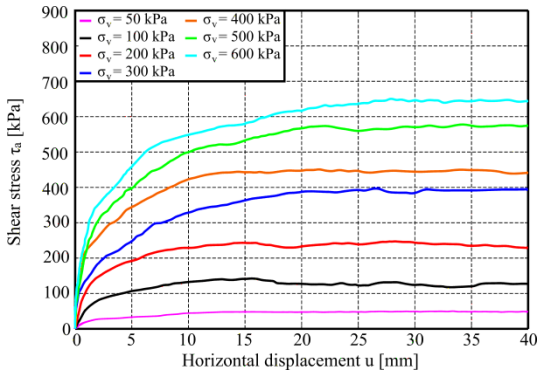


Figure 8 – *Shear stress–horizontal displacement curve due to direct shear testing of stone pebbles subjected to different vertical stresses* $\sigma_v$

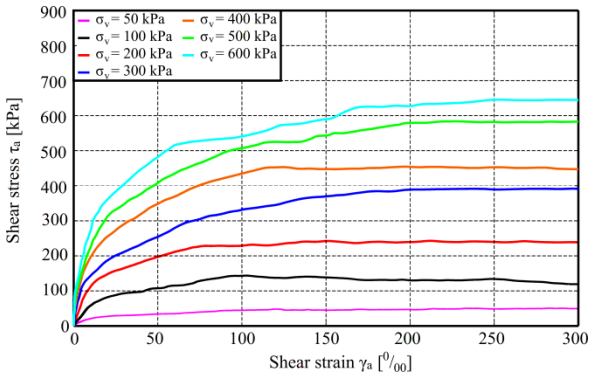


Figure 9 – *Shear stress–shear strain curve due to direct shear testing of stone pebbles subjected to different vertical stresses* $\sigma_v$

The actual (curvilinear) and previously defined uniform distribution of shear stress in the horizontal cross-section of the pebble sample is shown in Figure 10. The resulting shear force for both of these shear-stress distributions is equal (shear stress integral on the shear surface). The normal stress–shear stress relation is presented in Figure 11. For low levels of $\sigma_v$, this relation is approximately linear, while with increasing, $\sigma_v$ it is increasingly nonlinear. The slope of the normal stress–shear stress curve is the angle of internal friction of the pebbles $\varphi$, which decreases with increasing normal stress. The initial $\varphi$ is approximately $48^0$, which is close to the value experimentally determined by Indraratna *et al.* [2011] for similar gravel materials. For $\sigma_v$ = 0, the actual shear strength of the pebbles disappears. The experimentally determined strength for this case is due to the influence of the shear box, the loading speed, and other imperfections of the experiment. Once again, it is important to note that in this experiment, the pebbles were exposed to both vertical pressure and biaxial lateral pressure of

close to 50 % of the vertical pressure. Such a stress state does not correspond to the actual stress state of the pebbles under the building foundation, where they are predominantly exposed to uniaxial pressure and shear. Therefore, the relation $\sigma_v$-$\tau$ according to Figure 11 does not apply to the problem considered in Figure 1. The actual $\sigma_v$-$\tau$ relation for this problem is closer to the adopted diagram according to Figure 3 and is planned to be experimentally determined soon by a different approach.

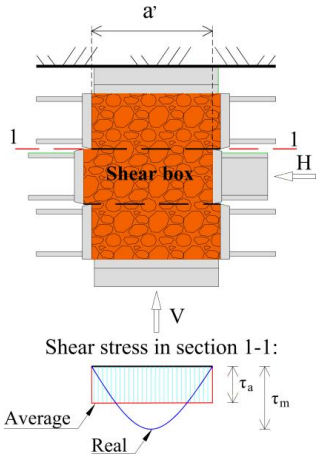


Figure 10 – *Shear stress distribution in section 1-1*

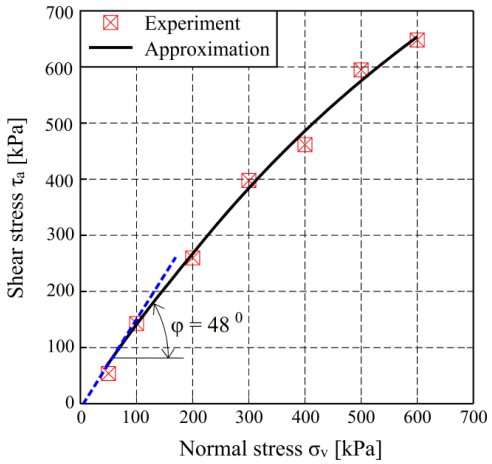


Figure 11 – *Shear stress–normal stress relation and frictional angle φ derived from direct shear testing*

The bulk density of the pebbles compacted to MS = 30 MPa was $\gamma_0$ = 1680 kg/m$^3$.

## 4.2 Some parameters of the foundation-pebble layer coupling surface

The friction angle $\varphi_c$ of the pebble layer subjected to different vertical stresses against a smooth prefabricated foundation interface was measured through experimental testing, as shown in Figure 12. A concrete prism with ground plan dimensions of 0.5 m x 0.5 m with variable additional weight at the top was adopted. The normal stress–shear stress relation derived from the previously mentioned experimental setup is presented in Figure 13. Based on the experimental results, $\varphi_c = 27^0$ was adopted. Clearly, there is a large difference between $\varphi_c$ and $\varphi = 48^0$.

The values of the parameters of the foundation-pebble layer coupling surface were calculated using the mechanical parameters of the pebble layer as

$$\tau_{0,c}=(\varphi_c/\varphi_0)\tau_m \tag{13}$$

$$G_c=(\varphi_c/\varphi_0)G \tag{14}$$

$$\gamma_{u,c}=(\varphi_0/\varphi_c)\gamma_u \tag{15}$$

where $\tau_m$, $G$, $\gamma_u$, $\varphi$ refer to the pebble layer, and $\tau_{0,c}$, $G_c$, $\gamma_{u,c}$, $\varphi_c$ to the foundation-pebble layer coupling surface behavior, respectively.

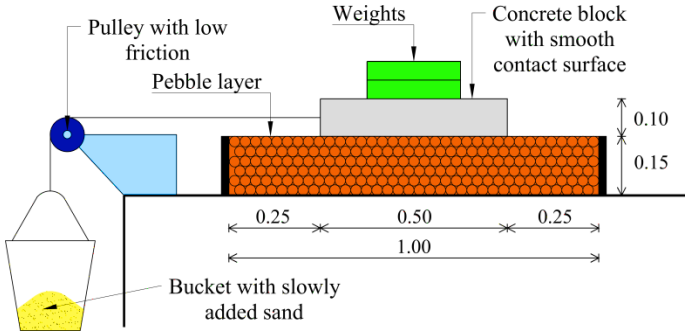


Figure 12 – *Experimental setup: rigid concrete block with smooth contact surface designed to slide against the pebble layer to determine friction angle* $\varphi_c$

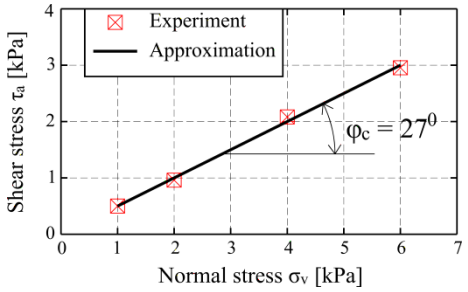


Figure 13 – *Normal stress–shear stress relation for experimental setup according to Figure 12*

## 5 Verification of the presented numerical model

The numerical model for dynamic analysis of planar structures presented in Section 3, with the developed constitutive models for the stone pebble layer and the foundation-layer contact surface, was verified using shake-table tests of simple structural models based on an aseismic layer of stone pebbles. In this study, only the model of a very stiff building $M_1$ and the model of a stiff building $M_2$ [Banović *et al.*, 2020b] are considered, whose data are shown in Figure 14.

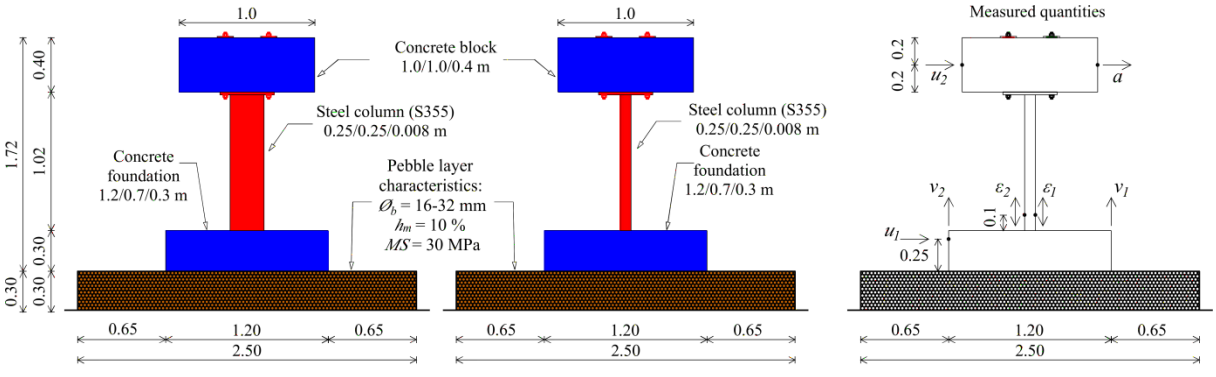


Figure 14 – *Considered models previously tested by shake-table: (a)Very stiff model* $M_1$*, (b) Stiff model* $M_2$*, (c) Measured quantities during shake-table testing*

The model column is made of a square cross-section steel tube, with a rigid concrete block of m = 1000 kg on the column top. The models have a concrete foundation, dimensions 1.2 m x 0.7 m x 0.3 m, which is based on an aseismic layer with the following characteristics: thickness $h_p$ = 0.3 m, fraction $\phi_b$=16-32 mm, compaction MS = 30 MPa and humidity $h_m$ = 10 %. A more detailed description of the conducted experimental tests can be found in [Banović *et al.*, 2020b].

The models were exposed to horizontal accelerations of four accelerograms (artificial accelerogram-AA, accelerogram Petrovac-AP, accelerogram Ston-AS, and accelerogram Banja Luka-ABL), as shown in Figure 15. All accelerograms were scaled to equal peak ground acceleration (PGA) = 0.3 g.

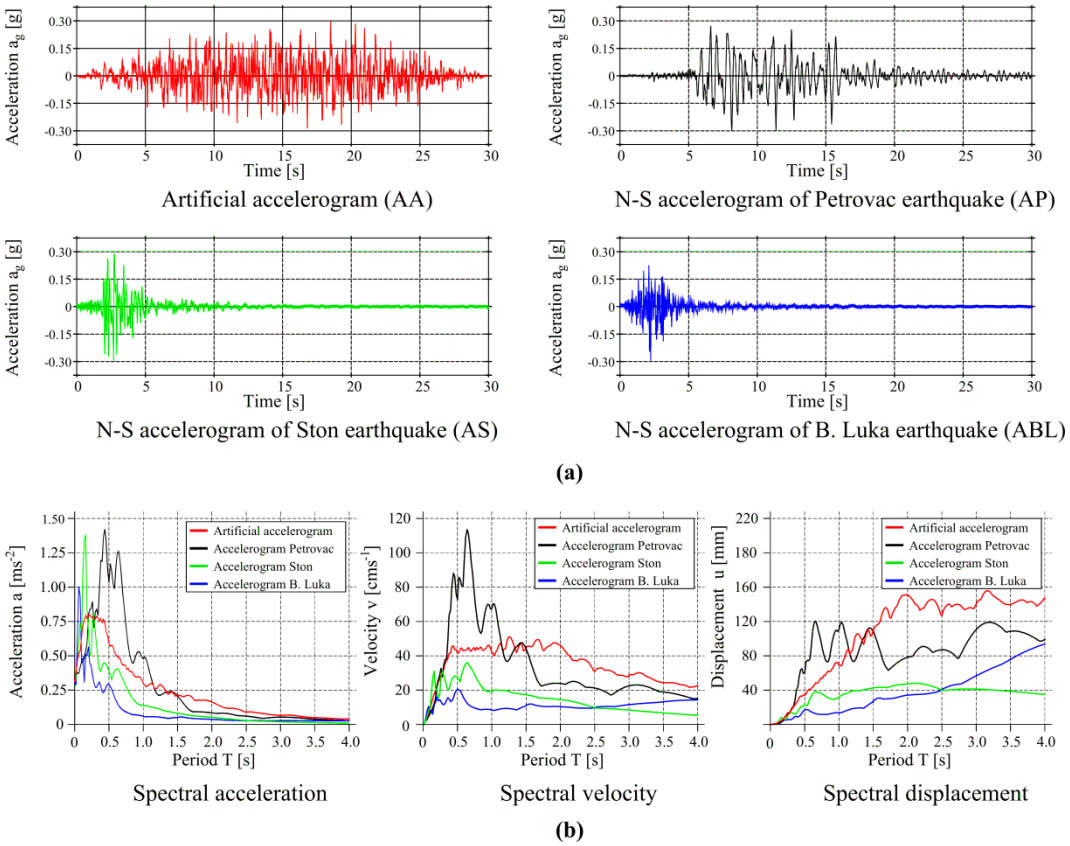


Figure 15 – *Applied horizontal base excitations: (a) Accelerograms, (b) Elastic response spectra*

The presented numerical model was verified using a simulation of 10 conducted experimental tests (Table 1). The spatial discretization of the models is presented in Figure 16.

Table 1- *Performed numerical simulations of experiments*

| Excitation | Model $M_1$ | Model $M_2$ | |
|---|---|---|---|
| AA | + | + | *One-time base excitation with PGA = 0.3 g* |
| AP | + | + | |
| AS | + | + | |
| ABL | + | + | |
| AA | + | + | *Successive application of AA excitation until model collapse* |

Thin contact elements were used at the foundation-pebble layer contact surface. A rather coarse mesh of regular finite elements was used. It should be noted that the concrete block at the top of the column and the concrete foundation are rigid. Therefore, these elements are

simulated with elastic behavior and extreme strengths to simplify and shorten dynamic analyses. The parameters of steel, stone pebbles, and contact element constitutive models are presented in Table 2.

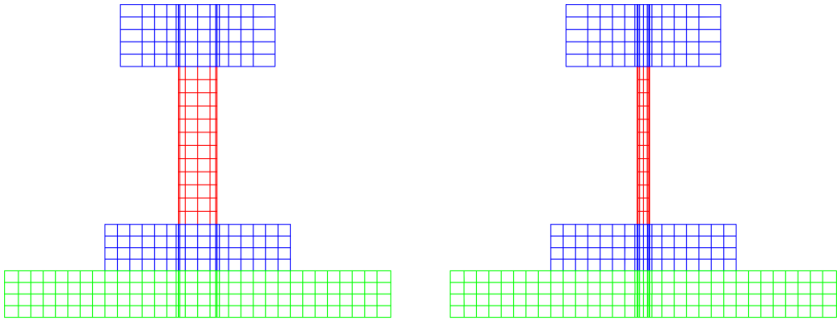

**(a)** **(b)**

Figure 16 – *Spatial discretization by FE: (a) $M_1$ model, (b) $M_2$ model*

Table 2- *Adopted basic parameters of steel, stone pebbles, and contact elements constitutive models*

| *Steel* | | | | | | | | | | | |
|---|---|---|---|---|---|---|---|---|---|---|---|
| $E$ (GPa) | | $f_{c,\,steel}$ (MPa) | | $f_{t,\,steel}$ (MPa) | | $\nu_{steel}$ | | $\varepsilon_{steel}$ [$^0/_{00}$] | | | |
| 200 | | 520 | | 520 | | 0.3 | | 20 | | | |
| *Stone pebbles* | | | | | | | | | | | |
| $E_v$ (MPa) | $E_h$ (MPa) | $f_v$ (MPa) | $f_h$ (MPa) | $\tau_m$ (MPa) | $\nu_v$ | $\nu_h$ | $\varepsilon_{u,v}$ [$^0/_{00}$] | $\varepsilon_{u,h}$ [$^0/_{00}$] | $G$ (MPa) | $\gamma_u$ [$^0/_{00}$] | $\varphi$ [$^0$] |
| 270 | 135 | 6.0 | 3.0 | 1.8 | 0.24 | 0.48 | 20 | 40 | 64.3 | 100 | 48 |
| *Contact element: foundation-pebble layer coupling surface* | | | | | | | | | | | |
| $E_c$ (MPa) | | $f_{v,c}$ (MPa) | | $\tau_{m,c}$ (MPa) | | $\nu_c$ | $\varepsilon_{u,c}$ [$^0/_{00}$] | | $G_c$ (MPa) | $\gamma_{u,c}$ [$^0/_{00}$] | | $\varphi_c$ [$^0$] |
| 270 | | 6.0 | | 1.01 | | 0.24 | 20 | | 36.17 | 177 | | 27 |

Only some results of the performed dynamic analyses are presented, and these are discussed below. A comparison of the time sequence of experimentally determined and numerically obtained results of measured accelerations, displacements, and strains for AA excitation at PGA = 0.3 g is presented in Figure 17. This sequence is quite identical for both models as well as the correlation of the measured peak values (see Table 3). Deviations in the "frequencies" of the time response of quantities $a$, $u_2$, $\varepsilon_1$ between the experiment and the numerical model is due to the difference in their stiffness and material properties, model parameters (spatial and temporal discretization, convergence criterion, etc.), and due to other influential parameters. It should be noted that the numerical model obtains a slightly stiffer construction of the physical model, resulting in slightly higher accelerations and strains and smaller displacements. This is probably due to the inadequacy of the adopted constitutive models of materials, overestimated values of strengths and modulus of elasticity, design parameters, etc.

Although the stresses on the bottom of the steel column are in the elastic region, owing to the nonlinear behavior of the seismic layer and the nonlinear behavior at the foundation-seismic isolation coupling surface, the obtained numerical results can be considered acceptable, especially the peak values according to Table 3.

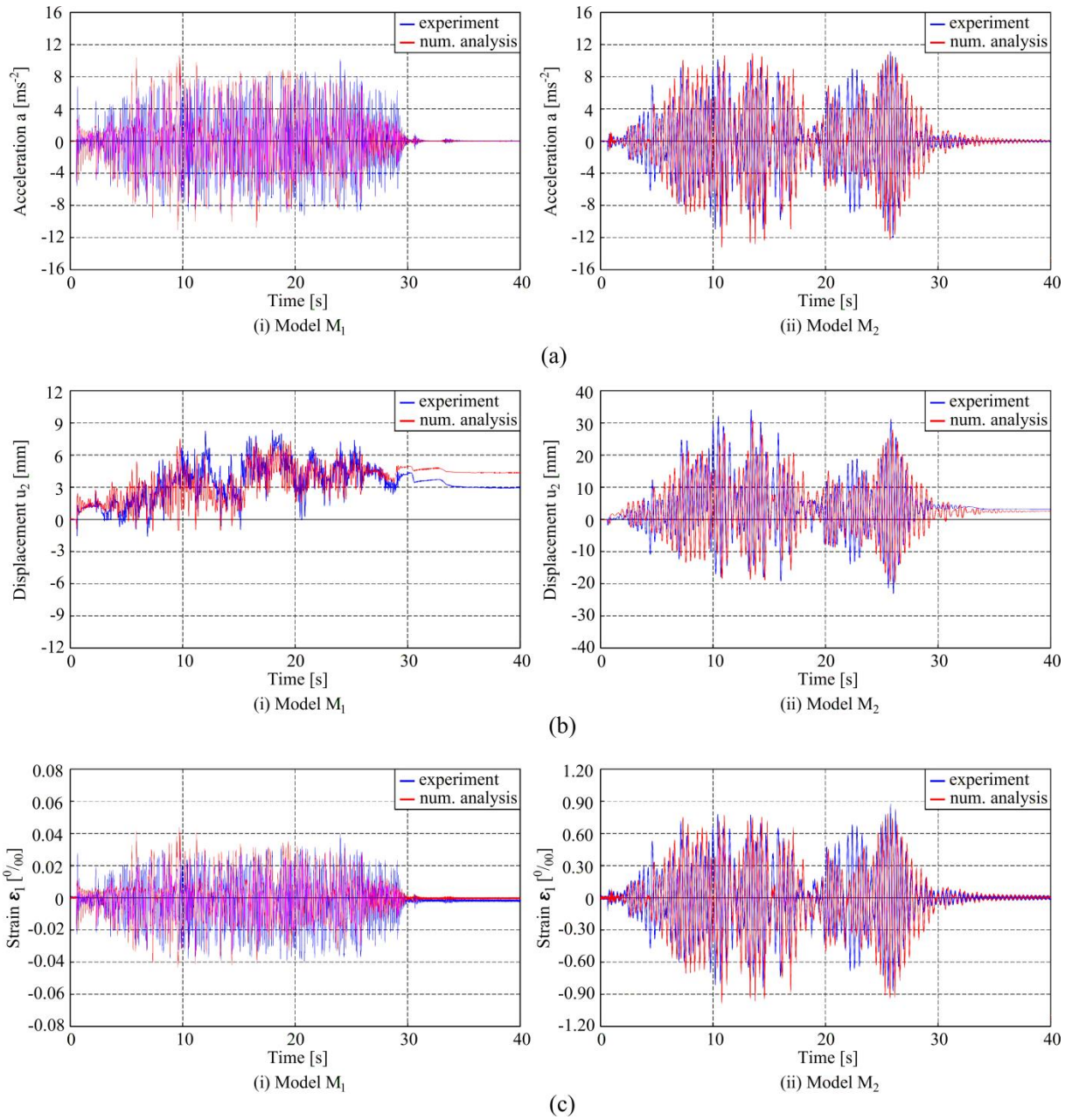


Figure 17 – *Comparison of experimentally determined and numerically obtained results for applied AA accelerogram (PGA = 0.3 g): (a) Horizontal acceleration of the mass at the column top, (b) Horizontal displacement of the mass at the column top, (c) Vertical strain on the right bottom side of the steel column*

A comparison of the time history of the experimental and numerical results for $a$, $u_2$, $\varepsilon_1$ under the action of an ABL accelerogram with PGA = 0.3 g is shown in Figure 18. A good agreement between the experimental and numerical results can also be spotted, similar to those in Figure 17 and Table 3 for the AA accelerogram.

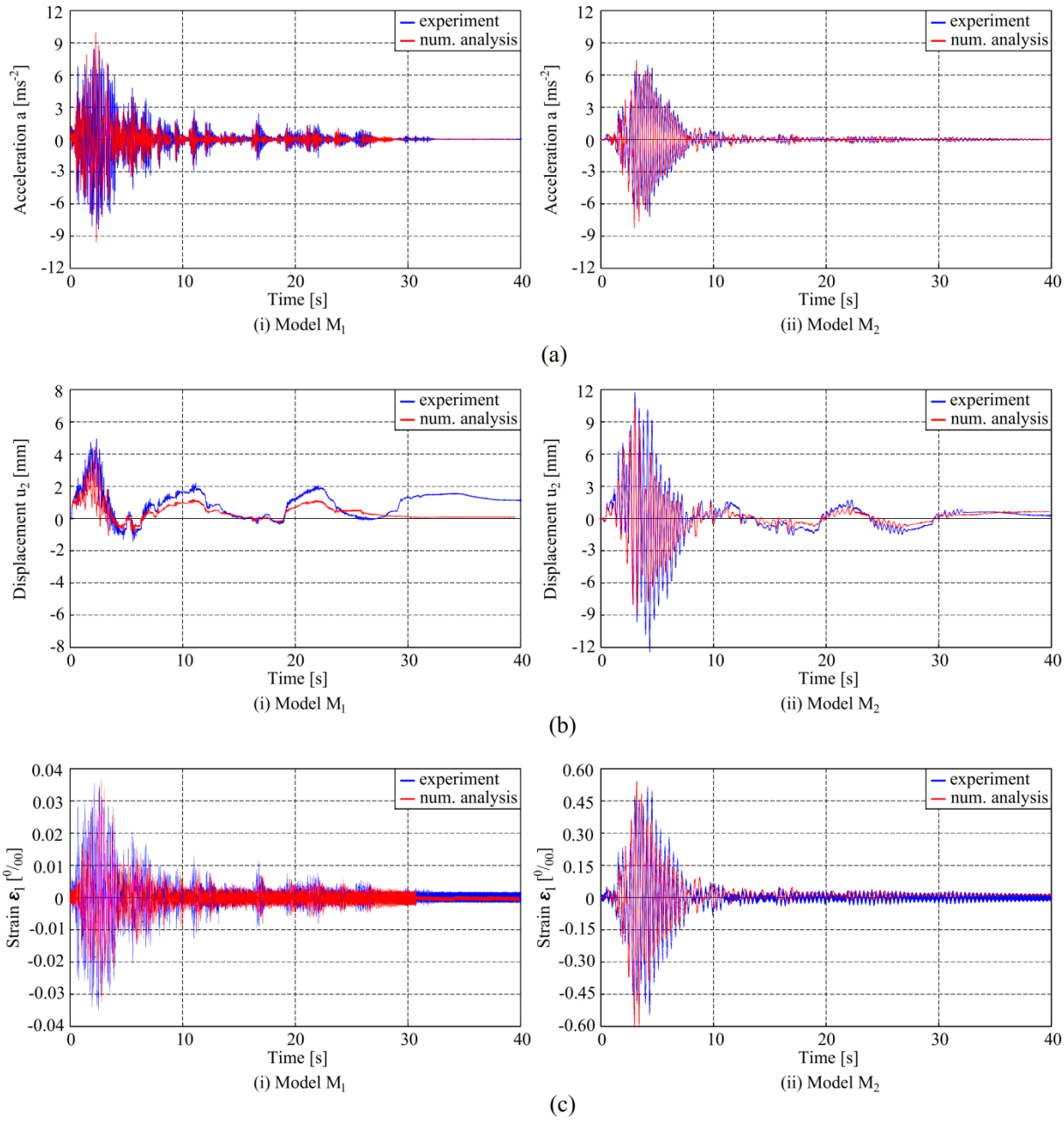


Figure 18 – *Comparison of experimentally determined and numerically obtained results for applied ABL accelerogram (PGA = 0.3 g): (a) Horizontal acceleration a of the mass at the column top, (b) Horizontal displacement $u_2$ of the mass at the column top, (c) Vertical strain $\varepsilon_1$ on the right bottom side of the steel column*

A comparison of the peak values of measured quantities determined using the experimental model and calculated using the presented numerical model for applied excitations at PGA = 0.3 g is presented in Table 3. It can be observed that for the short predominant period, impact accelerograms AS and ABL, the deviations of the experimental and numerical values are slightly larger than those for the accelerograms with a larger predominant period (AA and AP). Nevertheless, these deviations can still be considered within acceptable limits.

Table 3- *Comparison of some peak values of experimentally determined and numerically obtained results for one-time base excitation (PGA = 0.3 g)*

| | AA | | | AP | | | AS | | | ABL | | |
|---|---|---|---|---|---|---|---|---|---|---|---|---|
| Model $M_1$ | Exp. | Num. | Rel. error [%] | Exp. | Num. | Rel. error [%] | Exp. | Num. | Rel. error [%] | Exp. | Num. | Rel. error [%] |
| $a$ [ms$^{-2}$] | 10.18 | 11.17 | 9.7 | 9.90 | 10.74 | 8.4 | 10.73 | 12.34 | 15 | 8.41 | 9.96 | 18.4 |
| $\varepsilon_1$ [$^0/_{00}$] | 0.040 | 0.043 | 7.5 | 0.040 | 0.042 | 5.0 | 0.042 | 0.047 | 11.9 | 0.030 | 0.035 | 16.7 |
| $u_2$ [mm] | 7.95 | 7.52 | 5.7 | 5.20 | 4.81 | 7.5 | 7.00 | 5.97 | 17.2 | 5.00 | 4.42 | 13.1 |
| Model $M_2$ | | | | | | | | | | | | |
| $a$ [ms$^{-2}$] | 11.86 | 13.17 | 10.0 | 14.17 | 15.89 | 12.1 | 7.89 | 8.86 | 10.9 | 7.22 | 9.24 | 14.1 |
| $\varepsilon_1$ [$^0/_{00}$] | 0.870 | 0.962 | 11.1 | 1.020 | 1.121 | 9.9 | 0.587 | 0.660 | 12.4 | 0.537 | 0.606 | 12.8 |
| $u_2$ [mm] | 33.75 | 30.7 | 9.4 | 40.4 | 37.1 | 8.2 | 17.5 | 15.1 | 15.9 | 12.5 | 10.41 | 16.7 |

A comparison of the artificial accelerogram PGA at which the physical and numerical models collapsed, with a successive increase in the acceleration $\Delta a_{g,\,max}$ = 0.05 g, is presented in Table 4. It can be noted that the PGA values at the collapse of the experimentally tested model are slightly higher than the values at the collapse of the numerical model. Thus, in the considered examples, the numerically obtained PGA values are conservative in relation to the experiment, which may not be the case in many other examples. The difference in the experimental and numerical values of PGA is relatively small, especially when we consider that numerous nonlinearities in the structure progressively occur before its failure.

Table 4- *Comparison of the PGA of the artificial accelerogram at which the physical and numerical model collapsed*

| | Model $M_1$ | | Model $M_2$ | |
|---|---|---|---|---|
| | Exp. | Num. | Exp. | Num. |
| PGA [g] | 0.55 | 0.50 | 0.45 | 0.40 |

# 6 Conclusions

This paper briefly presents the previously developed numerical model for the dynamic analysis of planar concrete, steel, and masonry structures based on FEM. The model was then extended with developed constitutive models of the stone pebble aseismic layer behavior and the foundation-pebble layer coupling surface behavior. The simple numerical model is based on a relatively small number of parameters, and is intended for practical application. The verification of the numerical model was performed on several previously performed shake-table tests of simple models of very stiff and stiff building on an aseismic layer of pebbles, with four different earthquake accelerograms. A good agreement was observed between the experimental and numerical values of the measured accelerations, displacements, and strains/stresses, both for lower PGA levels and for structural collapse at higher PGA levels. However, further verification of this model is needed, as well as its improvement.

# 7 Acknowledgements

This work has been fully supported by the Croatian Science Foundation under the project *"Seismic base isolation of a building by using natural materials - shake table testing and numerical modeling*" [IP-06-2016-5325]. The work of doctoral student Ivan Banović has been fully supported by the *"Young researchers' career development project – training of*

*doctoral students"* of the Croatian Science Foundation funded by the European Union from the European Social Fund. The authors are grateful for the support.

## References

Amendola, A., Carpentieri, G., Feo, L., Fraternali, F. (2016a). Bending dominated response of layered mechanical metamaterials alternating pentamode lattices and confinement plates. Composite Structures. 157, 71-77.

Amendola, A., Smith, C.J., Goodall, R., Auricchio, F., Feo, L., Benzoni, G., Fraternali, F. (2016b). Experimental response of additively manufactured metallic pentamode materials confined between stiffening plates. Composite Structures. **142**, 254-262.

Anastasopoulos, I., Kourkoulis, R., Gelagoti, F., Papadopoulos, E. (2012b). Rocking response of SDOF systems on shallow improved sand: An experimental study. Soil Dynamics and Earthquake Engineering. **40**: 15-33.

Anastasopoulos, I., Loli, M., Georgarakos, T., Drosos, V. (2012a). Shaking table testing of rocking-isolated bridge pier on sand. Journal of Earthquake Engineering. **17**(1): 1–32.

Avossa, A. M., Pianese, G. (2017). Damping effects on the seismic response of base-isolated structures with LRB devices. Ingegneria Sismica. **34**(2): 3-30.

Azinović, B., Kilar, V., Koren, D. (2014). The seismic response of low-energy buildings founded on a thermal insulation layer –a parametric study. Engineering Structures. **81**: 398-411.

Azinović, B., Kilar, V., Koren, D. (2016). Energy-efficient solution for the foundation of passive houses in earthquake-prone regions. Engineering Structures. **112**: 133-145.

Azzam, W., Ayeldeen, M., El Siragy, M. (2018). Improving the structural stability during earthquakes using in-filled trench with EPS geofoam—numerical study. Arabian Journal of Geosciences. **11**(14): 395.

Baloević, G., Radnić, J., Grgić, N. (2019). Numerical model for dynamic analysis of masonry-infilled steel and concrete frames. Materialwissenschaft und Werkstofftechnik. **50**(5): 519-532.

Baloević, G., Radnić, J., Grgić, N., Matešan, D., Smilović, M. (2016b). Numerical model for nonlinear analysis of composite concrete-steel-masonry bridges. Coupled Systems Mechanics. **5**(1): 1-20.

Baloević, G., Radnić, J., Matešan, D., Grgić, N., Banović, I. (2016a). Comparison of Developed Numerical Macro and Micro Masonry Models for Static and Dynamic Analysis of Masonry-infilled Steel Frames. Latin American Journal of Solids and Structures. **13**(12), 2251-2265.

Bandyopadhyay, S., Sengupta, A., Reddy, G. R. (2015). Performance of sand and shredded rubber tire mixture as a natural base isolator for earthquake protection. Earthquake Engineering and Engineering Vibration. **14**(4): 683–693.

Banović, I., Radnić, J., Grgić, N. (2018b). Shake table study on the efficiency of seismic base isolation using natural stone pebbles. Advances in Materials Science and Engineering, Article ID 1012527, 20 pages

Banović, I., Radnić, J., Grgić, N. (2019). Geotechnical seismic isolation system based on sliding mechanism using stone pebble layer: shake-table experiments. Shock and Vibration, Article ID 9346232, 26 pages

Banović, I., Radnić, J., Grgić, N. (2020a). Effect of structural stiffness on the efficiency of seismic base isolation using layers of stone pebbles. Ingegneria Sismica, **37**(2): 66-91.

Banović, I., Radnić, J., Grgić, N. (2020b). Foundation size effect on the efficiency of seismic base isolation using a layer of stone pebbles. Earthquakes and Structures. **19**(2): 103-117.

Banović, I., Radnić, J., Grgić, N., Matešan, D. (2018a). The use of limestone sand for the seismic base isolation of structures. Advances in Civil Engineering. Article ID 9734283, 12 pages

Brunet, S., de la Llera, J. C., Kausel, E. (2016). Non-linear modeling of seismic isolation systems made of recycled tire-rubber. Soil Dynamics and Earthquake Engineering. **85**: 134–145.

Calvi, P. M., Moratti, M., Calvi, G. M. (2016). Seismic Isolation Devices Based on Sliding Between Surfaces with Variable Friction Coefficient. Earthquake Spectra. **32**(4): 2291-2315.

Castaldo, P., Ripani, M. (2017). Optimal design of single concave sliding bearings for isolated structures considering intermediate isolation degrees. Ingegneria Sismica. **34** (5): 5-24.

Chen, X., Xia, X., Zhang, X., Gao, J. (2020). Seismic performance and design of bridge piers with rocking isolation. Structural Engineering and Mechanics. **73**(4): 447-454.

Chung, Y. L., Du, L. J., Pan, H. H. (2019). Performance evaluation of a rocking steel column base equipped with asymmetrical resistance friction damper. Earthquakes and Structures. **17**(1): 49-61.

De Domenico, D., Ricciardi, G., Infanti, S., Benzoni, G. (2019). Frictional Heating in double curved surface sliders and its effects on the hysteretic behavior: an experimental study. Frontiers in Built Environment. **5**(74)

Dhanya, J. S., Boominathan, A., Subhadeep Banerjee. (2019). Performance of Geo-Base Isolation System with Geogrid Reinforcement. International Journal of Geomechanics. **19**(7).

Dhanya, J. S., Boominathan, A., Subhadeep Banerjee. (2020). Response of low-rise building with geotechnical seismic isolation system. Soil Dynamics and Earthquake Engineering. **136**

Doudoumis, I., Papadopoulos, P.,Papaliangas, T. (2002). Low-cost base isolation system on artificial soil layers with low shearing resistance. Proceedings of the 12th European Conference on Earthquake Engineering, London, UK

Fabbrocino, F., Amendola, A., Benzoni, G., Fraternali, F. (2016). Seismic application of pentamode lattices. Ingegneria Sismica. **1**:62-71.

Forcellini, D. (2017). Assessment on geotechnical seismic isolation (GSI) on bridge configurations. Innovative Infrastructure Solutions **2**(1), 9 pages.

Forcellini, D. (2020). Assessment of Geotechnical Seismic Isolation (GSI) as a Mitigation Technique for Seismic Hazard Events. Geosciences. **10**, 222.

Fraternali, F., Amendola, A., Benzoni, G. (2018). Innovative seismic isolation devices based on lattice materials: A review. Ingegneria Sismica. **4**:93-113.

Hadad, H. A, Calabrese, A., Strano, S., Serino, G. (2017). A base isolation system for developing countries using discarded tyres filled with elastomeric recycled materials. Journal of Earthquake Engineering. **21**(2): 246-266.

Hernández, E., Palermo, A., Granello, G., Chiaro, G., Banasiak, L. (2020). Eco-rubber Seismic-Isolation Foundation Systems: A Sustainable Solution for the New Zealand Context. Structural Engineering International. 1-9.

Hughes, T. J. R., Pister, K. S., Taylor, R. L. (1979). Implicit-explicit finite elements in nonlinear transient analysis. Computer Methods in Applied Mechanics and Engineering. **17–18**: 159–182.

Indraratna, B., Ngo, T., Rujikiatkamjorn, C. (2011). Behavior of geogrid-reinforced ballast under various levels of fouling. Geotextiles and Geomembranes. **29**(3): 313-322.

Kalpakcı, V., Bonab, A. T., Özkan, M. Y., Gülerce, Z. (2018). Experimental evaluation of geomembrane/geotextile interface as base isolating system. Geosynthetics International. **25**(1), 1-11.

Karatzia, X., Mylonakis, G. (2017). Geotechnical seismic isolation using eps geofoam around piles. 6th International Conference on Computational Methods in Structural Dynamics and Earthquake Engineering, Rhodes Island, Greece

Kelly, J. (1986). Aseismic base isolation: review and bibliography. Soil Dynamics and Earthquake Engineering. **5**(4), 202-216.

Koren, D., Kilar, V. (2016). Seismic vulnerability of reinforced concrete building structures founded on an XPS layer. Earthquakes and Structures. **10**(4), 939 -963.

Kuvat, A., Sadoglu, E. (2020). Dynamic properties of sand-bitumen mixtures as a geotechnical seismic isolation material. Soil Dynamics and Earthquake Engineering. **132**, 106043

Lomiento, G., Bonessio, N., Benzoni, G. (2013). Concave sliding isolator's performance under multi-directional excitation. Ingegneria Sismica. **30**:17-32.

Makris, N. (2014). A half-century of rocking isolation. Earthquakes and Structures. **7**(6), 1187-1221.

Makris, N. (2018). Seismic isolation: early history. Earthquake Engineering and Structural Dynamics. **48** (2), 269-283.

Mavronicola E., Komodromos P., Charmpis D. C. (2010). Numerical investigation of potential usage of rubber–soil mixtures as a distributed seismic isolation approach. Proceedings of the 10th International Conference on Computational Structures Technology, Valencia, Spain

Murillo, C., Thorel, L., Caicedo, B. (2009). Ground vibration isolation with geofoam barriers: centrifuge modelling. Geotextiles and Geomembranes. **27**(6), 423-434.

Naeim, F., Kelly, J. M. (1999). Design of seismic isolated structures: From theory to practice. John Wiley & Sons, Inc., New York.

OECD (2008) Costs of Inaction of Environmental Policy Challenges Report ENV/EPOC(2007)17/REV2

Panjamani, A., Devarahalli Ramegowda, M., Divyesh, R. (2015). Low cost damping scheme for low to medium rise buildings using rubber soil mixtures. Japanese Geotechnical Society Special Publication. **3**(2), 24–28.

Patil, S. J., Reddy, G. R., Shivshankar, R., Babu, R., Jayalekshmi, B. R., Kumar, B. (2016). Seismic base isolation for structures using river sand. Earthquakes and Structures. **10**(4), 829-847.

Petrone, G., Ferrentino, T., Alfano, G. (2017). Influence of PGA/PGV ratio on the seismic reliability of base-isolated system with FPS. Ingegneria Sismica. **34**(3): 39-62.

Pistolas, G. A., Pitilakis, K., Anastasiadis, A. (2020). A numerical investigation on the seismic isolation potential of rubber/soil mixtures. Earthquake Engineering and Engineering Vibration. **19**: 683–704.

Pitilakis, K., Karapetrou, S., Tsagdi, K. (2015). Numerical investigation of the seismic response of RC buildings on soil replaced with rubber–sand mixtures. Soil Dynamics and Earthquake Engineering. **79**: 237–252.

Radnić, J., Grgić, N., Matešan, D., Baloević, G. (2015). Shake table testing of reinforced concrete columns with different layout size of foundation. Materialwissenschaft und Werkstofftechnik. **46**(4-5): 348–367.

Radnić, J., Harapin, A., Matešan, D., Trogrlić, B., Smilović, M., Grgić, N., Baloević, G. (2011). Numerical Model for Analysis of Masonry Structures. Gradjevinar, **63**(6): 529-546.

Radnić, J., Markić, R., Grgić, N., Glibić, M., Banović, I. (2016). Comparison of numerical models for nonlinear static analysis of planar concrete frames based on 1D and 2D finite elements. Materialwissenschaft und Werkstofftechnik. **47**(5-6): 369-581.

Radnić, J., Matešan, D., Harapin, A., Smilović, M., Grgić, N. (2012). Numerical model for static and dynamic analysis of masonry structures. Mechanics and Properties of Composed Materials and Structures, Advanced Structured Materials, 1–33, Springer-Verlag, Berlin, Germany

Smilović Zulim, M., Radnić, J. (2020). Anisotropy Effect of Masonry on the Behaviour and Bearing Capacity of Masonry Walls. Advances in Materials Science and Engineering. 2020, 5676901

Smilović Zulim, M., Radnić, J., Grgić, N., Baloević, G. (2018). Effect of anisotropy of masonry on the behaviour of unreinforced and confined masonry walls under ground motion. Engineering Design Applications. Heidelberger, Springer, Cham, 173-183.

Smilović Zulim, M., Radnić, J., Harapin, A. (2019). Shear effect on seismic behaviour of masonry walls. Materialwissenschaft und Werkstofftechnik. **50**(5), 565-579.

Sorrentino, L., Masiani, R., Decanini, L. D. (2006). Overturning of rocking rigid bodies under transient ground motions. Structural Engineering and Mechanics. **22**(3), 293-310.

Sorrentino, L., Masiani, R., Griffith, M. C. (2008). The vertical spanning strip wall as a coupled rocking rigid body assembly. Structural Engineering and Mechanics. **29**(4): 433-453.

Tehrani, F. M., Hasani, A. (1996). Behaviour of Iranian low rise buildings on sliding base to earthquake excitation. Proceedings of the 11th World Conference on Earthquake Engineering, Paper 1433, Acapulco, Mexico

Titirla, M. D., Katakalos K., Zuccaro G., Fabbrocino F. (2017). On the mechanical modeling of an innovative energy dissipation device. Ingegneria Sismica. **34**(2): 126-137.

Tsang, H. H. (2008). Seismic isolation by rubber-soil mixtures for developing countries. Earthquake Engineering & Structural Dynamics. **37**(2): 283–303.

Tsang, H. H. (2009). Geotechnical seismic isolation. Earthquake Engineering: New Research. 55–87, Nova Science Publishers Inc., New York, NY, USA

Tsang, H. H., Lo, S. H., Xu, X., Neaz Sheikh, M. (2012). Seismic isolation for low-to-medium-rise buildings using granulated rubber-soil mixtures: numerical study. Earthquake Engineering & Structural Dynamics. **41**(14): 2009–2024.

Tsang, H. H., Pitilakis, K. (2019). Mechanism of geotechnical seismic isolation system: Analytical modeling. Soil Dynamics and Earthquake Engineering. **122**: 171-184.

Tsiavos, A., Alexander, N. A., Diambra, A., Ibraim, E., Vardanega, P. J., Gonzalez-Buelga, A., Sextos A. (2019a). A sand-rubber deformable granular layer as a low-cost seismic isolation strategy in developing countries: experimental investigation. Soil Dynamics and Earthquake Engineering. 125.

Tsiavos, A., Alexander, N. A., Sextos, A. (2019b). Numerical investigation of the sliding response of flexible structures founded on a deformable granular layer. 2nd International Conference on Earthquake Engineering and Post Disaster Reconstruction Planning, Bhaktapur, Nepal

Tsiavos, A., Haladij, P., Sextos, A., Alexander, N. A. (2020b). Analytical investigation of the effect of a deformable sliding layer on the dynamic response of seismically isolated structures. Structures. **27**: 2426-2436.

Tsiavos, A., Sextos, A., Stavridis, A., Dietz, M., Dihoru, L., Alexander, N. A. (2020a). Large-scale experimental investigation of a low-cost PVC 'sand-wich' (PVC-s) seismic isolation for developing countries. Earthquake Spectra.

Xiong, W., Li, Y. (2013). Seismic isolation using granulated tiresoil mixtures for less-developed regions: experimental validation. Earthquake Engineering & Structural Dynamics. **42**(14), 2187-2193.

Xiong, W., Yan, M. R., Li, Y. Z. (2014). Geotechnical Seismic Isolation System - Further Experimental Study. Applied Mechanics and Materials. **580-583**: 1490-1493.

Yegian, M. K., Kadakal, U. (2004). Foundation isolation for seismic protection using a smooth synthetic liner. Journal of Geotechnical and Geoenvironmental Engineering. **130**(11): 1121–1130.

Yegian, M. K., Lahlaf, A. M. (1992). Geomembranes as base isolation. Geotechnical Fabrics Report. **10**(6): 17-21.

Zhao, X., Zhang, Q., Zhang, Q., He, J. (2016). Numerical study on seismic isolation effect of gravel cushion. Proceedings of the 7th International Conference on Discrete Element Methods. **188**: 1055-1063., Dalian, China

Zorn, M. (2018). Natural Disasters and Less Developed Countries: Nature, Tourism and Ethnicity as Drivers of (De)Marginalization. Perspectives on Geographical Marginality, vol 3. Springer, Cham.